DOE/NASA/0153-3
NASA CR-174736
84AEPD004

Mod-5A Wind Turbine Generator Program Design Report

Volume III—Final Design and System Description
Book 1

General Electric Company
(Advanced Energy Programs Department)

August 1984

Prepared for
NATIONAL AERONAUTICS AND SPACE ADMINISTRATION
Lewis Research Center
Cleveland, Ohio 44135
Under Contract DEN 3-153

for
U.S. DEPARTMENT OF ENERGY
Conservation and Renewable Energy
Division of Wind Energy Technology
Washington, D.C. 20545
Under Interagency Agreement DE-AI01-79ET20305

DISCLAIMER

Printed in the United States of America
Available from:
National Technical Information Service
U.S. Department of Commerce
5285 Port Royal Road
Springfield, VA 22161

Volume I, Executive Summary

Volume I contains an overview of the MOD-5A Program. These topics are covered:

Objectives of the MOD-5A Program
Description of the Final Design (Model 304.2)
Cost of Energy
Power Output
Trade-Off Studies
Development Tests
Analyses of Loads and Dynamics
Manufacturing and Quality Assurance and Safety Plans

Volume II, Conceptual and Preliminary Design

These sections comprise Volume II, which is divided into two books, as follows:

Book 1
1.0 Summary
2.0 Introduction
3.0 Design Requirements
4.0 Conceptual Design Studies
5.0 Design, Development, and Optimization
6.0 System Dynamics Analysis
7.0 System Loads Analysis

Book 2
8.0 Development Tests
9.0 Design Criteria
Appendix A System Specification
Appendix B Design Load Tables

Volume III, Final Design and System Description

These sections comprise Volume III, which is divided into two books, as follows:

Book 1
1.0 Summary
2.0 Introduction
3.0 System Description - Model 304.2
4.0 Rotor Subsystem
5.0 Drivetrain Subsystem
6.0 Nacelle Subsystem
7.0 Tower and Foundation Subsystems

Book 2

8.0 Power Generation Subsystem

9.0 Control and Instrumentation Subsystems

10.0 Manufacturing

11.0 Site and Erection

12.0 Quality Assurance and Safety

13.0 FMEA, RAM and Maintenance

Appendix A C.F. Braun & Company - Foundation Design Criteria

Appendix B GE - Product Assurance Program Plan for the MOD-5A WTG Program

Appendix C GE - System Safety Plan for the MOD-5A Program

Appendix D GE - MOD-5A Configuration Management Plan

Appendix E GE - MOD-5A Defect Reports for Development Hardware

Appendix F GE - MOD-5A Program Quality Assurance Requirements for the Control of Raw Materials and the Blade Fabrication Process

Appendix G GE - Statement of Work for the Erection of the MOD-5A WTG Yaw, Nacelle and Blade Subsystems

Volume IV, Drawings and Specifications

This volume contains the numbered drawings and specifications for the final design of the MOD-5A wind turbine. The volume is divided into five books, as follows:

Book 1 47A380002 through 47A380030

Book 2 47A380031 through 47A380068

Book 3 47A380074 through 47A380126

Book 4 47A380128 through 47A387125

Book 5 47D381002 through 47D387130

MOD-5A WIND TURBINE GENERATOR
DESIGN REPORT
VOLUME III, BOOK 1

Section | Page

Section Page

Section | Page

LIST OF FIGURES

LIST OF FIGURES (Cont'd)

LIST OF FIGURES (Cont'd)

LIST OF FIGURES (Cont'd)

LIST OF FIGURES (Cont'd)

LIST OF FIGURES (Cont'd)

LIST OF FIGURES (Cont'd)

LIST OF FIGURES (Cont'd)

LIST OF FIGURES (Cont'd)

LIST OF FIGURES (Cont'd)

LIST OF TABLES

LIST OF TABLES (Cont'd)

LIST OF TABLES (Cont'd)

LIST OF TABLES (Cont'd)

LIST OF TABLES (Cont'd)

1.0 SUMMARY

1.0 SUMMARY

The baseline MOD-5A wind turbine generator (WTG), a 400 ft. diameter, aileron controlled, wood laminated rotor configuration (Model 304.2), that evolved as a result of the design activities described in Volume II, was analyzed in depth to establish final drawings and specifications by which the WTG could be procured and fabricated. That analysis process and the results of these design studies are presented in Volume III.

Section 3.0 presents a description of each of the major WTG subsystems as well as the overall system and environmental characteristics of the baseline Model 304.2 configuration.

Sections 4.0, 5.0, 6.0, 7.0, 8.0 and 9.0 present the results of the detailed design studies conducted to define the components and elements of the Rotor, Drivetrain, Nacelle, Power and Foundation, Power Generation and Control and Instrumentation Subsystems, respectively.

Section 10.0 summarizes the results of the manufacturing studies that were conducted to verify that the MOD-5A wind turbine could be produced within the cost and weight requirements.

Section 11.0 describes the site and erection studies and evaluations that were conducted to establish the operational installation and assembly plans for erecting the wind turbine.

Sections 12.0 and 13.0 summarize the quality assurance, safety and failure modes and effects analysis, reliability, availability and maintenance requirements necessary to assure that the fabricated hardware fulfilled the design requirements.

2.0 INTRODUCTION

2.0 INTRODUCTION

In 1973, a national Wind Energy Program was established to develop the technology to make wind energy systems cost competitive with conventional power generation systems, and to accelerate the commercialization and use of wind energy.

The United States Department of Energy (DOE) has overall management responsibility for this program. The NASA-Lewis Research Center has the responsibility for managing the development of large horizontal-axis wind turbines for the DOE.

Under contract to NASA, the Advanced Energy Programs Department of the General Electric Company (GE-AEPD) has been engaged in the development of an advanced multi-megawatt wind turbine generator designated the MOD-5A WTG. Participating in this program, as subcontractors to GE-AEPD are Gougeon Brothers, Inc. (GBI) for the wood laminae blades, Philadelphia Gear Corporation (PGC) for the gearbox, and the Chicago Bridge and Iron Company (CBI) for the steel shell tower, site work, foundation and erection.

The goal of the MOD-5A program was to develop a reliable, commercially feasible wind energy system, able to produce electricity at a cost of energy of 3.75 cents per kilowatt hour, or less, in mid-1980 dollars, at a site with an annual average wind speed of 14 mph.

The general approach to the implementation of the MOD-5A WTG Program was the initiation of a multi-phased, 71 month effort, consisting of 47 months for conceptual design, preliminary design, final design, fabrication, assembly, installation and checkout, followed by 24 months of Operational Support and Design Improvements. In addition, development and qualification testing of materials, parts, and components were included as part of the preliminary design phase to ensure that the MOD-5A would perform and endure, as designed.

The program began in July 1980. It was organized into three design phases: conceptual design, which was completed in March 1981, preliminary design, which was completed in May 1982, and final design, which started in June 1982.

Each design phase culminated in a comprehensive design review that had two main objectives: an in-depth review of the design's technical adequacy, and verification that the program's requirement for cost of energy was still being met.

During the conceptual design phase, comprehensive trade-off and system sizing studies were conducted around a baseline configuration. The goal of these studies was to arrive at a concept with the greatest potential to meet the project's objectives: a cost of energy of 3.75 cents per kilowatt hour in mid-1980 dollars, a 30-year life, and safe operation, with acceptable risk to the program and equipment. As part of this activity, a cost, cost of energy, and weight accounting procedure was developed. This procedure tracked the effects of the sizing and trade-off studies. In addition, a manufacturing plan was developed to support the projected program costs for the fabrication of the 100th MOD-5A production unit.

After NASA and the Department of Energy approved the conceptual design, the program progressed into the preliminary design phase. During this period the recommended baseline configuration, an upwind wind turbine, with a 400-ft., laminated wood and epoxy rotor and a power rating of 5.0 MW, was evaluated further. The outcome of the preliminary design would be used in the final development phases. In conjunction with the preliminary design activity, qualification of the wood-epoxy laminae blade materials, as well as key components and subsystems were conducted. These tests continued during the final design phase.

The development produced a wind turbine design rated at 7300 kW, with a 400-ft. rotor with lightweight, wood-epoxy laminated blades, aileron control and a tower and nacelle system designed for reliability and ease of maintenance. As a result of the optimum size and the numerous technical advances, this third-generation machine would be expected to achieve a cost of energy competitive with the cost of conventional forms of power generation. This volume, Volume III of the MOD-5A Design Summary Report, presents the results of the detailed design studies and evaluations that led to the establishment of final drawings and specifications by which the wind turbine hardware could be procured and fabricated.

3.0 SYSTEM DESIGN MODEL 304.2

3.0 SYSTEM DESCRIPTION - MODEL 304.2

3.1 GENERAL ARRANGEMENT AND CHARACTERISTICS

The model 304.2 configuration is shown in Figure 3-1 and Table 3-1. This was the last design configuration for the MOD-5A program and was rated at 7300 kW in a 32 mph wind.

The 400 ft. laminated wood-epoxy rotor has ailerons for torque control. A steel yoke supports the rotor on elastomeric teeter bearings. Two rolling element bearings support the yoke on the nacelle, which is supported on the tower by a three row yaw bearing. The 14.5 ft. diameter steel shell tower supports the nacelle and rotor at a hub height of 250 ft. The tower is flared at the base and anchored to a reinforced concrete foundation.

Wind energy is converted to electrical energy by a speed-increase gearbox and variable speed generator located in the nacelle. The rotor will operate at set speeds of either 13.2 or 16.2 rpm depending on the wind speed. Converter and interface equipment located on the ground permit the generator to operate over a small variable speed range above the set rotor speed, while connected to a constant frequency utility network.

The MOD-5A was designed for automatic, unattended operation. A controller, located in the nacelle, provides automatic sequencing, dynamic control, supervisory monitoring, and communication functions.

A brief description of the system is provided in the rest of this section. Design details are provided in subsequent sections of this volume.

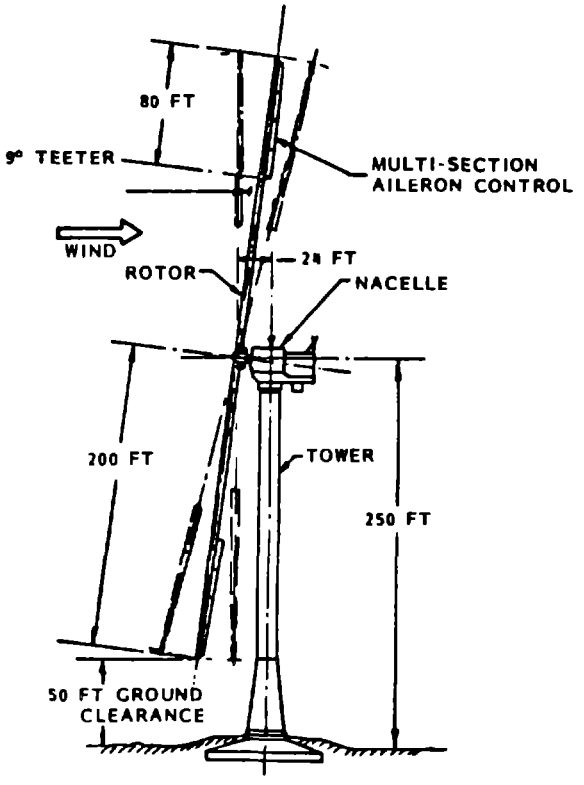

OPERATIONAL CHARACTERISTICS

RATED POWER	7300 KW AT 0.98PF
RATED WIND SPEED	32 MPH AT 250 FT
CUT-IN/CUT-OUT WIND SPEED	14/60 MPH AT 250 FT
MAXIMUM WIND SPEED (SURVIVAL)	130 MPH AT 250 FT
POWER CONTROL	MULTI-SECTION AILERONS
ROTOR RPM-SET SPEED	13.7/16.8 RPM (± 10%)
ENERGY CAPTURE/YR	21.3 X 10^6 KWH (NASA SPECIFIED WIND SPEED DURATION CURVE, 18 MPH AT 32 FT, 100 % AVAIL)
TOTAL WT ON FOUNDATION	1804 K-LB

FEATURES

- WOOD LAMINATE BLADES WITH HIGH PERFORMANCE AIRFOIL - UPWIND, TEETERED
- NON-ROTATING ROTOR SUPPORT
- HYBRID EPICYCLIC/PARALLEL SHAFT GEARBOX
- VARIABLE SPEED/CONSTANT FREQUENCY OPERATION, WITH 2 SET POINTS
- SOFT SHELL TOWER, TUNEABLE BELL SECTION

Figure 3-1 MOD-5A Model 304.2

Table 3-1 Model 304.2 Configuration

System Weight (lb)	1,803,926
Installed Cost (Volume, 1980 $)	4,111,805
Annual Energy (GWH, SOW wind, 0.96 AF)	21.2
Cost of Energy (Volume, 1980 cents/kwh)	3.69

Rotor 474,470 lb.

- o Upwind of tower
- o 400 ft. diameter
- o 352 ft/sec tip speed
- o 13.2-13.8/16.2-16.8 rpm two range variable speed operation
- o Laminated wood blades
- o Continuous wood blade, tip-tip
- o 64-XXX Airfoil, 300 in. root chord, 3.06% solidity
- o 40% (80 ft.) aileron control -90° motion 40% chord, 3 hydraulic actuators/blade
- o Steel yoke attachment at teeter axis
- o Teeter and brake shafts in bolster
- o Rotor stopping brake
- o Yoke-mounted hydraulic power unit
- o 7° tilt, ±9° teeter allowance
- o Elastomeric teeter bearings and brake type teeter restrictor.
- o Yoke supported on spindle with dual bearings

Drivetrain 259,636 lb.

- o Floating torque shaft from yoke to gearbox
- o Hybrid single ratio gearbox, 3.38 million ft.-lb. input torque
- o Planetary 1st and 2nd stage gearing, parallel shaft 3rd stage
- o In-line slipring access, shaft drive lube pump, inching drive
  Floating high speed shaft,
- o 7,300 kW, 960-1440 rpm wound rotor, induction generator

Nacelle 328,700 lb.

- o Bedplate type with wiring, piping runs under flooring
- o Box type rotor support structure with spindle, crane mount
- o Mountings for gearbox, generator, control electronics, high voltage cabinet
- o Insulated weather fairing
- o Lubrication system for gearbox and bearings on lower platform
- o Yaw structural adapters and bearing
- o Hydraulic power supply and push-pull yaw drive
- o Yaw slipring

Tower 653,120 lb.

- o 14.5 ft. diameter steel shell
- o 250 ft. to rotor hub
- o 50 ft. tapered bell for tuning
- o Internal traction elevator and ladder

Foundation

- o Spread footing, reinforced concrete
- o About 960 cubic yards
- o Anchor bolts for tower attachment

Electrical 88,000 lb.

- o Electrical equipment building with cycloconverter and switchgear and control
- o 7,300 kVA oil-filled transformer with fused switch
- o 69 kV nominal interface
- o 175 MVA radial feeder cluster, with 24 units

Maintenance

- o Permanent cluster crew

3.1.1 ROTOR SUBSYSTEM

The rotor subsystem of the MOD-5A wind turbine generator consists of all the rotating structures windward of the main rotor bearings. It is mounted by the main rotor bearings on the rotor support spindle, which is part of the nacelle assembly. The rotor subsystem is illustrated in Figure 3-2.

The major assemblies shown are the blade and ailerons. The rotor subsystem also includes the yoke, teeter bearings, brake subsystems, hydraulic subsystem and electrical subsystem. The yoke is a large steel fabrication that supports the blade from the teeter bearings to the main rotor bearings and the rotor support spindle. It transmits rotor torque through its forward shear web to the low speed shaft. The blade is attached to the yoke by the teeter bearing assemblies, which provide a degree of freedom to the blade perpendicular to the plane of rotation.

The laminated wood and epoxy blade is assembled from five segments: the center blade unit, two inner blade units and two outer units, which are bonded together in the field.

The ailerons form the trailing edge of the outer segments, from 60% to 100% of span. They modify the rotor lift and drag characteristics to modulate system torque and provide rotor speed control.

The rotor subsystem requires two braking subsystems, for teeter motion and for the rotor. The teeter brake subsystem stabilizes the teeter angle for low rotational speeds and high wind angle conditions. The teeter brake force is applied to four arms that are pinned to the blade bolster and slide through two sets of caliper brake assemblies for each arm. These calipers are mounted to the four corners of the yoke. They are actuated by the control subsystem. The rotor brake subsystem stops the rotor after the ailerons are deployed. The rotor brake torque is applied independently of the low speed shaft by means of a yoke-mounted brake disc and nacelle-mounted caliper brake sets.

The hydraulic subsystem which provides the required pressure to the ailerons and teeter brakes is mounted on the outside of the yoke, to simplify its interfaces.

The electrical subsystem provides all power, command and signal functions to tne rotor. Slip rings interface the rotating components with the non-rotating nacelle.

Lightning protection is built into the blades. A metal screen is used on the outer portion of the blade and conduit and conductors carry lightning currents to the yoke. The current is carried through the yoke to the nacelle and tower via a separate conduction path.

The five blade segments are assembled in the field. The ailerons are fit in the factory, but are installed in the field. Trailing edges, bolsters, hydraulic and electrical distribution systems and the teeter bearings and teeter shaft are also installed in the field. All subsystems are checked and the rotor is lifted as a unit into place on the yoke. The yoke assembly is also completed in the field, by installing the hydraulic power subsystem and associated hydraulic and electrical distribution lines. The yoke is installed on the nacelle support structure after the blade-to-yoke interface is validated on the ground. The installation of the blade to the yoke completes the assembly of the rotor subsystem.

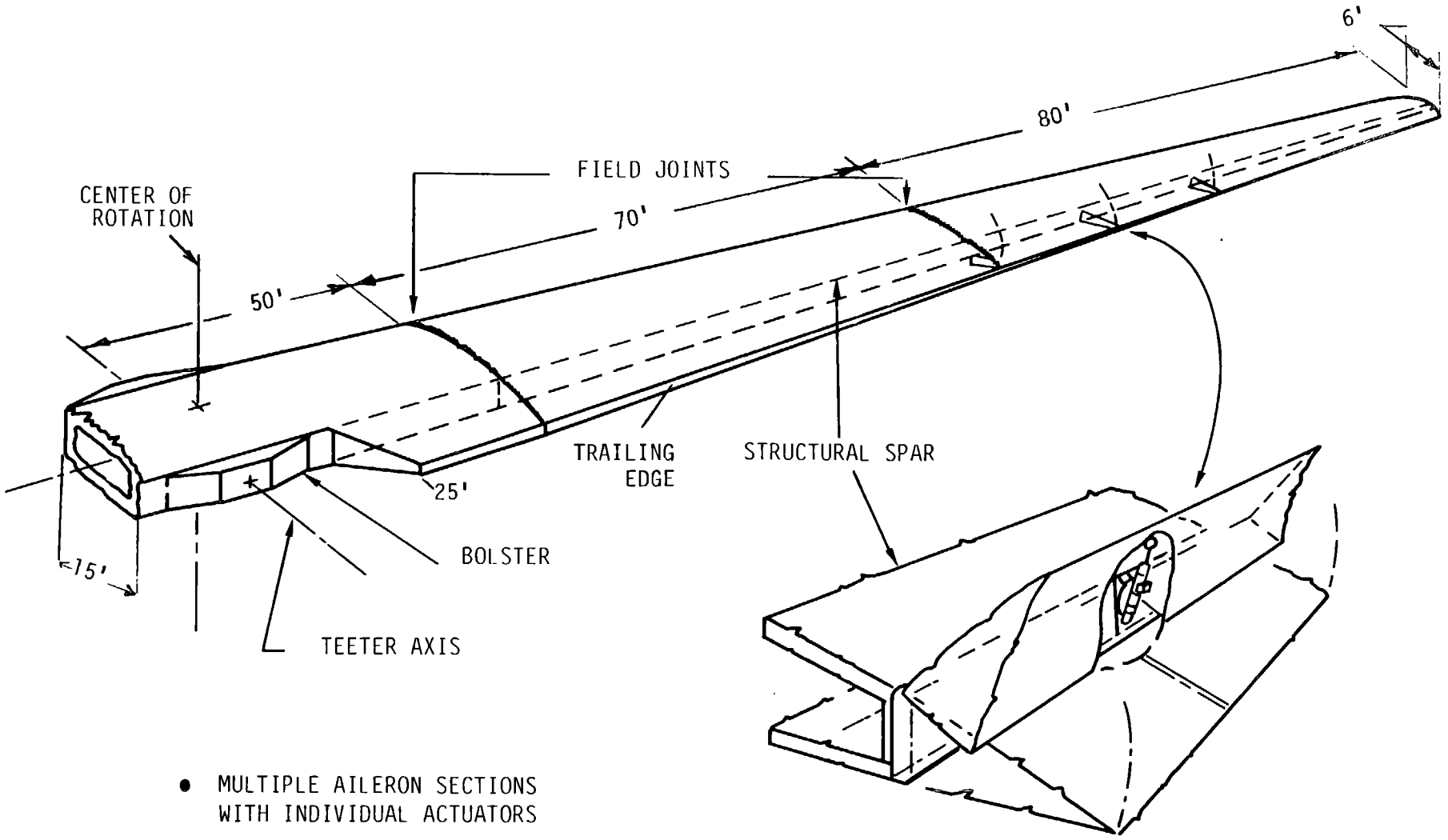

- MULTIPLE AILERON SECTIONS WITH INDIVIDUAL ACTUATORS
- FAIL-SAFE HYDRAULIC SYSTEM
- CONVENTIONAL, LIGHTLY LOADED WOOD/METAL JOINTS
- CONTINUOUS TIP-TO-TIP STRUCTURAL SPAR

Figure 3-2 Rotor Subsystem

3.1.2 DRIVE TRAIN SUBSYSTEM

The overall nacelle and drivetrain are shown in Figure 3-3. The drivetrain subsystem consisted of all the elements that transmit power from the rotor to the generator. Power from the rotor passed through the torque plate, low speed shaft, speed increaser gearbox, and the high speed shaft to the generator. The gearbox increased the shaft speed via a set of gears with a ratio of 1 to 82.14. For example, if the low speed shaft turned at 16.8 rpm, the high speed shaft would turn at 1380 rpm. The rotor support bearings supported the rotor and provided rotational freedom to the rotor.

The drivetrain was rated for 3.38×10^6 ft-lb of torque at the low speed shaft. Total system losses are approximately 10% at rated operating conditions and this torque rating provides 8,066 KW at 16.8 rpm (7,300 kW rating X 1.105 = 8,066 kW). Friction caused some power loss in the drivetrain. The maximum power loss in the gears and bearings of the speed increaser was 3%. No loss was expected in the low and high speed shaft and coupling assemblies. The rest of the losses occur in the generator and electrical subsystem.

The rotor was supported on a pair of tapered roller bearings in a horizontal "king post" arrangement. The bearings were mounted on a stationary spindle, which was part of the bedplate structure. The inner bearing races were stationary, and the outer races rotated with the yoke. In this arrangement the two bearings oppose the weight moment exerted by the rotor, the dead weight of the rotor, and the rotor thrust. The bearing arrangement is illustrated in Figure 3-4. The bearings were designed for grease lubrication. An automatic lubricator periodically injects a metered quantity of grease.

The torque plate transmits torque from the yoke to the low speed shaft. The outer diameter of the torque plate was bolted to the yoke, and the inner diameter of the torque plate interfaced with the low speed shaft via a splined connection. The low speed shaft is a forging with a concentric inner passage, which protected an electrical conduit. Electric power, control and

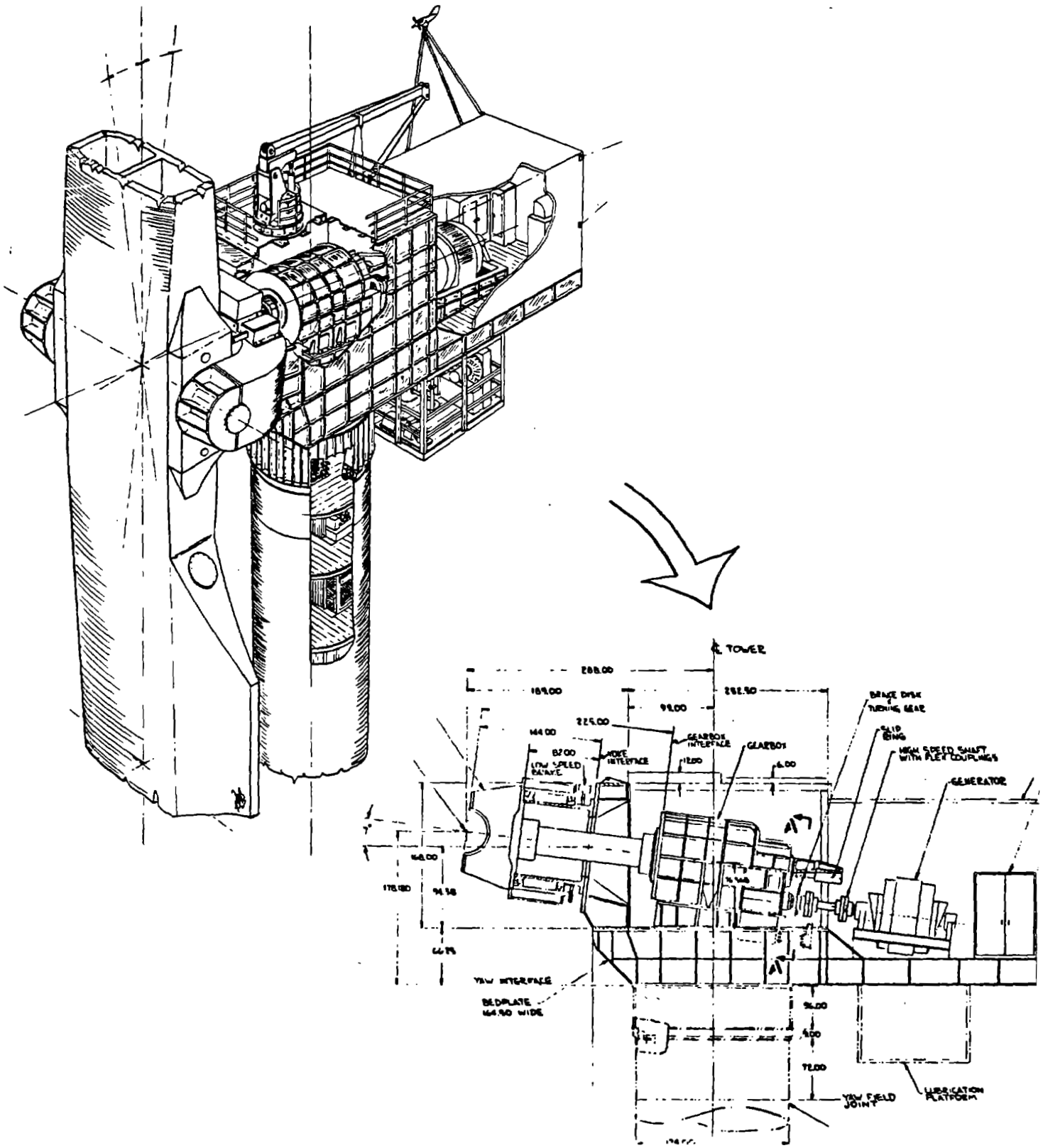

Figure 3-3 Overall Nacelle Profile

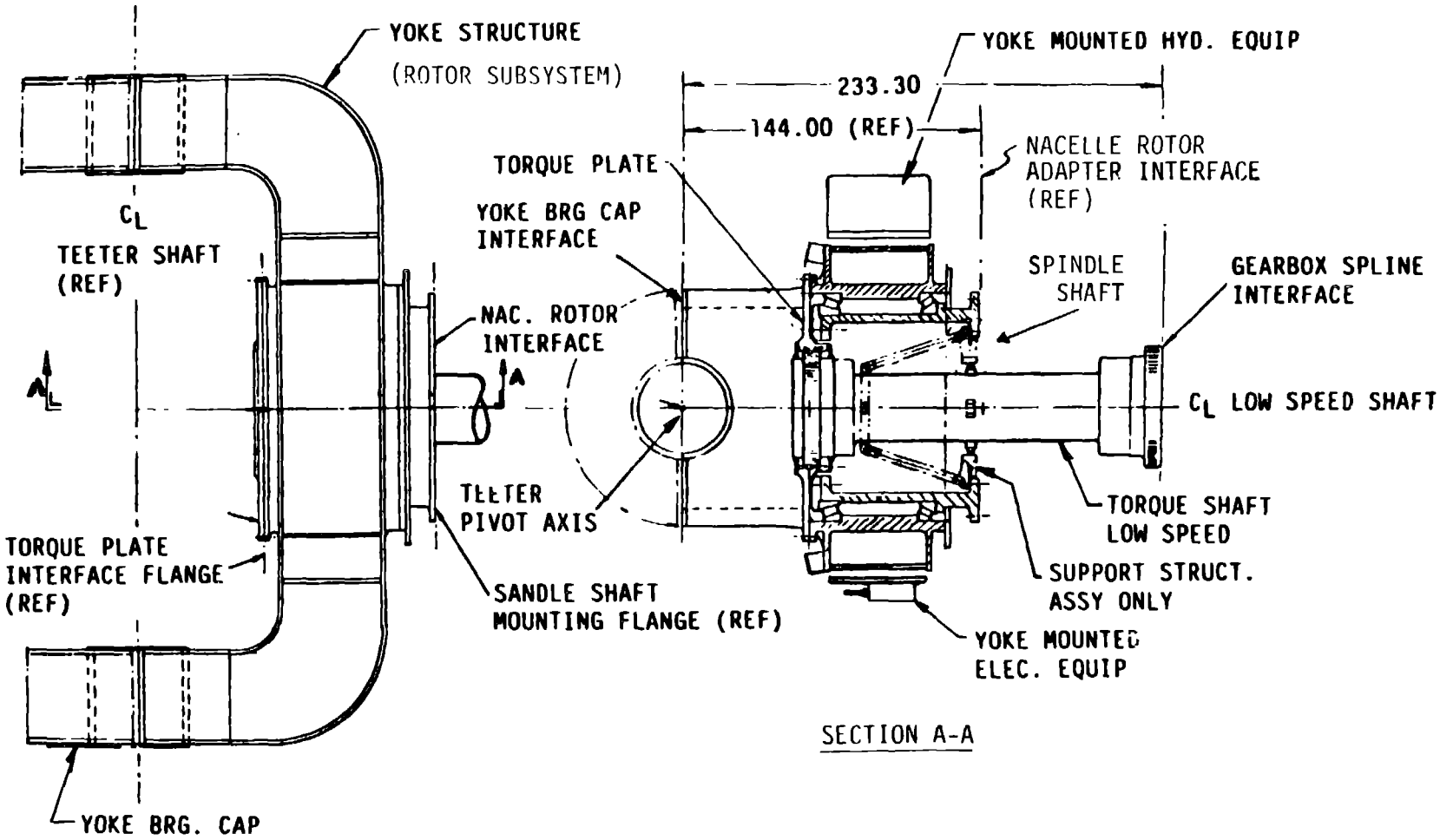

Figure 3-4 Rotor Support Assembly

instrumentation wiring ran from a slipring, mounted on the rear end of the gearbox, through the gearbox and low speed shaft to the rotor. They provided electric power and control to the hydraulic aileron actuation subsystem and other rotor controls.

The low speed shaft was connected directly to the first stage of the gearbox via a splined connection. The gearbox was a stand-alone, 3-stage unit. The first and second stages were epicyclic and the third stage was a parallel shaft design. The epicyclic stages are a conventional planetary arrangement, in which the input torque is transmitted to the planet cage and the output torque is transmitted by the sun wheel to the next stage. The output of the second stage was transmitted to the bull gear of the third stage. The bull gear turned a pinion, whose output drove the generator. The connection between the gearbox and generator was the high speed shaft assembly.

The gearbox and the splined interface between the gearbox and low speed shaft were lubricated by a central oil lubrication system. Two parallel pumps ensured that oil was available at all times. A motor-driven pump circulated oil during start-up and backed up the gear driven pump in the gearbox. The gear-driven pump circulated oil after the wind turbine reached operating speed. Mobil SHC630 oil was circulated through the gearbox at 160 gpm and 25 psi. The oil temperature was kept between $60^{o}F$ and $115^{o}F$ by heaters or coolers to maintain the proper viscosity for protecting the gears and bearings.

A 400 gallon oil reservoir was built into the gearbox. Other conditioning equipment, such as filters, heaters, and coolers were located either in the reservoir or on the lube subsystem platform.

The high speed shaft assembly used flex disc couplings to provide a low maintenance floating shaft configuration.

The low speed brake was designed to assist the ailerons in stopping the rotor, when the rotor speed was 10 rpm or lower. The brake also prevented rotation during maintenance and servicing. The low speed brake consisted of a 10.5 ft. diameter steel disc mounted on the rear of the yoke and eight Goodyear SLC 19 brake calipers, mounted on the front rotor adapter. The brakes supply a holding torque of 3,000,000 ft-lb.

3.1.3 NACELLE SUBSYSTEM

The nacelle subsystem has key structural, dynamic and protective functions. As a structure, the nacelle provides a load path from the rotor to the tower. The load is complex, consisting of equipment dead weight, overturning moments, thrust, rotor dynamics and wind induced forces. In designing the structural elements, in addition to ultimate load levels, fatigue was considered as a design driver. The nacelle provides the rotating interface between the rotor and gearbox in the form of a stationary spindle shaft, shown in Figure 3-4, and a pair of tapered roller bearings. The bearings support the 300,000 lb rotor and resist the associated dynamic forces, while providing rotational freedom to the rotor. And finally, the nacelle protects the drivetrain, generator, controls and power conditioning equipment from the environment. A profile of the nacelle subsystem is shown in Figure 3-3. The nacelle's structural arrangement is shown in Figure 3-5.

3.1.3.1 Description

The largest, and perhaps most critical element of the nacelle is the bedplate. The bedplate, shown in Figure 3-5, is a large weldment, made of structural shapes and the design includes details needed to meet the fatigue load environment. All key welds are full penetration, all changes in section are smooth and gradual and there are no sharp corners. The bedplate material is A572 GR 50 steel and is specified to have controlled grain size and minimal inclusions and must meet a rigorous low temperature Charpy V-notch test. Post-weld heat treatment was specified to assure that residual stresses are relieved. Similar design criteria were applied to the front adapter sections, side walls and roof sections.

The bedplate has a flat bottom made of 4 in. thick steel plate that is bolted to the flange of the upper yaw section. To reduce weight, lightly loaded sections of the bottom plate are made of 1 in. thick steel.

The spindle is a forging, made from ASTM A508, Class 4b steel with controlled inclusion shapes and restrictions on phosphorus and sulphur. The forging must meet a rigorous low temperature Charpy V-notch test. The spindle is bolted to the front face of the rotor adapter and supports the rotor on bearings.

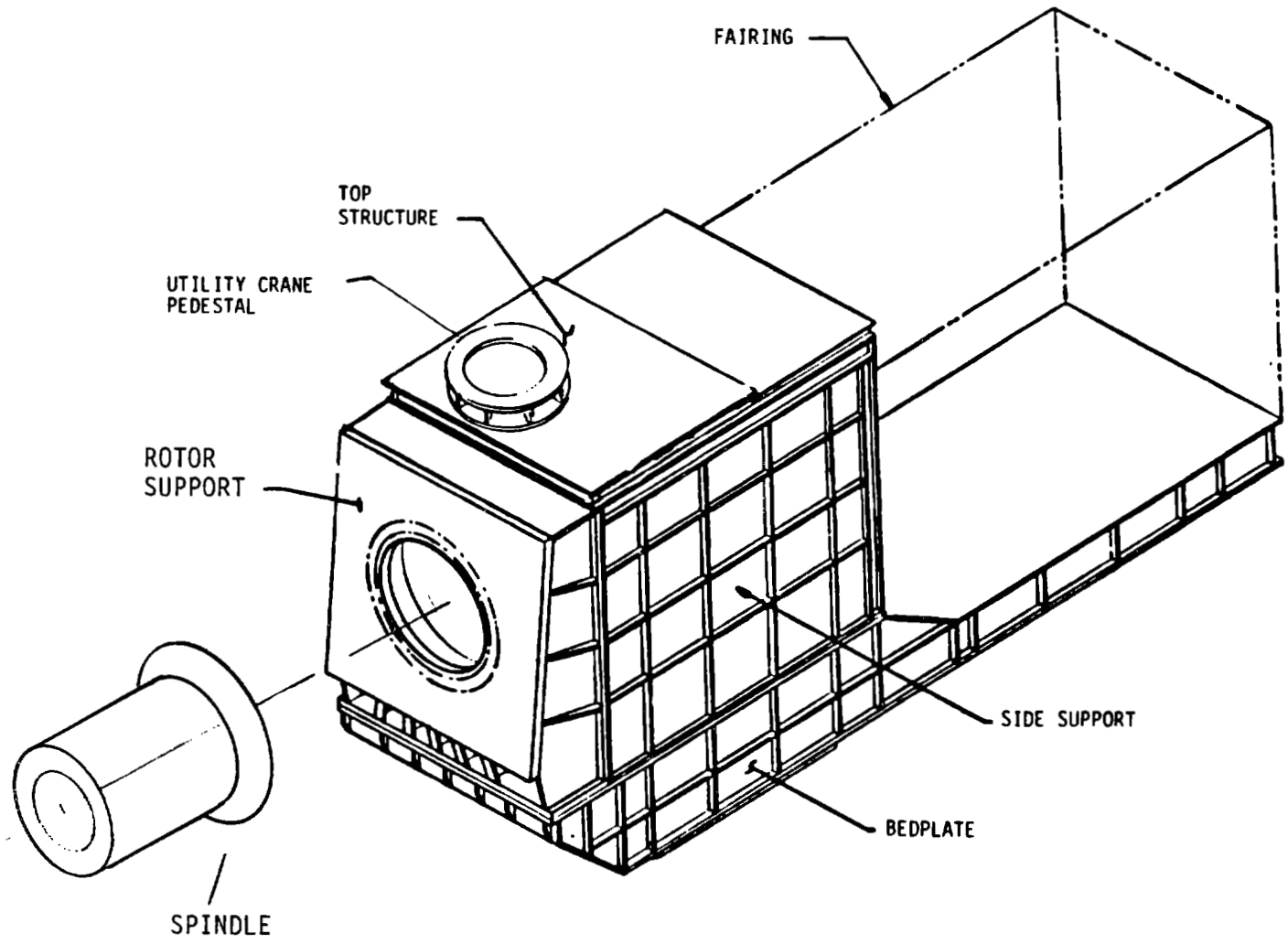

Figure 3-5 Nacelle Structural Assembly

The roof structure of the nacelle was designed to support a 5-ton utility crane. The crane is a service and maintenance tool and can reach and lift most of the generator and drivetrain components, such as pinions, bearings and couplings. Also, the crane provides a hoist point for blade inspection and teeter bearing maintenance.

A fairing covers the aft section of the nacelle to protect the generator, control cabinet and nacelle power conditioning equipment. The fairing is made of light-weight galvanized steel with thermal insulation. The fairing is designed to resist wind pressure and live loads on the roof. A louvered vent, air filters and an exhaust fan are attached to the fairing. The fairing has access hatches and supports two wind sensor masts and aircraft warning lights. The gearbox lubrication subsystem was attached to the bottom of the bedplate.

All sections of the nacelle subsystem were designed to meet shipping size and weight requirements. The sections are bolted together in the field to form the overall structure. All exposed metal surfaces areas are painted in the factory with two coats of zinc rich primer before the finish paint coat and touch-up paint are applied in the field.

3.1.4 TOWER AND FOUNDATION SUBSYSTEM

The tower and foundation are shown in Figure 3-6. The tower is a cylindrical welded steel structure made from formed plates. The cylinder has a 14.5-ft. diameter between the nacelle and an elevation of 50 ft. Below 50 ft. the structure is conical, spreading out to a diameter of 22.5 ft. at the base. There are 25 sections, most of which are slightly less than 10 ft. high. The thickness of each section, which was determined by fatigue or buckling allowable stress and the frequency criteria, is different. The frequency criteria required that the tower stiffness be such that the first bending frequency of the entire system would be approximately 0.34 Hz.

The tower base has reinforcements, called anchor chairs, that help distribute the tower loads into the 96 anchor bolts. The anchor bolts are embedded about 4 ft. into the reinforced concrete ring wall of the foundation. The foundation is a spread foundation, 72 ft. in diameter and 9 ft. below the original grade level. The design requires approximately 1,000 cubic yards of concrete. This design is a generic design; the foundation design should depend on the soil properties at the site. However, study has shown that except for some unusual sites, the design will be close to what is described here.

The elevator and support structure are inside the tower. The elevator is a traction elevator, often used in grain elevator applications. The elevator meets ANSI/ASME 17.1a Part XV and, consequently, it will be acceptable in over 90% of the states without special permit requirements. The elevator support structure is only attached at the top of the tower, and it stands on a pivoted base to minimize stresses induced as the tower flexes. There are platforms at the top and bottom for entrance to the elevator. The tower has a door at the bottom to allow entrance to the interior of the tower and access to the elevator.

At the top of the tower there are two sections called the lower and upper yaw adapter sections. Between these sections, a large slewing ring bearing is

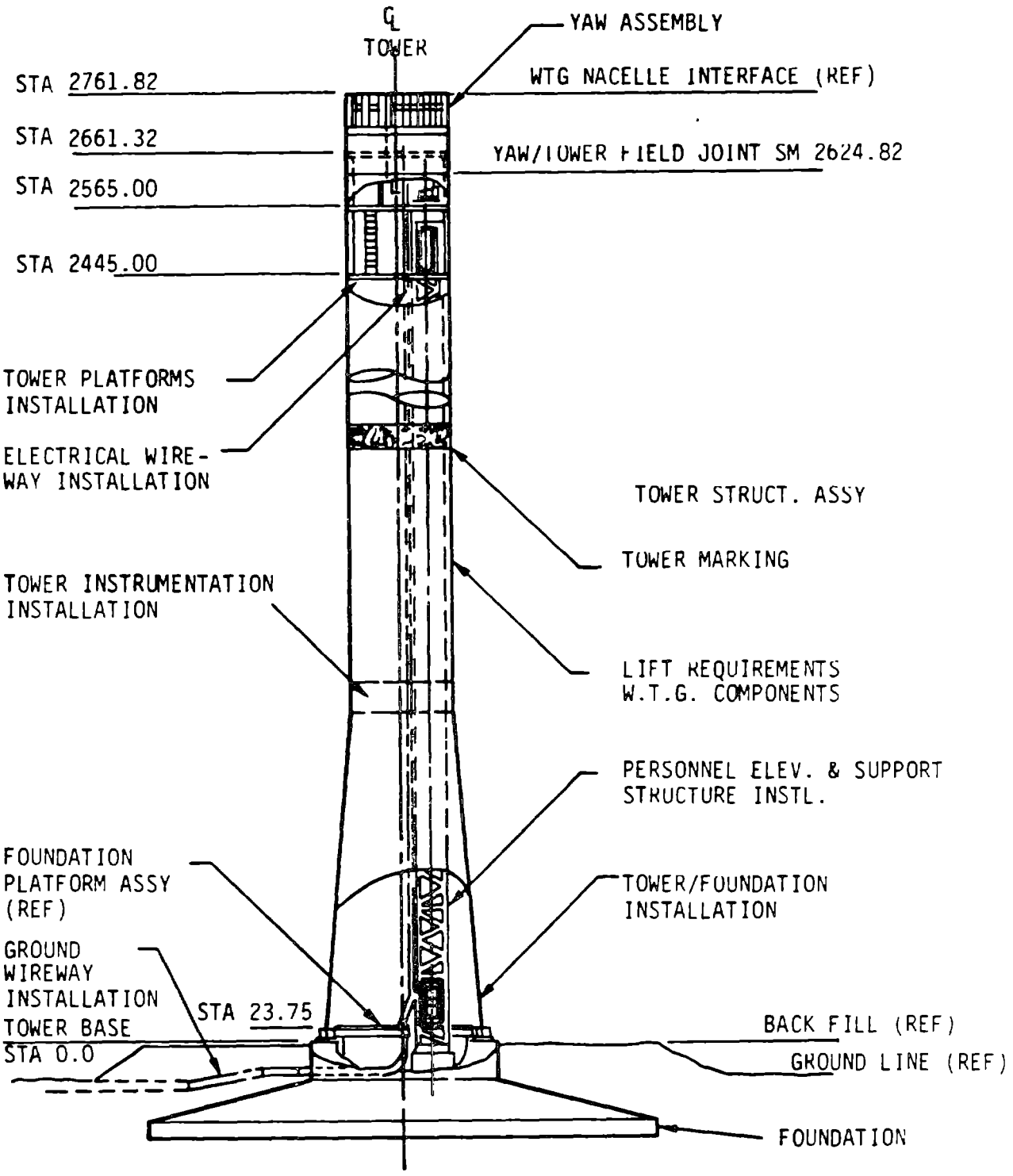

Figure 3-6 Tower And Foundation

mounted. The bearing allows the nacelle to rotate in the yaw azimuth, relative to the fixed tower. The yaw sections also include a yaw drive, yaw slipring, hydraulic power supply, and an automatic bearing lubrication system. All components are enclosed in the tower, to protect them from the weather. A ladder in the yaw section provides access to the nacelle through manholes in the bedplate floor.

3.1.5 POWER GENERATION SUBSYSTEM

A variable speed generator and its associated power conversion equipment converted the mechanical energy of the wind turbine to useful electrical energy. Equipment locations are shown in Figure 3-7. A simplified one-line diagram of the subsystem with protective relay numbers is shown in Figure 3-8.

The major components included the generator, sliprings, interconnections, power converter, harmonic filter, switchgear, step-up transformer, and station batteries. The components were chosen for 30-year life and a maintenance interval of 6 months or more.

The generator was a 7500 kVA wound-rotor, 6 pole machine with a 6300 kVA stator, and a 1500 kVA rotor. A static power converter and its associated control maintained the output frequency at 60 Hz while rotor speed varied. The stator and converter output was 4160 V. When singly excited, the generator also provided motoring duty to bring the rotor up to 3.5 rpm.

The converter and its controls were designed to regulate the generator's air gap torque, frequency and reactive power. This equipment was located in an enclosure near the base of the wind turbine tower. The switchgear for stator short, stator tie, and converter tie functions, and associated relays are also located in the enclosure.

All electrical circuits between the rotatable nacelle and the stationary support tower pass through the yaw slipring assembly.

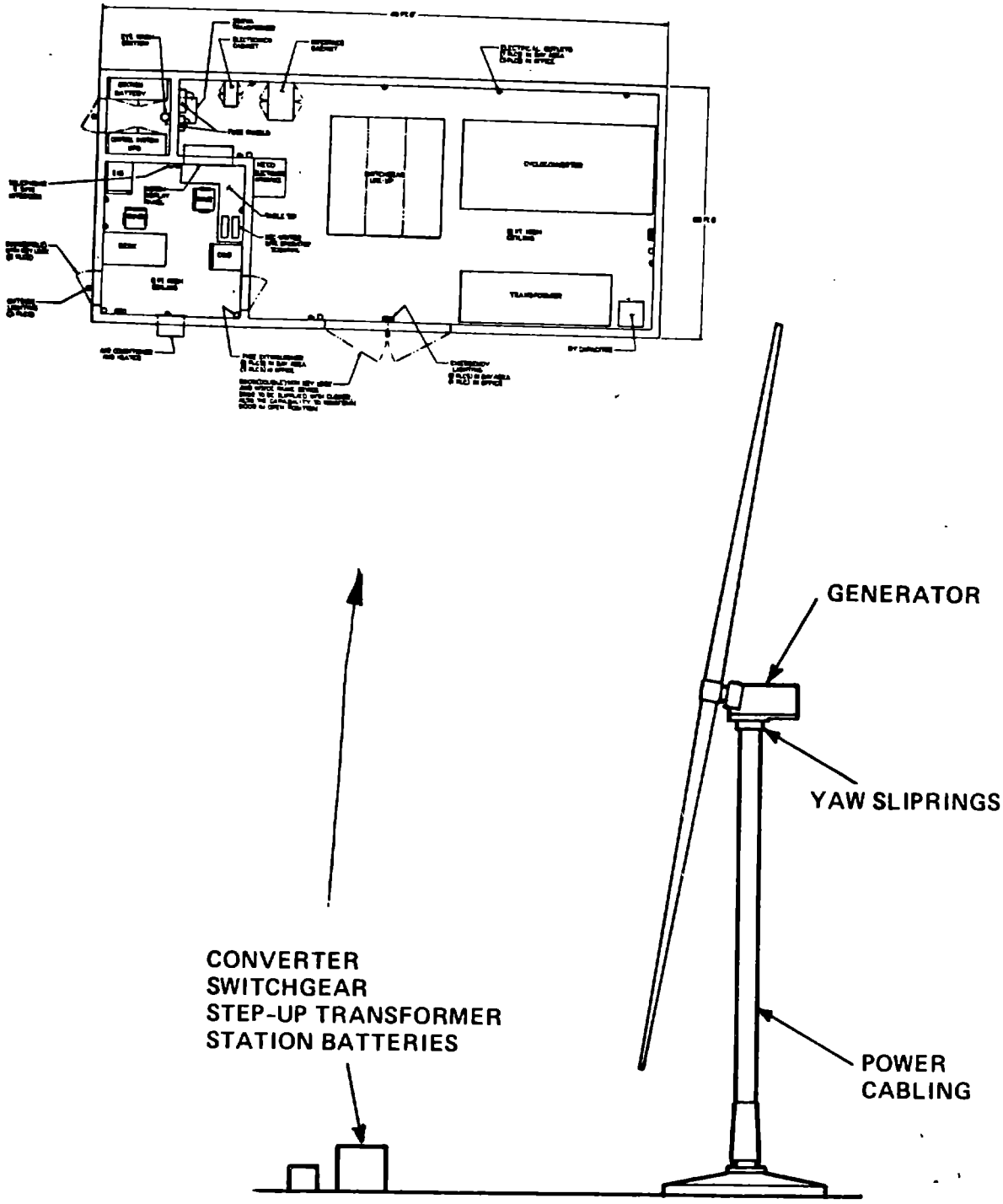

Figure 3-7. Electrical Equipment Location

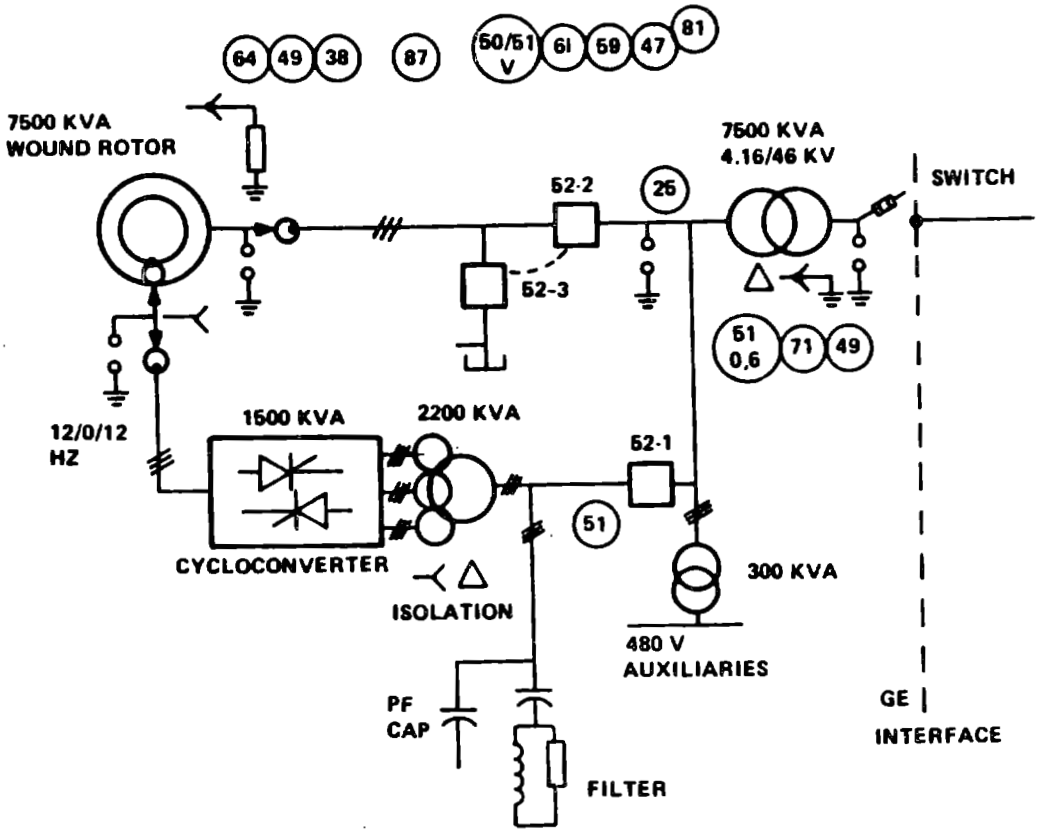

Figure 3-8 Power Generation Subsystem

3.1.6 CONTROL AND INSTRUMENTATION SUBSYSTEMS

The major subassemblies of the control and instrumentation system, shown in Figure 3-9 are the:

- o controller
- o signal conditioning
- o sensors
- o emergency shutdown
- o system display panel
- o operator terminal
- o engineering instrumentation system
  - controls data system
  - multiplexers

3.1.6.1 Control System Description

A block diagram of the control system is shown in Figure 3-10. The controller, signal conditioning, and the emergency shutdown are located in the nacelle in the controls equipment cabinet. Figure 3-11 shows the layout of the front panel of the controls equipment cabinet. The system display panel, operator's terminal, and the controls data system are located in the office of the electrical equipment building at the base of the tower. Figure 3-12 contains a floor plan of the electrical equipment building. There are 3 multiplexers; one is located in the yoke, one in the nacelle, and one in the electrical equipment building.

The controller is a microprocessor-based, programmable controller: the EPTAK 700, made by Eagle Signal. The basic functions of the controller are mode determination, automatic sequence operation, torque and speed control, and command and data interface.

The remote and site operator's terminals are "dumb" keyboard printers that print a summary of the operating data and transmit the operator's commands.

The control data system is an engineering instrumentation system that supports tests and initial operation. It receives operating data from the controller, and records and processes the data for a detailed report. The control data system transmits the operator's commands to interrogate controller RAM locations and to alter operating parameters.

MAJOR SUBASSEMBLIES

- o CONTROLLER
- o SIGNAL CONDITIONING
- o ESD
- o SENSORS
- o SYSTEM DISPLAY
- o OPERATOR TERMINAL
- o EIS (CDS, MUX)

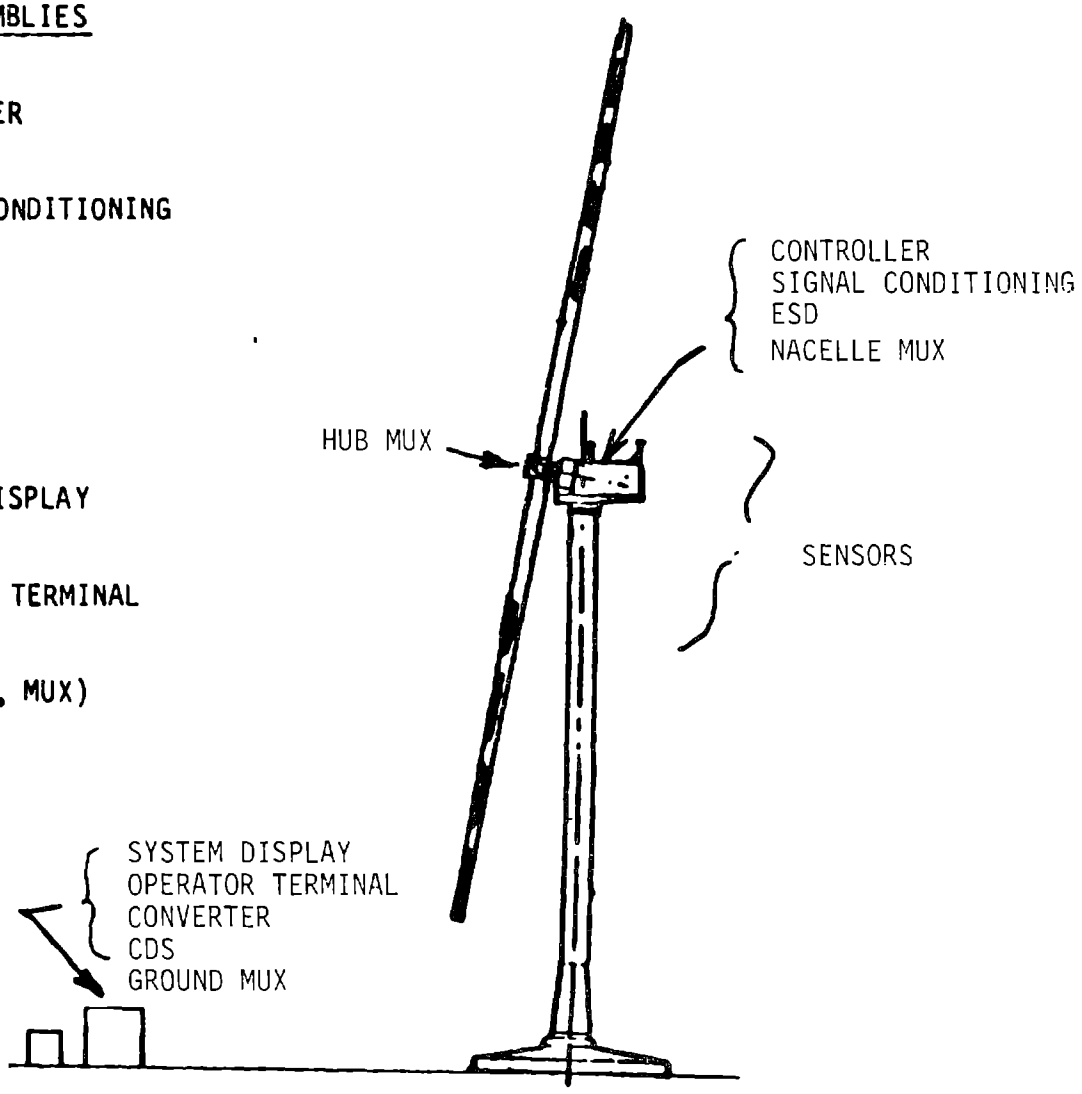

Figure 3-9 Instrumentation and Control Subassemblies

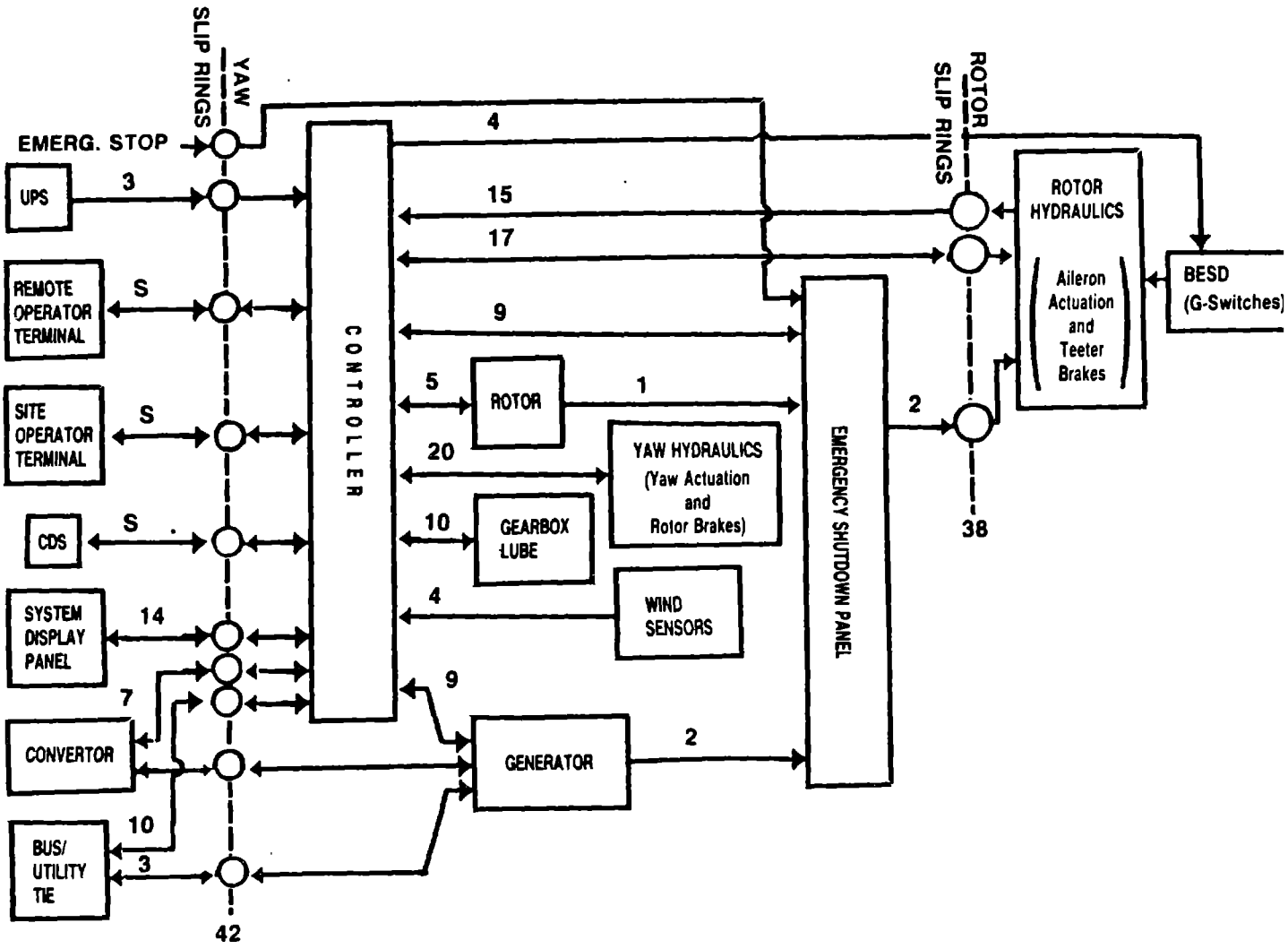

Legend:

UPS = Uninterruptible Power Supply
CDS = Control Data System
S = Serial data link

Numbers by lines indicate quantity of signals.

Figure 3-10 MOD-5A Control Systems Block Diagram

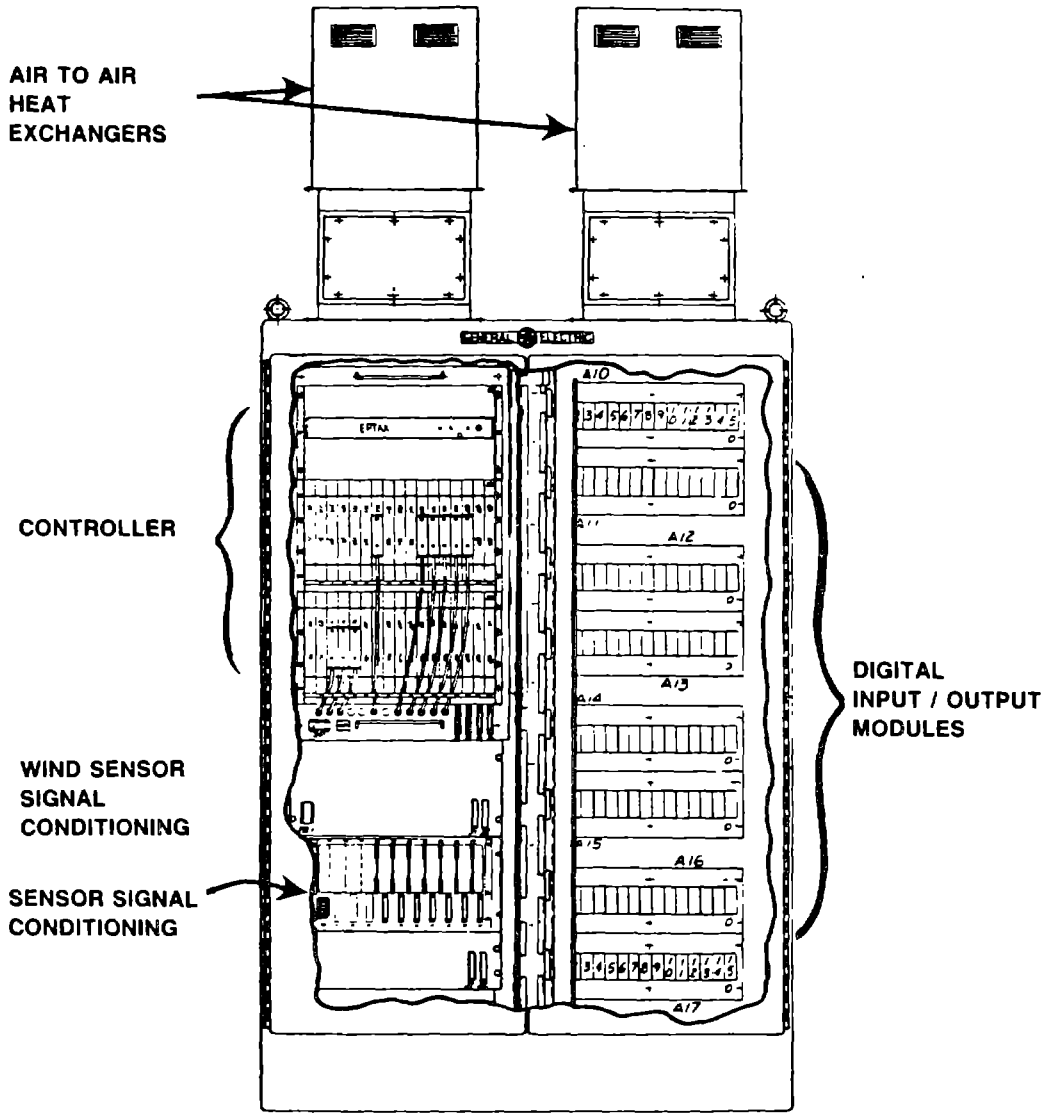

Figure 3-11 Front View of the Controls Equipment Cabinet

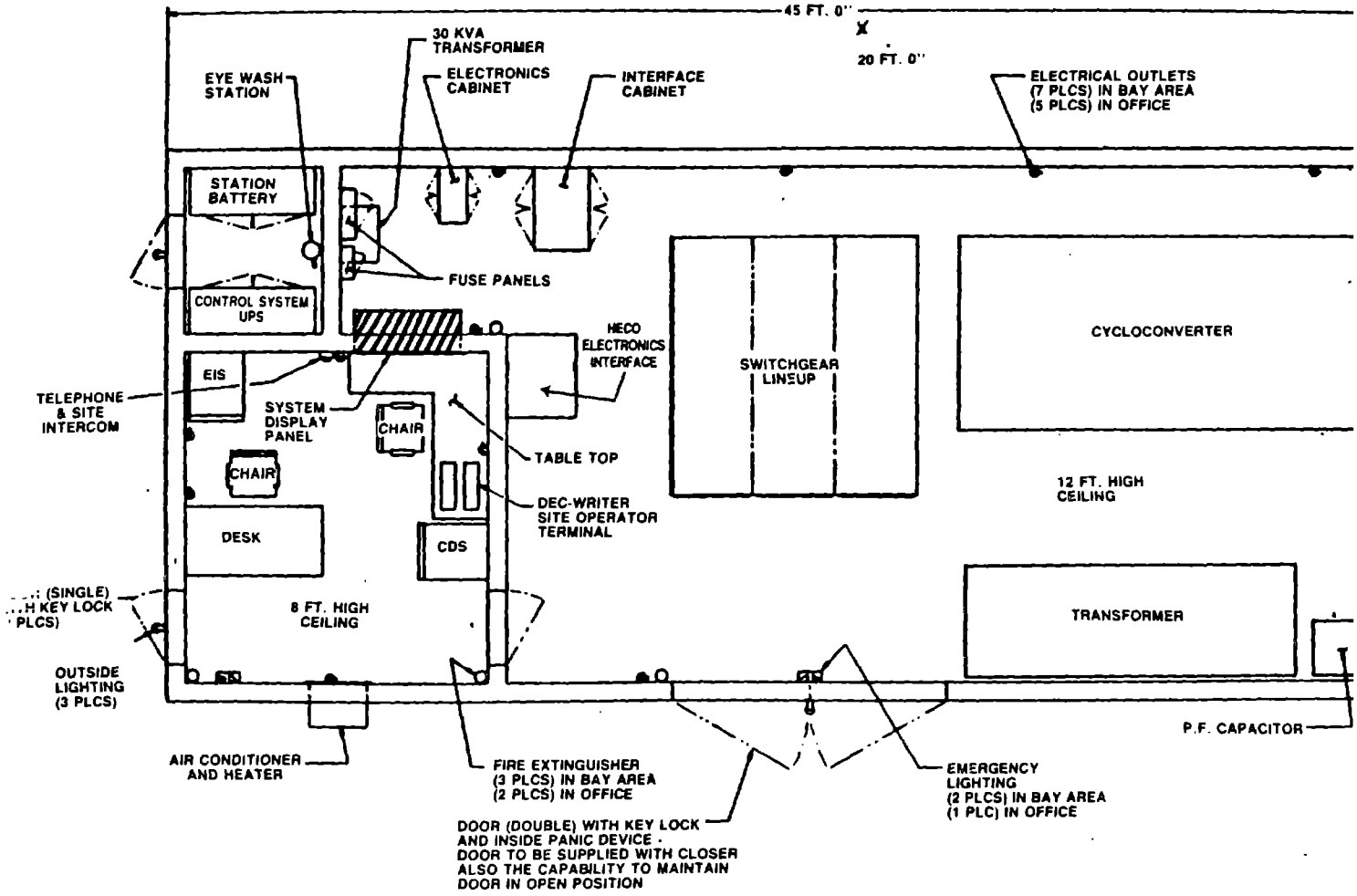

Figure 3-12 Electrical Equipment Building

The system display panel contains hardware functions for shutdown, manual mode select, and controller reset. Basic operating performance parameters are displayed in engineering units. TV video display and the intercom are located in the system display panel.

An interface for Hawaii Electric Co., which is specifically for the site in Oahu, interfaces with the system display panel and provides command and signal functions to the utility.

The emergency shutdown functions independently of the controller. The emergency shutdown energizes feather valves that enable the controller to operate hydraulic servo valves. When deenergized, the feather valves cause the ailerons to feather. When the emergency shutdown loses the signal, it deenergizes the feather valves for a shutdown that is analogous to a "deadman stick" operation.

3.2 SYSTEM PARAMETERS

3.2.1 PERFORMANCE

The performance of the MOD-5A model 304.2 was computed from full rotor power coefficients, mechanical and electrical losses, start-up and shutdown losses, and nomekeeping energy loses.

The design wind regime is defined as a Weibull distribution with a 32.8 ft. shape factor of 2.29 and a mean coefficient of 7.17 mps. The vertical wind distribution varies exponentially with elevation and the exponent varies with wind speed. At the hub height of 250 ft., the Weibull parameters are 2.75 and 10.46 mps. Hub height parameters were used as full immersion valves and the sub-rated energy capture was later reduced by 4.2% to account for rotor tilt, teeter, and vertical wind variation.

The baseline performance is shown in Figure 3-13 for the design wind at sea level, and at an elevation of 7000 ft. The net output power and wind speed at hub height are plotted against cumulative probability. At sea level, the cut-in wind speed is 14 mph, the rated wind speed is 32 mph and the cut-out wind speed is 60 mph. The predicted annual energy capture, at 96% availability, is 21.2 GWh at sea level, and 17.9 GWh at 7,000 ft.

The distribution of energy losses, with respect to the total energy in the wind passing through the rotor disk area, is shown in Table 3-2.

The predicted performance for the wind turbine in Kahuku, Oahu, HI, is shown in Figure 3-14. The strong trade winds in this area provide almost 2.5 times the operating time at the rating provided by the design wind. The predicted annual energy capture at 96% availability is 32.2 GWh.

In the design wind distribution, the 7300 kW rating is based on a relatively high power density, and the plant factor is, therefore, a low value: 33%.

The rotor performance predictions use the automatic control plan, where changes in speed are made while power is being delivered. A low speed range, from 13.2 to 13.8 rpm, and a high speed range, from 16.2 to 16.8 rpm, are used to maintain high rotor efficiency. Startup and shutdown losses are based on 1100 starts per year, at 15 minutes for each.

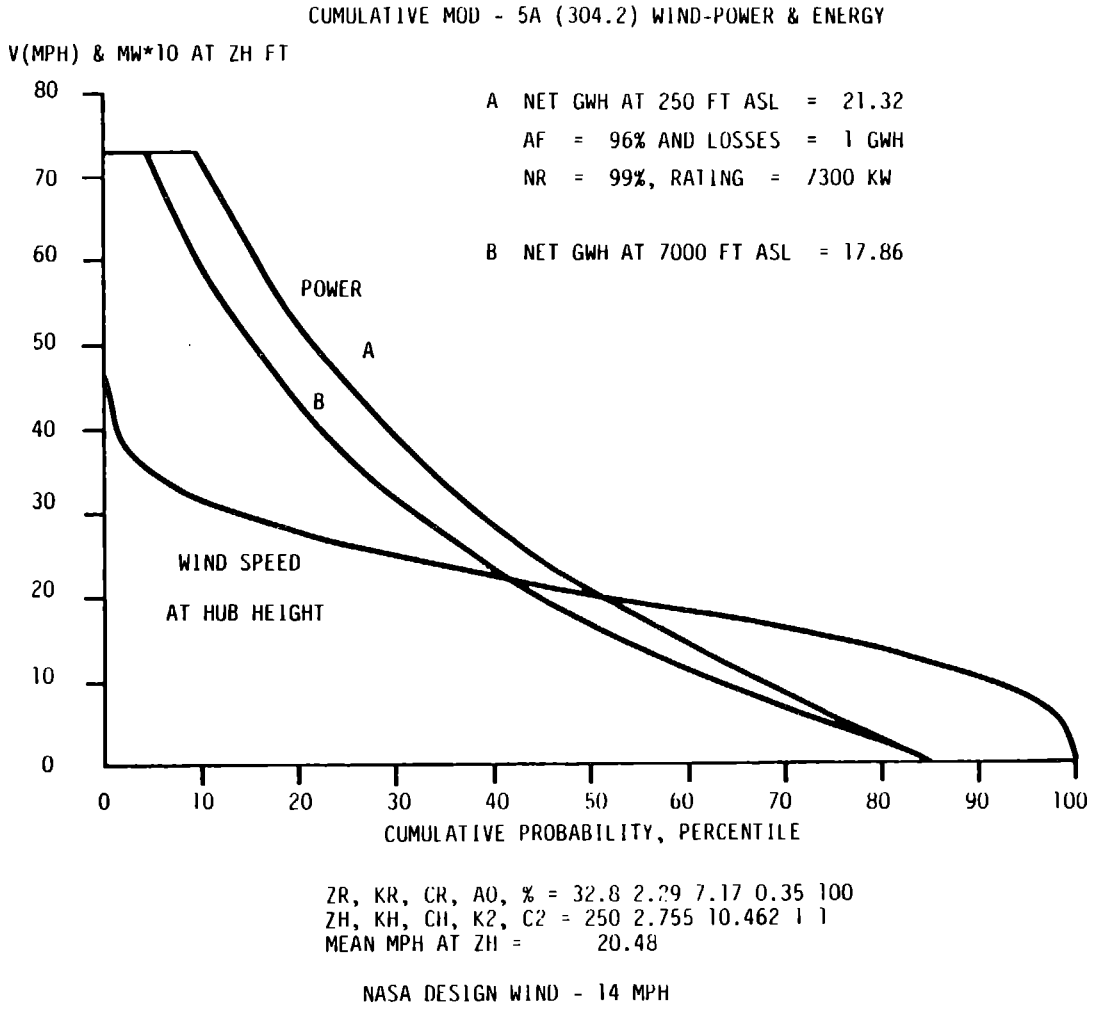

Figure 3-13 Power and Wind Speed Probability for the Design Wind Regime

Table 3-2 Design Energy Output

Item (Model 304.0)	Energy Loss -GWh/Year	Net Energy Output GWh/Year	Gross % of Wind Energy
Gross Wind Energy (12-60 mph)		72.34	100.0
Not Extractable	29.44		(40.7)
Maximum Theoretical Energy (Betz Limit)		42.90	59.3
Rotor Profile & Degradation	11.60		(16.0)
Rotor Power Limit (Above Rating)	4.57		(6.3)
Rotor Teeter, Tilt, Heading, Misc.	1.44		(2.0)
Rotor Startup, Shifting Losses	0.29		(0.4)
Rotor Output Energy		25.00	34.6
Transmission Losses	1.06		(1.5)
Generator Losses	0.99		(1.4)
Generator Output Energy		22.95	31.7
Accessory/Auxiliary Losses	0.58		(0.8)
Transformer Losses	0.11		(0.1)
Single Unit Output Energy		22.26	30.8
Interconnection Losses	0.21		(0.3)
Availability Losses	0.86		(1.2)
Net Utility Substation Output Energy		21.19	29.3

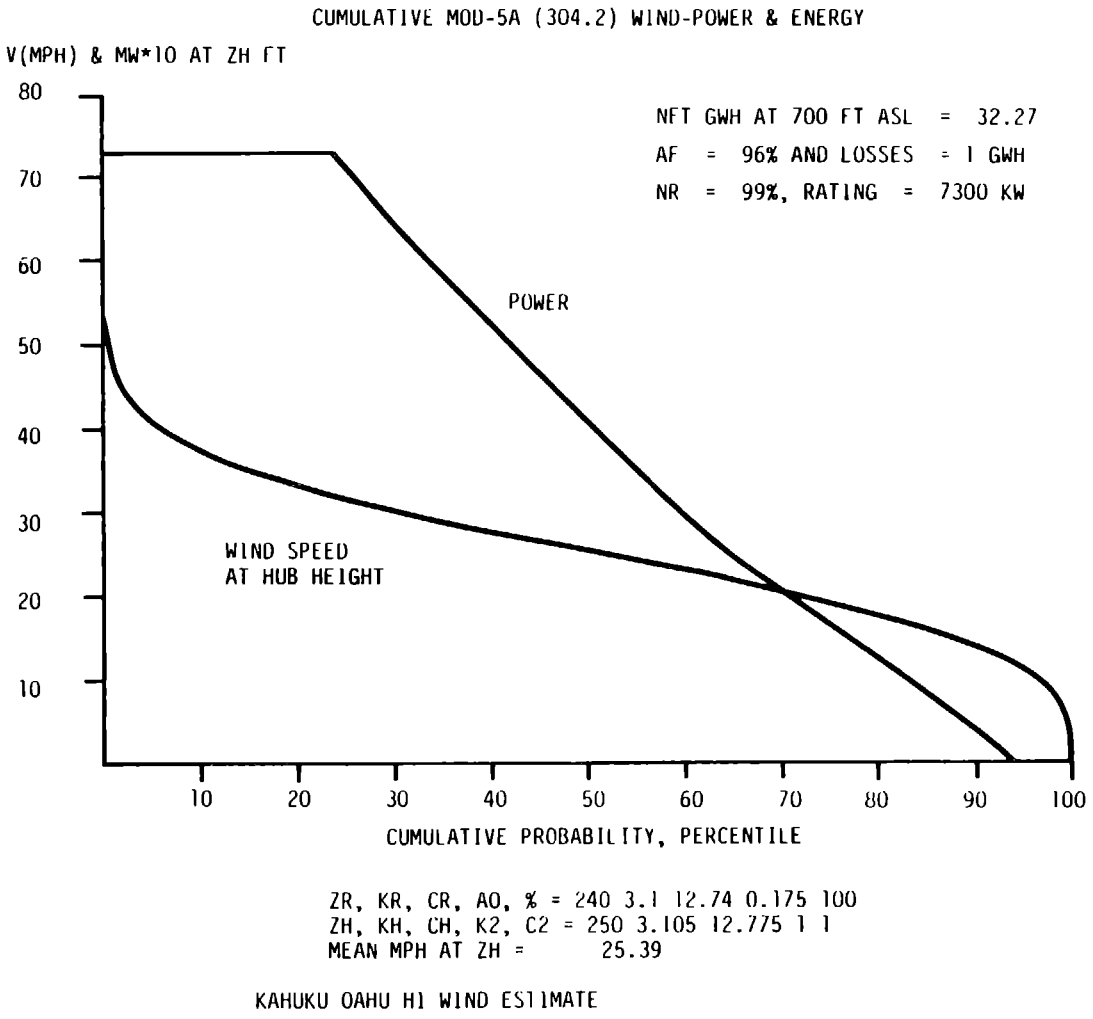

Figure 3-14 Power and Wind Speed Probability for the Wind Regime in Kahuku

3.2.2 WEIGHT SUMMARY

The model 304.2 equipment above ground level weighs 1,803,926 lb. Thirty-five percent of the weight is in the support tower and elevator, and 5% is in the ground electrical equipment. The electrical equipment building structure is not included in the weight breakdown. Nineteen percent of the weight is in the nacelle and yaw structure. Twenty-five percent of the weight is in the rotor, and 14% of the weight is in the drivetrain.

A weight breakdown by major subsystem is shown in Table 3-3.

3.2.3 COST SUMMARY

Cost summaries for the first, second third, the 100th unit in a single installation, and the 100th unit in a cluster installation are shown in Tables 3-4 through 3-8. The costs are in 1980 dollars.

3.2.4 COST OF ENERGY

Cost of energy values are shown in Tables 3-4 through 3-8. The predicted cost of energy for the clustered installation, in volume production, for a design wind regime and mature availability is 3.69 cents/kWh. This cost is below the maximum of 3.75 cents/kWh specified in the Statement of Work.

Table 3-3 Model 304.2 Weight Summary

Subsystem	Item	Weight (lb.)
Rotor	Blades	229,900
	Ailerons	9,760
	Yoke	150,000
	Teeter Bearing Assembly	45,670
	Other	39,140
	Subtotal	474,470
Drivetrain	Low Speed Shaft	66,700
	Gearbox	137,000
	Generator	47,200
	Other	8,736
	Subtotal	259,636
Nacelle	Bedplate, Supports	111,000
	Rotor Support	130,150
	Fairing	6,800
	Yaw	54,400
	Other	26,350
	Subtotal	328,700
Tower	Structure	609,120
	Lift	28,500
	Other	15,500
	Subtotal	653,120
Ground Electrical Equipment		88,000
Total Weight Above Grade		1,803,926

Table 3-4 Cost Summary for the First Unit

SUBASS. ABBREV.	ITEM NAME ABBREV.	REF. NUM.	WEIGHT # 1ST UNIT	COST (1980) 1ST UNIT	DOLLARS PER LB.	% OF TOTAL WT.	% OF COE	COE CONTRIB. (1980 CENTS)
SITE	FOUNDATION	110		$362,300.00			2.75	0.329
	GRD EQUIP.	120	68000	$725,500.00	$8.24	4.8781	5.50	0.658
	SPECIAL	130		$160,600.00			1.22	0.146
			68000	$1,248,400.00	N/A	4.8781	9.47	1.132
TRANSPORT.	TRANSPORT.	240		$306,664.62			2.33	0.278
ERECTION	INSTALL.	310		$605,200.00			4.59	0.549
	INTEG. & C/O	350		$1,194,700.00			9.06	1.084
				$1,799,900.00			13.65	1.633
ROTOR	BLADES	410	229900	$2,614,758.00	$11.37	12.7441	19.83	2.372
	ROTOR HYDR.	420	8418	$47,961.00	$5.70	0.4666	0.36	0.044
	AILERONS	425	9760	$188,846.00	$19.35	0.5410	1.43	0.171
	YOKE ASM/BRGS.	430	170962	$777,877.00	$4.55	9.4770	5.90	0.706
	TEETER ASM.	440	55430	$305,528.00	$5.51	3.0727	2.32	0.277
			474470	$3,934,870.00	$8.29	23.2288	29.84	3.569
DRIVE TRAIN	LOW SPEED SFT.	518	86700	$298,601.00	$4.48	3.8974	2.26	0.271
	TRANSMIS.	520	139730	$468,491.00	$3.50	7.7457	3.70	0.443
	HI SPEED	530	3000	$17,763.00	$5.92	0.1663	0.13	0.016
	GEN. & EXCIT.	540	50206	$320,716.00	$6.39	2.7831	2.43	0.291
			259636	$1,125,571.00	$4.34	6.6468	8.54	1.021
NACELLE	ROTOR SUPPORT	605	139150	$405,891.00	$2.92	7.7136	3.08	0.368
	BEDPLATE	610	116050	$338,866.00	$2.92	6.4330	2.57	0.307
	HYD. SYSTEM	620	6100	$18,118.00	$2.97	0.3381	0.14	0.016
	FAIR. & MISC.	645	6800	$90,326.00	$13.28	0.3769	0.68	0.082
	SLP, ELEC.	660	2970	$53,912.00	$18.15	0.1646	0.41	0.049
	INST. & CON.	670	3270	$114,752.00	$35.09	0.1813	0.87	0.104
	YAW SUBSYS.	680	54400	$354,999.00	$6.53	3.0156	2.69	0.322
			328740	$1,376,864.00	$4.19	18.2232	10.44	1.249
TOWER	TOWER	710	609120	$681,000.00	$1.12	33.7656	5.16	0.618
	PERS. LIFT	720	28500	$89,827.00	$3.12	1.5799	0.67	0.081
	CABLING	740	15500	$88,806.00	$5.73	0.8592	0.67	0.081
			653120	$858,633.00	$1.31	36.2047	6.51	0.779
REM. CONT.	LINE MODEM	810		$728.00			0.01	0.001
	REM. DISP.	820		$4,776.00			0.04	0.004
				$5,504.00			0.04	0.005
SPARES	SPARES	830		$117,496.00			0.89	0.107
SPECIAL	PROFIT	1010		$1,154,827.26			8.76	1.047
	ASM. & TEST	1020		$774,080.00			5.87	0.702
	GROWTH BUDGET	1030		$0.00			0.00	0.000
				$1,928,907.26			14.63	1.750
LAND	MTG LAND	1110		$0.00			0.00	0.000
	ROAD LAND	1140		$0.00			0.00	0.000
				$0.00			0.00	0.000
CLUSTER	SUBSTATION	1240		$0.00			0.00	0.000
	TRANSM. ETC.	1250		$0.00			0.00	0.000
				$0.00			0.00	0.000
O & M	YEARLY O & M	1340		$43,500.00			3.67	0.438
TOTAL OVERALL (NO O&M)								
REF. NUM. 100-1299			1803966 #	$12,703,099.88	7.0417	100.0000	100.00	11.960
				PRE-PROFIT (1980)	AF	GROSS	GWH/YR*E4	NET
PREPROFIT COST				$11,548,272.62	0.9	220500		198450

(2295A)

Table 3-5 Cost Summary for the Second Unit

SUBASS. ABBREV.	ITEM NAME ABBREV.	REF. NUM.	WEIGHT # 2ND UNIT	COST (1980) 2ND UNIT	DOLLARS PER LB.	% OF TOTAL WT.	% OF COE	COE CONTRIB. (1980 CENTS)
SITE	FOUNDATION	110		$333,316.00			3.08	0.302
	GRD EQUIP.	120	88000	$667,460.00	$7.58	4.8781	6.17	0.605
	SPECIAL	130		$128,480.00			1.18	0.117
			88000	$1,129,256.00	N/A	4.8781	10.43	1.024
TRANSPORT.	TRANSPORT.	240		$306,854.62			2.84	0.278
ERECTION	INSTALL.	310		$466,004.00			4.31	0.423
	INTEG. & C/O	350		$836,290.00			7.73	0.759
				$1,302,294.00			12.03	1.181
ROTOR	BLADES	410	229900	$1,961,068.50	$8.53	12.7441	18.12	1.779
	ROTOR HYDR.	420	8418	$43,164.80	$5.13	0.4666	0.40	0.039
	AILERONS	425	9760	$141,634.50	$14.51	0.5410	1.31	0.128
	YOKE ASM/BRGS.	430	170962	$684,531.76	$4.00	9.4770	6.32	0.621
	TEETER ASM.	440	55430	$259,698.80	$4.69	3.0727	2.40	0.236
			474470	$3,090,098.46	$6.51	23.2288	28.55	2.803
DRIVE TRAIN	LOW SPEED SFT.	518	66700	$238,880.80	$3.58	3.6974	2.21	0.217
	TRANSMIS.	520	139730	$439,641.80	$3.15	7.7457	4.06	0.399
	HI SPEED	530	3000	$14,210.40	$4.74	0.1663	0.13	0.013
	GEN. & EXCIT.	540	50206	$304,680.20	$6.07	2.7831	2.82	0.276
			259636	$997,413.30	$3.84	6.6468	9.22	0.905
NACELLE	ROTOR SUPPORT	605	139150	$345,007.35	$2.48	7.7136	3.19	0.313
	BEDPLATE	610	116050	$281,258.78	$2.42	6.4330	2.60	0.255
	HYD. SYSTEM	620	6100	$16,306.20	$2.67	0.3381	0.15	0.015
	FAIR. & MISC.	646	6800	$76,777.10	$11.29	0.3769	0.71	0.070
	SLP, ELEC.	660	2970	$48,520.80	$16.34	0.1646	0.45	0.044
	INST. & CON.	670	3270	$94,096.64	$28.78	0.1813	0.87	0.085
	YAW SUBSYS.	680	54400	$312,399.12	$5.74	3.0156	2.89	0.283
			328740	$1,174,365.99	$3.57	18.2232	10.85	1.065
TOWER	TOWER	710	609120	$626,520.00	$1.03	33.7656	5.79	0.568
	PERS. LIFT	720	28500	$79,944.30	$2.81	1.5799	0.74	0.073
	CABLING	740	15500	$81,701.52	$5.27	0.8592	0.75	0.074
			653120	$788,165.82	$1.21	36.2047	7.28	0.715
REM. CONT.	LINE MODEM	810		$684.32			0.01	0.001
	REM. DISP.	820		$4,393.92			0.04	0.004
				$5,078.24			0.05	0.005
SPARES	SPARES	830		$97,521.68			0.90	0.088
SPECIAL	PROFIT	1010		$944,838.57			8.73	0.857
	ASM. & TEST	1020		$557,337.60			5.15	0.506
	GROWTH BUDGET	1030		$0.00			0.00	0.000
				$1,502,176.17			13.88	1.363
LAND	MTG LAND	1110		$0.00			0.00	0.000
	ROAD LAND	1140		$0.00			0.00	0.000
				$0.00			0.00	0.000
CLUSTER	SUBSTATION	1240		$0.00			0.00	0.000
	TRANSM. ETC.	1250		$0.00			0.00	0.000
				$0.00			0.00	0.000
O & M	YEARLY O & M	1340		$38,715.00			3.87	0.390
TOTAL OVERALL (NO O&M)								
REF. NUM. 100-1299			1803966 #	$10,393,224.28	5.7613	100.0000	100.00	9.817
				PRE-PROFIT (1980)	AF	GROSS	GWH/YR*E4	NET
PREPROFIT COST				$9,448,385.71	0.9	220500		198450

Table 3-6 Cost Summary for the Third Unit

SUBASS. ABBREV.	ITEM NAME ABBREV.	REF. NUM.	WEIGHT # 3RD	WEIGHT # UNIT	COST (1980) 3RD	COST (1980) UNIT	DOLLARS PER LB.	% OF TOTAL WT.	% OF COE	COE CONTRIB. (1980 CENTS)
SITE	FOUNDATION	110			$317,050.80				3.28	0.270
	GRD EQUIP.	120		88000	$634,889.20		$7.21	4.8781	6.57	0.540
	SPECIAL	130			$112,380.13				1.16	0.096
				88000	$1,064,320.13		N/A	4.8781	11.01	0.905
TRANSPORT.	TRANSPORT.	240			$306,854.62				3.18	0.261
ERECTION	INSTALL.	310			$398,367.86				4.12	0.339
	INTEG. & C/O	350			$675,174.03				6.89	0.574
					$1,073,541.89				11.11	0.913
ROTOR	BLADES	410		223900	$1,650,173.17		$7.18	12.7441	17.08	1.403
	ROTOR HYDR.	420		8418	$40,520.64		$4.81	0.4666	0.42	0.034
	AILERONS	425		9760	$118,180.67		$12.21	0.5410	1.23	0.101
	YOKE ASM/BRGS.	430		170962	$633,891.17		$3.71	9.4770	6.56	0.539
	TEETER ASM.	440		55430	$235,570.71		$4.25	3.0727	2.44	0.200
				474470	$2,679,436.36		$5.65	29.2288	27.73	2.278
DRIVE TRAIN	LOW SPEED SFT.	518		66700	$208,946.57		$3.13	3.6974	2.16	0.178
	TRANSMIS.	520		139730	$412,709.61		$2.95	7.7457	4.27	0.351
	HI SPEED	530		3000	$12,429.68		$4.14	0.1663	0.13	0.011
	GEN. & EXCIT.	540		50206	$295,446.19		$5.88	2.7831	3.06	0.251
				259636	$929,532.06		$3.58	6.6468	9.62	0.790
NACELLE	ROTOR SUPPORT	605		139150	$312,953.42		$2.25	7.7136	3.24	0.266
	BEDPLATE	610		116050	$251,508.66		$2.17	6.4330	2.60	0.214
	HYD. SYSTEM	620		6100	$15,307.29		$2.51	0.3381	0.16	0.013
	FAIR. & MISC.	646		6900	$69,643.80		$10.24	0.3769	0.72	0.059
	SLP, ELEC.	660		2870	$45,548.43		$15.34	0.1646	0.47	0.039
	INST. & CON.	670		3270	$83,533.84		$25.55	0.1813	0.86	0.071
	YAW SUBSYS.	680		54400	$289,333.96		$5.32	3.0156	2.99	0.246
				328740	$1,067,829.49		$3.25	18.2232	11.05	0.908
TOWER	TOWER	710		609120	$595,947.00		$0.98	33.7656	6.17	0.507
	PERS. LIFT	720		28500	$75,046.94		$2.63	1.5799	0.78	0.064
	CABLING	740		15500	$77,714.64		$5.01	0.8592	0.80	0.066
				653120	$748,708.58		$1.15	36.2047	7.75	0.637
REM. CONT.	LINE MODEM	810			$659.38				0.01	0.001
	REM. DISP.	820			$4,178.50				0.04	0.004
					$4,838.89				0.05	0.004
SPARES	SPARES	830			$87,206.33				0.90	0.074
SPECIAL	PROFIT	1010			$841,990.17				8.71	0.716
	ASM. & TEST	1020			$457,633.53				4.74	0.389
	GROWTH BUDGET	1030			$0.00				0.00	0.000
					$1,299,623.70				13.45	1.105
LAND	MTG LAND	1110			$0.00				0.00	0.000
	ROAD LAND	1140			$0.00				0.00	0.000
					$0.00				0.00	0.000
CLUSTER	SUBSTATION	1240			$0.00				0.00	0.000
	TRANSM. ETC.	1250			$0.00				0.00	0.000
					$0.00				0.00	0.000
O & M	YEARLY O & M	1340			$36,100.50				4.15	0.341
TOTAL OVERALL (NO O&M)										
REF. NUM. 100-1299			1803966 #		$9,261,891.84		5.1341	100.0000	100.00	8.217
					PRE-PROFIT (1980)		AF	GROSS	GWH/YR*E4	NET
PREPROFIT COST					$8,419,901.68		0.96	220500		211680

Table 3-7 Cost Summary for the 100th Unit, Single Installation

SUBASS. ABBREV.	ITEM NAME ABBREV.	REF. NUM.	WEIGHT # 100TH UNIT	COST (1980) 100TH UNIT	DOLLARS PER LB.	% OF TOTAL WT.	% OF COE	COE CONTRIB. (1980 CENTS)
SITE	FOUNDATION	110		$227,949.83			4.83	0.194
	GRD EQUIP.	120	88000	$414,969.20	$4.72	4.8781	8.87	0.353
	SPECIAL	130		$39,613.31			0.86	0.034
			88000	$682,532.44	N/A	4.8781	14.75	0.580
TRANSPORT.	TRANSPORT.	240		$239,156.36			5.17	0.203
ERECTION	INSTALL.	310		$145,047.76			3.13	0.123
	INTEG. & C/O	360		$109,500.41			2.37	0.093
				$254,548.16			5.50	0.216
ROTOR	BLADES	410	223900	$380,488.89	$1.66	12.7441	8.22	0.324
	ROTOR HYDR.	420	8418	$23,676.26	$2.81	0.4666	0.51	0.020
	AILERONS	425	9760	$27,490.10	$2.82	0.5410	0.59	0.023
	YOKE ASM/BRGS.	430	170962	$330,327.58	$1.93	9.4770	7.14	0.281
	TEETER ASM.	440	55430	$102,838.89	$1.86	3.0727	2.22	0.087
			474470	$864,811.80	$1.82	23.2288	18.69	0.735
DRIVE TRAIN	LOW SPEED SFT.	518	66700	$66,956.72	$1.00	3.6974	1.45	0.057
	TRANSMIS.	520	139730	$241,146.73	$1.73	7.7457	5.21	0.205
	HI SPEED	530	3000	$3,983.08	$1.33	0.1663	0.09	0.003
	GEN. & EXCIT.	540	50206	$227,441.01	$4.53	2.7831	4.91	0.193
			259636	$539,527.55	$2.08	6.6468	11.66	0.459
NACELLE	ROTOR SUPPORT	605	139150	$136,620.61	$0.98	7.7136	2.95	0.116
	BEDPLATE	610	116050	$97,241.40	$0.84	6.4330	2.10	0.083
	HYD. SYSTEM	620	6100	$8,944.07	$1.47	0.3381	0.19	0.008
	FAIR. & MISC.	645	6800	$30,403.22	$4.47	0.3769	0.66	0.026
	SLP, ELEC.	660	2870	$26,614.01	$8.96	0.1646	0.58	0.023
	INST. & CON.	670	3270	$30,360.79	$9.28	0.1813	0.66	0.026
	YAW SUBSYS.	680	54400	$150,751.29	$2.77	3.0156	3.26	0.128
			328740	$480,935.39	$1.46	18.2232	10.39	0.409
TOWER	TOWER	710	609120	$447,943.66	$0.74	33.7656	8.68	0.381
	PERS. LIFT	720	28500	$43,650.02	$1.54	1.5799	0.95	0.037
	CABLING	740	15500	$50,794.98	$3.28	0.8592	1.10	0.043
			653120	$542,588.66	$0.83	36.2047	11.72	0.461
REM. CONT.	LINE MODEM	810		$480.94			0.01	.000
	REM. DISP.	820		$2,731.76			0.06	0.002
				$3,212.70			0.07	0.003
SPARES	SPARES	830		$75,862.78			1.64	0.065
SPECIAL	PROFIT	1010		$395,637.86			8.55	0.336
	ASM. & TEST	1020		$85,686.73			1.85	0.073
	GROWTH BUDGET	1030		$0.00			0.00	0.000
				$481,324.69			10.40	0.409
LAND	MTG LAND	1110		$4,859.00			0.09	0.004
	ROAD LAND	1140		$964.00			0.02	0.001
				$5,823.00			0.11	0.004
CLUSTER	SUBSTATION	1240		$48,708.00			1.05	0.041
	TRANSM. ETC.	1250		$132,886.00			2.87	0.113
				$181,594.00			3.92	0.154
O & M	YEARLY O & M	1340		$24,906.48			0.98	0.235
TOTAL OVERALL (NO O&M)								
REF. NUM. 100-1298			1803966 #	$4,352,017.52	2.4124	100.0000	100.00	3.935
				PRE-PROFIT (1980)	AF	GROSS	GWH/YR*E4	NET
PREPROFIT COST				$3,956,379.56	0.96	220500		211680

Table 3-8 Cost Summary for the 100th Unit, Clustered Installation

SUBASS. ABBREV.	ITEM NAME ABBREV.	REF. NUM.	WEIGHT # 100TH UNIT	COST (1980) 100TH UNIT	DOLLARS PER LB.	% OF TOTAL WT.	% OF COE	COE CONTRIB. (1980 CENTS)
SITE	FOUNDATION	110		$207,227.21			4.79	0.176
	GRD EQUIP.	120	88000	$414,969.20	$4.72	4.8781	9.59	0.353
	SPECIAL	130		$36,012.10			0.83	0.031
			88000	$658,208.51	N/A	4.8781	15.22	0.560
TRANSPORT.	TRANSPORT.	240		$179,816.81			4.16	0.153
ERECTION	INSTALL.	310		$105,047.76			2.43	0.089
	INTEG. & C/O	350		$109,500.41			2.53	0.093
				$214,548.16			4.96	0.182
ROTOR	BLADES	410	229900	$380,488.88	$1.66	12.7441	8.80	0.324
	ROTOR HYDR.	420	8418	$23,676.26	$2.81	0.4666	0.55	0.020
	AILERONS	425	9760	$27,480.10	$2.82	0.5410	0.64	0.023
	YOKE ASM/BRGS.	430	170962	$330,327.58	$1.93	9.4770	7.64	0.281
	TEETER ASM.	440	55430	$102,838.99	$1.86	3.0727	2.38	0.087
			474470	$864,811.80	$1.82	23.2288	19.99	0.735
DRIVE TRAIN	LOW SPEED SFT.	510	66700	$66,956.72	$1.00	3.6974	1.55	0.057
	TRANSMIS.	520	139730	$241,146.73	$1.73	7.7457	5.57	0.205
	HI SPEED	530	3000	$3,983.08	$1.33	0.1663	0.09	0.003
	GEN. & EXCIT.	540	50206	$227,441.01	$4.53	2.7831	5.26	0.193
			259636	$539,527.55	$2.08	6.6468	12.47	0.459
NACELLE	ROTOR SUPPORT	605	139150	$136,620.61	$0.98	7.7136	3.16	0.116
	BEDPLATE	610	116050	$97,241.40	$0.84	6.4330	2.25	0.083
	HYD. SYSTEM	620	6100	$8,944.07	$1.47	0.3381	0.21	0.008
	FAIR. & MISC.	645	6800	$30,403.22	$4.47	0.3769	0.70	0.026
	SLP, ELEC.	660	2870	$26,614.01	$9.26	0.1646	0.62	0.023
	INST. & CON.	670	3270	$30,360.79	$9.28	0.1813	0.70	0.026
	YAW SUBSYS.	680	54400	$150,751.28	$2.77	3.0156	3.48	0.128
			328740	$480,935.39	$1.46	18.2232	11.12	0.409
TOWER	TOWER	710	609120	$389,516.23	$0.64	33.7656	9.00	0.331
	PERS. LIFT	720	28500	$43,650.02	$1.54	1.5799	1.01	0.037
	CABLING	740	15500	$50,794.98	$3.28	0.8582	1.17	0.043
			653120	$484,161.22	$0.74	36.2047	11.19	0.412
REM. CONT.	LINE MODEM	810		$480.94			0.01	.000
	REM. DISP.	820		$2,731.76			0.06	0.002
				$3,212.70			0.07	0.003
SPARES	SPARES	830		$33,716.80			0.78	0.029
SPECIAL	PROFIT	1010		$373,214.27			8.63	0.317
	ASM. & TEST	1020		$85,686.73			1.98	0.073
	GROWTH BUDGET	1030		$0.00			0.00	0.000
				$458,901.00			10.61	0.390
LAND	MTG LAND	1110		$4,959.00			0.10	0.004
	ROAD LAND	1140		$964.00			0.02	0.001
				$5,923.00			0.11	0.004
CLUSTER	SUBSTATION	1240		$48,708.00			1.13	0.041
	TRANSM. ETC.	1250		$132,886.00			3.07	0.113
				$181,594.00			4.20	0.154
O & M	YEARLY O & M	1340		$19,926.18			5.12	0.188
TOTAL OVERALL (NO O&M)								
REF. NUM. 100-1289			1803966 #	$4,105,356.82	2.2757	100.0000	100.00	3.678
				PRE-PROFIT (1980)	AF	GROSS	GWH/YR*E4	NET
PREPROFIT COST				$3,732,142.66	0.96	220500		211680

3.3 ENVIRONMENTAL CHARACTERISTICS

3.3.1 SOUND

Initial MOD-5A sound predictions were made with a modified version of the SOUND code originally developed by NASA Lewis Research Center. This code agreed well with measurements on the downwind MOD-1 wind turbine. It was modified to include cylindrical tower shadow models for both upwind and downwind rotors. The tower shadow models are shown in Figure 3-15.

Measurements from the MOD-2 wind turbines, reported in ref. 3-1, indicated that sound characteristics from upwind rotors are broadband, rather than tonal. The tonal characteristic is more important for downwind rotors, where a significant tower wake is periodically cut by the blades. SOUND code predictions in the frequency range from 0.6 to 26.1 Hz are shown in Figures 3-16 through 3-19. The background sound model is shown in Figure 3-16. Near field characteristics at 800 ft. from the wind turbine are shown in Figures 3-17, 3-18, and 3-19 for downwind, MOD-1, and upwind tower shadows, respectively. The upwind shadow sound level is barely above the background value.

3.3.1.1 Broadband Sound

The broadband sound mechanisms are not completely determined, but ref. 3-2 indicates that they originate from fluctuating lift caused by the interaction of the blades and inherent wind turbulence, and the interaction of the trailing edge of the blade with the turbulent boundary layer of air flow along the chord of the blade. Theoretical directivity pattern analysis indicates a dipole source model, but field measurements indicate that an omnidirectional source model is more appropriate. Sound power levels were therefore assumed to decrease with radial distance from the MOD-5A wind turbine as:

$$L_A = L_B + 20 \log (X_B/X_A) \qquad (3\text{-}1)$$

where L_A, L_B = levels in decibels at locations A, B

X_A, X_B = distance from the wind turbine to locations A, B

This equation does not include the effects of ambient wind refraction and the effect of an ambient wind "shadow" typically found at a distance of several diameters upwind. It was conservative to neglect the upwind shadow effect and report only downwind spherical propagation.

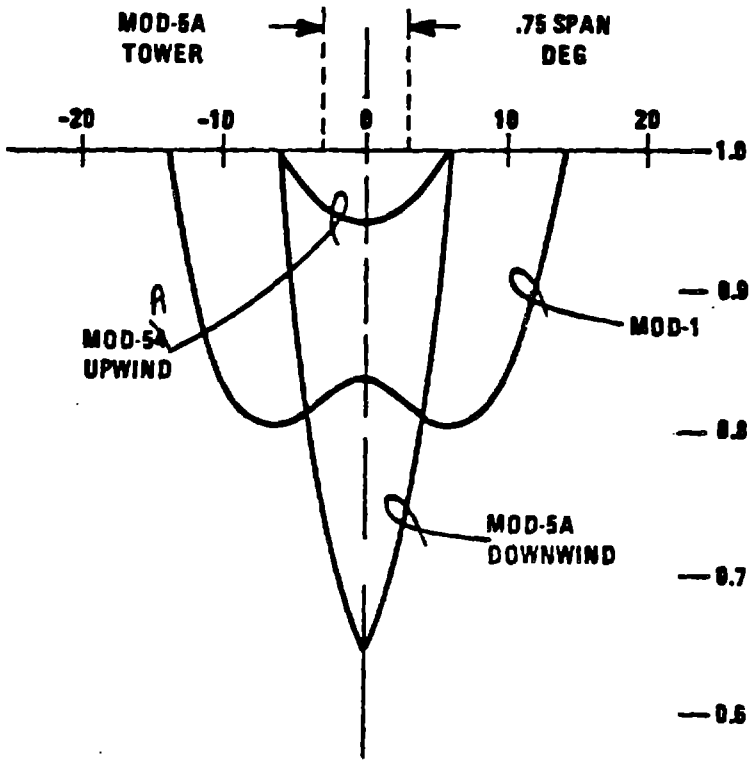

Figure 3-15 Tower Shadow Models

WIND TURBINE SOUND LEVEL PROGRAM

ROTOR THRUST, LBS	190,000
ROTOR TORQUE, FT-LBS	2,620,000
ROTOR SPEED, RPM	17.4
ROTOR RADIUS, FT	200
NUMBER OF BLADES	2
DISTANCE FROM ROTOR, FT	800
REFLECTION FACTOR	2
PITCH ANGLE, DEG	1
WIND SPEED AT HUB, MPH	26
HUB HEIGHT, FT	250
AZIMUTH, DELTA, DEG	175
ALTITUDE, PHI, DEG	21
CHORD LENGTH, FT	16.3

LAST MODIFIED 801216 RSB

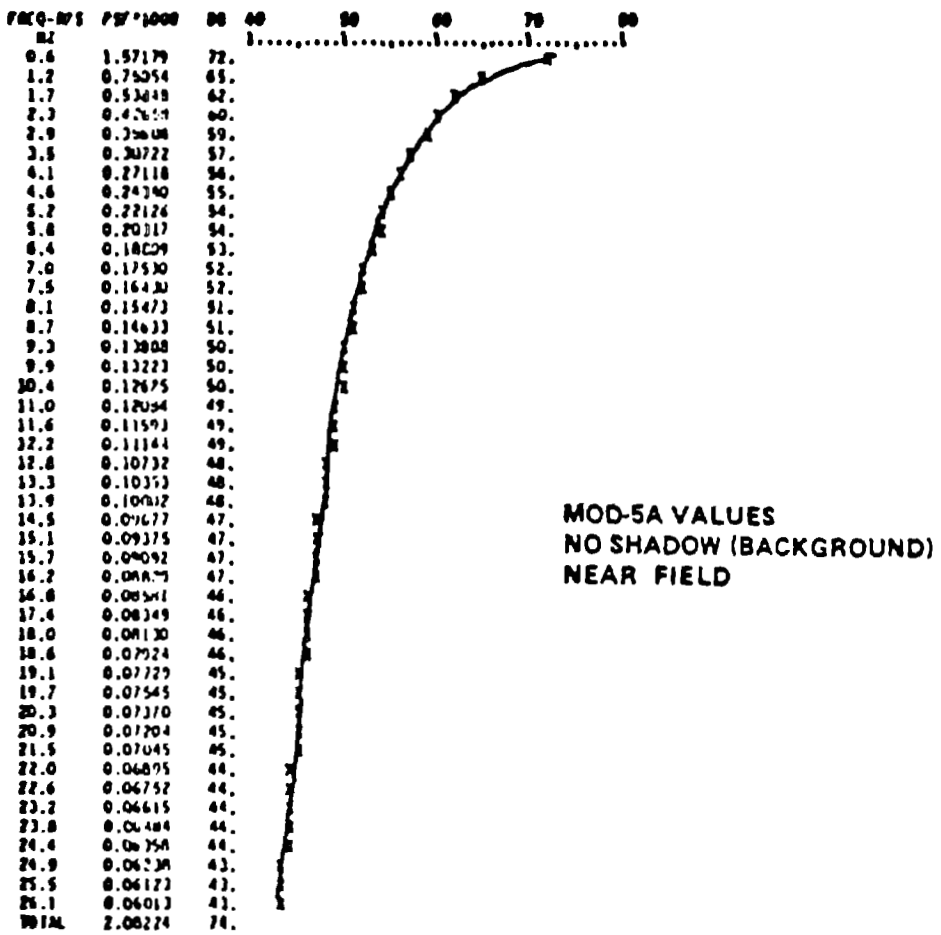

Figure 3-16 Background Sound in Near Field

WIND TURBINE SOUND LEVEL PROGRAM

ROTOR THRUST, LBS	190,000
ROTOR TORQUE, FT-LBS	2,620,000
ROTOR SPEED, RPM	17.4
ROTOR RADIUS, FT	200
NUMBER OF BLADES	2
DISTANCE FROM ROTOR, FT	800
REFLECTION FACTOR	2
PITCH ANGLE, DEG	1
WIND SPEED AT HUB, MPH	26
HUB HEIGHT, FT	250
AZIMUTH, DELTA, DEG	175
ALTITUDE, PHI, DEG	21
CHORD LENGTH, FT	16.3

LAST MODIFIED 801216 RSB

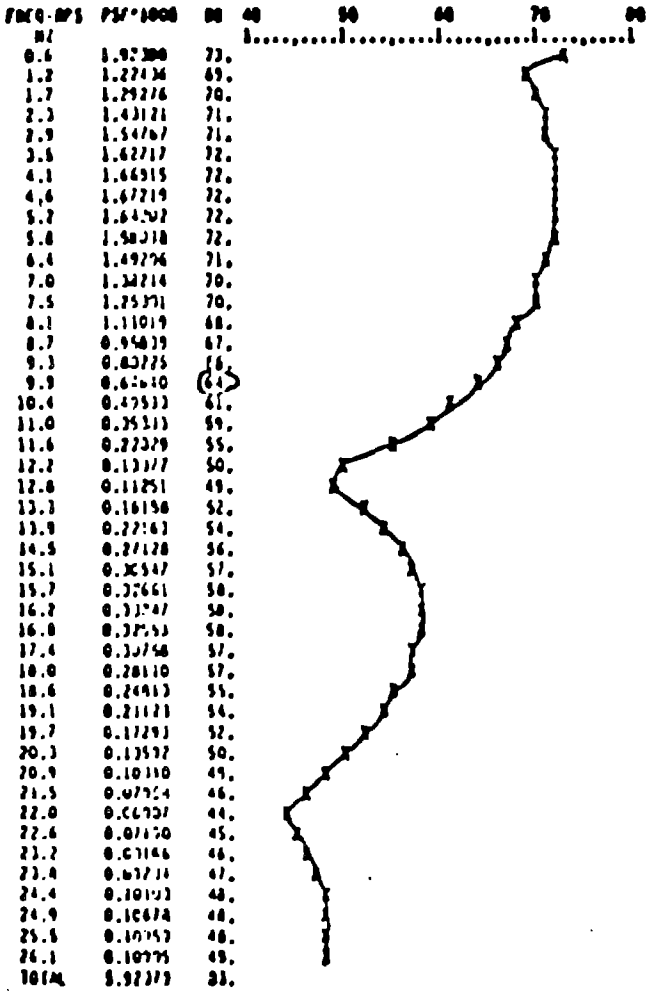

Figure 3-17 Sound with Downwind Tower Shadow in Near Field

WIND TURBINE SOUND LEVEL PROGRAM

ROTOR THRUST, LBS	190,000
ROTOR TORQUE, FT-LBS	2,620,000
ROTOR SPEED, RPM	17.4
ROTOR RADIUS, FT	200
NUMBER OF BLADES	2
DISTANCE FROM ROTOR, FT	800
REFLECTION FACTOR	2
PITCH ANGLE, DEG	1
WIND SPEED AT HUB, MPH	26
HUB HEIGHT, FT	250
AZIMUTH, DELTA, DEG	175
ALTITUDE, PHI, DEG	21
CHORD LENGTH, FT	16.3

LAST MODIFIED 80/2/6 RSB

FREQ-HZ	PSF*1000	DB
0.6	2.36673	75.
1.1	1.87864	73.
1.7	1.83570	73.
2.3	1.54873	71.
2.8	1.03959	68.
3.4	0.49613	61.
4.0	0.32560	58.
4.5	0.62695	64.
5.1	0.79978	66.
5.7	0.77149	65.
6.2	0.59253	63.
6.8	0.32144	59.
7.4	0.16960	52.
7.9	0.27969	57.
8.5	0.36155	59.
9.1	0.33571	58.
9.6	0.22627	55.
10.2	0.13403	50.
10.8	0.16458	52.
11.3	0.23387	55.
11.9	0.25094	56.
12.5	0.20683	54.
13.0	0.13397	50.
13.6	0.10412	48.
14.2	0.14170	51.
14.7	0.16788	52.
15.3	0.15527	51.
15.9	0.11534	49.
16.4	0.09751	46.
17.0	0.10450	48.
17.6	0.12803	50.
18.1	0.12860	50.
18.7	0.10652	48.
19.3	0.09104	46.
19.8	0.07809	45.
20.4	0.07003	47.
21.0	0.09542	47.
21.5	0.06583	46.
22.1	0.07194	45.
22.7	0.06824	44.
23.2	0.07443	45.
23.8	0.07720	45.
24.4	0.07358	45.
24.9	0.06775	44.
25.5	0.07134	43.
TOTAL	4.33271	80.

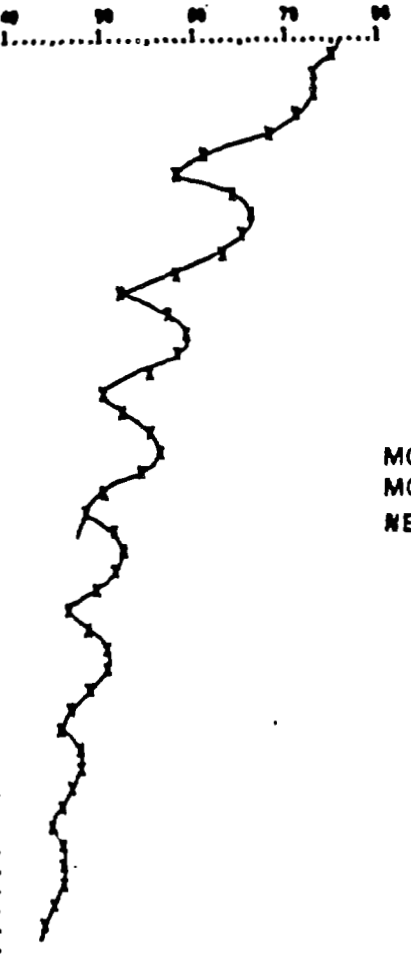

MOD-5A VALUES
MOD-1 SHADOW
NEAR FIELD

Figure 3-18 Sound with MOD-1 Tower Shadow in Near Field

WIND TURBINE SOUND LEVEL PROGRAM

ROTOR THRUST, LBS	190,000
ROTOR TORQUE, FT-LBS	2,620,000
ROTOR SPEED, RPM	17.4
ROTOR RADIUS, FT	200
NUMBER OF BLADES	2
DISTANCE FROM ROTOR, FT	800
REFLECTION FACTOR	2
PITCH ANGLE, DEG	1
WIND SPEED AT HUB, MPH	26
HUB HEIGHT, FT	250
AZIMUTH, DELTA, DEG	175
ALTITUDE, PHI, DEG	21
CHORD LENGTH, FT	16.3
LAST MODIFIED 801216 RSB	

FREQ-CPS HZ	PSF*1000	DB
0.6	1.61918	72.
1.2	0.77235	69.
1.7	0.56521	67.
2.3	0.46871	66.
2.9	0.41524	66.
3.5	0.38172	65.
4.1	0.35773	65.
4.6	0.33794	65.
5.2	0.31953	65.
5.8	0.30499	64.
6.4	0.29169	64.
7.0	0.28148	64.
7.5	0.27055	64.
8.1	0.25929	64.
8.7	0.24825	64.
9.3	0.23807	64.
9.9	0.22944	64.
10.4	0.22275	64.
11.0	0.21948	64.
11.6	0.21908	64.
12.2	0.21787	64.
12.8	0.21746	64.
13.3	0.21512	64.
13.9	0.21403	64.
14.5	0.21341	64.
15.1	0.21266	64.
15.7	0.21140	64.
16.2	0.20945	64.
16.8	0.20680	64.
17.4	0.20355	64.
18.0	0.20187	64.
18.6	0.20000	64.
19.1	0.20217	64.
19.7	0.20460	64.
20.3	0.20544	64.
20.9	0.20279	64.
21.5	0.20064	64.
22.0	0.20025	64.
22.6	0.20281	64.
23.2	0.20651	64.
23.8	0.20552	64.
24.4	0.20457	64.
24.9	0.20359	64.
25.5	0.20258	64.
26.1	0.20153	64.
TOTAL	2.25451	75.

MOD-5A VALUES
UPWIND .05 SHADOW
NEAR FIELD

Figure 3-19 Sound with Upwind Shadow in Near Field

The effect of ambient wind speed was treated as an increase in ambient or "background" sound level as the wind speed increases. As the sound generated by the wind turbine must be above the background sound to be noticed, a perception threshold distance model was appropriate.

The audible perception threshold model is expected to correlate with a negligible complaint probability, although periods of perception can occur during lulls in wind at the observer's location.

3.3.1.2 Sound Code Modification

The SOUND code was modified to predict broadband sound levels that occur at frequencies around 1000 Hz, as well as the original low frequency tonal predictions. An example of the modified output spectral plot and sound level prediction table is shown in Figure 3-20.

The broadband term is derived from the data presented in ref. 3-1, but uses spherical or omnidirectional spreading characteristics.

The peak broadband sound is modeled as:

$$SPL = 10 \log_{10} (KSN^{b}D^{b}) + 20 \log_{10} (D/X) \qquad (3\text{-}2)$$

where SPL = sound power level (dB)
K = empirical constant = 2.0×10^{-19}
D = rotor diameter = 400 ft for MOD-5A
N = speed of rotor = 13.8 rpm and 16.8 rpm for MOD-5A
X = distance from wind turbine (ft)
S = rotor solidity = .03 for MOD-5A

The original equation used blade area in place of the squared diameter and solidity terms, and speed at 90% of the span to the sixth power rather than speed times diameter to the sixth power. The K constant was adjusted for these changes. Unit conversions were included in the K constant. The second term is the same as equation 3-1, with the reference equal to one rotor diameter.

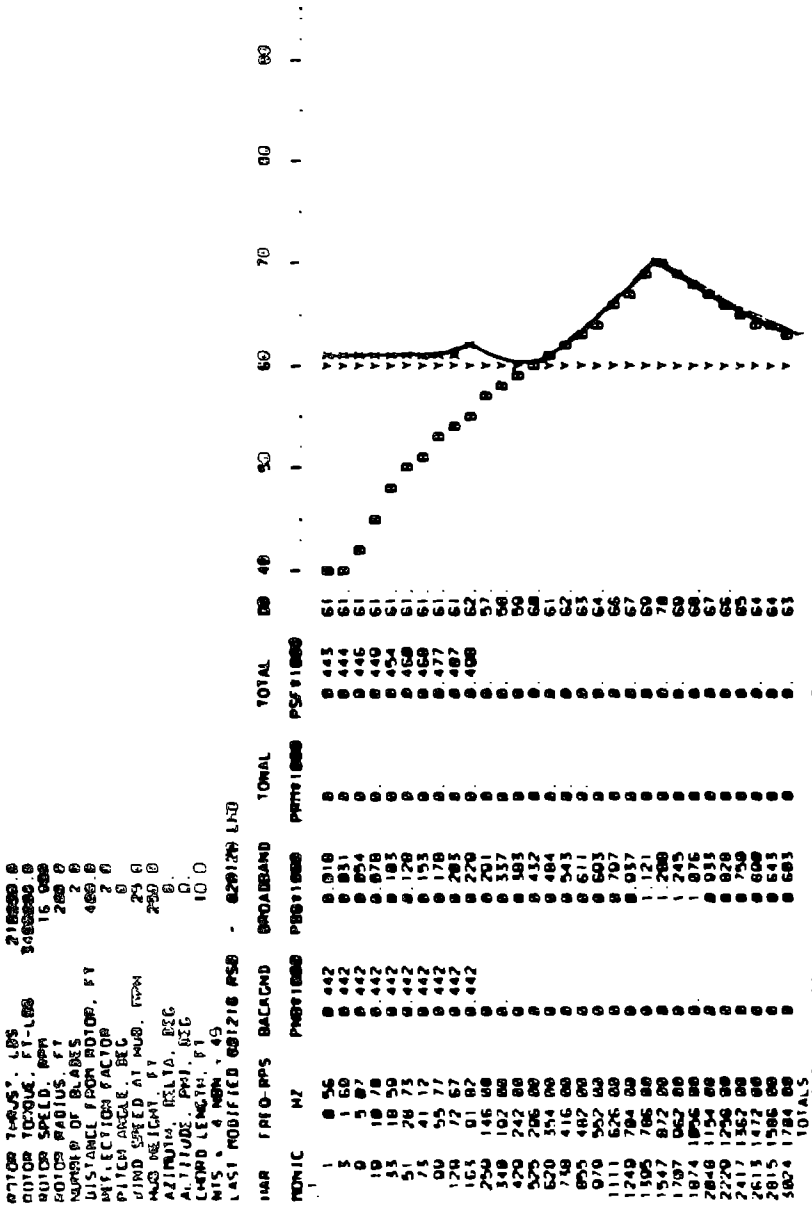

Figure 3-20 Broadband SOUND Code Prediction

Fan scaling was suggested as a way of verifying scaling laws or predicting sound levels of similar machines. One version indicates scaling by diameter to the seventh power and rotor speed to the fifth power, but is appropriate to axial flow, propeller-type fans with proportional loading. Since wind turbines do not always scale this way on loading, the more conservative higher powers of diameter and speed from equation 3-2 were used.

Note that the broadband sound prediction from the first term in equation 3-2 is independent of wind speed. Also, the spherical propagation model is assumed to be independent of wind speed at the frequency of roughly 1000 Hz that predominates. Reflections from atmospheric terrain, or structural discontinuities and site turbulence were estimated to produce a band of wind turbine sound at the observer site of ±6 dB around the prediction from equation 3-2. A similar band of ±6 dB around the ambient or background sound level was added to account for local wind turbulence. MOD-2 measurements indicate that ambient sound varies by 6.2 dB per 10 mph of wind.

3.3.1.3 Methodology Discussion

The goal of computing sound levels and propagation from a wind turbine source was to predict the likelihood of complaints in the worst case, or the perception distance in the benign case. Work on the MOD-1 wind turbine, and studies of gas turbines indicate that a sustained sound level of 10 dB above ambient produces a high probability of complaints.

The distance from a broadband sound source, where the rated source sound level just equals the ambient sound level, is computed. Ref. 3-2 indicates that this condition is at the threshold of detection if the ambient sound level is defined as the one-third-octave value at 1000 Hz, based on MOD-2 measurements.

Ref. 3-2 also indicates that the A scale weighing (dBA) definition of overall sound level is not suitable for predictability. Typical spectra of background noise from this reference are shown in Figure 3-21. The one-third-octave level at 1000 Hz is approximately 10 dB below the dBA level of these spectra, and it is possible that this difference may be useful in interpreting ambient dBA measurements.

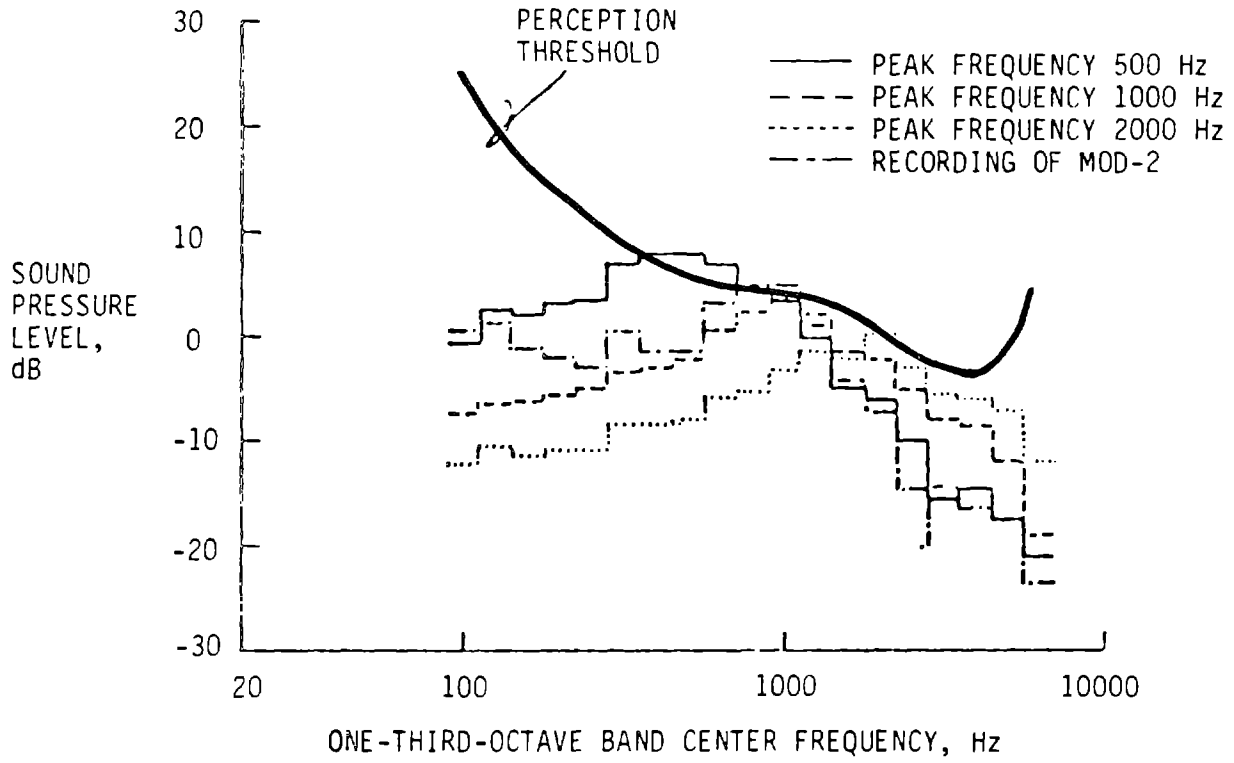

Figure 3-21 Perception Threshold Data

The perception versus distance results were calculated according to the following rules:

1. Assume broadband sound is characteristic of MOD-5A and disregard low frequency or tonal sound. Some measurements of sound from the MOD-0 wind turbine, which had ailerons, included a low frequency, cavity resonance sound, but this sound is believed to originate from the peculiar geometry of the test article, not the ailerons.
2. Compute a sound level typical of one rotor diameter from the wind turbine using the first term of equation 3-2.
3. Determine the reference sound level versus distance profile using the second term of equation 3-2.
4. Determine a turbulence-probability band of ±6 dB around the profile of item 3.
5. For a typical ambient sound level at zero wind speed, compute a wind speed profile using 6.2 dB per 10 mph slope.
6. Establish a turbulence/probability band of ±6 dB around the profile of item 5.
7. Determine the distance of threshold of perception for a particular wind speed.
8. Determine complaint probability for always audible and never audible distances for the wind speed of interest.
9. Repeat the sequence for other wind speeds.

3.3.1.4 Example

Refer to Figure 3-22, which is typical of the MOD-5A. The right curve set is basic and contains ±6 dB characteristics of predicted wind turbine sound versus distance. The left curve set is basic and contains ±6 dB characteristics of A scale background sound versus wind speed. A 40 dB level at zero wind curve was used because it is typical of a low background sound site.

To determine reference perception distance for a particular wind speed at the observer,

a) determine the ambient dB level at selected wind speed (Point A at 20 mph)

b) determine the distance at the ambient dB level of Point A (Point B at 22*400 ft. = 8,800 ft.).

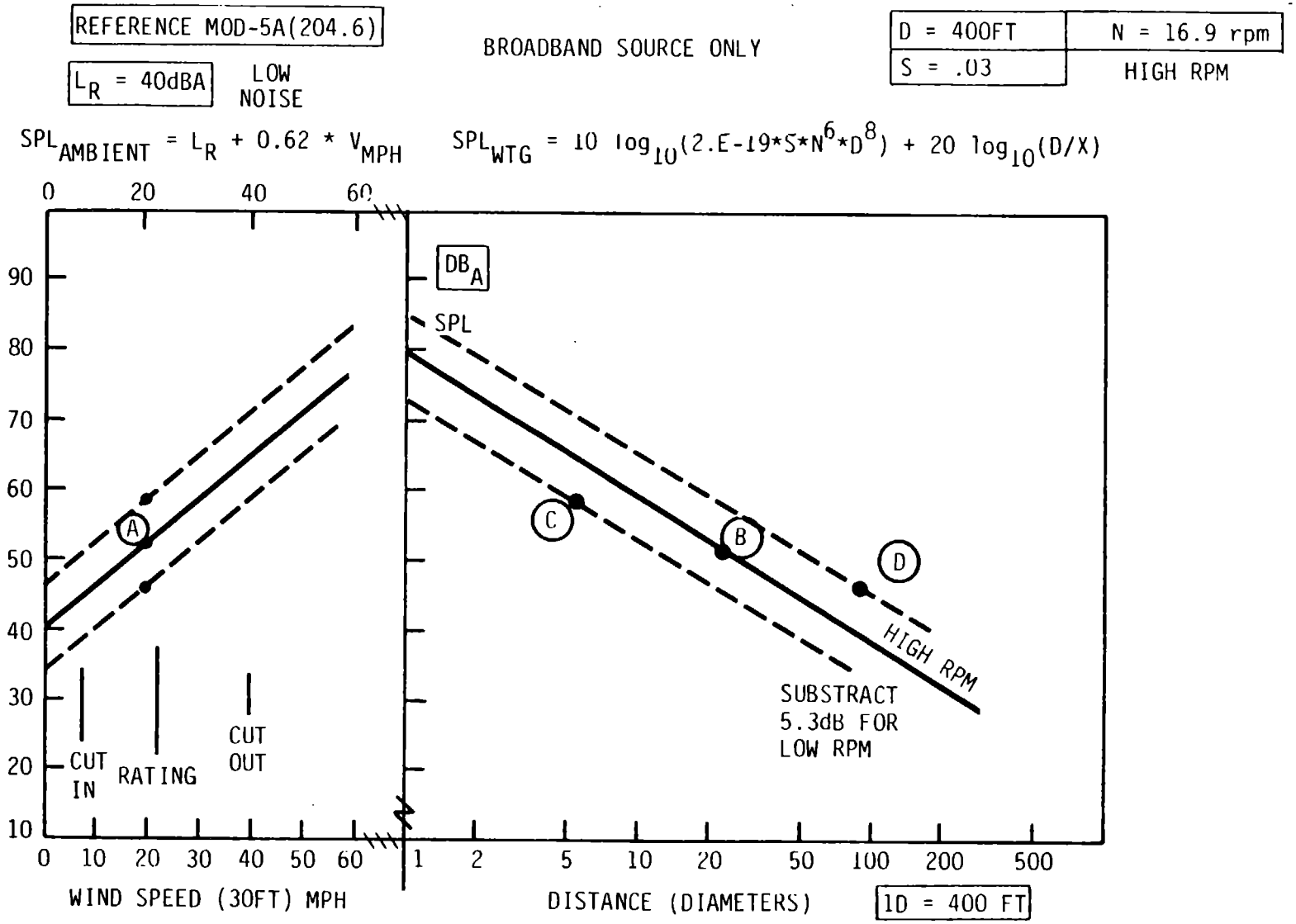

Figure 3-22 MOD-5A Sound Prediction Graph

Otner points labeled "C" and "D" represent distances where either high ambient and low wind turbine sound are always audible or low ambient and high wind turbine sound are never audible.

The wind speed-background may be adjusted for zero wind ambients at the observer of 30 dBA (quiet), 40 dBA (low), 50 dBA (moderate) and 60 dBA (noisy). Operation at a lower speed range is used to enhance energy capture when winds are below about 22 mph. This condition is represented by deducting 5.3 dB from the values on the right curve set.

The results of sound prediction studies are summarized as:

1. MOD-5A is characterized by broadband sound. Tonal sound levels are calculable as shown in Figure 3-20, but are neglected.

2. Approximate downwind distances to the threshold of perception for MOD-5A in a low noise ambient (40 dBA) vary from 30 to 50 diameters at the cut-in wind speed to 10 to 20 diameters at the rated wind speed.

3. Site ambient sound level measurements should be made at existing residences, particularly downwind, in the prevailing wind direction up to 50 diameters (3.8 miles) away. The ambient versus wind speed model should be adjusted to conform to the site.

4. The probability of complaints of sound from MOD-5A is negligible.

3.3.2 TELEVISION INTERFERENCE

Wind turbine generators can cause interference with television reception, resulting in video distortion. The blades are usually the main cause of television interference. They tend to reflect or scatter the TV signal, creating a secondary signal that combines with the primary signal to produce the interference. Regions where the interference is considered objectionable are defined as interference zones. An interference zone is shown in Figure 3-23 and incorporates the assumption that the turbine is oriented so as to direct the maximum scattered signal toward the receiver. The portion of the zone that is produced by specular reflection from the blades is called the backward interference region, and is shaped like a cardioid, centered at the turbine with its maximum radius, R1, pointing toward the transmitter. Forward scattering, in which the signals are blocked by the blades, results in a relatively narrow lobe of interference with its maximum radius, R2, directed away from the transmitter. In areas where TV reception is good, the maximum radius of the backward interference region will exceed that of the forward region. In areas where the signal is weak, the maximum radius of the forward interference region will be dominant and will determine the greatest interference distance.

Whether the interference is significant enough to be objectionable depends on the interaction of several factors, including the:

1. Height of the Tower - Laboratory and full scale tests for MOD-0, MOD-1, and MOD-2 indicate that blade scattering is mostly in the backward and forward direction, and is usually greatest when the blade is horizontal, at a height equal to that of the tower above the surrounding ground.

2. Length, area, and composition of the blades - Television interference increases with blade size. Metallic blades create more interference than non-metallic blades; however, non-metallic blades require metallic lightning conductors and piping, which generally contribute to interference.

3. Distance between the turbine and TV receivers - Television interference decreases with increasing distance between the turbine and the receiver.

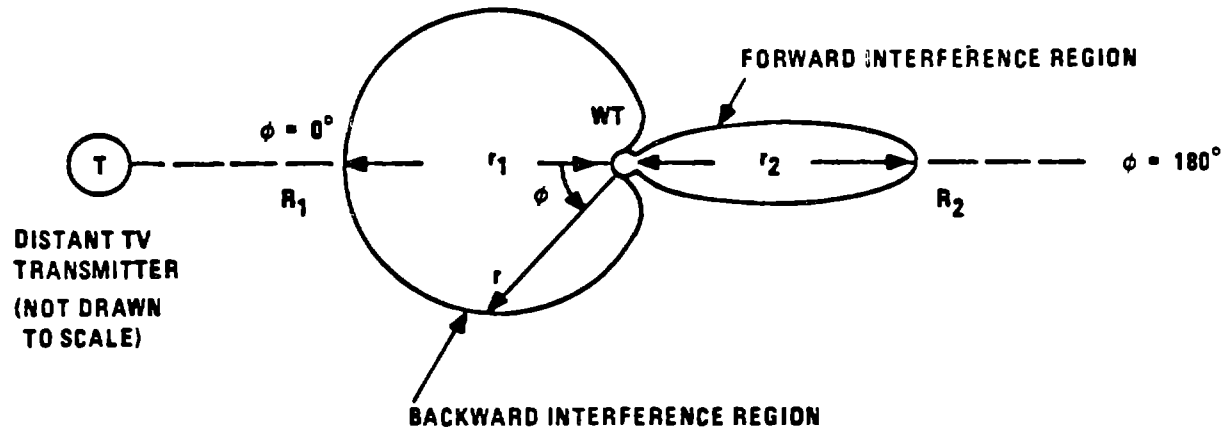

Figure 3-23 Television Interference Zone of a Wind Turbine

4. Distance between the turbine and transmitter - When the turbine is located above the radio horizon of the transmitter, the largest radius of interference is usually associated with the backward interference region; when the wind turbine is located beyond the radio horizon, in fringe reception areas, the largest radius of interference is usually associated with the forward interference region.

5. Frequency of TV signal - Television interference increases with the frequency of the TV signal, and therefore, is worse at the upper end of the UHF band.

6. Tilt of blades - Tilting the plane of blade rotation should reduce interference in the backward interference region. The reflected TV signal will either be directed up and away from TV receivers, or will be directed down so that the interference zone is shortened, depending on the orientation of the wind turbine with respect to the transmitter. The effect of blade tilt on interference in the forward region does not appear to be significant. Navigation aid interference was not evaluated, but should be considered at each site.

3.3.2.1 Analysis

The analysis was based on the technique developed from laboratory and field testing of the MOD-0, MOD-1, and MOD-2 wind turbines. The technique uses a graphical method to determine the maximum interference distances for the backward and forward regions, and incorporates the following assumptions:

1. The earth is smooth and spherical with no terrain effects.

2. The transmitting and receiving antennae are omnidirectional.

3. The blades rotate in a vertical plane.

For the evaluation of television interference from the MOD-5A, the results obtained for the MOD-0, MOD-1, and MOD-2 were extrapolated to account for the MOD-5A's greater tower height. Blade and tower characteristics of MOD-0, -1, and -5A are compared in Table 3-9 to show the increase in size of the MOD-5A over previous wind turbines.

Two different blade conditions were evaluated:

1. The effect of the lightning protection on television interference is insignificant and the reflected signal is that of wood blades. For this condition the field strength values of the reflected signal from

Table 3-9. Wind Turbine Blade and Tower Characteristics

MOD	BLADE					TOWER HEIGHT
	Length*	Planform Area	Scattering Efficiency	Scattering Area	Material	
	ft	ft^2	%	ft^2		ft
0	62.5	194	67	39	metal	100
1	100	678	63	430	metal	135
2	150	2153	70	1507	metal	200
5A	200	2443	30	733	wood	250
	200	2443	70	1710	metal	250

*Blade Length = .5 Rotor Diameter

the MOD-5A blade to the receiver were estimated by interpolating the corresponding values for MOD-0, -1, and -2 as a function of effective scattering area. A value of 30% was used for scattering efficiency, which is representative of non-metallic blades.

2. The lightning protection dominated the reflection characteristics and produced television interference approaching that of a metallic blade. For this condition the field strength values of the reflected signal from MOD-5A blades to the receiver were also estimated by extrapolating the corresponding values for MOD-0, MOD-1, and MOD-2 as a function of blade scattering area. A value of 70% was used for scattering efficiency and is representative of metallic blades.

An estimate of television interference distance, based on non-metallic distances plus 25% of the difference between non-metallic and metallic, is shown in Figure 3-24.

After the preceding analysis, the MOD-5A blade planform was increased slightly and the aerodynamic control was changed to ailerons. Metallic aileron construction was used as the baseline configuration. Both of these changes will increase the interference distance by an unknown amount. The analysis was not repeated with new parameters. Tilt, which was not included in the analysis, is expected to partly offset the affect of the changes.

The following summarizes the study of television interference:

1. The interference zone extends from less than 2 mi at the lower (50 MHz) end of the VHF range to over 125 mi at the upper (900 MHz) end of the UHF range.

2. At low frequency the interference distance is dictated by the backward reflection; whereas, at high frequency the forward scattering interference distance is greater and dominates in areas where TV reception is weak.

3. Metal blades or blades with lightning conductors tend to result in larger interference distances than non-metallic blades. At low signal frequency the difference in interference distance between metal and wood blades is less than 0.6 mi. At high frequency the difference can be as great as 13 mi. in areas where TV reception is good. In areas where TV reception is weak, the interference distances of the wood blade approaches that of the metal blade.

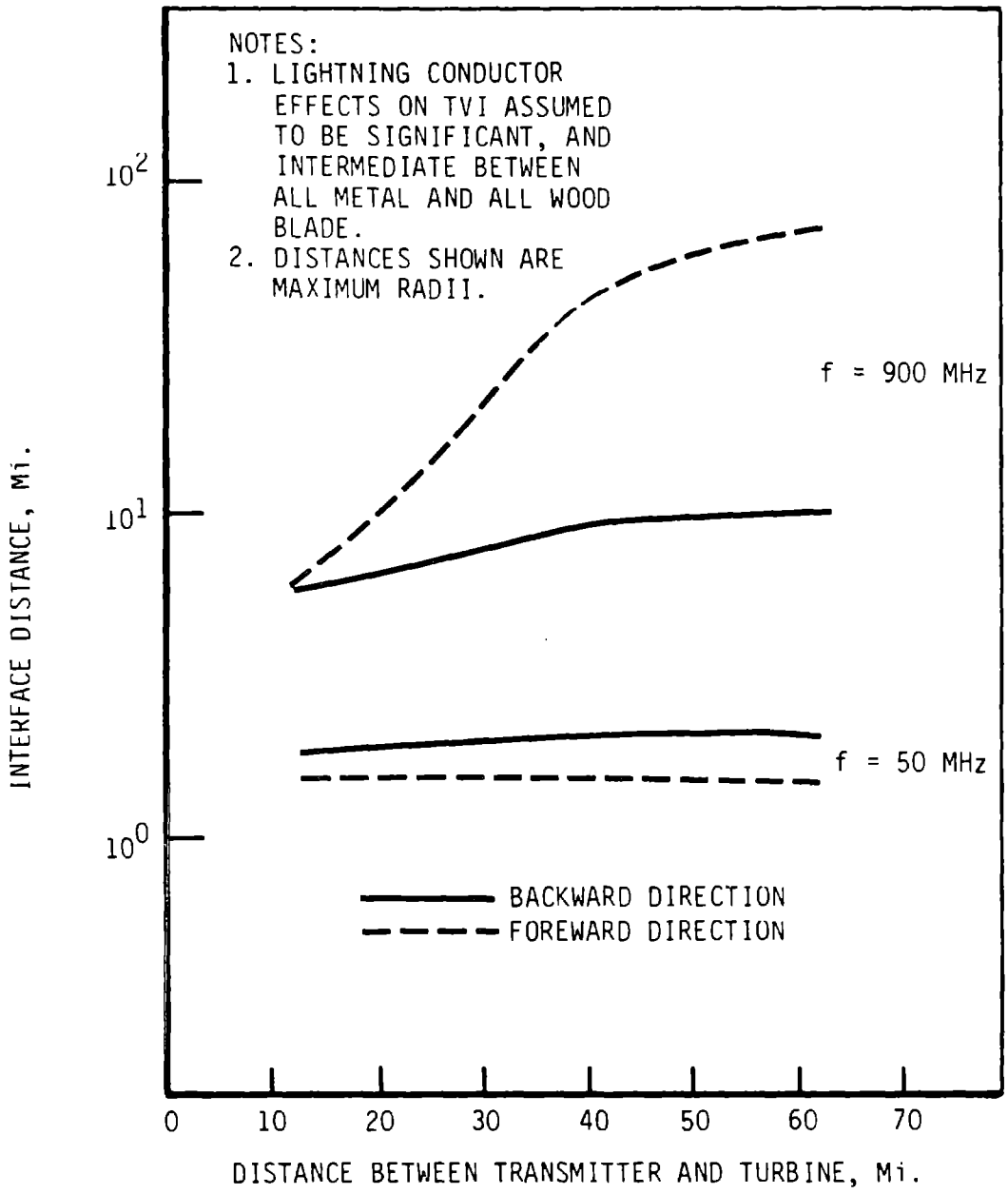

Figure 3-24 Television Interference Distances for MOD-5A

REFERENCES

3-1. H. H. Hubbard, K. P. Shepherd, F. W. Grosveld, "Sound Measurements of the MOD-2 Wind Turbine Generator", NASA Contractor Report 165752, Langley Research Center, July 1981.

3-2. K. P. Shepherd, D. G. Stevens, F. W. Grosveld, "Development of Wind Turbine Noise Criteria", Fifth Biennial Wind Energy Conference and Workshop, Proceedings Volume III, page 163, SERI/CP-635-1340, October 1981.

4.0 ROTOR SUBSYSTEM

4.0 ROTOR SUBSYSTEM

4.1 BACKGROUND AND HISTORY

Conceptual Design Phase - The first rotor studies determined the rotor diameter, blade material and shape, and the method of torque control. Because the rotor diameter, blade material, and blade shape were closely related, they were determined in parallel during the conceptual design phase. Each of these issues was related to other system parameters. The blade material was closely associated with the system cost but had to be treated independently of the rotor size, since the diameter was not known at that time. A parametric approach to the blade design process was used in order evaluate both size and material aspects of cost and strength.

Three blade materials were evaluated: epoxy and polyester bonded transverse filament tape (TFT) glass fiber, welded steel, and epoxy bonded laminated wood. All of these options used a steel hub at the center of the blade.

Each of these materials had been used in wind turbine applications. TFT glass fiber was used in a 150-ft., single blade, made by Kaman/SCI, which was statically tested. NASA-LeRC selected TFT glass fiber for a study of low-cost blade materials, which progressed to the fabrication of a blade set that was operated on NASA's MOD-0A machine. Welded steel was used by GE for the MOD-1 blades, and by Boeing for the MOD-2 blades. Laminated Douglas fir bonded with epoxy was another low-cost blade material selected by NASA LeRC for use on the MOD-0 blade. A set of wood and epoxy blades was in use on the MOD-0A machines.

The rotor was too large to ship in one piece. Field joints would, therefore, be necessary to construct the blade at the site. The parametric material study examined the influence of the joints on the structural integrity, the weight and the cost of the blade.

The shape of the blade, planform and airfoil, could not be determined at that point in the design process although these parameters and the blade material modulus were important in defining the natural frequency of the blade. Because of the limits on time for conceptual design, the blade trade-off studies did not relate stiffness to the possible rotational speed ranges defined by the variation in rotor diameter. The initial evaluations indicated

that all of the materials under consideration could be configured to meet the required range of blade frequencies.

Two methods of controlling rotor torque were studied: a fully rotatable tip (partial span control), and a hinged trailing edge control surface (ailerons on the outer span of the blade).

The torque control and blade material trade-off studies and the results are summarized in Section 4.0 of Volume II. The conceptual design studies indicated that a wood-epoxy blade and the partial span control subsystem (PSC) were the most cost effective configuration for the MOD-5A wind turbine generator.

Preliminary Design Phase -- During the preliminary design phase it became apparent that the decision to use wood laminae was appropriate, but the attachment of the main blade to the partial span control subsystem and to the steel hub were growing concerns.

The partial span control development resulted in an unanticipated increase in weight. The shaft and bearing designs were larger than expected, to meet the limit and fatigue load requirements. The ratio of the blade thickness-to-chord was increased to accommodate the larger shaft and bearing. As a result the weight of the partial span control structure increased. The increased mass, located at 75% of the span, reduced the natural frequency of the blade to an unacceptable value.

At the same time, the understanding of the 30-year design properties of wood laminae was changing. As the volume of stressed material increased, the permitted stress level had to be lowered. This discovery caused concern, so the materials development program examined the size effect.

The blade was redesigned to accommodate the increase in weight, decrease in natural frequency and the reduction in allowable stress. The blade chord was increased, but the ratio of the blade thickness-to-chord stayed the same in order to maintain performance. This change increased the natural frequency of the blade and reduced the stress level, so that both parameters were again acceptable.

The weight of the partial span control assembly increased again when the fatigue loads were redefined. The assembly weight increased from 20,000 lbs. to nearly 40,000 lbs. per blade or 80,000 lbs. for the rotor. These weights and their associated costs indicated that the question of partial span control vs aileron control should be reopened.

The partial span control exerted large reversing flap bending loads on the blade because of the negative lift coefficients that developed when the tip moved through large angles during shutdown. With an aileron, control surface deflection reduced the blade's lift coefficients and increased its drag coefficients. The loads associated with the aileron drag coefficients were applied principally in the plane of rotation, so they did not contribute much to the flap bending loads.

The results of the second torque control study showed that ailerons were the preferred design. The discontinuity in the primary structure, required by the partial span control shaft, was no longer necessary. Eliminating the discontinuity also eliminated a source of weight and a potential single failure point. Hydraulic, direct action aileron actuators were selected, based on schedule and cost requirements . The effect of the aileron installation on the main blade was examined. An acceptable configuration, well integrated with the blade subcontractor's design, was completed. Aileron control became the baseline configuration for torque control.

NASA Lewis and Wichita State University previously worked on the use of ailerons for wind turbine torque control. This data was not directly applicable to a system size of the MOD-5A, so more data was required. A program for wind tunnel testing of the MOD-5A aileron was designed, approved, and implemented. It provided a data base for designing various aileron configurations. The resulting aileron design was implemented on the MOD-0 wind turbine at Plumbrook, Ohio. Testing began in December, 1983. The results, to date, confirmed the performance predictions and indicated that the ailerons would be acceptable for rotor control. Wind tunnel and MOD-0 tests indicated that the ailerons could achieve acceptable reduction in rotor speed but might not be able to stop the blade completely. A low speed shaft brake was then designed for application at low rotor speeds. Disc caliper brake sets, similar to those used on the yaw system, were mounted on the forward

face of the nacelle support structure. They apply braking force to a yoke-mounted brake disc, separating the resulting brake load path from the low speed torque shaft.

A continuous, wood rotor design was developed to replace the steel hub and bolted-on blade concept defined earlier in the conceptual design phase. This change was the second major change in the preliminary design phase and was dictated by the structural and stiffness discontinuities created by the steel hub, which had posed serious design and fabrication problems. The design needed to match incremental chordwise spring rates between the wood blade and steel hub, to avoid major stress increases in both the hub and the blade. Complex analysis and development testing was required to validate the design. High manufacturing costs were created by the need to install, with very close tolerances, hundreds of steel studs to a planar steel interface.

The baseline steel hub rotor configuration contained eight chordwise joints. The continuous wood rotor required only six joints to fully satisfy fabrication, shipping and assembly requirements, reducing complexity and cost. The interface of the rotor and the nacelle was also changed from a hub-to-low-speed-shaft arrangement to a continuous, blade-to-yoke configuration. The yoke is a Y-shaped, box structure mounted with teeter bearings to the blade. Bolsters, or doublers, were provided on the blade faces, to distribute loads from the blade to the teeter bearings. The bolsters were augmented with glass fiber cloth, as required by the high load levels. Augmenting the bolster made extensive augmentation of the center blade unnecessary. This arrangement was advantageous, since the bolster is smaller and simpler than the center blade.

Final Design Phase -- Sections 4.3 through 4.6 describe the final rotor design for model 304.2., which is summarized below:

Blade	- 5 section laminated wood and epoxy with bolsters at the center
Torque Control	- hydraulically-actuated, three-section ailerons on each blade
Blade Support	- steel weldment yoke interfacing the blade bolsters through elastomeric teeter bearings

The following sections describe the trade-off studies in greater detail. Subsequent sections define and substantiate the final design for the blade, ailerons, and yoke.

4.1.1 MATERIAL SELECTION AND SUBSTANTIATION

4.1.1.1 General

An extensive trade-off study evaluated blades made of TFT reinforced glass fiber, steel, and wood lamina and epoxy, based on the cost of the 100th unit. The affect of the blade material on the cost of energy is described in section 4.1.1.2. The results of the study indicated that the wood lamina and epoxy was the most effective material for a rotor with a large diameter, TFT glass fiber was a close second, and steel was a distant third. Other composite materials, such as filament-wound glass fiber, were not evaluated because of the limits on resources and previous experience with cost, weight and performance.

4.1.1.2 Blade Material Selection

One of the major trade-off studies conducted during the conceptual design phase selected the most appropriate material for the blade. The minimum cost of energy at the 100th unit was the main system requirement for the blade material. Experienced fabricators provided credible cost information for the system design. The study also evaluated the affect of rotor diameter, rotor speed, solidity, airfoil shape, taper ratio, and joints on the cost of manufacturing blades of the three candidate materials.

Figure 4-1 is a flow plan of the major features of the blade material trade-off studies. GE performed these studies with three subcontractors: Chicago Bridge & Iron for steel; Structural Composites, Inc. for TFT glass fiber and Gougeon Brothers, Inc. for wood. The table and figure annotations, shown in Figure 4-1, summarize the results of various phases in the study. Material properties, listed in Table 4-2, were derived from existing data. A test plan was developed to augment and expand the data base (section 4.1.1.3).

Initial cost information from the subcontractors, in dollars per pound, based on their experience and judgment, was organized, as shown in Figures 4-4 and 4-5. The information was input to the SECTION program to begin the cost and system sizing calculations. This study is discussed in more detail in section

4.3.1. During this time, the subcontractors were given the loads for typical blade sections, listed in Table 4-3, and asked to develop a design and determine costs for these blade cross sections. The results are listed in Table 4-5. GE defined the blade joint interface constraints, so that the subcontractors could produce a design and costs for joining techniques that were compatible with their materials. These results are listed in Table 4-4.

The refined cost estimates became the basis for a second calculation, using the SECTION program, of the size, cost and contribution to cost of energy of the blade. The results of this calculation, shown in Figure 4-2, were plotted for the three materials.

The conceptual designs for the blade were supplied to the subcontractors. They determined blade and joint weights, and costs based on their methods of construction. These blade weights and costs, listed in Table 4-1, correlated with the results of the parametric study, shown in Figure 4-2. The results indicated that wood was the most cost effective blade material.

The blade material selection was then evaluated at the system level, Table 4-6. A wind turbine with wood and epoxy blades weighed 146,000 lbs. less than one with glass fiber blades. The costs of energy were similar, but experience indicated that the risks associated with a wood blade were less than those associated with a glass fiber blade. Wood and epoxy was selected as the blade material.

The following sections discuss the material selection process further.

Initial Cost Inputs - The "best estimate" costs defined by the subcontractors were used in early system cost evaluations, and the SECTION program was used to study the system. These costs were refined in support of the parametric costing and then, for the final cost.

Material Allowables - The definition of stress allowables was a greater effort for wood and TFT glass fiber than for steel. A test program was necessary to obtain data to be used in the definition of the allowables for TFT glass fiber and wood. SCI used polyester resin instead of epoxy, to reduce costs and this

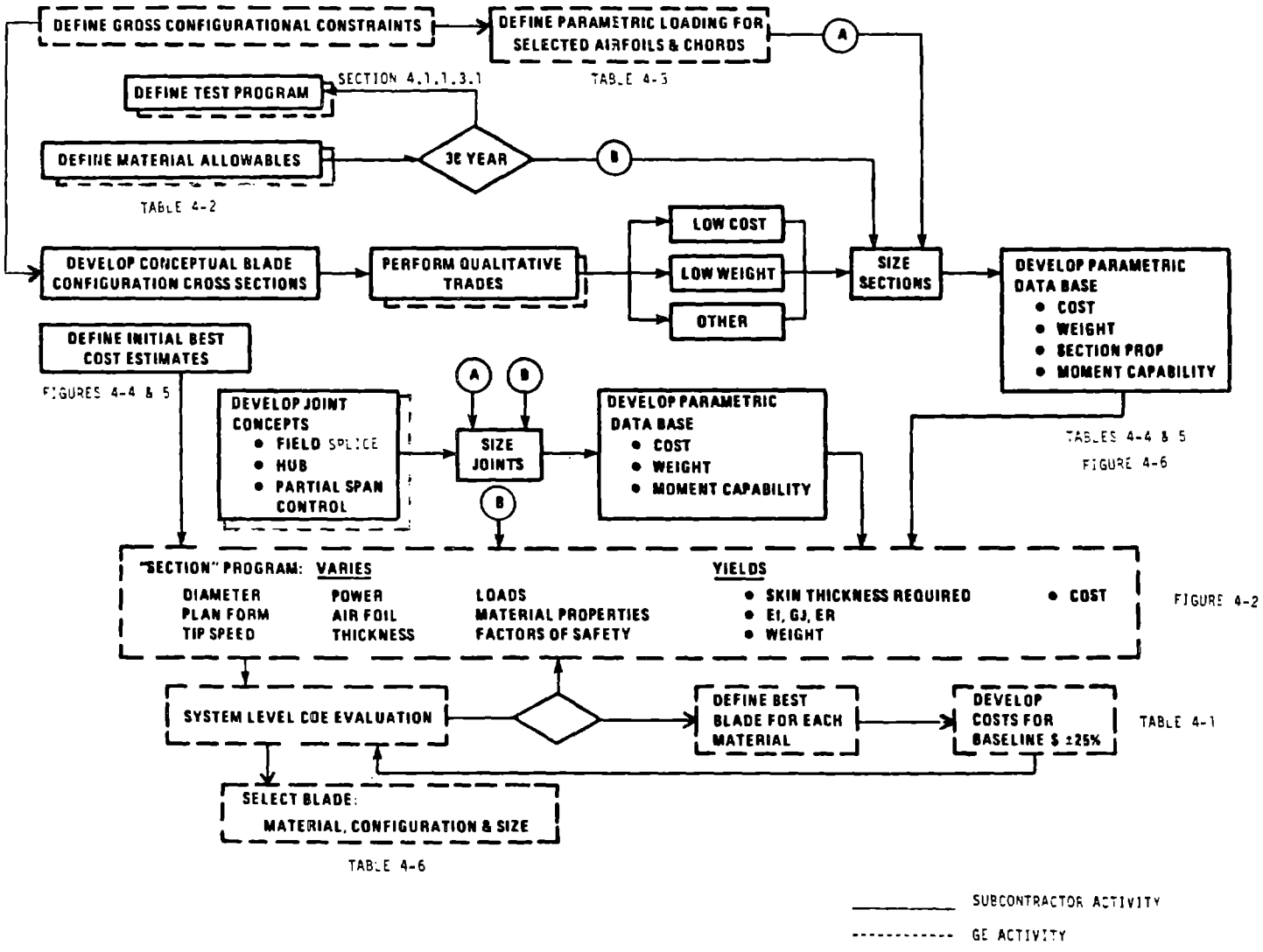

Figure 4-1 Blade Material Trade Study - Flow Diagram

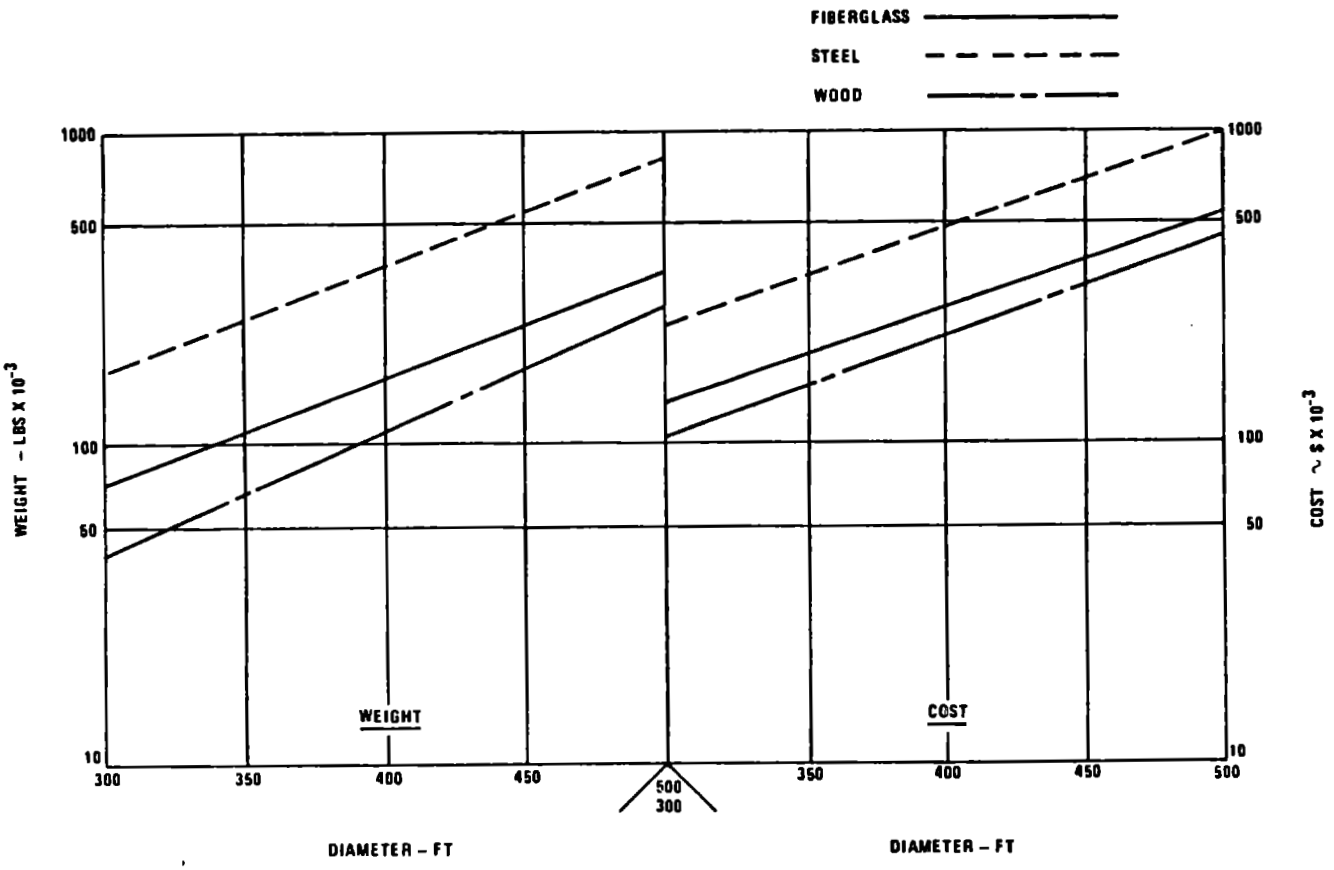

Figure 4-2 Blade Cost and Weight - Parametric Summary

Table 4-1 Conceptual Design - 100th Unit Cost and Weight

Diameter - Ft.	300	350	400	500
Field Joint Req'd.	No	No	Yes	Yes
Cost - K$				
Fiberglass	135.2	159.4	299.1	636.1
Wood	89.7	138.8	183.7	360.2
Steel	170.6	247.1	363.0	689.6
Weight - K-Lbs.				
Fiberglass	98.9	125.0	244.3	716.9
Wood	51.3	75.6	139.5	318.8
Steel	165.0	261.0	395.0	800.0

- Std. labor rates
  - S. E. U. S.
- Construct OH
  - Direct lab. support
  - Mat'l. burden
  - Dir. lab. OH
- Construct G&A
- Depreciation
  Plant - S. L. @ 30 yrs.
  Equip. - S. L. @ 20 yrs.
- Cost of money
  Assume 25% front
  Fin 75% @ 12%
  - Plant - 30
  - Equip - 20
- Profit 6% aft. tax
  - Assume 45% state & fed. tax

Notes: 1. Normalized 100th unit costs based on subcontractor's quotes
2. One rotor set: two blades and joints.

substitution required expediting testing glass fiber and polyester specimens. The steel allowables were based on MOD-1 and MOD-2 inputs, since the characteristics for steel are well known.

The resulting material properties are shown in Table 4-2. The subcontractors began to develop the blade and define any limitations on the section and materials. The initial configurations are shown in Figure 4-3. The incremental studies indicated modifications, which were made to improve the cost and weight efficiency of the sections.

C-2

Table 4-2 Material Allowables for Design Trades

Matl. ID No.	Description	Density Lb/in^3	E PSI X 10^{-6}	E Buckling PSI X 10^{-6}	G PSI X 10^{-6}	Allowables -PSI X 10^{-3}		
						Yield	Fatigue R=-1	Fatigue R=+1
1.	FRP 73-16-11 Polyester resin	0.07	3.69	2.64	0.61	30	5.93	30
2.	FRP 73-16-11 Epoxy resin	0.07	3.69	2.64	0.61	30	5.93	30
3.	STL A131A + PWHT	0.29	29	29	11	30.6 (1)	9.2	42.0 (3)
4.	WTL A633A + PWHT	0.29	29	29	11	37.8 (1)	9.2 (2)	42.0 (3)
5.	Douglas fir laminate and epoxy resin 12% moisture cont. (Gulf coast env.)	0.023	2.0	0.5	0.15	5.5	2.75	5.5
6.	Douglas Fir Laminate and epoxy resin 5% moisture cont. (nominal env.)	0.023	2.0	0.5	0.15	7.0	3.5	7.0
7.	FRP 73-16-11 Polyester resin (with adequate process cont. and material develop.)	0.07	3.69	2.64	0.01	55.0	11.0	55.0

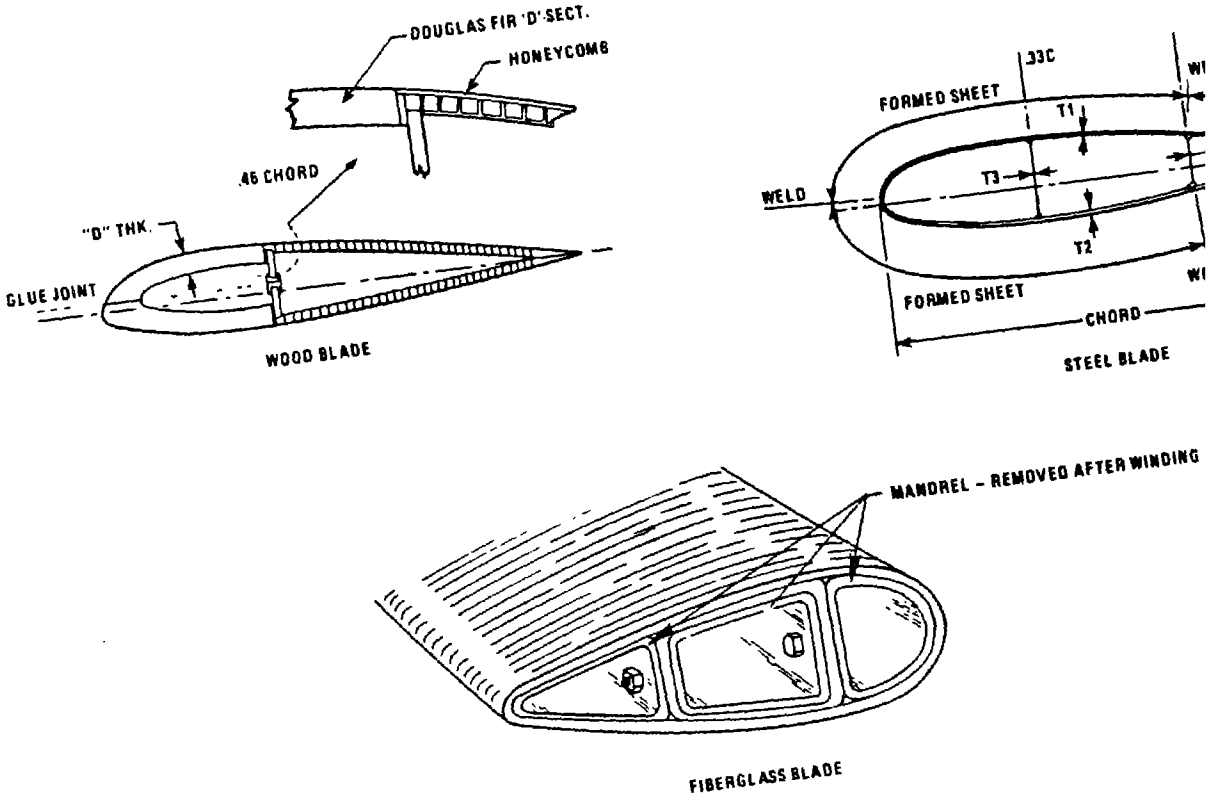

Figure 4-3 Typical Blade Cross-Sections

GE worked closely with each of the subcontractors, to make sure that each material would be used in the most advantageous design configuration. For example, on the laminated wood and epoxy blade, the wood skin depth was limited to approximately 15% of the maximum section depth. This depth appeared to be the point of diminishing return for the flap section modulus with respect to the weight of the added material. It was accepted as a design limit. The higher strength of both glass fiber and steel precluded similar limits for these materials and stiffnesses.

An early attempt to develop cost versus load capability based on the subcontractor's best estimate of cost is shown in Figures 4-4 and 4-5. Limit and fatigue flap bending moments are related to a bending element of the blade cross section, of a thickness "t", located at a flange distance of "h". The resulting cost, in dollars per inch of span per inch of chord, indicated that wood and epoxy was the best choice, but a greater flange distance "h" was required to achieve limit load ranges comparable to those of glass fiber and steel. This fact indicated that wood would impose a performance penalty because of its greater thickness in the same airfoil series. This penalty motivated the search for an airfoil family that would allow an increase in the structural thickness of the wood and epoxy blade without reducing its performance.

The subcontractors explored the blade configurations on the basis of minimum cost and minimum weight. The objective was to determine if a less costly blade could be defined and, if so, to evaluate the relative affects of cost and weight on the cost of energy. In summary, there was not much difference in the cost of the minimum weight and the minimum cost blades. For the wood blade, there is no difference, because each lamina must be placed in its optimum location. Hence, for wood, the minimum cost configuration is also the minimum weight configuration. The cost estimates for the glass fiber blade used both polyester and epoxy resins to define a cost difference with no weight difference. The glass fiber blade was also examined in a two-cell configuration similar to that used in the MOD-0A low cost blade program. The two-cell configuration was slightly heavier and more costly than the three cell baseline shown in Figure 4-3, so it was dropped from consideration.

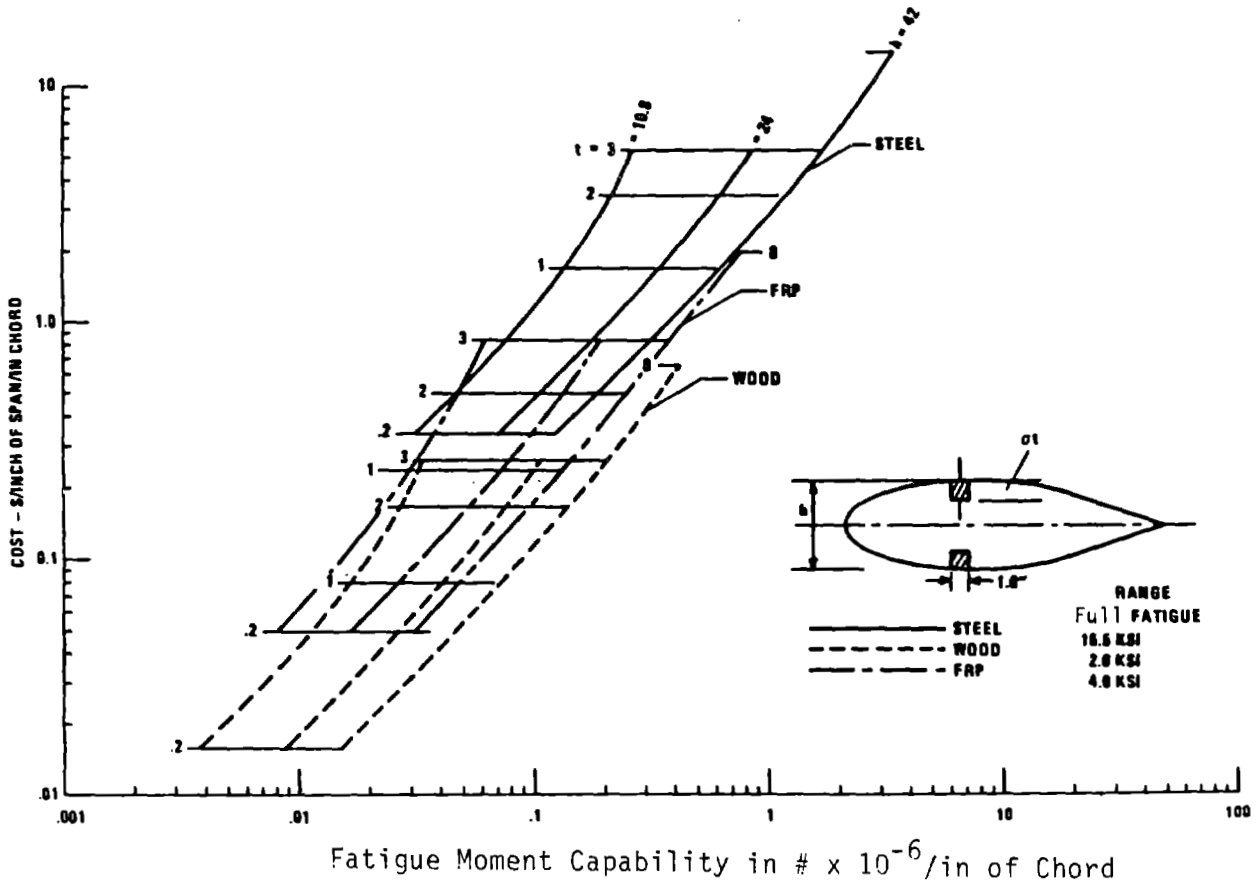

Figure 4-4 Flap Fatigue Moment Capability vs Cost

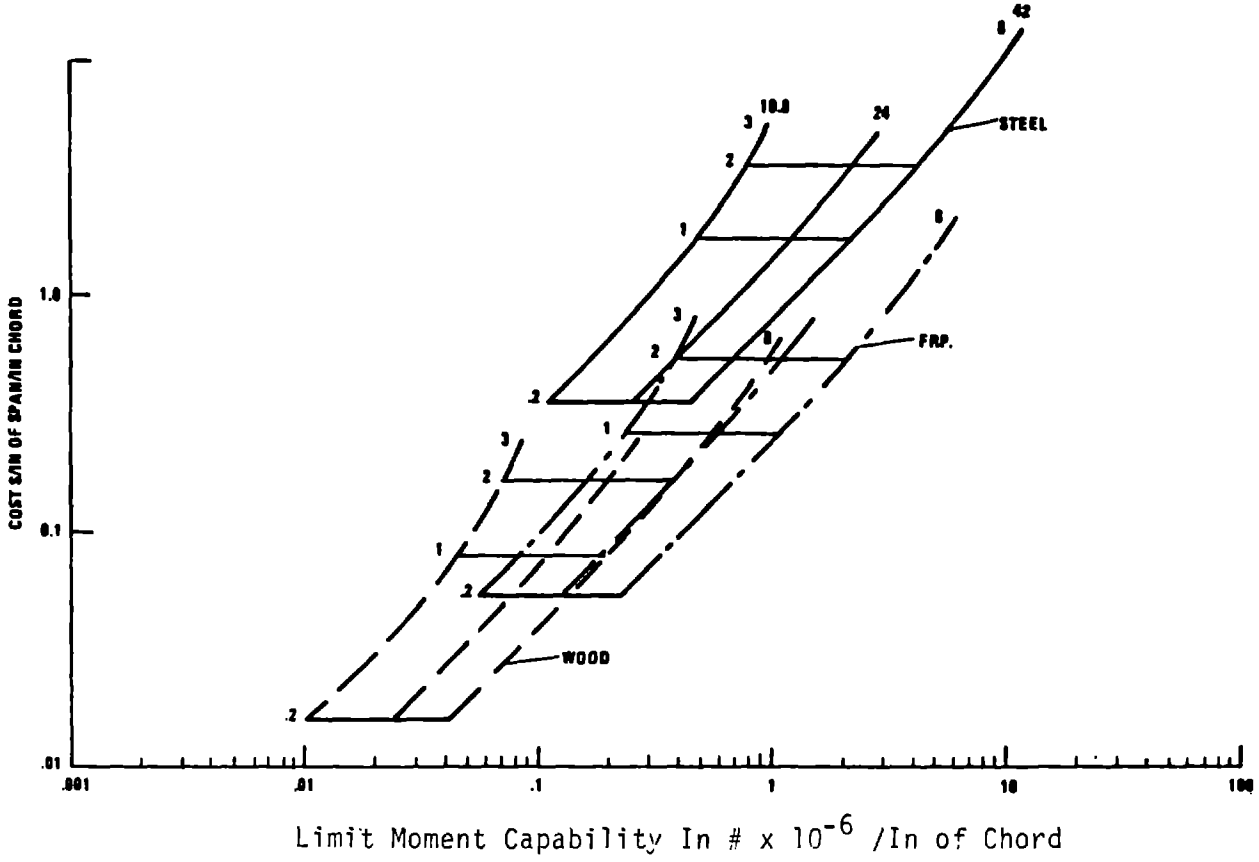

Figure 4-5 Flap - Limit Moment Capability vs. Cost

During the conceptual design phase the blade was defined as terminating at a steel hub assembly. Each blade subcontractor defined the cost and weight for a root joint that was a 23030 series airfoil with a 14-ft. chord. The loads on the joint are shown in Table 4-3.

Table 4-3 Design Loads for the Blade Subcontractors for the MOD-5A Blade Parametric Studies

Condition	Type Loading	14' Chord		10' Chord		6' Chord	
		M_{Flap}	M_{Chord}	M_{Flap}	M_{Chord}	M_{Flap}	M_{Chord}
Maximum Moment	Peak	440.	230.	75.	24.	10.	2.6
	ALT (±)	110.	200.	19.	20.	2.5	1.9
Minimum Moment	Peak	36.	12.	10.	1.3	1.0	0.14
	ALT (±)	9.	10.	2.5	1.0	0.25	0.10

Note: All moments expressed in units of inch - pounds x 10^{-6}

The costs and size of the field joint that allows the blade to be assembled in the field were also evaluated. The chord of the field joint was 10 ft., and the airfoil was a 23020 series. The root and partial span control joint interfaced with a steel assembly, whose configuration could be made compatible with the blade according to the subcontractor's recommendation. The field joint would allow each of the subcontractors to join their material to itself in the best way possible in the field.

The resulting costs and weight of the joints for each of the base blade materials were summarized so that the parametric variations could be incorporated into the SECTION program. This summary is shown in Table 4-4.

Table 4-4 Joint Cost Summary - Parametric Data Base

Section	Table 4-3 Load	Fiberglass		Wood		Steel	
		Cost K$	Wt - K#	Cost K$	Wt - K#	Cost K$	Wt - K#
14.0' Chord "Root Joint"	Max.	55.8	12.5	15.5	2.32	16.2	.145
	Min.	8.1	1.2	6.2	.86	10.3	-0-
10.0' Chord "Field Joint"	Max.	2.8	0.24	2.3	.27	13.5	.135
	Min.	2.7	0.8	2.2	.23	10.3	-0-
6.0' Chord "Tip Joint"	Max.	0.2	.1	3.1	.35	Built-In	Built-In
	Min.	0.18	.1	1.6	.24	Built-In	Built-In

The results of the blade section evaluations were summarized in a similar manner, as shown in Table 4-5. This summary reflects the inputs received from tne three subcontractors in November and December, 1980. The cost per pound of the labor-intense wood and steel constructions are greater at the small chord sections and smaller at the large chord sections, for which much larger quantities of material are used with a modest increase in labor. Glass fiber reflects material costs more directly and shows higher unit costs where most of the material is, at the larger chord sections and in the presence of higher loads.

A summary of the blade and joint cost data for this study is shown in Figure 4-6. The data clearly notes the result when the skin depth of wood was limited to 15% of the maximum section depth. The data shows that the more dense material, with higher material allowables, can span the design load ranges defined for various chords. The data also indicates that glass fiber is the most cost effective material for the given geometry, wood is a close second, and steel is a distant third.

The subcontractor's cost and weight data for the 6, 10 and 14 foot chordal section were organized as an input to the SECTION program. Current loads, blade geometries, tip speeds and load factors were also defined an input to the SECTION program. Many detailed blade skin and spar thickness variations for each of the three materials were evaluated for blade lengths between 300 and 500 ft. Joint costs and weights were factored into these results for each material and blade diameter.

The steel and glass fiber blade configurations had the same thickness-to-chord ratio (t/c). The t/c for the wood blade was increased to compensate for the lower packaging efficiency of the wood. This increase in t/c, which did not include drag and performance losses, was possible because a NACA 64XXX series airfoil was adopted in place of the NACA 23XXX series used in the steel and glass fiber Blades. The reduced drag coefficients of the 64XXX series allow the t/c to increase 30-50%, although the performance is the same as that of the 23XXX series.

Table 4-5 Summary of Parametric Costs and Weights for the 100th Unit Base

Configuration & Material	Chord Ft.	Load	Cost $/In Span	Cost $/#	Weight #/In Span
Fiberglass & Polyester 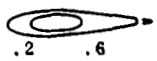 .2 .6 SCI	6	Min	3.40	1.21	2.80
		Max	10.30	1.17	8.80
	10	Min	11.40	1.17	9.70
		Max	31.70	1.23	25.70
	14	Min	19.00	1.16	16.30
		Max	89.00	1.19	6.60
Fiberglass & Epoxy  -2 -6 SCI	6	Min	3.90	1.39	2.80
		Max	12.20	1.38	8.80
	10	Min	13.50	1.39	9.70
		Max	37.60	1.46	25.70
	14	Min	23.40	1.43	16.30
		Max	97.30	1.49	66.00
A131A Steel & PWHT  .2 .67 CBI	6	Min	31.00	2.58	12.00
		Max	48.00	1.30	37.00
	10	Min	54.00	1.68	32.00
		Max	102.00	1.12	91.00
	14	Min	85.00	1.51	56.00
		Max	153.00	1.07	142.00
A633A Steel & & PWHT  .2 .67 CBI	6	Min	32.00	2.66	12.00
		Max	47.00	1.38	34.00
	10	Min	55.00	1.71	32.00
		Max	104.00	1.14	91.00
	14	Min	86.00	1.53	56.00
		Max	156.00	1.09	142.00
Douglas Fir & Epoxy  .4 .6 GB	6	Min	8.47	3.41	2.48
		Max	10.59	2.44	4.34
	10	Min	15.87	1.84	8.59
		Max	20.08	1.54	12.96
	14	Min	23.02	1.59	14.39
		Max	48.35	1.31	36.63

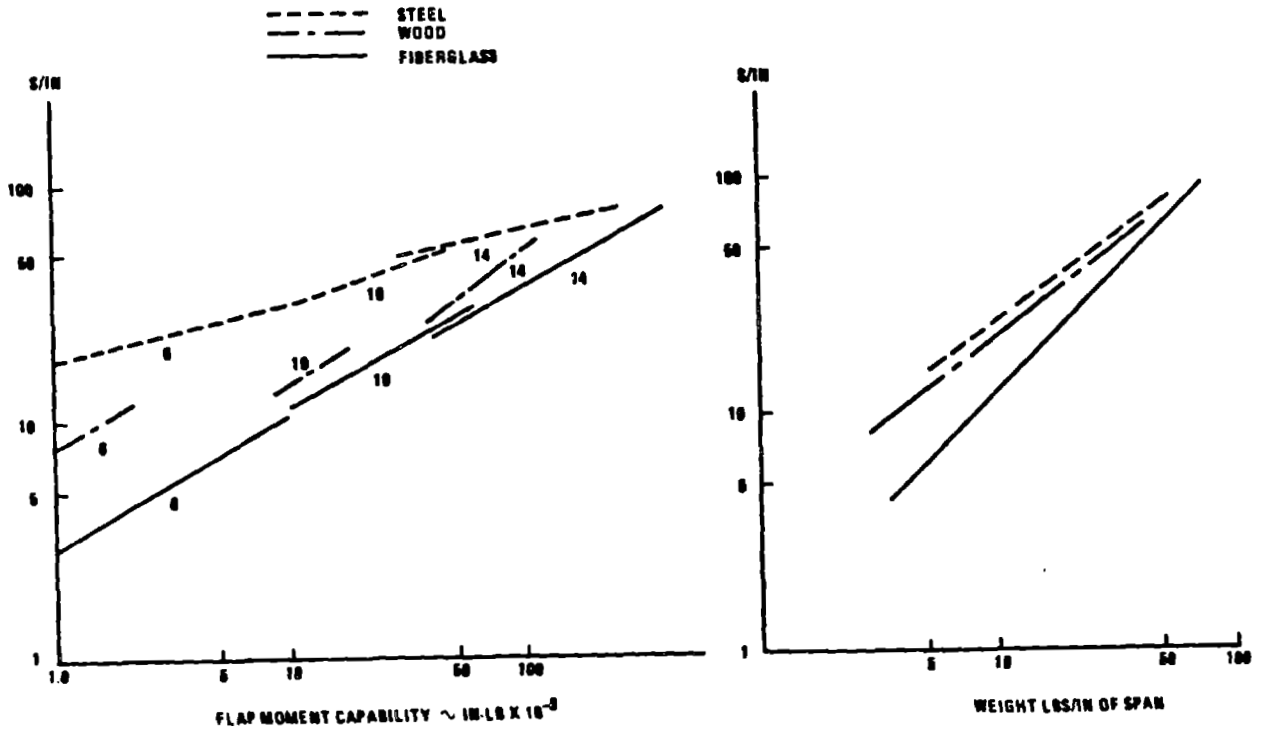

Figure 4-6 Cost and Weight vs. Flap Moment Capability Parametric Summary

The 64XXX series has concave airfoil sections, which can be fabricated without additional cost on the wood blade because the construction of the wood blade used female moulds. The concave surface would incur additional costs on the steel and glass fiber blades, so it was not used with these materials.

The results of the studies of blade material and diameter, based on parametric data from the subcontractors, are shown in Figure 4-2. The three materials were ranked as they were before the studies: wood was the lightest, glass fiber slightly heavier, and steel was the heaviest and most expensive. In a complex trade-off, such as this one, assumptions are always made and data is always manipulated, so these rankings were corroborated by inputs from the subcontractors.

GE defined blades of various diameters, based on sizing calculations using SECTION, to each of the subcontractors. The subcontractors were asked to determine costs and weights for the 100th unit of each design. They produced conceptual designs for each blade, including joints and other manufacturing features. The weights and costs are listed in Table 4-1. The designs correlated with the results of the parametric study. The ranking of wood, glass fiber and steel were not changed. However, the cost and weight of the glass fiber blade increased, making the choice between wood and glass fiber more clear. Wood was chosen as the most cost effective material.

Wood blades were also evaluated at the system level, as shown in Table 4-6. Qualitatively, wood was considered to be the least risky of the possible materials. Quantitatively, it resulted in the lowest system weight and lowest cost of energy.

The choice of laminated wood and epoxy was based on these trade-off studies, a preliminary blade design and the wood material substantiation, which is described in the following section.

4.1.1.3 Material Substantiation

The selection of laminated wood and epoxy as the most cost effective blade material created an immediate need for a materials development program to substantiate the material in a 4×10^8 cycle, fatigue environment. The

Table 4-6 System Blade Material Trade-Off Summary

Item	Units	Baseline	A	B	Remarks
Blade Material		Fiberglass	Wood	Steel	
Complexity	Qual	Baseline	Less	Less	Process control
Transportation .	K $	Baseline	23 less	26 more	Weight dependent
Reliability	Qual	Baseline	Same	Same	
Maintainability, O&M	Qual	Baseline	Same	More	Painting
Availability	%	Baseline	Same	Same	.96 goal
Enviromental	Qual	Baseline	Same TVI Less sound	Worse TVI Less Sound	Material dependent Speed dependent
Safety	Qual	Baseline	Same	Less	Single steel load path
Risk	Qual	Baseline	Less	Same	MOD-OA history
Diameter	Ft	402	400	400	
Tip speed	Ft/Sec	400	350	325	Wood, Fiberglass Optimized
Weight	K LB	1349	1209	1627 (A)	3/81 WCER 100th unit
Installed cost	K $ (1980)	3602	3366	4100 (B)	3/81 WCER 100th unit
Annual energy capture	GWH	20.56	19.21	19.80 (C)	Lower wood CP - λ
Cost of energy	¢/KWH(1980)	3.33	3.32	3.90	Wood has least cost, risk

A Based on parametric data
B Based on 3/81 cost data
C Extrapolated

Wood Handbook, published by Forest Products Laboratory or the U.S. Department of Agriculture, and its references were the key sources used in defining allowables for the parametric study.

All the existing data was derived from testing small, clear grained specimens. This data needed to be expanded to account for increases in dimensions and for the use of laminated wood, rather than solid stock. The carefully selected wood veneer, bound with an epoxy matrix was assumed to be equal to or better than solid material. This assumption was based on: (1) the ability of the epoxy to create a cohesive bond to the wood laminae which was stronger than the laminae in cross-grain tension; (2) the ability to limit defects in each lamina by a careful inspection before bonding.

4.1.1.3.1 Basic Properties

The materials test program was structured to measure tensile, compressive and shear properties under static and fatigue loads, in a variety of humidities and temperatures. The last two parameters had been shown to be important in wood design in the MOD-0A service.

As the test program progressed, concerns about a phenomenon known as "size effect" developed. The size effect tends to reduce the allowable strength of an assembly, in proportion to its increasing stressed volume. It is based on the premise that as the amount of material increases, the probability of a large defect or a critical array of smaller defects also increases. The size of the defects would limit the strength of the total assembly. The use of qualified laminae and a rigidly controlled bonding process would bias the size of the critical defect to a lower limit. A series of tests to evaluate the impact or size effect were designed and performed and their results applied to the material allowables.

Wood allowables are also affected by the duration of the applied load i.e., the shorter the duration of the load, the higher the allowable. Standard test practices base quoted allowables on a five-minute load-to-failure ramp. This technique was used in all static testing, so that this data would be consistent with other data bases. Limited resources, both time and funds,

prevented any attempt to characterize the load duration effect on the wood laminae. The allowables were adjusted to the expected thirty-year life, based on existing data from the Forest Products Laboratory.

4.1.1.3.2 Component Testing

The test program included a series of laminated wood and epoxy component development tests, in addition to the materials characterization tests.

This phase of the test program addressed the features determined by joining and assembly constraints and requirements. Static and fatigue tests at various temperature were performed on:

a) Field Joints - a series of close tolerance interlocked triangular fingers, factory machined into the end grain of the blade and bonded with epoxy in the field.

b) Stud Joints - a machine steel stud with a machine threaded shank and a taper machined body which is bonded with epoxy into a taper hole drilled into the end grain of the blade material.

c) Longitudinal Bonded Joints - required to factory assemble the blade segments. These joints are approximately parallel to the grain direction of the laminated assemblies.

d) Teeter Area Joints - consisted of scale model testing of the center blade area involving the bolsters, teeter bearings and teeter brake restraints.

A detailed description of tests and their results is contained in Volume II, Section 8.0, entitled Development Tests. The allowable design properties used for the final blade design are discussed and summarized in Section 4.3. Their application to the design is directed by the structural design criteria, which is defined and discussed in detail in Volume II, Section 9.0.

4.1.2 BASIC GEOMETRY

A review of the history of the rotor gives a fuller understanding of the rotor geometry shown in Figure 4-7. The rotor design was controlled and paced largely by the blade design. Because the blade was the front-end of the machine, from the physical, technological and manufacturing standpoints, there were many constraints on the rotor design. The form of the blade was important in achieving a balanced wind turbine design. The blade shape and resulting aerodynamics had to be compatible with the blade material and manufacturing programs. The major departure from the original approach was

the adoption of the NACA 64XXX series airfoil in place of the NACA 230XX series. The laminated wood molding process provided excellent control of the reflexed trailing edge and allowed an increase in the thickness of the blade, without incurring drag losses. This increase was especially important because it allowed an efficient structural section modulus for the relatively poor volume-efficiency laminated wood.

The span of the blade, 400 ft, was not changed during the program, but the planform and thickness changed significantly. The continued load refinement, based on the operating history of other large wind turbines, and the evolving mass and stiffness characteristics of the blade, were major sources of change. The results of the development tests of the laminated wood and a broader knowledge of wood failure phenomena, resulted in a reduction of the blade's mechanical properties. The simultaneous increase in loads and decrease in allowables changed the blade design drivers from strength criteria to stiffness criteria. The design was forced into a classical weight and stiffness iteration mode, which was further complicated by the higher than anticipated growth of the weight of the partial span control assembly.

All of these factors resulted in the increase of the thickness and chord of the blade, to achieve acceptable strength and stiffness characteristics, and to maintain adequate aerodynamic performance. The aerodynamic chord of the center section grew from 180 in. to 300 in., though the tip chord was maintained at 73 in. This increase in the chord was one of the reasons for adopting the continuous wood blade, which replaced the original steel hub. This trade-off study is discussed in Section 4.1.2.1.

At 300 in., manufacturing and shipping problems affected the design of the large center chord of the blade. Consequently, it was determined that the center blade would consist of a 180 in. structural box section with fairings, which would be assembled in the field, to increase the aerodynamic chord to 300 in. The depth of the structural chord, 180 in., affected the design of the supporting yoke. Structural reinforcement was necessary, to maintain acceptable stresses in the laminated wood at the yoke interface. Several concepts were considered, but for manufacturing ease and cost effectiveness a bolster concept was selected.

The bolsters, a laminated assembly of wood and glass fiber, were the interface between the blade and the yoke. They allow the basic blade structural section to continue, with only minor interruptions, through the blade center. The bolsters avoid large holes in the blade for the teeter interface. The bolsters did complicate the interface of the blade and yoke by forcing another increase in the span of the yoke, from 180 in. to 224 in. Also, because 180 in. is about the maximum length of a blade that can be shipped in one piece, the bolsters would have to be installed in the field. Major particulars of the blade assembly are discussed in section 4.3.

The yoke was the subject of both configuration and design studies. The major configuration study, described in Section 4.5.3, addresses the interfaces between the yoke, nacelle and low speed shaft. In the initial design, the yoke was attached to the forward face of the low speed shaft. The low speed shaft was supported by a main rotor bearing, mounted rigidly to the nacelle structure. Concern about the life of the low speed shaft, which worked as a rotating cantilever beam, was the motivation for seeking another design. In the current configuration a bearing set is mounted between the yoke and the non-rotating rotor support spindle. The alternating loads associated with the weight of the rotor are applied to the yoke, but not to the support. A torque plate mounted to the forward face of the yoke, and splined to the low speed torque shaft, transmits rotor torque to the first stage of the gearbox.

The change from partial span control to trailing edge ailerons for rotor control was the last major change to affect the rotor geometry. The trade-off for this change is discussed in Section 4.2. Because this change occurred late in the program, its effect was confined to the blade. Slight modifications were made in the thickness-to-chord ratio of the outer blade and the weight was reduced. The weight reduction resulted in a new blade skin schedule, but did not affect the blade and yoke attachment or the yoke.

The final rotor design is shown in Figure 4-7. The 400 ft. blade contains one center section, two inner sections and two outer sections. Segmented ailerons form the trailing edge of the outer blade sections over the outer 40% of the span and 40% of the chord. Finger joints allow the blade sections to be assembled in the field. Elastomeric teeter bearings mount the blade to the

U-shaped steel yoke. The dimensions were determined in the final design phase. A more detailed discussion of the blade and aileron aerodynamic shape and geometry is given in Section 4.2.

4.1.2.1 Continuous Blade Trade-Off Study

The first preliminary design task for the rotor was a review of the configuration of laminated Douglas fir. This review highlighted the problems associated with joining the laminated wood to steel. The joint area for both wood and glass fiber was identified as difficult in the conceptual design phase.

The baseline rotor, shown in Figure 4-8a, contained a steel center hub, and inner and outer and tip sections on each side of the blade. The rotor assembly had seven sections, six steel-to-wood joints, and two wood-to-wood joints.

The teetered rotor support allows the major flap loads to be reacted nearly symmetrically through the hub of the rotor. The hub joint, at 7.5% of the span, was not necessary to the configuration, but it was a way to simplify fabrication and assembly of the rotor. The wood-to-steel joint, shown in Figure 4-8a, used steel studs, which were bonded with epoxy to the wood and bolted to a steel-ended rib of the hub, for structural continuity. A similar arrangement was used successfully on the MOD-0A. Test results from NASA's prototype wood blade indicated that a joint efficiency of 50-60% could be achieved, where joint efficiency is the ratio of the stress in the wood associated with the stud, to the allowable stress in the wood. (Ref. 1) However, the higher MOD-5A flap bending loads required a stud with an efficiency between 80 and 90%.

An extensive development program examined the potential for such a joint. The moduli of wood and steel are not compatible: 2×10^6 and 30×10^6 lbs/in^2, respectively. The development of a high-efficiency joint between such materials would be difficult to achieve and risky to costs and schedules. A wood-to-wood, outboard joint, which would reduce flap loads and eliminate the incompatible moduli, was considered instead. The flap loads were reduced by

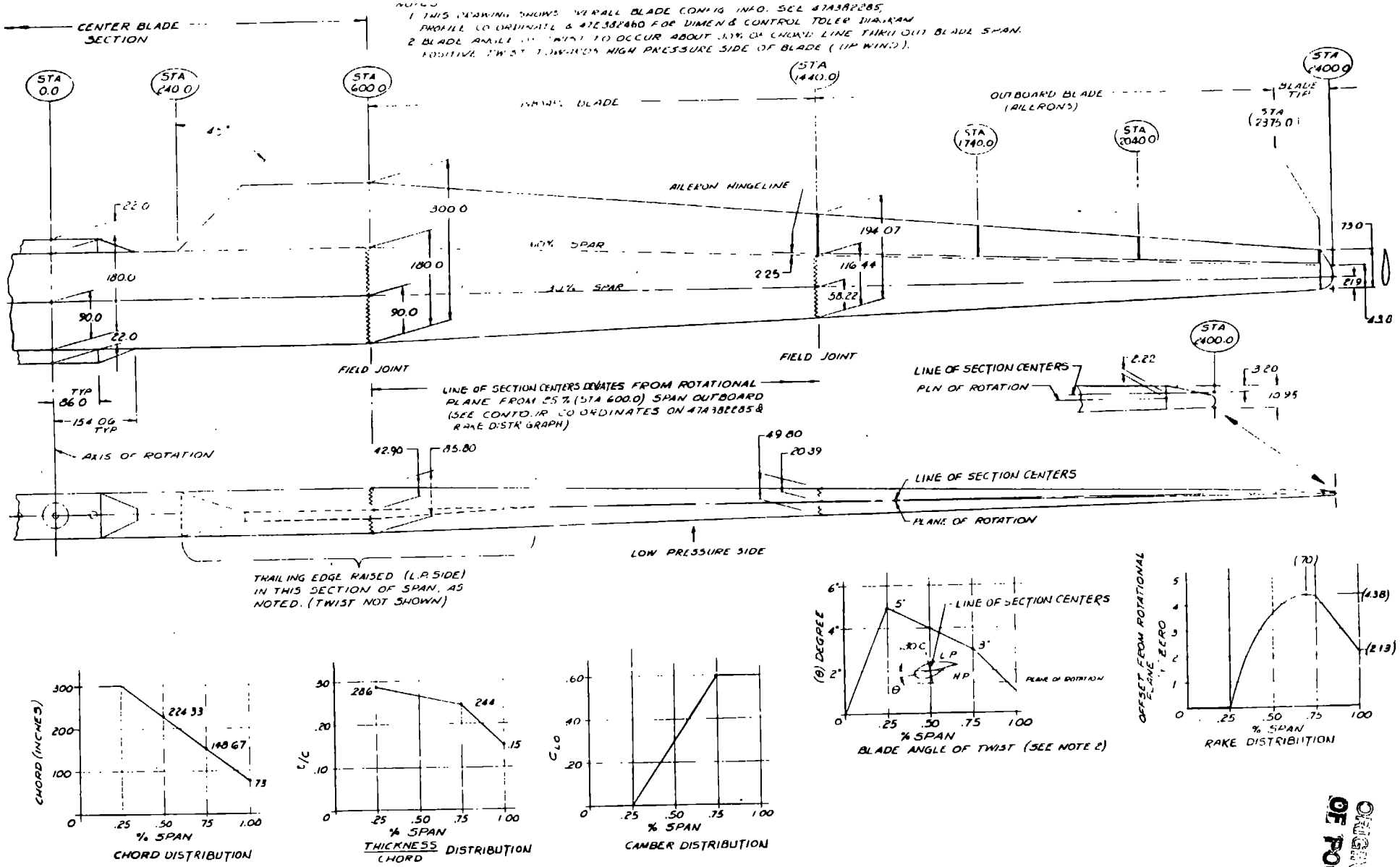

Figure 4-7 Final Rotor Geometry

positioning the joint outboard, since flap bending moments are approximately a cubic function of the outboard span, and the cover loads are a squared function of the chordal depth.

Analysis showed that a joint at 25% of the span could be configured within the constraints of the airfoil, if an efficiency of approximately 80% could be achieved. Data from the Forest Products Laboratory indicated that finger joints with this efficiency had been made. Increasing the thickness of wood at the joint would satisfactorily transfer the load across the joint in even the most conservative load conditions.

To avoid the potential risks associated with the development of a highly loaded, bonded stud-to-steel joint, a continuous hub configuration was chosen. It consisted of a five-section rotor assembly, using four wood-to-wood joints and four steel-to-wood joints, as shown in Figure 4-8.

The steel-to-wood joints, at the inboard and outboard interfaces of the partial span control assembly, required studs with only slightly higher performance than those used successfully in the MOD-OA. They were considered to be a much lower risk than the larger root joint studs. This configuration eliminated a major development risk and allowed the rotor to be made in five, rather than seven, sections.

The structural integrity of the rotor in the fatigue-dominated hub was kept almost intact by this approach. Another stud trade-off study determined how to mount the rotor to the low speed shaft so that the shaft would accept thrust, torque and weight from the blade. The flapwise and chordwise bending stresses were no longer the main consideration in the design of the hub for a continuous blade.

There were two approaches to mounting the rotor to the low speed shaft:

- o an internal teeter bearing arrangement, similar to the steel hub, which required piercing the flap surfaces of the blade with the low speed shaft, as shown in Figure 4-9, and
- o an external arrangement, which used a yoke between the low speed shaft and the teeter bearings, as shown in Figure 4-10.

The interruption of the flapwise bending cover with the internal bearing arrangement partially eliminated the gains associated with the continuous wood structure. This trade-off was the major consideration in choosing the yoke approach. Therefore, the external yoke was selected based on weight, cost and risk trade-offs. The yoke design also interrupts the wood structure with a steel teeter shaft, which interfaces with the teeter bearings. However, this discontinuity is introduced into the chordwise bending covers, which experience less stress than the flapwise covers. The teeter shaft, which is bonded in the chordwise covers, physically capturing the blade, does not create the major discontinuity that an open hole in the flapwise covers does. The resulting preliminary design, including the teeter brake shafts and teeter restraint brakes, is shown in Figure 4-11.

The cost of the continuous wood rotor was assessed after the preliminary design. The cost was less than the cost of the steel hub rotor, as summarized in Table 4-7. The continuous wood rotor also weighed less than the steel hub rotor, as shown in Table 4-8. The lower cost and weight produced a lower cost of energy.

Eliminating the two large, steel-to-wood joints reduced risks associated with the rotor. Deleting the complex primary load transition in the steel hub and reducing any risks associated with the rotor were the main reasons for choosing the continuous wood rotor and yoke combination.

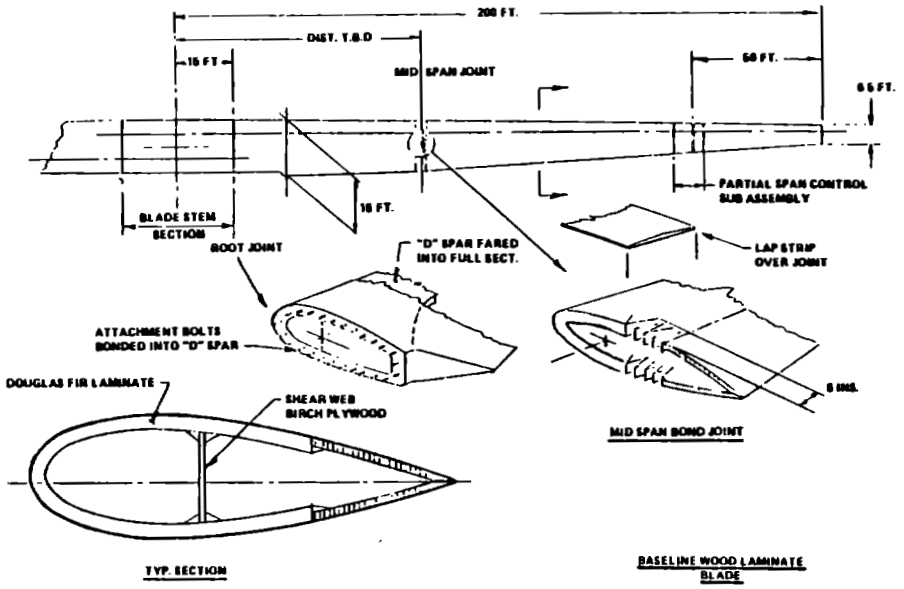

a) Conceptual Design - Steel Hub

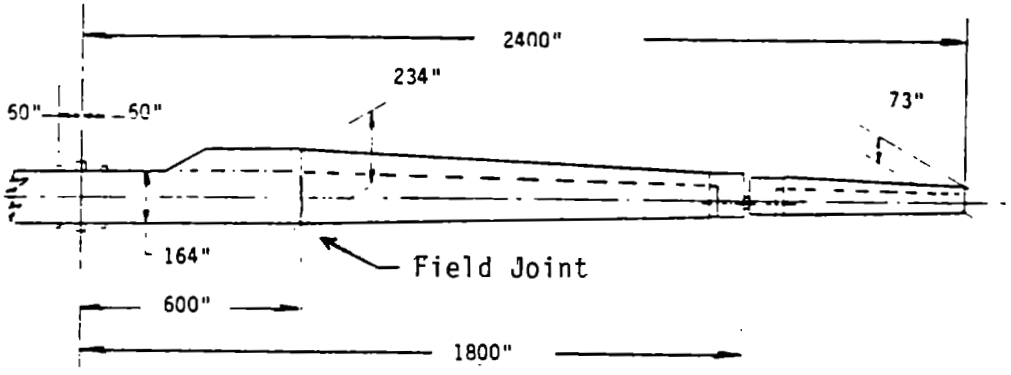

b) Preliminary Design - Continuous Wood Hub

Figure 4-8 Rotor Details and Joints

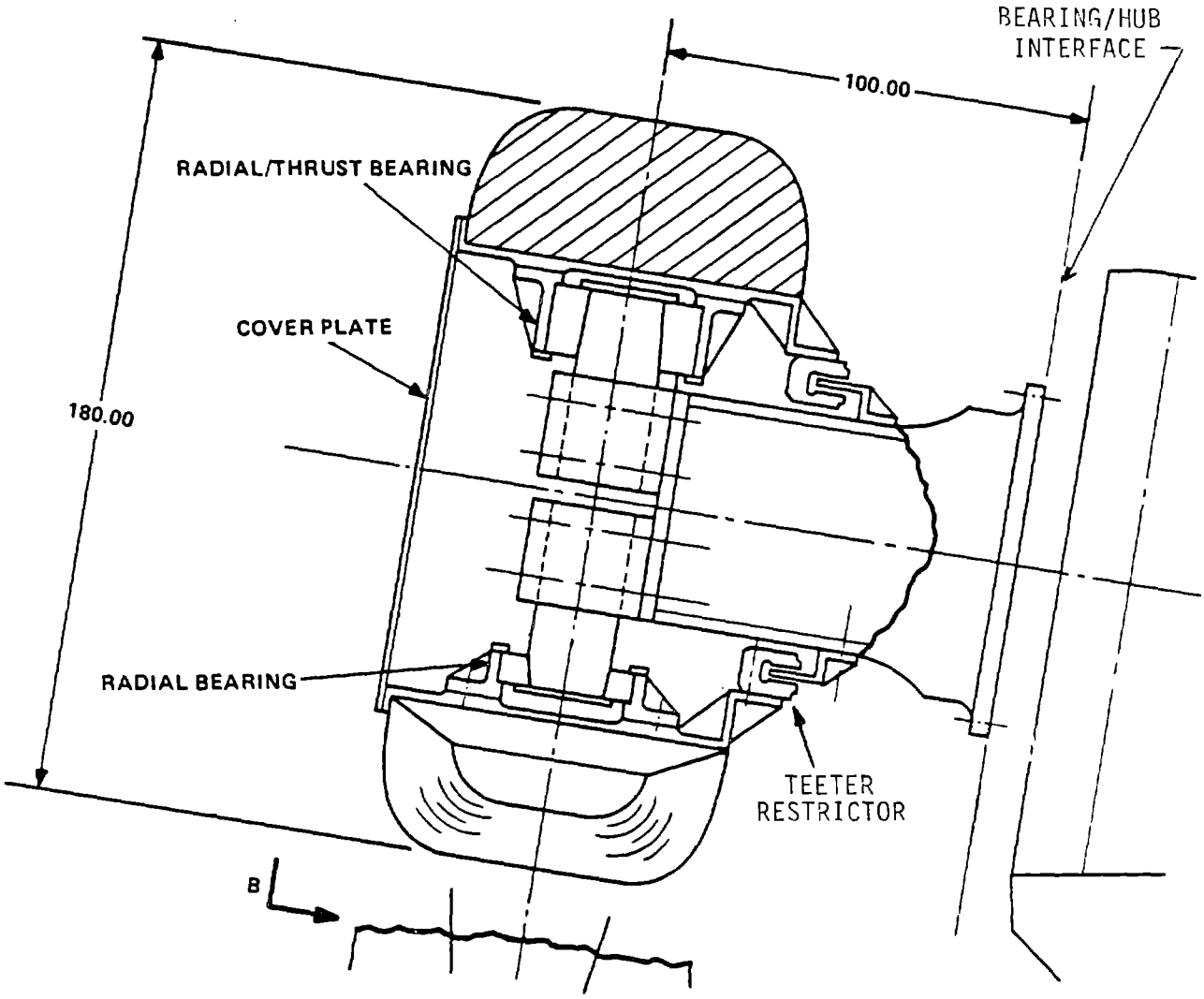

Figure 4-9 Continuous Wood Blade with Internal Teeter Bearing Option

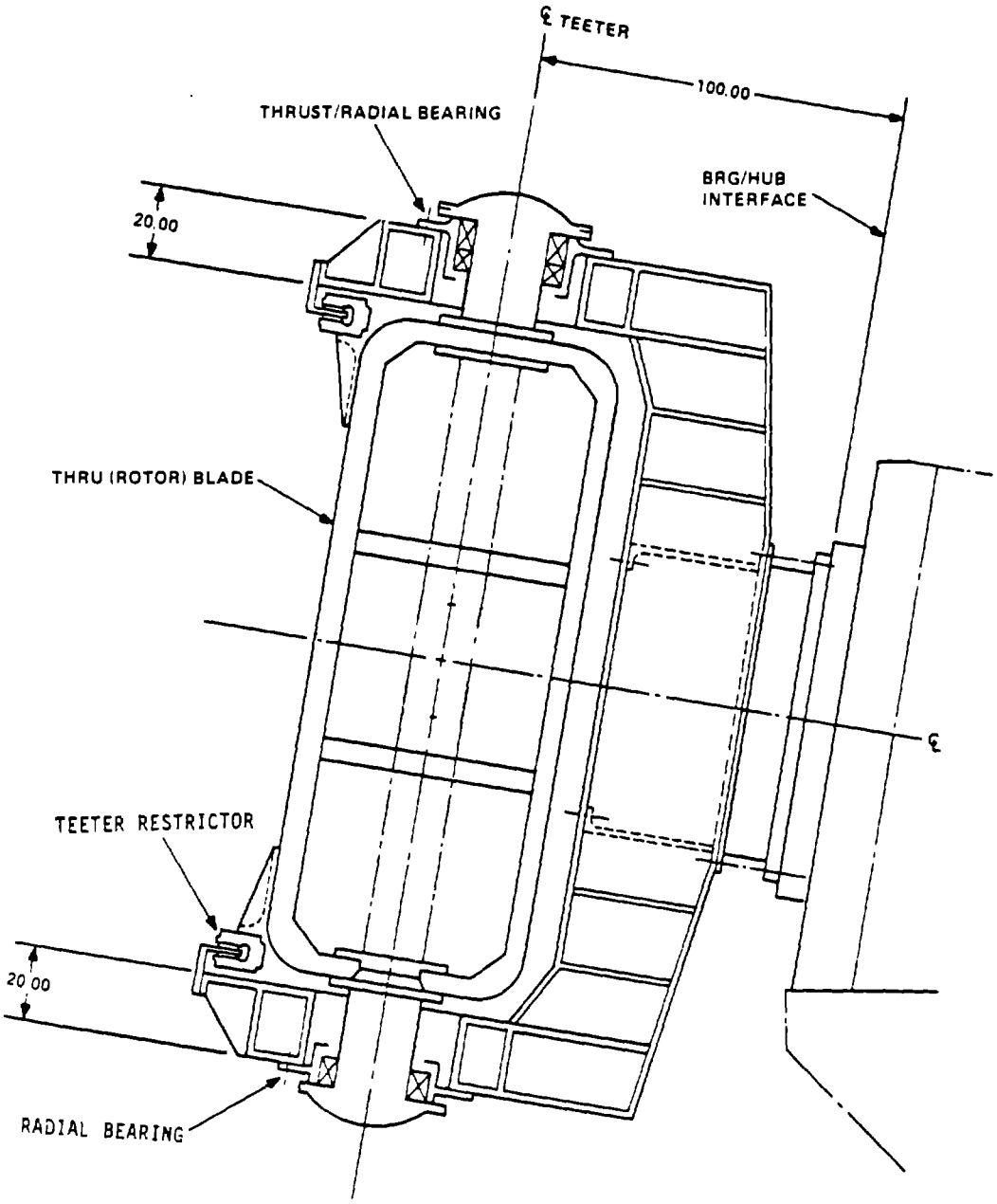

Figure 4-10 Continuous Wood Blade with External Teeter Option

Table 4-7 Continuous Blade Cost Comparison

CONFIGURATION ITEM	BASELINE - STEEL HUB 100 TH UNIT $K	1 ST UNIT $K	TOOLING $K	CONTINUOUS BLADE; STEEL YOKE 100 TH UNIT $K	1 ST UNIT $K	TOOLING $K
STEEL HUB	134.8	246.9	130.0 (2)			
LS SHAFT	24.0	52.7				
TEETER SHAFT	31.0 (3)	49.6 (3)		23.3	37.2	
YOKE & LS SHAFT				69.8	116.6	40.0
BLADE (2)	219.0	1285.0	1350.0	235.6	1436.0	1393.0
TOTAL	408.8	1634.2	1480.0	328.7	1589.8	1433.0

(1) ROTOR COSTS THAT ARE NOT NOTED REMAIN THE SAME.

(2) INCLUDES ASSEMBLY TOOLING AT $1.00/LB. OF FINISHED ASSEMBLY, $100K.

(3) TO BE CONSISTENT WITH CONTINUOUS BLADE, WHICH WAS SIZED FOR CURRENT TEETER STOP LOADS.

LS = LOW SPEED

Table 4-8 Continuous Blade Weight Comparison

CONFIGURATION ITEM	BASELINE - STEEL HUB LBS x 10^3	CONTINUOUS BLADE/ STEEL YOKE LBS x 10^3
STEEL HUB	87.0	-
LOW SPEED SHAFT	13.0	-
TEETER SHAFT	20.0	15.0
YOKE AND LOW SPEED SHAFT	-	45.0
BLADE	123.3	152.7
TOTAL	243.3	212.7

(1) ROTOR WEIGHTS THAT WERE NOT NOTED REMAIN THE SAME, FOR EXAMPLE 43,000 LBS FOR THE TEETER BEARING, SNUBBERS AND PARTIAL SPAN CONTROL.

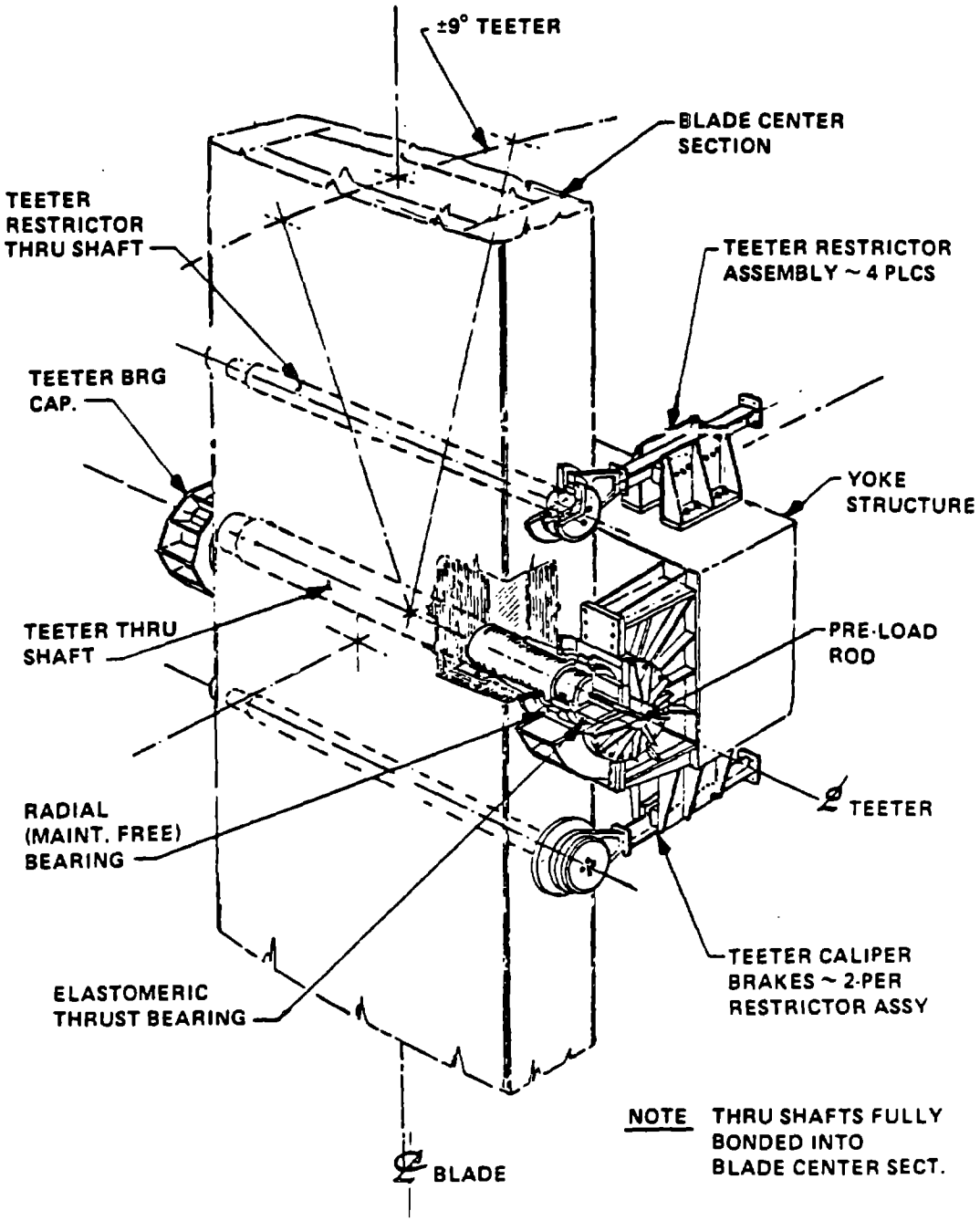

Figure 4-11 Continuous Wood Blade with Teeter Shaft/Rotor

4.2 AERODYNAMICS

4.2.1 BLADE DESIGN DESCRIPTION

The MOD-5A blade design was developed using knowledge gained from the MOD-1 development, and several proposal studies and successive designs. These studies showed that the cost and weight of large wind turbine generator systems are very sensitive to the rotor torque. The design torque for the rotor affects the low speed shaft, bearings and gearbox. These components are major contributions to the cost and weight of the drivetrain system, so they force the rotor design to low torque. A low torque rotor requires high rotor speed and low rotor solidity to achieve the rated power efficiently. Low solidity depends on narrow blades, which must be thick enough to provide the necessary strength and stiffness. However, thickness creates high drag and lowers the rotor's performance.

The aerodynamic and structural design of the blades required a series of trade-off studies that balanced thickness, stiffness, performance, control and construction methods. For example, the method for fabricating laminated wood blades limited mechanical twist to 0.1° per foot, or 5° of twist at 25% of the span. The aerodynamic design added effective twist by cambering and raising the trailing edge of the airfoil. This section discusses the aerodynamic design of the blades and ailerons.

4.2.1.1 Blade Aerodynamics

4.2.1.1.1 Blade Section Geometry

The geometric characteristics of the blade are tabulated in Table 4-9 and depicted in Figures 4-12 and 4-13. The effective rotor solidity is the solidity of both blades at 70% of the span, and is .0310.

Figure 4-14 shows the very substantial variation in the thickness-to-chord ratio (t/c) from the tip, where t/c=.15, to 25% of the span, where t/c=.29. In selecting airfoil sections, this large change in ratio was considered.

4.2.1.1.2 Blade Section Kinematics

In the region from the cut-in wind speed to the rated wind speed, the wind turbine can capture energy in proportion to its maximum power coefficient at any wind speed. The range of wind speeds below the rating can be regarded as

Table 4-9 Geometry of the MOD-5A Blade

RADIAL STATION (X/R)	RADIAL STATION (IN)	TWIST ANGLE (DEG)	THICKNESS (IN)	THICKNESS (RATIO)	CHORD (IN)	DESIGN CAMBER	T.E. UPPER ORDINATE (IN)	T.E. TOTAL THICKNESS (IN)
.25	600	5.0	85.80	.2860	300.00	0.000	17.045	17.109
.30	720	4.8	80.28	.2818	284.87	0.100	9.651	9.945
.35	840	4.6	74.88	.2776	269.73	0.175	3.459	3.926
.40	960	4.4	69.63	.2735	254.60	0.238	1.220	1.797
.45	1080	4.2	64.49	.2693	239.47	0.297	0.770	1.385
.50	1200	4.0	59.47	.2651	224.33	0.350	0.576	1.161
.55	1320	3.8	54.58	.2609	209.20	0.400	0.537	1.076
.60	1440	3.6	49.82	.2567	194.07	0.450	0.498	0.996
.65	1560	3.4	45.20	.2526	178.93	0.500	0.460	0.919
.70	1680	3.2	40.69	.2484	163.80	0.550	0.421	0.842
.75	1800	3.0	36.31	.2442	148.67	0.600	0.382	0.764
.80	1920	2.6	30.10	.2254	133.53	0.6	.343	.686
.85	2040	2.2	24.45	.2065	118.40	0.6	.305	.610
.90	2160	1.8	19.38	.1877	103.27	0.6	.266	.532
.95	2280	1.4	14.88	.1688	88.13	0.6	.227	.454
1.0	2400	1.0	10.95	.1500	73.0	0.6	.188	.376

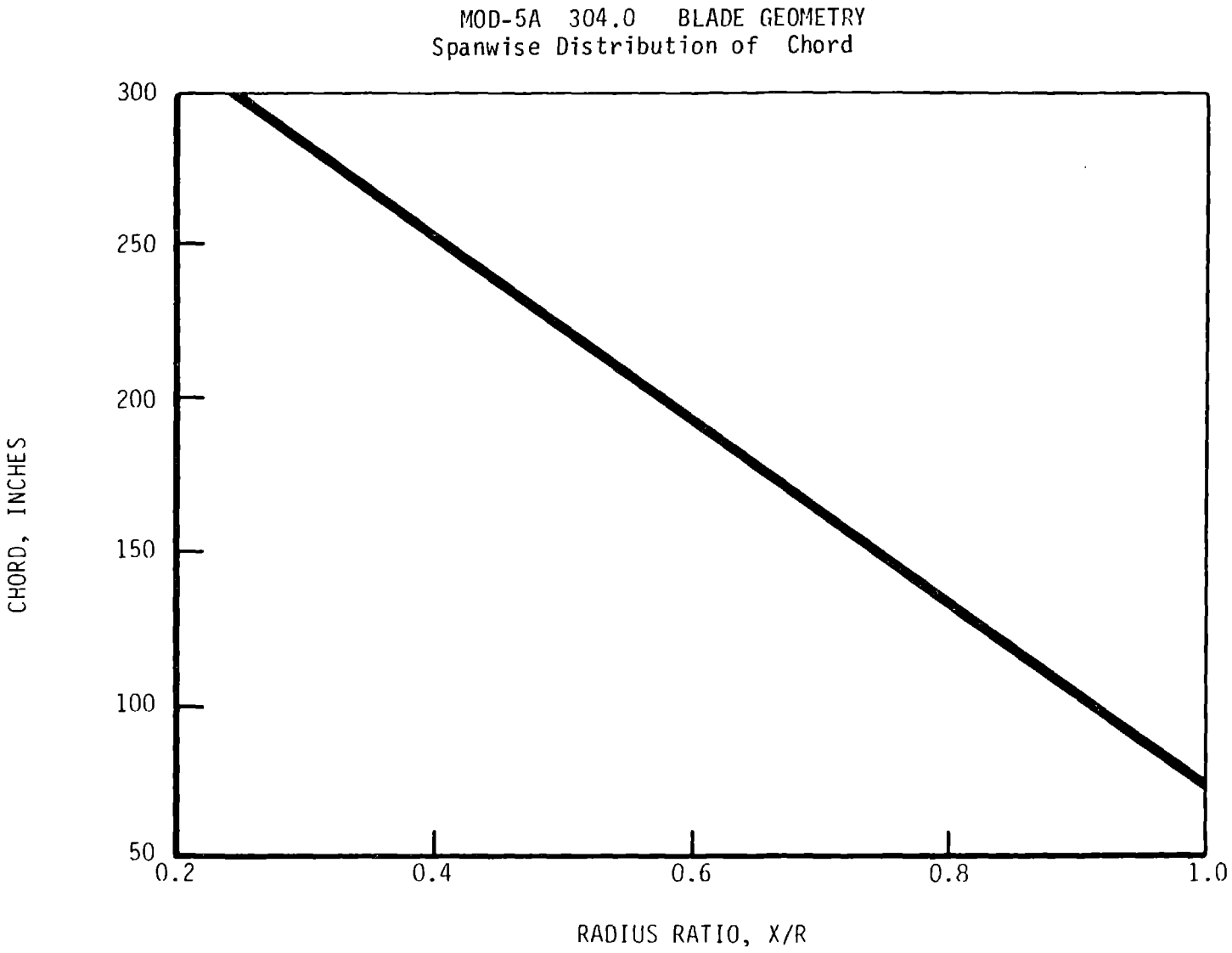

Figure 4-12. Blade Chord Distribution

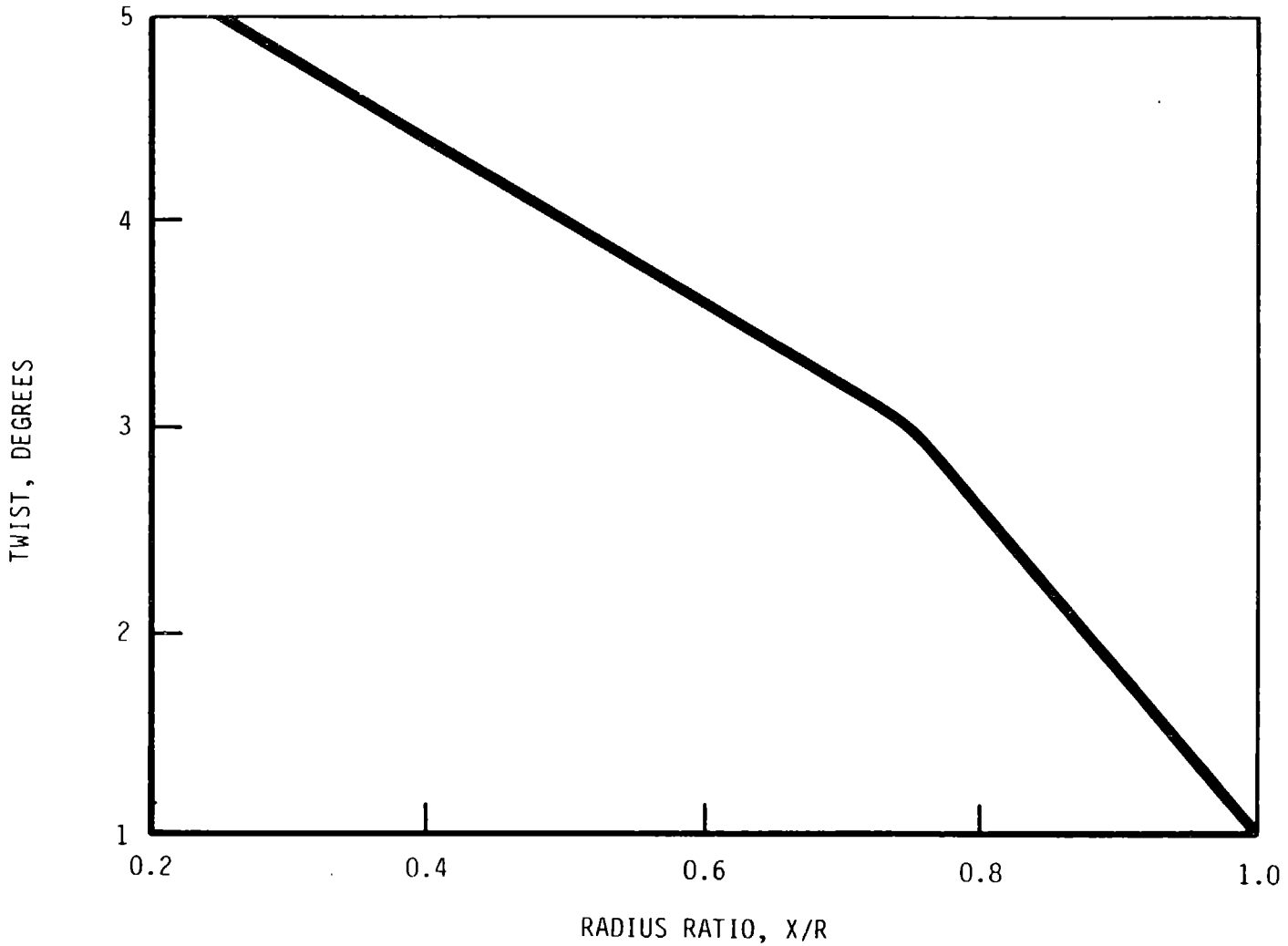

Figure 4-13. Blade Twist Distribution

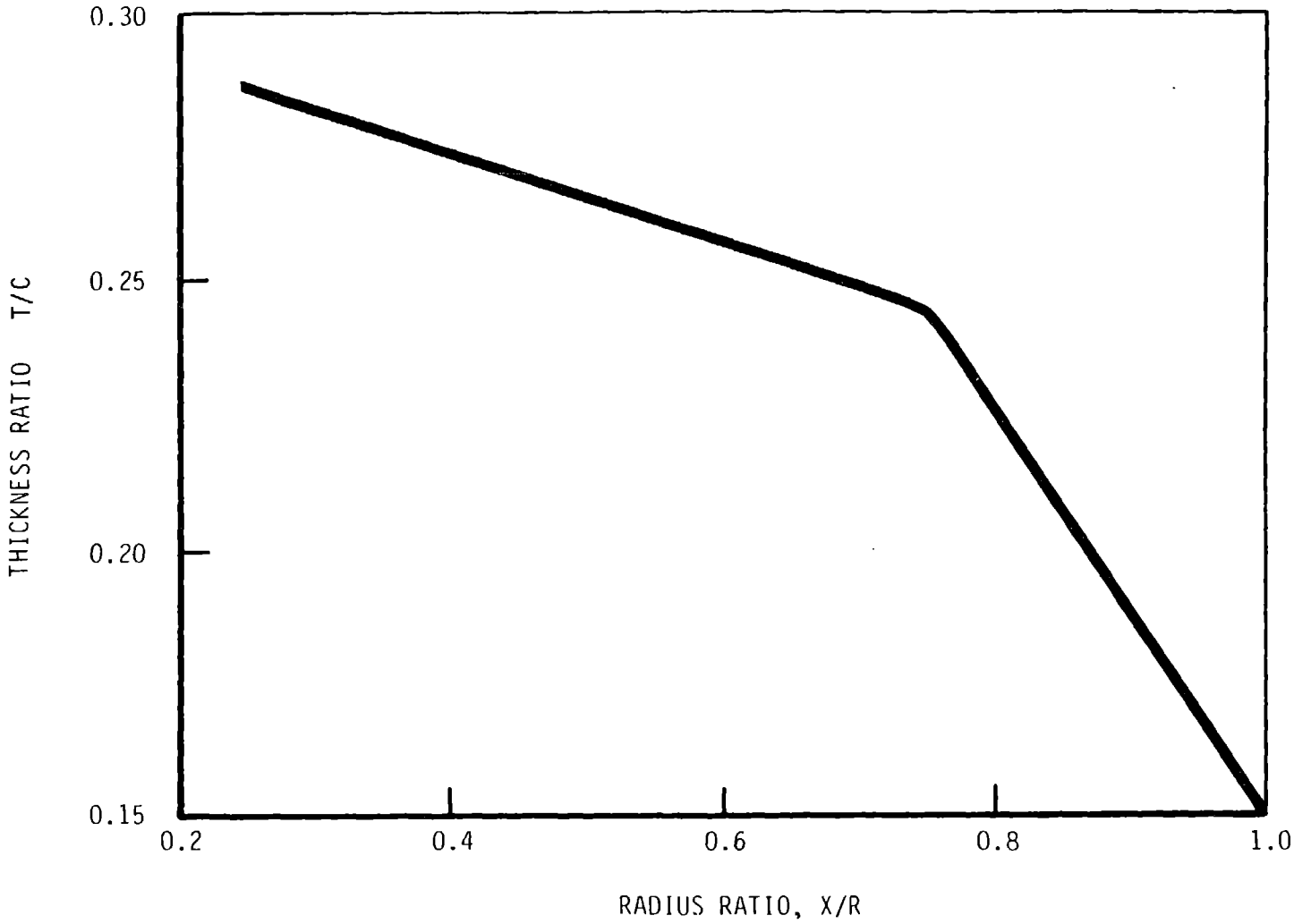

Figure 4-14. Blade Thickness Ratio Distribution

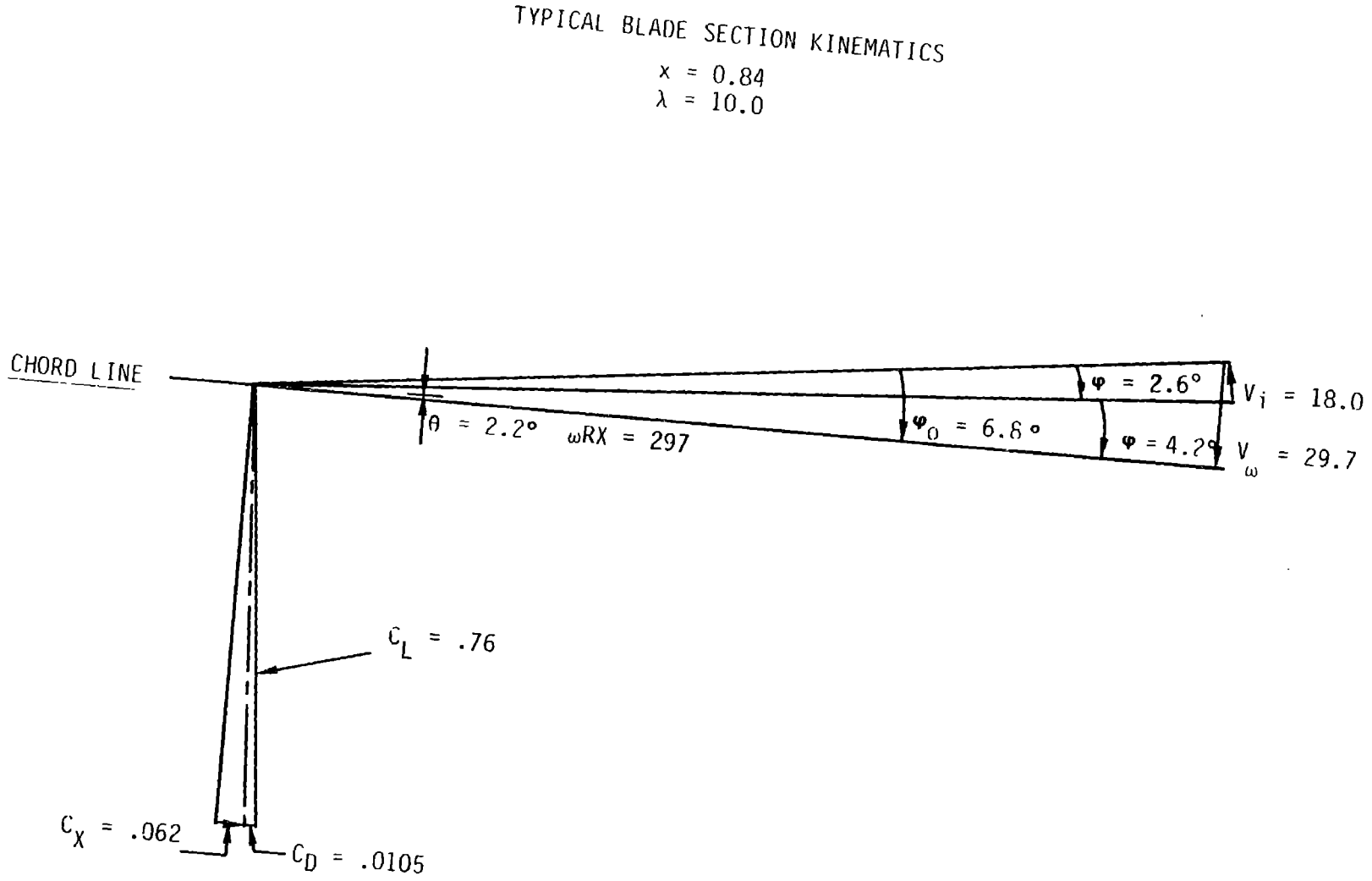

Figure 4-15. Typical Blade Section Kinematics

the performance region because at wind speeds greater than the rating, the turbine must shed power and its energy capture is independent of the rotor's potential efficiency.

The basic interactions between the blade velocity and the force it produces are illustrated in Figure 4-15. This figure is a scaled illustration of the actual conditions at 84% of the span with a tip speed ratio of λ=10. The MOD-5A is designed to capture 60% of its energy at wind speeds below the rated wind speed. The rated wind speed at the height of the hub is 30 mph. This speed corresponds to a tip speed ratio of 8. Hence, λ=10 corresponds to a wind speed of 24 mph. The figure emphasizes that at speeds up to the rated speed all the air angles are so small that the angle of attack is almost entirely due to the retarded wind velocity, and the dynamic pressure is almost entirely due to the tangential velocity. The figure also indicates that the torque, C_X, is produced by a small component of the lift (the lift multiplied by sin ϕ) minus the drag.

Under these conditions, the optimum airfoil sections are required to produce high values of the lift-to-drag ratio at smaller angles of attack than those for which airfoils are usually designed.

The actual distributions of the angle of attack, for wind speeds between the cut-in and rated speeds, is shown in Figure 4-16. Here the angles of attack lie in two regions: the outer region, where the angles are small and slowly changing, and the inner region where the angles are larger and increase substantially both inwardly along the blade span and with increasing wind speed (decreasing tip-to-speed ratio). These two regions were treated differently in the airfoil optimization process.

4.2.1.1.3 Airfoil Section Optimization

A review of data on families of NACA and other airfoil sections under consideration, including the LS(1)( ),04XX, the 230XX and the 63XXX, 64XXX and 65XXX sections, evaluated their suitability. The 64XXX adapted best to the requirements of the MOD-5A. This family of airfoils had a well documented data base, spanning the wide range of camber and thickness-to-chord ratios. The database only included thickness-to-chord ratios of up to 21%, however,

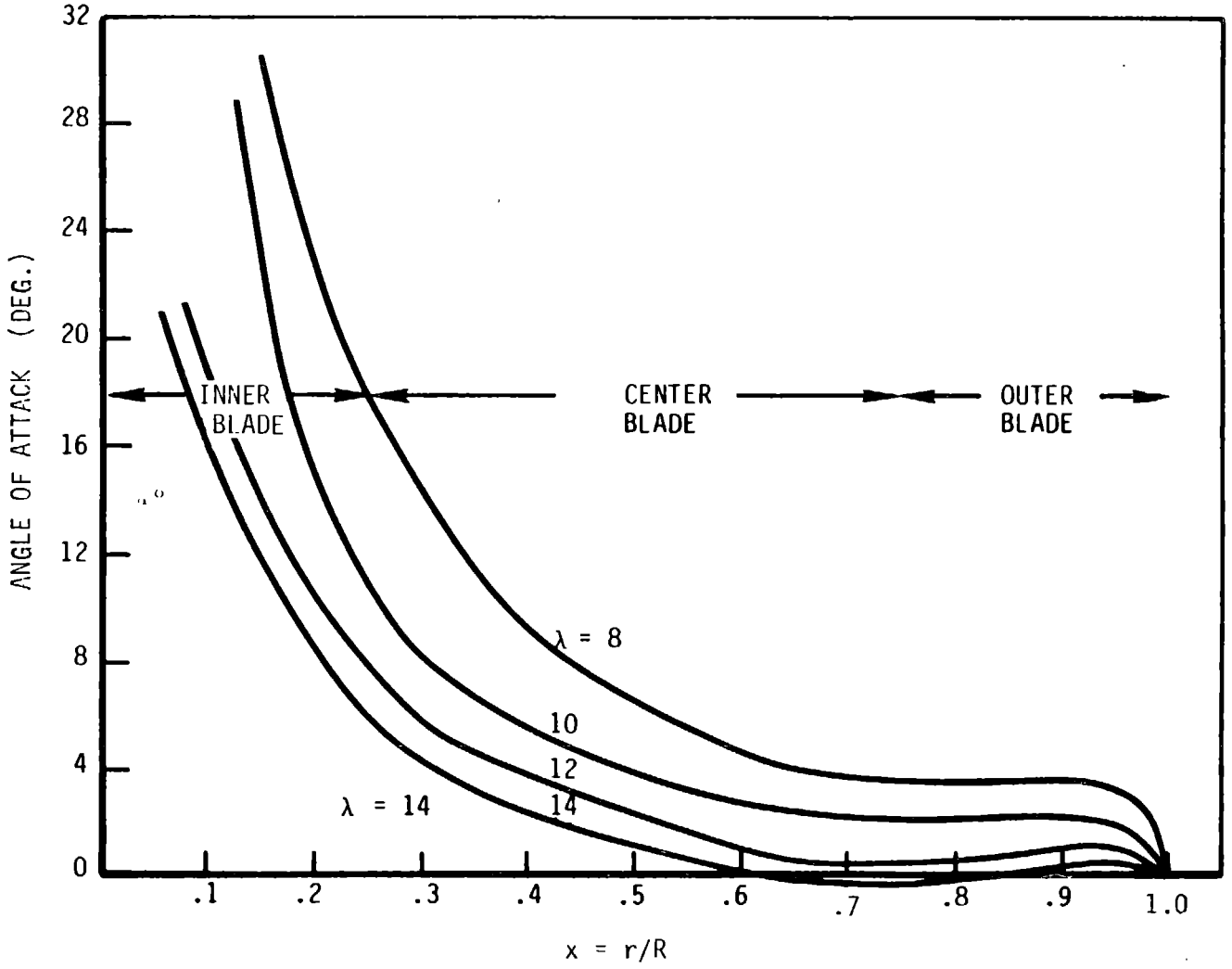

Figure 4-16. Angle of Attack Distribution Along Blade From Low Cut-in to Rated Wind Speed

and wind tunnel tests were made to obtain data for ratios up to 29%, as described in Volume II, section 8.4. A high lift-to-drag ratio in the range of angles of attack that corresponded to the performance region was used as the criteria for airfoil selection.

Outboard Region -- The angle of attack varies little in the outer 25% of the blade. Therefore, this region is well served by airfoil sections of constant camber and nearly constant pitch angle. The very low operating angles of attack in the region between the cut-in and rated speeds requires a highly cambered airfoil section. A camber corresponding to a design lift coefficient of 0.6 was selected because this amount of camber produced optimum lift-to-drag ratios at low angles of attack ($\alpha \sim 2.0°$). The distribution along the blade is illustrated in Figure 4-17, with camber shown as a change in design lift coefficient.

Figure 4-18 shows the lift and drag characteristics of the 64621 profile. The leading edge was tripped and the Reynolds Number is 4×10^6. This profile of a section at 84% of the span is representative of the outboard region. In the region between the cut-in and rated wind speeds, this section operates at reasonable lift coefficients below stall and in the low drag region of the section. Figure 4-19 displays the angle of attack distribution and the lift-to-drag ratios along the outboard span for two significant tip-speed-ratios. Negative angles of attack were estimated and used only during analysis. The lift-to-drag ratios, which range from 60 to 100 in these conditions, are as good as or better than the ratios that can be achieved by other airfoil sections of the same thickness operating at the same angles of attack. For comparison, the 21% thick LS (1) airfoil discussed in NASA TM X-72843, which would be located at x=0.94, at λ=8 and 10, yields lift-to-drag values of 55 and 51 respectively, at a Reynolds number of several million.

The Inboard Region -- From Figure 4-16 shows that the angle of attack, α, increases rapidly inboard and with decreasing tip-to-speed ratios. The trend can be countered along the span, by applying twist to keep each section at a moderate angle of attack. However the manufacturing method adopted for the MOD-5A precludes pitch angles greater than 5° at 25% of the span. An effective aerodynamic twist of 4° is achieved by reducing the camber from a lift coefficient of 0.6 at x=0.7 to an uncambered airfoil at x=0.25.

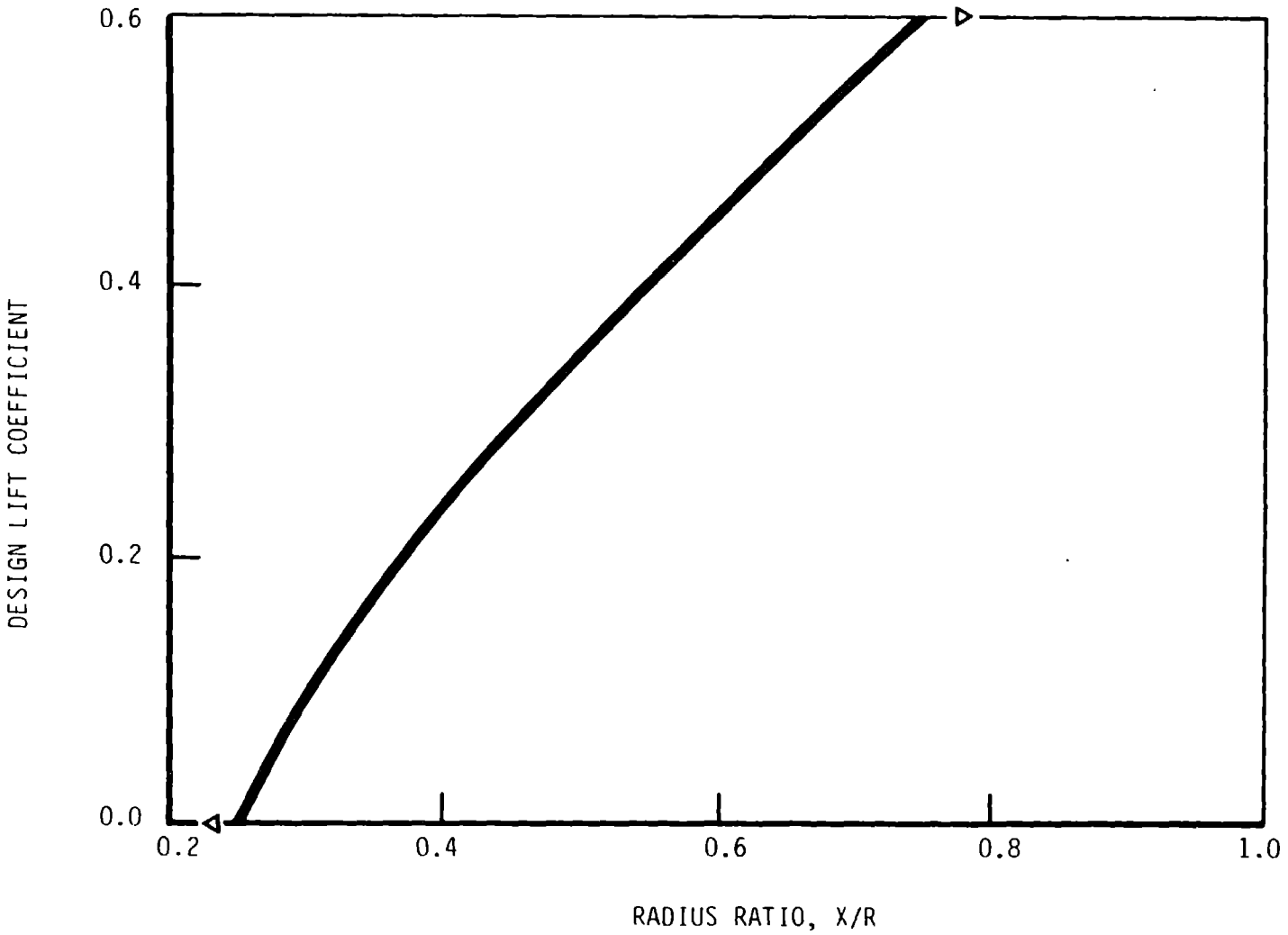

Figure 4-17. Spanwise Camber Distribution

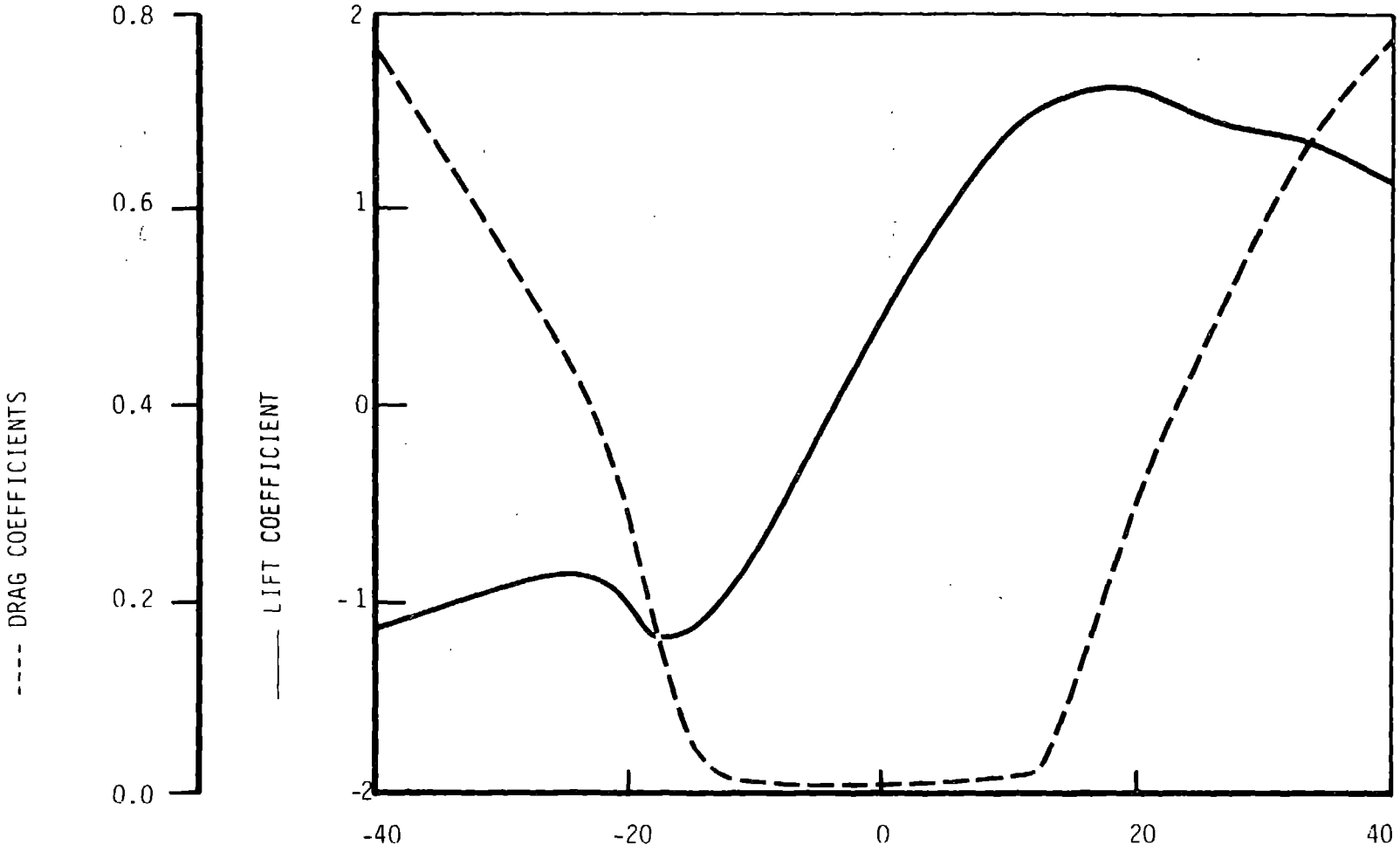

Figure 4-18. Lift and Drag of 64621 Section at 0.84 Span (Leading Edge Tripped, Reynolds No. = 4 million)

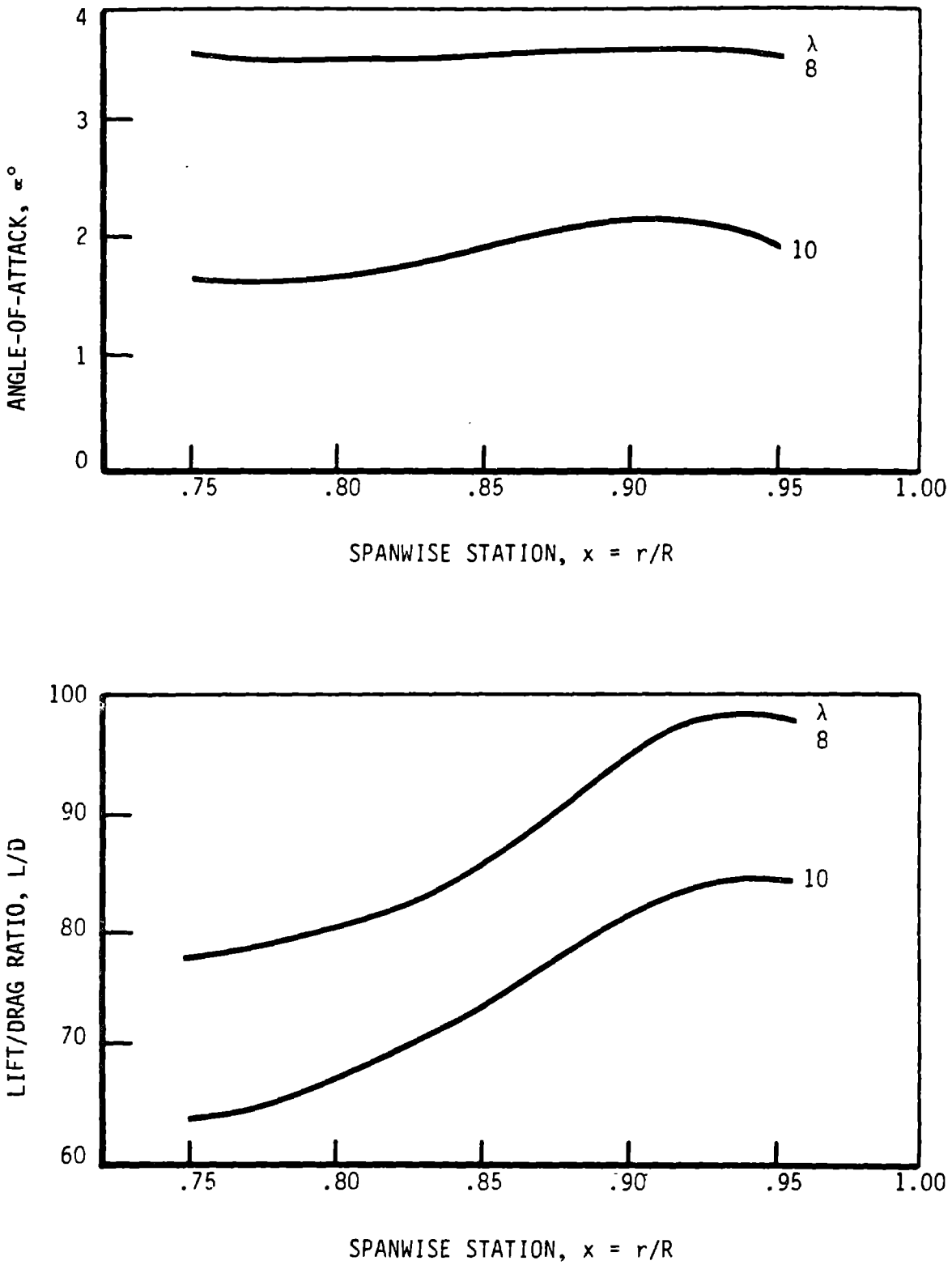

Figure 4-19. Angle of Attack and Lift-to-Drag Ratio Distributions

(1856A)

Based on the data gathered in the wind-tunnel tests, discussed in section 8.4.1 of Vol II, the effective camber of the inboard region was decreased. Stall was avoided in the region between the cut-in and rated wind speeds by using raised trailing edges, which reduce the camber of the airfoil sections. Data from Hoerner was used to establish the optimum trailing edge thickness-to-chord ratio of .005. This is the thickest trailing edge that can be employed with no increase in profile drag. The resultant raised and lowered trailing edge distributions are documented in Figure 4-20.

Lift and Drag Characteristics of the Rotor -- The lift and drag coefficients in the angle of attack range between -40° and +40° are presented in tables and graphs. They are given for four spanwise stations in each of the three blade regions: outer blade ($0.76<x<1.00$), center blade ($0.25<x<0.76$) and inner blade ($0.10<x<0.25$). The tabulations are given in Tables 4-10, 4-11, and 4-12 for the outer, center and inner regions respectively. The graphs are in Figures 4-21 through 4-26. The information is based on wind tunnel test data and interpolation. Some bumps appear in the otherwise smooth curves because of the wind tunnel drag measurement procedure. The data was not smoothed, and the bumps do not influence the rotor's performance.

For completeness, the lift and drag coefficients for the region $40<\alpha<320°$ are given in Figures 4-27 and 4-28. This single representation is used for all of the sections because such high angle properties are substantially independent of section geometry.

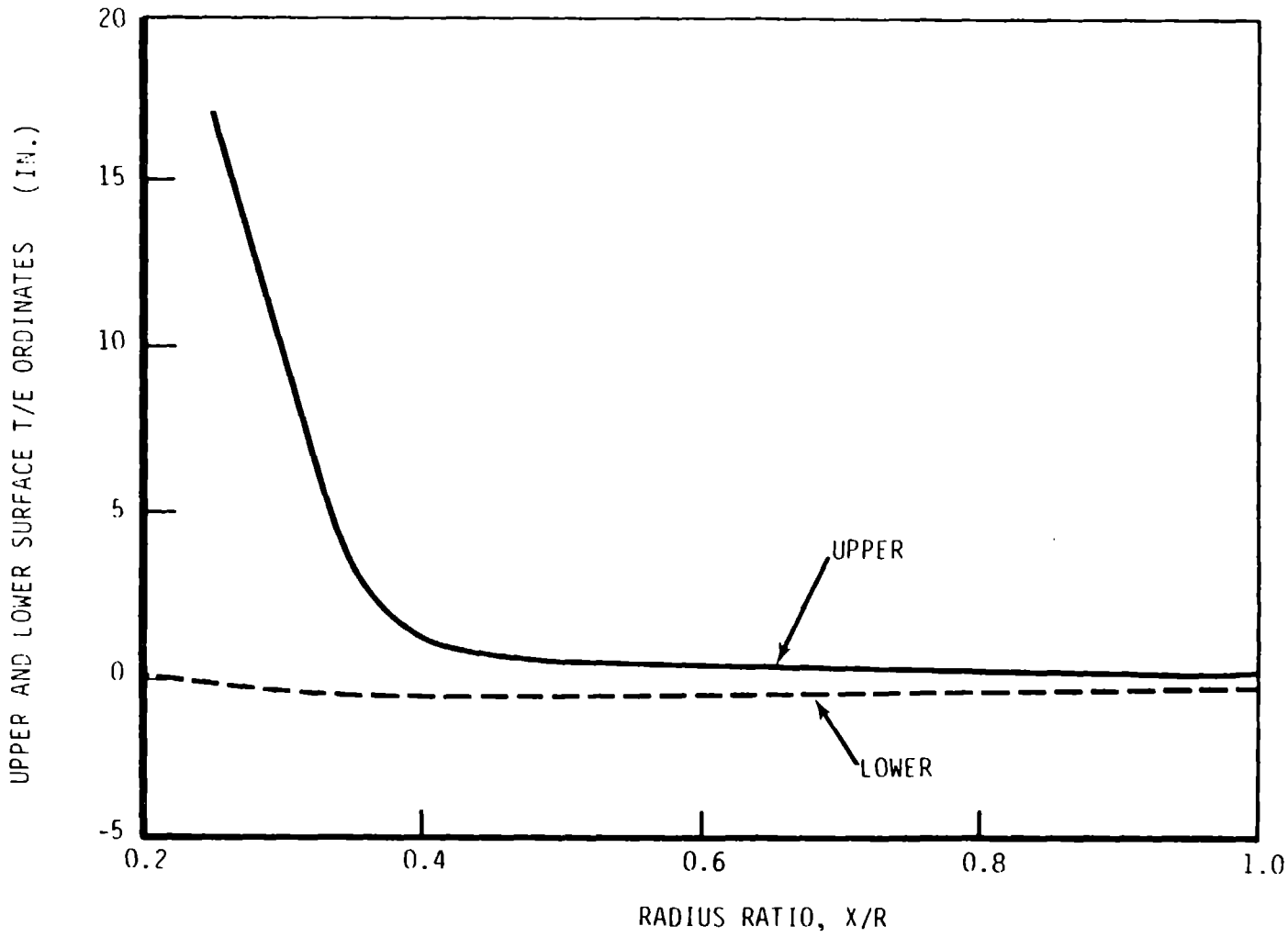

Figure 4-20. Trailing Edge Ordinate Distribution

Table 4-10 Lift and Drag Characteristics of the Outboard Blade Region

	x=0.76		x=0.841		x=0.92		x=1.0	
α^o	C_L	C_D	C_L	C_D	C_L	C_D	C_L	C_D
-40.0	-1.094	0.7760	-1.150	0.7768	-1.150	0.7748	-1.154	0.7747
-38.0	-0.964	0.7563	-1.180	0.7566	-1.105	0.7309	-1.111	0.7309
-36.0	-0.939	0.7305	-1.197	0.7304	-1.060	0.6873	-1.066	0.6874
-34.0	-0.938	0.6927	-1.190	0.6920	-1.017	0.6444	-1.021	0.6445
-32.0	-0.906	0.6368	-1.146	0.6353	-0.975	0.6024	-0.977	0.6026
-30.0	-0.838	0.5568	-1.053	0.5543	-0.936	0.5617	-0.936	0.5619
-28.0	-0.761	0.4527	-0.898	0.4489	-0.899	0.5218	-0.898	0.5220
-26.0	-0.675	0.3481	-0.698	0.3437	-0.869	0.4795	-0.867	0.4797
-24.0	-0.595	0.2729	-0.580	0.2691	-0.863	0.4307	-0.852	0.4308
-22.0	-0.542	0.2454	-0.602	0.2438	-0.898	0.3710	-0.861	0.3708
-20.0	-0.471	0.2392	-0.460	0.2376	-1.010	0.2928	-0.906	0.2923
-18.0	-0.498	0.2091	-0.367	0.2058	-1.190	0.1923	-0.985	0.1921
-16.0	-0.789	0.1279	-0.826	0.1229	-1.182	0.0952	-1.047	0.0955
-14.0	-0.987	0.0679	-1.089	0.0533	-1.072	0.0359	-1.038	0.0358
-12.0	-0.927	0.0492	-0.906	0.0260	-0.939	0.0175	-0.938	0.0161
-10.0	-0.750	0.0283	-0.726	0.0162	-0.742	0.0149	-0.746	0.0122
-8.0	-0.523	0.0145	-0.524	0.0129	-0.500	0.0114	-0.501	0.0103
-6.0	-0.280	0.0126	-0.271	0.0117	-0.250	0.0091	-0.243	0.0086
-4.0	-0.034	0.0114	-0.038	0.0107	-0.001	0.0079	0.013	0.0076
-2.0	0.233	0.0098	0.224	0.0099	0.242	0.0074	0.262	0.0072
0.	0.516	0.0105	0.520	0.0096	0.475	0.0076	0.497	0.0074
2.0	0.788	0.0152	0.791	0.0106	0.696	0.0080	0.712	0.0076
4.0	1.032	0.0186	1.031	0.0118	0.900	0.0088	0.900	0.0085
6.0	1.236	0.0136	1.237	0.0132	1.084	0.0109	1.065	0.0102
8.0	1.389	0.0124	1.393	0.0152	1.250	0.0144	1.251	0.0140
10.0	1.479	0.0836	1.485	0.0137	1.395	0.0185	1.440	0.0209
12.0	1.515	0.0806	1.516	0.0215	1.500	0.0236	1.540	0.0233
14.0	1.521	0.0989	1.512	0.0564	1.553	0.0650	1.620	0.0609
16.0	1.527	0.1448	1.522	0.0882	1.580	0.1399	1.690	0.1417
18.0	1.537	0.2100	1.543	0.1152	1.604	0.2201	1.727	0.2204
20.0	1.538	0.2863	1.535	0.1584	1.600	0.2996	1.716	0.2995
22.0	1.532	0.3657	1.521	0.1721	1.550	0.3705	1.648	0.3705
24.0	1.506	0.4399	1.500	0.1743	1.494	0.4397	1.542	0.4396
26.0	1.416	0.5027	1.450	0.2605	1.450	0.5011	1.451	0.5010
28.0	1.226	0.5550	1.419	0.4330	1.423	0.5540	1.413	0.5539
30.0	1.025	0.6000	1.400	0.5971	1.400	0.6000	1.399	0.6000
32.0	0.914	0.6403	1.369	0.6778	1.366	0.6410	1.373	0.6411
34.0	0.892	0.6770	1.326	0.6942	1.322	0.6780	1.331	0.6781
36.0	0.939	0.7112	1.273	0.6891	1.269	0.7121	1.277	0.7121
38.0	1.031	0.7435	1.213	0.7055	1.211	0.7441	1.216	0.7441
40.0	1.146	0.7750	1.150	0.7861	1.150	0.7752	1.150	0.7752

Table 4-11 Lift and Drag Characteristics of the Center Blade Region

	x=0.250		x=0.293		x=0.445		x=0.760	
α°	C_L	C_D	C_L	C_D	C_L	C_D	C_L	C_D
-40.0	-1.150	0.7747	-1.149	0.7749	-1.150	0.7746	-1.094	0.7760
-38.0	-0.926	0.7088	-1.058	0.7295	-1.079	0.7273	-0.964	0.7563
-36.0	-0.724	0.6487	-0.972	0.6846	-1.010	0.6812	-0.939	0.7305
-34.0	-0.565	0.6003	-0.898	0.6411	-0.946	0.6375	-0.938	0.6927
-32.0	-0.470	0.5693	-0.840	0.5995	-0.888	0.5974	-0.906	0.6368
-30.0	-0.461	0.5616	-0.806	0.5605	-0.838	0.5620	-0.838	0.5568
-28.0	-0.560	0.5745	-0.801	0.5233	-0.798	0.5308	-0.761	0.4527
-26.0	-0.781	0.5719	-0.827	0.4820	-0.778	0.4961	-0.675	0.3481
-24.0	-0.991	0.5091	-0.882	0.4291	-0.811	0.4484	-0.595	0.2729
-22.0	-0.984	0.3414	-0.948	0.3613	-0.889	0.3805	-0.542	0.2454
-20.0	-0.861	0.1141	-0.990	0.2840	-0.872	0.2936	-0.471	0.2392
-18.0	-0.808	0.0846	-0.998	0.1840	-0.796	0.1906	-0.498	0.2091
-16.0	-0.906	0.0808	-0.991	0.0939	-0.698	0.0968	-0.789	0.1279
-14.0	-0.811	0.0650	-0.981	0.0808	-0.601	0.0637	-0.987	0.0679
-12.0	-0.980	0.0566	-0.950	0.0295	-0.528	0.0665	-0.927	0.0492
-10.0	-0.921	0.0578	-0.870	0.0174	-0.499	0.0587	-0.750	0.0283
-8.0	-0.626	0.0554	-0.730	0.0144	-0.466	0.0308	-0.523	0.0145
-6.0	-0.441	0.0446	-0.558	0.0121	-0.343	0.0144	-0.280	0.0126
-4.0	-0.364	0.0321	-0.366	0.0109	-0.154	0.0122	-0.034	0.0114
-2.0	-0.324	0.0252	-0.161	0.0103	0.012	0.0131	0.233	0.0098
0.	-0.237	0.0248	0.050	0.0140	0.157	0.0118	0.516	0.0105
2.0	-0.046	0.0265	0.263	0.0150	0.369	0.0114	0.788	0.0152
4.0	0.204	0.0280	0.482	0.0147	0.601	0.0118	1.032	0.0186
6.0	0.441	0.0275	0.672	0.0156	0.793	0.0108	1.236	0.0136
8.0	0.638	0.0238	0.791	0.0174	0.908	0.0110	1.389	0.0124
10.0	0.920	0.0177	0.889	0.0181	0.915	0.0359	1.479	0.0836
12.0	0.985	0.0231	0.795	0.0345	0.865	0.0628	1.515	0.0806
14.0	0.806	0.0523	0.762	0.0541	0.866	0.0549	1.521	0.0989
16.0	0.912	0.0964	0.786	0.0687	0.932	0.1175	1.527	0.1448
18.0	0.807	0.1349	0.834	0.0790	1.040	0.2387	1.537	0.2100
20.0	0.859	0.1331	0.916	0.0970	1.157	0.3040	1.538	0.2863
22.0	0.986	0.1480	0.983	0.1363	1.250	0.3695	1.532	0.3657
24.0	0.993	0.2099	0.931	0.1810	1.285	0.4302	1.506	0.4399
26.0	0.781	0.3062	0.720	0.2191	1.229	0.4894	1.416	0.5027
28.0	0.558	0.4459	0.725	0.3655	1.092	0.5471	1.226	0.5550
30.0	0.458	0.5996	0.993	0.5983	1.012	0.5999	1.025	0.6000
32.0	0.466	0.7075	1.200	0.7615	0.986	0.6450	0.914	0.6403
34.0	0.561	0.7669	1.290	0.8396	0.996	0.6835	0.892	0.6770
36.0	0.722	0.7898	1.292	0.8537	1.032	0.7168	0.939	0.7112
38.0	0.925	0.7886	1.236	0.8253	1.087	0.7468	1.031	0.7435
40.0	1.150	0.7752	1.151	0.7755	1.150	0.7751	1.146	0.7750

Table 4-12. Lift and Drag Characteristics of the Inboard Blade

α°	x=0.10		x=0.15		x=0.20		x=0.25	
	C_L	C_D	C_L	C_D	C_L	C_D	C_L	C_D
-40.0	-1.146	0.7744	-1.146	0.7744	-1.150	0.7754	-1.150	0.7747
-38.0	-1.097	0.7048	-1.097	0.7048	-0.926	0.7439	-0.926	0.7088
-36.0	-1.053	0.6421	-1.053	0.6421	-0.724	0.7095	-0.724	0.6487
-34.0	-1.018	0.5931	-1.018	0.5931	-0.565	0.6693	-0.565	0.6003
-32.0	-0.998	0.5647	-0.998	0.5647	-0.470	0.6204	-0.470	0.5693
-30.0	-0.996	0.5638	-0.996	0.5638	-0.461	0.5598	-0.461	0.5616
-28.0	-1.011	0.5840	-1.011	0.5840	-0.560	0.4852	-0.560	0.5745
-26.0	-1.038	0.5660	-1.038	0.5660	-0.781	0.3967	-0.781	0.5719
-24.0	-1.050	0.4371	-1.050	0.4371	-0.991	0.2948	-0.991	0.5091
-22.0	-1.022	0.1979	-1.022	0.1979	-0.984	0.1802	-0.984	0.3414
-20.0	-0.955	0.0828	-0.955	0.0828	-0.861	0.0948	-0.861	0.1141
-18.0	-0.865	0.0859	-0.865	0.0859	-0.808	0.0865	-0.808	0.0846
-16.0	-0.773	0.0808	-0.773	0.0808	-0.906	0.0791	-0.906	0.0808
-14.0	-0.691	0.0651	-0.691	0.0651	-0.811	0.0656	-0.811	0.0650
-12.0	-0.619	0.0567	-0.619	0.0567	-0.980	0.0568	-0.980	0.0566
-10.0	-0.555	0.0576	-0.555	0.0576	-0.921	0.0577	-0.921	0.0578
-8.0	-0.502	0.0557	-0.502	0.0557	-0.626	0.0553	-0.626	0.0554
-6.0	-0.446	0.0458	-0.446	0.0458	-0.441	0.0446	-0.441	0.0446
-4.0	-0.356	0.0331	-0.356	0.0331	-0.364	0.0322	-0.364	0.0321
-2.0	-0.204	0.0235	-0.204	0.0235	-0.324	0.0252	-0.324	0.0252
0.	0.001	0.0201	0.001	0.0201	-0.237	0.0248	-0.237	0.0248
2.0	0.205	0.0233	0.205	0.0233	-0.046	0.0265	-0.046	0.0265
4.0	0.357	0.0335	0.357	0.0335	0.204	0.0280	0.204	0.0280
6.0	0.444	0.0471	0.444	0.0471	0.441	0.0275	0.441	0.0275
8.0	0.500	0.0569	0.500	0.0569	0.638	0.0238	0.638	0.0238
10.0	0.555	0.0562	0.555	0.0562	0.920	0.0177	0.920	0.0177
12.0	0.620	0.0566	0.620	0.0566	0.985	0.0232	0.985	0.0231
14.0	0.690	0.0723	0.690	0.0723	0.806	0.0523	0.806	0.0523
16.0	0.771	0.0615	0.771	0.0615	0.912	0.0964	0.912	0.0964
18.0	0.863	0.0897	0.863	0.0897	0.807	0.1348	0.807	0.1349
20.0	0.956	0.2492	0.956	0.2492	0.859	0.1332	0.859	0.1331
22.0	1.029	0.3506	1.029	0.3506	0.986	0.1480	0.986	0.1480
24.0	1.059	0.4497	1.059	0.4497	0.993	0.2099	0.993	0.2099
26.0	1.038	0.5229	1.038	0.5229	0.781	0.3064	0.781	0.3062
28.0	1.002	0.5679	1.002	0.5679	0.558	0.4460	0.558	0.4459
30.0	0.987	0.6001	0.987	0.6001	0.458	0.5993	0.458	0.5996
32.0	0.994	0.6321	0.994	0.6321	0.466	0.7068	0.466	0.7075
34.0	1.019	0.6661	1.019	0.6661	0.561	0.7662	0.561	0.7669
36.0	1.055	0.7016	1.055	0.7016	0.722	0.7893	0.722	0.7898
38.0	1.100	0.7380	1.100	0.7380	0.925	0.7883	0.925	0.7886
40.0	1.149	0.7750	1.149	0.7750	1.150	0.7753	1.150	0.7752

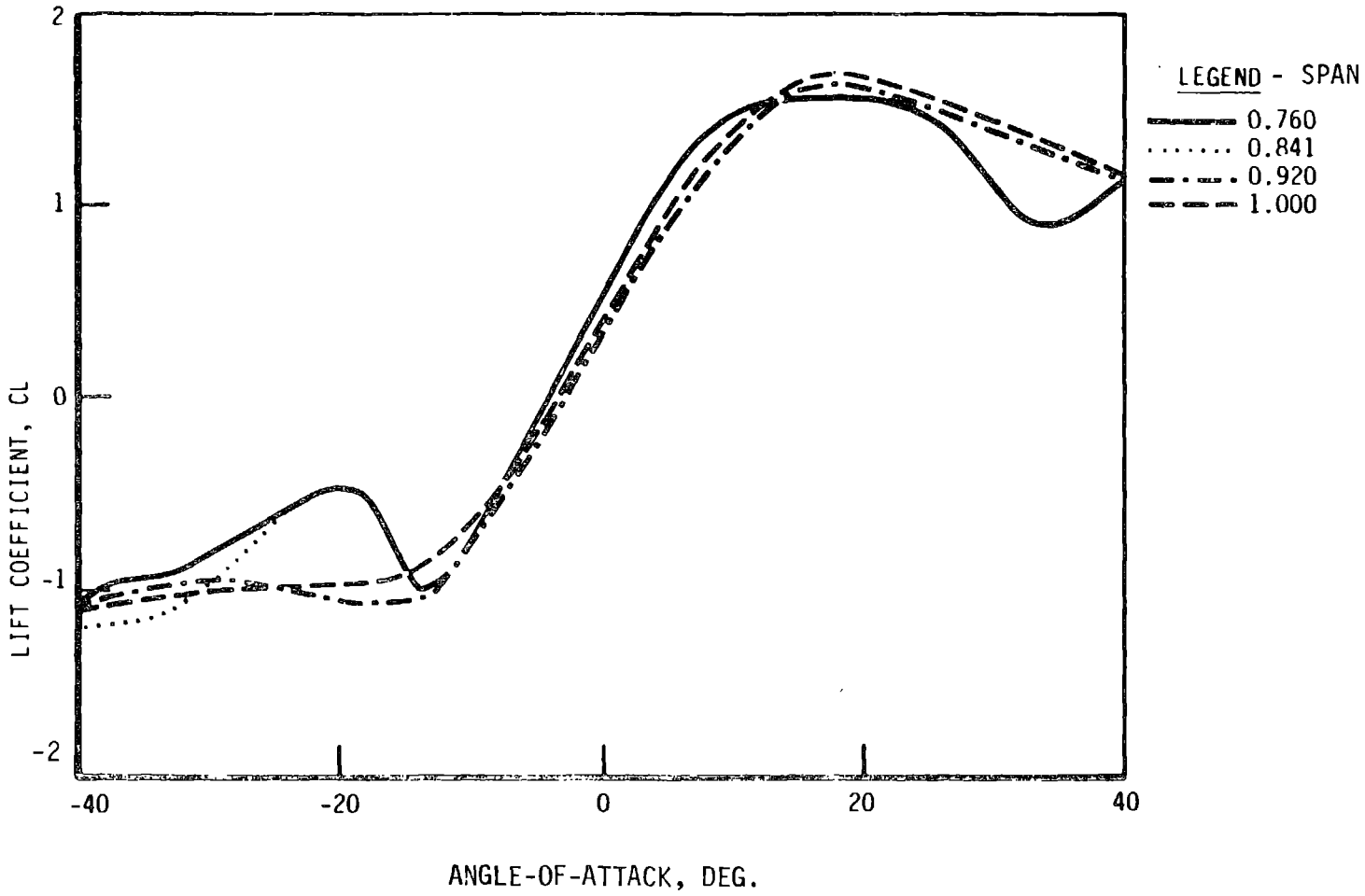

Figure 4-21. Outer Region Lift Characteristics

(Leading Edge Tripped, Reynolds No. = 4 Million)

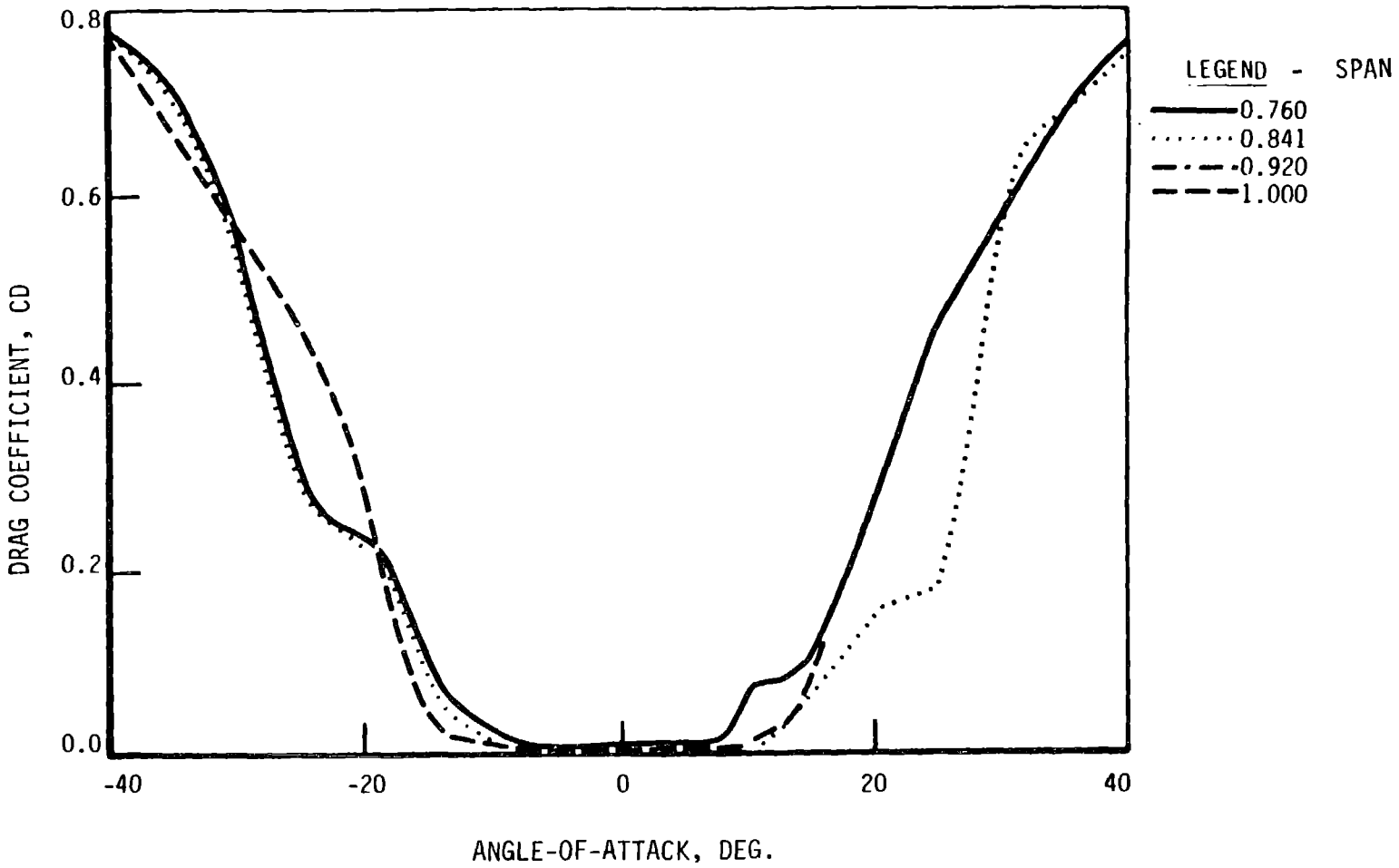

Figure 4-22. Outer Region Drag Characteristics
(Leading Edge Tripped, Reynolds No. = 4 Million)

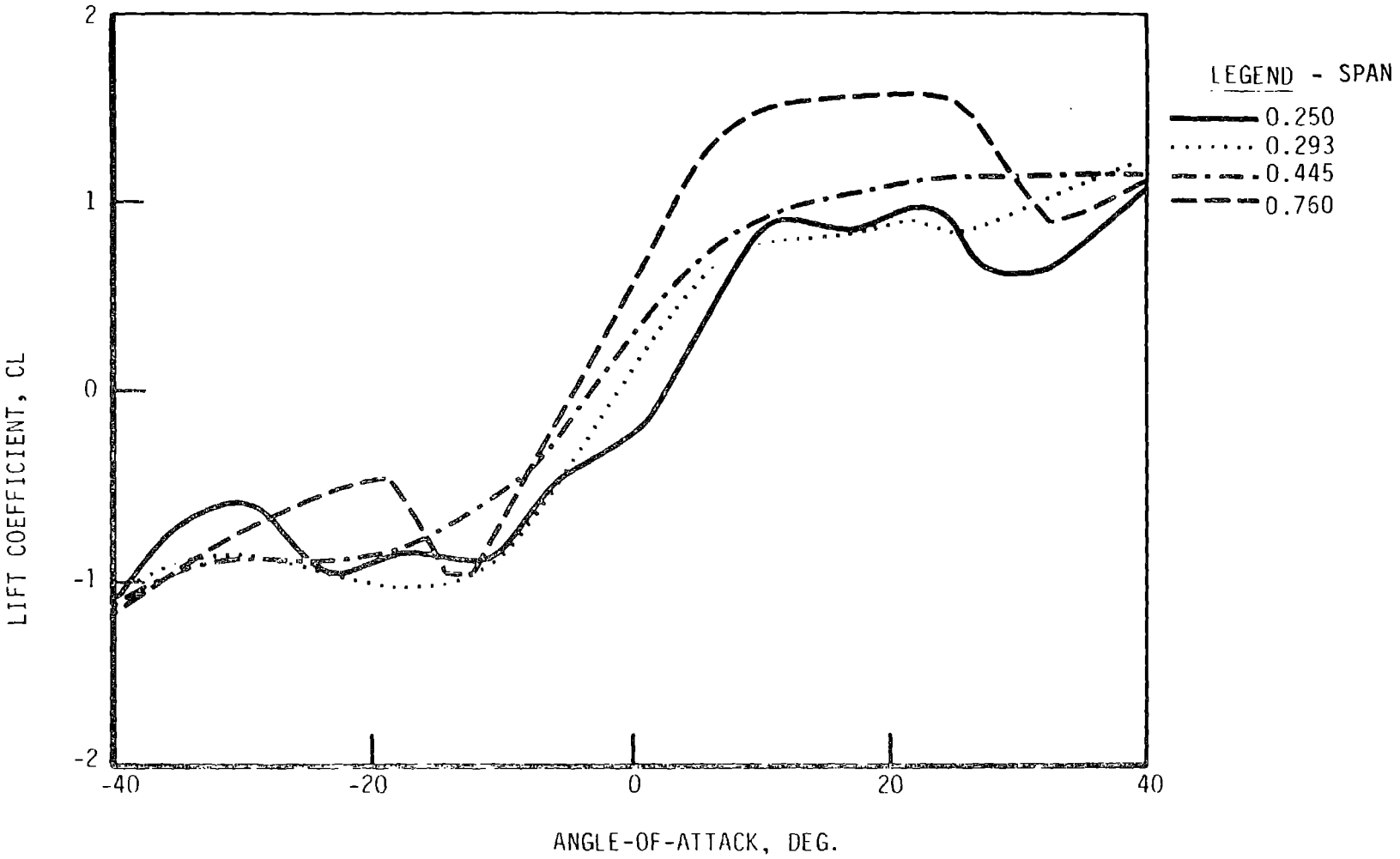

Figure 4-23. Center Region Lift Characteristics

(Leading Edge Tripped, Reynolds No. = 4 Million)

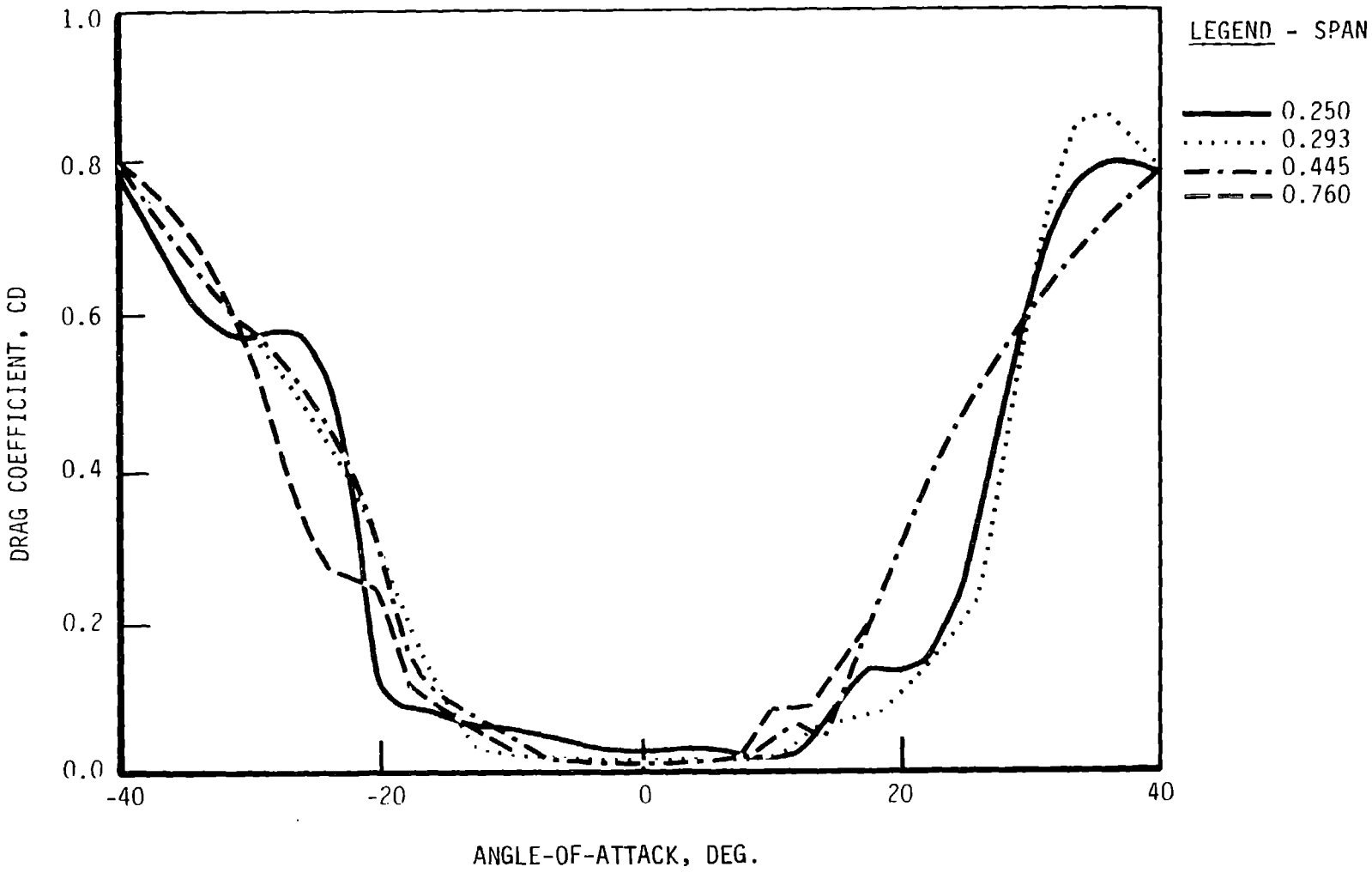

Figure 4-24. Center Region Drag Characteristics
(Leading Edge Tripped, Reynolds No. = 4 Million)

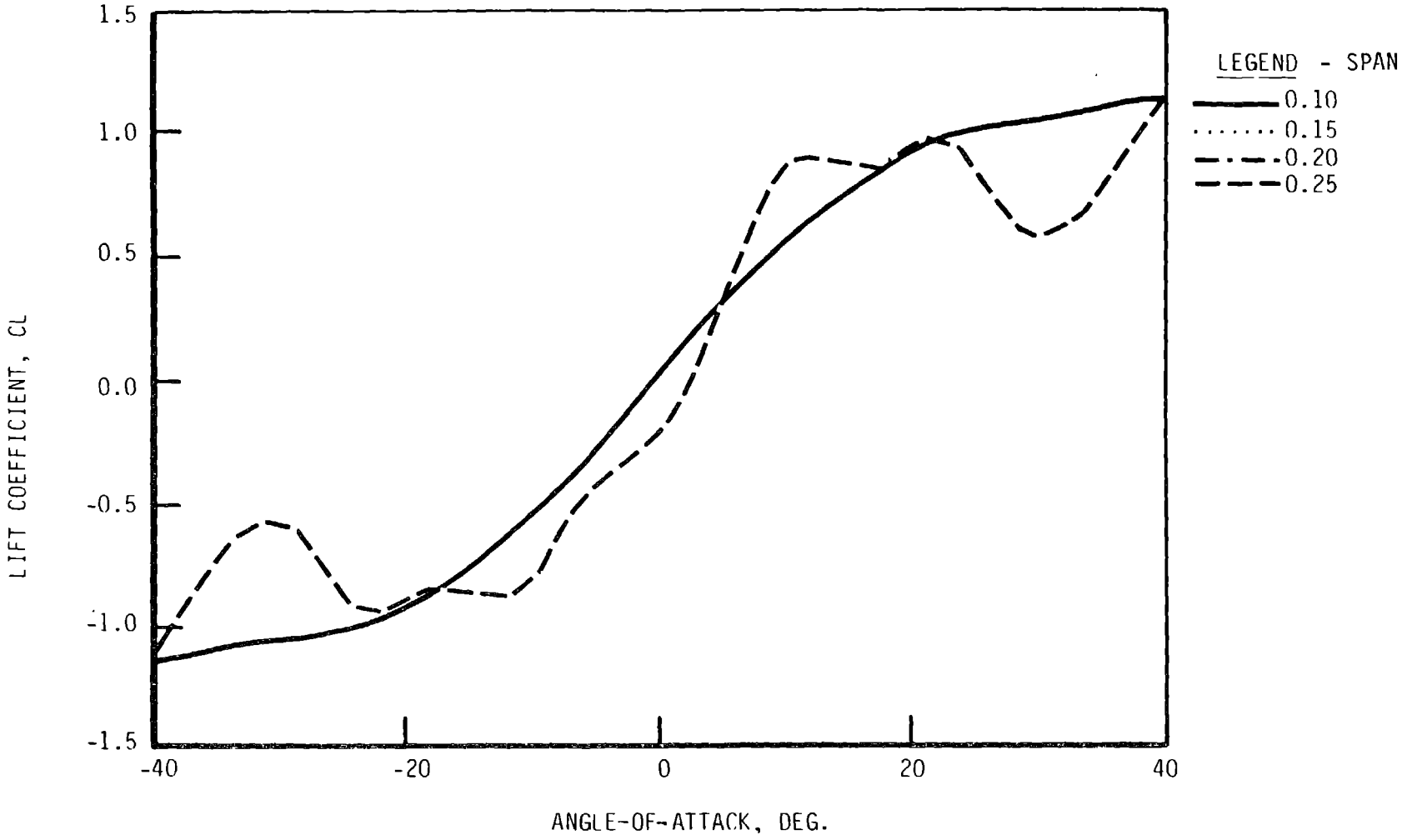

Figure 4-25. Inner Region Lift Characteristics
(Leading Edge Tripped, Reynolds No. = 4 Million)

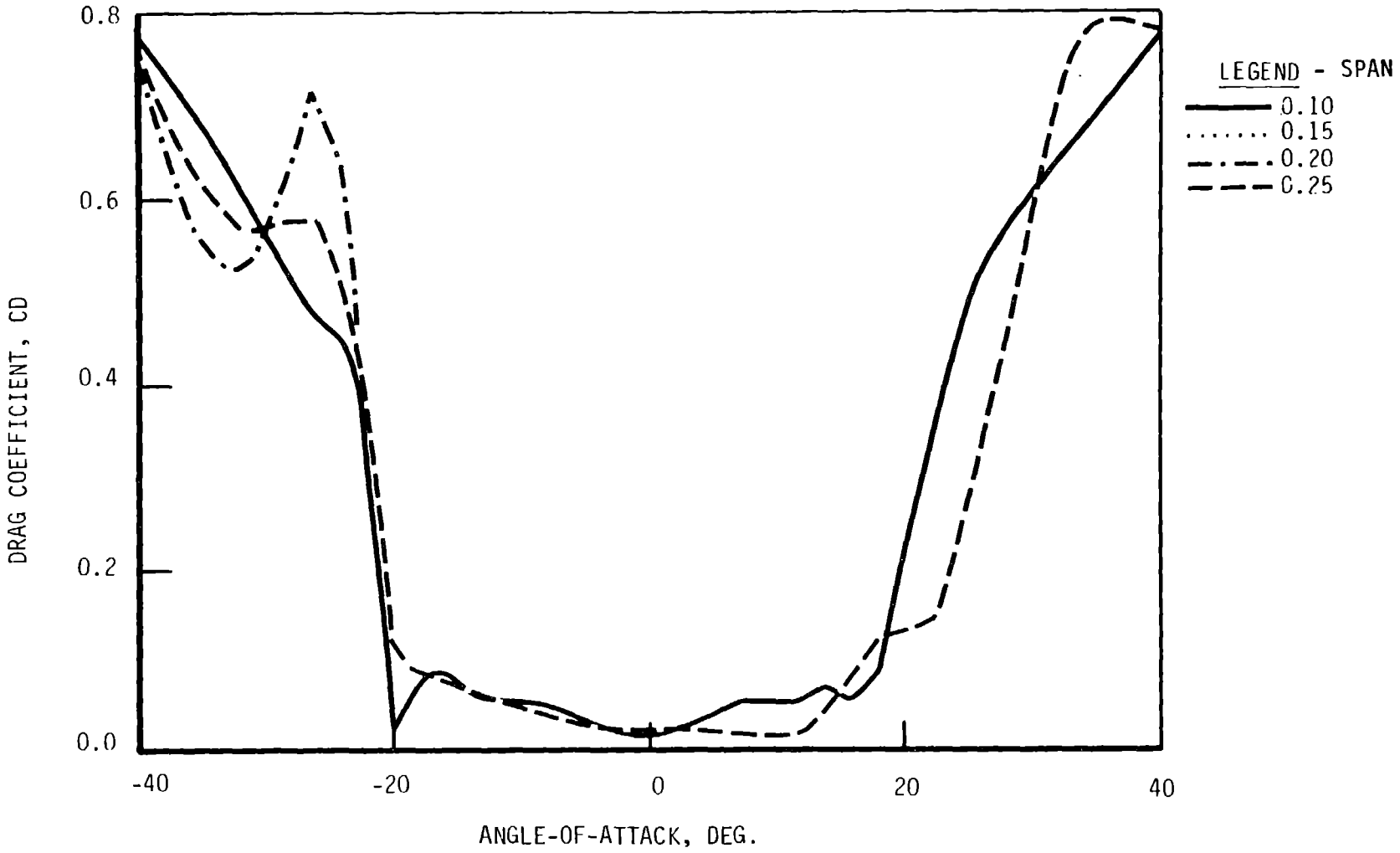

Figure 4-26. Inner Region Drag Characteristics

(Leading Edge Tripped, Reynolds No. = 4 Million)

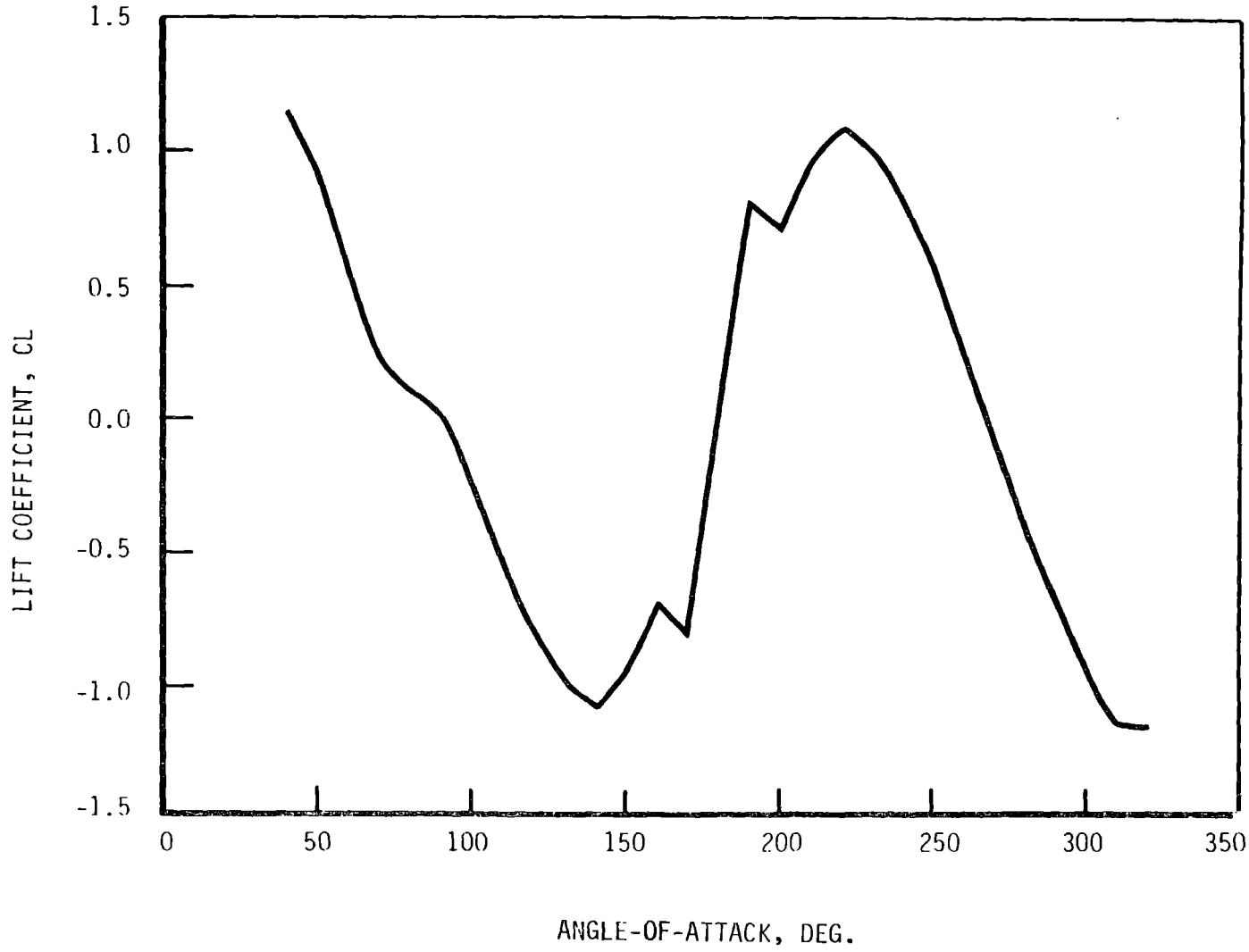

Figure 4-27. Common Region Lift Characteristics
(Leading Edge Tripped, Reynolds No. = 4 Million)

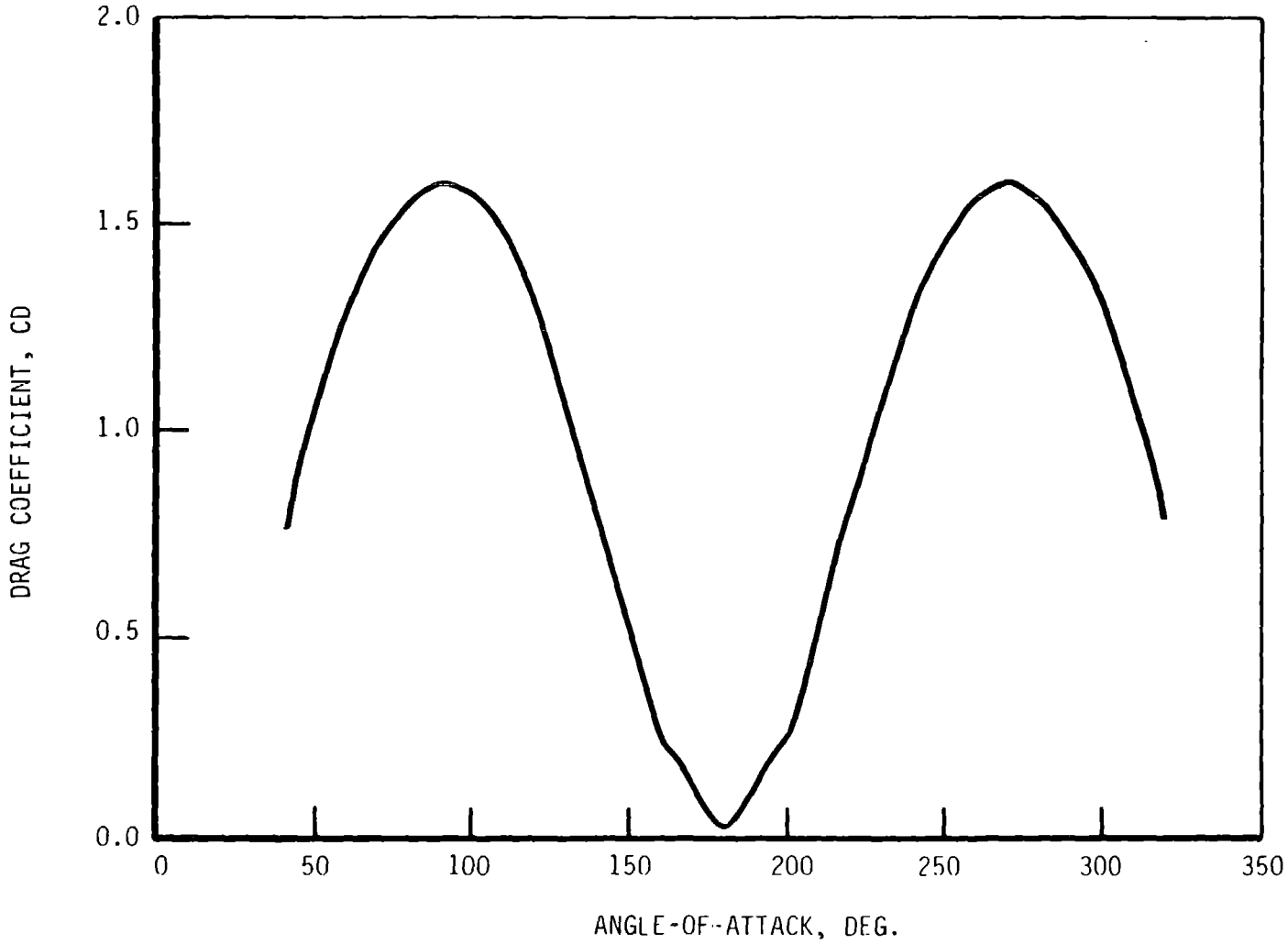

Figure 4-28. Common Region Drag Characteristics
(Leading Edge Tripped, Reynolds No. = 4 Million)

4.2.1.2 Blade Configuration

The blade configuration shown in Table 4-9 and Figures 4-12 through 4-14 is the result of a series of trade-offs between the desired shape, the required structure, the manufacturing limitations associated with laminated wood, and the shipping and assembly constraints. The goal of these trade-offs was to achieve the most cost-effective blade shape for the 400-ft. rotor.

The previous section discussed the aerodynamics of the blade. This section will relate that discussion to the blade shape and will describe other influences on the blade shape.

The limitations imposed by the material was a major consideration in establishing the blade geometry. Some of these considerations were established during previous work with wooden blades and others, such as the blade twist and the center section transitions, were developed during the MOD-5A program. Note that very complex surfaces have been developed from laminated wood. Boat hulls, with rapid section changes and recurving areas, are an excellent example of the sophisticated shapes that are possible with wood. Such shapes are achieved by painstakingly scribing and trimming each of the sub-elements of the shape to ensure conformance. This technique requires that every piece of veneer used in the blade be trimmed precisely, which would be extremely expensive. This fact prompted a blade shape that could be achieved within the geometrical limits imposed by the use of uniformly trimmed veneer panels, laid in a female mould. These transition limits closely approximate the type of transition that can be achieved with plywood. This concept became GE's basic approach to blade formation and transition.

The blade consists of a primary and a secondary structure within the airfoil envelope. The primary structure extends from the leading edge, 0% chord, to the rear spar, 60% chord. It provides the blade with spanwise strength and stiffness. The secondary structure extends aft from the rear spar to the trailing edge, 100% chord. It receives the local air loads and transmits them to the primary structure for spanwise distribution. The portion of this secondary structure on the outer span, from 60% to 99% of the span, is hinged at the upper surface of the rear spar, providing ailerons for rotor torque control. From 25% to 60% of span the secondary structure has the configur-

ation of an airfoil, and is rigidly mounted to the rear spar. From 10% to 25% of the span, the trailing edge has a modified airfoil shape compatible with the overall blade structural transition. The trailing edge ends with a diagonal taper between 100% and 60% of the chord, and between 10% and 5% of the span. From 60% to 100% of span, the trailing edge is an integral part of the aileron surfaces.

Construction methods limited the structural twist to 5° from the center of rotation to 25% of the span. However, the airfoil base lift coefficient, at an angle of attack of 0°, increases from 0.0 at 25% of the span, to 0.6 at 60% of the span and beyond. This aerodynamic effect reduces the structural twist the blade requires to operate efficiently.

As the leading edge of one blade becomes the rear spar of the other, the center blade, which is primary structure, must twist a total of 10°. The outer surface must change from a symmetrical airfoil at 25% of the span to a rectangular cross-section at the center of rotation, as shown in Section 4.3.

Initial geometrical calculations, and the subcontractor's experience indicated that these transitions could be achieved. A quarter scale model was built to verify the geometry and the relationships. It clearly demonstrated that both the 10° of total twist and the reversed airfoil development could be achieved within the established cost base.

The location of field joints at the 25% of span points were the result of two considerations -- the inboard extent of the true airfoil, and shipment size. Aerodynamically, the inboard quarter of the blade contributed little torque but could be responsible for significant losses. The quarter span, true airfoil termination, was augmented by a trailing edge geometry modification, keep these losses within reasonable limits and maintained the maximum shipping dimension to a length of 100 ft. The trailing edge modification consisted of lifting the low pressure surface of the airfoil, to thicken the trailing edge from 38% of the span and inboard.

This aerodynamic enhancement created another blade surface transition at 38% of the span, where the normal airfoil contour was blended to the increasing thickness of the trailing edge. Numeric and lofting evaluations established a curvature that could be accomplished without veneer trimming. The increased thickness of the aft half of airfoil also increased the modulus of the inboard portion of the blade, a desired effect.

The final blade design, sizing, arrangement, functional features and interfaces are discussed in detail in Section 4.3. Studies that investigated the final configuration are also discussed in that section.

4.2.2 AILERON DESIGN DESCRIPTION

Aerodynamic controls on the wind turbine limit the loads experienced by the system's components, and provide a means for shutting down the system. The controls may also contribute to increasing energy capture at wind speeds below the rated speed.

Details of the aileron subsystem are described in section 4.4 of Volume III. The ailerons are plain flaps, with the hinge line at 62% of the airfoil chord, and no overhang or balance. They extend from 60% to 99% of the span. The ailerons on both blades operate in the same direction, not differentially, as airplane wing ailerons do. The wind tunnel test program used in the development of these controls is documented in section 8.4.2 of Volume II. For the mechanical and geometrical characteristics and dimensions of the ailerons and aileron control system, see section 4.2.2.2.

4.2.2.1 Aileron Aerodynamics

4.2.2.1.1 Section Characteristics

The aerodynamic characteristics of the aileron section were derived from the wind tunnel tests described in section 8.4.1.1 of Volume II. The basic airfoil data ($\delta = 0$) was subtracted from the data obtained with the aileron deflected. From these tests, the incremental lift and drag caused by aileron deflection were deduced. The lift coefficient increments are shown in Table 4-13, and the drag coefficient increments are shown in Table 4-14. Graphs of these control functions, interpolated to include points at every 2° of control angle, are illustrated in Figures 4-29 through 4-36.

Table 4-13 Incremental Lift Coefficient of the MOD-5A Aileron as a Function of Angle of Attach and Aileron Deflection

ALPHA/DELTA	0.	5.	10.	15.	20.	25.	30.	35.	40.	45.
0.	0.	-0.340	-0.740	-1.120	-1.310	-1.450	-1.580	-1.890	-2.250	-2.500
6.	0.	-0.340	-0.740	-1.120	-1.310	-1.450	-1.580	-1.890	-2.250	-2.500
9.	0.	-0.450	-0.700	-1.040	-1.240	-1.370	-1.470	-1.650	-1.930	-2.230
12.	0.	-0.400	-0.520	-0.770	-0.930	-1.060	-1.210	-1.360	-1.580	-1.840
15.	0.	-0.300	-0.400	-0.560	-0.720	-0.820	-0.880	-1.010	-1.160	-1.350
18.	0.	-0.250	-0.370	-0.480	-0.540	-0.590	-0.630	-0.690	-0.770	-0.890
21.	0.	-0.190	-0.290	-0.370	-0.400	-0.420	-0.450	-0.490	-0.540	-0.630
24.	0.	-0.110	-0.180	-0.280	-0.310	-0.320	-0.330	-0.360	-0.390	-0.460
27.	0.	-0.050	-0.100	-0.200	-0.215	-0.230	-0.240	-0.250	-0.270	-0.320
30.	0.	-0.030	-0.070	-0.140	-0.155	-0.175	-0.180	-0.180	-0.200	-0.230
33.	0.	-0.010	-0.050	-0.085	-0.100	-0.110	-0.120	-0.125	-0.125	-0.120
36.	0.	-0.005	-0.030	-0.045	-0.055	-0.060	-0.065	-0.066	-0.068	-0.070
40.	0.	-0.121	-0.248	-0.350	-0.317	-0.258	-0.211	-0.159	-0.108	-0.063
45.	0.	-0.086	-0.172	-0.250	-0.227	-0.198	-0.174	-0.151	-0.126	-0.102
50.	0.	-0.052	-0.100	-0.150	-0.151	-0.140	-0.138	-0.135	-0.132	-0.129
90.	0.	-0.052	-0.100	-0.150	-0.151	-0.140	-0.138	-0.135	-0.132	-0.129

	50.	55.	60.	65.	70.	75.	80.	85.	90.
0.	-2.620	-2.710	-2.760	-2.790	-2.840	-2.880	-2.890	-2.910	-2.920
6.	-2.620	-2.710	-2.760	-2.790	-2.840	-2.880	-2.890	-2.910	-2.920
9.	-2.440	-2.600	-2.710	-2.790	-2.850	-2.910	-2.930	-2.950	-2.970
12.	-2.080	-2.290	-2.450	-2.630	-2.730	-2.830	-2.850	-2.860	-2.880
15.	-1.580	-1.840	-2.130	-2.370	-2.510	-2.640	-2.660	-2.680	-2.700
18.	-1.050	-1.270	-1.560	-1.930	-2.210	-2.480	-2.500	-2.530	-2.550
21.	-0.800	-1.030	-1.320	-1.730	-1.990	-2.250	-2.280	-2.300	-2.330
24.	-0.610	-0.800	-1.070	-1.410	-1.690	-1.970	-2.000	-2.040	-2.070
27.	-0.440	-0.625	-0.870	-1.100	-1.300	-1.440	-1.580	-1.681	-1.760
30.	-0.265	-0.310	-0.381	-0.445	-0.530	-0.740	-0.785	-0.940	-1.260
33.	-0.135	-0.140	-0.165	-0.200	-0.245	-0.300	-0.365	-0.450	-0.700
36.	-0.075	-0.080	-0.105	-0.115	-0.160	-0.200	-0.260	-0.400	-0.500
40.	-0.015	0.033	0.080	0.104	0.129	0.157	0.181	0.206	0.230
45.	-0.077	0.	0.055	-0.030	0.001	0.031	0.061	0.087	0.118
50.	-0.125	-0.123	-0.119	-0.095	-0.046	0.	0.025	0.006	0.037
90.	-0.125	-0.123	-0.119	-0.095	-0.046	-0.025	0.006	0.037	0.070

Table 4-14 Incremental Drag Coefficient of the MOD-5A Aileron as a Function of Angle of Attack and Aileron Deflection

ALPHA°/DELTA°	0.	5.	10.	15.	20.	25.	30.	35.	40.	45.
0.	0.	0.	0.005	0.002	0.005	0.079	0.112	0.154	0.196	0.238
6.	0.	0.	0.005	0.002	0.025	0.079	0.112	0.154	0.196	0.238
9.	0.	0.003	0.	0.006	0.035	0.062	0.085	0.132	0.174	0.213
12.	0.	0.040	0.017	0.009	0.030	0.054	0.080	0.116	0.157	0.198
15.	0.	0.025	-0.020	-0.045	-0.018	0.008	0.035	0.069	0.102	0.138
18.	0.	0.015	-0.030	-0.065	-0.043	-0.029	-0.010	0.015	0.048	0.070
21.	0.	0.025	-0.030	-0.065	-0.095	-0.095	-0.077	-0.052	-0.025	0.
24.	0.	0.025	-0.030	-0.065	-0.098	-0.125	-0.162	-0.200	-0.227	-0.257
27.	0.	0.025	-0.030	-0.065	-0.098	-0.125	-0.162	-0.200	-0.267	-0.265
30.	0.	-0.083	-0.182	-0.270	-0.346	-0.419	-0.472	-0.512	-0.538	-0.550
33.	0.	-0.115	-0.228	-0.329	-0.422	-0.491	-0.546	-0.586	-0.614	-0.620
36.	0.	-0.146	-0.288	-0.410	-0.507	-0.585	-0.640	-0.672	-0.696	-0.697
40.	0.	-0.192	-0.370	-0.510	-0.618	-0.700	-0.752	-0.789	-0.801	-0.795
45.	0.	-0.227	-0.420	-0.540	-0.655	-0.720	-0.775	-0.810	-0.860	-0.860
50.	0.	-0.235	-0.435	-0.540	-0.660	-0.745	-0.785	-0.825	-0.870	-0.879
55.	0.	-0.225	-0.415	-0.520	-0.640	-0.720	-0.775	-0.820	-0.860	-0.860
60.	0.	-0.200	-0.370	-0.475	-0.595	-0.690	-0.745	-0.790	-0.820	-0.820
65.	0.	-0.167	-0.322	-0.400	-0.530	-0.625	-0.700	-0.745	-0.700	-0.700
70.	0.	-0.133	-0.260	-0.320	-0.460	-0.555	-0.620	-0.695	-0.560	-0.560
75.	0.	-0.100	-0.198	-0.240	-0.380	-0.460	-0.560	-0.620	-0.420	-0.420
80.	0.	-0.067	-0.145	-0.160	-0.270	-0.350	-0.430	-0.500	-0.280	-0.280
85.	0.	-0.033	-0.175	-0.160	-0.130	-0.210	-0.300	-0.350	-0.140	-0.140
90.	0.	0.	0.	0.	0.	0.	0.	0.	0.	0.

	50.	55.	60.	65.	70.	75.	80.	85.	90.
0.	0.280	0.322	0.365	0.405	0.443	0.490	0.597	0.700	0.810
6.	0.280	0.322	0.365	0.405	0.443	0.490	0.597	0.700	0.810
9.	0.255	0.297	0.338	0.379	0.420	0.464	0.562	0.671	0.775
12.	0.235	0.275	0.314	0.353	0.392	0.432	0.527	0.625	0.725
15.	0.174	0.210	0.245	0.281	0.317	0.353	0.440	0.530	0.625
18.	0.102	0.135	0.168	0.200	0.233	0.265	0.346	0.428	0.510
21.	0.030	0.056	0.080	0.106	0.135	0.160	0.220	0.292	0.375
24.	-0.270	-0.275	-0.265	-0.230	-0.180	-0.128	-0.070	0.	0.060
27.	-0.295	-0.335	-0.360	-0.370	-0.350	-0.320	-0.270	-0.210	-0.155
30.	-0.545	-0.530	-0.510	-0.485	-0.454	-0.417	-0.381	-0.352	-0.300
33.	-0.610	-0.592	-0.570	-0.543	-0.519	-0.490	-0.456	-0.422	-0.390
36.	-0.670	-0.645	-0.618	-0.593	-0.566	-0.540	-0.515	-0.488	-0.465
40.	-0.765	-0.738	-0.712	-0.685	-0.659	-0.632	-0.605	-0.577	-0.550
45.	-0.830	-0.780	-0.712	-0.688	-0.667	-0.646	-0.624	-0.602	-0.580
50.	-0.850	-0.820	-0.707	-0.691	-0.667	-0.646	-0.624	-0.602	-0.580
55.	-0.850	-0.820	-0.705	-0.694	-0.684	-0.673	-0.662	-0.651	-0.640
60.	-0.800	-0.780	-0.702	-0.697	-0.692	-0.686	-0.681	-0.675	-0.670
65.	-0.700	-0.700	-0.700	-0.700	-0.700	-0.700	-0.700	-0.700	-0.700
70.	-0.560	-0.560	-0.560	-0.560	-0.560	-0.560	-0.560	-0.560	-0.560
75.	-0.420	-0.420	-0.420	-0.420	-0.420	-0.420	-0.420	-0.420	-0.420
80.	-0.280	-0.280	-0.280	-0.280	-0.280	-0.280	-0.280	-0.280	-0.280
85.	-0.140	-0.140	-0.140	-0.140	-0.140	-0.140	-0.140	-0.140	-0.140
90.	0.	0.	0.	0.	0.	0.	0.	0.	0.

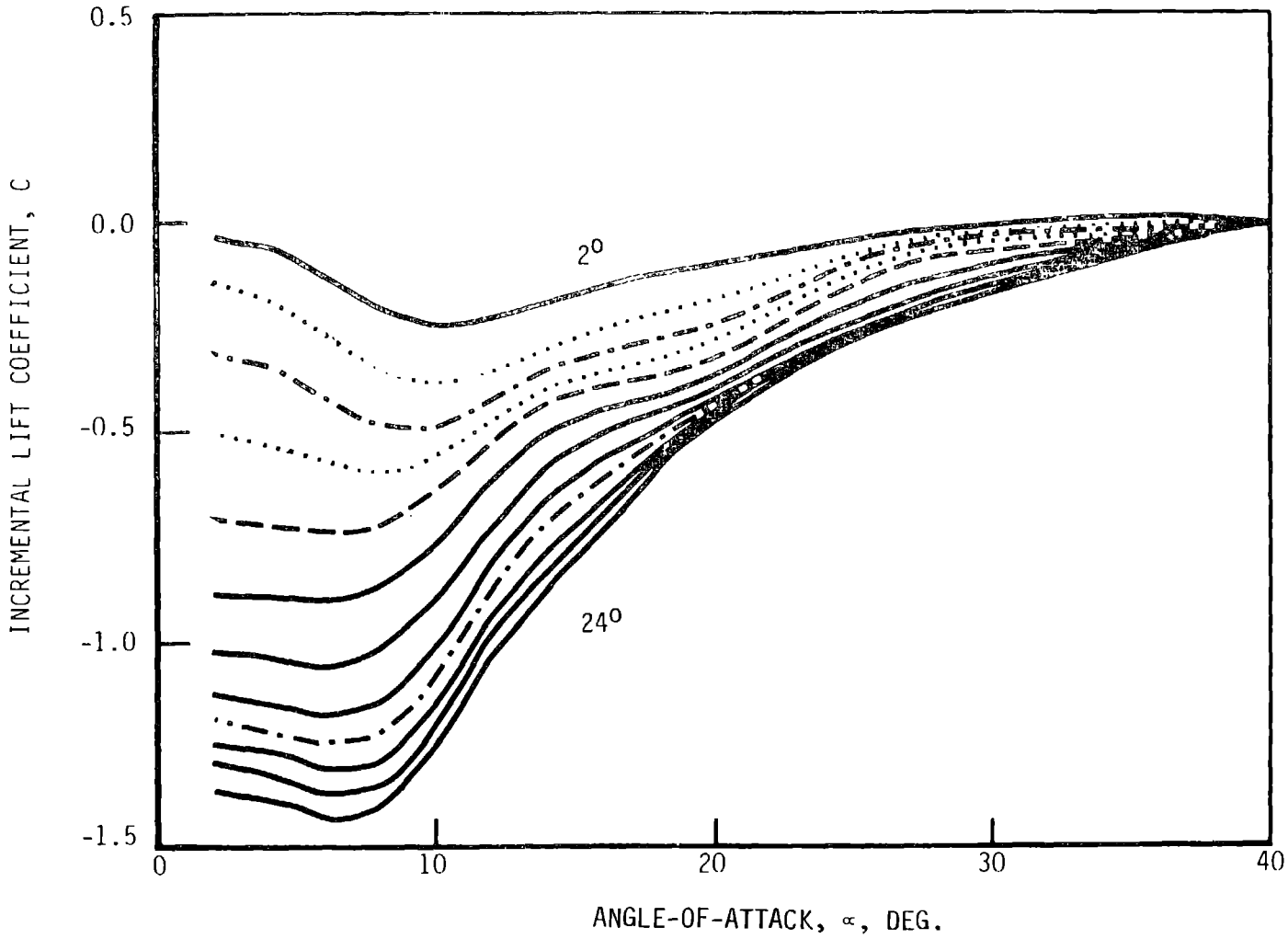

Figure 4-29. Aileron Lift - Control Angle Characteristics, 2 - 24°

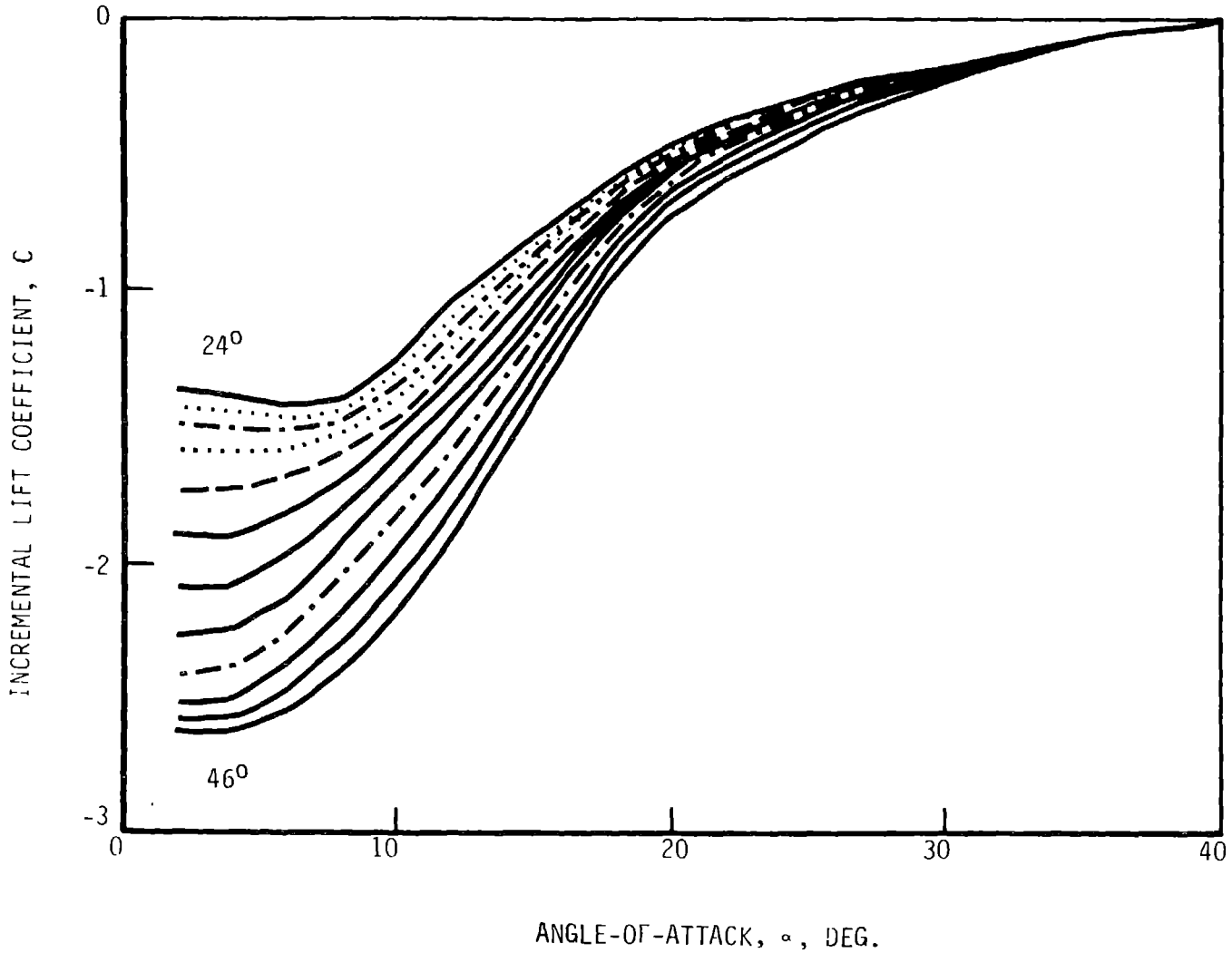

Figure 4-30. Aileron Lift - Control Angle Characteristics, 24-46°

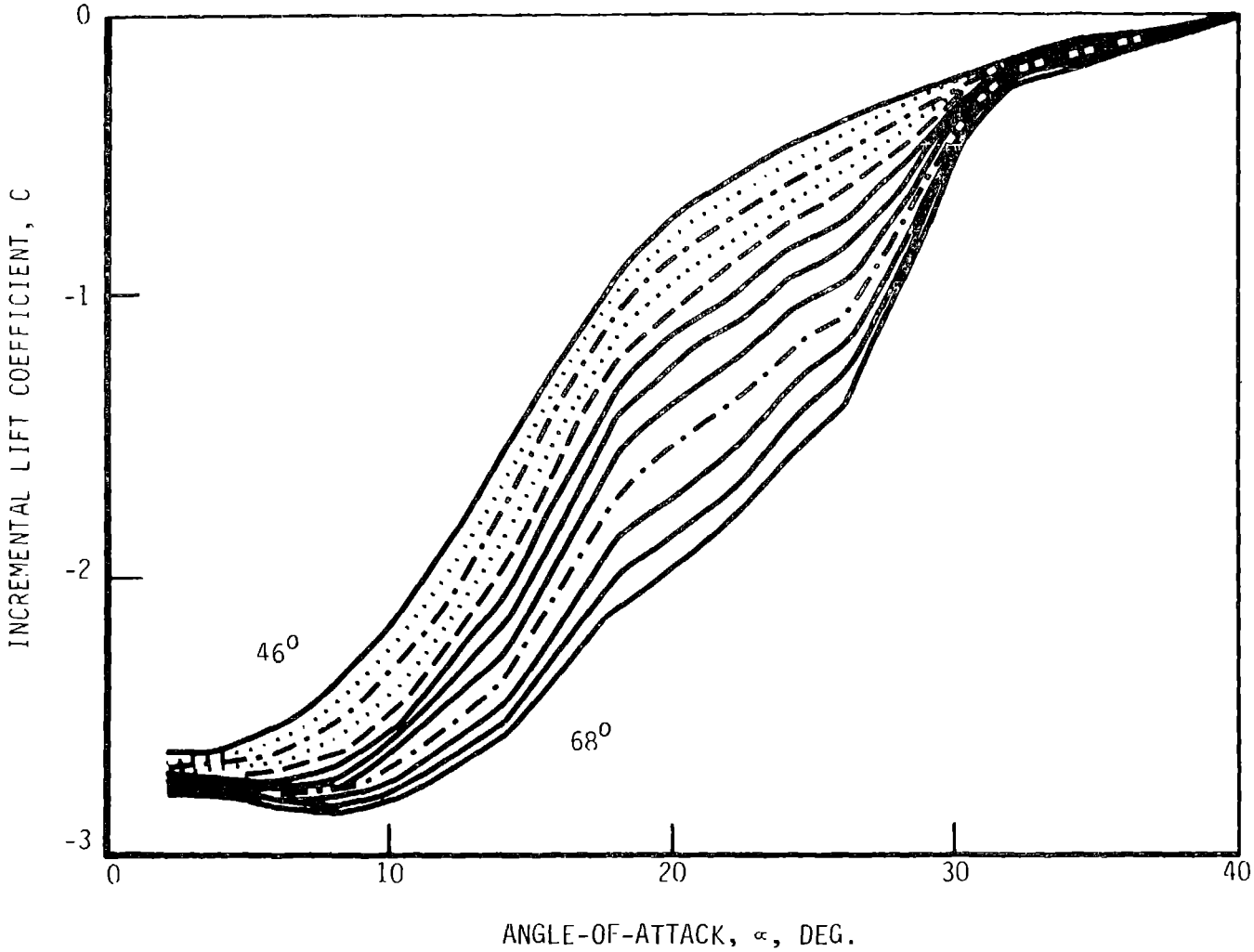

Figure 4-31. Aileron Lift - Control Angle Characteristics, 46-68°

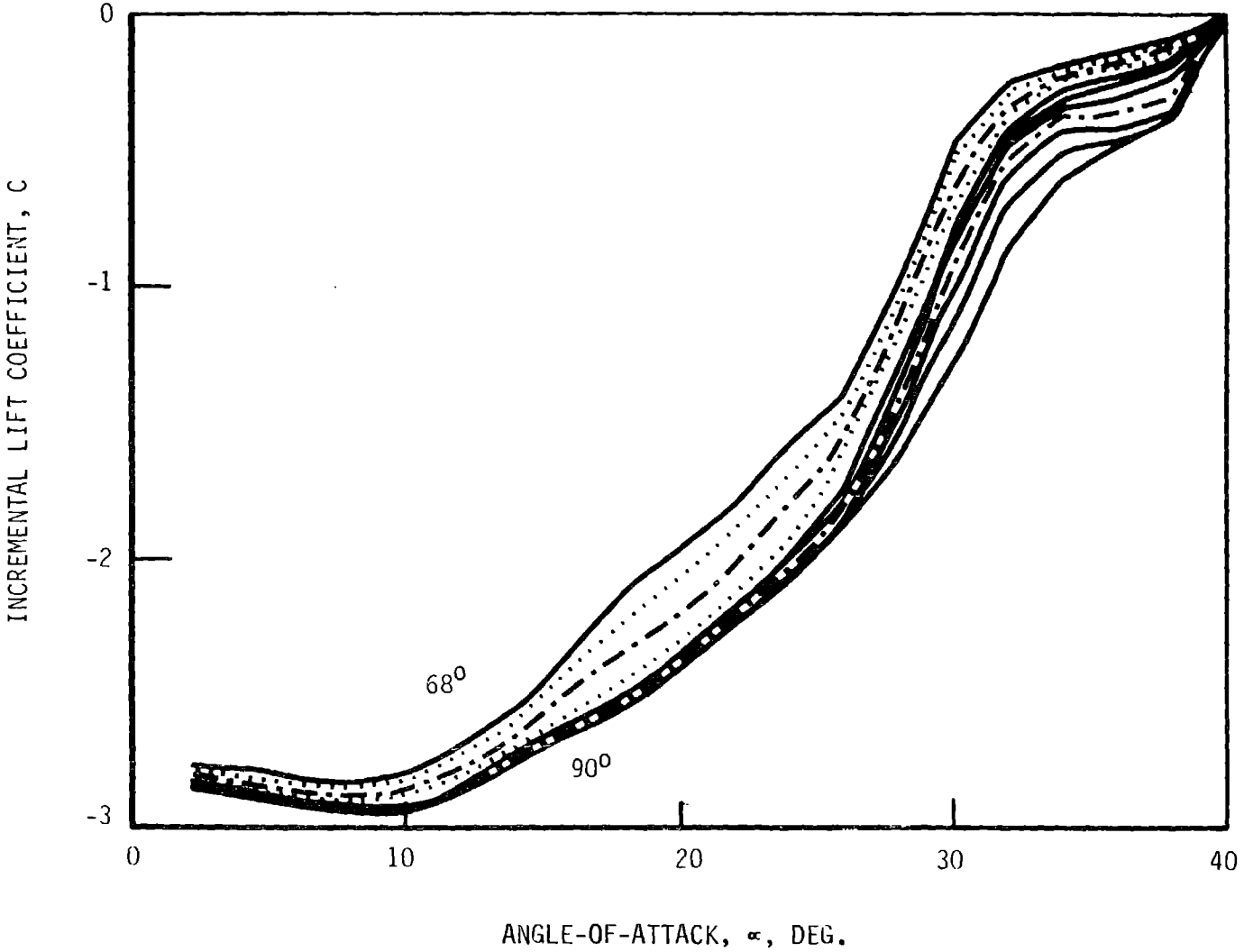

Figure 4-32. Aileron Lift - Control Angle Characteristics, 68-90°

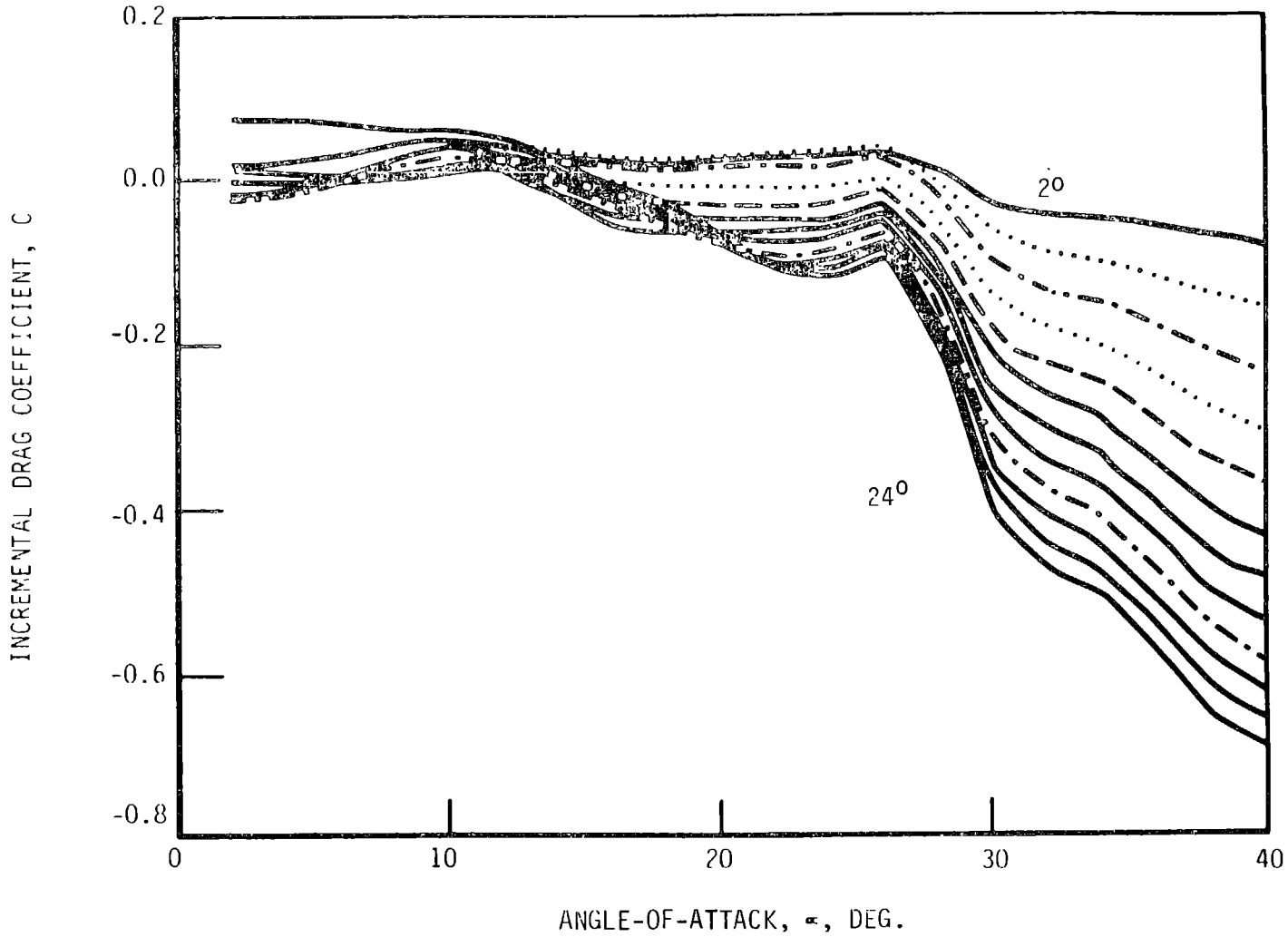

Figure 4-33. Aileron Drag - Control Angle Characteristics, 2-24°

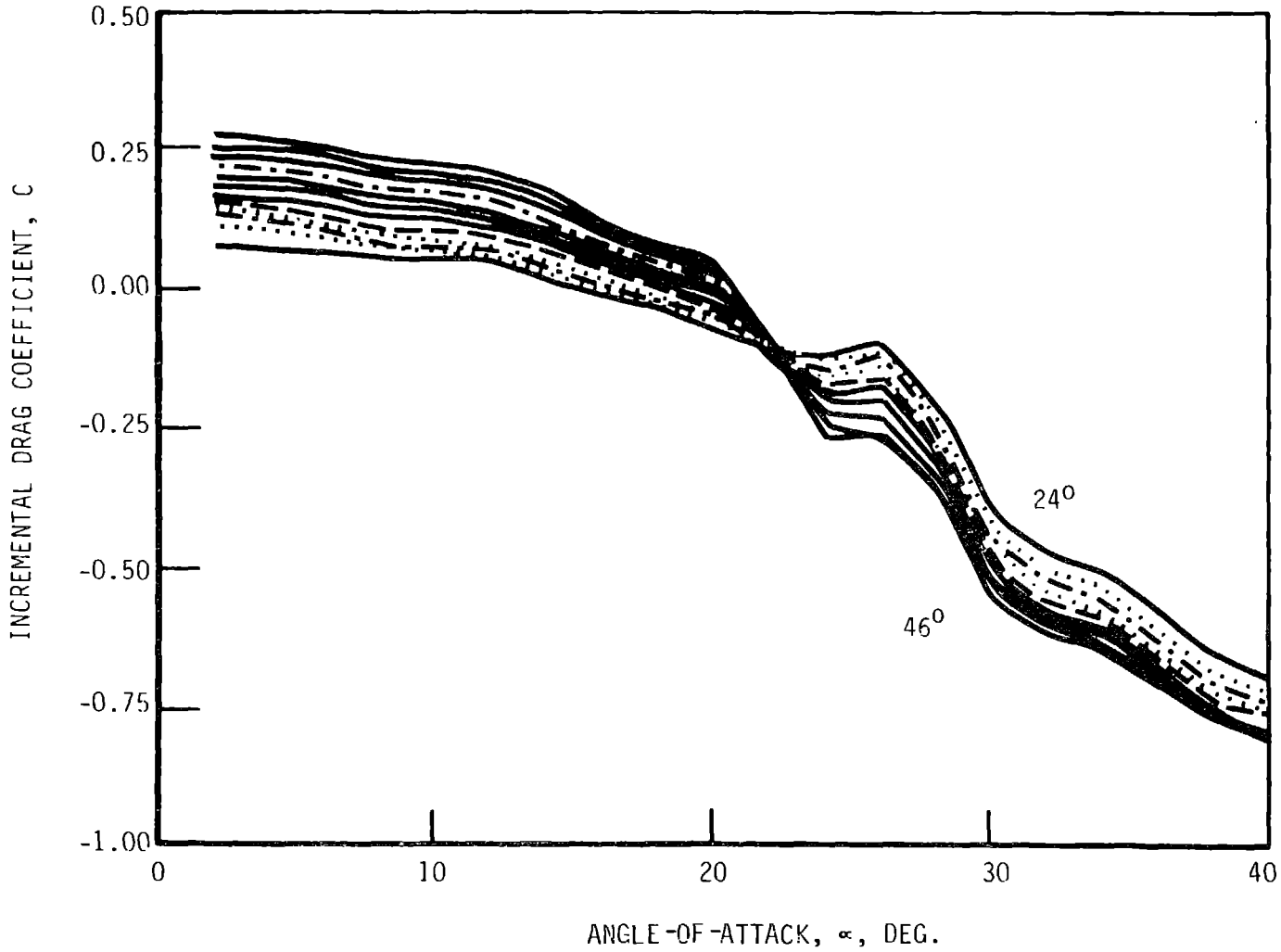

Figure 4-34. Aileron Drag - Control Angle Characteristics, 24-46°

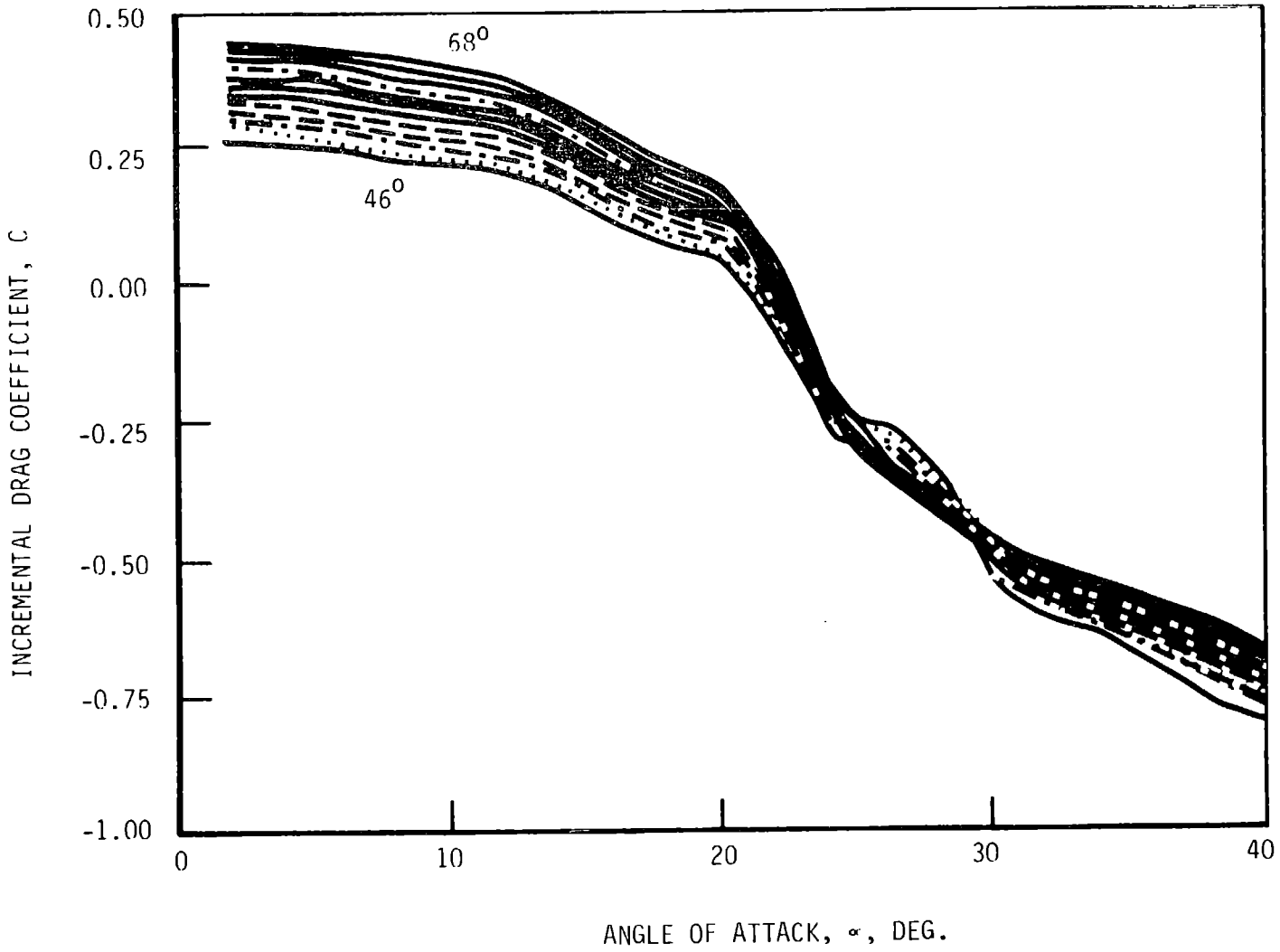

Figure 4-35. Aileron Drag - Control Angle Characteristics, 46-68°

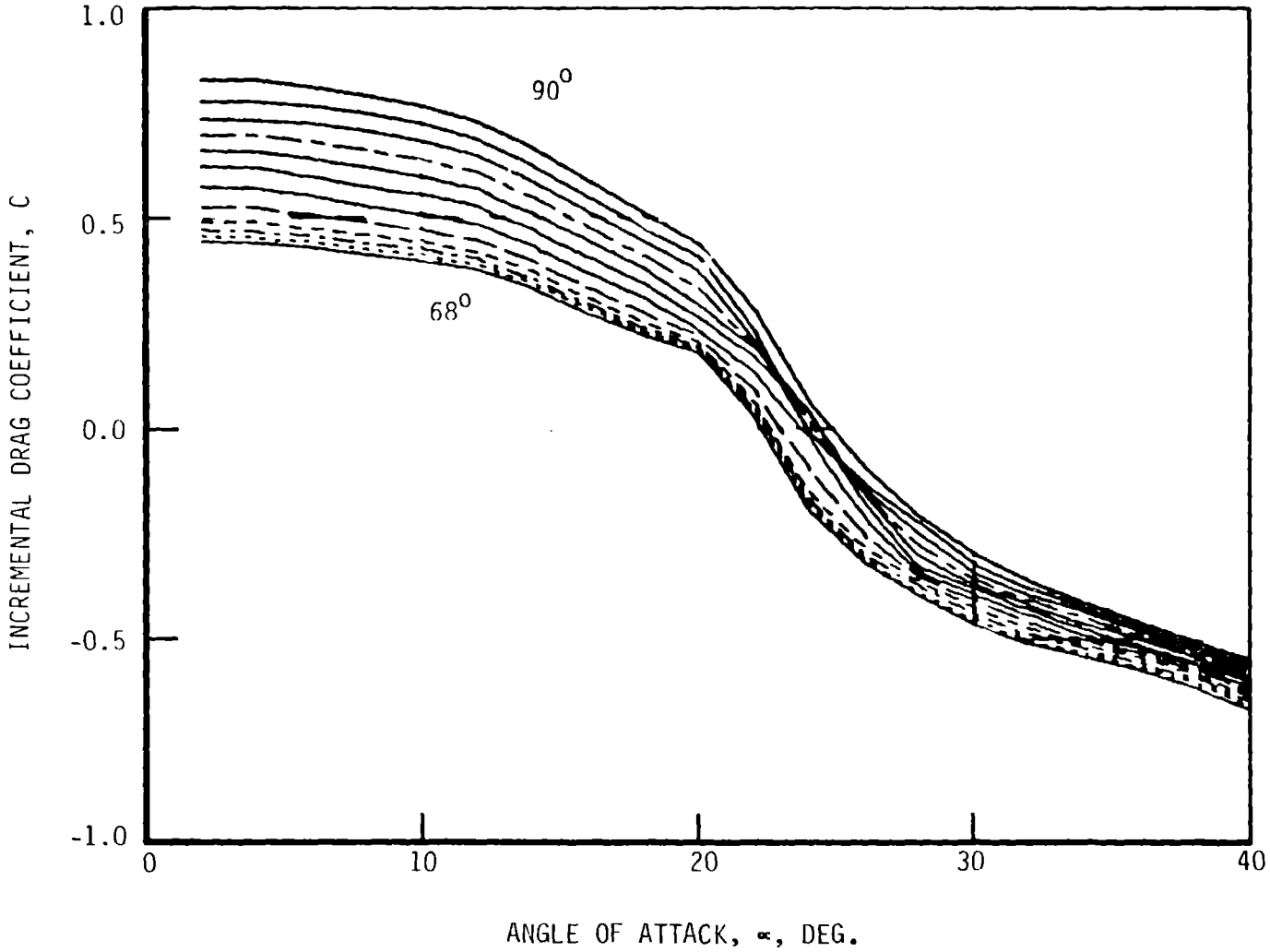

Figure 4-36. Aileron Drag - Control Angle Characteristics, 68-90°

4.2.2.1.2 Control Characteristics

The computer code AEOLUS was modified to include the effects of the deflected aileron. The estimated control characteristics of the MOD-5A, based on computations using this code, are presented in Figures 4-37 through 4-40. Tables 4-15 through 4-18 contain the same data in numerical form.

Figures 4-37 and 4-38 show that at very low wind speeds, a small deflection of the aileron increases rotor torque and power output. The cause of this effect is shown in Figure 4-41, where the positive chord force increases at a deflection of -5° and small angles of attack. Except for this small region, the control characteristic is regular, monotonic and well behaved.

4.2.2.1.3 Trim Characteristics

The control setting required to trim any required power setting can be derived from the curves in Figure 4-38. Figure 4-42 shows the variation of the control angle required to trim the rotor power with wind speed and tip speed ratio. Near the rated wind speed the control parameter, $\partial\delta_a/\partial V_w$ becomes large.

This characteristic reflects the fact that near the peak of the $C_p - \lambda$ curve, power is inherently insensitive to the control setting. The decrease in control power with increasing angle of attack is manifested by the increase in $\partial\delta_a/\partial\lambda$ for wind speeds between 40 and 60 mph, from λ=6 to $\lambda = 4$. For the range in which control power is needed, the variation of the trim angle with wind speed goes from 3.5° to 9.8°, an easily manageable range.

Figure 4-43 displays the change in the torque coefficient distribution along the blade at trim for different windspeeds between the rated and cut-out speeds.

4.2.2.1.4 Aileron Control Stopping Power

In addition to controlling the power, or rotor torque, the ailerons are used to slow the rotor for shutdown. At high wind speeds this is a severe demand on the aileron's ability to provide negative torques to the rotor, because of the high angle of attack and wind speed on the one hand, and the decreasing rotor speed on the other. Since the effectiveness of upper surface trailing edge controls deteriorates at high angles of attack, as noted in section 8.4.1.2, Vol. II, the conditions encountered in high wind speed shutdowns are the most challenging to the aileron control system.

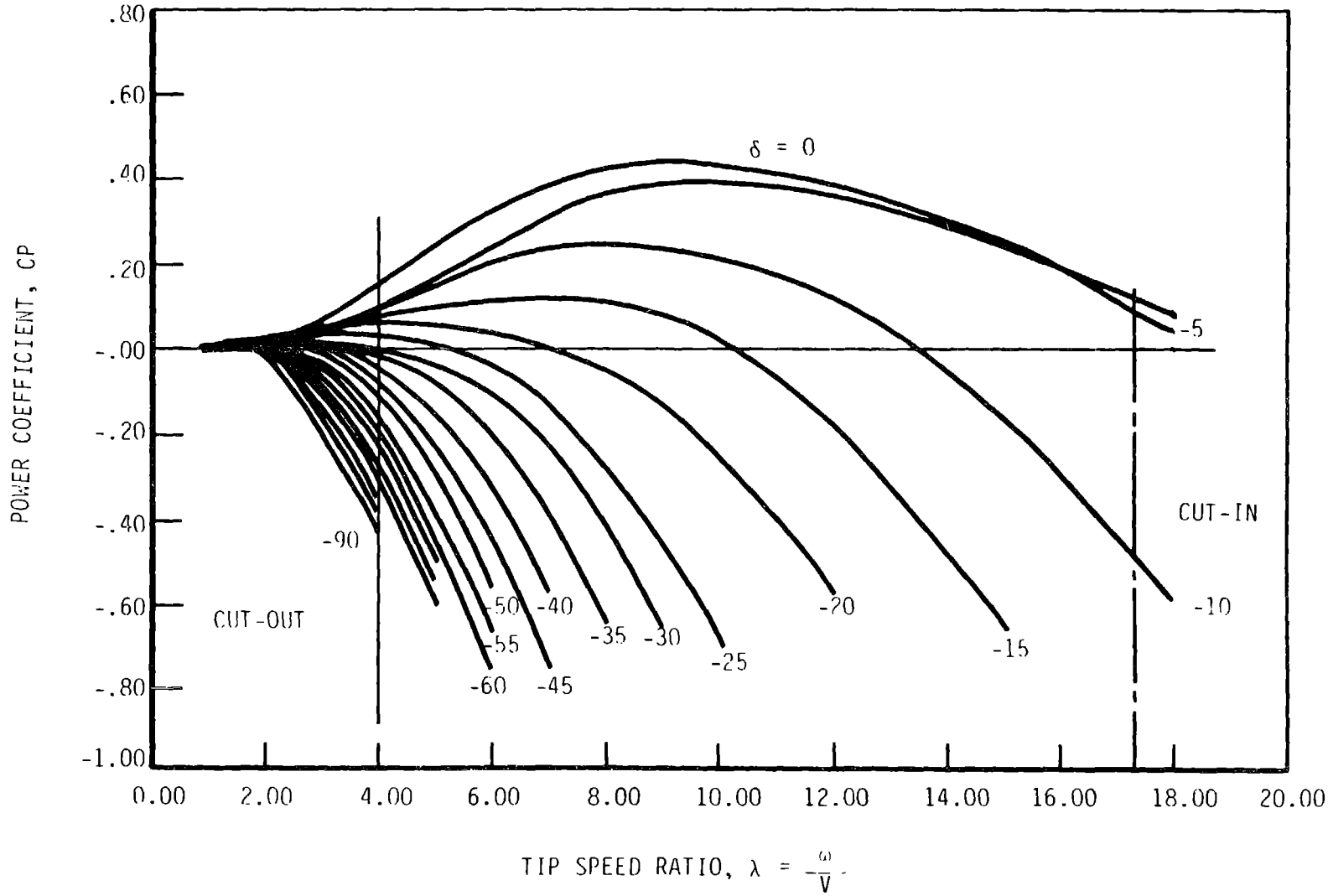

Figure 4-37. Effect of Aileron Control Deflection on MOD-5A Rotor Power

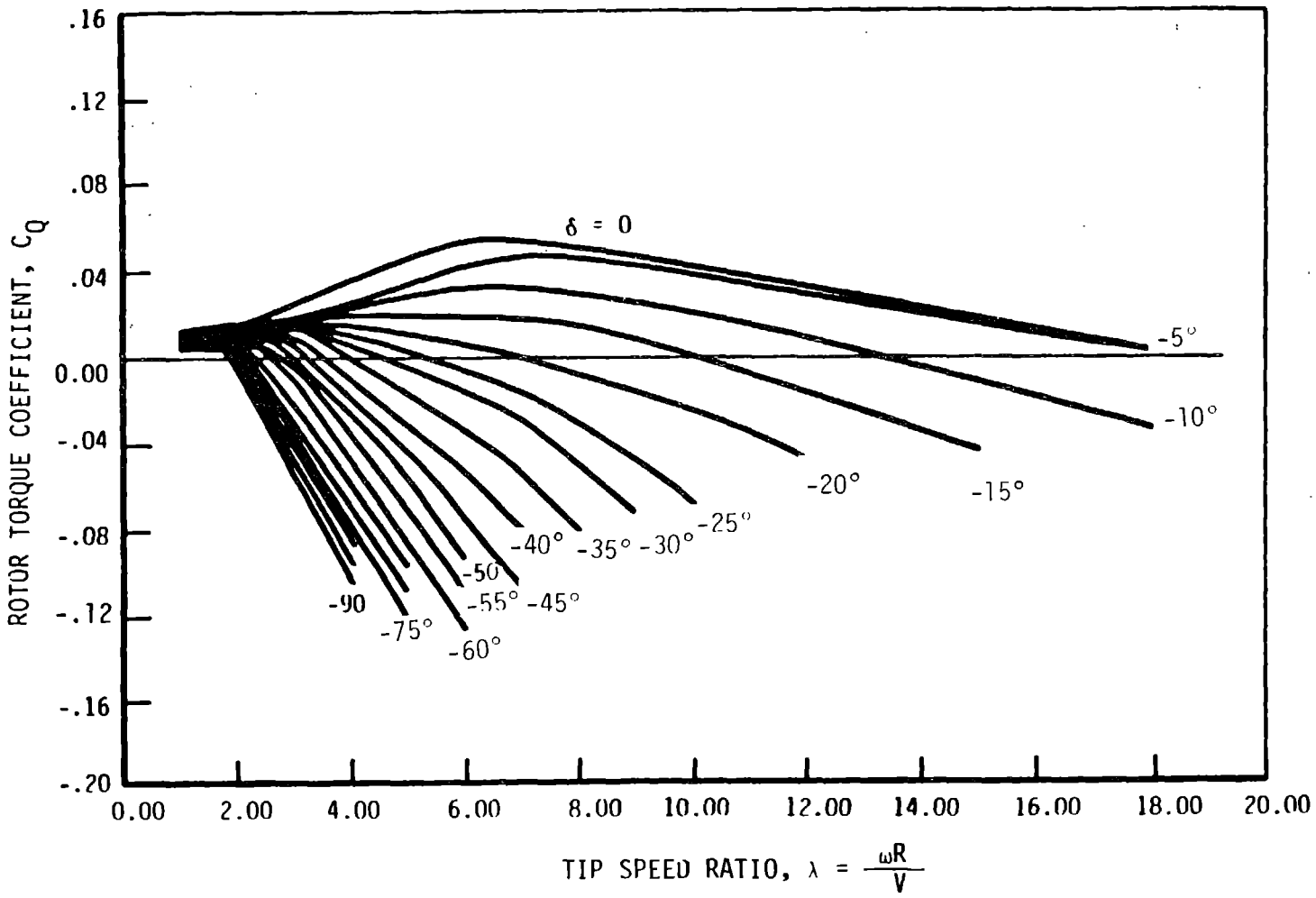

Figure 4-38. Effect of Aileron Control Deflection on MOD-5A Rotor Torque

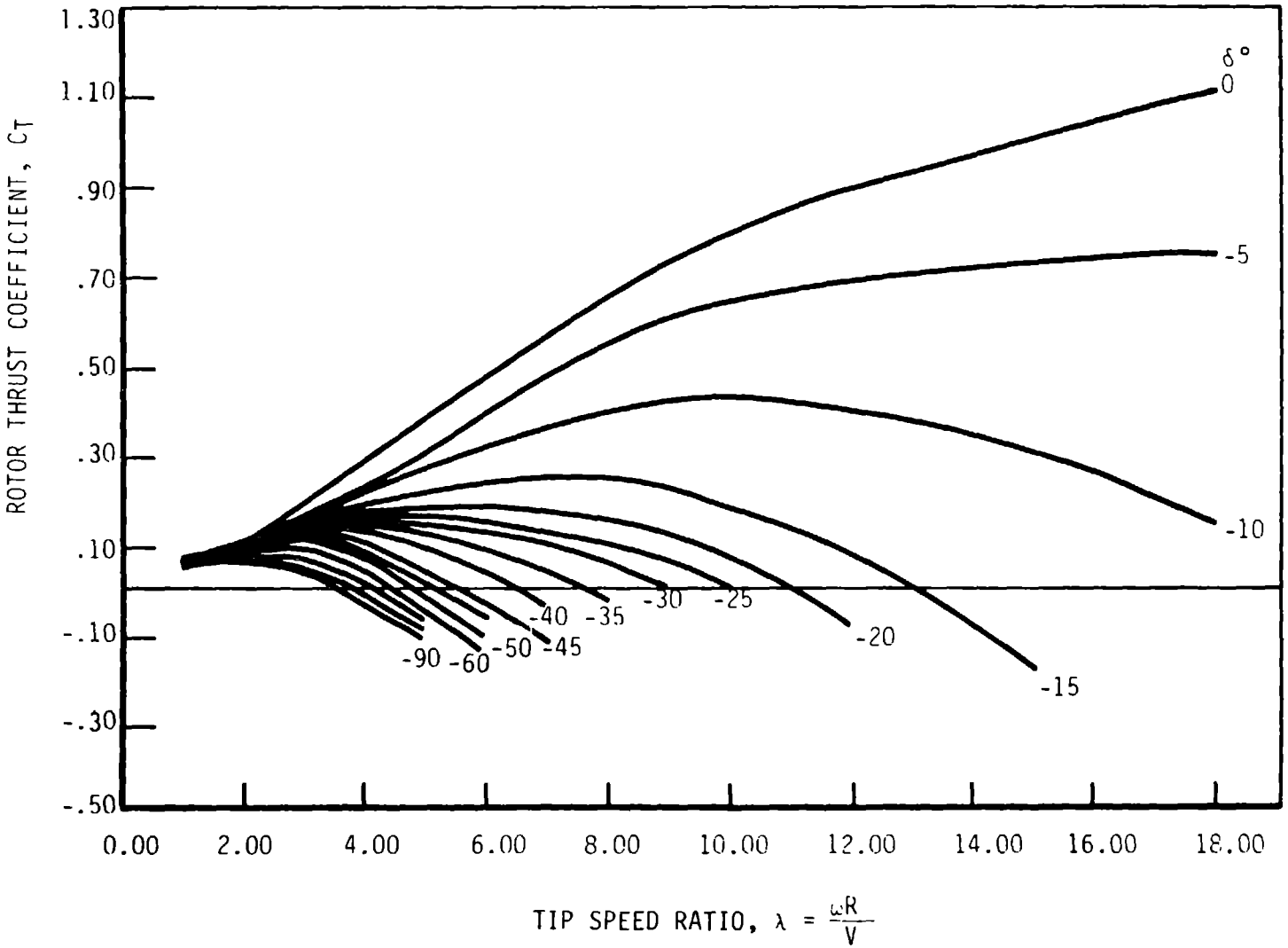

Figure 4-39. Effect of Aileron Control Deflection on MOD-5A Rotor Thrust

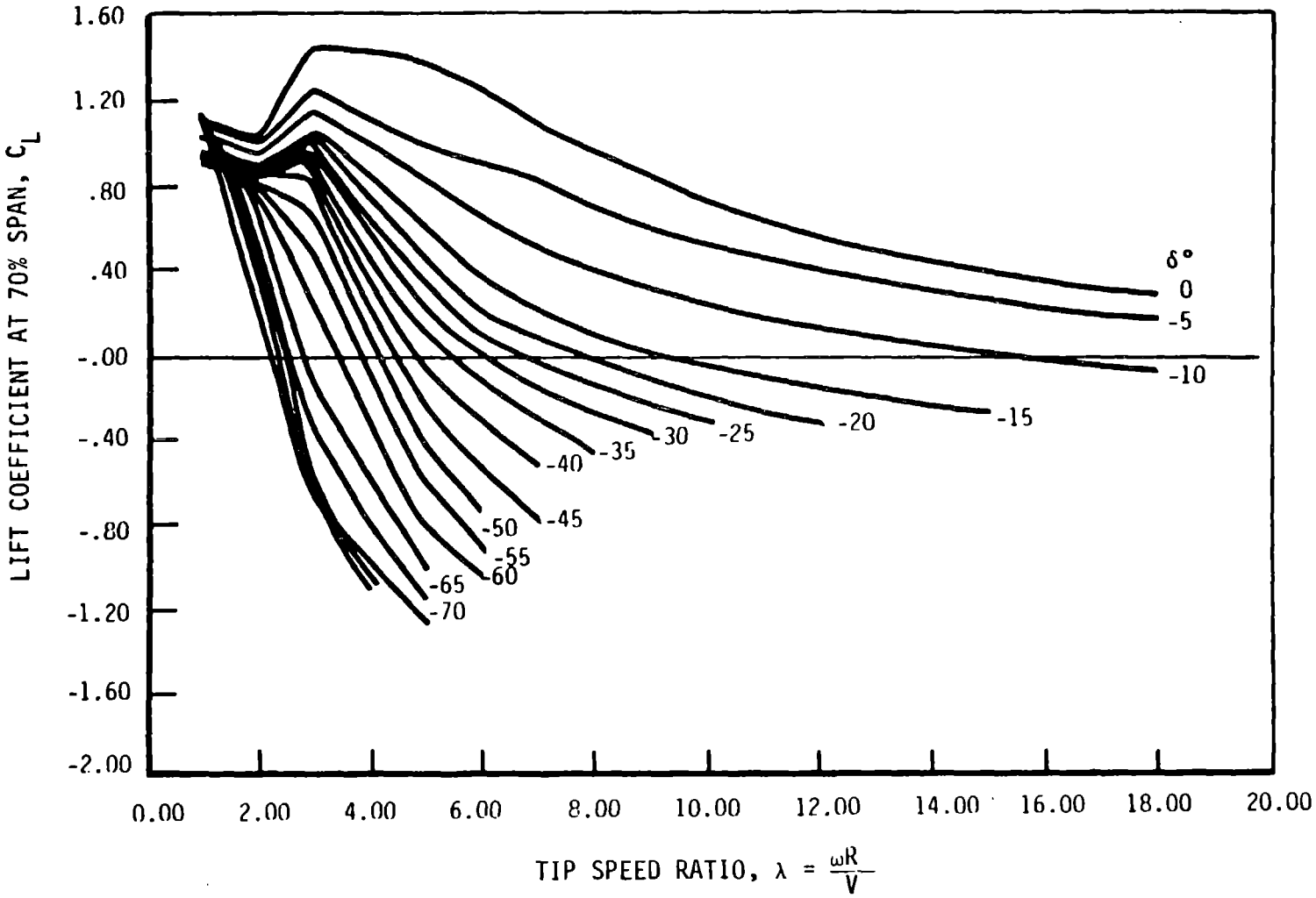

Figure 4-40. Effect of Aileron Control deflection on the Section Lift Coefficent at 70% Span

Table 4-15 MOD-5A Power Coefficient Variation With Control Setting and Tip-Speed Ratio

LAMBDA / DELTA	2.0	4.0	6.0	8.0	10.0	12.0	14.0	16.0	18.0
0.	0.019	0.147	0.311	0.406	0.420	0.383	0.304	0.186	0.030
-5.	0.018	0.099	0.250	0.361	0.380	0.350	0.287	0.192	0.062
-10.	0.021	0.099	0.192	0.243	0.207	0.101	-0.066	-0.301	-0.613
-15.	0.021	0.086	0.114	0.113	0.010	-0.192	-0.483	-0.877	-1.382
-20.	0.024	0.061	0.031	-0.047	-0.247	-0.577	-1.030	-1.625	-2.377
-25.	0.026	0.041	-0.039	-0.257	-0.695	-1.363	-2.292	-3.519	-5.081
-30.	0.028	0.022	-0.099	-0.401	-0.994	-1.867	-3.073	-4.661	-6.681
-35.	0.030	-0.005	-0.204	-0.649	-1.492	-2.716	-4.382	-6.567	-9.337
-40.	0.031	-0.035	-0.325	-0.924	-2.022	-3.661	-5.868	-8.739	-12.367
-45.	0.031	-0.070	-0.449	-1.191	-2.497	-4.465	-7.140	-10.619	-15.008
-50.	0.029	-0.107	-0.559	-1.427	-2.897	-5.102	-8.124	-12.063	-17.039
-55.	0.026	-0.146	-0.665	-1.646	-3.273	-5.703	-9.044	-13.407	-18.924
-60.	0.021	-0.191	-0.760	-1.840	-3.612	-6.251	-9.881	-14.630	-20.642
-65.	0.016	-0.238	-0.860	-2.022	-3.921	-6.742	-10.622	-15.709	-22.151
-70.	0.011	-0.275	-0.941	-2.191	-4.222	-7.235	-11.376	-16.809	-23.690
-75.	0.005	-0.313	-1.026	-2.370	-4.554	-7.791	-12.243	-18.086	-25.486
-80.	0.000	-0.349	-1.158	-2.688	-5.182	-8.887	-13.997	-20.704	-29.207
-85.	-0.006	-0.387	-1.293	-3.031	-5.845	-10.008	-15.746	-23.287	-29.484
-90.	-0.015	-0.425	-1.433	-3.366	-6.501	-11.145	-17.553	-25.979	-30.873

*

Table 4-16 MOD-5A Torque Coefficient Variation With Control Setting and Tip-Speed Ratio

LAMBDA / DELTA	2.0	4.0	6.0	8.0	10.0	12.0	14.0	16.0	18.0
0.	0.009	0.037	0.052	0.051	0.042	0.032	0.022	0.012	0.002
-5.	0.009	0.025	0.042	0.045	0.038	0.029	0.020	0.012	0.003
-10.	0.010	0.025	0.032	0.030	0.021	0.008	-0.005	-0.019	-0.034
-15.	0.011	0.021	0.019	0.014	0.001	-0.016	-0.035	-0.055	-0.077
-20.	0.012	0.015	0.005	-0.006	-0.025	-0.048	-0.074	-0.102	-0.132
-25.	0.013	0.010	-0.007	-0.032	-0.069	-0.114	-0.164	-0.220	-0.282
-30.	0.014	0.005	-0.017	-0.050	-0.099	-0.156	-0.220	-0.291	-0.371
-35.	0.015	-0.001	-0.034	-0.081	-0.149	-0.226	-0.313	-0.410	-0.519
-40.	0.016	-0.009	-0.054	-0.116	-0.202	-0.305	-0.419	-0.546	-0.687
-45.	0.015	-0.017	-0.075	-0.149	-0.250	-0.372	-0.510	-0.664	-0.834
-50.	0.014	-0.027	-0.093	-0.178	-0.290	-0.425	-0.580	-0.754	-0.947
-55.	0.013	-0.037	-0.111	-0.206	-0.327	-0.475	-0.646	-0.838	-1.051
-60.	0.011	-0.048	-0.127	-0.230	-0.361	-0.521	-0.706	-0.914	-1.147
-65.	0.008	-0.059	-0.143	-0.253	-0.392	-0.562	-0.759	-0.982	-1.231
-70.	0.005	-0.069	-0.157	-0.274	-0.422	-0.603	-0.813	-1.051	-1.316
-75.	0.002	-0.078	-0.171	-0.296	-0.455	-0.649	-0.875	-1.130	-1.416
-80.	0.000	-0.087	-0.193	-0.336	-0.518	-0.741	-1.000	-1.294	-1.623
-85.	-0.003	-0.097	-0.216	-0.379	-0.584	-0.834	-1.125	-1.455	-1.638
-90.	-0.007	-0.106	-0.239	-0.421	-0.650	-0.929	-1.254	-1.624	-1.715

Table 4-17 MOD-5A Thrust Coefficient Variation With Control Setting and Tip-Speed Ratio

LAMBDA / DELTA	2.0	4.0	6.0	8.0	10.0	12.0	14.0	16.0	18.0
0.	0.113	0.286	0.482	0.667	0.806	0.905	0.985	1.056	1.122
-5.	0.110	0.244	0.390	0.550	0.649	0.700	0.729	0.747	0.754
-10.	0.107	0.229	0.317	0.400	0.435	0.412	0.357	0.272	0.157
-15.	0.102	0.205	0.237	0.251	0.210	0.097	-0.064	-0.269	-0.516
-20.	0.100	0.189	0.194	0.175	0.092	-0.068	-0.282	-0.550	-0.870
-25.	0.099	0.179	0.166	0.122	0.010	-0.184	-0.441	-0.754	-1.122
-30.	0.097	0.170	0.141	0.076	-0.068	-0.297	-0.592	-0.950	-1.371
-35.	0.096	0.158	0.103	-0.018	-0.248	-0.567	-0.961	-1.429	-1.972
-40.	0.095	0.143	0.047	-0.131	-0.441	-0.873	-1.390	-1.992	-2.685
-45.	0.093	0.124	-0.011	-0.234	-0.589	-1.083	-1.682	-2.381	-3.180
-50.	0.090	0.103	-0.057	-0.304	-0.678	-1.193	-1.824	-2.565	-3.414
-55.	0.086	0.082	-0.097	-0.360	-0.750	-1.281	-1.934	-2.703	-3.588
-60.	0.081	0.056	-0.128	-0.400	-0.798	-1.336	-1.996	-2.780	-3.682
-65.	0.077	0.029	-0.161	-0.433	-0.832	-1.372	-2.036	-2.826	-3.737
-70.	0.073	0.010	-0.181	-0.457	-0.865	-1.417	-2.095	-2.901	-3.832
-75.	0.070	-0.009	-0.201	-0.481	-0.895	-1.456	-2.142	-2.960	-3.905
-80.	0.068	-0.008	-0.200	-0.480	-0.893	-1.452	-2.137	-2.953	-3.896
-85.	0.066	-0.007	-0.196	-0.478	-0.893	-1.454	-2.142	-2.961	-4.188
-90.	0.061	-0.006	-0.194	-0.476	-0.891	-1.450	-2.135	-2.952	-4.446

*

Table 4-18 MOD-5A CLX=0.7 Coefficient Variation With Control Setting and Tip-Speed Ratio

LAMBDA / DELTA	2.0	4.0	6.0	8.0	10.0	12.0	14.0	16.0	18.0
0.	1.012	1.414	1.241	0.933	0.700	0.540	0.431	0.352	0.293
-5.	0.987	1.098	0.892	0.701	0.509	0.370	0.276	0.209	0.161
-10.	0.948	1.001	0.646	0.405	0.230	0.117	0.035	-0.025	-0.073
-15.	0.890	0.848	0.362	0.101	-0.059	-0.165	-0.237	-0.293	-0.334
-20.	0.876	0.705	0.203	-0.058	-0.208	-0.314	-0.383	-0.434	-0.474
-25.	0.859	0.619	0.098	-0.172	-0.321	-0.422	-0.493	-0.542	-0.580
-30.	0.853	0.569	0.002	-0.269	-0.424	-0.527	-0.595	-0.645	-0.683
-35.	0.852	0.467	-0.139	-0.463	-0.665	-0.777	-0.843	-0.893	-0.930
-40.	0.838	0.354	-0.344	-0.695	-0.922	-1.065	-1.139	-1.186	-1.223
-45.	0.820	0.215	-0.568	-0.921	-1.129	-1.260	-1.345	-1.394	-1.430
-50.	0.794	0.054	-0.754	-1.082	-1.257	-1.369	-1.444	-1.493	-1.530
-55.	0.765	-0.134	-0.921	-1.215	-1.364	-1.458	-1.521	-1.569	-1.605
-60.	0.715	-0.357	-1.054	-1.311	-1.439	-1.516	-1.568	-1.610	-1.647
-65.	0.667	-0.613	-1.209	-1.393	-1.494	-1.557	-1.600	-1.635	-1.671
-70.	0.606	-0.820	-1.300	-1.454	-1.545	-1.605	-1.646	-1.677	-1.713
-75.	0.483	-1.042	-1.393	-1.516	-1.594	-1.648	-1.685	-1.712	-1.747
-80.	0.438	-1.041	-1.411	-1.535	-1.609	-1.661	-1.696	-1.721	-1.755
-85.	0.340	-1.088	-1.421	-1.551	-1.628	-1.679	-1.714	-1.740	-1.772
-90.	0.114	-1.106	-1.440	-1.570	-1.644	-1.692	-1.725	-1.749	-1.781

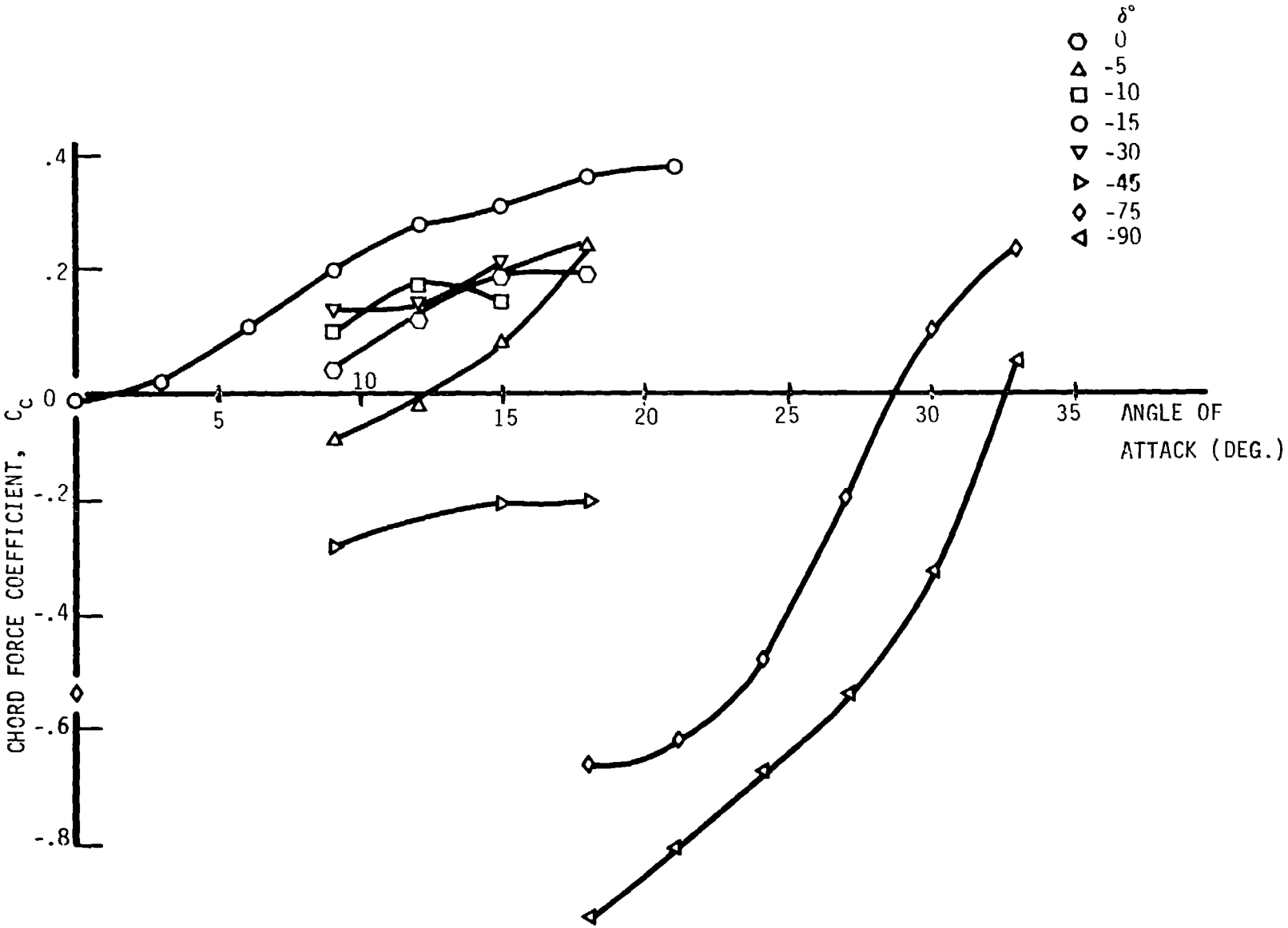

Figure 4-41 Variation of the Plain Aileron Section Chord Force Coefficient with Angle of Attack and Control Deflection - Wind Tunnel Tests at OSU

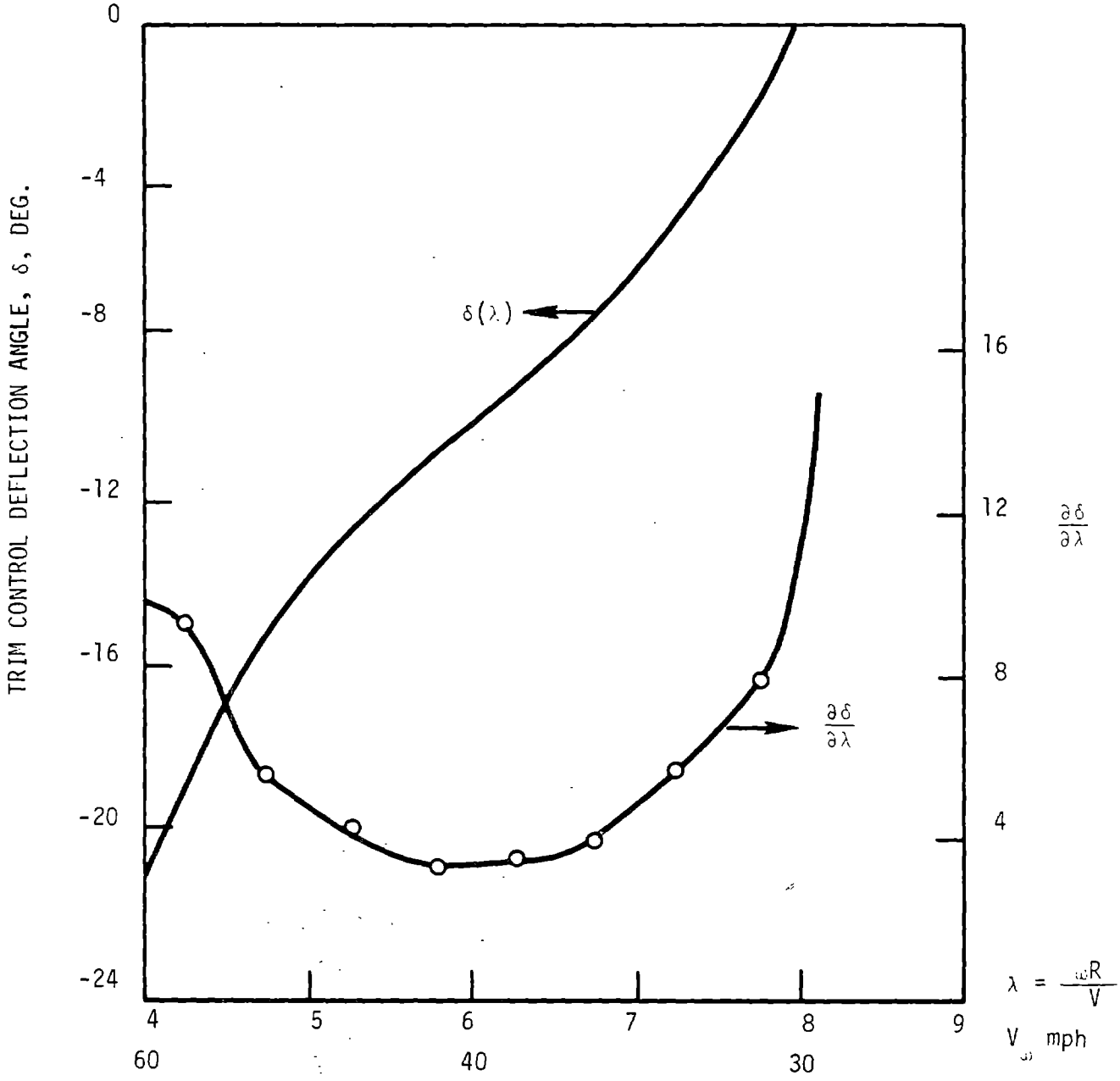

Figure 4-42. Control Trim Characteristics at Rated Power

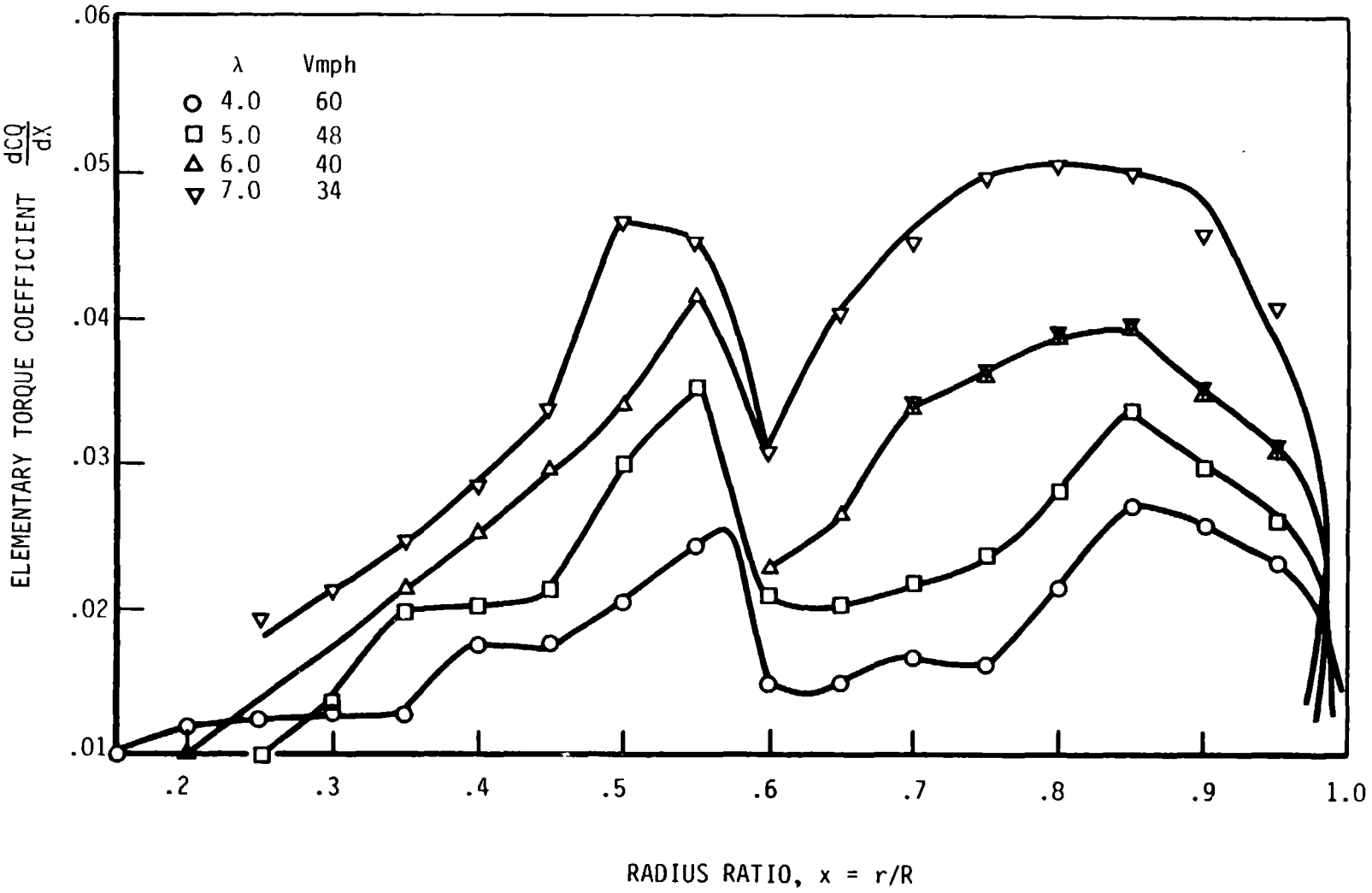

Figure 4-43. Torque Coefficient Distribution at Trim

The aileron control stopping power is illustrated in Figure 4-44. The figure illustrates that the rotor can be brought to an equilibrium tip-speed ratio of 1.5 by deflecting the ailerons -90°. This ratio corresponds to a rotor speed of 6.3 rpm at the cut-out windspeed of 60 mph.

4.2.2.1.5 Hinge Moment Characteristics of the Aileron Control

The hinge moment is the result of the displacement of the aileron's center of pressure from the hinge line. Because the hinge line is located at the leading edge of the aileron, the center of pressure will always be aft of it, so the hinge moment arm is negative. Positive normal forces produce negative hinge moments and negative normal forces produce positive hinge moments. Positive normal forces point from the lower surface of the aileron toward the upper surface, and positive hinge moments and control deflection point from the trailing edge down. Figure 4-45 is a correlation of the aileron's normal force coefficient versus the hinge moment coefficient. The aileron's normal force coefficient is defined as

$$C_{N_a} = \frac{N_a}{1/2\ \rho\ V^2 c_a}$$

where N_a is the aileron's normal force per unit of span and c_a is the aileron chord. Similarly, the aileron hinge moment coefficient is defined as:

$$C_{H_a} = \frac{H_a}{1/2\ \rho\ V^2 c^2_a}$$

The correlation curve passes through the origin, indicating that there is no significant effect of the aileron camber on the hinge moment.

The slope $\partial C_H/\partial C_N$ is the ratio X_{cp}/c_a where X_{cp} is the center of pressure offset from the hinge line. Figure 4-45 shows that $X_{cp}/c = -.29$ whether the normal force is produced by angle of attack or control deflection angle, since all of the points correlate around a single line.

Figure 4-46 shows the floating angle of the MOD-5A aileron. This is the equilibrium angle that the aileron will seek if no hydraulic actuator load is applied. This condition will exist if the hydraulic system fails, leading to loss of pressure. Under these conditions, the aileron position will be the unique function of tip-speed ratio (angle of attack) shown in the figure.

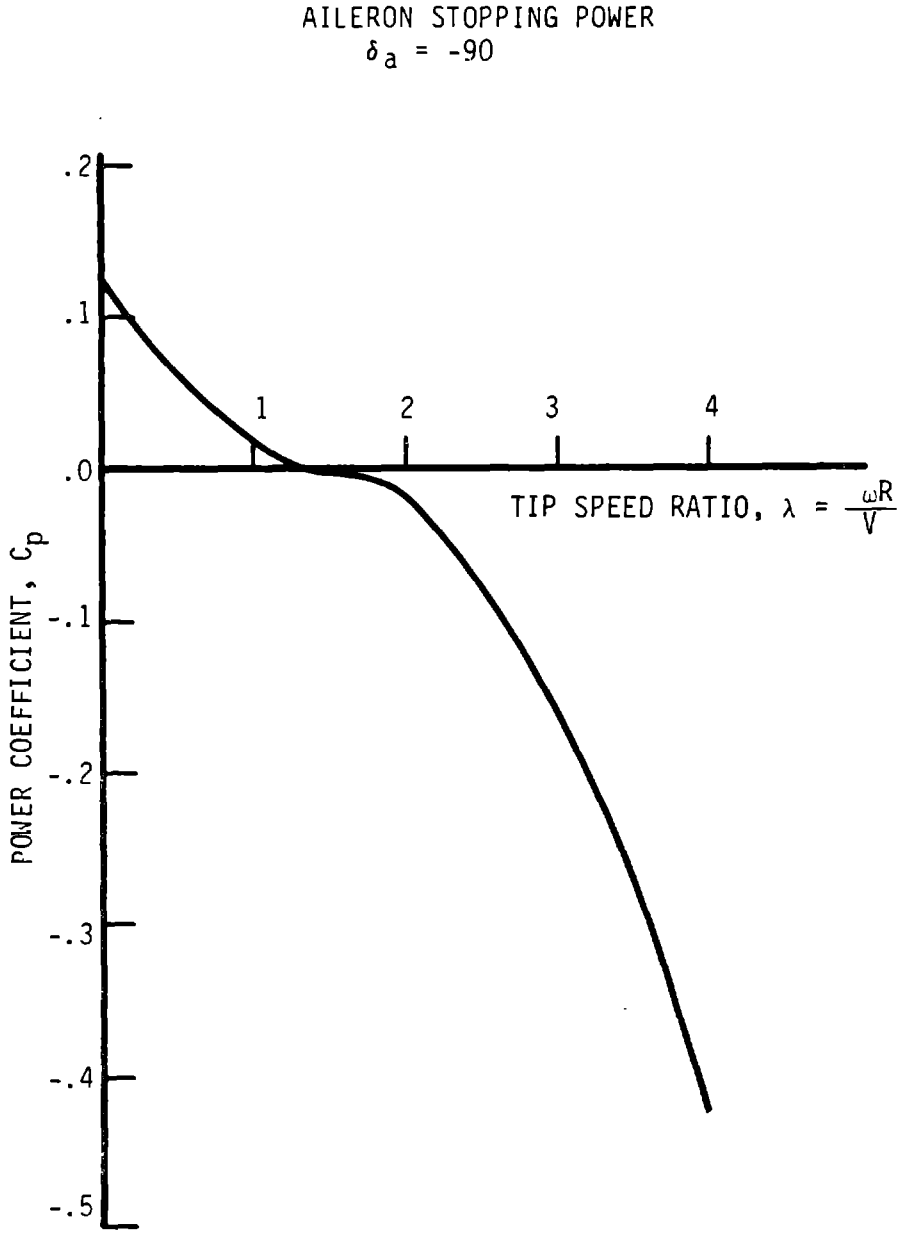

Figure 4-44. Aileron Stopping Power

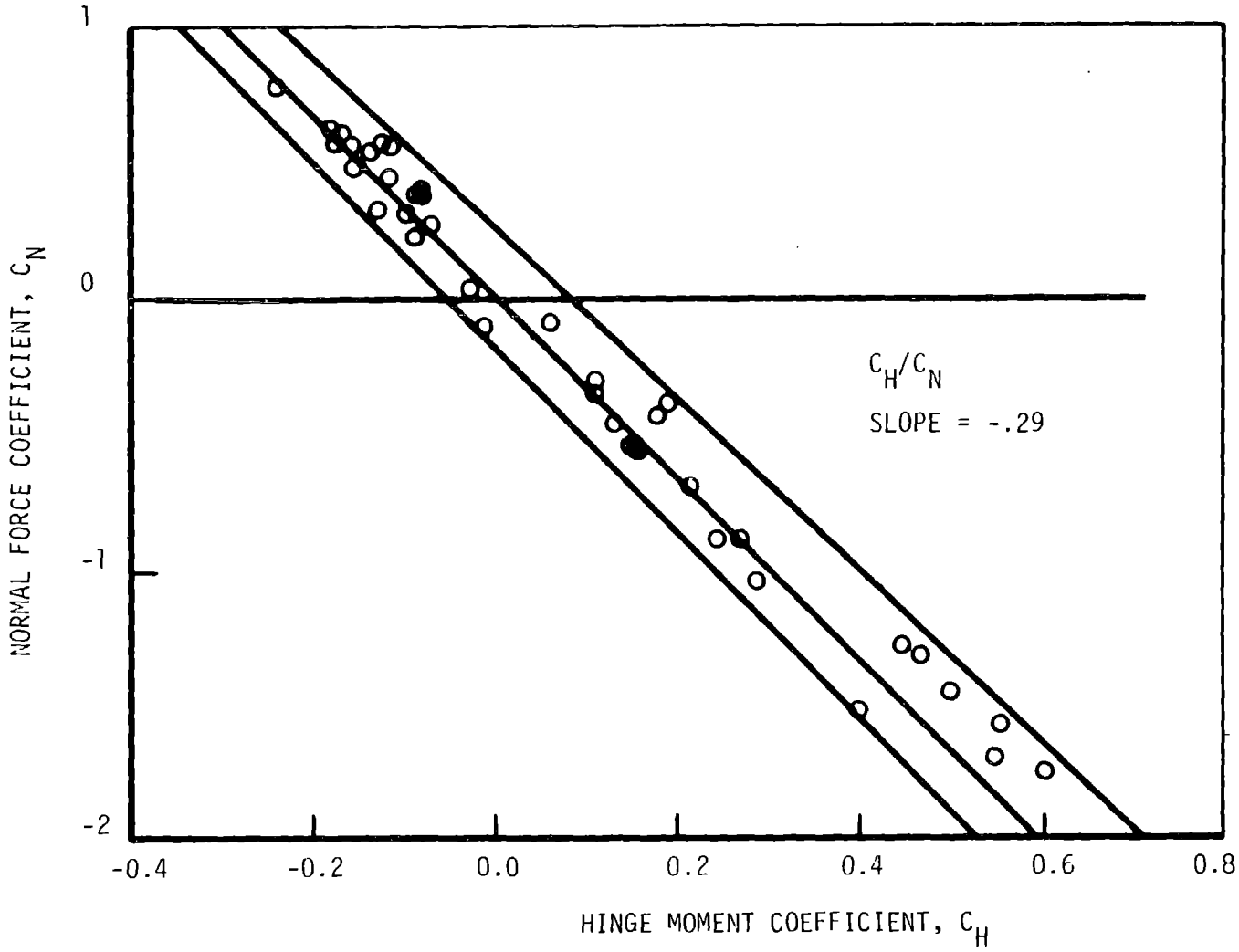

Figure 4-45. Aileron Normal Force - Hinge Moment Characteristics

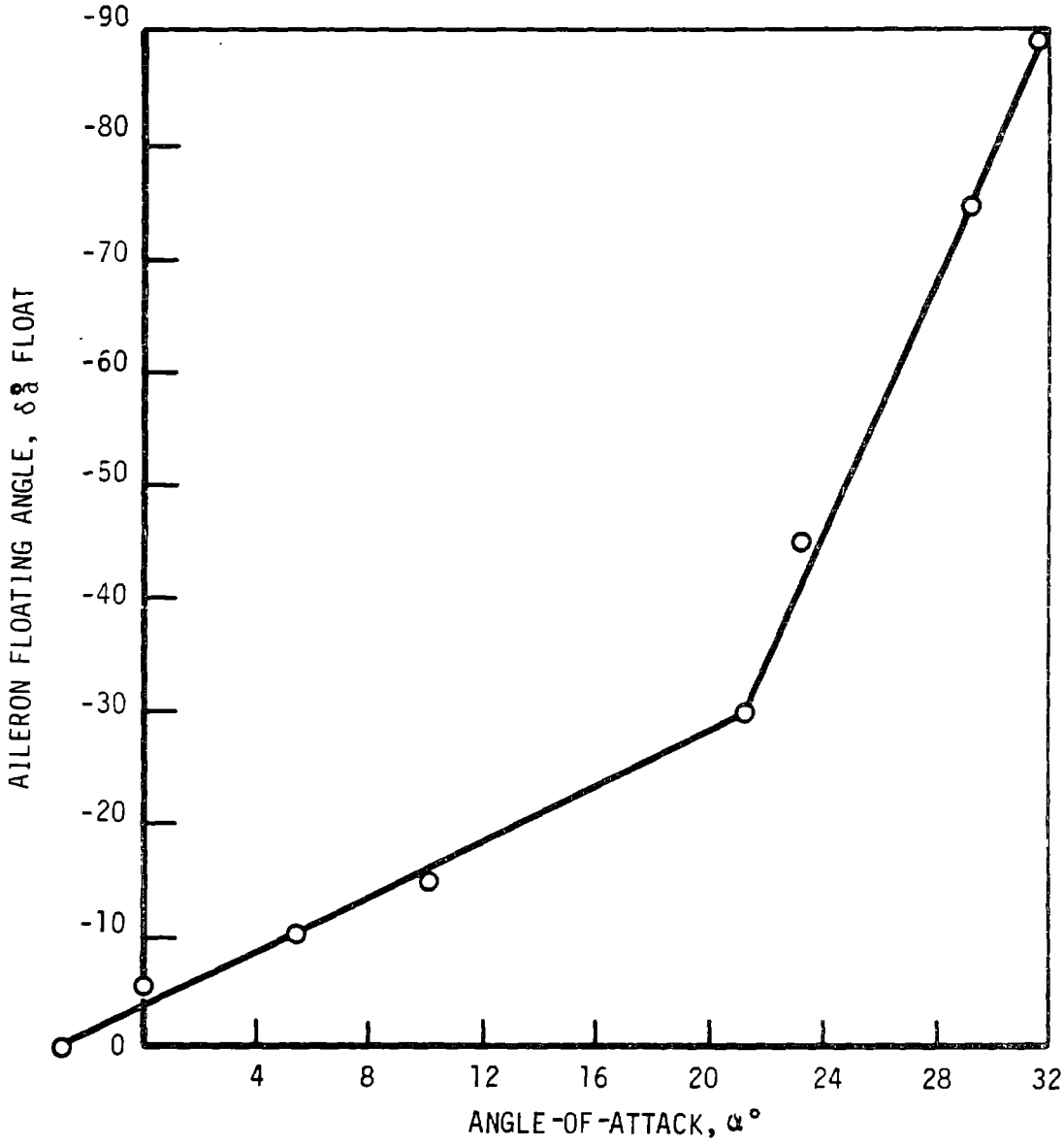

Figure 4-46. Aileron Floating Angle Characteristics

With the ailerons floating, the rotor has the power characteristic shown in Figure 4-47. Since the power coefficient with the ailerons floating never becomes negative, the ailerons will need further actuation to achieve shutdown if the hydraulic system fails. This capability is supplied by individual accumulators provided for each aileron actuator.

4.2.2.2 Aileron Configuration

Section 4.2.1.2 outlined the location and approximate size of the ailerons in the outer segment of the trailing edge. This section contains a more detailed description and discussion of the ailerons, and of the considerations that lead to this design. The aileron design is shown in Figure 4-48.

Ailerons were introduced to the MOD-5A design late in the final design phase. Ailerons imposed a new constraint on the configuration of the blade. Ailerons were designed and developed simultaneously with the partial span control so that the blade tooling and major molds for both designs would be compatible. This course of action was prudent, since the wind tunnel and MOD-0/5A test data was not available until late in the program.

The same external shape of the center and inner blade segments was used in both configurations. The outer panel, whose molds had the least influence on the schedule and cost, were allowed to vary in response to the design. It was intended to build the inner blade mold of a length that would accommodate the partial span control, between 25% and 71% of the span, but only to use the portion between 25% and 60% of the span for the aileron configuration. The thickness-to-chord ratio for the aileron outer panel was matched to the ratio of the inner blade at 60% of the span and then decreased linearly, to coincide with the ratio of the partial span control at 100% of the span. This approach limited changes in the outer blade segment and allowed the aileron and partial span controls designs to be compatible.

Two types of ailerons were considered, plain and balanced, as shown in Figure 4-49. Both surfaces of the plain aileron are located aft of the hinge line. The crown surface of the balance aileron extends forward of the hinge line.

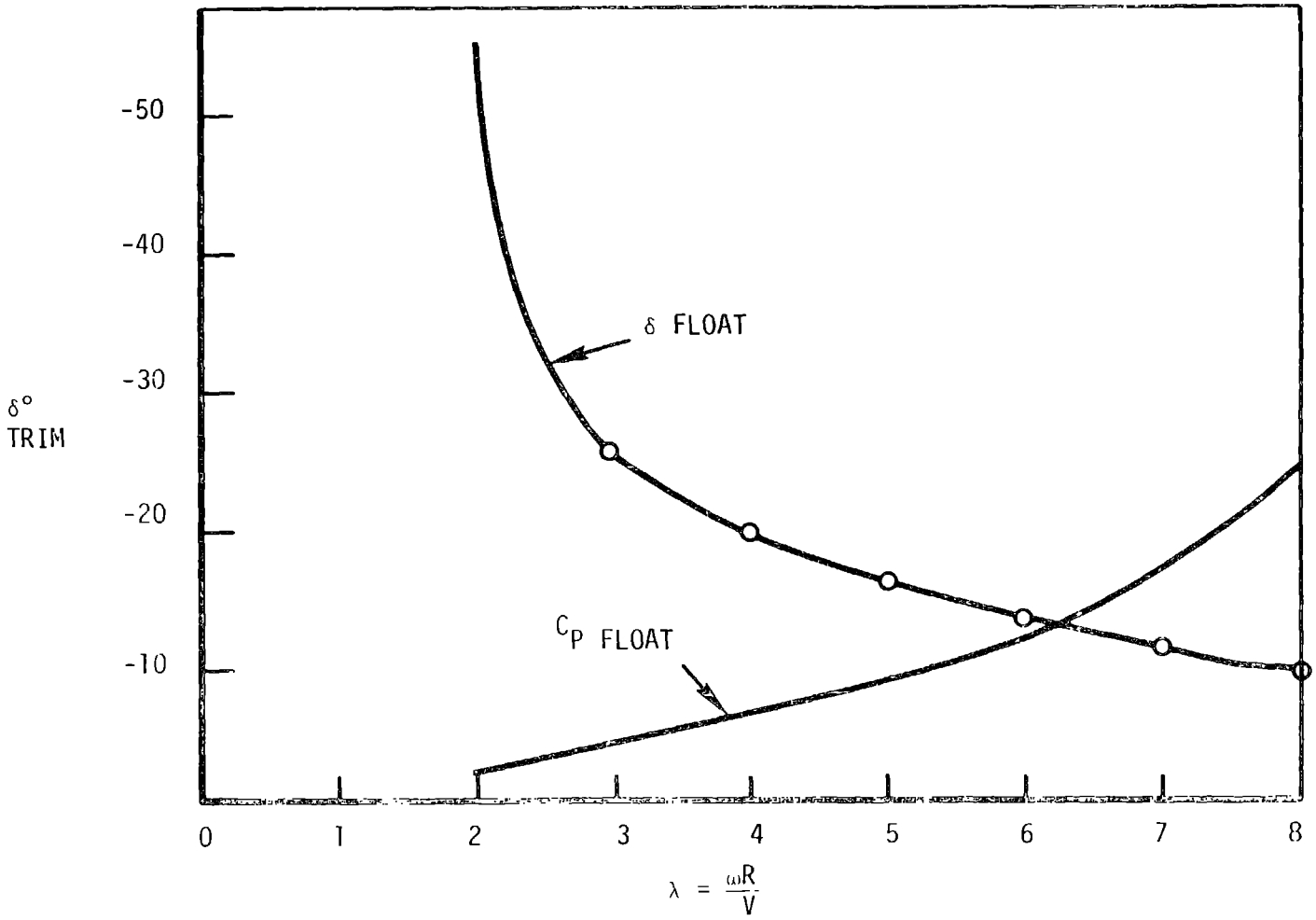

Figure 4-47 Aileron Characteristics at the Floating Angle

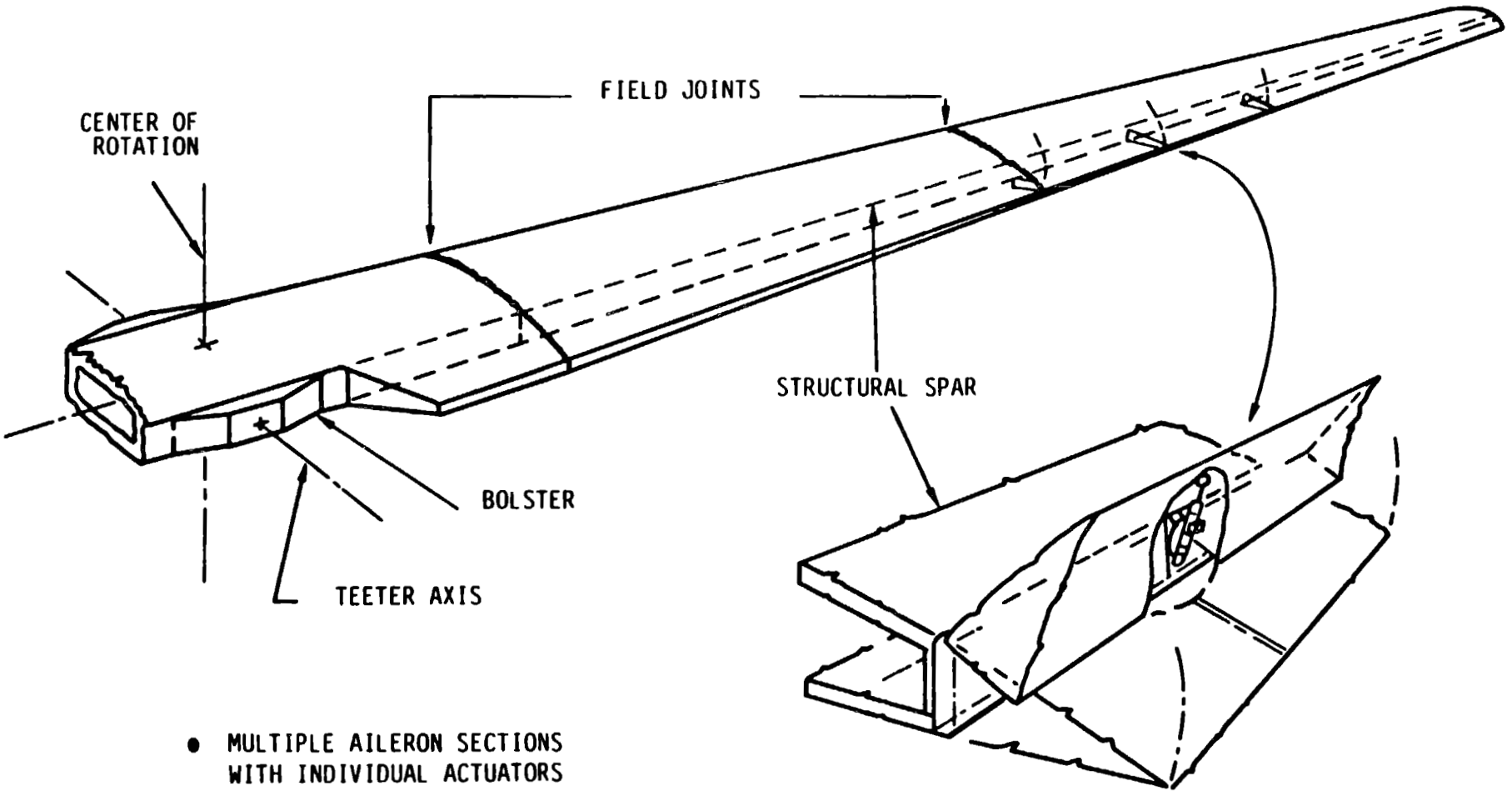

- MULTIPLE AILERON SECTIONS WITH INDIVIDUAL ACTUATORS
- FAIL-SAFE HYDRAULIC SYSTEM
- CONVENTIONAL, LIGHTLY LOADED WOOD/METAL JOINTS
- CONTINUOUS TIP-TO-TIP STRUCTURAL SPAR

Figure 4-48. Aileron Planform

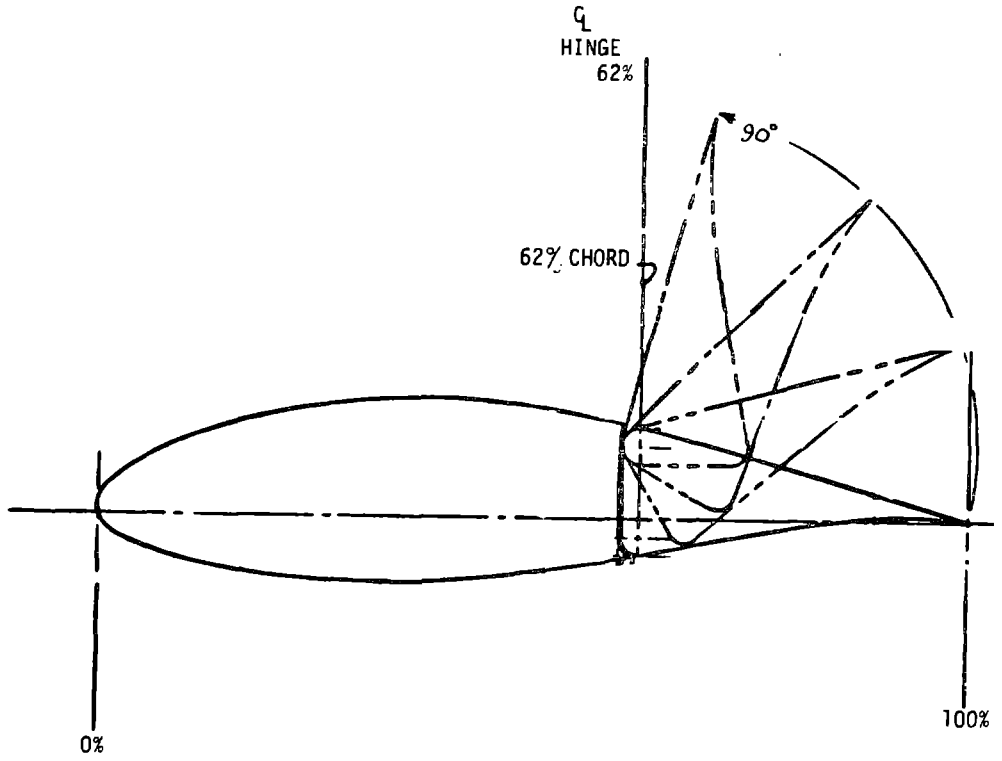

Figure 4-49a. Aileron Types Considered - Plain

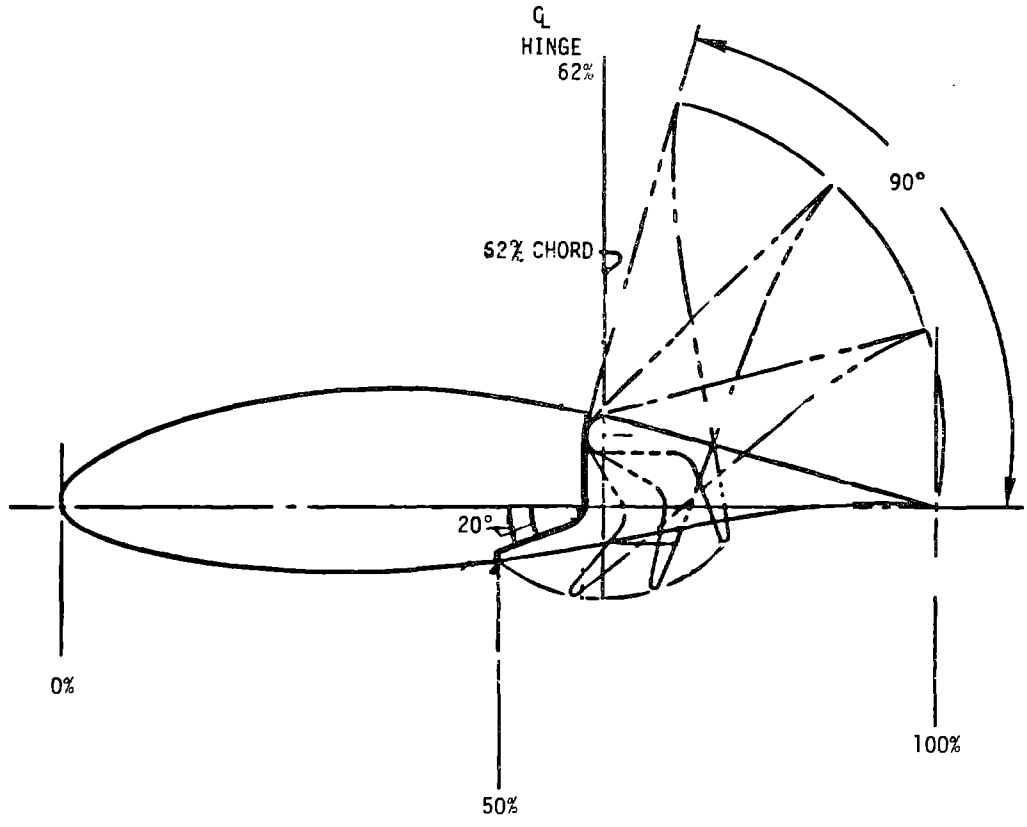

Figure 4-49b. Aileron Types Considered - Balanced

The plain ailerons have the least effect on the design of blade; they simply replace the secondary trailing edge structure described in section 4.2.1.2. They are attached to the primary structure, however, much differently. The fixed structure was mounted in a continuous fashion to the primary structure on both the high and low pressure sides of the airfoil at the rear spar location, 60%C (C is the chord). The ailerons on the other hand, are attached to a single surface at discrete points. The blade must accept and redistribute the concentrated loads associated with discrete hinge points. The chordwise moment capability, or aileron torque, is resisted as a couple between the hinge line and an actuator reaction point located on the rear spar. Chordwise ribs, which are attached to the rear spar, mid spar and inside surface of the blade skins, redistribute the concentrated loads. The rear spar thickness was also increased for adequate strength and stiffness. The aerodynamics and the structural constraint of the main structure of the blade were not affected by the plain aileron design.

The balanced ailerons required the same chordal internal structure for redistributing loads, but the shape of the primary blade structure was altered. The portion of the balanced aileron forward of the hinge-line, which was within the airfoil contour when not deployed, displaced a portion of the primary blade structural cross section, and made a change to the rear spar arrangement necessary. This arrangement made the design and construction of the basic blade more complicated and more expensive.

Both the plain and balanced ailerons were compatible with the blade, but the plain aileron was preferred because it cost less. However, before it was chosen, it had to meet all the performance requirements.

The salient differences between the plain and balanced ailerons were failsafe considerations, required actuator force and noise generation. Each of the aileron configurations had a characteristic float angle: an angular displacement toward the low pressure side of the blade that was associated with a zero hinge moment. The float angle of the balanced ailerons was great enough to slow the rotational speed of the rotor if an actuator failed. The plain aileron did not provide the same measure of protection, and consequently, another means of providing the adequate deployment angles was required.

The actuator force required for the balanced configuration was lower than that of the plain aileron. The difference in force was not great enough to allow the number of actuators to be reduced, but it did influence the size of the actuator. The main variable in the equation for the system cost was the number of actuators, not the size of the actuator. The cost for the aileron configurations was practically equal.

The noise generated by the ailerons was an undefined but important consideration. Other wind turbines, particularly the MOD-1, created noise. The frequency and volume of the noise ranged from annoying to unacceptable, according to residents in the area. Past experience indicated that the cleaner aerodynamic configuration, the plain ailerons, generate the least noise. Tests of both configurations on the MOD-0/5A unit were planned to provide data on this subject.

The plain ailerons were selected as the baseline configuration because they performed acceptably, cost less, had less influence on the design of the main blade and generated less noise.

The chord length and spanwise extent were both 40%, and the deployment angle was 90°. These values were based on the requirements defined in the discussion of aerodynamics in Section 4.2.1.2. The number of aileron actuators was determined by consideration of cost, failure modes, aileron torsional stiffness and packaging efficiency. A single actuator would cost the least, but if it failed, the control of one blade would be lost. Furthermore, one actuator has a large torsional deflection angle. The deflection angle is a function of aileron load and center of pressure, which can affect the control characteristics adversely. Consequently, a consider- ation of the failure characteristics determined that more than one actuator was required. Since the cost of the actuators is a function of the number of actuators, the minimum number of actuators must be determined. One requirement was that all the actuators had to be identical, to minimize development, spares and maintenance costs. The studies were now guided by considerations of packaging volume -- less outboard, stroke and column stability, failure effects, aileron torsional deflections, primary structural interfaces and handling and maintenance with emphasis on the removal aloft and the replacement of an

actuator or aileron segment. The detailed studies, which resulted in three actuator and six aileron segments per blade, are discussed in Section 4.4.

4.3 BLADE

The rotor assembly comprises a blade, ailerons, and a yoke, as shown in Figure 4-50. The forces of the wind on the blade surface create an aerodynamic torque that is transmitted to the generator through the blade and yoke structures. Because it is a major component of the wind turbine generator system, which directly affects the performance, cost, and reliability of the system, the blade design is very important.

This section describes the key features of the blade design. The subsections discuss each component in more detail. Copies of drawings referred to in the discussions are included in Volume IV.

A set of design, fabrication, and test requirements were developed for the blade. The requirements reflect GE's and NASA's experience, and the blade material and aerodynamic contour studies discussed in Volume II. The complete specification is included in Volume IV, and the key requirements are listed in Tables 4-19 and 4-20, and Figure 4-51. The rotor blade designed to meet these requirements is shown in Figure 4-52. The blade is a 400-ft structure, made from Douglas fir laminae.

A NACA 64XXX series airfoil defines the outside mold line of the blade cross-sections along its span. The specification for the required tolerances are shown on Figure 4-55. Typical cross-sections of the blade are shown in Figures 4-53a and b. The true airfoil, 4-53a, is modified inboard of 38% of the span by raising its upper surface as shown in 4-53b, to increase the aerodynamic torque contribution from this section of the assembly. Inboard of 10% of the span, the airfoil shape is truncated at 60% of its chord and becomes a rectangular shape at the center of rotation. At its maximum point, the airfoil is 25 ft. long and 86 in. thick. This dimension tapers to a minimum at the tip, where the chord is 73 in., and the thickness is 10.5 in. As shown in Figure 4-53a and b, the airfoil is twisted into the wind to produce the maximum aerodynamic torque.

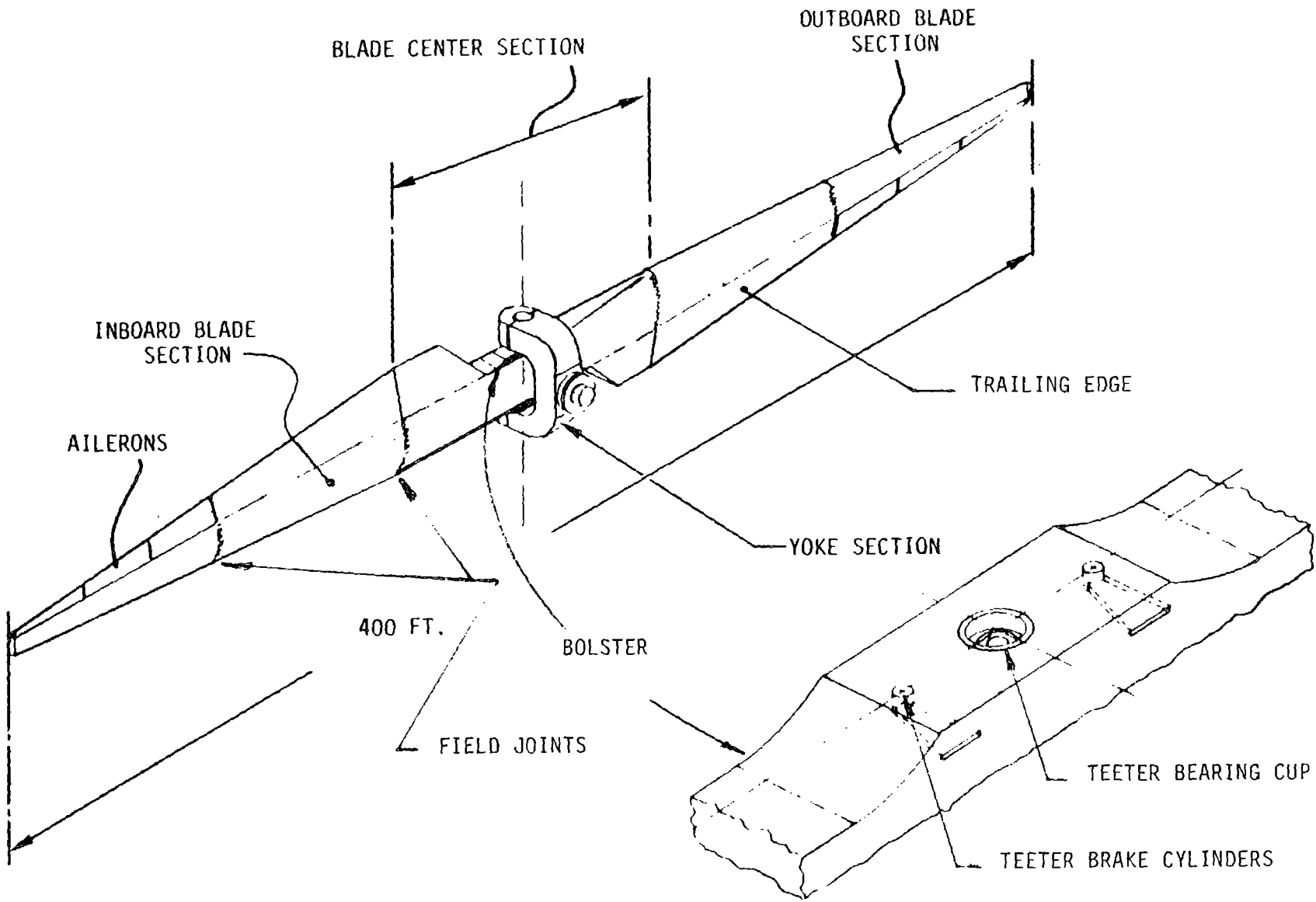
BLADE CENTER SECTION
OUTBOARD BLADE SECTION
INBOARD BLADE SECTION
AILERONS
TRAILING EDGE
YOKE SECTION
400 FT.
BOLSTER
FIELD JOINTS
TEETER BEARING CUP
TEETER BRAKE CYLINDERS

Table 4-19 Key Blade Design Requirements

- The blade will be designed to operate in the following environment for 30 years, or 4 X 10^8 cycles:
  - a) in winds up to 60 mph.
  - b) in 0° to 100°F ambient temperatures.
  - c) in rain, 4 in./hr.
  - d) in hail, 1 in. in diameter, 50 lb/ft^3, 66.6 ft/sec.
  - e) in snow, 21 lb/ft^2.
  - f) withstand lightning strikes.
  - g) withstand impact from birds, 4 lb. at 35 mph.

- The blade will be designed to withstand the following environments when not operating:
  - a) ambient temperatures of -40°F to 120°F.
  - b) loads imposed during transportation. Limit load factors are as follows:

Longitudinal	(In direction of travel)	±3 (truck) ±9 (rail)
Lateral	(Perpendicular to direction of travel	±1
Vertical		±3

  - c) wind velocities up to 130 mph.
  - d) a 2 in. coating of ice at 60/ft^3.

- The structural design of the blade will meet the following requirements:
  - a) withstand frequent and occasional limit loads without yielding. The minimum factor of safety will be, with regard to yield stress, 1.5 for frequent and 1.25 for occasional limit loads.
  - b) withstand catastrophic limit loads without exceeding the ultimate capability of the blade material.
  - c) withstand all loads without buckling. A minimum factor of safety, with regard to the theoretical critical buckling load, will be 1.5.

Table 4-19 (Cont.) Key Blade Design Requirements

d) preclude detrimental deflections caused by resonance.

e) withstand fatigue load histograms without exceeding a Miner's number of 1 with respect to the 95% confidence lower boundary for fatigue data, with consideration of stress ratio.

o The blade design will incorporate the following features:

a) the aerodynamic contour and aerodynamic profile coordinates.

b) use Douglas fir laminae, bonded with epoxy, as the main structural material of the blade.

c) be suitable for both rail and truck transport. General constraints are shown in Table 4-20 and Figure 4-51.

d) provisions to detect a layer of ice between .055 and .10 in.

e) provisions to install hydraulic and electrical conduits.

f) provisions to obtain a static balance about the rotational axis.

g) a means to attach and transfer loads to the rotor yoke through the elastomeric teeter radial bearing and thrust bearing.

h) a means to mount ailerons and aileron actuators and to transfer resultant loads and control forces to the blade structure.

Table 4-20 General Transportation Constraints*

ITEM	RAIL	TRUCK
Maximum weight	260,000 lb. (200,000 lb.)	70,000 lb.
Maximum length (120 ft.)	85 ft. (150 ft.)	50 ft.
Maximum width	Figure 4-51 (14 ft.)	12 ft.
Maximum height	Figure 4-51 (12 ft.)	10 ft.

* The values in parenthesis are possible with special routing, escorts and permits, at an added cost. Rail limitations are more severe in the northeast.

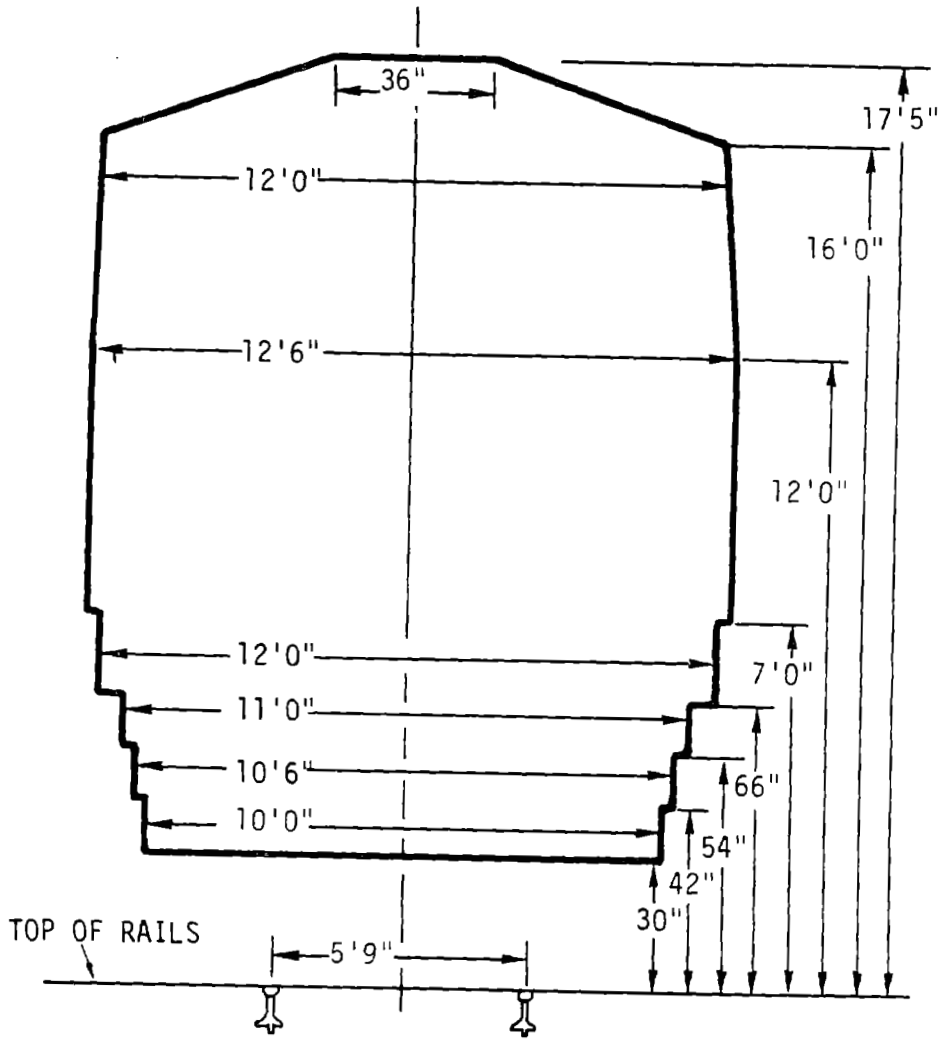

Figure 4-51. Maximum Railroad Shipping Clearances in the U.S.

(Except in New England)

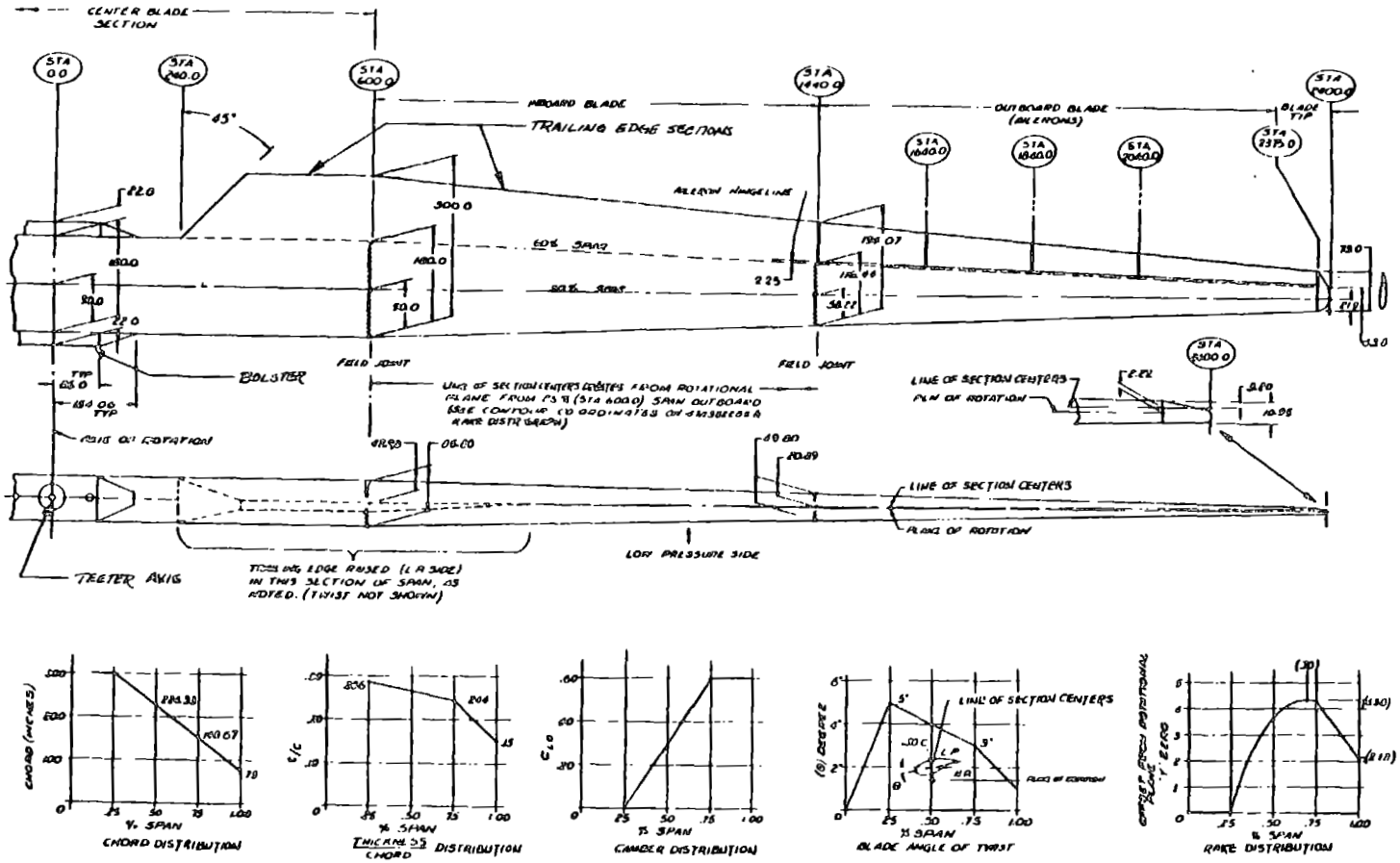

Figure 4-52. MOD-5A Rotor Blade Assembly

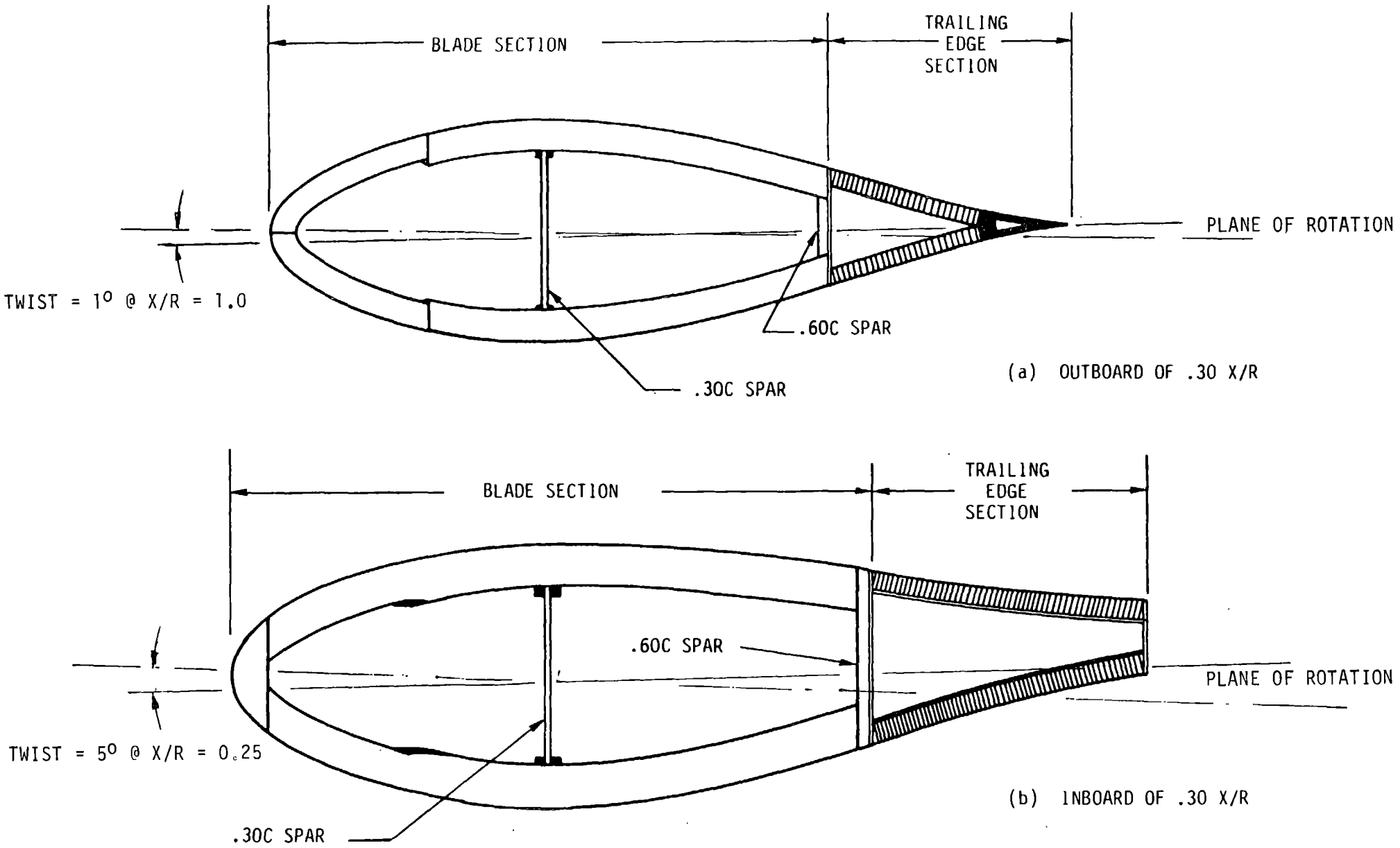

Figure 4-53 Typical Blade Cross-Sections

The materials used to fabricate the blade are shown in Figure 4-54a. Laminae of .10 in. thick Douglas fir, bonded with epoxy, are used in the structural portion of the airfoil shell, which runs from 0% to 60% of the chord, and the spars located at 30% and 60% of the chord. A detailed view of the laminae is shown in Figure 4-54b. The secondary structural portion of the airfoil shell, which is the trailing edge from 60% to 100% of the chord, is made from a paper honeycomb core with glass fiber faces. A 30-mil layer of glass fiber cloth covers the exterior and interior surfaces of the wood veneer, to protect the edge from the environment.

The blade assembly consists of three major subassemblies, the center, inner, and outer blade sections. The center blade section is the center 100 ft. of the span. Bolsters with steel fittings are bonded to the center blade, and form the center blade assembly. The bolsters and the teeter shaft have the necessary features to attach the blade assembly to the yoke. The inner blade occupies the portion of the blade between 25% and 60% of the span on either side of the center of rotation.

The non-structural trailing edge sections are attached to the center and inner blade sections. These sections are installed in the field because of restrictions on the shipping envelope shown in Table 4-20 and Figure 4-51. The outer blade sections make up the rest of the blade span. The aileron surfaces are affixed to the outer blade. A removable, contoured tip section terminates the outer blade section. It provides a gradual decrease in the load and access to provisions for adjustable ballast.

The continuous blade structure is formed by bonding the subassemblies at the site, using the field joint, which is a pattern of fingers at the interfaces. Conduits mounted at the 60% of the spar in the trailing edge sections transmit hydraulic and electrical power to the ailerons and sensors. The hydraulic lines are fabricated in the field by welding individual pieces, to eliminate the leaks associated with hydraulic union-type connectors.

The blade and the electrical system are protected from lightning. The protection is an aluminum screen and leading edge strips, below the blade's outer glass fiber layer. The screen and strips provide a path to ground. The blade assembly weighs approximately 273,000 lbs, as shown in Table 4-21.

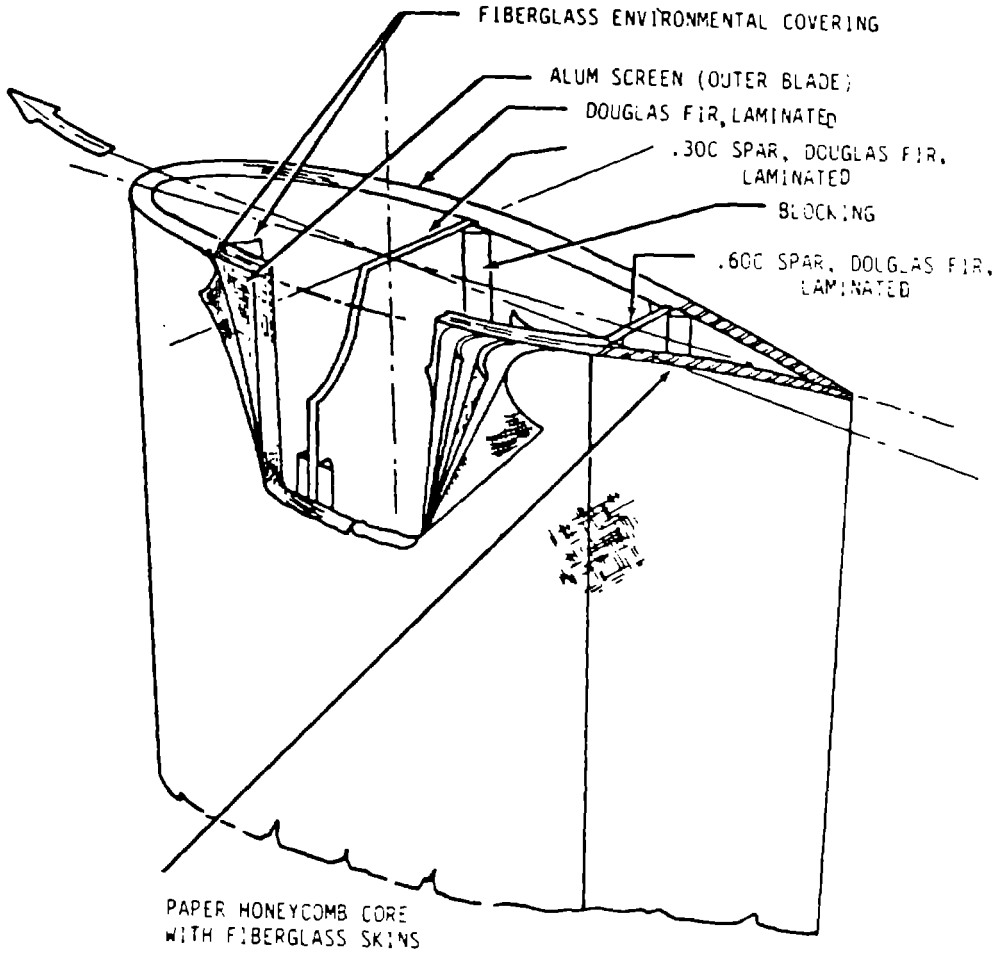

a) ARRANGEMENT

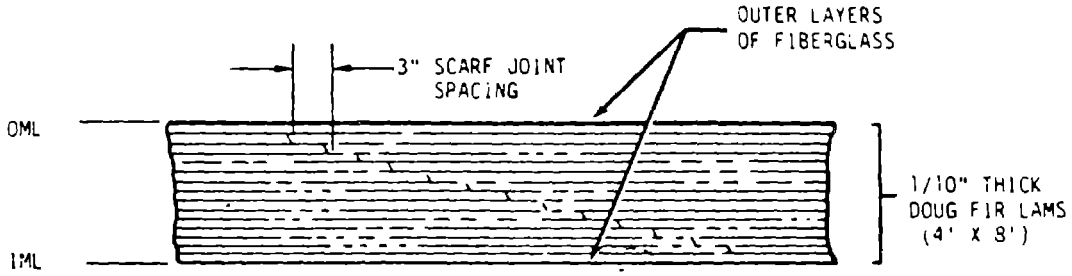

b) LAMINATE DETAIL

Figure 4-54 Blade Materials

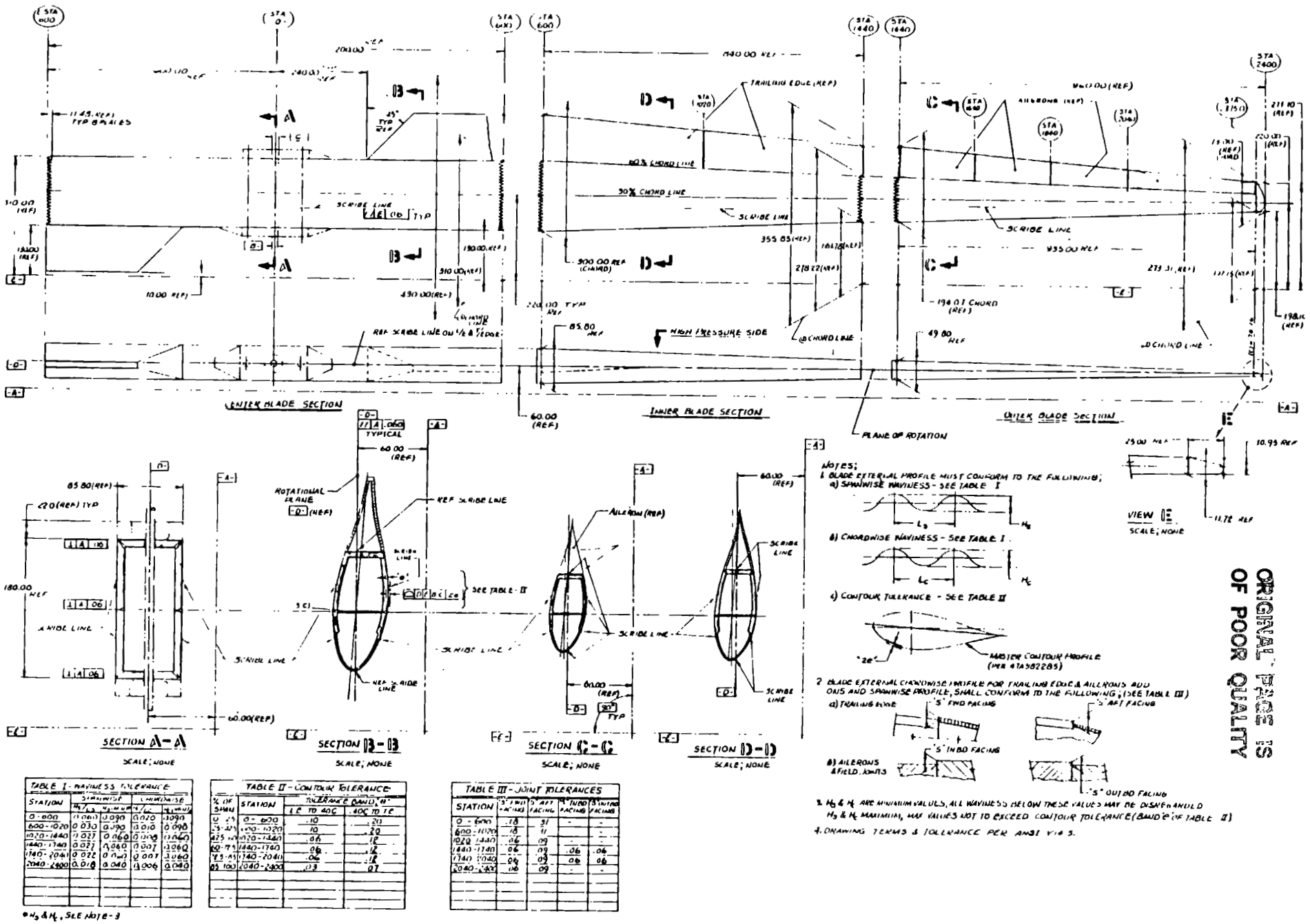

Figure 4-55 Blade Geometry & Tolerances

Table 4-21 Blade Weight

	UNIT WEIGHT, LBS.	# REQD.	TOTAL
CENTER BLADE ASSY		1	145,490
- CENTER BLADE	104,380	1	104,380
- CENTER BLADE WEBBING	4,600	1	4,600
- BOLSTER (INCLUDING INSERTS)	14,340	2	28,680
- TEETER SHAFT	5,900	1	5,900
INNER BLADE SECTION		2	78,920
- INNER BLADE	39,460	2	78,920
OUTER BLADE ASSY		2	35,420
- OUTER BLADE AND TIP	14,610	2	29,220
- AILERONS	3,100	2	6,200
TRAILING EDGE ASSEMBLY	2,395	2	4,790
HYDRAULIC INSTALLATION	930	2	1,860
ELECTRICAL INSTALLATION	1,090	2	2,180
ICE DETECTOR INSTALLATION	100	2	200
LIGHTNING PROTECTION INSTALLATION	470	2	940
BALLAST INSTALLATION	5,500 (Max)	1	5,500
			273,370

4.3.1 BASIC STRUCTURE

The cross-sections of the center, inner and outer blade sections have an outer mold line that is described by the structural portion of the airfoil. The aft surface of this shape is formed by the spar at 60% of the airfoil chord. There is another spar placed at 30% of the chord. The inner mold line of each section is determined by the wall and spar thicknesses required to meet the limit, fatigue, buckling margin of safety, and stiffness requirements. This section will discuss the approach used to design a structure with the minimum weight that satisfies these requirements.

The blade can be visualized as a cantilevered beam supported at the center of rotation. As shown in Figure 4-56, distributed shear loads act in the Y and Z directions and an axial force, representing the centrifugal force, acts in the X direction. The combination of these loads produces a spanwise stress equal to:

$$\left(\frac{\pm Mc}{I_y}\right) + \left(\frac{\pm Mc}{I_z}\right) + \left(\frac{P}{A_x}\right) \qquad \text{equation 4-1}$$

The stress at any point around the perimeter of the airfoil is composed of a flapwise, chordwise, and axial component. Because of the airfoil shape, the distance from the Y and Z neutral bending axes to the extreme fiber is a variable. This condition will produce a maximum stress at only one chordal point for a chord section of constant wall thickness. For a minimum weight design, the stress at all points should be equal to the allowable stress. This condition can be approached by varying the thickness of the wall at each chordal point in proportion to its distance from the neutral axes. The amount of weight saved must be balanced against the difficulties encountered in producing a complex shape.

Finally, since the blade is subjected to bending loads, tension and compressive stresses are produced. A buckling tendency is induced as a result of the compressive stress. This tendency can be controlled by increasing the wall thickness, by installing additional spars, or both. The final design represents a trade-off between the weight savings and manufacturing complexities of each approach.

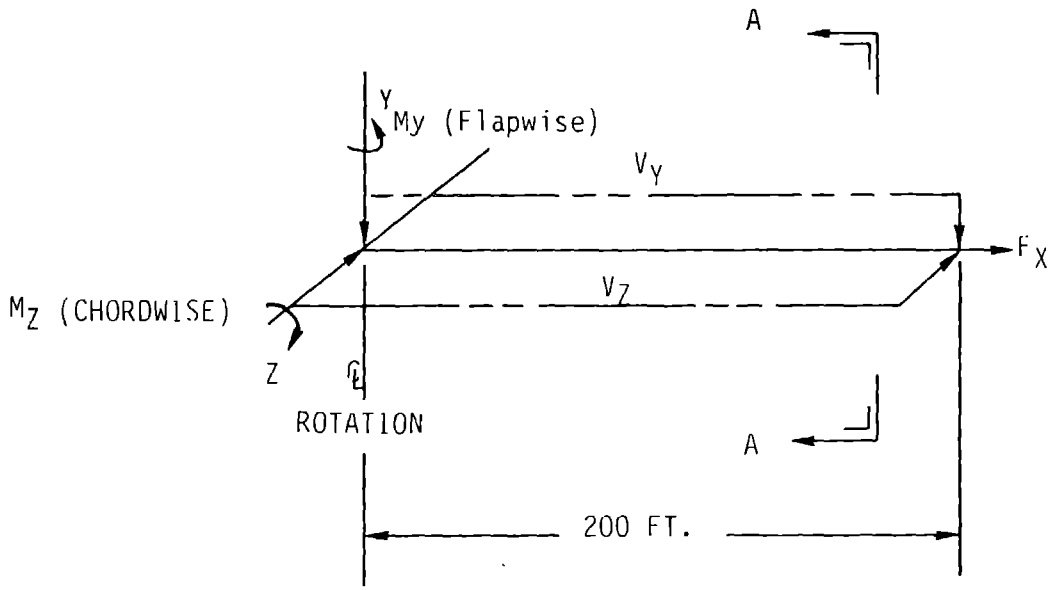

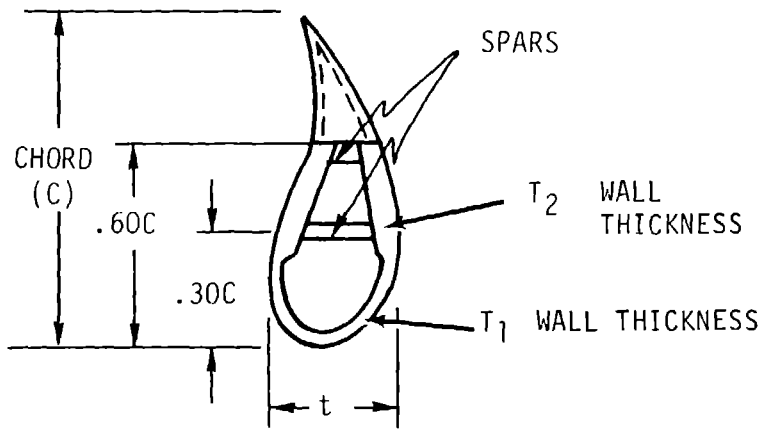

SECTION A-A

Figure 4-56. Conceptual Diagram of Blade Loading

A computer program, called SECTION, was developed to assist in evaluating the many trade-offs. The program equates the allowable stress to the first two terms of equation 4-1, and for a given set of geometry constraints, determines the value of the wall and spar thicknesses that yield a minimum weight. To simplify the program, the third term of equation 4-1 was ignored, since it represents only 5% of the total stress. The program methodology is shown in Figure 4-57.

The geometrical restraints include the spanwise definitions for the airfoil chord length, thickness ratio, wall thickness ratio, spar locations and the chordal locations where the wall thickness is to change. The final values for these restraints are shown in Table 4-22.

The material properties to be entered include density (.023 lb/in^3), modulus of elasticity (2.25 x 10^6 psi), and the limit and fatigue allowables. The stress allowables were discussed in section 8.1.8, Vol. II, and are repeated in Table 4-23. They represent the working strength of the wood parallel to the grain, its strongest direction. To take full advantage of its strength, the blade sections are fabricated with the grain in the direction of loading.

The M_y and M_z limit and fatigue loads described in section 7.5, Vol. II, are also entered. A typical loads input for the final blade design is shown in Table 4-24. The histogram of fatigue loads versus cycles, for each spanwise location, is divided into 24 intervals to facilitate a Miner's number summation.

After the program performs a series of load and sizing calculations the resultant skin and spar thicknesses and other blade characteristics are printed. The schedule of final thicknesses and the stress summary as determined by the program are shown in Table 4-25 and 4-26, respectively. This data is adjusted to reflect the results of finite element modeling, local reinforcement requirements, and the addition of the centrifugal force component, term three of equation 4-1.

Using SECTION to determine the blade thicknesses is satisfactory for the continuous run of material, such as the inner blade. However, cutouts and joints in the center, outer blade, and bolsters require special attention. Detailed calculations supported by finite element modeling are presented in the following sections.

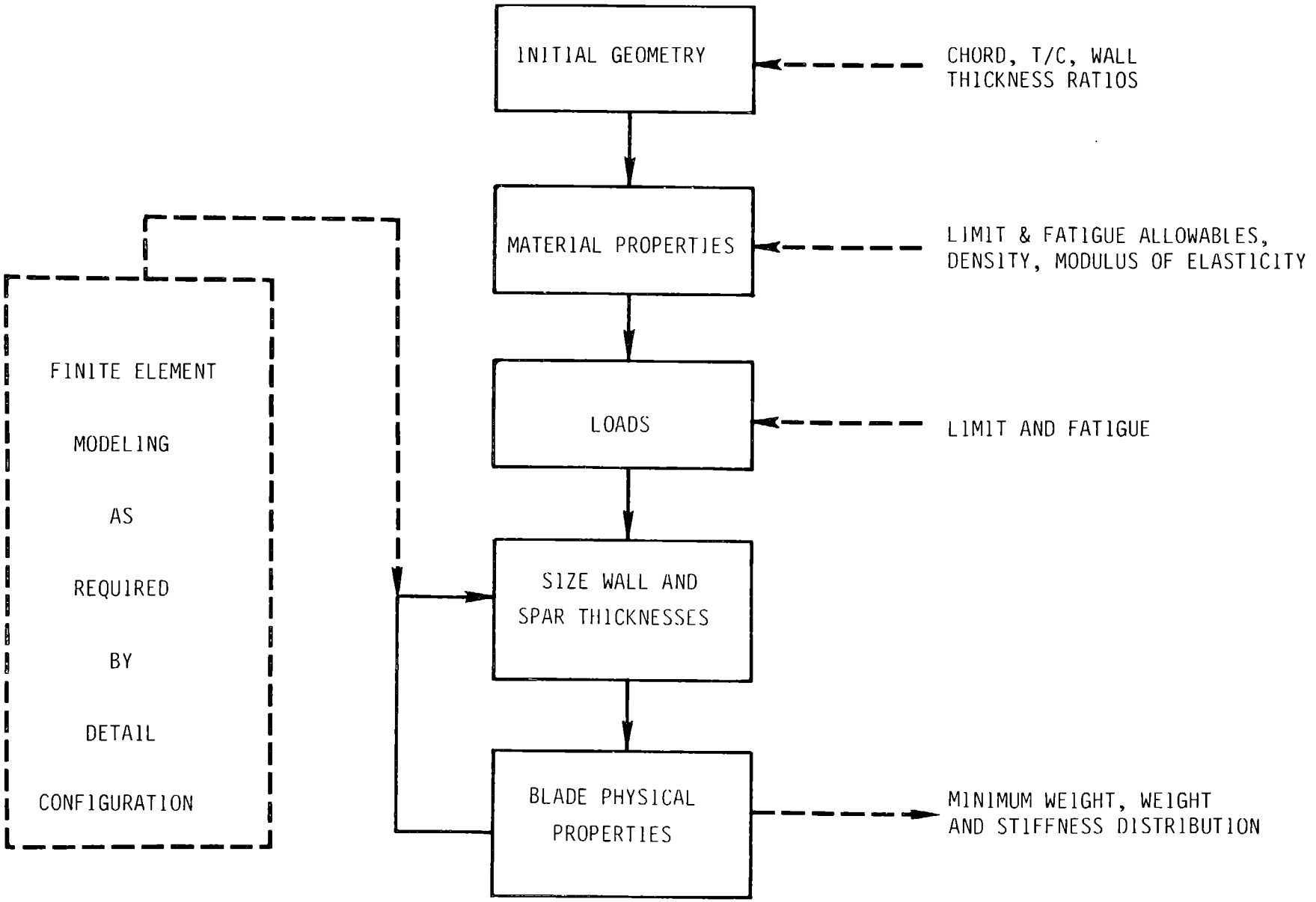

Figure 4-57. SECTION Execution Methodology

Table 4-22 Summary of Final Blade Geometry Characteristics

Airfoil Chord Length, in.	300 at 0 $^{x}/R$* 300 at .25 $^{x}/R$ 73 at 1.0 $^{x}/R$
Thickness to Chord Ratio	.286 at 0 $^{x}/R$ .286 at .25 $^{x}/R$ .224 at .75 $^{x}/R$ .150 at 1.0 $^{r}/R$
Spar Locations	.30 Chord .60 Chord
Wall Thickness Ratio, T1/T2	1.0 at 0 $^{x}/R$ .67 at .25 $^{x}/R$ .46 at .60 $^{x}/R$
Location of Wall Thickness Change	Blended between 0 $^{x}/R$ & .25 $^{x}/R$ .20 Chord at .25 $^{x}/R$ .20 Chord at 1.0 $^{x}/R$

* Rotor Structure Truncated to 180 in. at 0 $^{x}/R$

Table 4-23 Summary of Wood Allowables used in SECTION's Sizing

Tension Parallel To Grain

One Time Limit	4700 psi
Frequently Occurring Limit	4100 psi

Fatigue

Life Line, Cycles	Alt. Stress, psi	Mean Stress, psi
4.0×10^8	0.128×10^4	0.
	970.	460.
	764.	934.
	520	0.146E 04
	0.	0.320E 04
1.0×10^7	0.165×10^4	0.
	0.133×10^4	610.
	0.104×10^4	0.127×10^4
	720.	0.20×10^4
	0.	0.476×10^4
1.0×10^6	0.194×10^4	0.
	0.160×10^4	730.
	0.125×10^4	0.153×10^4
	880.	0.250×10^4
	0.	0.517×10^4
1.0×10^5	0.228×10^4	0.
	0.192×10^4	880.
	0.152×10^4	0.185×10^4
	0.105×10^4	0.296×10^4
	0.	0.534×10^4
1.0×10^4	0.267×10^4	0.
	0.233×10^4	0.107×10^4
	0.184×10^4	0.224×10^4
	0.122×10^4	0.345×10^4
	0.	0.547×10^4

Table 4-24 Typical Loads Definition for Final Blade Design

Spanwise Location .25 X/R

One Time Limit Load

Flapwise Moment	.228E9 in-lbs
Chordwise Moment	.101E9 in-lbs

Fatigue Loads

			Average Load in Bar Width			
			Flapwise Moment		Chordwise Moment	
Bar No.	Commul. %' Tile	No. of Cycles	Mean	Cyclic	Mean	Cyclic
1	5%	0.1800E 08	0.6610E 08	0.2900E 07	-0.6380E 07	0.1680E 08
2	10	0.1800E 08	0.6780E 08	0.6180E 07	-0.6690E 07	0.3400E 08
3	25	0.1800E 08	0.6910E 08	0.6850E 07	-0.6800E 07	0.3460E 08
4	20	0.1790E 08	0.7010E 08	0.7390E 07	-0.6830E 07	0.3500E 08
5	25	0.1800E 08	0.7100E 08	0.7870E 07	-0.6800E 07	0.3530E 08
6	30	0.1800E 08	0.7190E 08	0.8320E 07	-0.6740E 07	0.3570E 08
7	35	0.1800E 08	0.7270E 08	0.8760E 07	-0.6660E 07	0.3590E 08
8	40	0.1790E 08	0.7340E 08	0.9210E 07	-0.6570E 07	0.3620E 08
9	45	0.1800E 08	0.7400E 08	0.9650E 07	-0.6450E 07	0.3650E 08
10	50	0.1800E 08	0.7470E 08	0.1010E 08	-0.6310E 07	0.3670E 08
11	55	0.1790E 08	0.7530E 08	0.1060E 08	-0.6260E 07	0.3700E 08
12	60	0.1800E 08	0.7580E 08	0.1110E 08	-0.6260E 07	0.3720E 08
13	65	0.1790E 08	0.7630E 08	0.1160E 08	-0.6250E 07	0.3750E 08
14	70	0.1800E 08	0.7690E 08	0.1220E 08	-0.6380E 07	0.3780E 08
15	75	0.1790E 08	0.7740E 08	0.1290E 08	-0.6650E 07	0.3800E 08
16	80	0.1790E 08	0.7780E 08	0.1370E 08	-0.6810E 07	0.3840E 08
17	85	0.1800E 08	0.7820E 08	0.1470E 08	-0.6840E 07	0.3880E 08
18	90	0.1790E 08	0.7970E 08	0.1600E 08	-0.6800E 07	0.3930E 08
19	95	0.1800E 08	0.8230E 08	0.1800E 08	-0.6750E 07	0.4000E 08
20	97	0.7180E 07	0.8400E 08	0.2020E 08	-0.6740E 07	0.4070E 08
21	99	0.7180E 07	0.8790E 08	0.2320E 08	-0.6700E 07	0.4150E 08
22	99.9	0.3230E 07	0.9420E 08	0.2940E 08	-0.5720E 07	0.4300E 08
23	99.99	0.3230E 06	0.7790E 08	0.4270E 08	-0.1250E 08	0.4480E 08
24	Typ III	0.3540E 05	0.6060E 08	0.6480E 08	0.1140E 08	0.5550E 08

Table 4-25 Thicknesses for Blade Design Determined by SECTION

	Thickness, in.			
X/R	T1	T2	.30 Spar	.60 Spar
0.00	9.3	9.3	1.9	9.3
.10	6.5	7.5	1.4	8.2
.20	4.7	6.4	1.2	7.7
.25	3.9	5.9	1.1	7.3
.30	3.6	5.7	1.0	6.5
.40	3.5	6.1	1.0	5.6
.50	3.4	6.6	1.0	4.7
.60	2.9	6.3	1.0	3.2
.70	2.5	5.5	.8	2.3
.80	1.7	3.7	.5*	1.3*
.90	.9	2.0	.2*	.6*
1.00	.7	1.4	.2*	.4*

* Later increased based on detailed stress analysis

Table 4-26 Critical Stress Summary for Final Blade Design, Determined by SECTION

Desired Miner's No. Summation < 1.0
Desired Limit Margin-of-Safety > 0.00
Desired Buckling Margin-of-Safety > 0.00

	Miner's No. Summation					Limit Stress			Buckling Stress	
X/R	Max	Crit	Crit/Max	MOS	Location % C	Actual (PSI)	MOS	Location % C	Avg. (PSI)	MOS
0.00	.974	1.000	1.03	.00	.60	3820	.23	.60	1270	3.05
.10	.973	1.000	1.02	.00	.01	4040	.16	.60	3390	1.49
.20	.971	1.000	1.03	.00	.60	4180	.13	.60	3500	.28
.25	.964	1.000	1.04	.00	.60	4320	.09	.55	3310	.39
.30	.966	1.000	1.01	.00	.60	4560	.03	.50	3490	.27
.40	.360	1.000	2.78	.09	.55	4680	.10	.45	3510	.39
.50	.138	1.000	7.22	.18	.50	4530	.04	.45	3290	.73
.60	.123	1.000	8.14	.19	.50	4670	.01	.45	3290	.66
.70	.025	1.000	40.31	.36	.50	4530	.04	.45	3110	.79
.80	.017	1.000	57.79	.40	.45	4670	.01	.45	2740	.45
.90	.021	1.000	48.18	.38	.40	4200	.12	.40	2880	-.32*

* A positive margin was found in detailed analysis

4.3.1.1 Center Blade

The center blade is the expanse of the blade between + .25R and - .25R (where R is the radius), shown in Figure 4-58. At its extremities, the cross-section is a truncated airfoil, 180 in. along the chord, and twisted so that the leading edge is 5° into the wind. The shape gradually becomes a rectangular cross-section with no twist at the center of rotation. A center spar, located at 30% of the chord, decreases the unsupported span of the chordal panels and improves their buckling stability. The aft spar, located at 60% of the chord, and the center spar are foreshortened at the ends of the blade to provide clearance for field assembly tooling. Rib and keel support structures, shown in Figure 4-58, are installed inside at the center of rotation to transfer loads to the teeter shaft and rotor yoke. These secondary structures are bonded with wood fillets to increase the load carrying capability at the joint and to reduce the stress concentration.

Sealed manholes on the leading edge on each side of the center of rotation and cutouts in the center spar, ribs, and keels provide access to the inside of the blade. The manhole and cutout perimeters are wrapped with layers of style 7781 glass fiber cloth for transferring loads around the perturbance. In addition, these areas are reinforced locally with glass fiber cloth, to compensate for the material that was removed.

A pattern of fingers is cut into each end of a center blade section, with a congruent pattern of fingers on the adjacent inner blade section. The blade is assembled in the field by bonding the mating finger surfaces. The area of the fingers is reinforced with style 7781 FRP cloth between each layer of wood, to provide dimensional stability throughout the environmental changes during storage and transportation. See section 8.0 of Volume II for a detailed presentation of blade stability test results. Also, the wall and spar thickness in this area of the blade are increased by 20% over the minimum requirements determined by SECTION, to account for the structural joint efficiency. Affixed to the aft spar, between ± .10R and .25R, are trailing edge sections that are explained in section 4.3.3. The sections are bonded with epoxy, then screwed in place during field assembly.

The ends of the center blade are rotationally symmetric. This symmetry permits the blade section to be designed as the spanwise assembly of two

identical C-shaped subassemblies, as shown in Figure 4-58. The subassembly comprises three molded panels with beveled spanwise edges. The subassembly is fabricated by positioning the individual panels in a fixture so that the outer mold line has the proper dimensions. The adjacent edges are bonded together by inserting a wedge-shaped, wood filler into the V-shaped cavity formed by the beveled edges. See section 8.0 and 10.4 of Volume II for additional details. This type of bonding ensures good epoxy coverage and the exclusion of air from the joint, and eliminates the need to position large, heavy pieces very quickly during the short curing time of the epoxy. The joining of the subassemblies is done in similar fashion. Gravity assists the flow of material in all bonding assemblies. Alignment marks, which are scribed into the mold surface and reproduced on the panel piece parts, are used to align the subassemblies to meet the aerodynamic shape tolerances.

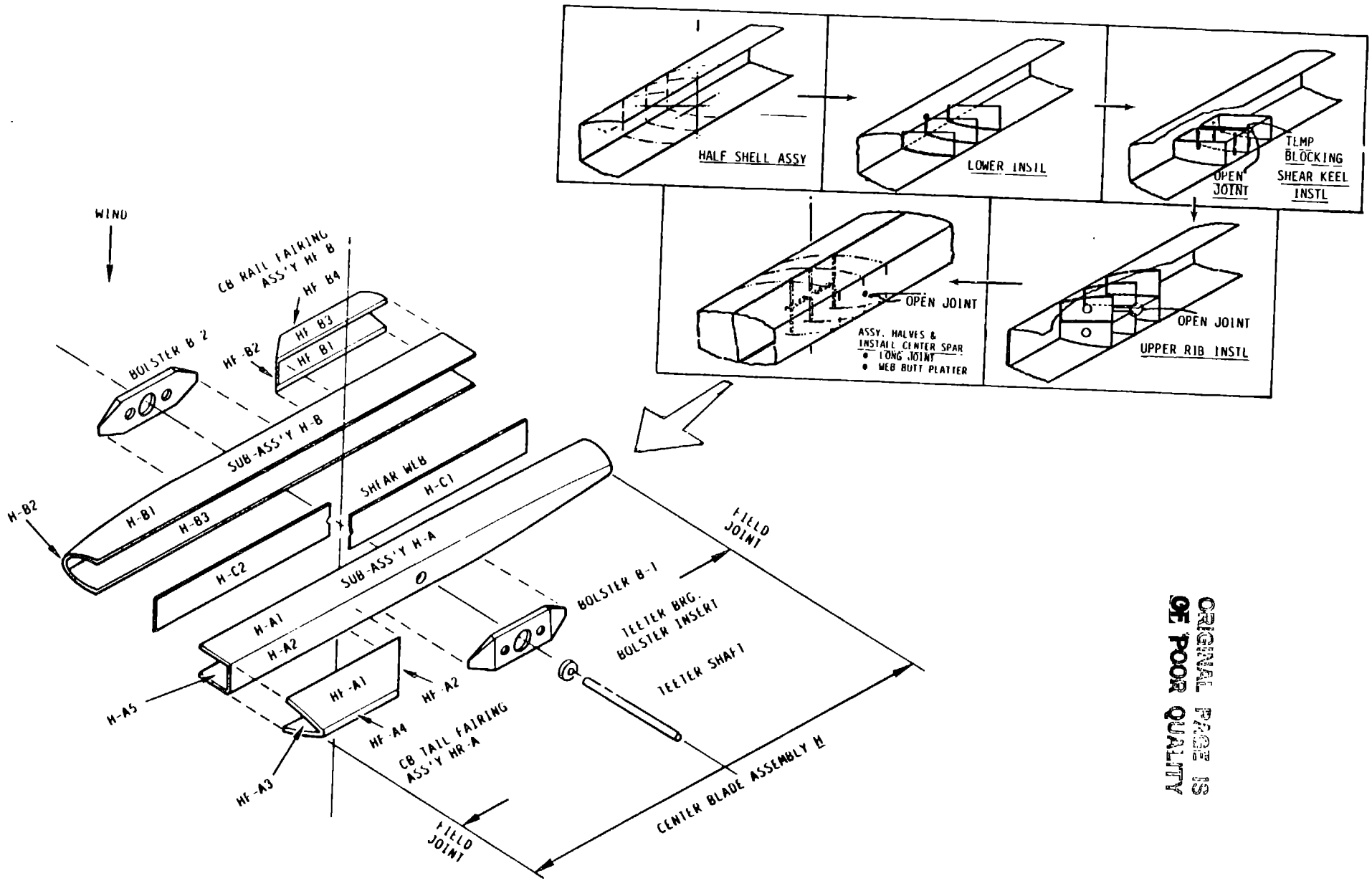

Figure 4-58 Center Blade Assembly

4.3.1.1.1 Center Blade Analysis

The center blade with bolsters was analyzed using a NASTRAN finite element model to determine local stress distributions. The access holes, internal shear bulkheads with holes, bolster tip taper, and steel fittings in the bolster received the most attention.

Except for local effects, the stress levels in the three-dimensional finite element model agreed well with beam theory and SECTION. Most local stress peaks can be controlled by design features, such as augmenting the wood with glass fiber cloth between the veneer at access holes. The effectiveness of more extensive changes, such as redundancy in the brake attachment fitting is uncertain, but the recommendation should work well. Local analysis, which evaluated the brake attachment in the bolster, is described in 4.3.1.2.1.

The double linear taper of the bolster must be replaced during detailed design by a quadratic tip taper. This taper eliminates the 90° notches and reduces the peel stresses. The quadratic taper produces less than half the stress peak, shown in Figure 4-67. The blade section must be overdesigned at the bolster tip, station 100 to 200, to reduce the rated stress to compensate for the remaining tip stress riser.

The following recommendations were made on the basis of the stress analysis. The changes were incorporated into the final drawings, unless otherwise noted.

- Augment all places penetrated by holes with 0.01 in. of style 7781 cloth between each layer of veneer. The cloth should extend one diameter or further into the surrounding wood (Final drawings were not updated).
- Line all holes with glass fiber to reduce the risk of separation of the layers.
- Change the bolster tip taper (to be incorporated).
- Use a redundant fitting that penetrates the spar for teeter brake load reactions. (Final drawings were not updated).
- Locally, from station 100 to 200 transition to increase section modulus of carry-through section by a factor of 1.5 at station 150 to reduce sensitivity to bolster tip stress peak.
- Increase the teeter cup inner wall thickness epoxy to 5.5 in.

- o Use ± 45° ply orientation for interior bulkheads in the Y-Z plane at stations zero and 70 in. (See Figure 4-56.)
- o Use plywood with 0°/90° ply orientation for interior shear web in the X-Y plane. (See Figure 4-56).
- o Use balanced stacking sequence for all multidirectional layering.

The approach and analysis that led to these recommendations are discussed in the following paragraphs. The modelling features are shown in Figures 4-59 through 4-62. Blade twist was modelled. The thicknesses are consistent with a configuration coded VSECT85 and loads published according to system coupled dynamic response analysis. Figure 4-59 shows all the elements. Blade 1 is defined from the center to +600 in., or 25% of the span. Blade 2 is defined to -240 in., and a load transfer transformation to -600 in. At -600 in. a small member is used to locate a concentrated mass that balanced the center of gravity.

The X, Y, Z coordinates of the center of mass of the 151,500 lb. model are 0, 0, -1.187 in. The center of gravity of the entire rotor is offset a little in the -Z direction, and should be computed to locate the teeter shaft.

Teeter Brake Attachment Zone -- Figure 4-61 shows the location of steel in the model. The brake reaction fittings were modeled in two ways. The two rings in the +Y bolster were given independent slopes, representing a loose fit with the connecting pin. The ring in the -Y bolster represents a tight fit with the connecting pins. In both bolsters, the brake fitting is embedded in the bolster and shears against the spar. As shown in Figure 4-63, there is a rolling shear stress peak at these fittings, caused by the smallness, incompatible modulii of elasticity and discontinuous shape. The combined stress also includes a high cross-grain tension of 632 psi. in the wood and glass fiber. Redistribution calculations show 193 psi. in tangential cross-grain tension on the wood, which has a working allowable of 100 psi. Therefore, the size of this fitting was recalculated and the new configuration was analyzed, as discussed in 4.3.1.2.1.

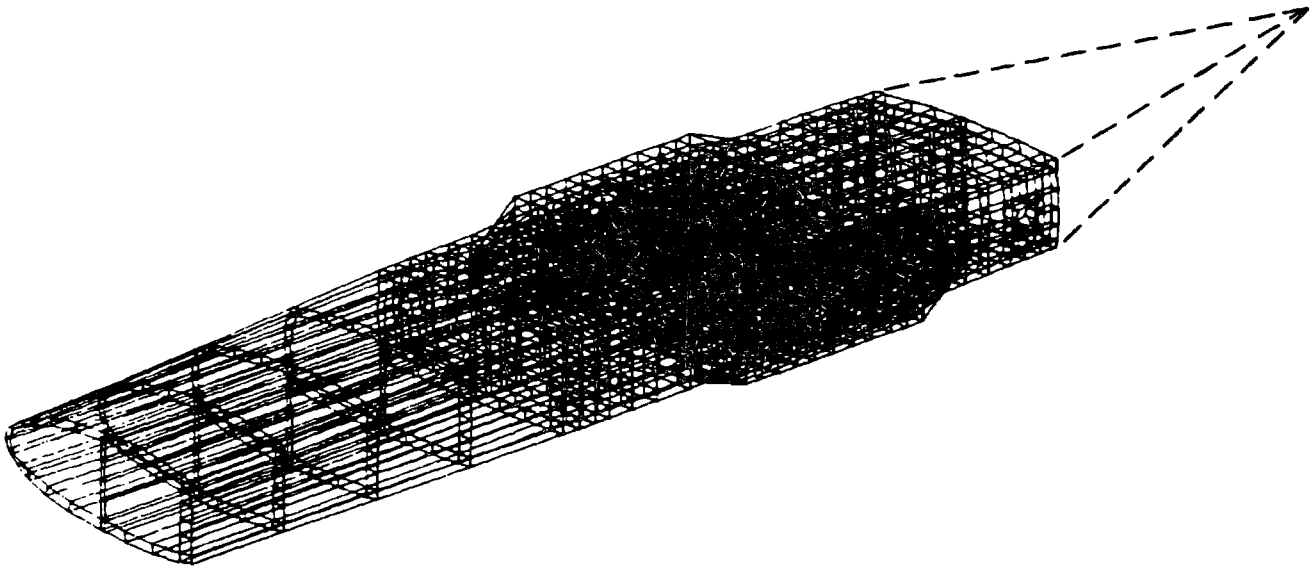

TYPE	NUMBER
HEXA8	1216
PENTA	96
QUAD4	384
GRIDS	2539

Figure 4-59. All Elements

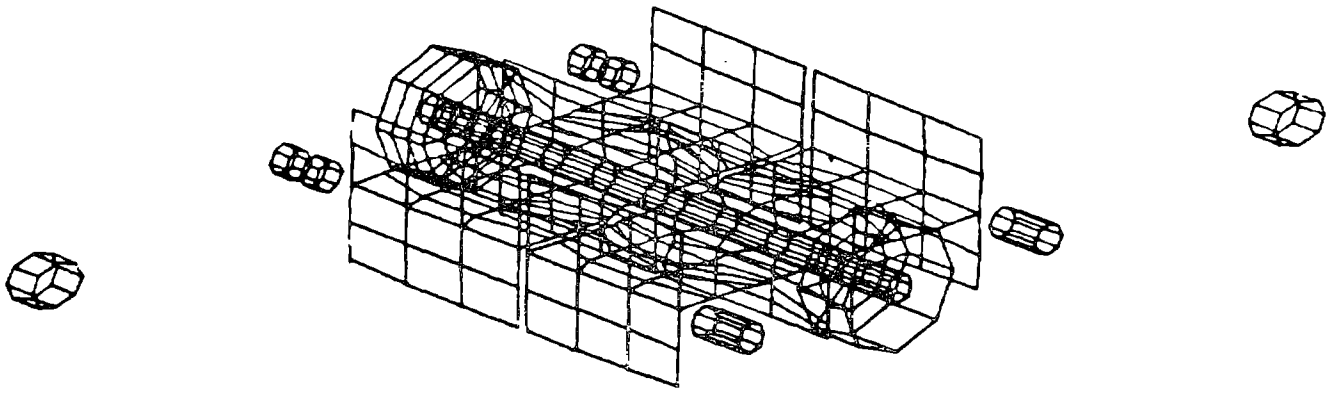

Figure 4-60. All Quadratic Elements

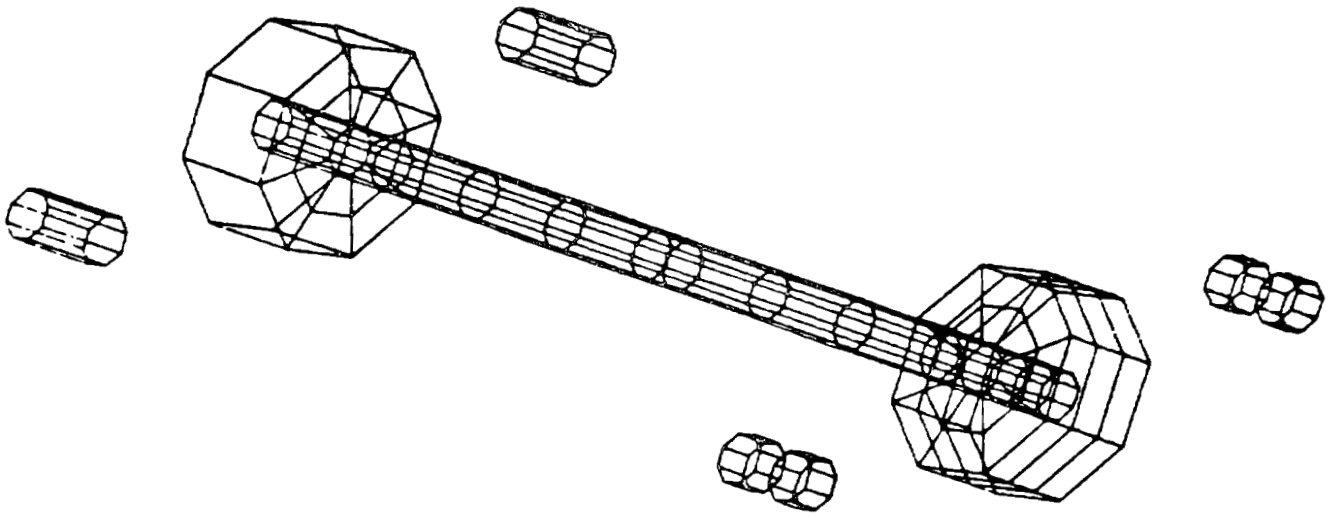

Figure 4-61. All Steel at Center

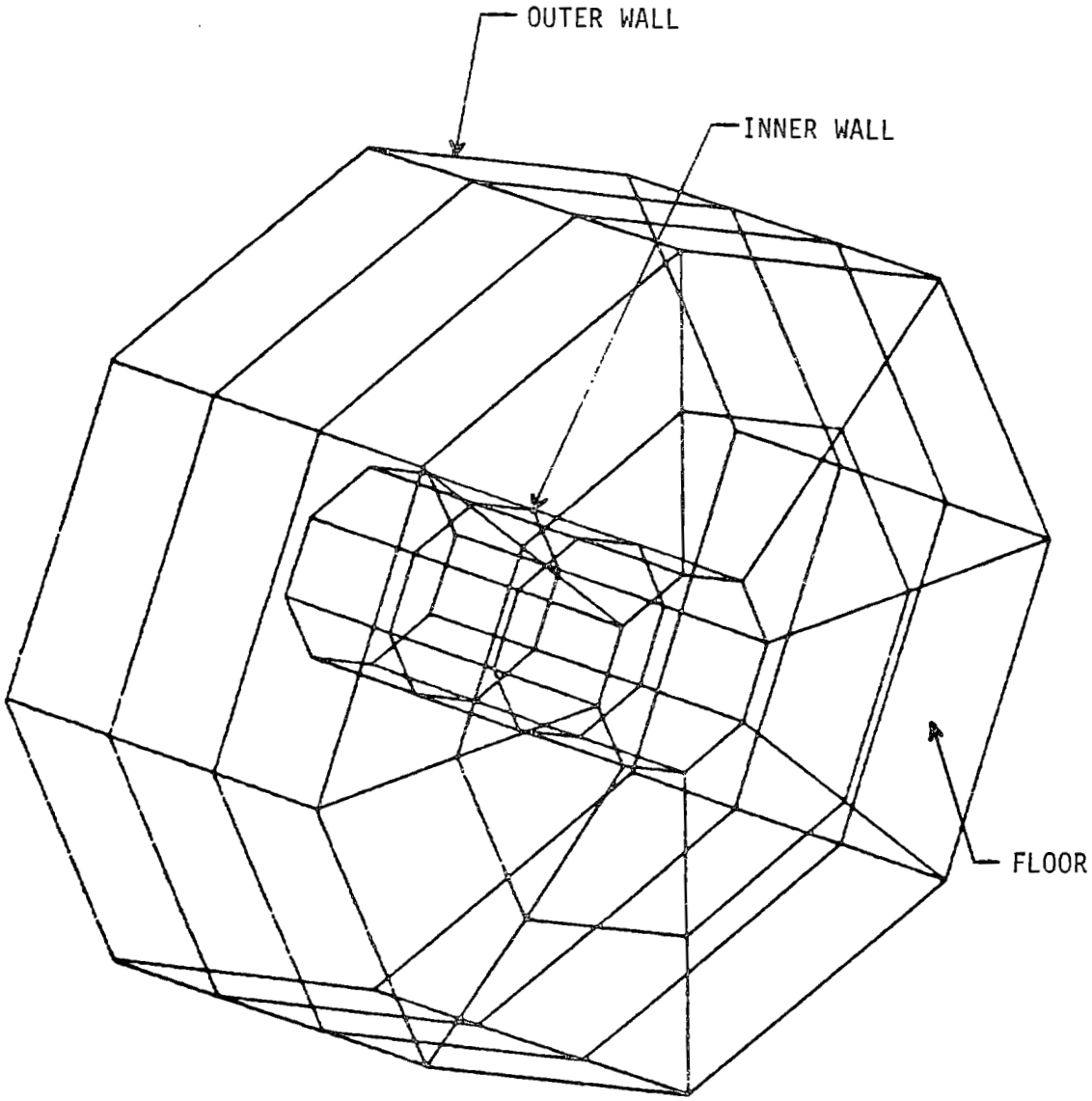

Figure 4-62. Steel Cup at Center

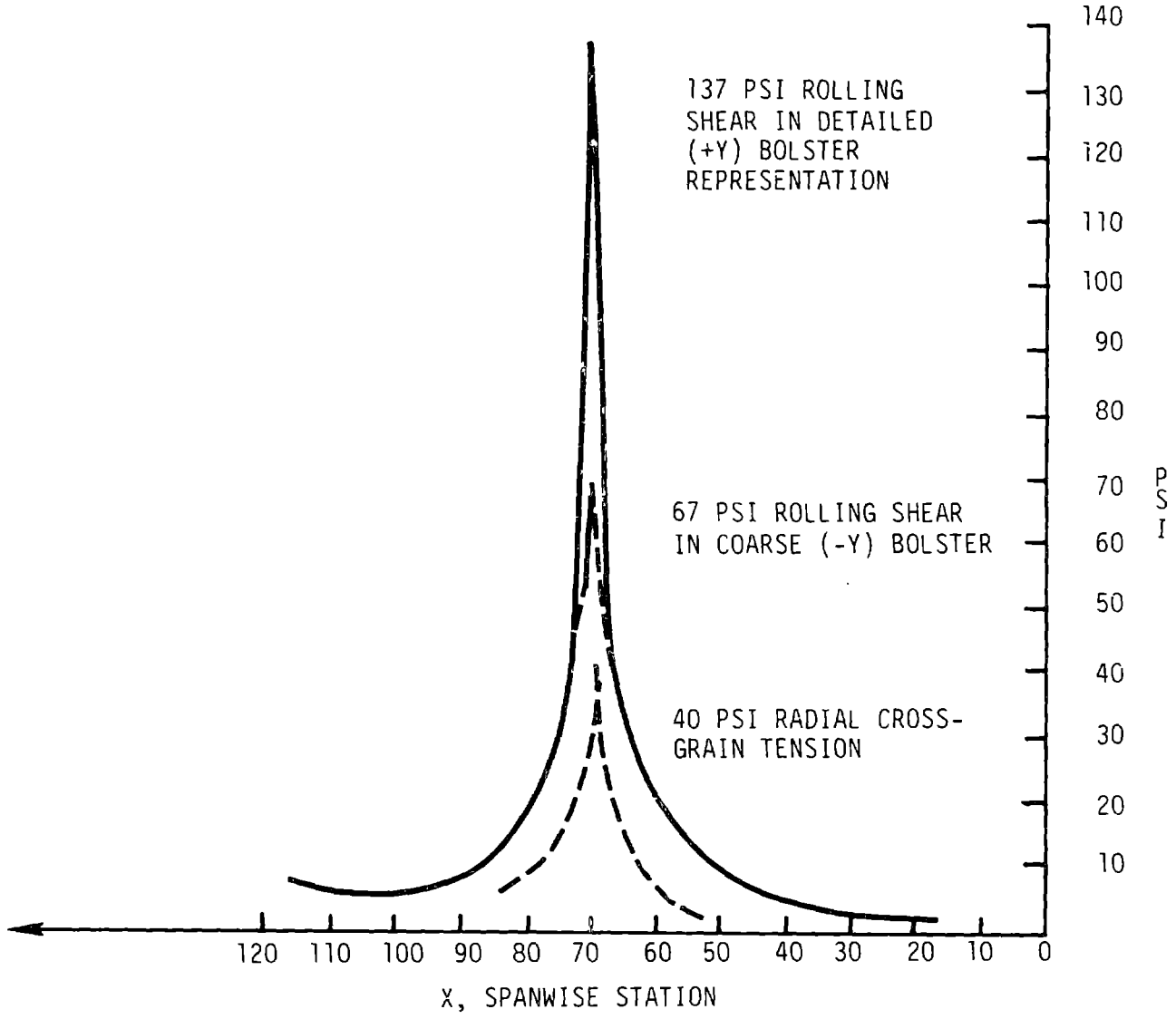

Figure 4-63. Cross-Grain Stresses at the Teeter Brake Fittings Predicted by the Finite Element Model of the Center Blade

Teeter Bearing Fitting Zone -- Stresses in the bolster are satisfactory at the teeter bearing cup. The teeter cup bonded to the augmented wood has a larger surface area than the brake fittings. The maximum rolling (YZ) shear is 105 psi. and the maximum radial (Y) cross-grain tension is 80 psi. Both are less than the working allowables, which are 110 and 190 psi., respectively. The stresses in the augmented directions are also less than allowables as listed in Tables 4-27 and 4-28.

The steel cup was modelled separately. The design had a 4.5 in. thick floor, 2 in. thick outer wall and a 7 in. thick bearing support tube. However, the model did not include the surrounding wood, so the center blade model analyzed the use of a 4 in. thick inner wall and 4 in. floor. This part of the center blade model is shown in Figure 4-62.

Table 4-29 shows that the 4 in. thick inner wall is unsatisfactory. The allowable alternating stress for this steel is ± 12,000 psi., but the inner wall would experience ± 18,771 psi. Figures 4-64 through 4-66 are plots of the detailed bearing fitting model and results for the teeter cup with the 7 in. thick inner wall. It experiences an alternating stress of ± 13,000 psi. in the floor plate, where this model did not include support from the wood. The principle stress in the 7 in. wall is predicted to be 3,413 ± 8,756 psi.

Examination of the detailed force distribution showed that about 50% of the wall stress is induced by plate bending. The plate thickness was increased, to avoid plate bending. The new plate bending stresses are proportional to thickness squared. The rest of the stress is associated with membrane forces. For these forces, the new thickness is linearly related to plate thickness, as shown in the following equation:

$$S_{NEW} = 1/2\ S_{OLD}\ (t_{OLD}/t_{NEW})^2 + 1/2\ S_{OLD}\ (t_{OLD}/t_{NEW})$$

The new inner wall is about 5.5 in. thick. The floor is 4 in. thick and the outer wall, 2 in. thick. The radius in the fillets joining these three zones is 2 in. These dimensions are associated with stresses of 24 ksi for the integrally machined forged cup.

Table 4-27 Stress Redistribution For Douglas Fir Veneer, 0.10 in. thick Augmented by 0.01 in. Glass Fiber, Bidirectional Cloth, Style 7781

(1)	COMPOSITE (PSI)	WOOD (PSI)	FRP (PSI)
L	1,000	961	1,393
T	0	12.5	-125
LT	0	0	0
L	0	-45	445
T	1,000	305	7,953
LT	0	0	0
L	0	0	0
T	0	0	0
LT	1,000	813	2,867

(1) L = Longitudinal, parallel to grain.
T = Tangential to tree, normal to grain, in veneer plane.

Table 4-28 Allowable Stresses

PARALLEL TO GRAIN	MAXIMUM		FATIGUE AT 4 X 10^8 CYCLES			
	D. FIR.	AUGMENTED	D. FIR.		AUGMENTED	
			R=-1	R=+1	R=-1	R=+1
TENSION	4100	4240	1280	3200	1324	3309
COMPRESSION	-4430	-4581	-1280	-3700	-1324	-3826
SHEAR LT	900	1107	±300	730	±369	898
SHEAR LR	1139	1139	±300	730	±300	730
PERPENDICULAR TO GRAIN						
TENSION R	190	190	±60	150	±60	150
TENSION T	100	328	±30	75	±98	246
COMPRESSION R	-230	-230	-120*	-200	-120*	-200
COMPRESSION T	-440	-1443	-260*	-330	-852*	-1082
ROLLING SHEAR RT	110	110	±40	90	±40	90

(VALUES IN PSI)

*THESE ALLOWABLES ARE ON THE MINIMUM STRESS AXIS AT A MAXIMUM STRESS OF ZERO

EACH VENEER IS AUGMENTED BY 0.01 IN. OF 7781 GLASS FIBER CLOTH, WITH THE WARP PARALLEL TO THE GRAIN

Table 4-29 Element Stress Summary, Uncorrelated Maxima

LOCATION	X (L)	Y (R)	Z (T)	XY (LR)	YZ (RT)	ZX (TL) (1) (2)
AUGMENTED WOOD AT BRAKE FITTING	803	40	632	47	270	403
AUGMENTED WOOD AT TEETER CUP	1914	80	286	17	105	189
WOOD AT BOLSTER TIP (W/O K_t)	3300	43	60	-31	-28	-141
WOOD AT R = 210 ACCESS HOLE (W/O K_t)	2319	67	204	23	38	224
FRP ACCESS HOLE LINER	2612	-160	-	414	-	-
PLYWOOD YZ WEB AT R = ± 70	-	408(L)	134(L)	-	-130 (LT)	-
PLYWOOD YZ WEB AT R = 0	-	398(L)	208(L)	-	-118 (LT)	-
PLYWOOD XY WEB AT Z = 0	244 (L)	199(T)	-	234(LT)	-	-

STEEL IN TEETER CUP, 7 in. wall = 3413 ± 8756; floor = 5500 ± 13000 psi.

STEEL IN TEETER CUP, 4 in. wall = 7991 ± 18771; floor = 4800 ± 10987 psi.

Notes (1): See Figure 4-56 for coordinate definition.
(2): L = Parallel to grain
R = Normal to grain in a radial direction with respect to growth rings
T = Normal to grain in a tangential direction with respect to growth rings

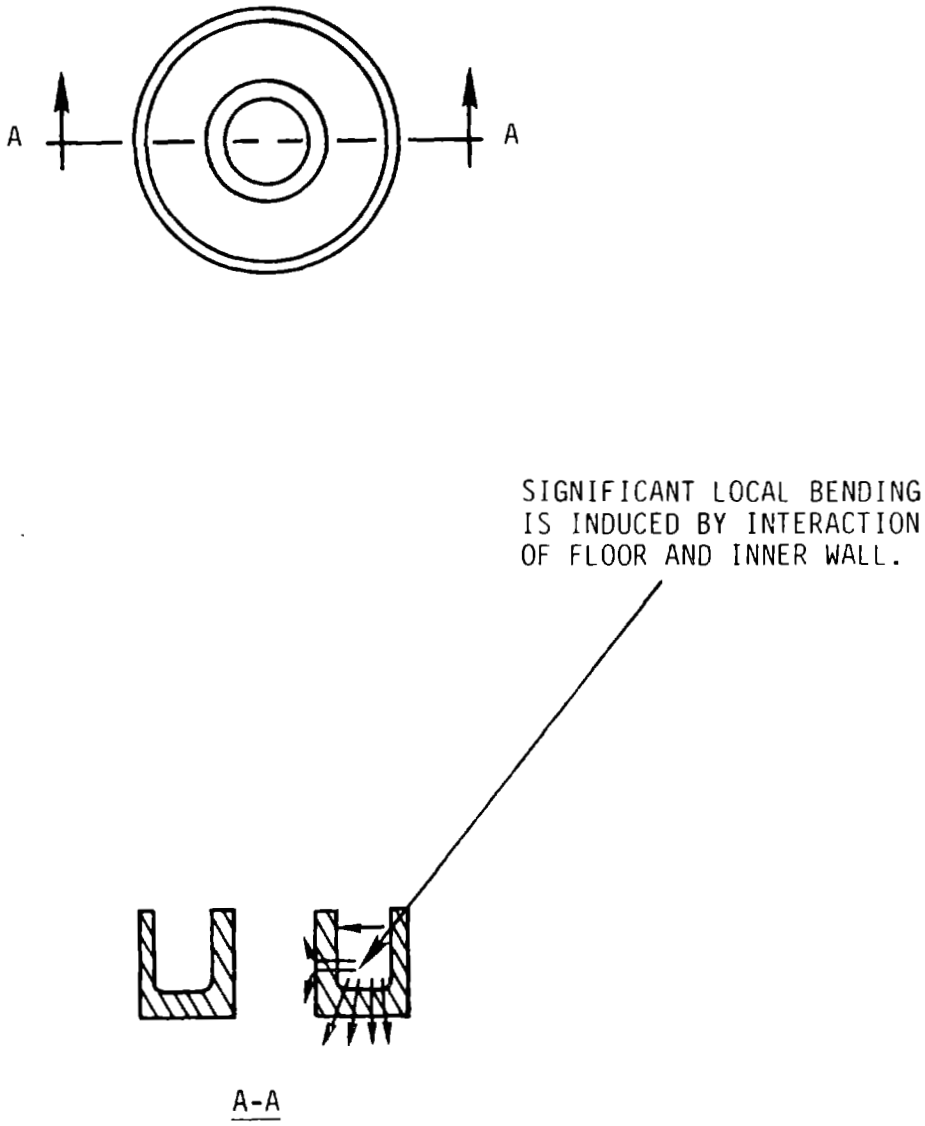

Figure 4-64 Teeter Cup Analysis

Steel Cup Housing For Radial Teeter Bearing

Maximum Deflection 20.7 mils, Maximum Alternating Loads

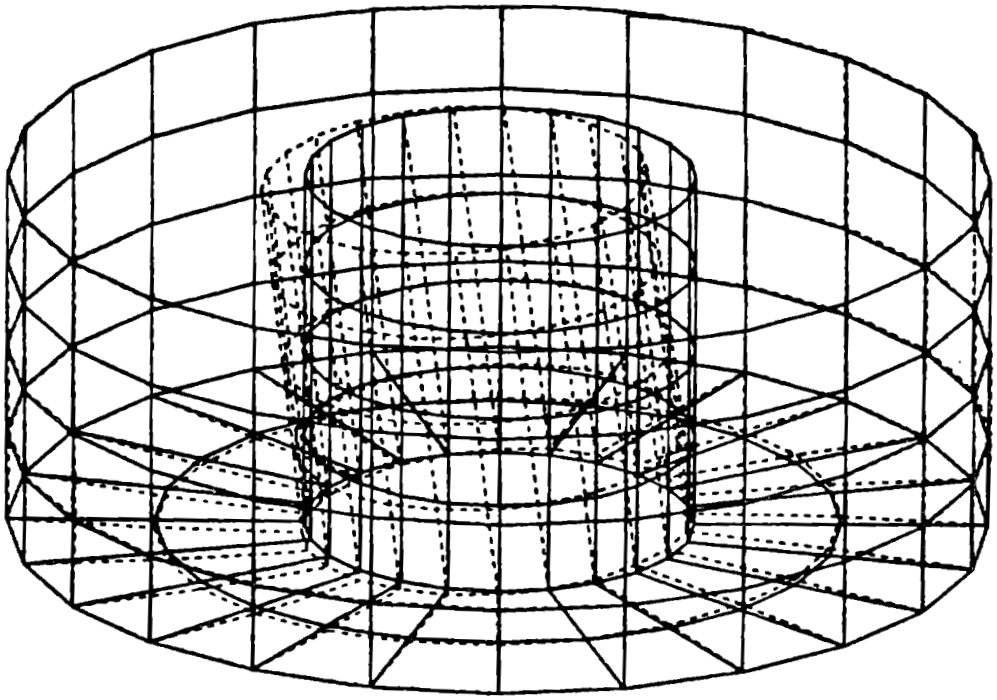

Figure 4-65. Refined Model of Teeter Cup and Deformation Under Maximum Fatigue Loads

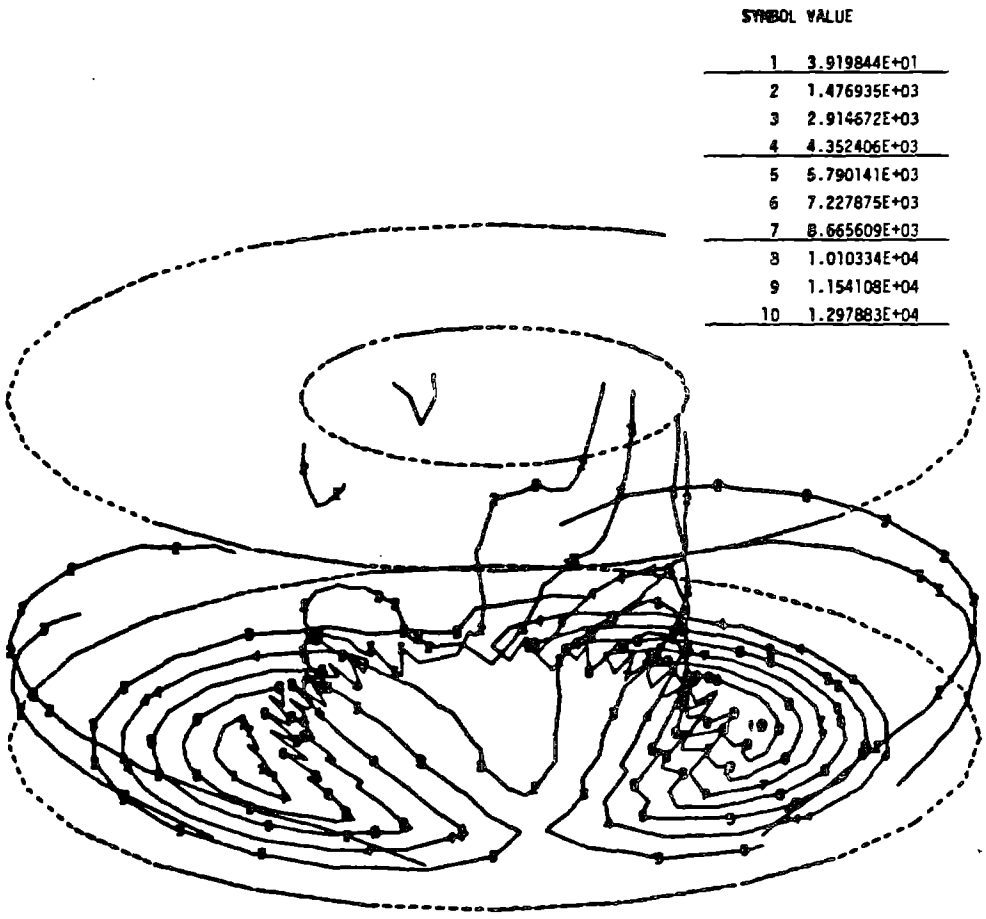

Figure 4-66. Maximum Principle Alternating Stress Caused by Maximum Fatigue Loads

Bolster Tip Zone -- Table 4-29 shows an unconcentrated, maximum spar stress parallel to the grain of 3,300 psi. This stress occurs with the rotor horizontal at rated power, in response to a severe limit gust. A separate series of models estimated the concentrated stress at the bolster tip. The results are summarized in Figure 4-67. The baseline double linear taper is expected to split from the spar during such a limit gust. The fatigue life is unsatisfactory because ± 1,000 psi. parallel to the grain in the spar will probably develop at the bolster termination. This stress is estimated to develop a cross-grain tensile stress greater than the static strength and far greater than the fatigue allowable. Consequently, the bolster tip taper must be a quadratic form that spans the full spar, rather than a form that tapers to 22 in. wide. The subscale static test confirm this assessment, because the bolsters split off the spar at 60% of the strength of a spar. See section 8.0 of Volume II for detailed test results.

Interior Shear Webs -- The stress for 4 in. thick plywood webs is low. The stress is associated with the direction of the grain, as noted in Table 4-29. The Y and Z stress columns for the YZ webs were adjusted for L-direction stress redistribution in the ± 45° layup. Although the thickness could be reduced, since this area is relatively unrepairable, it was overdesigned for the prototype. Field stress measurements will be used to recalculate the size of webs for subsequent units. Access ways must be locally augmented and lined.

Access Holes at Station 210 -- These holes permit entry to the rotor for inspection and maintenance. The stresses listed in Table 4-29 show that the holes are placed satisfactorily, but they should be augmented, to resist the 204 psi. cross-grain tension. The hole should be augmented by one layer of 7781 cloth between each veneer. The hole should also be lined with 1 in. of 7781 glass fiber cloth, so that the veneer doesn't separate from the edge.

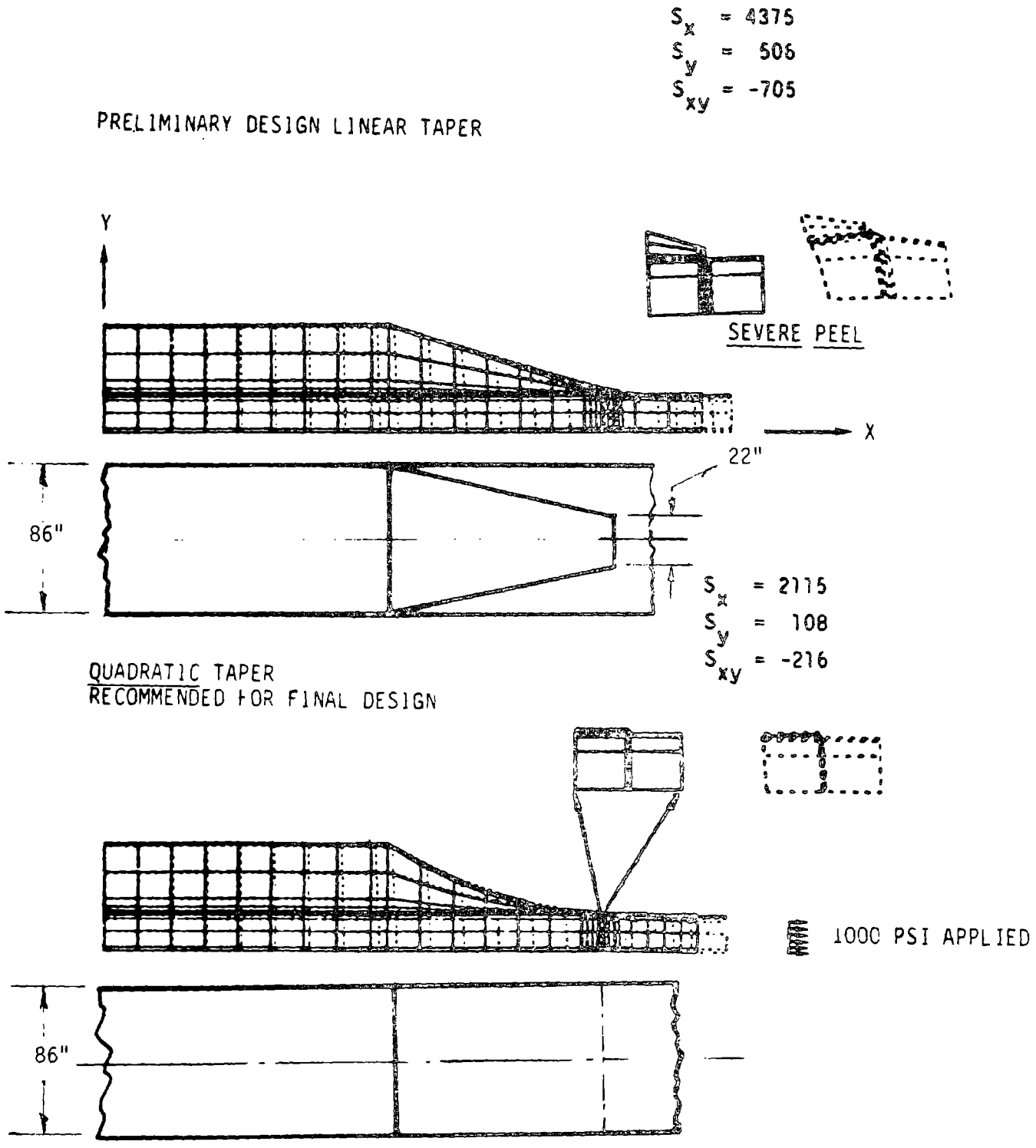

Figure 4-67. Bolster Taper and Stress Concentration at the Tip, for 1,000 psi in Spar.

4.3.1.2 Bolster

The bolster structure is bonded to the center blade leading and trailing surfaces during field assembly. The bolster is shown on Figure 4-68. The bolsters transfer the aerodynamic torque, thrust, and blade gravity loads to the yoke with as little disturbance to the primary center blade structure as possible.

The bolster is made of alternate layers of Douglas fir veneer and style 7781 bidirectional glass fiber cloth. The grain of the wood is parallel to the primary stress caused by the torque and gravity loads. The glass fiber cloth gives the laminated wood enough cross-grain strength to ensure positive margins of safety for stresses induced in this direction from the wind thrust load. The warp of the cloth is parallel to the wood grain, to take advantage of its continuous length in this direction, and to eliminate joints along the span.

The cross-section has a quadratic taper from the maximum thickness of 22 in., to 0.2 in. A featner edge, made by sanding during final assembly, is blended with the main span. This tapering reduces the stress concentration at the bolster tip and the cross-grain stresses discussed in the previous section.

Three holes are built into the bolster. The center hole provides clearance for the teeter shaft and a cavity to install the yoke's radial bearing interface fitting, the teeter cup. The remaining holes are used to install the teeter restraint shown in Figure 4-69. These fittings provide a slip fit for a pin, which captures the teeter restrictor arm in the triangular cavity at each hole. Each cavity is lined with glass fiber cloth and incorporates corner radii to provide structural continuity and to reduce stress concentrations.

The interface between the center blade and the bolster is a flat surface. The bolster is bonded to the center blade. A uniform bond gap is created by duplicating the surface contour variations of the center blade and bolster, using matched and coordinated tooling. Scribe lines are etched onto the part to assist in the assembly and installation of the teeter cup and teeter

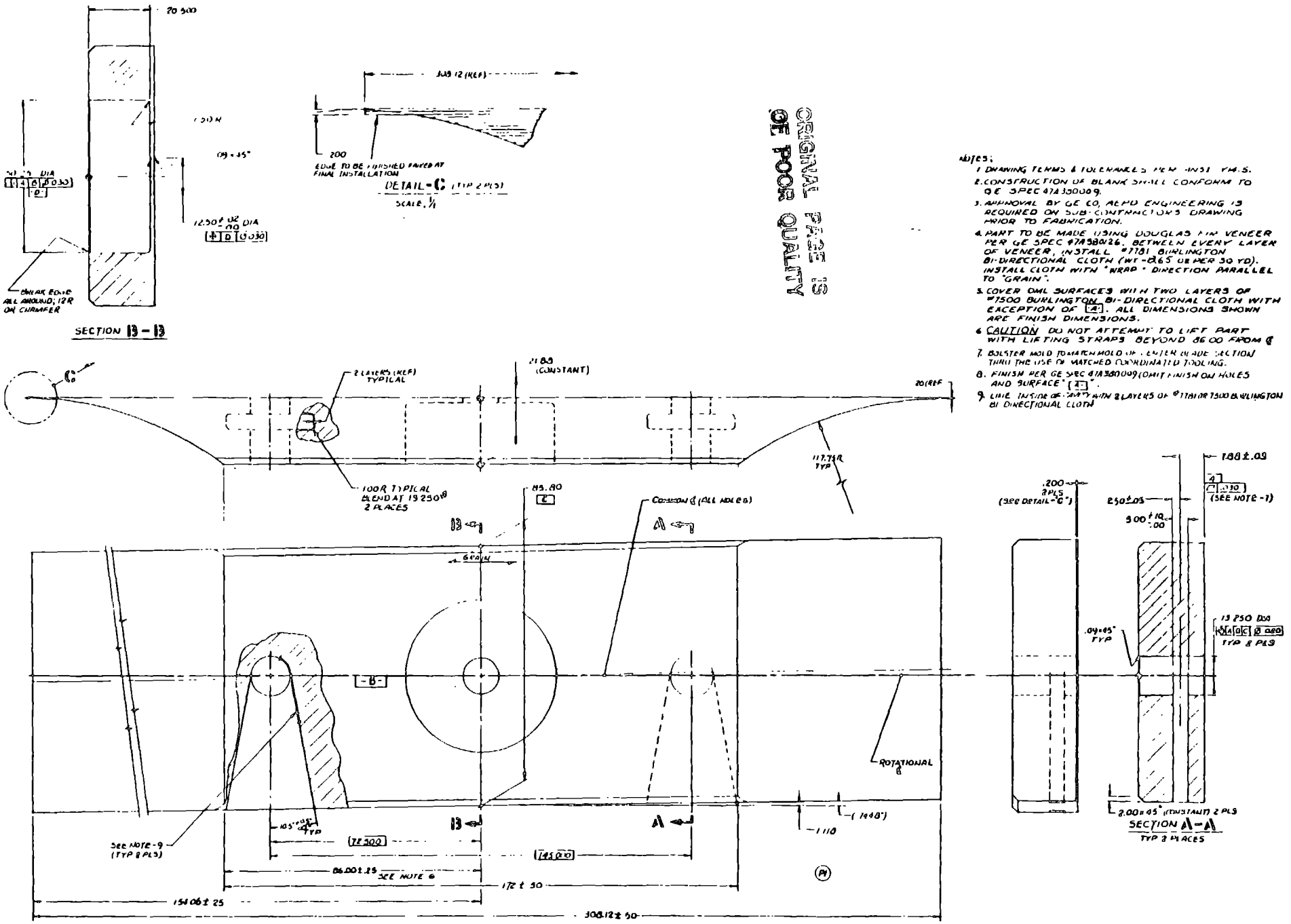

Figure 4-68 Bolster Assembly

restraint fittings. The external surface of the bolster is protected from the environment by two layers of glass fiber cloth. The finished bolster assembly is coated with a white polyurethane paint that resists ultraviolet light.

4.3.1.2.1 Teeter Brake and Bolster Interface Structural Analysis

The interface between the teeter brake and the bolster recommended in this section resolves overstress conditions described in section 4.3.1.1.1. A tubular shell with a dome should be bonded into the bolster and spar, to eliminate the sharp edges of the independently bonded rings and to minimize rolling shear stresses in the wood.

Recommendations -- Figure 4-69 shows a suitable arrangement for the steel details that are bonded permanently into the bolster and spar. The cylinder has a 20.0 in. outer diameter, a 0.375 in. minimum wall thickness, a 90° by 5 in. slot and a hemispherical end cap. The end cap intrudes 5.0 in. into the spar and has a 10.0 in. radius.

The inner diameter of the maintenance-free bearing is about 6.3 in. The pin should have an outer diameter of 6.3 in., an inner diameter of 3.5 in. and an effective span of 10.0 in.

The disks inside the cylinder, which support the pins, should be at least 1.0 in. thick and spaced 10.0 in. apart, on center. The disks should be lightly shrunk into the cylinder with a 0.005 to 0.010 in. diametrical interference. There should be replaceable bushings between the pin and the disks. There should be positive mechanical retention features for the pin, the bushings, and the disks.

Analysis -- Traditional analysis techniques were used to evaluate the drag link and to estimate dimensions for the steel details bonded into the bolster. A finite element model predicted stress levels in the wood and verified the size of the steel shell. The analyses of the drag link and other brake hardware are discussed in section 4.5.5.1.

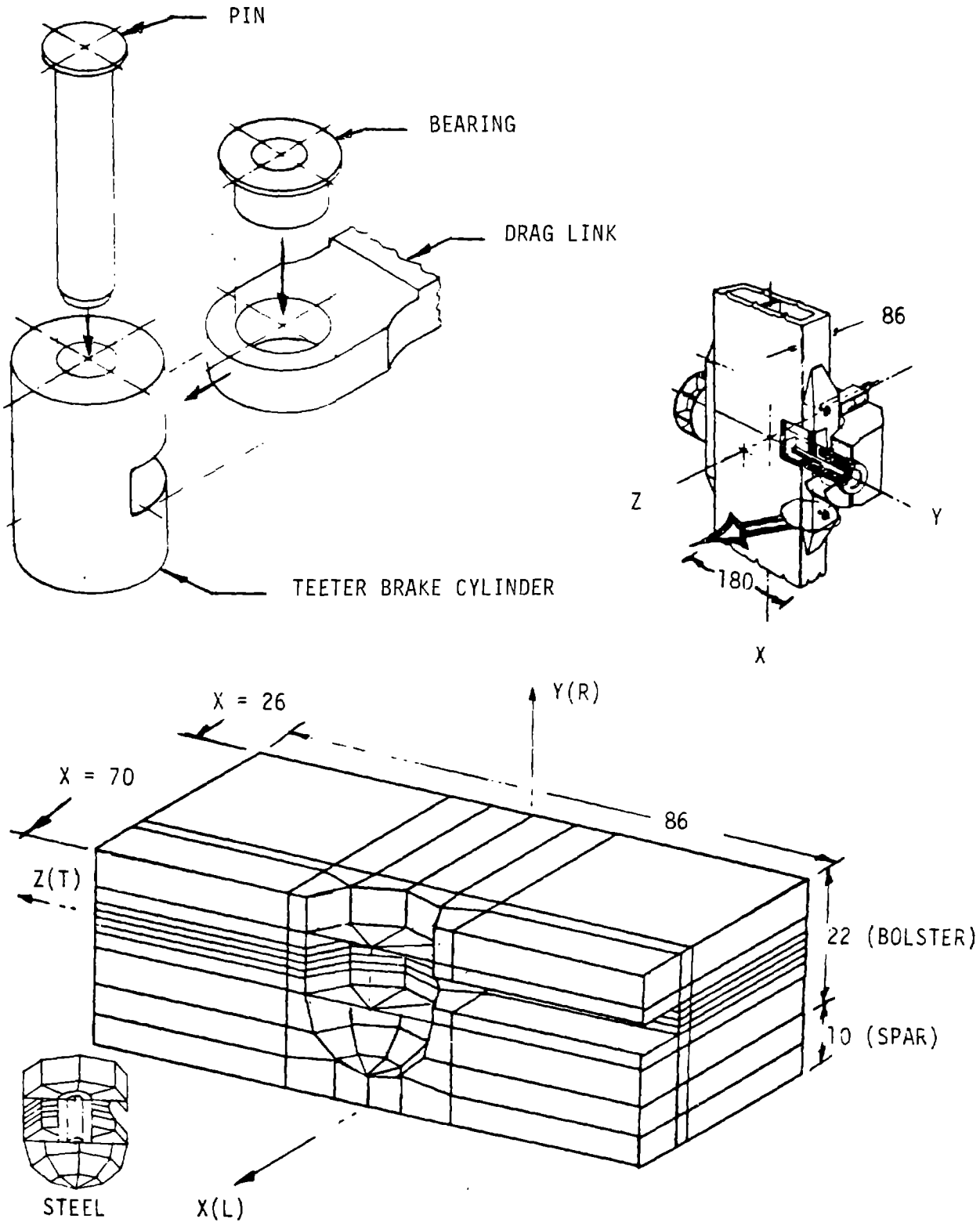

Figure 4-69. Model and Section Through the Brake Attachment Steel-to-Wood Fitting

Shell and Fittings in the Bolster -- Calculations of direct bearing, bending, and shear stress led to the dimensions analyzed with a NASTRAN finite element model. Predicted shear stress in the steel shell determined the wall thickness.

Figure 4-69 and Table 4-30 show the results of the NASTRAN model. The model predicts satisfactory stresses in the wood and in the steel. The table lists the maximum stresses.

Steel Shell and Disks -- The fatigue loading from full-force teeter braking occurs less than 5×10^5 times in an expected 35000 start-stop cycles. The maximum braking force occurs for a few cycles during inflow conditions at low rotor speed. In a tabular histogram in the teeter bearing specification, the angle that triggers full-force braking is listed 110700 times in a spectrum of 1467300 cycles of teeter motion. Half-force brake action occurs 1356600 cycles. The maximum loads occur fewer than 40,000 times during the full-force braking cycles.

The shell and disks are loaded by the surrounding wood deformations in normal operation and in teeter braking. The fatigue spectrum for the shell and disks includes up to 4×10^8 cycles at various amplitudes. This spectrum is defined as AISC condition 4 in ref. 4-1, more than 2×10^6 cycles. As shown in Table 4-30, the maximum alternating stresses in this spectrum are greater than the average mean stress, but the spectrum has a variable stress ratio. The data contributing to Figure 4-70 included many stress ratios. According to references 4-1, 4-2, and 4-3, the design may be evaluated by the stress range and the mean stress may be disregarded. The stress range allowed for AISC condition 4 is 24 ksi for Category A, 16 ksi for Category B and 8 ksi for shear.

The applied stress ranges are twice the alternating values, shown in Table 4-30. The shell and disk stress ranges satisfy the AISC design criteria.

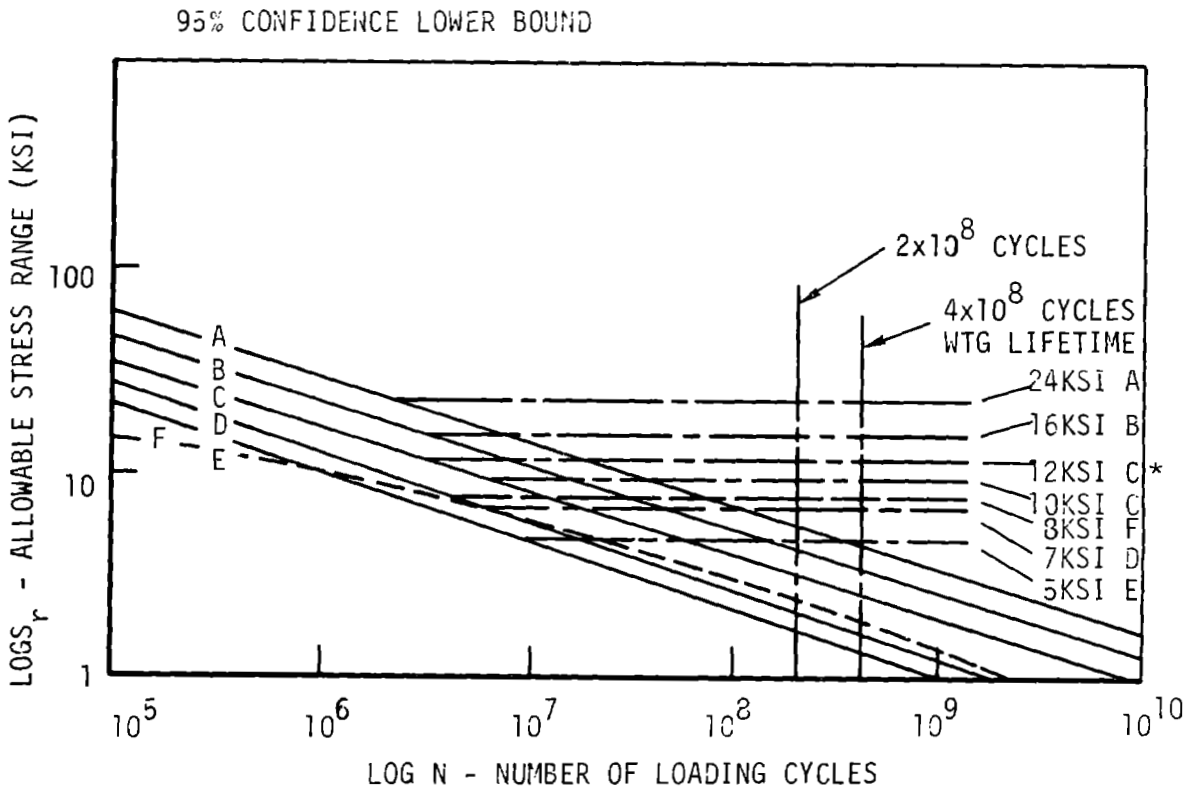

Figure 4-70. Stress vs. Number of Cycles for Various Weld Categories

Table 4-30 Brake Location Finite Element Model Results

	AUGMENTED WOOD					
LOAD CASE	S_L	S_R	S_T	S_{LR}	S_{RT}	S_{TL}
TEETER BRAKING[a]	±1000	±117	±235	±113	±26	±259
LIMIT UPGUST	1320	75	116	109	19	147
AVERAGE MEAN	562	60	40	74	10	63
MAXIMUM ALTERNATING[b]	±528	±25	±56	±38.6	±8	±56.9

	STEEL					
LOAD CASE	SHELL		PIN		DISKS	
	S_1	SHEAR	S_B	SHEAR	S_1	SHEAR
TEETER BRAKING[a]	±8335	±3891	±13507	±5568	±6133	±3053
LIMIT UPGUST	7959	3780	-	-	4613	3130
AVERAGE MEAN	2804	1654	-	-	1546	1056
MAXIMUM ALTERNATING[b]	±3712	±2030	-	-	±2261	±1523

(a) EXPECTED TO OCCUR 10^5 TIMES IN A FORGE-LIMITED SPECTRUM OF 1.5×10^6 CYCLES

(b) 99.99^{TH} PERCENTILE IN A SPECTRUM OF 4×10^8 CYCLES

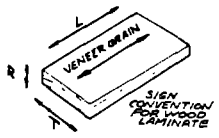

A flaw size for non-destructive examinations can be defined using facture mechanics.

$$\Delta K = \Delta S \, F_S \, F_E \, F_W \, F_G \sqrt{\pi a}$$

Considering a semi-circular surface flaw, normal to the principle stress field, the coefficients are initially:

F_S = 1.12 at front free surface
$F_E = 2/\pi$
F_W = 1.0 far from back free surface
F_G = 1.0 uniform stress

From reference 4-4, the flaw growth threshold could be 5.5 ksi $\sqrt{IN}$. The flaw radius for growth at less than 10^{-9} in. per cycle is then,

$a = [(\pi\ 5.5)/(2(16.670))]^2/\pi$
$a = 0.085$ in. where a = 1/2 the crack length.

The shell and disks will be inspected, to preclude indications greater than 0.1 in. on the surface, according to GE Specification 47A380054. The inspector would have to miss a flaw 1.7 times larger than the rejectable defect before it would propagate. Also, the stress level required to propagate the postulated flaw if a = 0.05 is:

$\Delta S = 5.5\ \pi/(2\ (\pi\ 0.05)^{1/2})$
$\Delta S = 21.8$ ksi

The margin of safety with successful a non-destructive examination is:

$$\frac{21.8}{2(8.335)} - 1 = +0.31$$

NASTRAN shell stress contours for the maximum load case are shown in Figure 4-71. The Category B welds in the shell are located away from the location of the maximum predicted stress.

Augmented Wood

Table 4-31 shows stress redistribution using lamination theory (ref. 4-5) for Douglas fir augmented with .01 or .02 in. thick glass fiber cloth between each veneer. The 10% augmentation has the allowable stresses shown in Table 4-32. The maximum stresses in Table 4-30 are less than the allowables except for cross grain tensile fatigue. The minimum strength in cross-grain tensile fatigue with 20% augmentation is expected to be 675 psi

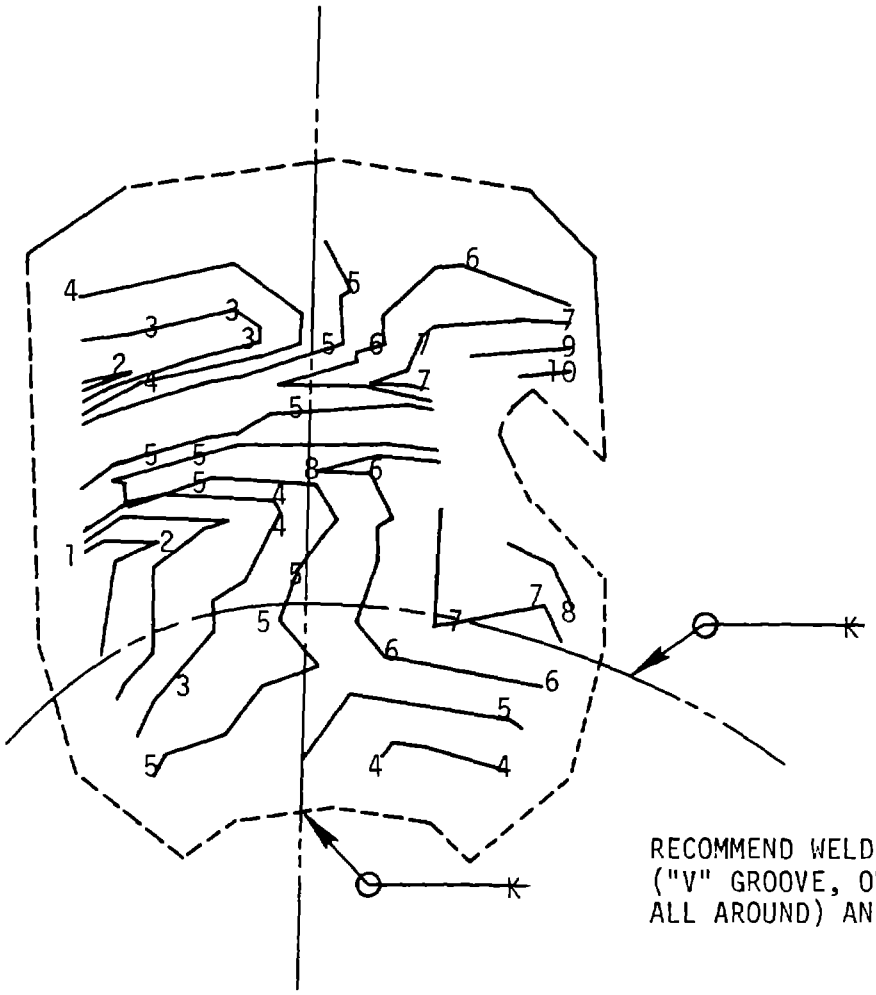

NOMENCLATURE

5 = 5000 PSI MAXIMUM PRINCIPAL STRESS

Figure 4-71. Example of Stress Contour Output of Finite Element and Weld Location Recommendation

Table 4-31. Stress Redistribution For Douglas Fir Veneer, .1 in. Thick Augmented with 0.01 in. Glass Fiber Bidirectional Cloth, Style 7781

	COMPOSITE (PSI)	90% WOOD (PSI)	80% WOOD (PSI)	10% FRP (PSI)	20% FRP (PSI)
L	1,000	961	947	1,393	1212
T	0	12.5	15	-125	-66
LT	0	0	0	0	0
L	0	-45	-50	445	199
T	1,000	305	148	7,953	4467
LT	0	0	0	0	0
L	0	0	0	0	0
T	0	0	0	0	0
LT	1,000	813	664	2,867	2342

Table 4-32. Allowable Stresses

PARALLEL TO GRAIN	MAXIMUM		FATIGUE AT 4 X 10 CYCLES			
	PLAIN WOOD	AUGMENTED	PLAIN WOOD		AUGMENTED	
			R=-1	R=+1	R=-1	R=+1
TENSION	4100	4240	1280	3200	1324	3309
COMPRESSION	-4430	-4581	-1280	-3700	-1324	-3826
SHEAR LT	900	1107	±300	730	±369	898
SHEAR LR	1139	1139	±300	730	±300	730
PERPENDICULAR TO GRAIN						
TENSION R	190	190	±60	150	±60	150
TENSION T	100	328	±30	75	±98	246
COMPRESSION R	-230	-230	-120*	-200	-120*	-200
COMPRESSION T	-440	-1443	-260*	-330	-852*	-1082
ROLLING SHEAR RT	110	110	±40	90	±40	90

(VALUES IN PSI)

*The compressive value occurs on the axis of compressive minimum stress and zero maximum stress.

The wood is augmented by .1 in. of 7781 glass fiber cloth between each veneer, with the warp parallel to the grain.

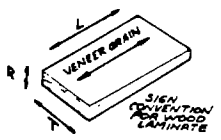

static and ±202 psi at 4×10^8 cycles, based on the Douglas Fir allowables divided by the redistribution factor of 0.148. As drawn in Figure 4-72, the stress margin of safety with 20% augmentation is +0.4.

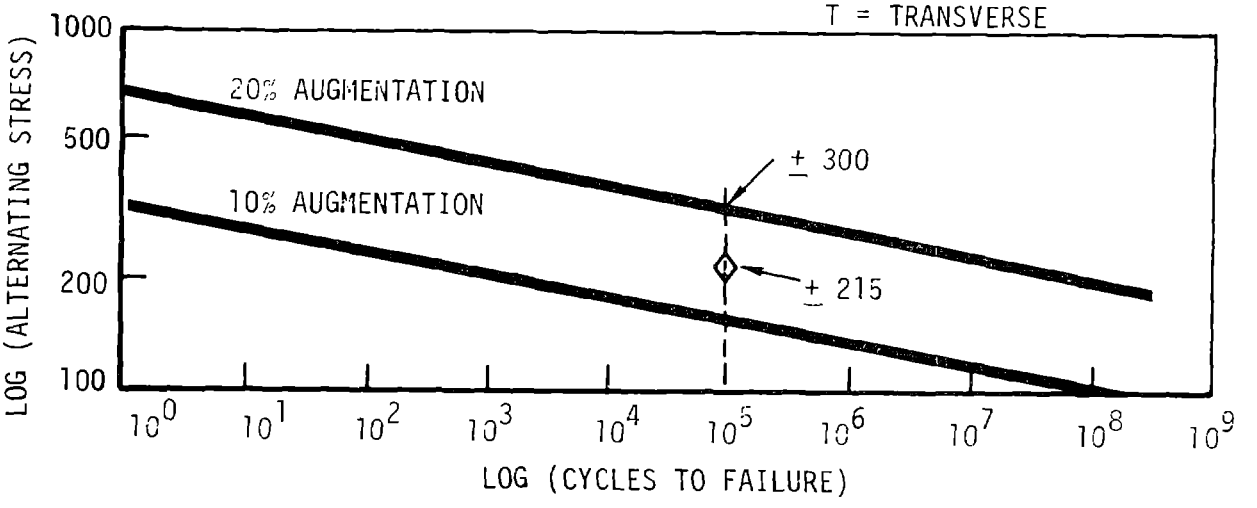

Figure 4-72. Augmented Douglas Fir Cross-Grain Fatigue

$S_{min}/S_{max} = -1$

Stress Margin Summary

Bearing Pin Fatigue	0.37
Shell and Disk, Condition 4	0.45
Shell and Disk Flaw Growth	0.31
Bolster, Cross-grain Fatigue	0.40

4.3.1.3 Center Blade Assembly

The center blade assembly consists of the bolster structures, steel inserts, the teeter shaft, and the center blade, as shown in Figure 4-73. Because of the shipping envelope and the tolerance requirements, these parts are assembled in the field.

An overview of the assembly sequence is presented here. More detailed information is provided in section 10.7.1.

The assembly sequence begins by supporting the center blade, so that the chordal dimension is in the vertical position. The first of the two bolsters is lifted to the top. After applying epoxy to the mating surfaces and coating the center blade interface surface with asbestos-filled epoxy, the bolster is lowered into position and aligned, using the scribe lines and alignment marks. Precise alignment is not necessary, since key interface dimensions are established by fittings, which are installed later and which were designed to compensate for tolerance relief.

Three methods for establishing the bolster/center blade bond gap were identified. Each method is designed to avoid bond voids. The first uses a glass fiber cloth layer between the center blade and bolster, which acts as a wicking medium for trapped air. The second method forces air out of the region with a mound of thickened epoxy. The mound is pushed forward as the bolster lowers, using one of its edges as a pivot. The third method pumps epoxy into the bond gap.

After the appropriate set-up time, the center blade is rotated 180°, and the other bolster is attached. The teeter shaft assembly is then installed through the clearance holes in the bolsters and center blade and temporarily supported while the center blade is re-oriented to a horizontal position for the teeter shaft alignment and bonding.

Optical tooling is used to position the teeter shaft so that the angle of twist established by its centerline and the actual mean chord line of the

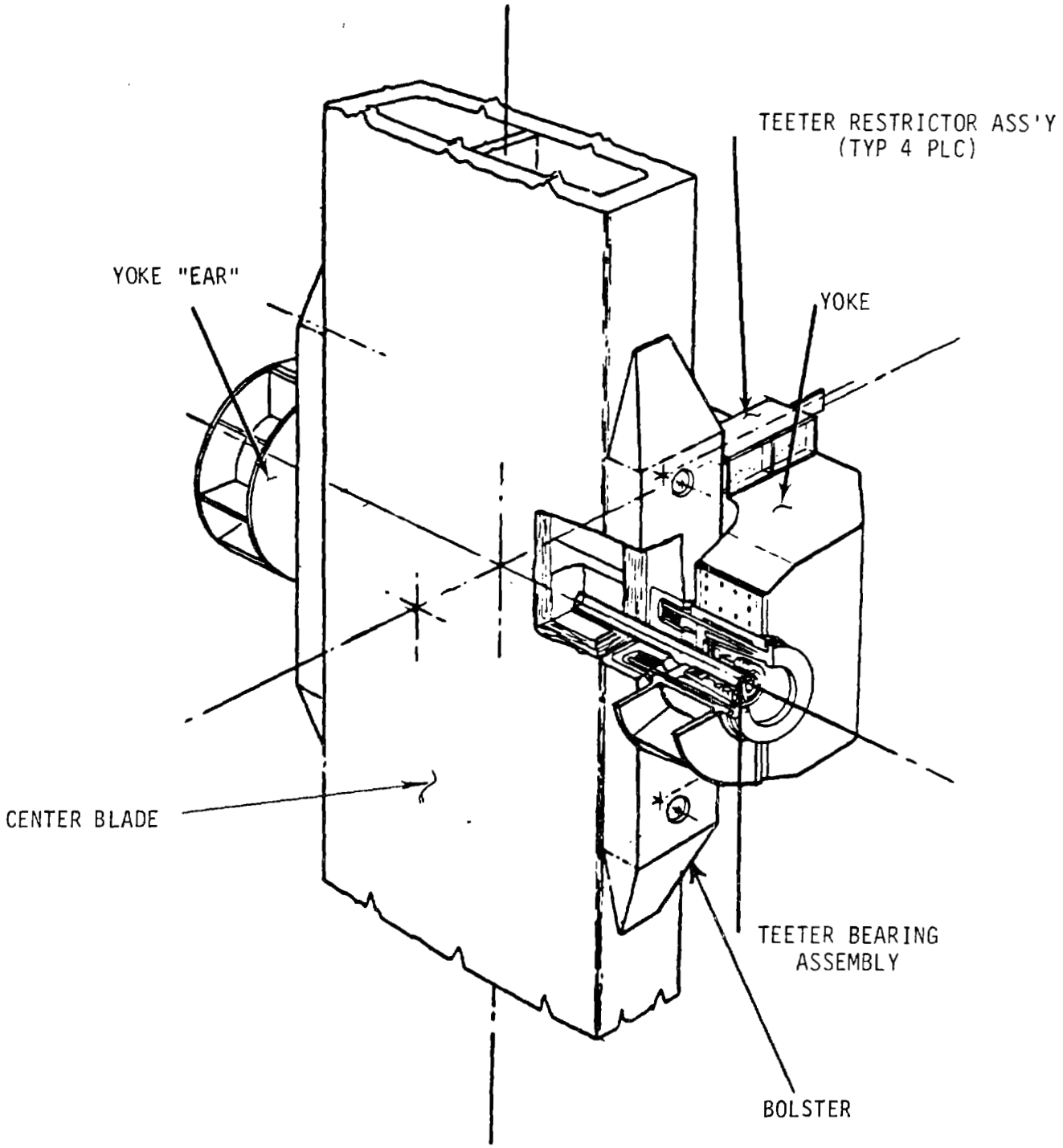

Figure 4-73 . Center Blade Assembly

airfoils at ±.25R (R is the radius) are identical. This position ensures even torque production from the blade sections on either side of the center of rotation. Once aligned, the shaft is bonded to the shear webs, keels, and .30C spar inside the center blade. Thickened epoxy and incremental lengths of congruently shaped wood fillets are used.

The center blade is rotated again so that the chordal dimension is vertical. Using the teeter shaft as a locating pin, the teeter bearing cup is bonded in place. Like the teeter shaft, the cup is wrapped with glass fiber cloth impregnated with epoxy to enhance the adhesion of the additional epoxy in the bond gap. The relatively wide bond gap allows the use of large tolerances for locating the cup in the bolster. The large tolerances make assembly quicker and easier. The annular bond gap can be filled by either pumping epoxy into the gap or by allowing the weight of the fitting to displace a volume of epoxy placed in the bottom of the cavity.

The upper and lower teeter restrictor fittings on either side of the teeter cup are installed. After curing, the assembly is rotated 180°, and the process repeated for the remaining fittings.

4.3.1.4 Inner Blade Assembly

The inner blade is the portion of the rotor between .25R and .60R, on each side of the center blade. Its typical cross-section, as shown in Figure 4-75, is a truncated airfoil with the .60C spar as its aft surface. A main spar, located at .30C, spans the length of the blade section. Blade grade #1 Douglas fir veneer, the strongest available, is used on the outer half of the wall thickness and .60C spar, which is the highly stressed portion of the airfoil shell. Other areas of the blade are made from blade grade #2 veneer. The blade is covered externally and internally with two layers of 7781 bi-directional glass fiber cloth reinforced with epoxy. The epoxy seals the wood from the environment and the glass fiber distributes the load at joints in the outer and innermost laminae of the airfoil shell. This covering also protects the wood from abrasion and erosion.

A pattern of fingers is machined into each end of the blade section. The fingers match a corresponding pattern on the center and outer blade sections. The thickness of the laminae in these areas is 20% greater than the minimum

requirements determined by SECTION, to account for the structural joint efficiency. These areas are also reinforced with type 7781 FRP cloth between each veneer, to provide dimensional stability for any environment. At .25R, spars are foreshortened, providing clearance for the tooling needed to assemble the center and inner sections.

The hydraulic and electrical conduits are installed against the aft surface of the .60C spar. Clamps used to support the conduits are secured, by fasteners torqued into the inserts bonded into the spar as shown in Figure 4-74. The dimensions of the insert provide a bonding surface area large enough to react shear pullout forces, which occur during turbine operation. Preload torque is prevented from stressing the wood by installing the insert slightly above the spar surface, which also eliminates concerns about loss of preload from creep. The conduit installations were not completely designed at the time of this report, therefore, the inner blade drawing does not show the requirement for inserts.

Continuous lengths of wood blocking are bonded and screwed to the aft surface of the .60C spar, as shown in Figure 4-75. These pieces provide a mounting surface for the trailing edge sections installed at the site. The birch laminae installed into the spanwise kerf provide a large surface area, which shears the trailing edge loads into the main blade structure, minimizing tension on the bond line. Birch has greater cross grain properties than Douglas fir. The location of this kerf also minimizes any interference with the most highly stressed wood fibers of the airfoil shell.

Provisions for mounting balance weights on the .30C spar at .50R are shown in Figure 4-76. An internal rib is installed at this location to support the spar and to transfer the load due to the weight of the ballast into the airfoil shell. The centrifugal force of the ballast weight is transmitted to the spar through the bonded steel bushings. It is transferred to the airfoil shell by shear along the spar/shell interface. The spar thickness is locally increased to accommodate the imposed bearing and bending loads.

The inner blade is designed as the assembly of three components: the high and low pressure side chordal covers and the .60C spar. The covers are bonded together at the leading edge of the airfoil with a flat, spanwise,

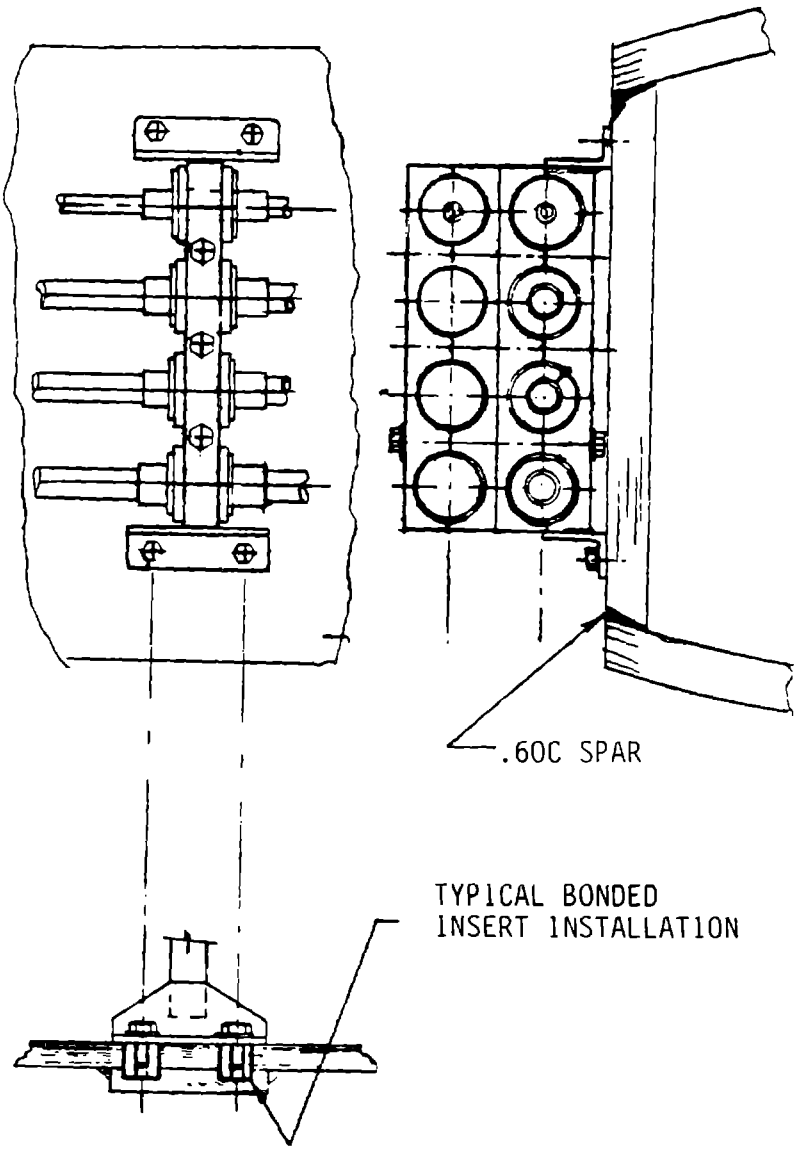

Figure 4-74. Hydraulic and Electrical Conduit Mounting Provisions

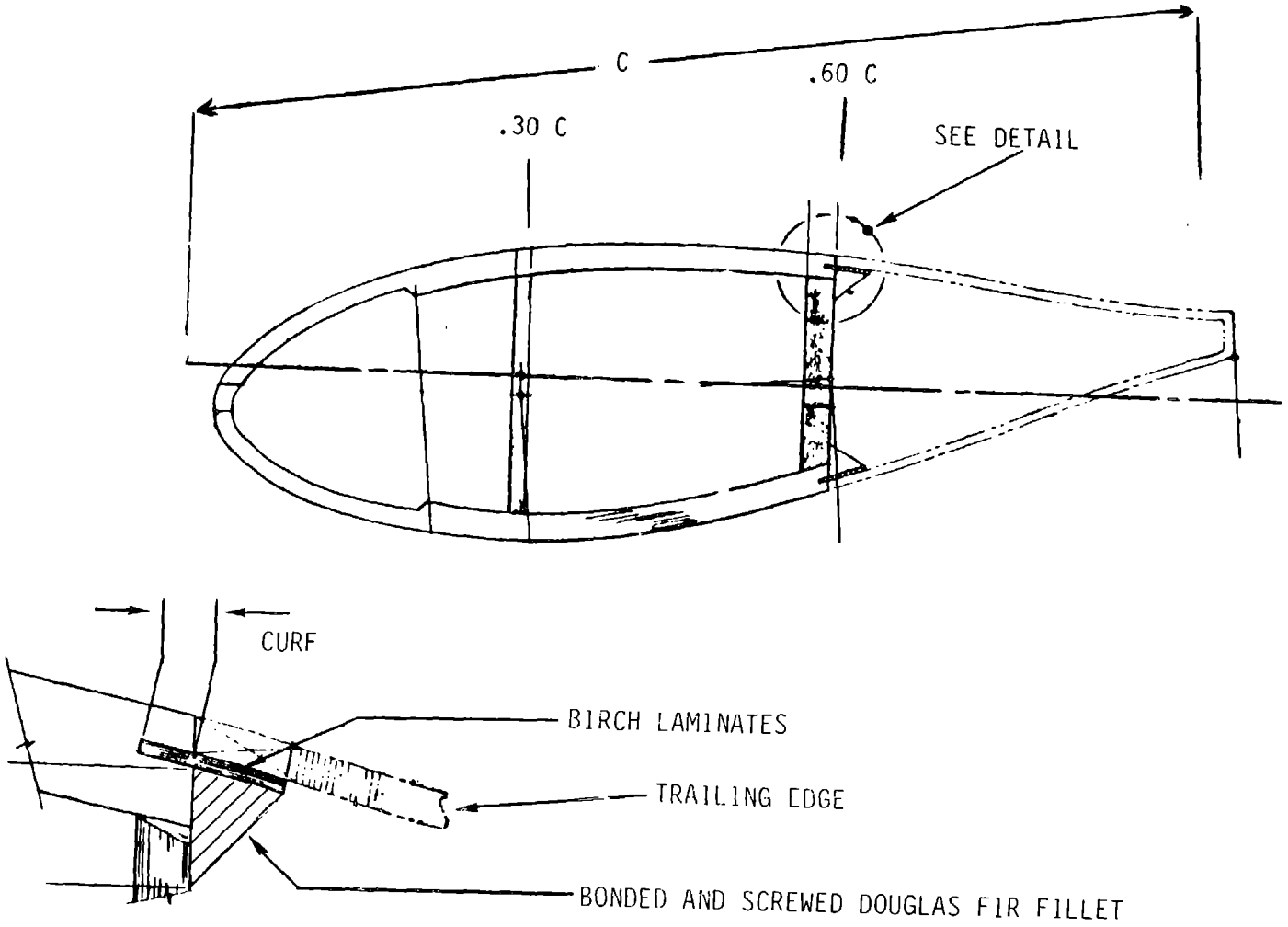

Figure 4-75 Typical Cross Section and Trailing Edge Mounting Provisions

longitudinal joint. The joint is made using incremental lengths of laminated wood wedge fillers, like the method used to bond the .60C spar. This method allows the parts to be properly positioned before the bonding operation, eliminating the handling of heavy pieces and removing the time constraint on completing the joint.

The inner blade was analyzed during the preliminary design phase using an orthotropic plate-element numerical model to assess the design produced by SECTION. As expected, the stresses parallel to the grain were in agreement; however, spar thickness was too thin and shear fatigue margins of safety were low in that design. Subsequent sizing procedures for the spars have led to satisfactory shear strength, fatigue resistance, and buckling stability in the inner blade.

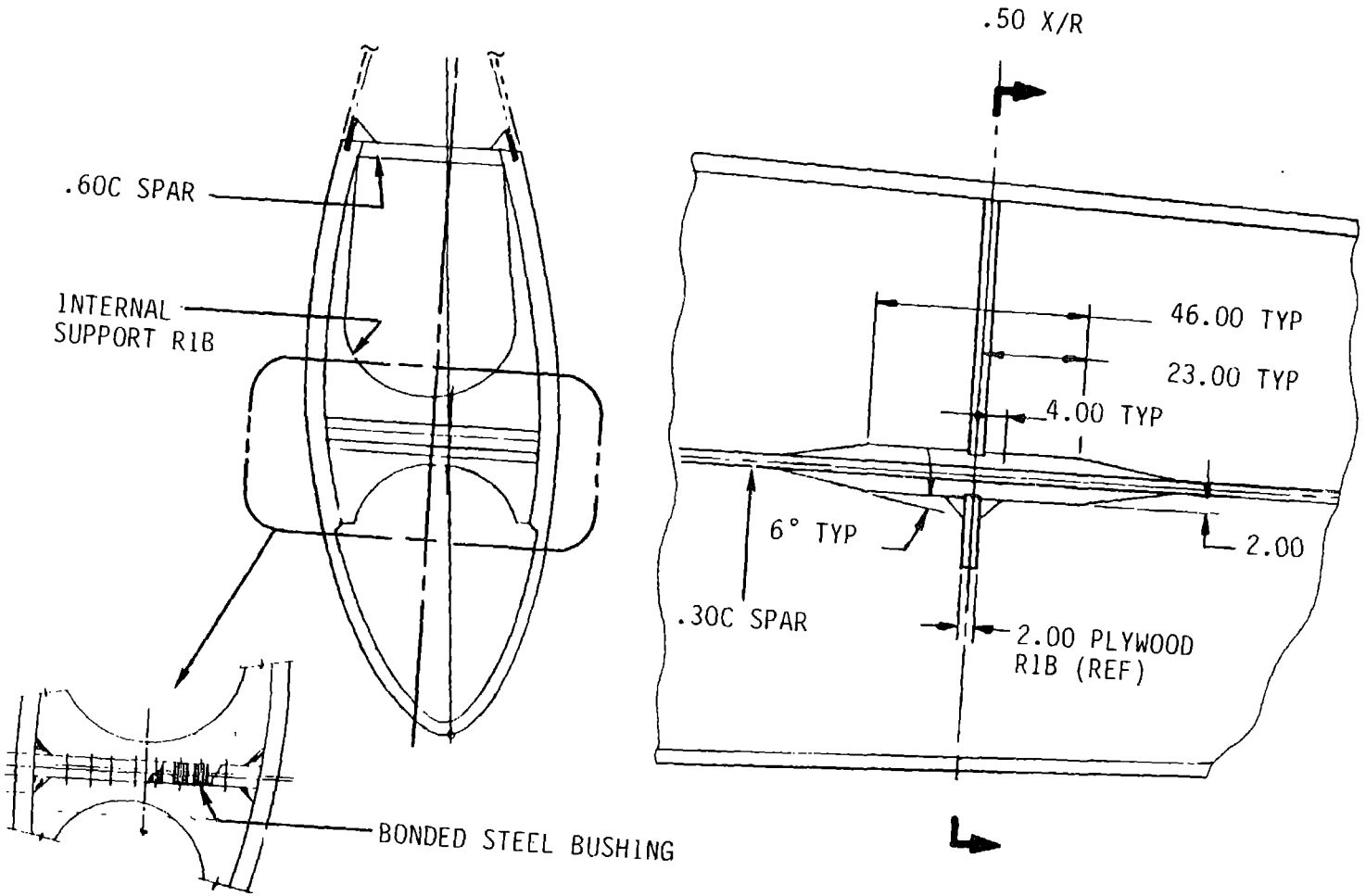

Figure 4-76. Ballast Mounting Provisions

4.3.1.5 Outer Blade Assembly

The outer blade assembly and the tip section make up the outer 80 ft of the blade. The aileron surfaces are mounted on the aft spar. The configuration of the outer blade is similar to that of the inner blade, in that both sections have a truncated airfoil cross-section that is composed of three molded parts. The materials of the two sections are also similar. Blade grade #1 veneer is used in the outer half of the shell and grade #2 is used elsewhere. A pattern of fingers interfaces the outer and inner blades. Like other portions of the blade with this feature, the shell thickness is locally increased by 20%, and reinforced with interlaminar glass fiber cloth. Conduits protect the electrical wiring and hydraulic lines connected to the ailerons, and are mounted to the aft face of the .60C spar. The conduits are supported as they are on the inner blade.

The lightning protection for Model 304.2 was not completed at the time of this report. However, much of the design developed for Model 204.6 is applicable. This design includes installing a bright clad aluminum mesh screen, 18 X 16 X .012" Ø wire, between the two exterior layers of glass fiber cloth. The screen is electrically connected to the grounded conduits mounted on the aft face of the .60C spar, to provide a path to ground for lightning strikes.

The outer blade ends at a removable tip section. Provisions to attach the tip are shown in Figure 4-77. Wood laminae at the end of the blade section are stepped back from the outer molded line to create a landing area for the tip. Ten threaded inserts are installed around the airfoil perimeter in this area. The inserts are located by match drilling the fastener clearance holes in the tip. The inserts are bonded slightly above the surface of the lamina to prevent fastener preload torque from stressing the wood.

Removal of the tip provides access to the ballast installation which balances the static moment of the rotor. The internal structure that supports the ballast container is shown in Figure 4-78. The weight of the installation is supported by the two partial ribs, which transfer any bending load to the airfoil shell through shear parallel to the grain. The centrifugal load is transferred to the shell by a parallel to the grain shear along the interface with the partial spars. This design minimized rolling shear stresses in the ribs. The spars can also react torsional moments.

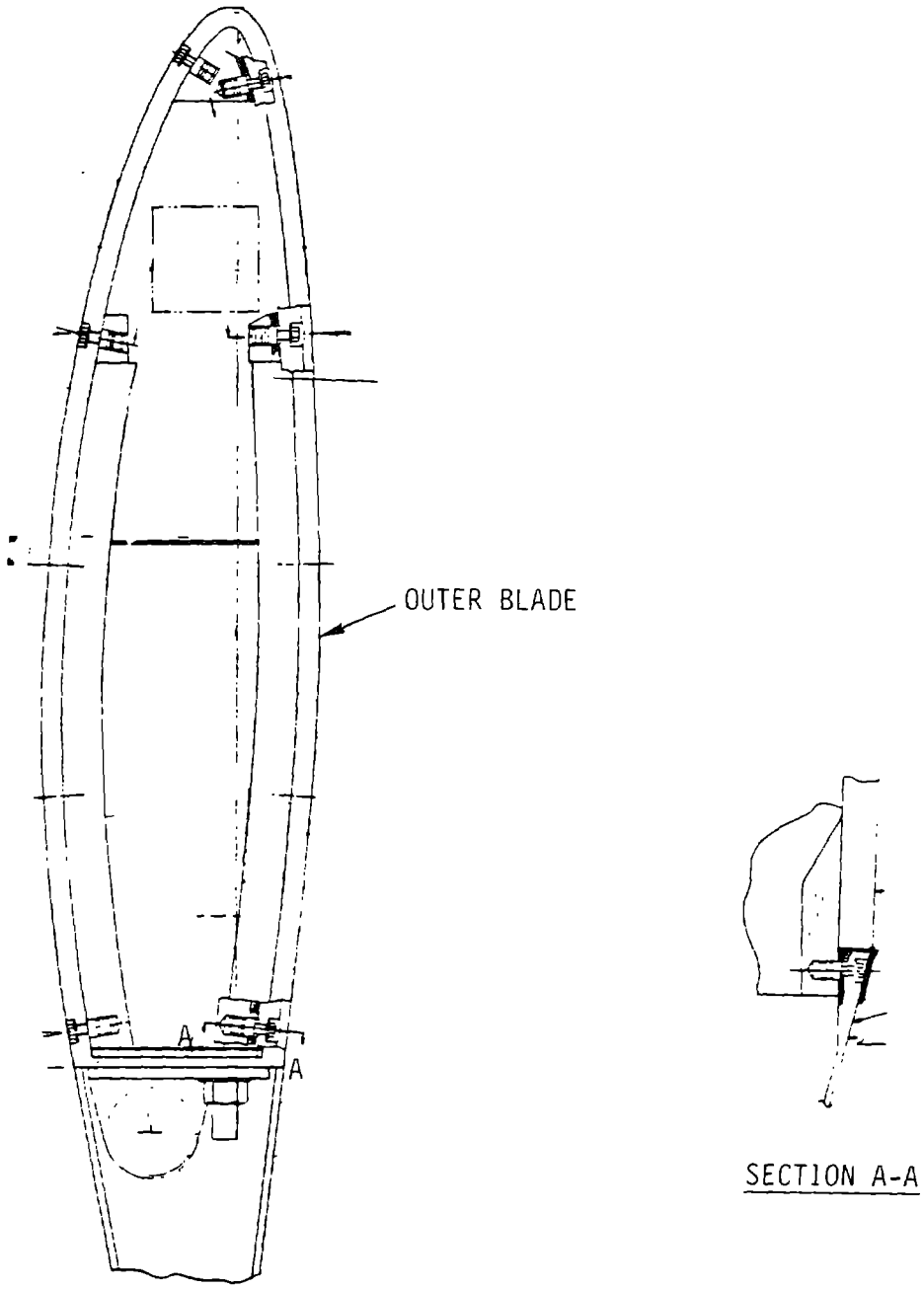

Figure 4-77. Tip Mounting Provisions

The most important feature of the outer blade is the method of securing the ailerons surfaces. The design must transfer the imposed loads efficiently into the airfoil shell. The aileron interface fittings are attached to the blade section with steel studs bonded into internal ribs as shown in Figure 4-79. At the three actuator locations, stations 1449.0, 1740.0 and 2040.0, the rib spans the full cross-section of the airfoil. The loads are imposed on the studs, which transmit them to the shell by shear along the interface with the rib. Each mounting stud is installed to protrude slightly above the aft surface of the .60C spar to avoid preloading the surrounding wood when the aileron attachment fitting is secured.

The stud design, as shown in Figure 4-80, provides enough surface area to shear imposed axial loads into the surrounding wood along its length. The tapered stud body gradually reduces the stud stiffness and consequently improves the rate of load transfer to the wood. This shape and the locally voluminous adhesive pocket reduce the stress concentration at the tip. Spiral grooves are machined into the body of the stud to serve as a locking feature after bonding, to minimize the dependence on adhesion to the steel surface for 30 years. A separately installed threaded shank (as opposed to an intregral machined shank) is used to obtain the recommended ratio of length to diameter, to ensure adequate preload retention and eliminate the stress concentrations that would be present in a machined shank configuration. The ultimate and fatigue axial performance of this design has been evaluated and the results are reported in section 8.2.3 of Volume II.

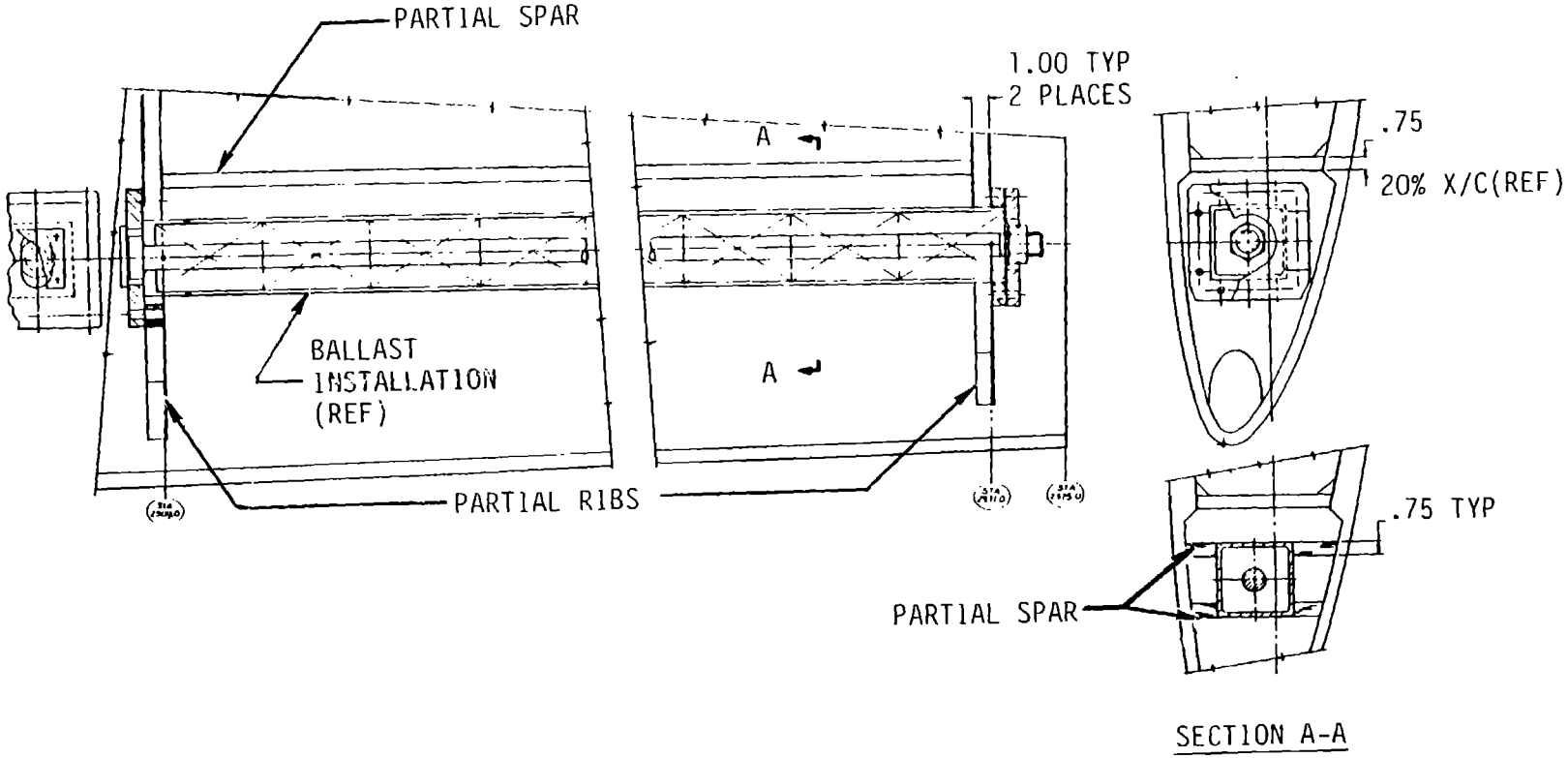

Figure 4-78. Ballast Installation Support Structure

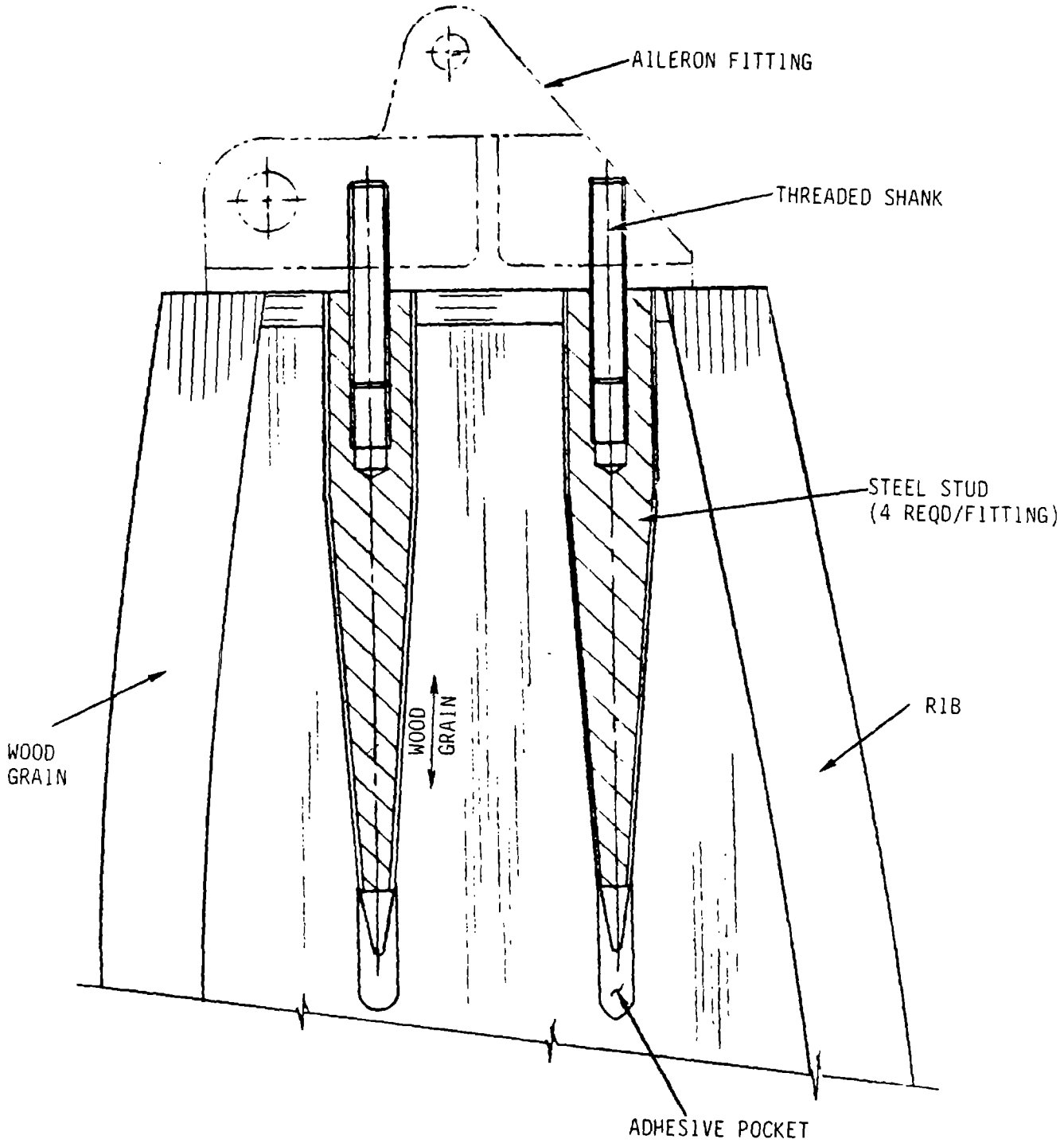

Figure 4-79. Attachment of Aileron Fitting to Outer Blade Section

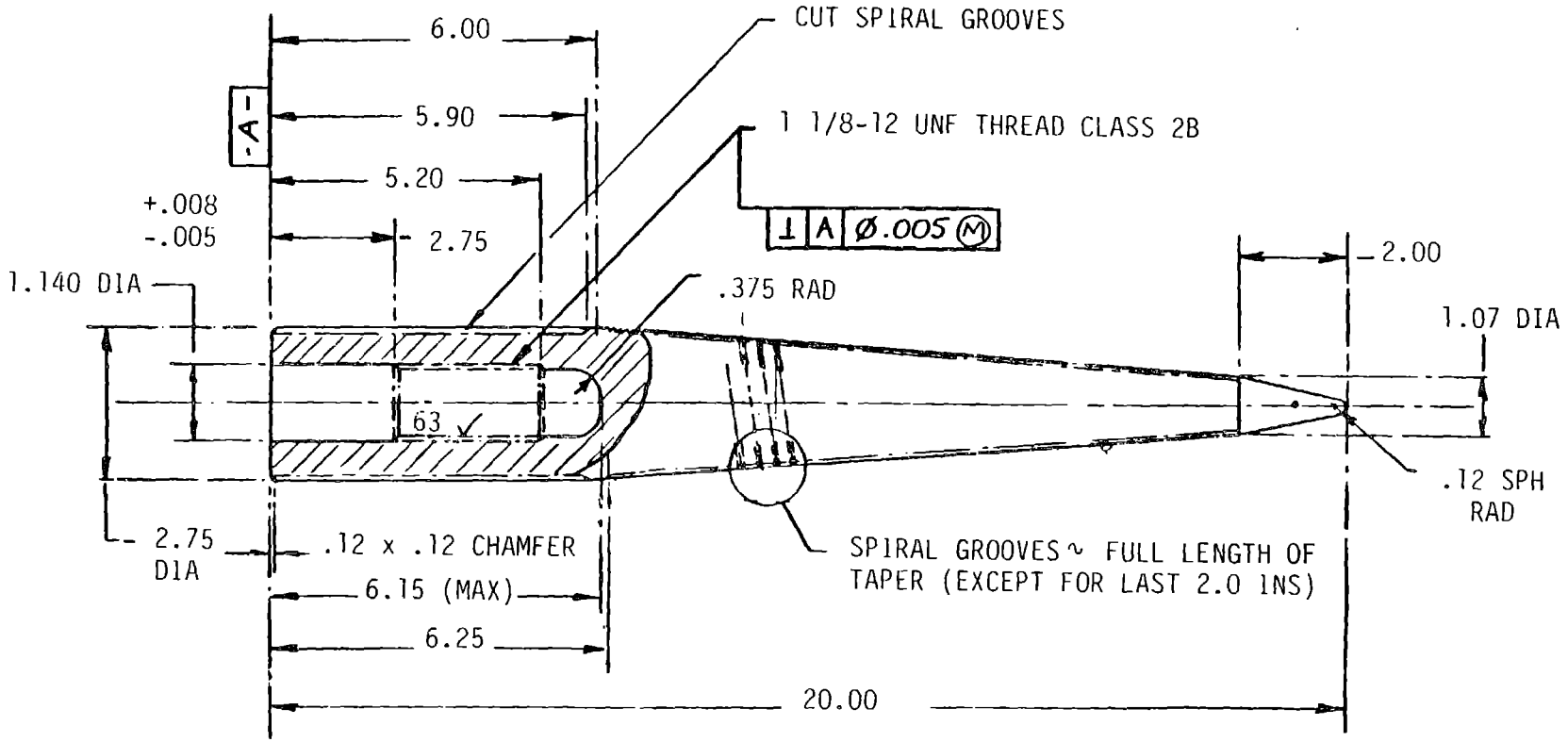

Figure 4-80. MOD-5A Stud Design

4.3.1.5.1 Outer Blade Cross-Grain and Shear Stress Analysis

The outer blade skin and spar thickness shown in Table 4-25 were determined by the flap and chord bending load conditions. It was necessary to analyze these thicknesses for the effects of local pressures and concentrated loads introduced by the ailerons. The outer blade, which experienced the highest surface pressures and the lowest bending moments, is the most susceptible to the effects of surface pressure.

The pressure differential across the most critical surface with the lowest pressure was conservatively assessed at 2 psi. This value accounts for internal pressure, caused by centrifugal forces and venting, and external pressures, caused by aerodynamic forces. When the low pressure surface was treated as a flat orthotropic plate surface supported by spar and aileron ribs, it had a spar-to-spar stiffness approximately 80 times that of the rib-to-rib bending stiffness. Therefore, the skin was treated as a unit width beam between spar. The highly curved leading edge shell was assumed to be inherently self-reinforced shear parallel to the grain and bending. An analysis of the unit width beam for the pressure differential of 2 psi showed that 0.03 in. of 7781 glass fiber cloth on both sides of the low pressure skin from station 1440 to the tip would provide an ample margin of safety. The cloth was also applied to the high pressure skin to simplify manufacturing. From station 1440 inboard, the skin thickness increases and the differential pressure decreases. 0.02 in. of glass fiber cloth provides an acceptable margin of safety in this region.

The 30% of chord spar reacts the differential skin pressures, and it is stressed in a cross-grain tension loading, with negligible bending. The minimum thickness for this loading was 0.6 in, so the thickness of the spar outboard of station 1920 was increased to 0.6 in, rather than the 0.5 in. listed in Table 4-25. The 60% of chord spar experiences a bending moment caused by internal pressure superimposed in cross-grain tension strain. The minimum thickness for this condition is 1.0 in. The thickness of the spar outboard of station 2160 was increased to 1.0 in, rather than the listing in Table 4-25.

The spars and the aileron ribs transmit aileron fitting loads to the blade. The 60% of chord spar experiences the highest shear loads, which are critical at the tip support, station 2390, because the spar depth is the smallest there. At this location, the 60% of chord spar is 1.0 in. thick, to satisfy the limit load condition. This thickness provides a margin of safety of +0.25 for shear fatigue.

The spars must be augmented at the holes where the aileron is attached to the internal ribs by studs. Holes in wood develop a shear stress of 70% to 80% of the far-field stress applied parallel to the grain stress and a cross-grain stress equal to about 20% of the parallel to the grain stress also develops. The blade encountered such stresses from overall chordwise and flapwise bending and from centrifugal force. These stresses superpose with the direct shear and cross-grain stresses estimated in this report. Augmentation prevents splitting at the attach point. Spars inboard of station 1920 did not require changes from the preliminary sizes.

4.3.1.5.2 Aileron Attachment Analysis

A detailed analysis of the fitting and preliminary design for an aileron attachment showed that the concept is feasible. Maximum and fatigue stresses in all locations and directions were satisfactory for this stage of the design. The critical locations are at the spars that react the hinge moment, and at both stud locations. These locations are at each spanwise station, where aileron actuators are mounted.

Loads from the system coupled dynamic analysis were applied to the model shown in Figure 4-81 80% span, and to the fitting portion of the model, shown in Figure 4-82. The limit load cases included two hurricane conditions and 50% overspeed. The aileron loads represented both the undeflected and the fully deflected positions in the two storm cases. The aileron deflection simulated in the overspeed case was 45°, which is a position of maximum hinge moment predicted from the transient dynamic analysis. Fatigue load cases were average mean loads and maximum alternating loads. The alternating loads were described as the 99.99th percentile of the loading spectrum and were 1.58 times as large as the 99.9% loads. This large difference in aileron hinge moment and attachment forces is less damaging than a constant amplitude fatigue load. Finally, a load case in which only aileron attachment forces

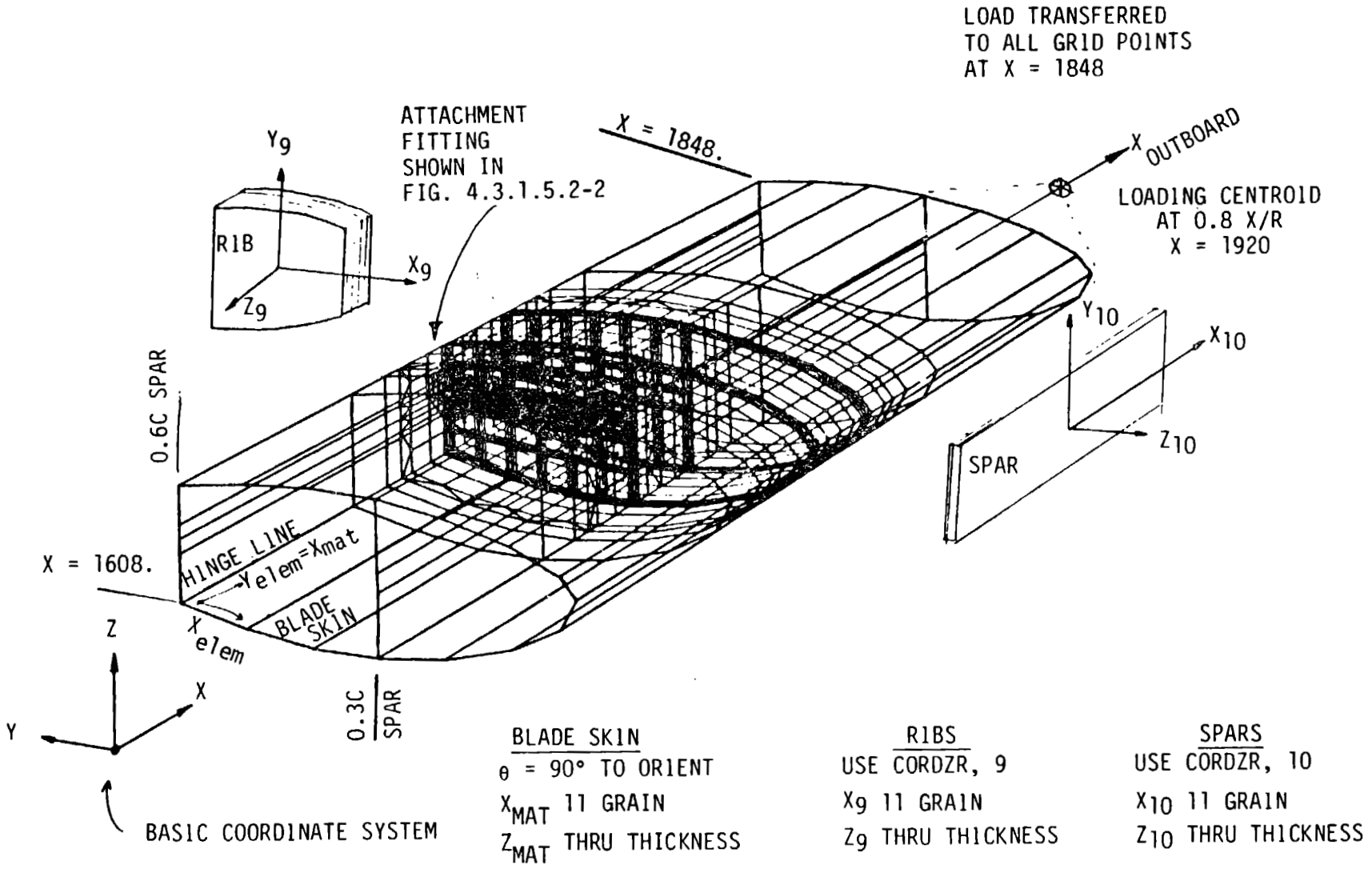

Figure 4-81. Finite Element Model of the Aileron Attachment

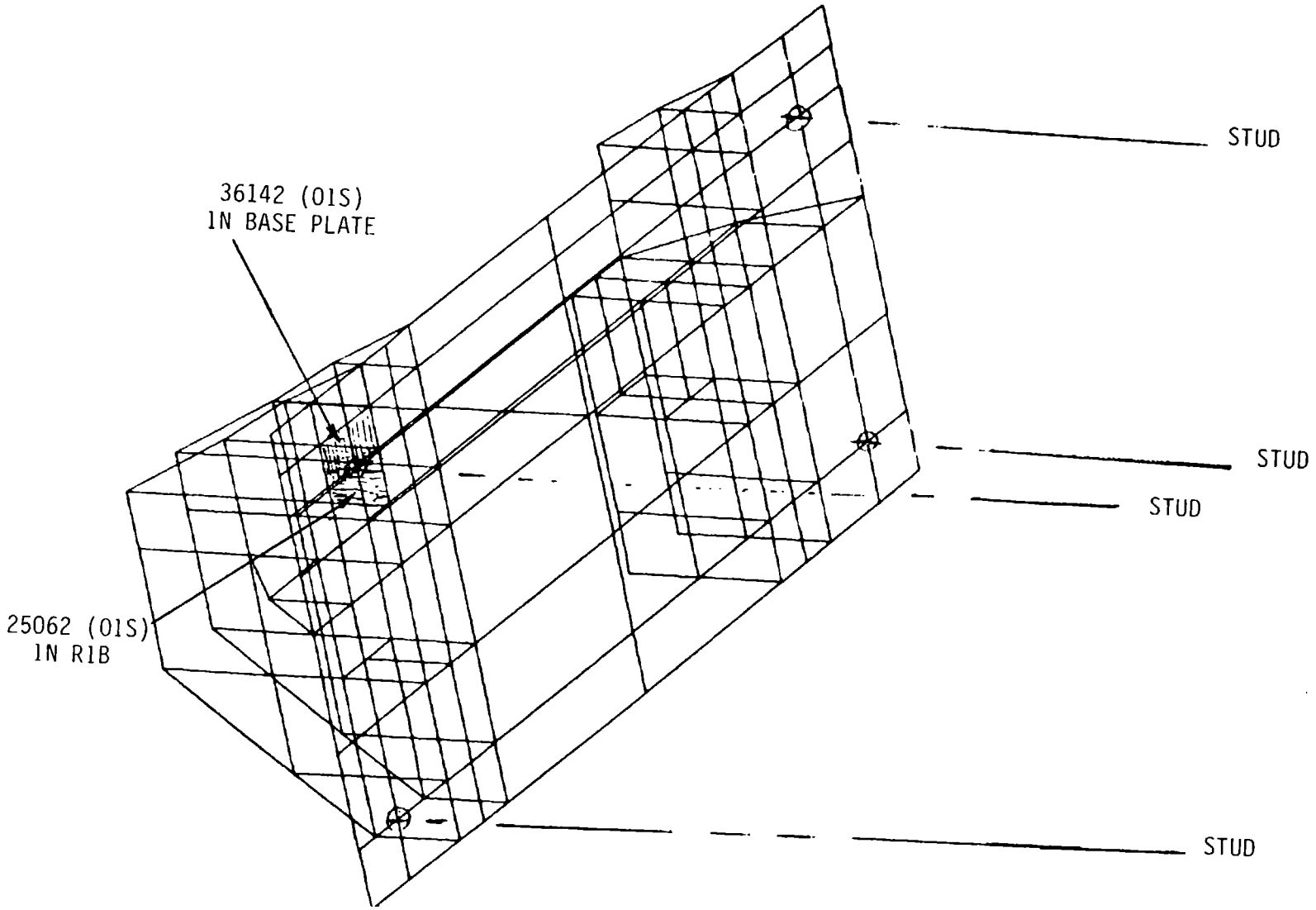

Figure 4-82. Finite Element Model of the Attachment Fitting

Table 4-33 Summary of Aileron Attachment Analysis of the Preliminary Design

Location	50% Overspeed Stress (psi)	M.S.	Fatigue Stress (psi)	M.S.
Upper Skin	-3470 (L)	0.28	-97±559	1.29
	98 (T)	0.02	29± 48	-0.38
	210 (LT)	3.29	-54±157	0.91
Lower Skin	3882 (L)	0.06	910±486	1.64
	91 (T)	0.10	91± 47	-0.36
	197 (LT)	3.57	51±150	1.00
Fitting Base	36140 (HVM)	0.29	8462±12260	0.06
Spar at 0.6C	3445 (L)	0.19	594±656	0.95
	125 (T)	-0.20	108±70	-0.57
	715 (LT)	0.26	-252±234	0.28
Spar @ 0.3C	3366 (L)	0.22	190 ±133	8.62
	88 (T)	0.14	7±43	-0.30
	391 (LT)	1.30	-82±243	0.23
Ribs	-698 (L)	5.35	180±255	4.02
	94 (T)	0.06	27±38	-0.21
	110 (R)	0.73	27±23	1.61
	411 (LT)	1.19	-99±134	1.24
	51 (TR)	1.16	-12±18	1.22
	-224 (RL)	4.08	50±76	2.95

L = Longitudinal, parallel to grain
T = Tangential to tree, perpendicular to grain, in veneer plane
R = Radial to tree, perpendicular to grain, through veneer thickness
LT, TR, RL = Shears
HVM = Henky-Von Mises equivalent stress

were applied was run. The aileron loads produced almost all the stress in the aluminum fitting, studs and ribs, and about 50% of the stress in the 0.6C spar at the stud penetrations.

The results of the 50% overspeed finite element analysis of the most critical load conditions are summarized in Table 4-33. Tensile stress perpendicular to the grain of the Douglas fir and shear stress parallel to the grain were significantly greater at the aileron attachment, compared to the rest of the rotor. The style 7781 glass fiber cloth between each veneer of the 0.6C spar and on the inside and outside surface of each skin is essential, to minimize the risk of splits in the wood. Since this region is very important to the control of the wind turbine, a full-scale mock-up from 65% to 77% of span was under consideration for testing. Testing of such a section would run for one million cycles with the 99.99% loads applied to the fitting and to the blade. Then the maximum expected service loads would be applied, and finally the test article would be loaded to destruction, to assess residual strength and failure modes.

In the analysis, the aluminum fitting was composed of 1.25 in. thick webs, ribs, and plates. This fitting should be integrally machined from a tough, fatigue resistant alloy, such as 7075. The T73 heat treatment is preferable, since it minimizes the risk of stress corrosion cracking. However, the T6 heat treatment could work, provided there are no high steady stresses, such as those caused by press-fitted parts or clamping residual stresses in the hinge pin mounting lugs. The fatigue margin noted for the fitting is with respect to the typical constant life line for ten million cycles for 7075-T6 with a notch factor of 1.5. Since the design maximum alternating stress should occur less than 323,000 cycles, the probability of successfully detailing the fitting for a satisfactory fatigue life is high.

4.3.1.6 Tip

The extreme ends of the rotor span are enclosed by aerodynamically shaped tip structures. The tips reduce drag to increase energy capture. Estimates indicated the additional energy provides an acceptable return on the initial cost of fabricating and installing the tip structures. The tips are attached to the outer blade at approximately STA 2375, and extend along the spar to STA 2400. The tip is attached to the blade over 4 ft of the chordwise length. Ten fasteners engage inserts, which are imbedded in the edge of the outer blade. These fasteners are extractable, so the tip can be removed to provide access to the ballast installation.

The tip design is shown in Figure 4-83. The outside dimensions of the tip were determined to provide the best aerodynamic performance for the given constraints on manufacturing and shipping. The tip is fabricated from a polyester and glass composite, with an aluminum screen embedded for lightning protection. The screen extends to the outer blade and connects with the main lightning protection system on the blade.

The size of the tip was determined using aerodynamic pressures resulting from normal operation. The windward surface was modeled as a plate, supported as shown in Figure 4-84, conservatively and uniformly loaded by the largest estimated aerodynamic pressure. The leeward skin was checked for buckling stability using the model shown in Figure 4-84. Finally, the bearing stresses at the fastener locations were checked. The resulting margins of safety are shown in Table 4-34. The allowable stress was taken as 60% of the average yield stress, derived from the vendor's data. Further work would be required to ensure the accuracy of this estimation. Fatigue and limit load analyses were not performed on the tip before the project was terminated. Some adjustment of skin thicknesses might be required as a result of these loading conditions.

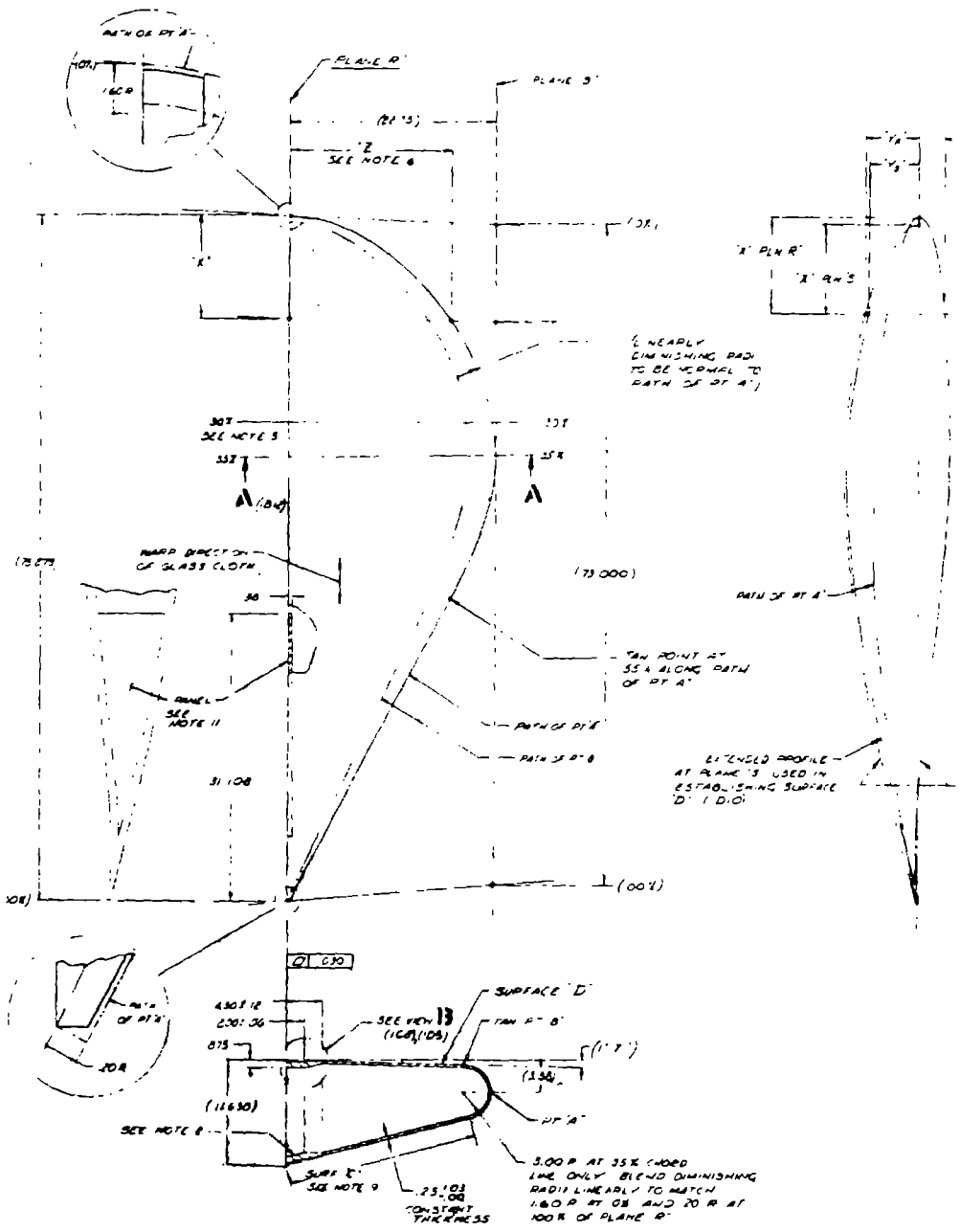

SECT A-A (16.5)

Figure 4-83. Tip Design

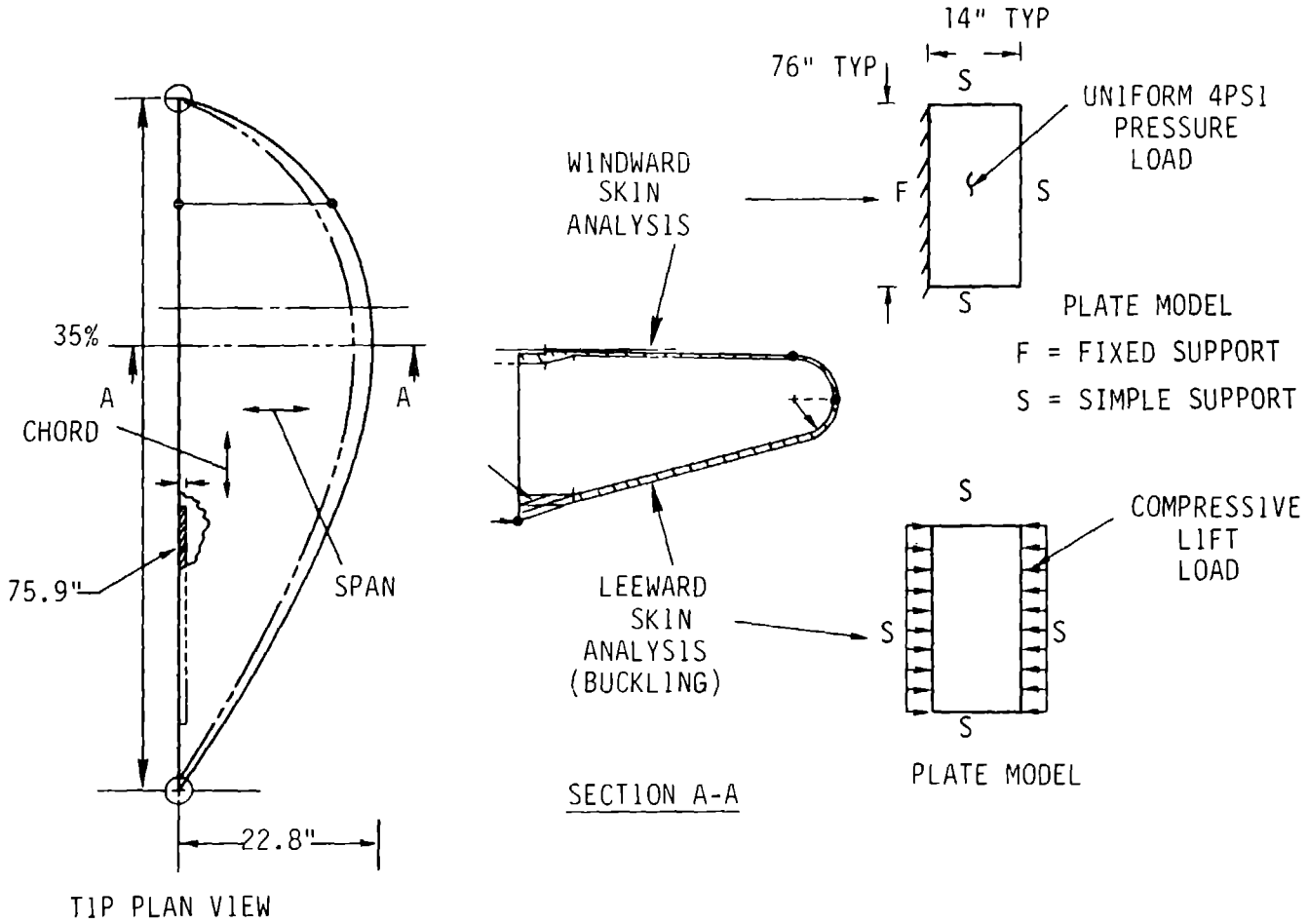

Figure 4-84. Tip Design Analysis

Table 4-34 Margin Summary

	Calculated Value (psi)	Allowable Stress (psi)	MS
Tensile Stress	10,200	18,000	.76
Buckling Stress	70	630	Large
FRP Bearing Stress	8,000	18,000	1.25

4.3.2 FIELD JOINT

The continuous rotor structure is fabricated by bonding individual blade sections at the site. The main functional requirement of the joint design is that it be able to transfer loads throughout the life of the blade. There are three methods for joining adjacent members: butt joints, finger joints, and scarf joints. Butt joints were eliminated from consideration because they cannot transmit tensile loads. Finger joints were favored over scarf joints because they are easier to fabricate, although the scarf joint has some performance advantages. Mechanical designs that would join the assemblies were also considered. The major problem with these design is that the load concentrates at the fastener locations. This characteristic produces large stress and relatively low joint efficiency. For these reasons, finger joints were chosen as the baseline design.

The final finger configuration is shown in Figure 4-85. It has a slope of 1/10 (rise/run) and a pitch of 2.701 in. The pitch reflects a bond gap of 37 mils.

The impact of slope, pitch and bond gap on the performance of the joint were parametrically determined as part of the finger joint configuration development test program discussed in section 8.2.1, Volume II. The program indicated that performance improves as the slope decreases, which can be accounted for by the resulting reduction in the cross-grain stress component. However, the rate of improvement diminishes beyond a slope of 1/10. The test program also indicated that large pitch dimensions are beneficial. The tip and root of the finger joint are typified as butt joints. Keeping these dimensions constant while increasing the pitch results in a larger area for transmitting tensile loads. This benefit is maximized in the final design by specifying root and finger length dimensions that represent the minimum and maximum manufacturing capabilities, respectively, at a finger slope of 1/10.

The results of the finger joint bond gap tests illustrated that the joint performance improved as the gap size decreased. However, the gap must be large enough to prevent an interference fit during enlargement of the fingers. The bond gap was determined by achievable manufacturing, dimensional stability and alignment tolerances. Stability of the finger-to-finger dimensions was a key consideration. The value used for the stability factor

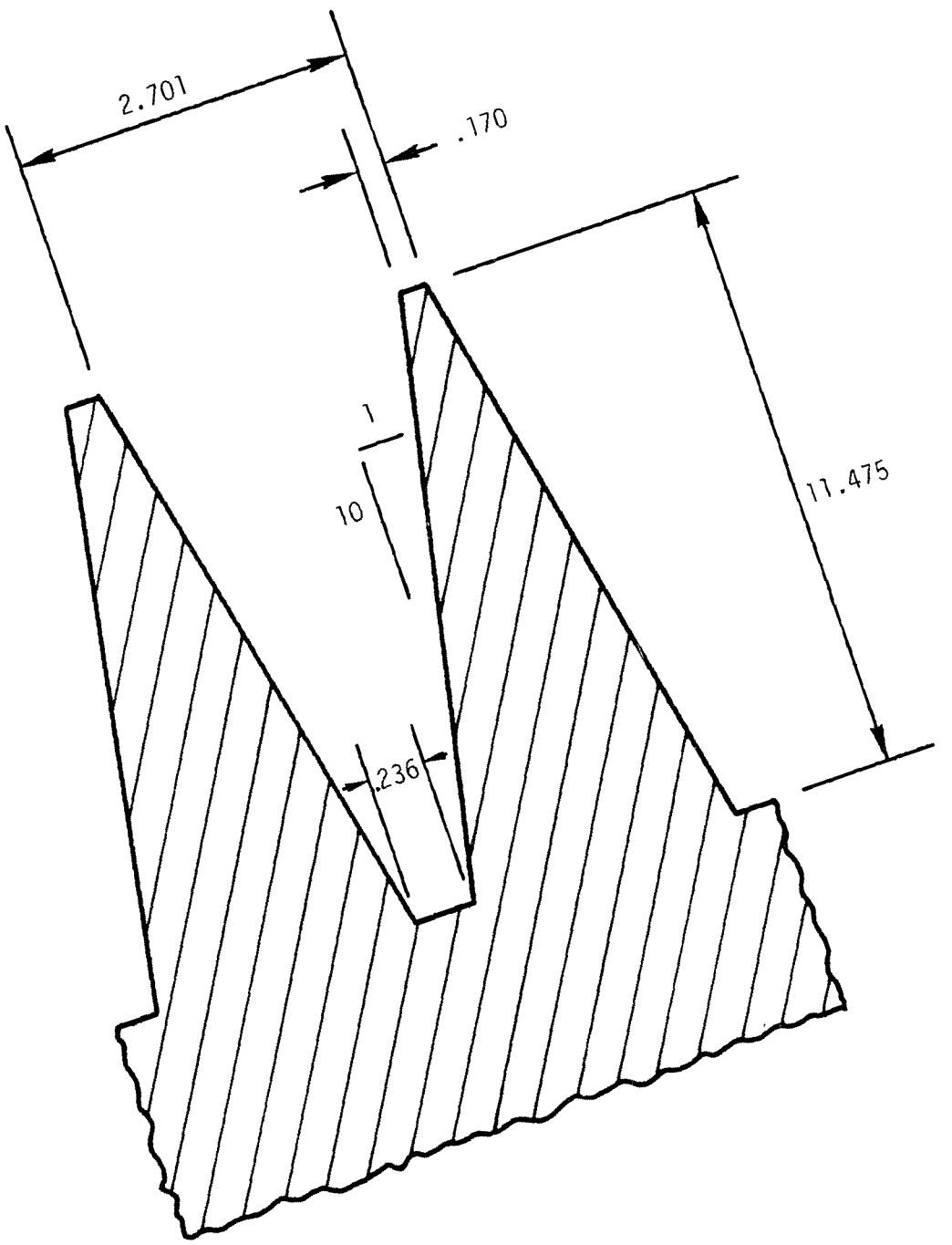

Figure 4-85. Finger Joint Configuration

reflects the results of tests discussed in Volume II, section 8.1.5.3, which measured the change in the cross-grain dimensions of the blade during shipment and storage. The contribution of each of these factors is shown in Table 4-35.

The shell thickness is increased around the field joint. Based on the limit and fatigue performance test results, a set of corresponding stress allowables were developed. They are illustrated in Table 4-36. The percent difference between the basic wood allowable represents the increase in thickness required. This computation indicates a 0% increase for field joints designed according to limit loads and a 18% increase for the field joints designed according to fatigue loads. These increases would have been larger considering the combined product of the joint efficiency and bond gap factor alone. However, since the stressed volume of the field joints is so much smaller than the volume of the blade on each side, their reduction in strength because of size effects is smaller than for the basic wood allowable. The field joint is analogous to an aluminum link joining two steel link chains together. The probability of having a single aluminum link weaker than a given allowable is much less than the strength of one of many steel links being below the allowable. As the steel chain gets longer, its allowable stress can become lower than the allowable stress of the single aluminum link.

Tne assembly procedure, as discussed in section 10.7.1, positions, aligns, and dry fits the sections together before the epoxy is applied to the interfaces. The tooling needed for the assembly of the joint at .25R is temporarily installed inside the blade. The .30C and .60C spars are foreshortened to allow the installation and removal of the tooling. The spars are made continuous after the joint is completed, by splicing in the rest of the spar, using scarf joints. The tooling required for the field joint at .60R must be installed on the exterior of the blade, since there is not working space inside. Fingers are cut into the spars so the assembly operations were performed on full-scale simulations of the .25R blade sections as part of the blade development program. The results verified that the large surface area of the interface could be successfully bonded in one operation. Test samples were fabricated from the simulated sections to verify that the performance of the joint is consistent with the results obtained during the finger joint configuration development tests. Details of these tests may be found in Volume II, section 8.0.

Table 4-35 Finger Joint Bond Gap Allowances

FACTOR	ALLOWANCE (In.)
o Assembly	
- angular alignment of adjacent sections	(± .005) x 2
o Cutting Tolerances	
- location	(± .004) x 2
- shape variations	(± .004) x 2
o Stability	
- variation in pitch	± .010
- variation in root	± .001
	± .037

Table 4-36 Finger Joint Allowable Tensile Stress

	Limit			Fatigue (R = .1) at 7716 psi		
Tension Parallel To Grain	Test Value	Adjustment Multiplier	psi	Test Value	Adjustment Multiplier	Max psi
Test Mean	12% M.C		11023(1)	10% M.C.	10^6 cyc	7716
Moisture	10%	1.032		10%	1.0	
Proportional limit	N/A	1.0		N/A	1.0	
Size effect factor	1460 in^3	.87		1460 in^3	.69	
-2σ	15% cov	.70		5% cov	.90	
Temp., °F	68°F	1.0		Spectrum	.975	
Load duration	N/A	1.0		N/A	1.0	
Efficiency	N/A	.96		N/A	.56	
Bond gap discount	N/A	.95		N/A	.90	
4 x 10^8 discount	N/A	1.0		N/A	.609	
Factor of safety	SDC	.67		N/A	1.0	
Allowable			4200			1436
Ref Basic Wood Allowable			(4200)			(1700)

(1) Phase A lamina testing, BG #1 Veneer, no joints.

(2) Full detailed discussion of "Adjustment Multiplier" see Volume II, section 8.0.

4.3.3 TRAILING EDGE

The trailing edge of the blade is the portion of the airfoil between .60C and 1.0C. The blade has a fixed trailing edge section between .10R and .60R on either side of the center of rotation. Its spanwise length comprises three sections. Each section is bonded and screwed to the rest of the airfoil section during the assembly of the blade. The spanwise joints between the blade section and the trailing edge sections, and the chordwise joints between the trailing edge sections are covered with a layer of glass fiber cloth to provide an environmental seal. Workers can reach the interior of the trailing edge through manholes at .10R. Internal pressure, which could build up stress, is prevented by vents at .10R and .60R. Condensation passes through the vents and strategically placed weep holes.

The trailing edge is designed to be structural along the chord and non-structural along the span. This arrangement eliminates the need to assemble a high-quality, spanwise structural joint in the field. This design allows the trailing edge to be lightweight, and allows more freedom in the choice of materials. The construction of the trailing edge uses a paper honeycomb core with glass fiber faces. A typical cross-section is shown in Figure 4-86. The core has .25 in. cells, uses 60 weight kraft paper and is impregnated with phenolic resin to protect against moisture. The glass fiber faces are 30 mils thick through the span of the trailing edge. The use of wood veneer was considered for the face material, but it would require that the veneer be placed in the fabrication mold with its weakest direction along the chord for proper compliance with the mold surface. Unfortunately, in this arrangement the weakest direction of the veneer is parallel to the stress field. To satisfy the structural criteria a wood design requires more weight and higher costs than the glass fiber design.

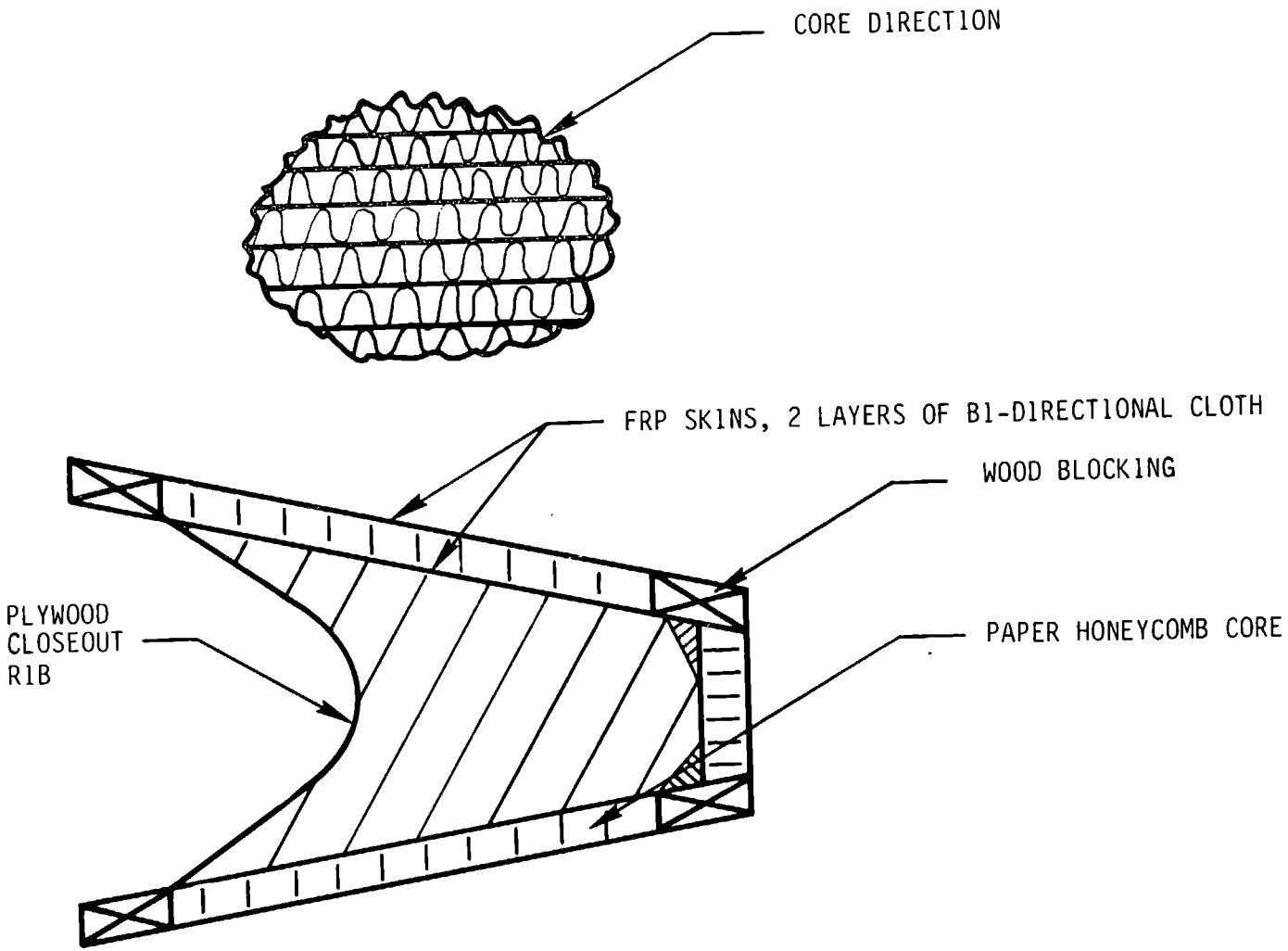

Figure 4-86. Typical Trailing Edge Cross-Section

The face and core thicknesses were determined by chordwise stresses produced by hurricane winds. Hurricane winds of 130 mph impose a positive pressure of .345 psi on the windward surface and a negative pressure of -.138 psi on the leeward surface. The total pressure difference was calculated using equation 4-2.

$$\Delta p = C_1 \, C_2 \, q \qquad 4\text{-}2$$

Where

q = dynamic pressure = .30 psi
C_1 = load contingency factor = 1.15
C_2 = average drag coefficient = 1.4

The loads and reactions are illustrated in Figure 4-87. Reactions and maximum moments were determined from a unit width beam finite element model assuming fixed joints. The reactions and moments are summarized in Table 4-37. The core thickness was the maximum required to satisfy equations 4-3 and 4-4.

$$C = \frac{M}{fFb} - f \qquad 4\text{-}3$$

$$C = \frac{V}{Sb} - f \qquad 4\text{-}4$$

Where

C = core thickness, in.
M = moment, in-lbs
F = facing stress allowable = 12,500 psi
f = face thickness = .03 in.
b = panel width = 1 in.
V = total shear load, lbs
S = core shear stress allowable = 20 psi

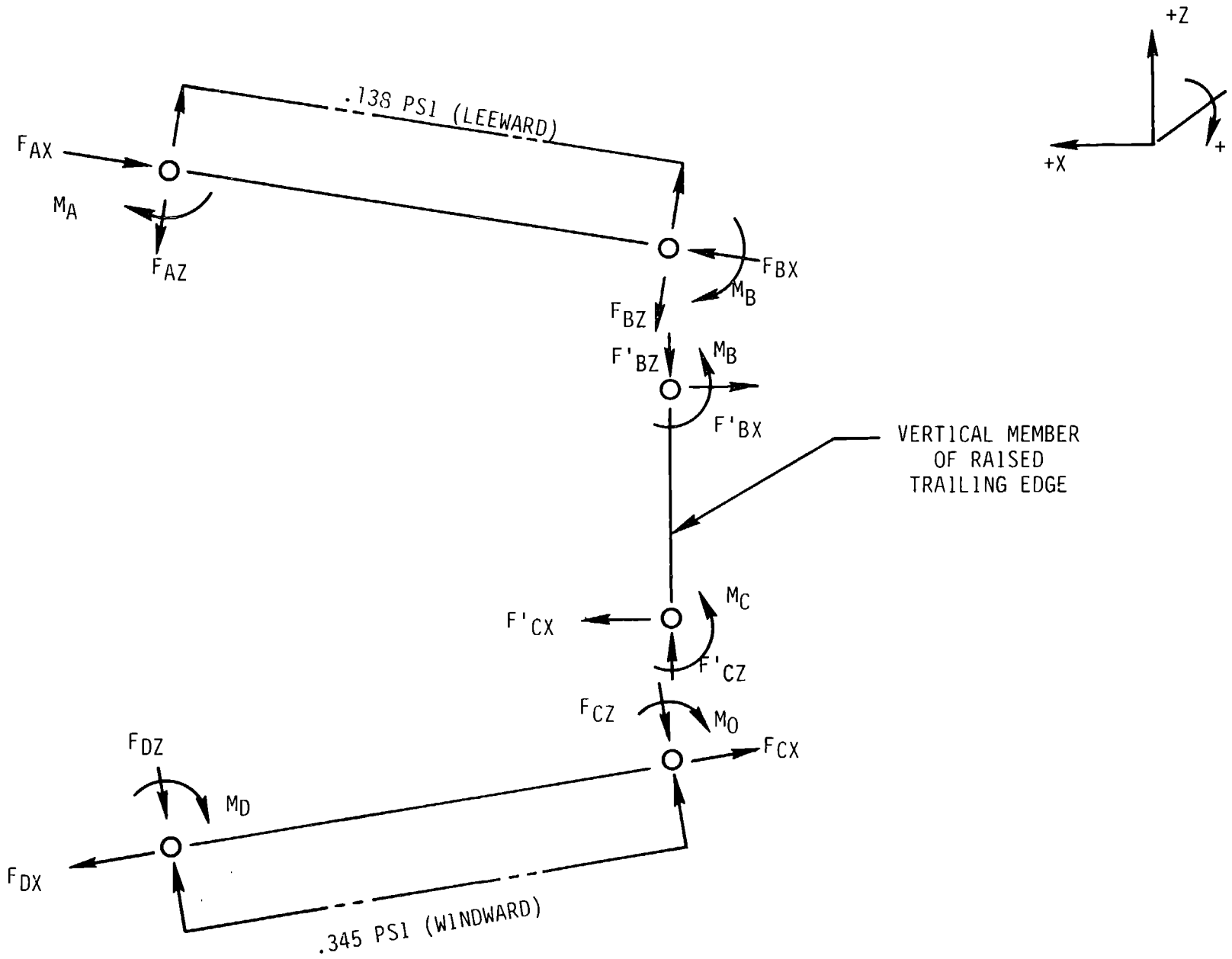

Figure 4-87. Free Body Diagram of Trailing Edge

Table 4-37 Summary of Trailing Edge Reaction Loads and Core Maximum Shear and Moments

Leeward Panel

X/R	F_{AX}, lbs(1)	F_{AZ}, lbs	M_A, in-lbs	F_{BX}, lbs	F_{BZ}, lbs	M_B, in-lbs	CORE V_{MAX}, lbs	CORE M_{MAX}, in-lbs
.10	-34.9	-16.3	571	34.9	- .4	393	16.3	571
.425	-39.8	-10.3	234	39.8	-4.0	89	10.3	234
.60	-32.2	- 8.0	143	32.2	-3.2	52	8.0	143

Vertical Panel

X/R	F'_{BX}	F'_{BZ}	M_B	F'_{CX}	F'_{CZ}	M_C	CORE V_{MAX}	CORE M_{MAX}
.10	-34.5	-4.8	-393	34.5	4.8	-196	34.5	393

Windward Panel

X/R	F_{DX}	F_{DZ}	M_D	F_{CX}	F_{CZ}	M_C	CORE V_{MAX}	CORE M_{MAX}
.1	32.3	-30.7	898	-32.2	-13.1	196	30.7	898
.425	37.1	-21.2	418	-37.1	-14.7	-89	21.2	418
.60	30.2	-16.5	253	-30.2	-11.4	-52	16.5	253

(1) See Figure 4-87 for coordinate definition.

The allowable stress in the glass fiber skins is 42% of the minimum average compressive strength specified by MIL-R-7575 for a composite of style 7781 glass fiber cloth and polyester resin. The allowable core shear stress is based on the manufacturer's test data and includes a factor of safety of 4. To minimize the number of different core thicknesses, a constant size is used from .10R to .425R and from .425R to .60R. To ensure the proper safety factors, the size of the core between these stations was determined using maximum loads. The results of these calculations are summarized in Table 4.3.3-2.

Table 4-38 Trailing Edge Sizing Results Based on Hurricane Limit Load

X/R	Max Shear lb/in	Max Moment in-lb/in	Core Thickness in	MARGIN OF SAFETY Core shear	MARGIN OF SAFETY Face Stress
.1 .425	30.7	898	2.50	.65	.06
.425 .60	21.8	418	1.12	.06	.03
(1)	34.5	393	1.88	.11	.82

(1) Vertical panel of trailing edge between .1R and .425R

The margin of safety for fatigue stresses along the chord for the face material were not determined at the time of this report. The average steady state pressure distribution on the leeward and windward surfaces is shown in Table 4-39. Since a pressure of .345 psi was used to determine the size of both surfaces, a mean face stress would be between 4,717 psi and 9,100 psi, based on the pressure reductions shown in the table. Depending on the magnitude of the alternating pressure, the face and core dimensions may need to be adjusted.

Table 4-39 Average Steady-State Pressure Distribution on Trailing Edge Surfaces at Rated Power

X/R	P_I, psi(2)	P_U, psi	P_L, psi	P_U-P_I	P_L-P_I
.25	14.57	14.67	14.69	.10	.12
.55	14.82	14.59	14.75	-.23	-.07

P_I = internal pressure
P_U = pressure on leeward surface
P_L = pressure on windward surface

(2) Variations in internal pressure occur because of centrifugal pumping of air.

Spanwise limit and fatigue stresses are imposed on the trailing edge because of the blade flapwise and chordwise bending loads. These stresses, and the buckling stability, were approximated assuming that the trailing edge was continuously attached along the blade span. This assumption yields a conservative result because it increases the load on the trailing edge. The strains of the structural portion of the airfoil and the trailing edge were equated and multiplied by the effective spanwise modulus of the glass fiber and core composite. The results are summarized in Table 4-40. All margins of safety are positive. The buckling margin of safety is reported for general buckling. Margins of safety for intercell, shear, and face buckling are higher. The buckling loads were calculated according to MIL-HNBK-23.

Table 4-40 Spanwise Limit and Fatigue Face[1] Stresses in Trailing Edge

xR	LIMIT[2] Stress, psi	M.S.	BUCKLING[3] Stress, psi	M.S.	FATIGUE Stress, psi	M.S.[5]
.1	4850	1.60	4850	.41	1550 ± 990	1.92
.2	5000	1.50	5000	.37	1580 ± 970	1.95
.3	5300	1.36	5300	.44	1620 ± 960	1.95
.4	5200	1.41	5200	.79	1510 ± 850	2.29
.5	5020	1.49	5020	1.39	1440 ± 750	2.66
.6	5140	1.43	5140	2.12	1440 ± 730	2.73

(1) Assume the trailing edge is continuously attached

(2) Stress at .60C
Seldom occurring limit load case
$E_{TE}/E_W = 1.20$
Compression allowable for face material = 12,500 psi

(3) General buckling assumes simply supported edges
$F_{allow} = F_{CR}/1.5$
F_{CR} per MIL-H-23

(4) Fatigue stresses at .60C caused by 99 percentile loads

(5) M.S. = Margin of Safety = $\frac{\text{Allowable}}{\text{Actual}} - 1$

The joint between the structural portion of the airfoil and the trailing edge is a key structural feature. The loads shown in Table 4-37 were applied to tne joint. The margins of safety were determined using the section properties of only the blocking and birch insert. Figure 4-88 illustrates the application of the maximum loads to typical joint designs for the center and inner blade sections. The results of the analysis are shown in Table 4-41. All margins of safety are positive. The redundant load-carrying capability of the retention screws and glass fiber overlap was ignored, as a simplifying assumption.

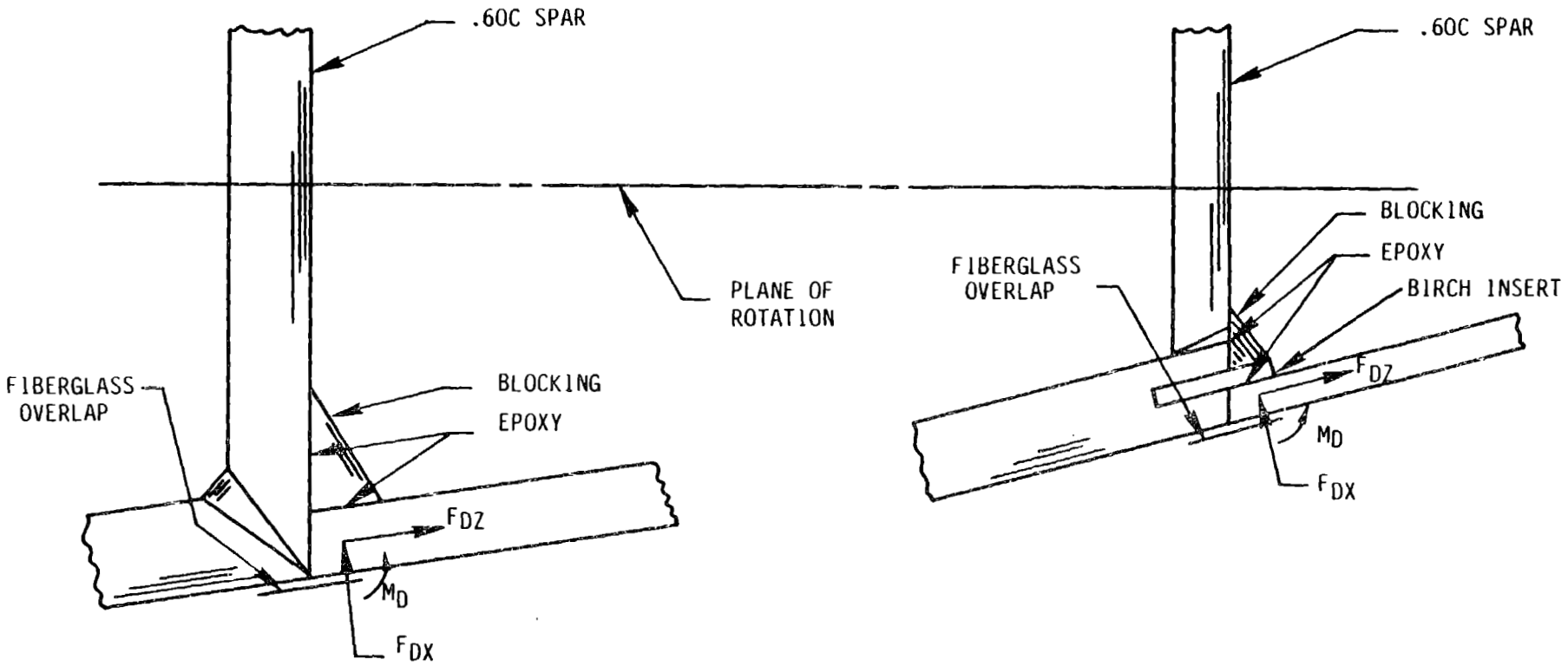

Figure 4-88. Applied Loads to Trailing Edge Joint

Table 4-41 Results of Trailing Edge Joint Analysis

Stress Component	RADIAL STATION .1R PSI	.1R M.S.	.25R PSI	.25R M.S.(2)
o Wood				
maximum cross-grain tension in the radial direction	174	.3	150	3.2(1)
maximum rolling shear	12	10.4	5	Large
o Epoxy				
maximum tensile	230	11.2	150	17.7
maximum shear	9	Large	5	Large

(1) Maximum cross-grain stress occurs in birch insert. Birch cross-grain allowable equals 630 psi.

(2) M.S. = Margin of Safety = $\frac{\text{Allowable}}{\text{Actual}} - 1$

4.3.4 HYDRAULIC INSTALLATION

The aileron's hydraulic system, shown schematically in Figure 4-140, consists of several modules containing control or power supply components. The yoke mounted power supply unit is the largest module. It contains an electrical motor-driven pump, reservoir, accumulators, filters, heaters and alarm switches for high temperature, control, and low pressure. These elements are packaged in an assembly about 30 in. x 51 in. x 173 in., as shown in Figure 4-89. The unit is designed to operate in an environment of alternating g-loads, which are produced by the rotation of the yoke. To prevent sloshing and air flow into the pump, the hydraulic reservoir consists of two low pressure bladder accumulators, nitrogen pressurized to about 3 psi when hydraulic fluids are fully discharged. These bladder accumulators enable the fluid to tumble without foaming. When fully charged with hydraulic fluid, even on the hottest day, the nitrogen charging pressure increases to 15 psi. The fluid follows this circuit through the system: the 3000 psi, 5 gpm pressure compensated pump delivers hydraulic fluid to the lines and accumulators serving the two blades. A 5 micron filter removes contaminants larger than 25 microns from the fluid. The fluid proceeds to the actuator modules on both blades and fills the main and emergency feather accumulators. During normal operation, only the pump supplies fluid to the actuators. During rapid aileron motion, which occurs during emergency feathering, the accumulators supplement the flow. The pump and main accumulator also provide pilot valve flow. The return line collects the discharge from the servo and actuator package and pilot lines and returns the fluid to the reservoir. To prevent complete discharge of the return line above the rotor centerline when the blade is stationary in the vertical position, a 75 psi relief valve is installed in the return line. To maintain acceptable fluid viscosity, immersion heaters, to keep the fluid temperature above 60°F at the inlet to the pump are placed in the return line between the accumulators and pump.

Conversely, the heat generated during operation is dissipated in the supply and return lines by convective air currents. To protect the pump, there is a 150 micron filter just upstream of the pump inlet.

The hydraulic supply system also provides pressure to the eight teeter snubber brakes. The two snubber manifolds, each with its own accumulator, are charged continuously through a back pressure sensing regulator that closes the lines

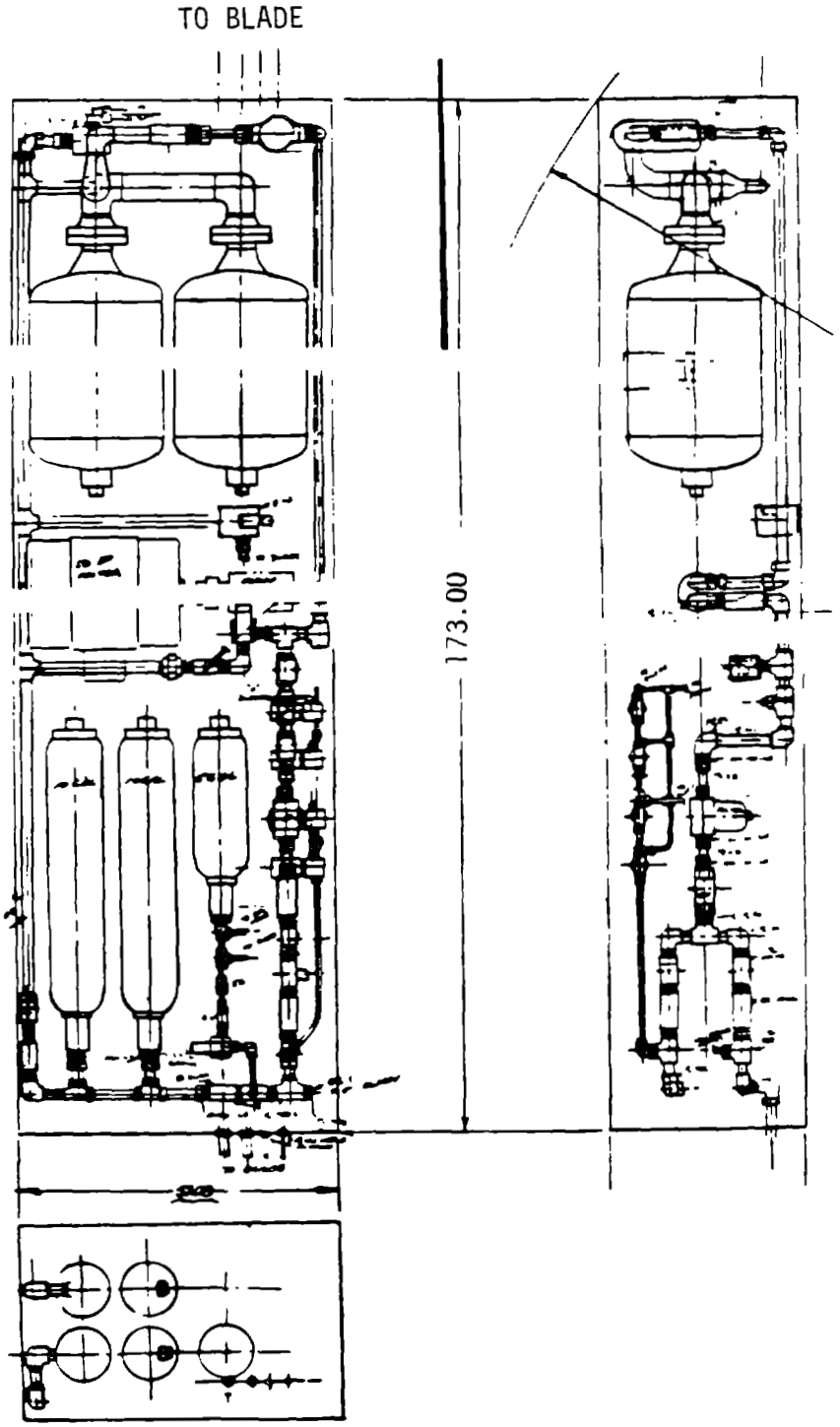

Figure 4-89. Hydraulic System Arrangement

when the brake accumulators are fully charged at 1500 psi. Check valves prevent the brake accumulators from being discharged when the pump is off. All solenoid valves in the hydraulic power supply package are shear-seal valves.

All the tubing that connects components is stainless steel with a minimum safety factor of 6. Connecting fittings are Lenz or SAE 37° flared fittings.

4.3.4.1 Hydraulic Supply Line Installation

Drawings defining the installation of the hydraulic conduits for Model 304.2 were not developed. However, the installation would be similar to that developed for Model 204.6. The hydraulic conduits are supported by clamps mounted to the aft face of the .60C spar, as shown in Figure 4-90. The installation avoids subjecting the conduits to compression or buckling stresses by fixing the conduit at the innermost support and allowing the load caused by centrifugal effects to pull, rather than push, the fitting. The fittings are placed near the neutral axis along the flap, to minimize bending stresses. At other clamp locations, the conduit is free to slide, which accommodates any differential movement with the blade. To assist the sliding action, the outside of the conduits is encased in a sleeve of Teflon. The conduits and mounting provisions can be inspected by entering the trailing edge through the manhole at .10R and walking along the .60C spar.

Where flexing occurs, flexible hose is used. Flexible hose supplies two locations: the interface between the rotor-mounted hydraulic supply module and the blade, and each aileron actuator. These hoses must be compatible with petroleum-based hydraulic fluid, such as MIL-H-5606 or Dexron. They must also have high burst strength and a short bending radius. Aeroquip 2757 and FC136 meet these requirements. Straight runs of stainless tubing in the blade are made by welding commercially available 20 ft. lengths. At transitions between stainless and flexible hose, 37° flared fittings are used.

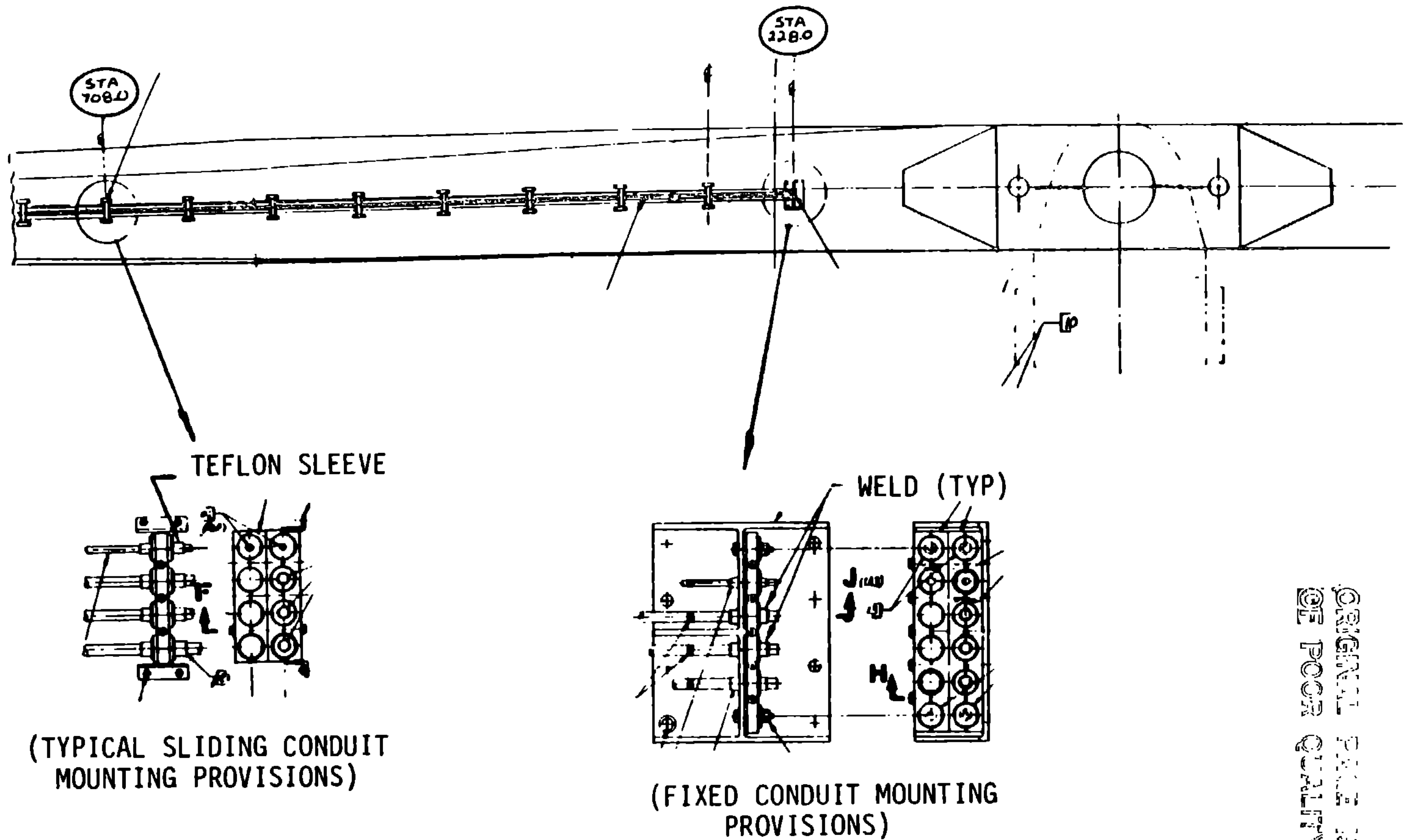

Figure 4-90. Blade Hydraulic Installation

4.3.4.2 Hydraulic Line Sizes

The diameter and thickness of hydraulic tubing is a function of the required flow rate and pressure. These parameters are a function of the actuation rate and piston diameter, both of which are a function of the load the actuators must overcome. In the case of the aileron actuators, the rates are 5°/sec for normal operation and 10°/sec for shutdown operation, with a hinge moment of 27,500 ft.-lb. The corresponding maximum actuator force is 55,000 lb, based on a minimum moment arm of 7 in. At a maximum differential pressure of 3,000 psi across the piston, the required net piston area is 18.33 $in.^2$. For a 10-in. stroke and a configuration representative of the aileron actuator, the actuator design standards dictate a rod diameter of 2.5 in.

The corresponding piston diameter (D) can be calculated from the expression:

$$[D^2 - (2.5)^2]\ \pi/4 = 18.33$$

$$D = 5.4399 \text{ (or 5.5 in. in round numbers).}$$

The rate of flow (Q) into and out of the actuator at the shutdown rate of 10°/sec, and with a 10 in. stroke, corresponding to a 90° aileron deflection is derived as follows:

$Q = \alpha \times G_L \times A_P$

α = aileron rate G_L = actuator linkage gain.

A_P = actuator piston area

$$10°/\text{sec} \times \frac{10 \text{ in.}}{90°} \times 18.33 \text{ in.} = 20.367 \text{ in.}^3/\text{sec}$$

This value is converted into conventional flow rate units expressed in gpm as follows:

$$20.367 \text{ in.}^3/\text{sec} \times \frac{60 \text{ sec}}{\text{min}} \times \frac{1 \text{ gallon}}{232 \text{ in.}^3} = 5.28 \text{ gpm}$$

Based on a fluid velocity of 25 ft./sec., the maximum recommended for aircraft hydraulic systems, the inner diameter of the flow passage must be 3/8 in., to feed the actuator. Consequently, the hoses adjacent to the actuators have inner diameters of 3/8 in. To provide this inner diameter for the stainless steel tubing, with a safety factor of 6, the outer diameter and the wall thickness is 5/8 in. X .095. It should be kept in mind that these dimensions

are for hydraulic lines feeding individual actuators. A line feeding two actuators, using similar design parameters, has an outer diameter of 7/8 in. and a wall thickness of .12 in. A line feeding all three actuators has an outer diameter of 1 in., and a wall thickness of .134 in.

The pilot lines have outer diameters of .25 in. and wall thicknesses of .035 in. They feed individual control modules. The pilot line that feeds two modules has 3/8 in. outer diameters and a .049 in. wall. A pilot line that feeds 3 modules has a .5 in. outer diameter and a .065 wall.

4.3.4.3 Functional Description

In Figure 4-140, all solenoid and hydraulic pilot operated valves are shown in the off position. When the valves are in the off position, the emergency feather system drives the ailerons to the feathered position by placing the shuttle valve spool so that the emergency feather accumulator is directly connected to the feather side of the actuator piston, and the power side is connected to the return line. The full pressure in the accumulator is brought to bear on the actuator to move the aileron. Flow rate, and aileron deployment rate is controlled by flow rate control valves in each feed line between the accumulator and actuator. Energizing feather valves A and B on each blade resets the shuttle valve, so that the connection between the emergency feather accumulator and actuator is blocked, but the lines between the servo valve and actuator are open. This set-up permits the on-board control system to command and control the aileron position through the servo valve. The pump normally supplies fluid to the servo valve; the supply is supplemented by the 5-gal. accumulator when the flow demand is high. The two emergency feather pilot valve sets, A and B, are connected in a fail-safe "semi-parallel-series" arrangement. This arrangement requires that both valves are on for the system to operate, but if either one drops out it will cause emergency feathering. Valve set A is controlled by the emergency shutdown panel and may be tripped by a number of malfunctions. Valve set B is tripped by a g-switch, during an overspeed.

The solenoid valves in the teeter snubber brake lines are also fail-safe, in that upon loss of electrical power the brakes will engage.

4.3.5 ELECTRICAL INSTALLATION

Permanent blade electrical circuits are routed in metal conduits that are supported by clamps along the 60% of chord blade spar. The conduits are located next to the hydraulic piping and use the same clamp attachments. Flexible conduit sections are located at the yoke and field joints to accommodate teeter motion and any other elongations. Junction conduits are located along the main conduits where the aileron actuators, strain sensors, thermal sensors, and ice detectors are connected.

Strain gage instrumentation leads are also routed in conduits along the blade, but are connected to the sensors with surface mounted shielded ribbon cable rather than through conduit. The ribbon cable is expendable in the event of a lightning strike.

Conduits are factory installed on each section of the blade. After the blade sections are bonded together in the field, the conduit sections are connected and the wiring is pulled into them. Aileron actuator circuits are connected as the aileron sections are installed on the ground. All circuits will be functionally checked both before and after the wire support and trailing edge structures are mounted.

4.3.6 Lightning Protection

The blade must be protected against structural damage caused by lightning strikes, for reliable, safe operation. This protection is provided by a path to ground for an electrical discharge. A preliminary set of requirements were defined for Model 204.6 by Lightning Technology Incorporated (LTI), based on the current history illustrated in Figure 4-91 and explained in Table 4-42. LTI limited the occurrence of structural damage of the main blade sections to once in 1000 years, and recommended:

1) a sacrificial tip section, since it is more cost effective to replace the tip than to prevent structural damage,

2) the surface of the outer blade section be covered with a wire mesh screen below the glass fiber layer, to limit repair to resurfacing the glass fiber. The inner and center blade sections do not require a mesh layer.

3) leading edge conductors be provided along the inner and outer blade sections,

4) trailing edge rods or the equivalent be provided at several spanwise locations to prevent a strike from puncturing the trailing edge,

5) the wire mesh, tip, leading edge conductors and trailing edge rods be connected electrically to a conduit, mounted on the aft face of the .60C spar.

These recommendations are equally applicable to Model 304.2 and are shown in Figure 4-92. The tip section is an expendable glass fiber part with an embedded aluminum screen, 18" x 16 x .012", covering the outer surface. This screen is connected to the embedded screen in the outer blade, as shown in Figure 4-93. The installation of the screen in the outer blade uses the same techniques demonstrated during a similar installation in the MOD-0A blades. The leading edge conductors, also embedded, are fabricated from .032 in. thick 5052-0 aluminum and have a cross-sectional area equivalent to AWG #4 copper wire. The same material is used to connect these conductors and the wire screen to the conduit, and to protect the trailing edge, as shown in Figure 4-94.

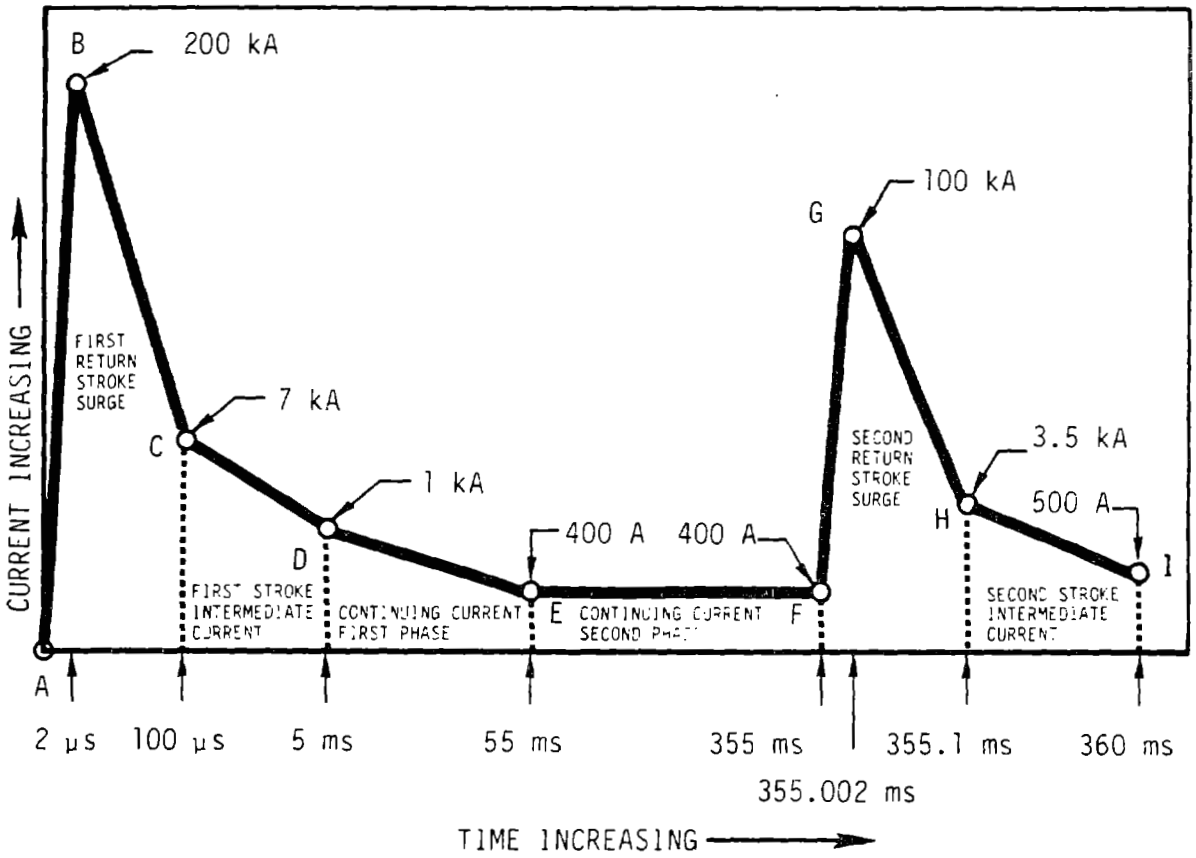

μs = microsecond, .000001 sec.

ms = millisecond, .001 sec.

KA = kiloAmperes, 1000 amperes

A = Amperes

(See Table 4-42 for Definition of Terms)

Figure 4-91. Diagrammatic Representation of Lightning Model

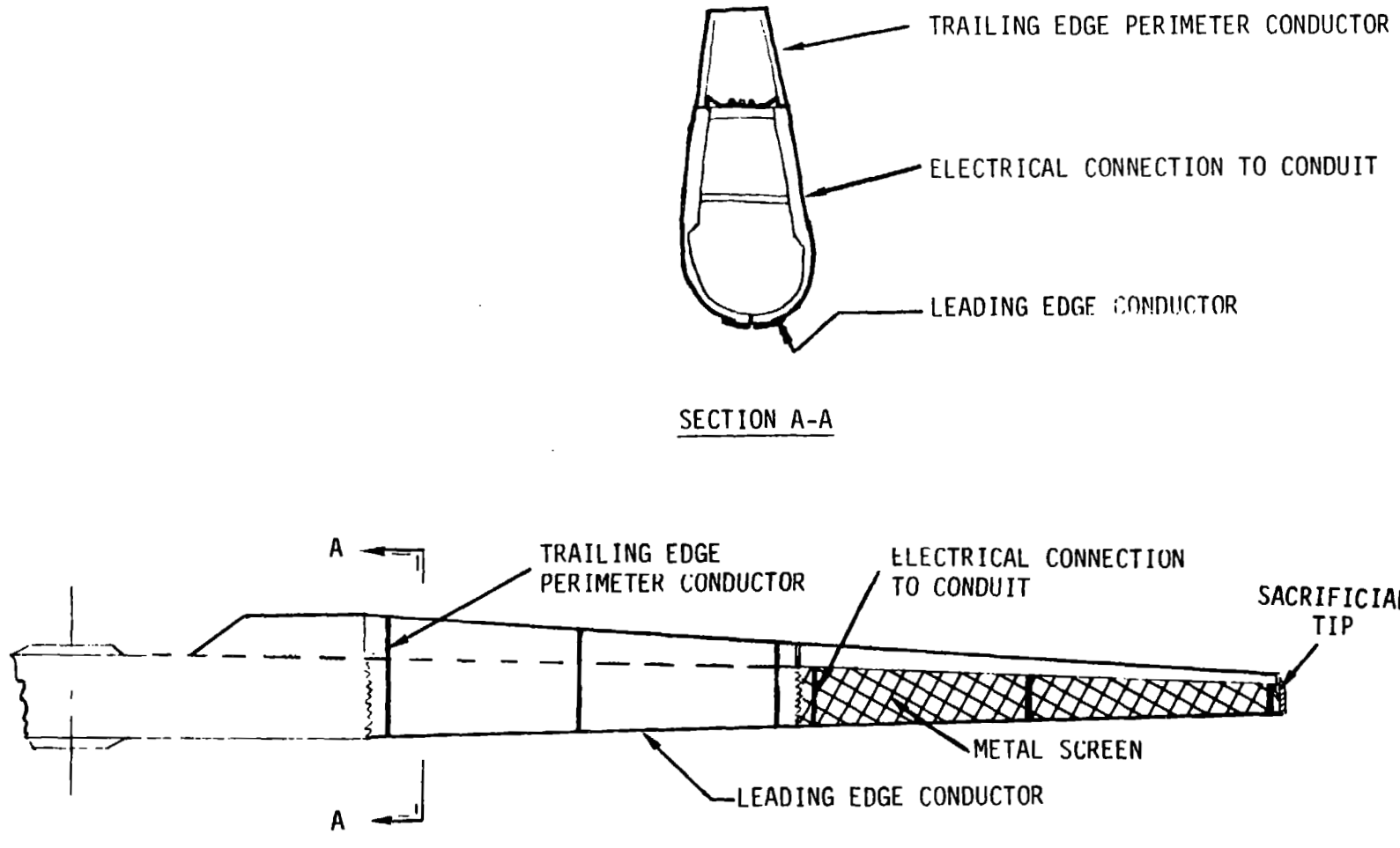

Figure 4-92. Blade Lightning Protection System

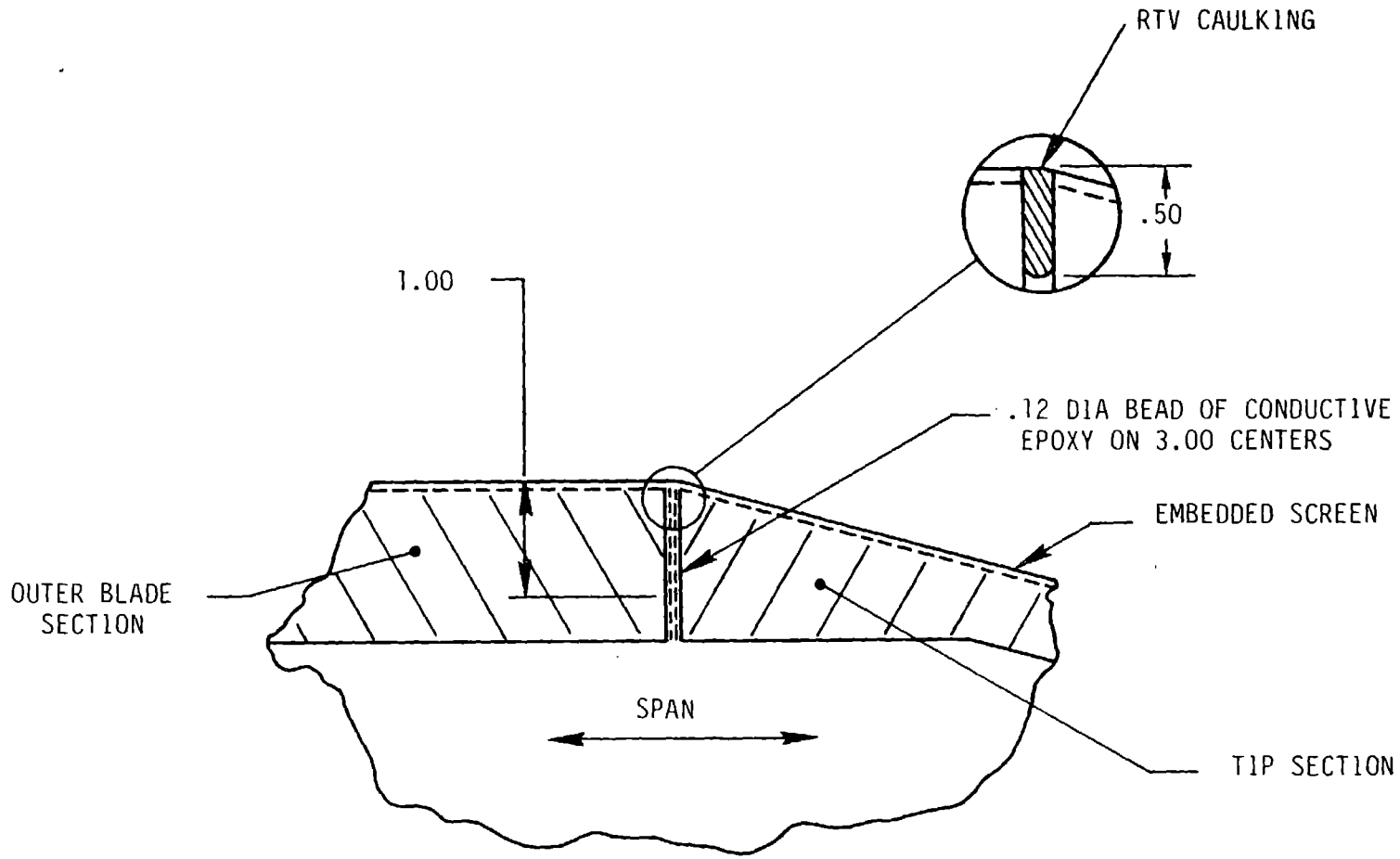

Figure 4-93. Electrical Connection Between Tip and Outer Blade

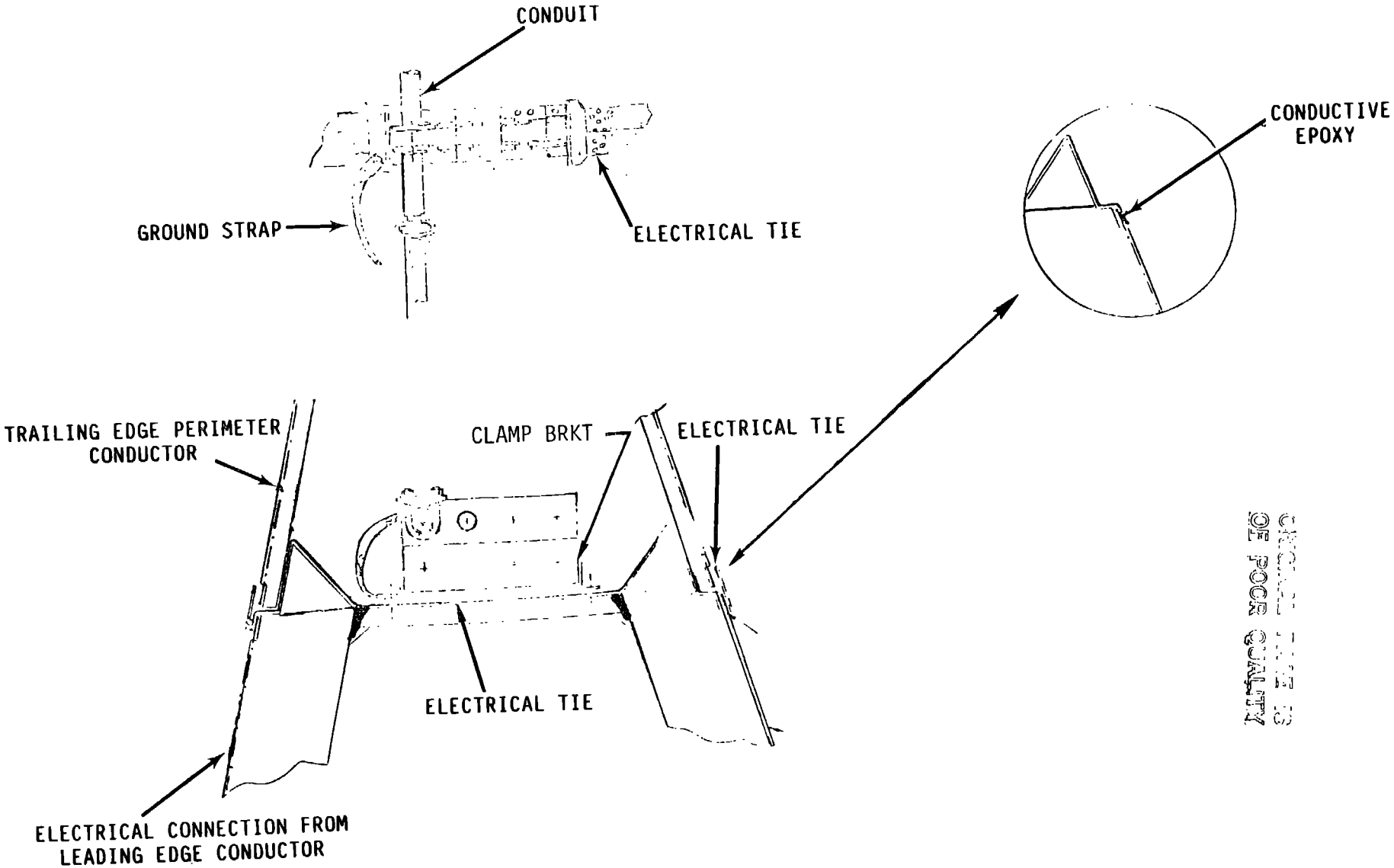

Figure 4-94. Electrical Connection to Conduit

Table 4-42 Details of Lightning Model

Stage	Key Points		Rate of Current Change	Charge Passing
1. First return stroke surge	t = 0 t = 2 ms t = 100 ms	i = 0 i = 200 kA i = 7 kA	Linear rise - 100 kA/ s Linear fall - 193 kA in 98 ms	0.2 C ~10.2 C
2. First stroke intermediate current	t = 100 ms t = 5 ms	i = 7 kA i = 1 kA	Linear fall - 6 kA in 4.9 ms	19.6 C
3. Continuing current - first phase	t = 5 ms t = 55 ms	i = 1 kA i = 400 A	Linear fall - 600 A in 50 ms	35.0 C
4. Continuing current - second phase	t = 55 ms t - 355 ms	i = 400 A i = 400 A	Steady current	120.0 C
5. Second return stroke surge	t - 355 ms t = 355.002 ms t = 355.1 ms	i = 400 A i = 100 kA i = 3.5 kA	Linear rise 50 kA/ ms Linear fall - 96.5 kA in 98 ms	~0.1 C ~5.0 C
6. Second stroke intermediate current	t = 355.1 ms t = 360 ms	i = 3.5 kA i = 500 A	Linear fall - 3 kA in 4.9 ms	9.8 C

Key: t = time
s = micro-second
ms = milli-second
i = current
A = Amps
kA = 1000 Amps
C = Coulomb

4.3.7 BALLAST INSTALLATION

The static and natural frequency imbalances that may occur because of manufacturing and operational biases must be controlled so that the dynamic loads produced on either side of center of rotation on the blade are equal. Ballast added to the inner and outer blades controls the static and natural frequency imbalances.

The ballast provisions for the inner blade are shown in Figure 4-95. Pieces of steel ballast weighing 50 lbs. are installed on the .30C spar at .50R to remove a static imbalance of up to 500,000 ft-lbs. Workers enter the blade through a manhole at .09R.

Figure 4-96 illustrates the installation of up to 500 lbs. of tungsten ballast in the outer blade. This ballast is used for fine tuning the blade properties. Removing the tip assembly provides access to the ballast cavity. The spanwise location of each 50 lb. piece in the ballast canister can be adjusted by installing a cylindrical spacer in the unused volume. The ballast is preloaded in the canister without inducing load on the wood support structure.

An analysis determined the possible variation in the blade weight, to ensure that there is enough ballast capability. The parameters that could cause a variation in weight included the wood density, the epoxy spread rate, and the thickness of the wood veneer. The thickness of the airfoil wall specified on the blade drawings is converted to an equivalent number of veneers during the manufacturing process. This system eliminates the need to inspect the dimensions of each veneer. The variation in the thickness of the veneer varies the cross-sectional area and blade weight. The statistical characteristics of these variables are shown in Table 4-43. The weight of the blade is calculated by multiplying the wood volume by an equivalent density ρ_e.

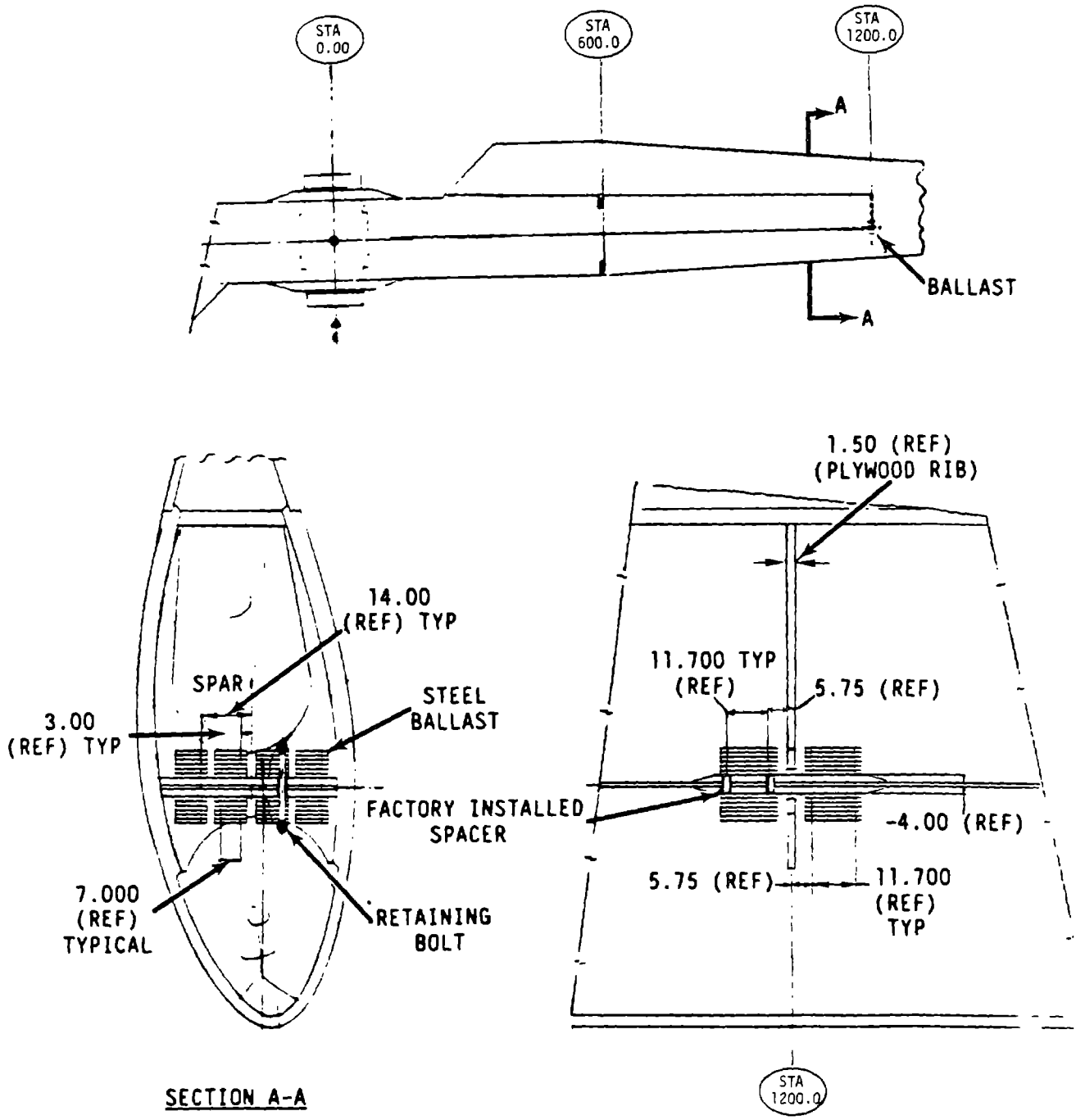

Figure 4-95. Ballast Installation in the Inner Blade

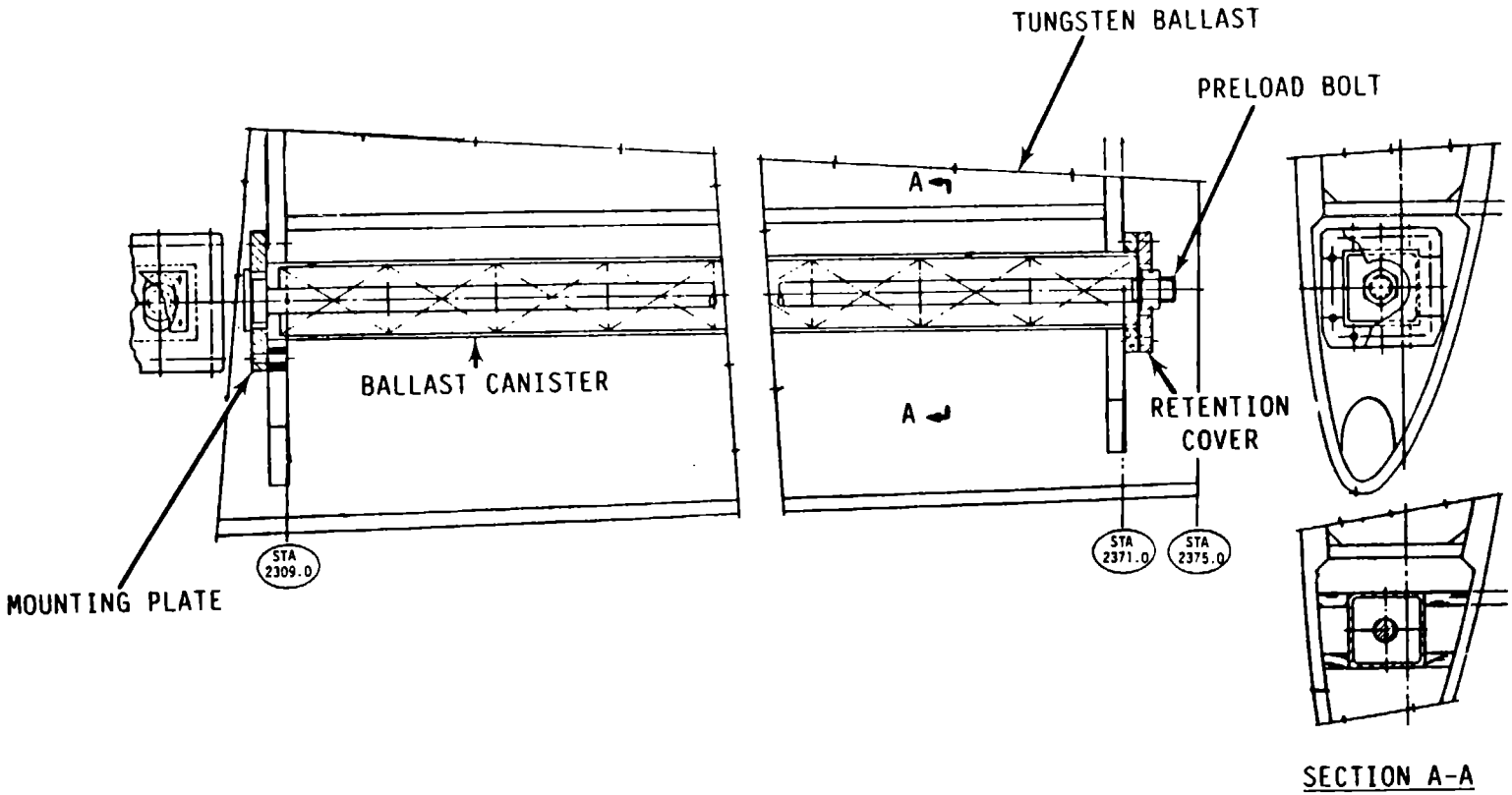

Figure 4-96. Ballast Installation in the Outer Blade

Table 4-43 Characteristics of Variables Used in Computing Variations in Blade Weight

Variable	Rating	Standard Deviation S	Coefficient of Variation
Wood Density, ρ_w	33.18 lb/ft^3	1.66	± 5%
Epoxy Spread Rate, A (1)	7.2 lb/ft^3	.18	± 2.5%
Veneer Thickness, t	.100 in.	.005	± 5%

(1) 60 lbs./1,000 ft^2 of double glue line normalized to 1 ft^3 of .1 in. thick veneer.

$$\rho_e = A + f_t \rho_w \qquad 4\text{-}5$$

Where

A = lbs of epoxy per ft^3 of .1/in. veneer. One ft^3 of .1 in. thick veneer has a l x w product equal to 120 ft^2. Therefore, the glue spread rate multiplied by 120 ft^2 equals pounds of epoxy per ft^3. The value is 7.2.

ρ_w = wood density, lbs/ft^3. The value is 33.18 for a moisture content 7%.

f_t = ratio of actual and rated thickness. The normal value equals 1.0.

Equation 4-5 yields a rated blade density of 40.38 lb/ft^3 for the rated values. The actual distribution of the weight in the blade depends on the statistical characteristics of the three variables. The standard deviation, S_e, for ρ_e is defined by equation 4-6. (Ref. 4-9)

$$S\rho_e = \left(S_A^2 + f_t^2 S\rho_w^2 + \rho_w^2 S_t^2\right)^{\frac{1}{2}} \qquad 4\text{-}6$$

Substituting the values from equation 4-5 and Table 4-43 in equation 4-6 yields a standard deviation for the blade, $S_{\rho e}$, of 1.68 lbs/ft^3. If the density of half the blade assembly is the rated density, and the density of the other half is at the +2 $S\rho_e$ limit, the difference in weight will be 8%. This difference results in a static moment imbalance of 524,966 ft-lbs, as shown in Table 4-44. The ballast provisions at .50R and .975R provide a balance capability of 598,460 ft-lbs, which represents a 14% margin.

Table 4-44 Design Point For Ballast Installation

R	Weight Distribution, lb/ft	Moment Arm, ft.	8% Imbalance ft-lb
0 - .10	1,249	10	19,987
.10 - .20	966	30	46,254
.20 - .25	789	45	28,405
.25 - .30	696	55	30,624
.30 - .40	618	70	69,216
.40 - .50	548	90	78,912
.50 - .60	459	110	80,784
.60 - .70	346	130	71,968
.90 - .80	224	150	53,760
.80 - .90	112	170	30,464
.90 - 1.0	48	190	14,592
			524,966

4.3.8 ICE DETECTOR INSTALLATION

The operation of the wind turbine is inhibited or halted if ice accumulates on the blade. A Rosemount ice detector, Model 871FA222SP5, shown in Figure 4-97, detects ice if the depth of the ice is greater than .2 in. The detector senses a difference in the oscillating frequency of the sensing probe. This detector is similar to the model used successfully on the MOD-1 wind turbine.

The detector must be oriented so that the sensing probe faces the wind when the wind turbine is not operating and so that the chord of its airfoil-shaped base strut is parallel to the wind during operation. The detector must be in a spanwise location that limits its steady-state operation to 15 g's. These requirements are met by the installation shown in Figure 4-98.

As shown in Figure 4-98, the detector is mounted on the high pressure side of the trailing edge at 0.65C and .58R. A housing assembly is bonded to the reinforced circular cutout provided in the trailing edge with its ice detector mounting holes properly oriented. The detector is installed into the housing assembly and secured with the retainer and screws. A gasketed fit provides an environ- mental seal. The housing also supports the conduit, and prevents loads on the ice detector's electrical connector.

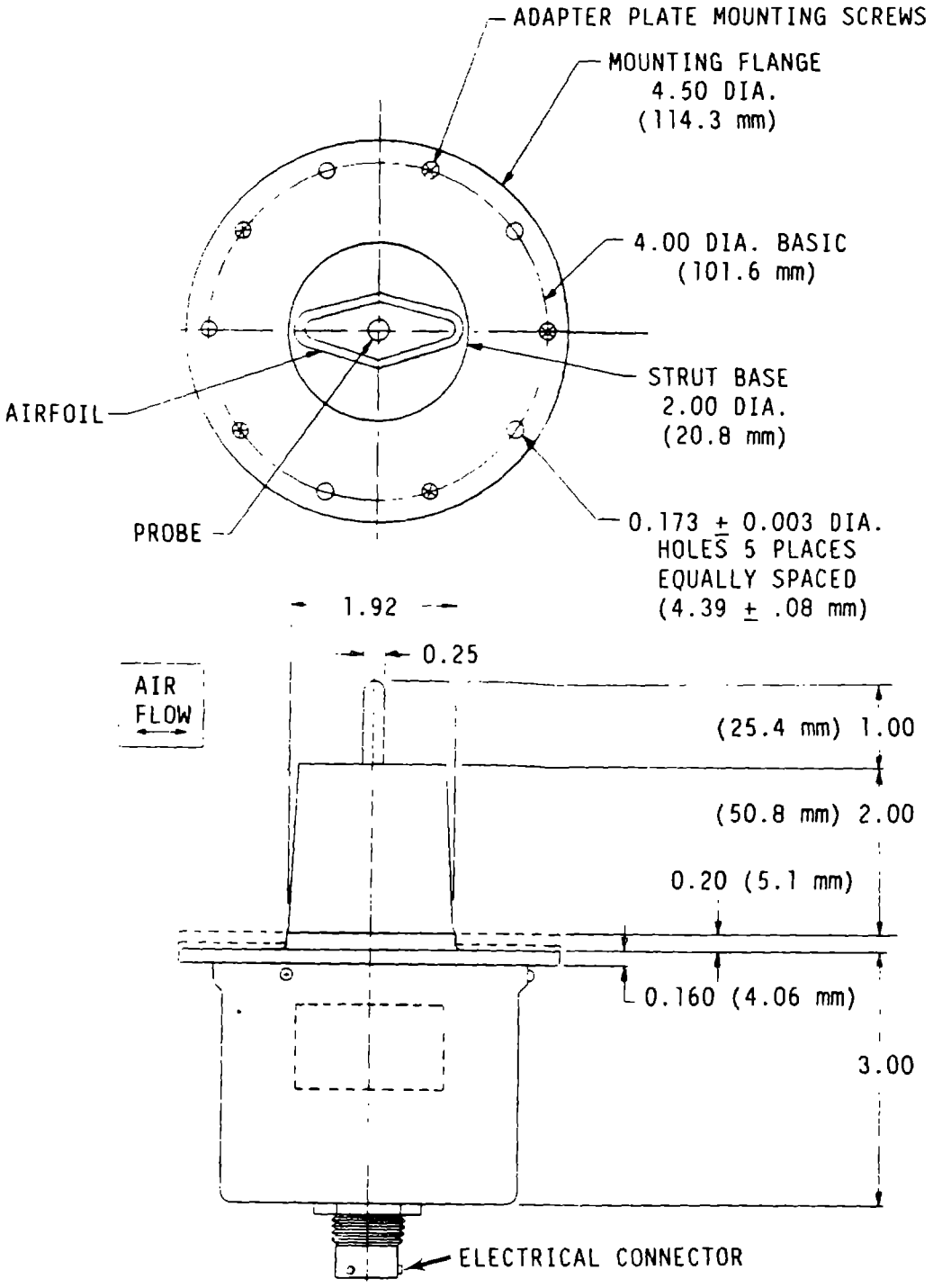

Figure 4-97. Ice Detector Assembly

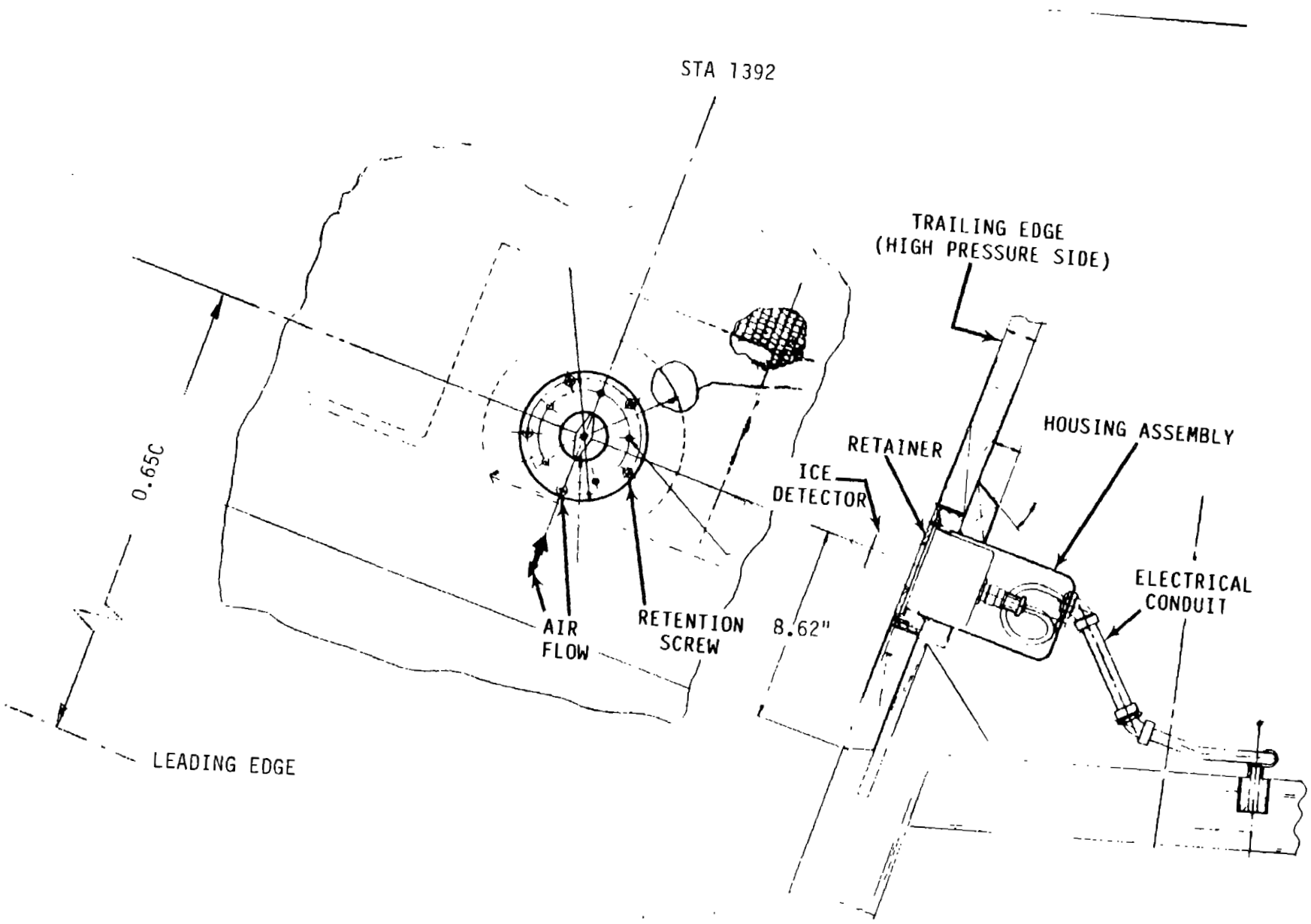

Figure 4-98. Ice Detector Installation at ± .58R

4.3.9 INSTRUMENTATION INSTALLATION

At the time of this report, the details defining the installation of the blade and aileron instrumentation, defined in Section 9, was not documented.

Strain gage locations are required at the following areas:

	Location	Min. No.	Purpose
1.	Actuator Pistons	3	Hinge Moment Evaluation
2.	Torque Links	3	Hinge Moment Evaluation
3.	Forward Spar	3	Normal & Torsional Load Determination
4.	Upper & Lower Skins	6	Normal & Torsional Load Determination
5.	Max Compression Skin	4	Skin Stability Assessment

Sine the the ailerons of each blade are symmetrical, instrumentation will be limited to one blade.

4.3.10 INTERFACES

There are many interfaces between the blade and other systems of the wind turbine. These interfaces are:

Teeter bearing	Blade and yoke subsystem
Teeter restraint	Blade and yoke subsystem
Hydraulic and electric lines	Blade, and hydraulic and electrical subsystems
Aileron support	Blade and aileron subsystems
Tether attach points	Blade to erection operation and maintenance

The bolster and blade teeter bearing cup interface is shown in Figure 4-99. The design of the bolster and teeter bearing cup were discussed in sections 4.3.1.1.1 and 4.3.1.2. The interface between the teeter restraint and bolster, shown in Figure 4-135, was discussed in section 4.3.1.2 and 4.3.1.2.1. The hydraulic and electrical service interface, shown in 4-90, was discussed in sections 4.3.4.1 and 4.3.5. The interface between the aileron and the blade, shown in Figure 4-79, was treated in the discussion of the outer blade assembly, and will also be discussed in section 4.4.

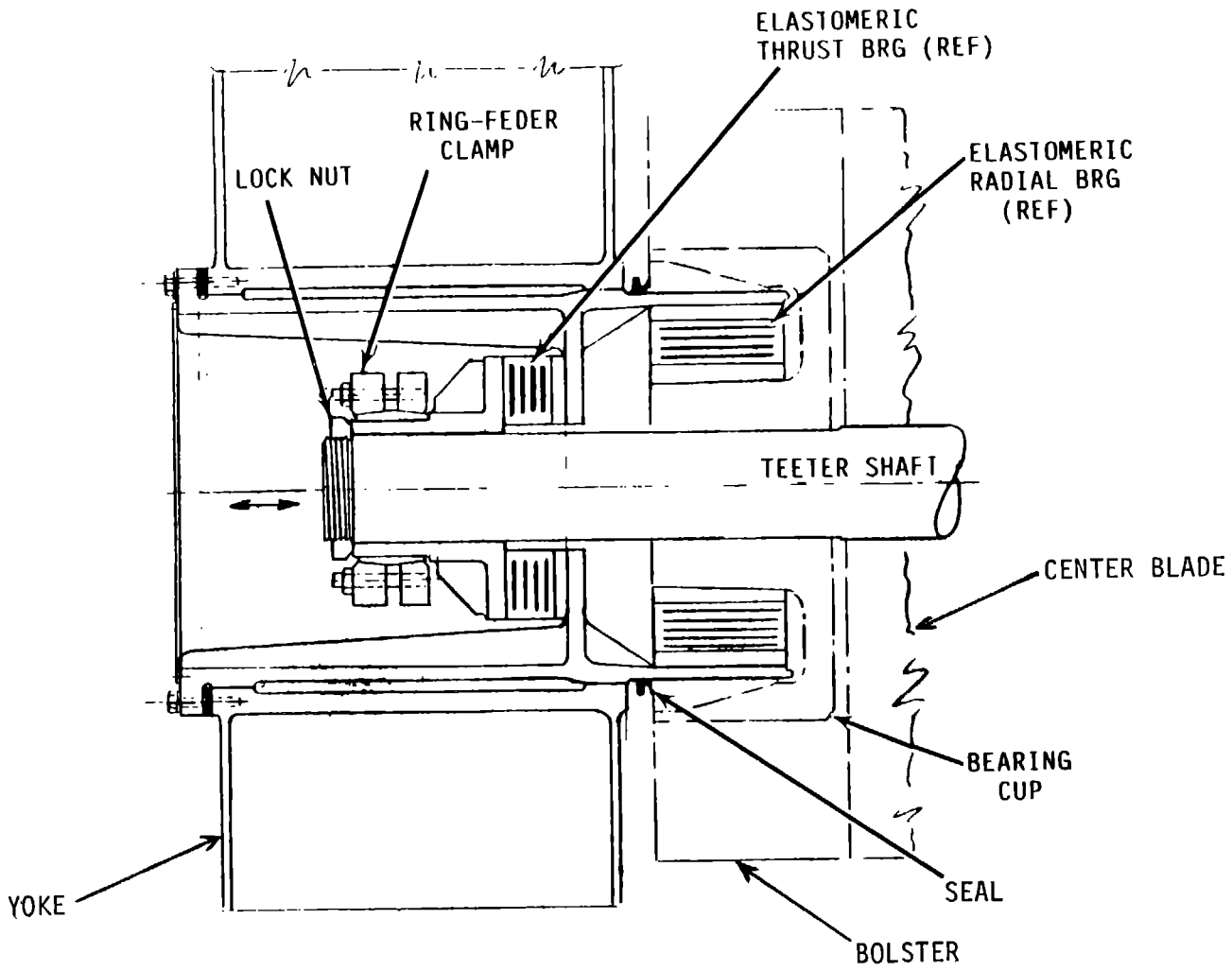

Figure 4-99. Radial and Thrust Bearing Interfaces with Blade

The blade required tether attachment points, to facilitate handling, erection and maintenance. The plan was to locate the tether attachment points in the aileron support fittings, to take advantage of the existing point-load introduction capability. However, the program was terminated before detailed work was done in this area.4.3.11

4.3.11 DESIGN IMPLICATIONS OF BLADE MANUFACTURING

There are several limitations on the manufacturing process for the blade. The limits on the angle of twist were especially important. Wood veneer could conform to the female mold surface if the change in the angle of twist was not more than 1.5° per chord length. Beyond this limit, the veneer must be spilled or trimmed, which would increase the blade cost by several times.

Furthermore, the blade could not be made or shipped in one continuous piece. A finger joint is incorporated at points where the curve describing the angle of twist changes slope. In determining the location of these joints, the maximum length of shipped components must be considered. Because of these requirements, and the need for 0° of twist at the center of rotation, the center blade was designed with a maximum twist of 5° at the finger joints.

The shape of the blade sections between the rectangular shape at .0R, and the airfoil shape at .25R, reflect the results of trial veneer layering, performed on a 1/4-scale model of the center blade. The purpose of the trials was to define the set of outer mold line coordinates that provided the shape restraints at .0R and .25R, and that minimized the compound curvature necessary to make the transition.

The last restraint was the need for V-type longitudinal bond joints. The large bond area required to bring together parts made from separate molds, necessitates a sequential bonding operation, which eliminates a time constraint, allows proper fixturing, and facilitates the inspection of the bonded joint. The V-joint allows all of these requirements to be met. Test data for the V-joint is contained in section 8.0 of Volume II. The manufacture of the joint is discussed in section 10.5.5.

4.4 AILERON SUBSYSTEM

Model 304.2 was a significant departure from the previous wind turbine generator configuration. The aerodynamic rotor control surfaces were changed from partial span control to aileron control, because the partial span control design caused growths in weight and cost. A second examination of the trade-offs performed during the conceptual design phase reversed the conclusions about the control system. The complexity of multiple aileron structures and actuators, which was considered a disadvantage in the earlier trade-offs, was eventually balanced by the benefits of removing the partial span control structure from the primary blade structure. The partial span control structural design and dynamic load analysis resulted in an increase of approximately 26,000 lbs. per blade.

The use of ailerons removed the aerodynamic control mechanism from the primary blade load path and distributed it as secondary blade structure, which interfaced the blade at the spar at 60% of the chord. The estimated weight of the aileron subsystem was less than 5000 lbs. per blade, much lower than the estimated weight of the the partial span control system, which was 40,000 lbs. per blade. A wind tunnel test program obtained initial aileron performance data. Functional, operation and performance development testing of the aileron system was conducted with the MOD-0 wind turbine generator, which had blades with ailerons. The results of these tests are presented in Volume II, section 8.4.2.

4.4.1 BASELINE AILERON DESIGN DESCRIPTION

The ailerons are aerodynamic control surfaces, which are used to control and shut down the rotor. The ailerons extend from 60% of blade span (Station 1440) to 99% of blade span (Station 2375), a length of 78 ft. The aileron is formed by the airfoil from 60% of the chord to the trailing edge. The aileron pivots up to -90° (towards the low pressure surface) about a hinge axis 2.75 in. below the low pressure blade surface, as shown in Figure 4-100. The aileron control surfaces are divided into three sections; each section is separated into two segments to accommodate blade flexure. The inboard segments of each section, which is closest to the rotor rotational axis, is driven by a linear hydraulic actuator with a slider-crank three-bar mechanism. The actuators and inboard pivot hinge of the aileron sections are located at Stations 1440, 1740 and 2040. The hinges at these stations have

spherical self-aligning plain and radial bearings, which react aerodynamic shear loads and actuator loads. The centrifugal forces from blade rotation are reacted at the hinge points between the pair of segments for each section (Stations 1590, 1890, and 2208). A pair of angular contact, spherical, self-aligning plain bearings are used at this hinge location because these bearings must carry axial, as well as radial loads. The central hinge point locates the aileron segments in the blade radial axis and the other hinges permit relative axial motion of the aileron with respect to the blade.

The outboard hinge point for each aileron section consists of one spherical self-aligning plain bearing. This bearing, with its angular and axial freedom, compensates for misalignment and deflections caused by the effects of loads, thermal expansion and moisture changes in the wood.

Each pair of segments are connected by a torque link that permits independent axial and radial alignment of each segment with the blade. The link also drives the outboard segment along with the inboard segment when the aileron is deployed. The loads induced at these hinge locations because of the torque link arrangement are significantly less than those at the actuator. This difference is because the effective moment arm for the torque link is much longer than the moment arm for the actuator. For example, at station 2208 the effective moment arm for the torque link is approximately 3 ft. and for the actuator at station 2040 the maximum moment arm is only 7 in. In addition, the hinge moment at the torque link is only about 50% of the moment at the actuator.

The aileron sections are structurally attached to the 60% spar of the blade at the hinge location. The hinge brackets are mounted to load distribution ribs in the blade by four tapered wood studs. The studs are 20 in. tapered steel rods with a maximum diameter of 2.75 in. They are mounted in a rectangular pattern approximately, 23 by 7 in. The blade structural interface and the tapered steel studs are discussed in Section 4.3.1.5, Outer Blade.

The actuator is a double ended rod-type hydraulic cylinder with a 4.4 in. bore and a 10 in. stroke. The actuator has a maximum capability of 50,000 lbs. at a supply pressure of 3000 psi. The double-ended rod arrangement provides

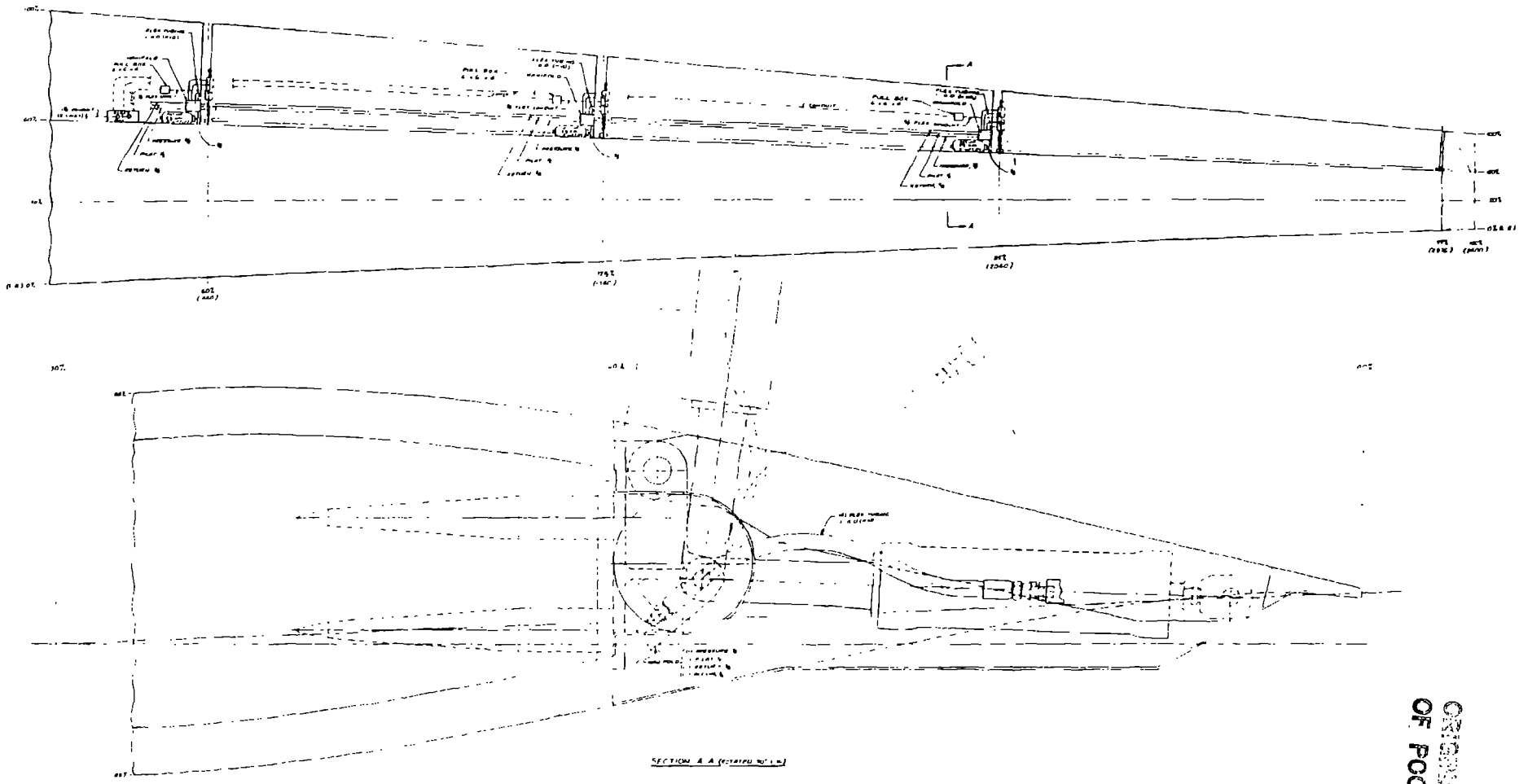

Figure 4-100 Aileron Arrangement and Schematic

lateral support and reduces bearing loads in the high g environment. The hydraulic control valves are integrated into the cylinder body and four hydraulic flexible hoses connect the actuator to the blade hydraulic system. The cylinder end is attached to the rear spar at the hinge bracket and is attached to the aileron rib structure at the rod end. Spherical self-aligning plain bearings are utilized in both connections. The effective moment arm of the actuator varies from 5 in. at 0° and -90° deployment up to 7.0 in. at 45° deployment of the ailerons in a sinusoidal curve, as shown in Figure 4-101.

The hydraulic piping and electrical service conduits are mounted to the aft surface of the 60% spar. The forward structure of the aileron is recessed to clear this piping and conduit and the hydraulic accumulator mounted at each actuator. An arrangement of this hardware is shown in Figure 4-100. In this figure the hardware is shown out of position; it is actually mounted to the spar. The flexible lines connecting the actuator to the hydraulic system are shown in Figure 4-102. The arrangement was selected to permit the components to be assembled to the outer blade section in the factory, before shipping. The lines would be connected via flexible hose or conduit at blade joint at 60% of the span in the field, after the blade sections were assembled. The flexible lines at each actuator hinge point accommodate differential expansions between the blade and piping. Access to the hardware for service and maintenance is obtained by parking the ailerons in the -90° position in which the entire aft surface of the blade spar and the aileron hardware mounted to the spar are exposed.

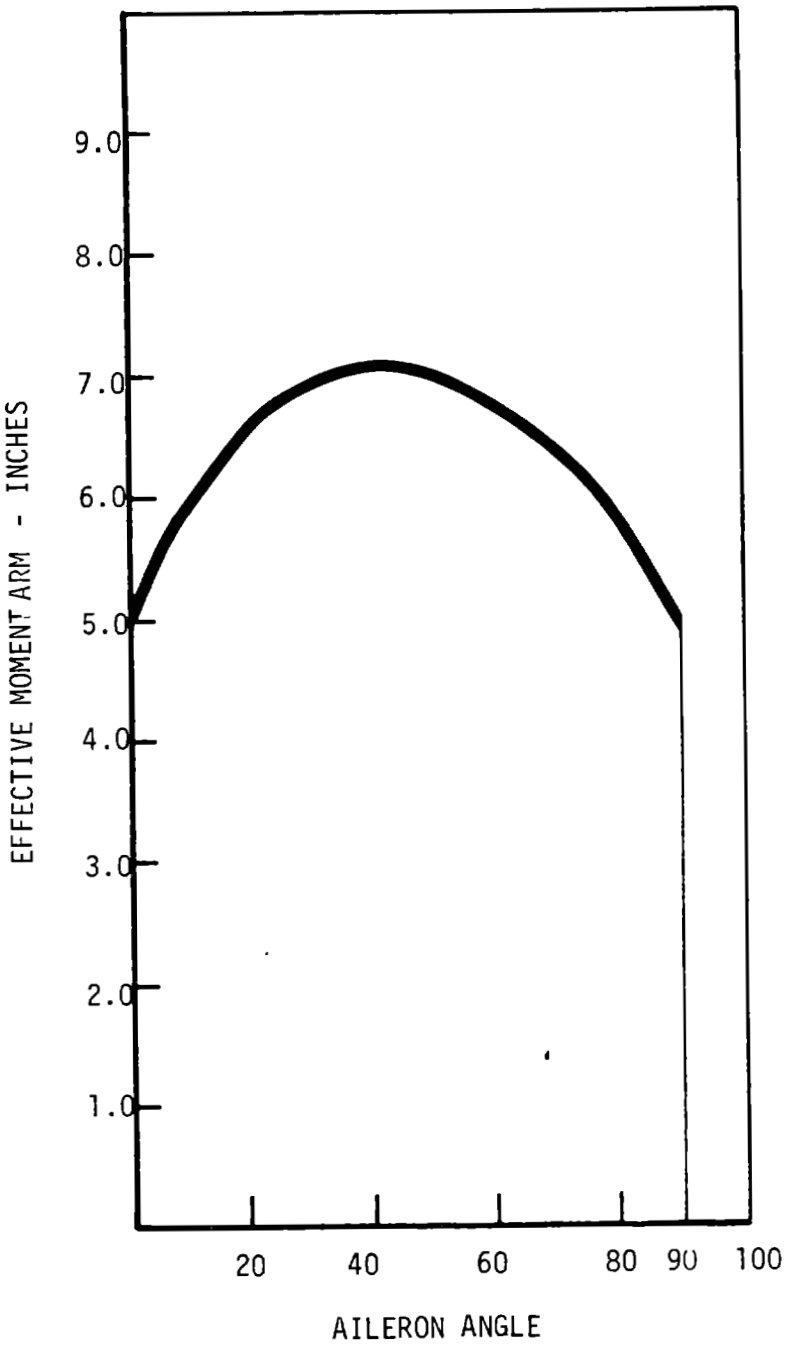

Figure 4-101. Actuator Effective Moment Arm

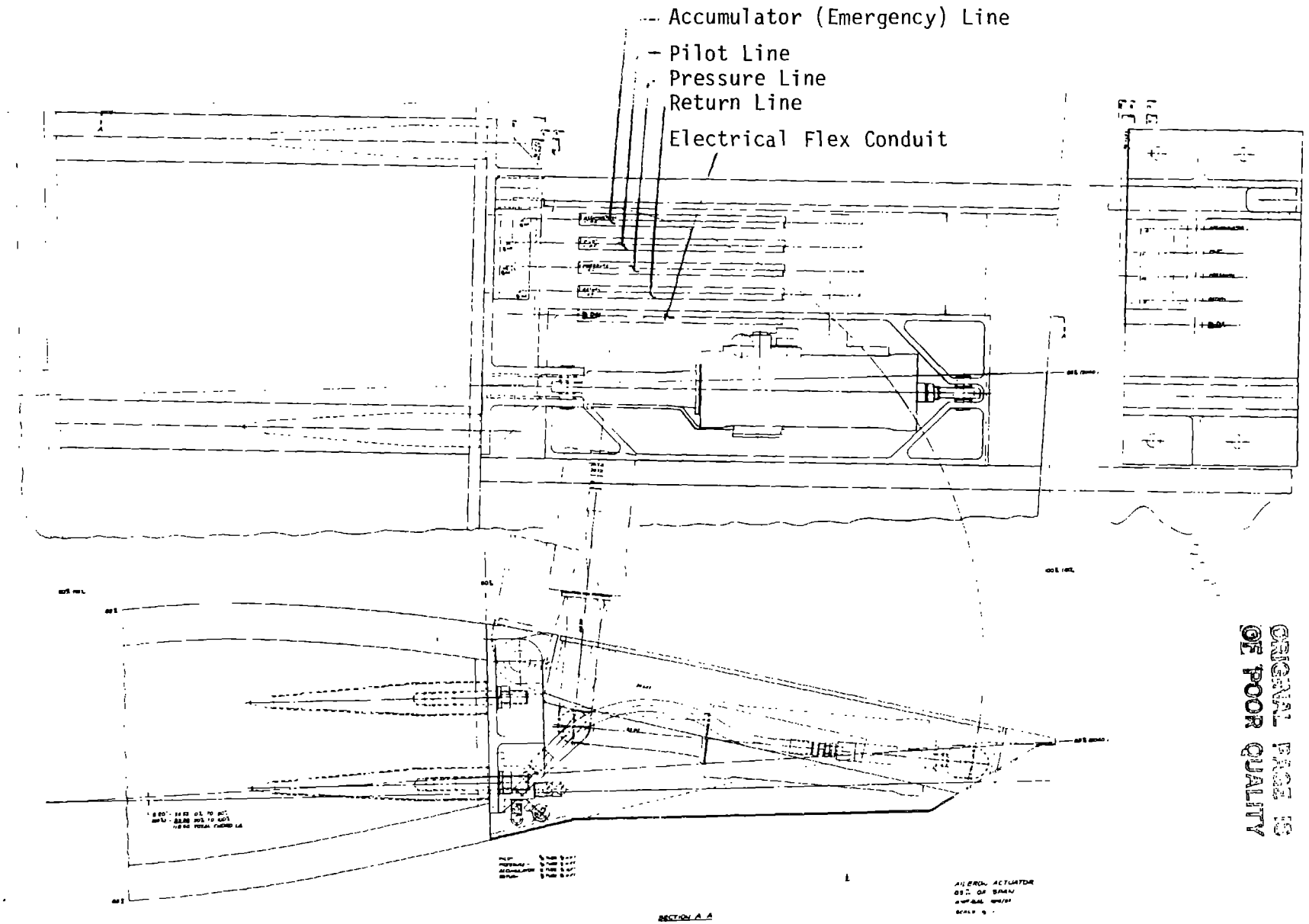

Figure 4-102. Aileron Hydraulic Flexible Line Arrangement

4.4.2 AILERON STRUCTURAL ANALYSIS

A typical aircraft wing construction was evaluated for the ailerons. It consisted of an aluminum skin, 0.1 in. thick, supported by a series of ribs and longitudinal stiffeners running through the ribs. This approach led to a preliminary definition of weights and structural complexity. The final design was to be generated by a vendor selected in a competitive technical proposal and bid review. The vendor would be free to use their own design and material system, subject to GE's review and approval.

The preliminary analysis considered stiffness, strength, fatigue strength, buckling stability, and reactions at the fittings to the outer blade, caused by various load cases. Various loads defined by an analysis of the system's dynamics and by the aerodynamic pressure distributions across the chord and span of the ailerons were chosen. Hurricane, overspeed, mean operational and normal operating variable loads were used. The maximum expected stresses, mean stresses and an alternating stress spectrum were calculated.

The material selected for the preliminary analysis was an aluminum alloy, 2024-T6 or T8. The -T3 temper of 2024 could not be used, because it is sensitive to stress corrosion. The properties used are described in MIL-H-5C.

Good torsional stiffness was found. The outboard aileron is the most flexible. Under normal operation its maximum structural angular uncertainty is less than 0.6° for the 99.99th percentile hinge moments.

The important design factors were local skin buckling stability and skin fatigue. Rib spacing of 12 in. and stringer spacing of 10 in. on the center were needed at important locations. Safety factors of 1.5 against buckling and yielding, and a Miner's summation of 1.0, including a fatigue notch factor of 2.0 were used. Because of the high dynamic air pressure, the skin thickness of 0.1 in. must linearly increase to 0.2 in. from 0.6R to 1.0R, to meet these factors of safety. Because there are six ailerons, the skin thickness should increase by 0.02 in. per aileron segment beginning with 0.1 in. at the aileron located at 0.6R. Variable rib and stringer spacing for weight optimization was not pursued in this preliminary analysis.

The analysis showed that the air pressure on the ailerons and bending of the ailerons are severe for the rib and stringer construction. On the compressive skin, the beam-column effect exaggerates the stress caused by air pressure alone. Closely spaced ribs and stringers are necessary to avoid damage.

A vertical shear through the airfoil thickness of 500 lb/ft, and a hinge moment of 1,000 ft-lb/ft of span, were typical load magnitudes. Air pressure on the skin varies with span and load type, between 0.3 and 1.7 psi. With the hinge points about 12 ft. apart, and because of the tapered blade geometry and the greater tangential velocity at the tip, stresses in the outer aileron were severe. Loading during storm or overspeed conditions was even more severe, as discussed in section 7.5 of Volume II.

4.4.3 AILERON TRADES

The aileron trade-offs examined the performance and the function of the aileron design. Aerodynamic considerations determined the required performance of the aileron. These considerations were discussed more fully in section 4.2.2. The performance requirements for an aerodynamic control surface were satisfied by a plain aileron extending from 60% of the span to 99% of span and from 60% of the chord to the trailing edge. This control surface formed a trapazoid, approximately 78 ft. long, 6 ft. wide inboard, and 2.5 ft. wide outboard. When deployed -90° toward the airfoil low pressure surface about the 60% chord axis, this control surface provided enough retarding torque to control the rotor. Various designs were evaluated to determine how the aileron design could be implemented in a mechanical system. The type and number of actuators, the actuator locations, the number of aileron structural sections and the number of segments in each section were evaluated.

Actuator

When ailerons replaced partial span control as the rotor torque control system, the actuation mechanisms had to be redesigned. When new torque level and frequency response requirements changed, a number of configurations were evaluated.

The main trade-off studies concerned linear and rotary electrical vs. linear and rotary hydraulic systems. The simplicity of the electrical systems was attractive. However, there was a large difference in the actuation rates of normal and emergency feather operation, for both linear and rotary actuators. The difference was so great that an electrical system selected for normal operation would not meet emergency feather requirements, and a system selected for emergency feathering would be inefficient in normal operation. The large gear reduction required to reduce the driving motor rates (1200 - 1800 rpm) to the aileron rates (.5 to 5 rpm) was another problem. Both electrical systems required a reducing gear (for rotary drive) or jack screw (for a linear actuator), both of which require maintenance. A review of the applicable industries, including aircraft design, indicated that hydraulic actuation is used when variable actuation rates are required.

One system design was based on an electric motor drive that allowed high emergency feather rates. This design involved a spring loaded clutch and motor brake. In normal operation the motor drove the ailerons, via a clutch. When emergency feathering was required, the brake was applied to the electric motor, and the clutch was released to allow the aileron to feather by means of a helper spring. The design and cost of this system was evaluated, but it was not cost effective and too complex for reliable operation.

A similar trade-off study evaluated linear and rotary hydraulic actuators. The rotary units were ruled out, because their rotor and seal construction made them prone to failure in the high g environment.

The linear hydraulic actuator was selected as the aileron actuation mechanism.

Aileron Structure

Aerodynamic considerations determined the configuration of the control surface. Structural considerations and the actuator's capacity determined the aileron segmentation, the interface between the ailerons and the main blade, and the number of sections driven by an each actuator. Several aileron arrangements, shown in Figure 4-103, were evaluated before the multiple actuator, split section baseline was selected.

Arrangements "a" through "f", shown in Figure 4-103, depict three or four actuators. A four-actuator arrangement was selected initially because of its capacity versus size characteristics, and to a lesser extent, because of aileron versus blade structural deflection concerns. The actuator vendors considered 50,000 lbs. to be approximately the largest capacity that would be feasible with a 10-in. stroke. This limit accommodated the high g environment on the blade and the resulting side load on the actuator. The side loads, and the axial loads on the actuator were a major influence on the design for the actuator structure and bearings. A favorable capacity and actuator weight relation was felt to exist at approximately the 50,000 lb. and 10-in. stroke size. This actuator size was within the capabilities of typical aerospace vendors. With these actuator parameters, an integration of the aileron distributed hinge line moment loads, as shown in Figure 4-104. would have

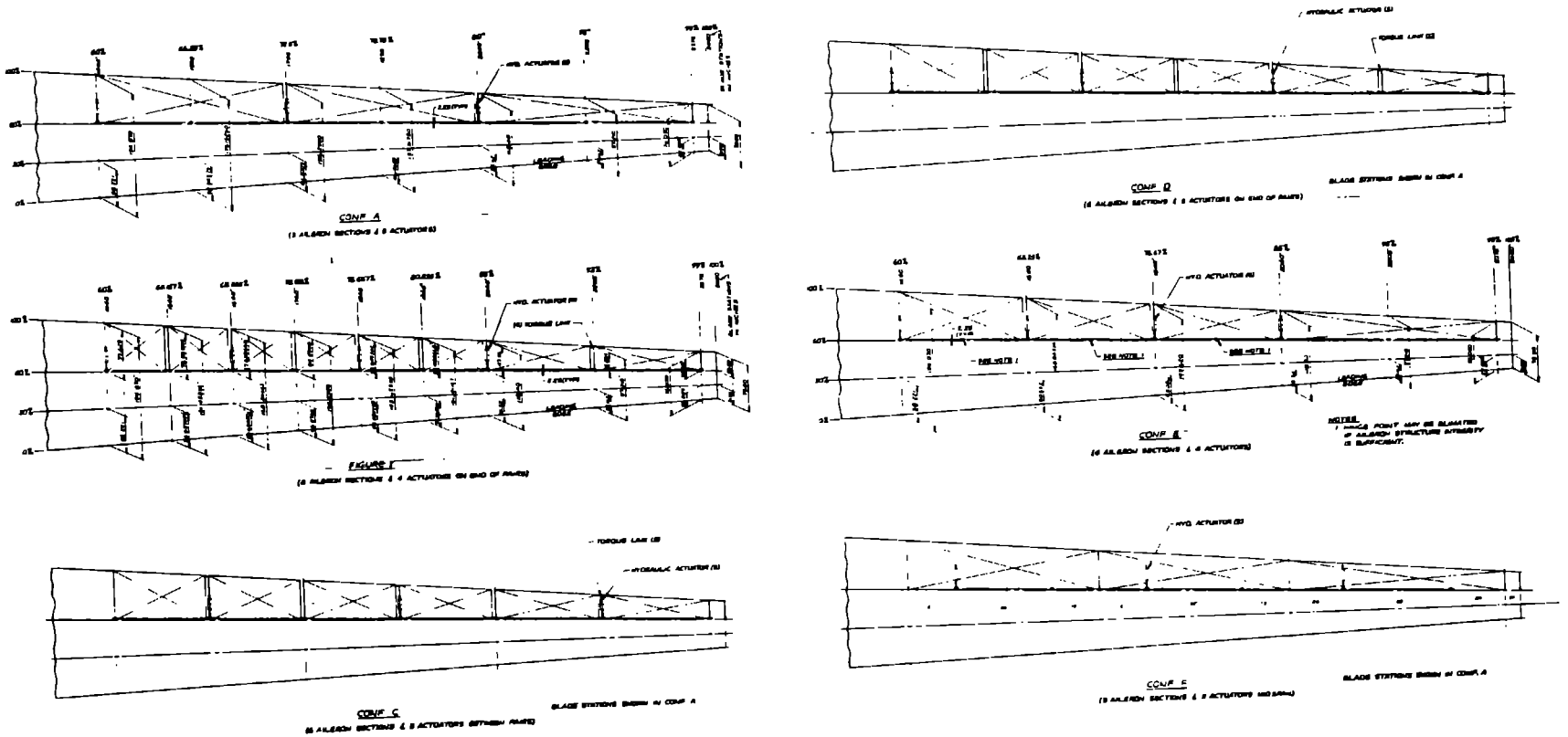

Figure 4-103. Aileron Geometry

required four actuators and ailerons per blade. This configuration is shown in arrangements b and e of Figure 4-103. There were cost and reliability incentives to reduce the number of actuators per blade from four to three. A force limiting actuator concept was developed to achieve this goal while maintaining a maximum actuator force of 50,000 lbs. The initial load requirements, shown in Figure 4-104, were based on full deployment of the aileron for rotor shutdown. Normal aerodynamic operating and control loads and aileron deflection angles were significantly less. Further analysis determined that a full deployment of the aileron surface at high rotor speed was not necessary for rotor shutdown. An angle of only -39° and moment of 20,000 ft.-lbs. would be required to start shutdown or autorotation. This requirement assumed one non-functional outboard aileron and an initial 50% overspeed of 25 rpm in a 79 mph wind. Additional margin loads for inertia, friction, and wind gusts were included to arrive at the 50,000 lb. requirement for shutdown. The actuator exerts enough force to deploy the ailerons to start rotor shutdown. The actuator increases the aileron angle as the rotor slows and the aerodynamic loads decrease, eventually reaching -90°. This control concept permitted aileron systems with three, 50,000 lb. actuators, instead of four.

The designs using three aileron sections, shown in a, c, d, and f, of Figure 4-103, were analyzed further to determine their sensitivity to differential deflections and thermal expansion. The load distribution, especially at the main blade wood interface, was the parameter that received the most attention. The tapered steel stud developed earlier was selected as the interface. The steel stud was developed extensively to qualify as a high strength interface fastener to the laminated wood blade (reported in section 4.3.1.5.1). In all aileron arrangements the actuator was located at a hinge point to minimize load transfer through the studs and the structure. Hinge moment loads and accumulated aerodynamic axial and shear loads are transmitted to the wood interface. Actuator forces are reacted within the closed-loop consisting of the hinge bracket aileron rib and actuator.

Arrangement "a" of Figure 4-103, consisted of three aileron sections, each driven on the inboard end by an actuator. The spanwise location of the

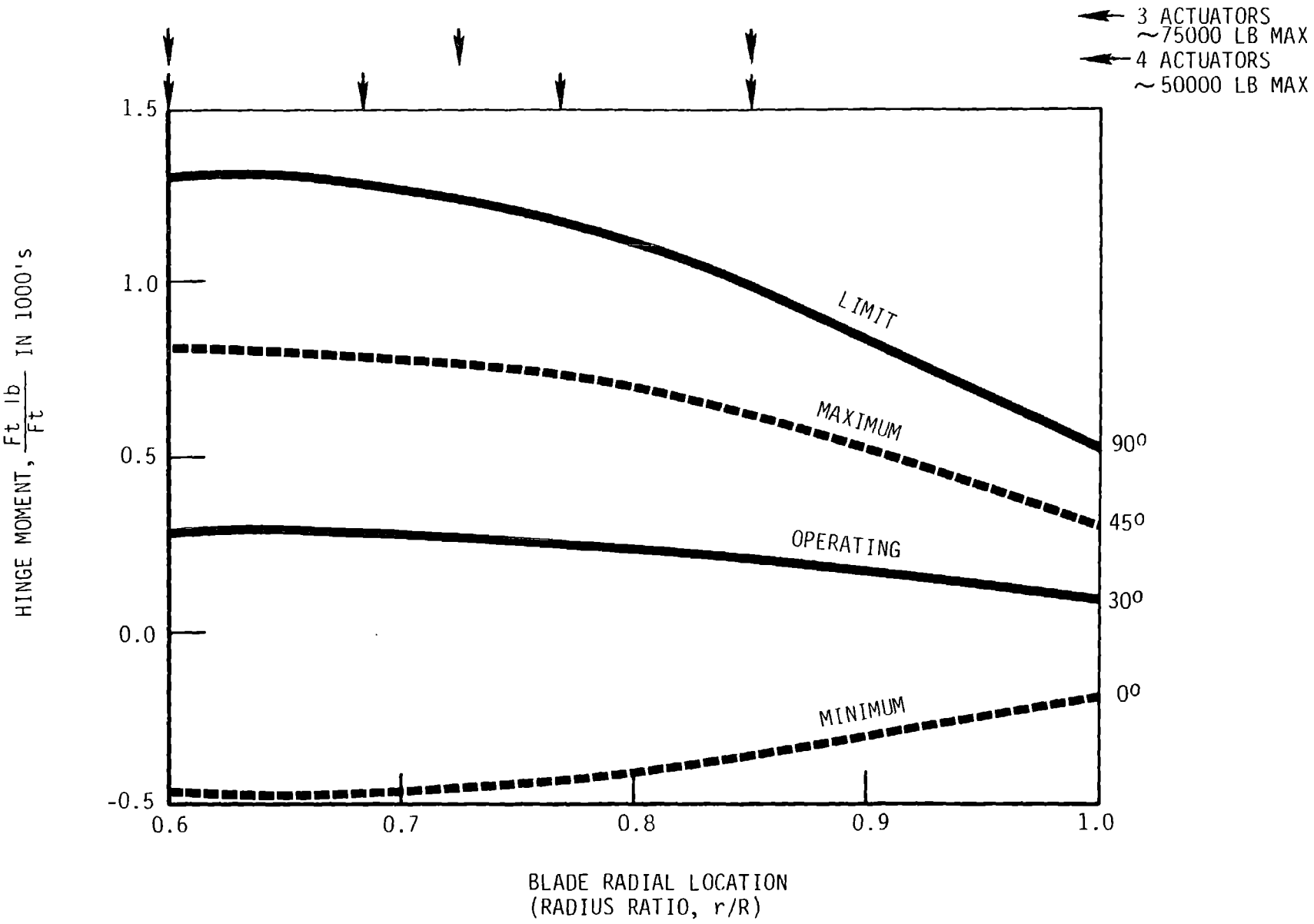

Figure 4-104. Aileron Design Hinge Moments - Actuator Location

actuators was selected to equalize the force on each actuator. The identical actuator is used at each location. This arrangement minimized development, qualification costs and scheduling difficulties. The operational spares inventory and potential maintenance costs were also reduced.

The three hinge-point interface between each aileron section and the blade became a problem. The outboard section is 28 ft. long and the inner sections are each 25 ft. long. Each section, required at least three hinge-point structural supports. Three bearings along an axis would be subject to high loads exerted by differential deflections or expansions of the blade and ailerons. A floating hinge for the outboard hinge was considered to alleviate this problem. This hinge, shown in Figure 4-105, provides only one degree of restraint by inserting a floating link between the two hinge brackets. If the link is installed with its axis perpendicular to the plane of the blade, the link restrains the aileron in the flapwise direction, but permits motion in the chordwise direction. The chordwise freedom between the aileron structure and the blade would accommodate some flapwise motion between the structures. The arc described by the link pivoting motion allows flapwise aileron motion.

The floating hinge reduced, but did not eliminate the load exerted by differential deflections during aileron deployment. The single degree of restraint imposed by the floating hinge caused the outer portion of each aileron structure to cantilever at the inner two bearing points. Because of this feature, the single piece, three bearing, aileron structural section was not considered any further.

The approach which eventually was developed into the baseline configuration was to segment the aileron sections as shown in "d" of Figure 4-103. The single structural section, shown in "a", was divided into two segments at the middle hinge point. Bearings at the ends of the segments connect the segment to the main blade. This simple support accommodated the blade-aileron differential deflections. The outboard, or slave segment, was driven by the inner or master segment through a torque link connection. The master segment was controlled by the actuator located at the inboard end of each section. The major reason for locating the actuator at the inboard end, rather than at the midpoint of each section as shown in "c", of Figure 4-103, was to minimize

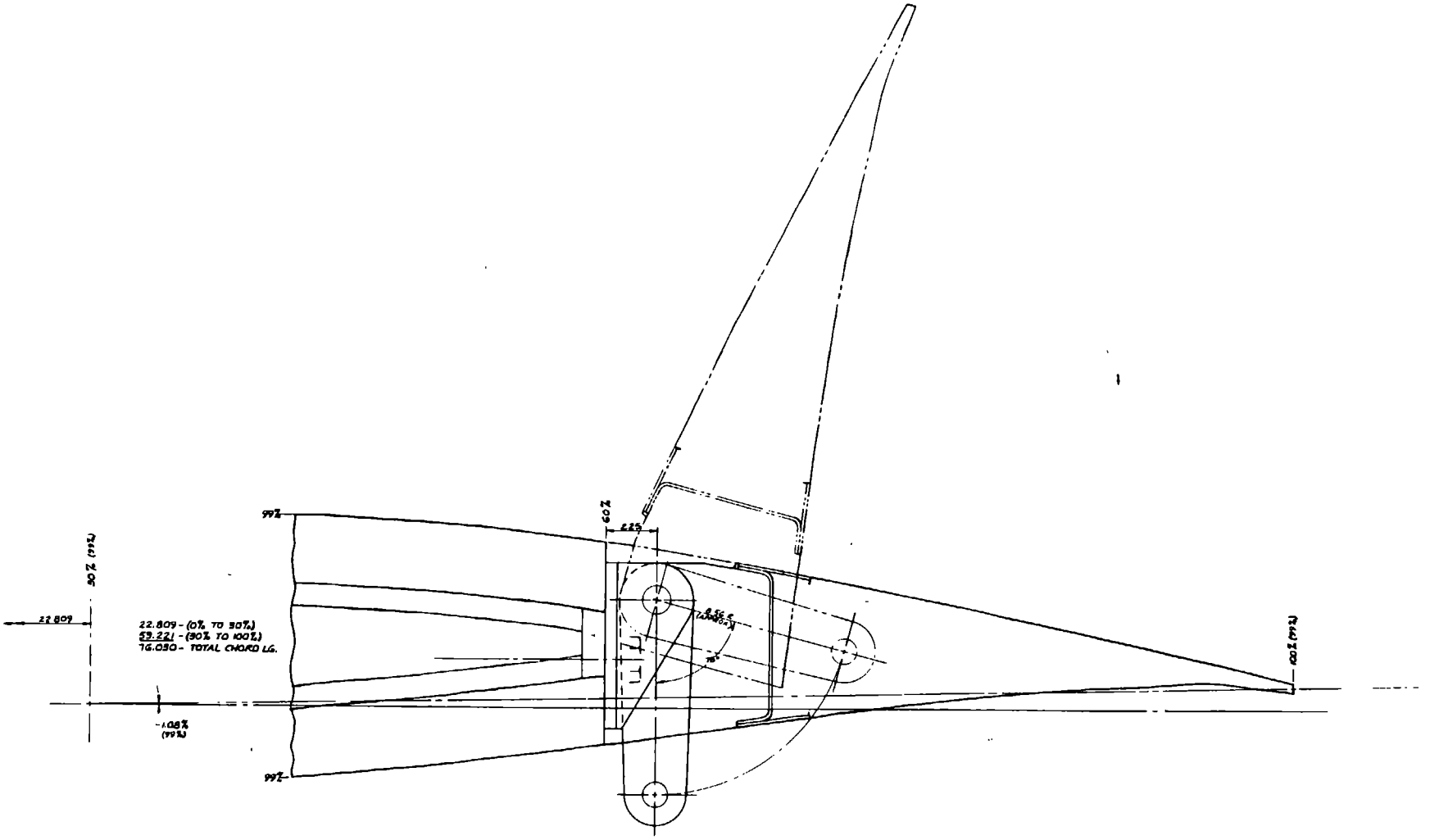

Figure 4-105. Floating Link

the g loads. The centrifugal acceleration on the outer section during normal operation is 18 g's at 92% of the span, but only 16.5 g's at 85% of the span. In addition, the space available for the actuator was significantly smaller at 92% of the span, so the actuator would have protruded outside the airfoil surface.

Hinge-Actuator Assemblies

Many hinge and actuator designs were evaluated. Three of them are illustrated in Figures 4-106, 4-107 and 4-108. One design used a rotary actuator to drive a pair of aileron surfaces through a parallel crank four bar linkage assembly, as shown in Figure 4-106. The assembly consisted of a crank driven by the rotary actuator via the coupler link. The follower crank was part of the hinge bracket of the aileron structure. This mechanism would accommodate aileron misalignment and deflection because it had self-aligning bearings at the aileron hinge points and the coupling ends. The many bearings and connections, however, caused strong concern. Bearing life, lubrication and assembly backlash were considered to be major detriments in this design. The design was abandoned because of these problems.

The other two designs illustrated in Figures 4-107 and 4-108 use a linear hydraulic actuator and deploy ailerons with a three-bar, slider crank, mechanical assembly. Several requirements were imposed on the mechanical assembly. The interface between the hinge assembly and the 60% blade spar should minimize violation of the spar's integrity. Protrusions beyond the airfoil surface should be minimized. Enough space for the hydraulic and electrical components should be available. The actuator rod should be extended only when the ailerons are deployed, to minimize the deterioration of the actuator rod caused by the environment.

The design shown in Figure 4-107 consists of a hinge bracket and structural support, extending from the 60% spar to the blade trailing edge. The cylinder end of the actuator is mounted at the trailing edge of the bracket and the cylinder body follows the low pressure airfoil surface. The rod end of the cylinder is attached to the aileron at the aileron hinge bracket. The bracket is the crank arm of the slider crank mechanism. The cylinder rod extends

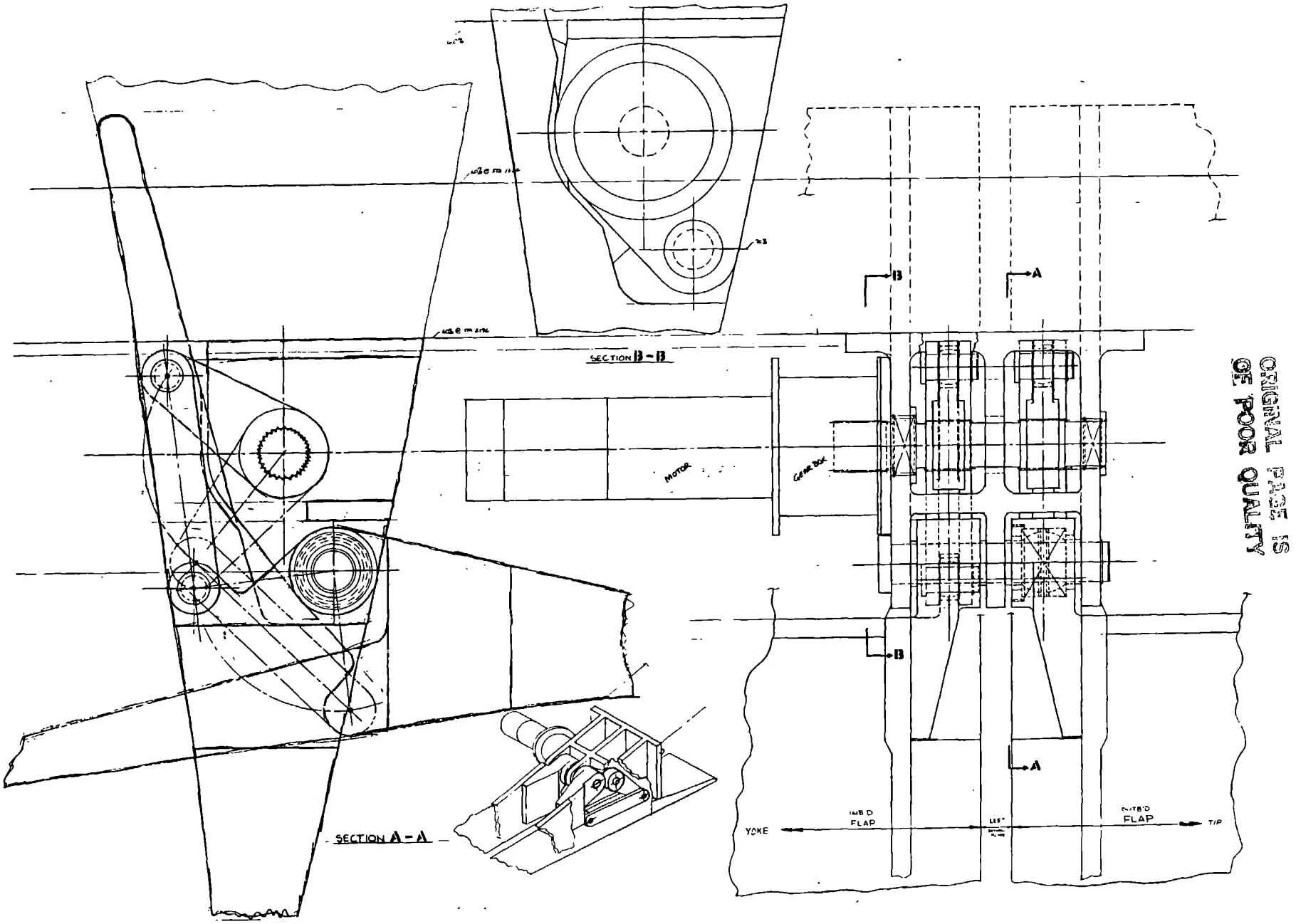

Figure 4-106. Rotary Actuator

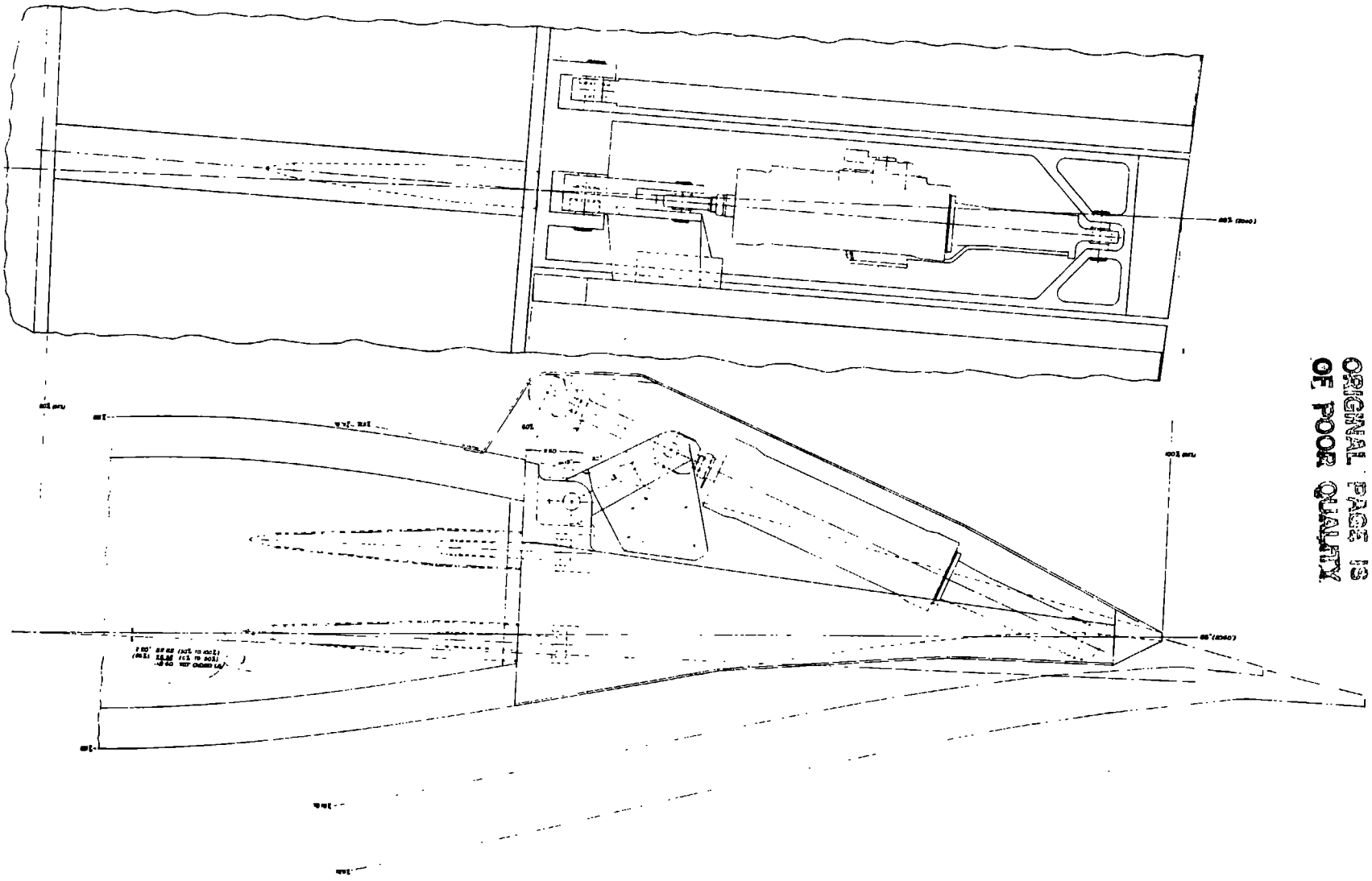

Figure 4-107. Hydraulic Actuator

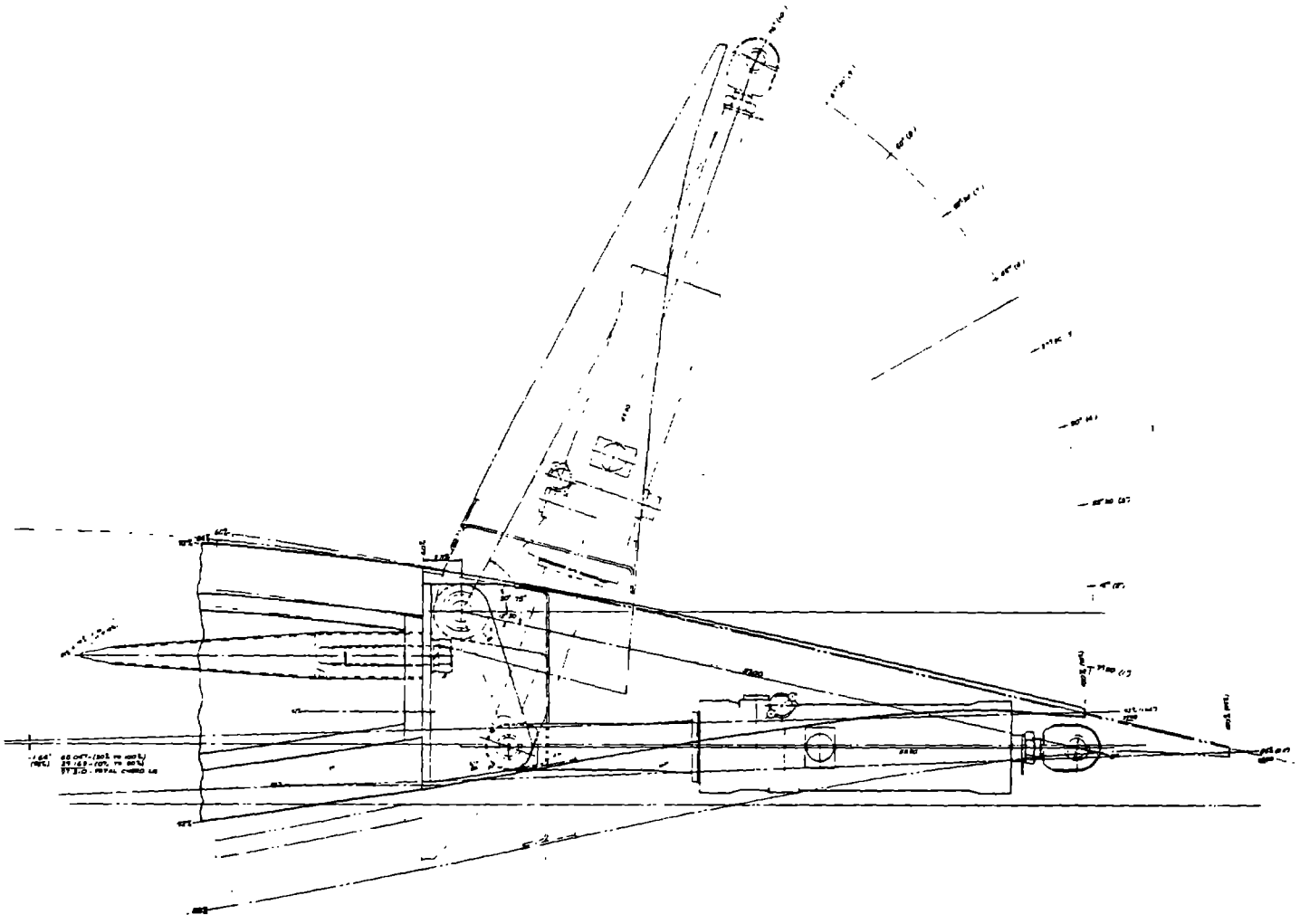

Figure 4-108. Hydraulic Actuator (Preferred Concept)

along the aileron surface hinge axis to deploy the aileron. The undesirable aspects of this design included the cantilevered structure supporting the actuator, restricted access to the actuator and other components and the extensive violation of the airfoil upper surface (the low pressure surface). The main advantage of the concept is the small arc, about 5°, that the actuator traveled when the ailerons are deployed. This deflection can be readily accommodated with hydraulic and electrical flex lines.

The cylinder end of the actuator was attached to the hinge bracket near the 60% spar for the preferred concept shown in Figure 4-108. The rod end was attached to the aileron near the trailing edge. This design minimized protrusions on the airfoil profile and located the actuator below the hinge axis. The aileron hinge bracket was structurally more efficient, because it resisted the actuator loads without restricting access to the actuator. The actuator travelled 90° as it extended to deploy the ailerons, and this caused some concern. The travel required significant flexibility in the hydraulic and electrical lines to the actuator. Discussion with vendors and further design alleviated this concern, so this design was selected as the baseline.

4.4.4 AILERON STRUCTURAL DESIGN

The structural design requirements for the aileron were compiled and a preliminary design was created. The aileron structure was analyzed, to quantify requirements and to provide a baseline for the evaluation of vendor's proposals. The preliminary design concentrated on a conventional aileron design, to provide a baseline. The final selection would have been based on responses to a formal request for quotes from vendors specializing in structural composite materials and conventional metallic airframe construction. The structural design described in the following paragraphs was completed in enough detail to show that the design requirements could be met.

Structures

The aileron configuration is shown on Figure 4-109. The structural design consists of a conventional riveted airframe fabrication of 2024-T3 aluminum. A single spar is located approximately 6 in. aft of 60% of the chord, and ribs are spaced on 12 in. centers to form the internal structure for the skins, which are .10 in. thick. Longitudinal stiffeners prevent the skin on the outer aileron segments from buckling. The spars and ribs are .10 in. thick, with appropriate lightening holes to reduce weight.

The portion of the aileron forward of its spar forms a U-shaped region aft of the 0.6C blade spar for hydraulic and electrical components. These components are mounted to the blade spar and are fully exposed with the ailerons deployed. A sealing system between the aileron segments and the main blade to enhances aerodynamic performance, especially when the aileron is not deployed. The logical location for such a seal is the interface region near the hinge axis at the low pressure surface of the aileron and main blade. The seal would be made of elastomeric material to accommodate differential deflection between the aileron structure and main blade and the aileron rotation.

The end rib configuration of the aileron structures varies to suit the particular hinge interface. The outermost end rib of an aileron section (as in Station 1740, 2040, or 2376) consists of an extended rib structure containing the radial bearing. Only chordwise and flapwise shear loads are directed at this bearing. The bearing is free to move in the spanwise direction to compensate for load deflections and differential thermal expansions between the blade and ailerons. All bearings are spherical, self-aligning, plain bearings with no maintenance requirements. This type of bearing permits angular misalignment of the inner and outer race and uses Teflon PTFE, or similar materials, for low friction sliding surfaces rather than conventional rolling elements and grease.

The structural end ribs at the hinge location between aileron segment pairs are interfaced by a pair of angular contact plain bearings. The pair of bearings provides restraint to the aileron structures in the radial direction; in centrifugal acceleration these ribs also absorb some of the chordwise and flapwise load. The inner races of the pair of bearings are fixed along the axis of the blade hinge bracket via thrust spacers around the hinge pin. The outer bearing races are assembled into the aileron rib hinge bracket to trap the inner bearing races and thus restrain the aileron segments. This segment end rib must also transfer hinge moment loads to the adjacent end rib through torque links. The torque link is a short connecting rod with spherical self-aligning bearings that are pinned to each segment end rib. This torque link compensates for aileron deflections with only minor relative alignment changes between segments. The preliminary analysis of the angular contact bearings (45 mm bore) indicated that they would last about 25 years. A controlled environment is very important for this long service. Seals and a grease packing to keep moisture and contaminants from the bearings are specified for all bearings.

The inboard segment mates with a separate structure at the actuator hinge locations. This structure is the crank of the slider-crank 3-bar mechanism. This crank structure is the primary load path for actuator forces of up to 50,000 lbs. It transfers the hinge moment to the aileron segments. The structure is formed by the low pressure surface and two parallel flanges that straddle the actuator, made from .5 in. thick 2024T3 aluminum. This U-shaped cross-section is structurally necked down at both ends to contain the hinge bearing at one end and the actuator rod end pin at the other. The hinge bearings are plain radial bearings that permit axial and angular alignment of the aileron segment with the blade. The life of this bearing (45 mm bore) was estimated to exceed 30 years.

The aluminum baseline structure had several advantages over others under consideration. The affects of a coastal environment on this material are well known. The conductive skin protects against lightning. Material strengths, both static and fatigue, are well documented. The development of a dissimilar structural material interface was not required. The preliminary aileron weight estimate is an acceptable 3,000 lbs., as shown in Table 4-45.

Several structural requirements have to be met during the final design phase, but they should be attainable. The control dynamic analysis established torsional stiffness requirements such that structural angular deflection must be less than 0.5° from the section inboard end to the outboard end under design hinge moment loads. A minimum torsional resonant frequency of 45 Hz was also established. These requirements are significant design factors and would have been closely watched when the vendor's proposals were reviewed and during the final design.

Hinge Brackets

The blade hinge brackets provide the mechanical interface between the 60% spar and the aileron segments. Two types of brackets are used, with some dimensional variations. The brackets are made of machined 2024 or type 7075 aluminum. The hinge brackets at Stations 1590, 1890 and 2208 must support

aileron aerodynamic shear loads and aileron centrifugal loads. The actuatorhinge brackets at stations 1440, 1740 and 2040 must support aileron aerodynamic shear loads and the hinge moment reaction loads. The outermost hinge bracket at Station 2376 supports only aileron aerodynamic shear loads. The incorporation of the Station 2376 hinge point into a combination hinge, blade tip and blade balance weight assembly was planned. The hinge brackets are attached through four wood studs to distribute the load into ribs in the blade. (See Section 4.3.1.5.1.) The location of the studs and the configuration of the brackets was varied at each location to accommodate geometry of the blade.

Table 4-45 Estimated Weights

	Detail Weights (lbs.)	Number Required	Subsystem Weight (lbs.)
AILERON SUBSYSTEM			(9,760)
Aileron Set			
(Including Fitting Aileron Side)	3,000	2	
Actuator	100	8	
Actuator/Hinge Fitting (Blade Side)	140	8	
Blade Mounted Accumulators	60	8	
Attachment Studs	25	32	
Hydraulic Flex Lines and Fittings	35	16	

4.4.5 ACTUATOR

The ailerons comprise three sections; the first section starts at 60% of the span, the second section at 72.5% and the third section at 85%, as illustrated in Figure 4-109. Each section is powered by its own valve and actuator module, which also includes a 2.5 gallon accumulator that contains enough hydraulic fluid to deploy the aileron from the power to the feather position. Each actuator has an electro-hydraulic servo-valve shuttle valve LVDT assembly, a latching assembly, a thermal relief valve and an electronic controller (servo-valve driver) built integrally into its housing. All of these components and associated fluid passages are contained in a single manifold assembly, for increased reliability.

The maximum hinge moment on each aileron panel was 20,000 ft.-lb. To account for inertia and friction, 22,000 ft.-lb. was chosen as the design moment. To meet this requirement at 2000 psi differential pressure with respect to the 3000 psi supply pressure and over a moment arm of 7 in., the actuator has a bore of 5.5 in. and a rod diameter of 2.5 in. The geometry of the aileron and blade requires an actuator stroke of 10 in. to move the aileron 90°.

Tests performed on the partial span control actuator showed that single-ended designs are subject to rod seal failure. This failure is caused by excess loads on rod end bearings in high g environments, as was discussed in section 8.3.1 in Vol II. For this reason, the aileron actuator was designed as a double-ended unit, to eliminate the effect of the moment load at the rod end bearings. The unit is suspended on self-aligning bearings between the aileron and the stationary blade. The blind end of the actuator is connected to the stationary blade, and the rod end to the aileron. The total weight of the actuator and valve assembly is less than 100 lbs.

The servo-valve is mounted with its spool transverse to the actuator axis, parallel to the direction of rotation. In this position the g-loads on the spool, caused by centrifugal force, are minimized, as shown in Figure 4-110. The housing, piston assembly and heads are made of 15-5 PH CRES forgings, to minimize the weight.

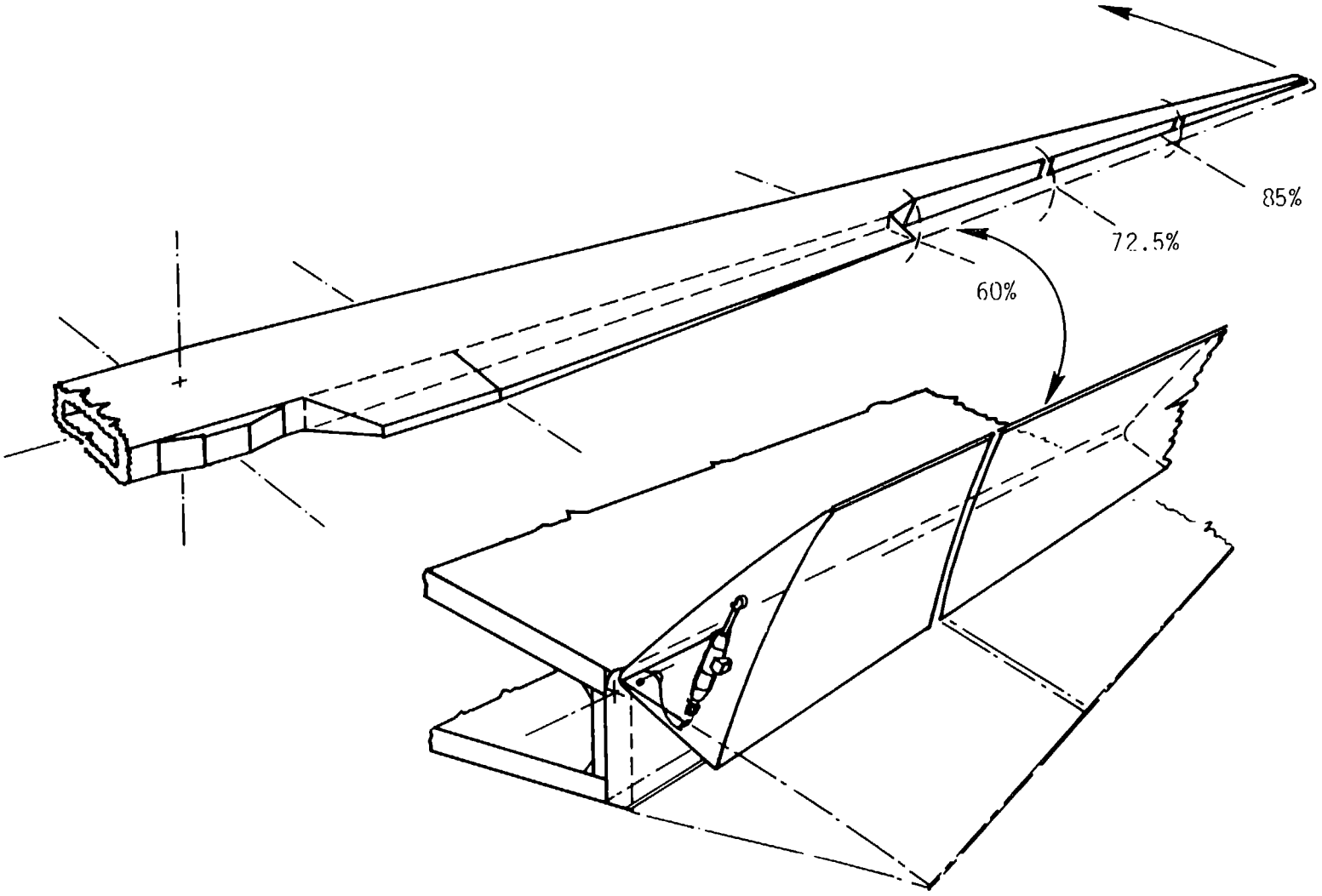

Figure 4-109. Aileron Arrangement

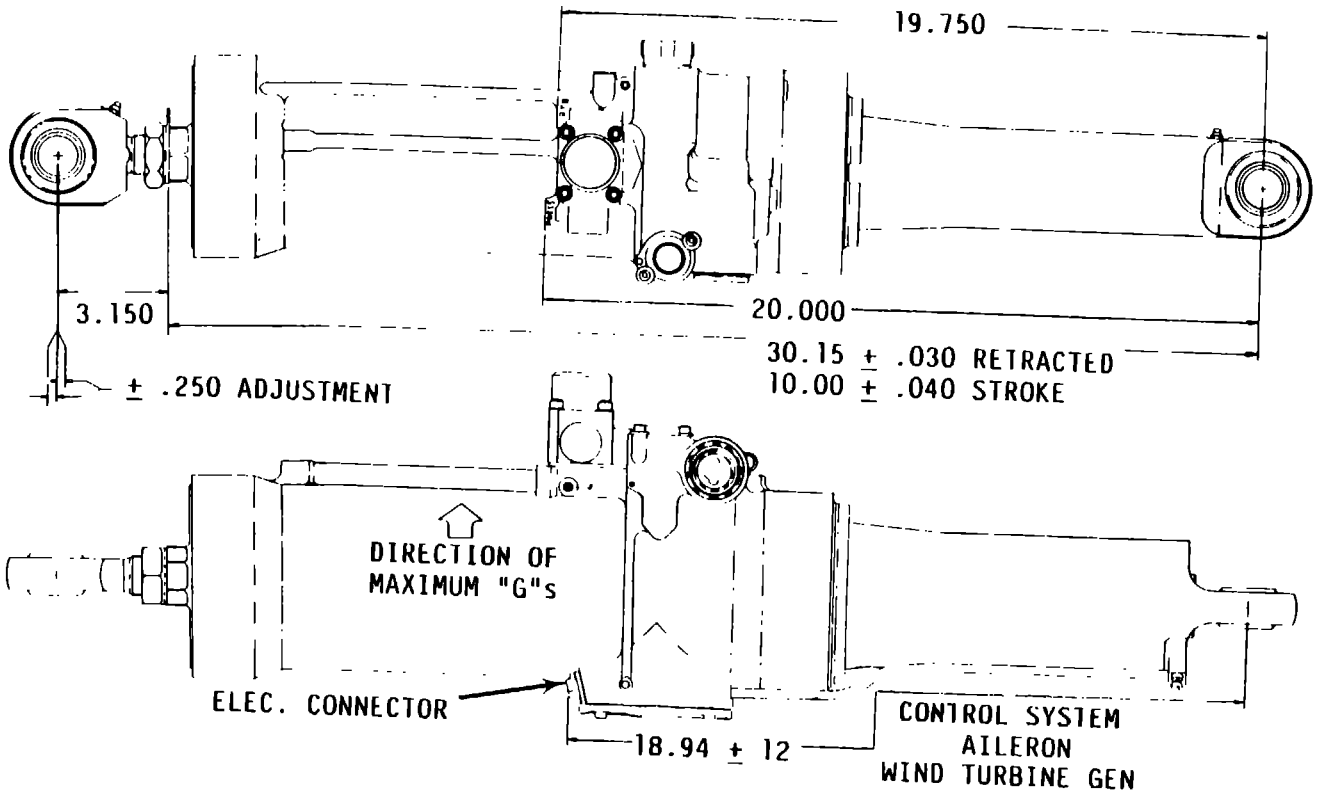

Figure 4-110. Aileron Actuator With Servovalve And Electronics

4.5 YOKE SUBSYSTEM

4.5.1 GENERAL DESCRIPTION

4.5.1.1 Subsystem Components

The yoke subsystem supports the blade against all gravitational and dynamic forces, provides rotational and teeter motion, and transmits the rotor torque to the low speed drivetrain. The yoke, two teeter bearing assemblies and four teeter restrictors comprise the yoke subsystem.

The yoke is a welded fabrication, made of steel plates of various thicknesses, forming a U-shaped structure around a large forged tube, as shown in Figure 4-111. The design consists of this central tube, onto which plates are welded to form the U-shaped structure with various interior bays. The central tube rotates on two main rotor bearings spaced along a stationary spindle shaft. All loads applied by the rotor, except torque, are transferred from the central yoke tube, through the main rotor bearings, into the spindle. The torque loads are transmitted from the forward face of the yoke to the low speed shaft through a gear coupling. The yoke fits around the blade at the center of rotation and is attached to it by teeter bearing assemblies, one in each "ear" of the yoke, as shown in Figure 4-112. The transfer of the loads from the blade to the yoke takes place through the two teeter bearing assemblies. Each assembly contains one radial and one thrust bearing. Both bearings must be preloaded in compression, so there is a constant compressive stress on the front and inside plates of the yoke, and a tensile stress on the back and outside plates. The four teeter restrictors also connect the rotor and yoke. Each restrictor consists of a link that is attached on one end to the blade, and engaged on the other end by two hydraulic caliper brakes mounted to the yoke. These brakes are activated to restrict teeter motion during startup and shutdown. The four restrictors are placed symmetrically about the blade, as shown in Figure 4-112.

4.5.1.2 Constraints on the Yoke Design

The yoke design was significantly influenced by the external structure that attached the blade to the yoke, and by the size of the blade. The smallest dimensions of the U-shaped structure were determined by the required cross-sectional dimensions of the blade at the center of rotation. In the spindle support area, the maximum yoke depth, 80 in., was fixed by the rail shipping envelope, while the center tube had to be large enough to accommodate the

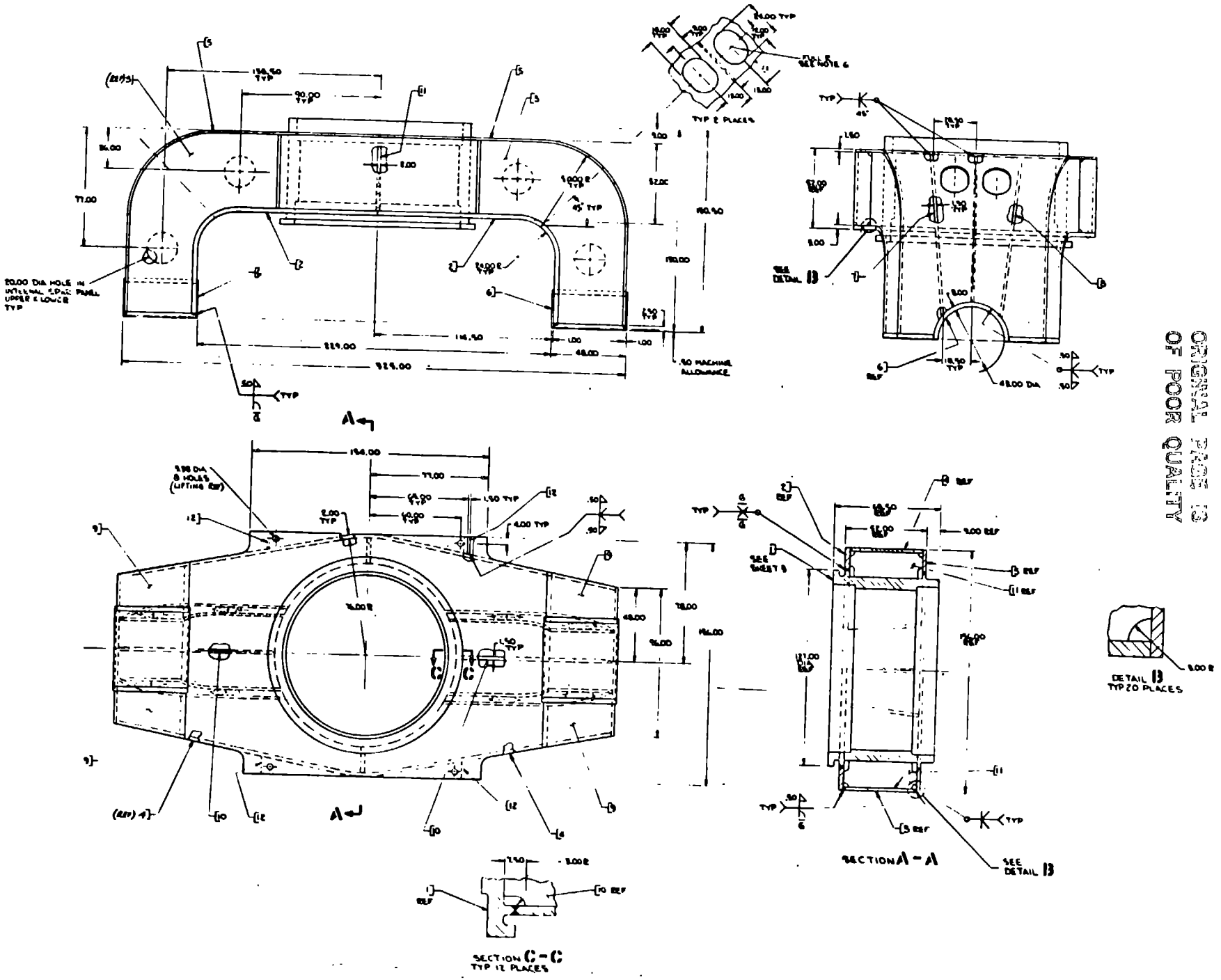

Figure 4-111. Yoke Weldment Drawing

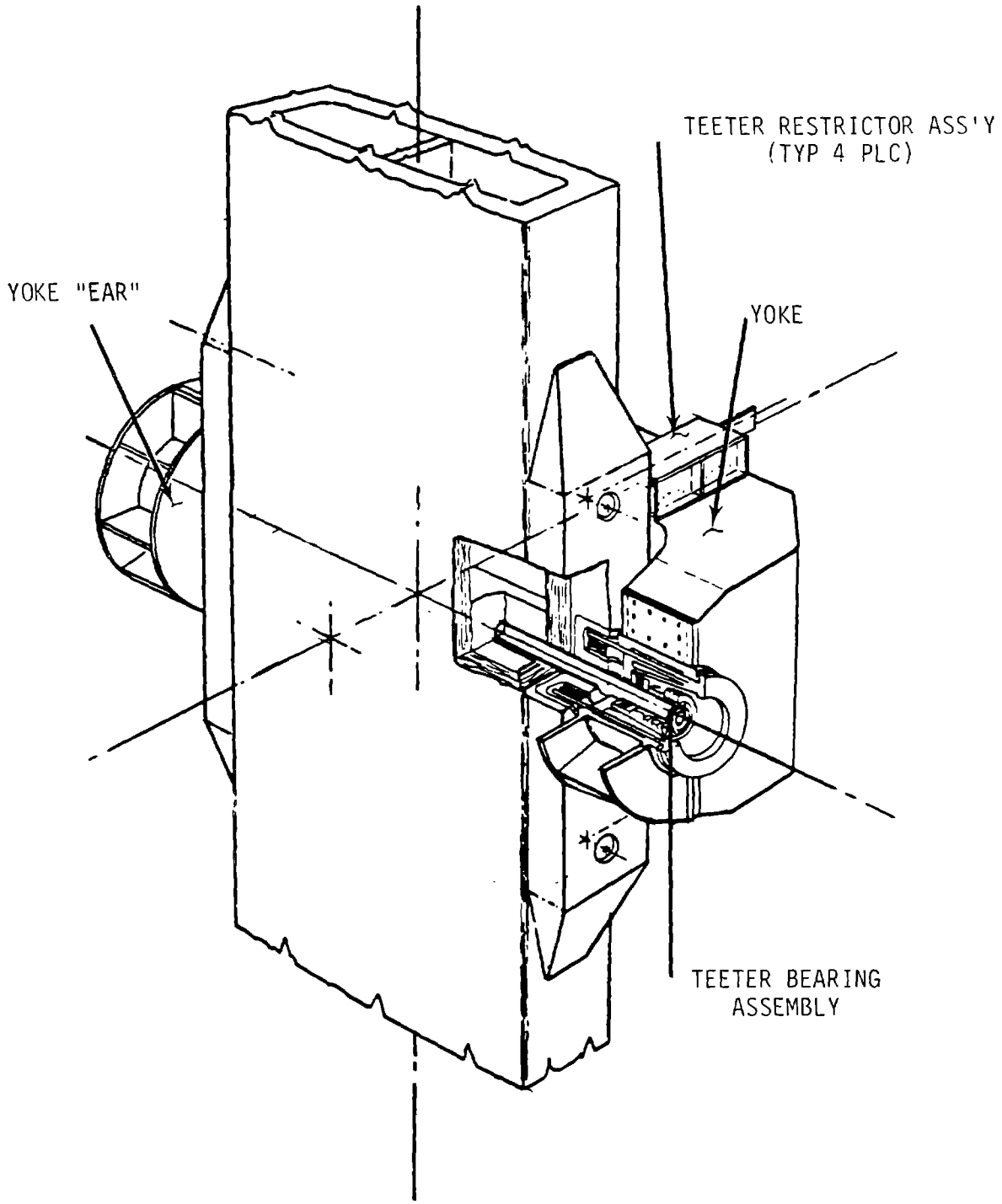

Figure 4-112 Yoke and Rotor Interface

outer race of the main rotor bearings. The large distances between the teeter bearings and rotor bearings, and the reaction loads, created correspondingly high bending and torsional moments that had to be transmitted through the yoke structure. The size of the yoke decreased its structural effectiveness, and required internal members to reinforce the "box", which increased the weight.

4.5.1.3 Yoke Design Concepts

Producibility, materials characteristics, reliability, weight and cost were considered in the yoke design. A study performed by Chicago Bridge and Iron (CBI), under contract to GE, confirmed that the production of the yoke design was feasible. The materials selected were ASTM A508 class 2 for the center bearing tube forging and ASTM A633 Grade C for the plate stock. These steels were to be purchased according to a GE specification, which contains stricter requirements than the standards of the industry. The specification imposes requirements on material quality, to minimize the risk of the material cracking during manufacture and service. A thorough non-destructive inspection plan would be used to be sure that the work complied with the flaw size requirements of GE's specifications. Sections 4.5.2 and 4.5.3 discuss the development, which minimized the weight and cost of the yoke. The baseline design, shown in Figure 4-111, satisfies the design requirements. A more detailed examination would be required to approve the design for construction.

4.5.2 LOADS AND STRESS ANALYSIS

4.5.2.1 Loads

The yoke is loaded by the blade dynamic weight, torque, wind thrust, and teeter pitching moments, all of which fluctuate as the blade and yoke rotate. The blade weight results in an alternating fully-reversing load cycle on the yoke, which makes a complete cycle for each blade revolution. Wind and torque fatigue loads cycle twice per revolution. The nomenclature and coordinate systems used in the analysis are described in Figures 4-113 and 4-114.

Estimates of the loading for all cases were obtained from analyses of the system's dynamics. The critical fatigue design case coincided with the critical limit case. Therefore, the reliability of the structure was effectively determined by the fatigue case loads, shown in Figure 4-114.

PLACE	IDENT
A	TOP PLATE
B	OUTSIDE PLATE
C	INSIDE PLATE
D	FRONT PLATE
E	SPAR PLATE
F	BACK PLATE
G	BULKHEAD PLATE
H	BOTTOM PLATE

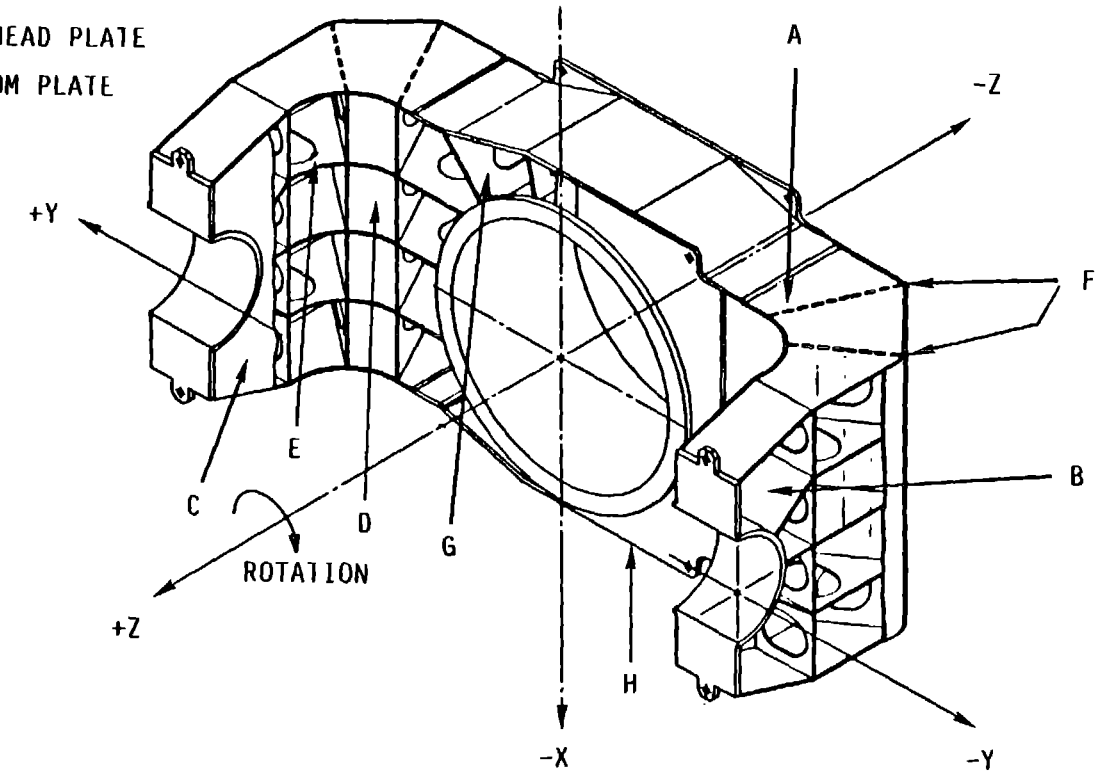

Figure 4-113. Preliminary Finite Element Yoke Model Analysis Summary

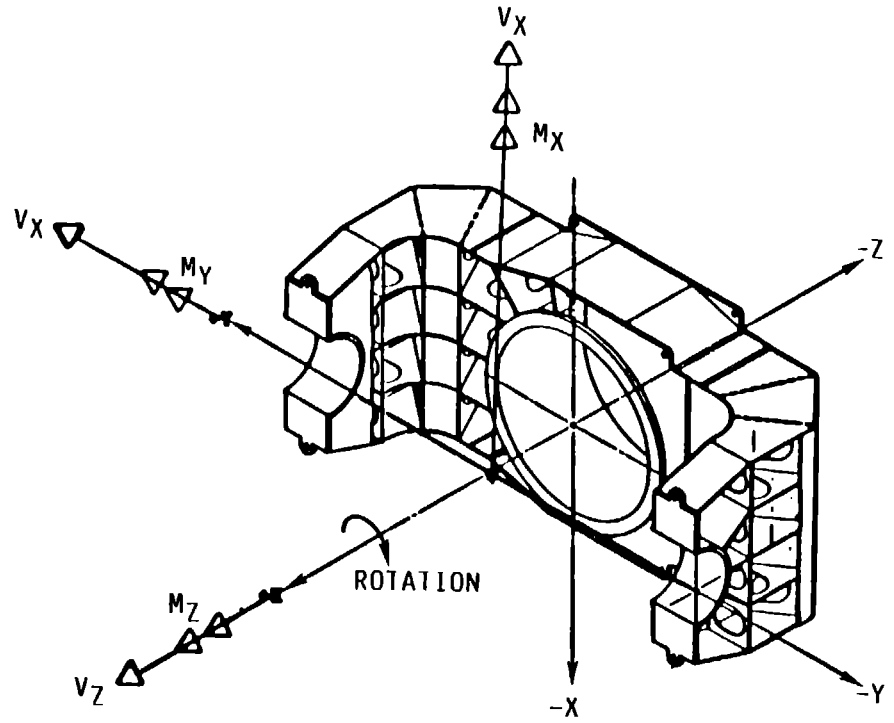

	BLADE VERTICAL	BLADE HORIZONTAL
Vx (Lbs)	$-.708 \times 10^3 \pm .407 \times 10^6$	$-.708 \times 10^3$
Vy (Lbs)	$-.276 \times 10^2$	$-.276 \times 10^2 \pm .449 \times 10^6$
Vz (Lbs)	$-.191 \times 10^6 \pm .110 \times 10^6$	$-.191 \times 10^6 \pm .110 \times 10^6$
Mx (Ft-Lbs)	$.686 \times 10^5 \pm .101 \times 10^7$	$.686 \times 10^5 \pm .101 \times 10^7$
My (Ft-Lbs)	$-.287 \times 10^5 \pm .811 \times 10^5$	$-.287 \times 10^5 \pm .811 \times 10^5$
Mz (Ft-Lbs)	$-.203 \times 10^7 \pm .238 \times 10^7$	$-.203 \times 10^7 \pm .238 \times 10^7$

Figure 4-114. Preliminary Finite Element Yoke Model Fatigue Loading

4.5.2.2 Allowable Stresses

The fatigue design life was 4 x 10^8 cycles of stress in 30 years of operation. The allowable stresses defined in the Structural Design Criteria Volume II, section 9 were developed from a combination of a crack growth threshold approach using fracture mechanics and the American Institute of Steel Construction (AISC) design criteria for welded structures.

The AISC criteria identify allowable stress ranges for various weld categories. The allowable stress range used for the yoke design is the stress level below which fatigue life of more than 2 million cycles is expected. The relationship between the stress range and the fatigue life for an AISC category C weld detail is shown in Figure 4-115. The alternating stress design limit designated by the crack growth threshold method, is more than 9 ksi for this category. For the typical wind turbine generator stress histogram, there could be a few stress cycles greater than the AISC allowable value, but the root mean cube stress for this histogram indicates an acceptable fatigue life. The yoke loading profile follows a narrow stress histogram, however, and the yoke was designed for all stress cycles to fall below the AISC allowable and well below the crack growth threshold. Using this the AISC allowables provides stress intensities with extremely small crack growth rates and satisfies the Structural Design Criteria. As shown in Figure 4-115, however, the yoke fatigue stress that meets the crack growth threshold requirements does not meet the requirements of the root mean cube method. The yoke is the only substructure of the wind turbine generator that requires the use of the crack growth threshold criteria to obtain a practical structure. Further explanation of the design approach can be found in section 9.0 of Volume II.

Use of the crack growth threshold in the design is justified by the requirement of both a non-destructive inspection plan and a fracture mechanics analysis of the growth characteristics of undetected defects. The inspection plan is to reliably find and repair all surface defects greater than 0.1 in. during shop inspections of critical weld zones. The final stress analysis would provide data for identification on the drawing of the level of inspection required for different areas of the yoke.

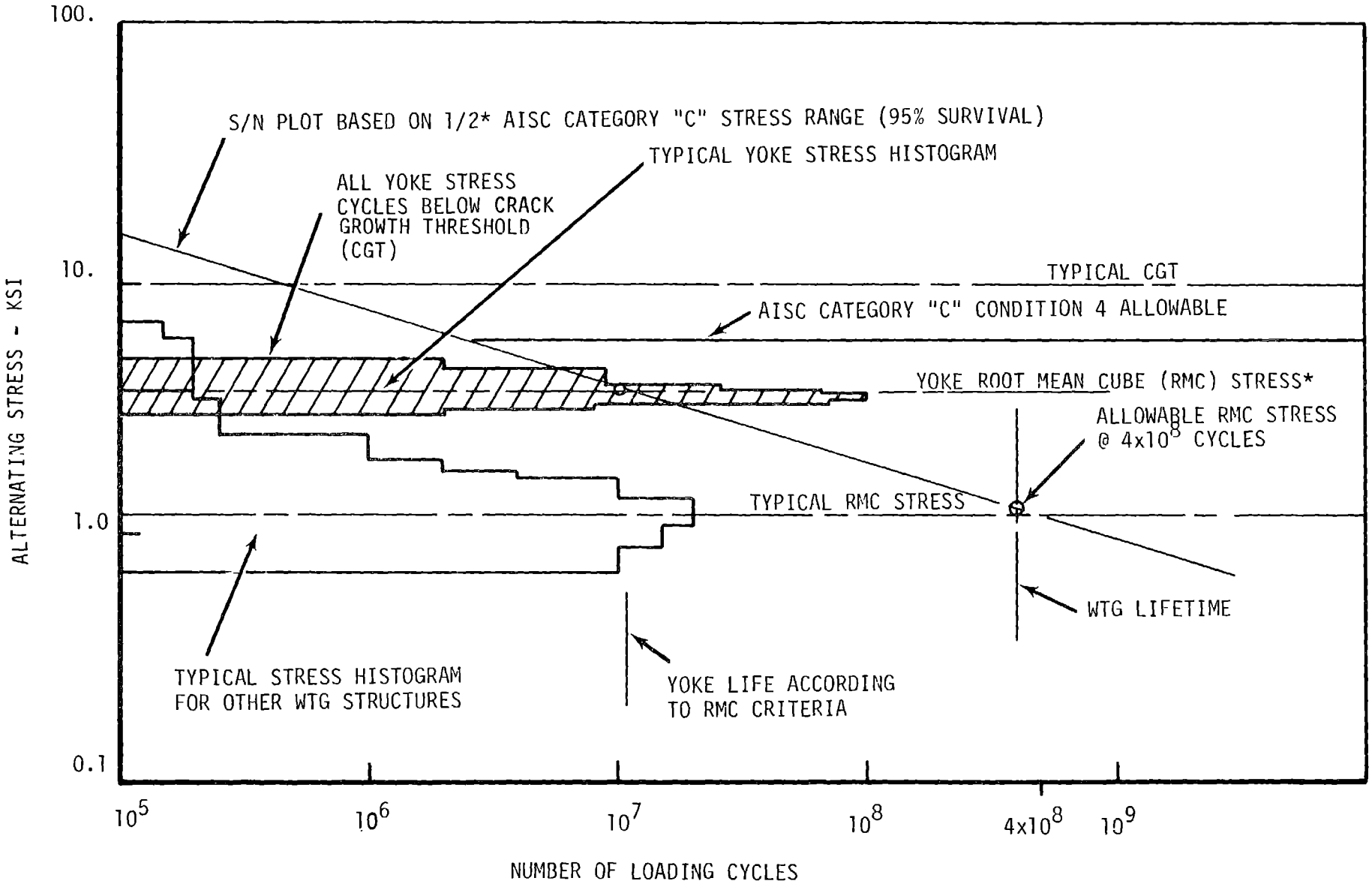

Figure 4-115. Stress Histogram - Yoke

4.5.2.3 Design Analysis

The changes in the blade width and the addition of bolsters to the rotor significantly affected the yoke and teeter bearing assemblies, which were already designed. The following design analysis was performed after these changes. The yoke design is depicted isometrically in Figure 4-111. The design featured the U-shaped outside box structure, supported internally by spar plates and perpendicular bulkhead plates.

A linear elastic finite element model, using 4,666 grid points and 6,067 elements, was developed using the MacNeal-Schwendler NASTRAN program, version 62A, as shown in Figure 4-116. The model was used to obtain estimates of the range of the alternating stress. The largest alternating stress levels occurred at the following two yoke positions: (1) when the yoke is horizontal, and the blade is vertical, (X-up), the torque load and dynamic weight load add on one ear and act on the strong axis of the yoke ear and elbow. (2) when the yoke is vertical, and the blade is horizontal, (Y-up), the torque load acts on the strong axis and the rotor weight acts on the smaller section of the ear and elbow.

The results of the finite element analysis of the preliminary yoke design are summarized in Tables 4-46, 4-47, and 4-48, and Figures 4-117, 4-118, and 4-119. This analysis quantified the degree to which some areas were structurally deficient and reinforcement was added where necessary. These locations are shown in Figure 4-113 and Table 4-46.

Preliminary sizing calculations were based on straight beam theory. A review of the present finite element model and several simpler finite element models shows that the yoke has the characteristics of both a frame and a beam. Beam theory assumes the reaction is at the beam center line; in this case midway between the front and back plates. However, the reactions are at the bearing tube where the front and back plates are connected. The front plate, which is

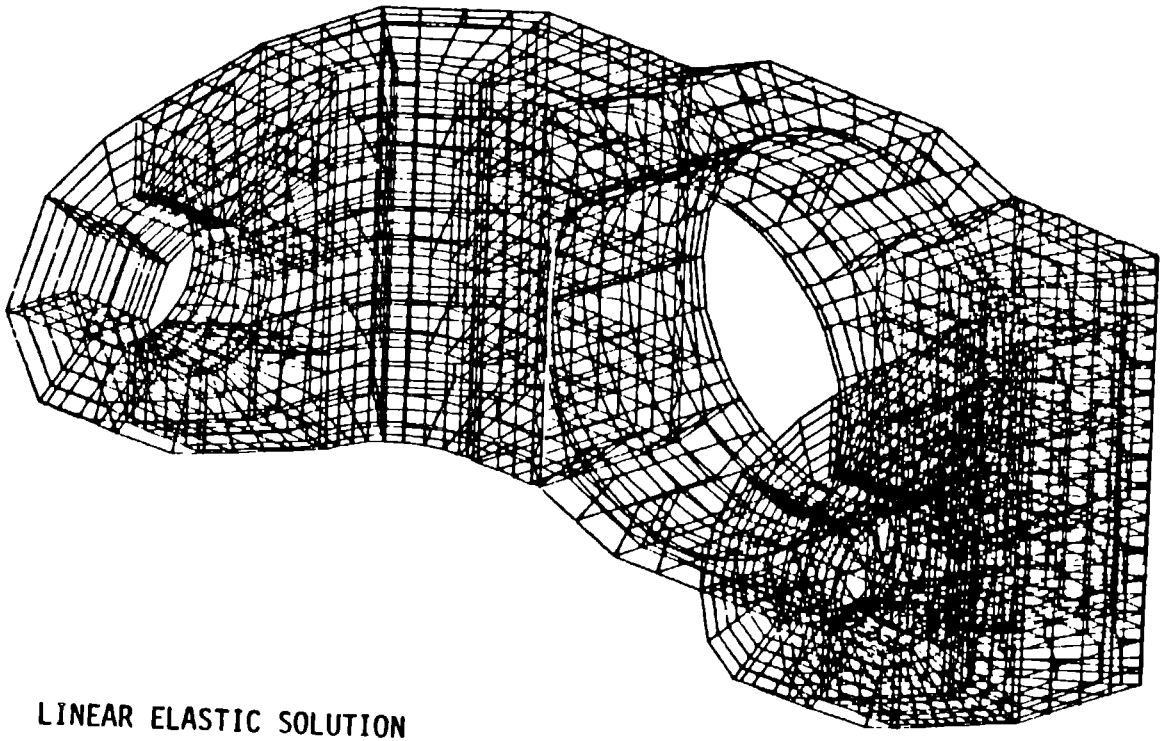

Figure 4-116. Yoke Finite Element Model

Table 4-46 Preliminary Finite Element Yoke Model
Fatigue Analysis Summary

IDENT.(1)	PLACE	RECOMMENDED CHANGE	CONCERN
A	TOP PLATE	INCREASE THICKNESS	HIGH BENDING
H	BOTTOM PLATE	TO 1.5 IN	STRESSES
B	OUTSIDE PLATE	INCREASE THICKNESS TO 2.0 IN INCREASE SECTION WIDTH	HIGH SHEAR STRESSES
C	INSIDE PLATE	INCREASE THICKNESS TO 2.0 IN INCREASE SECTION WIDTH	HIGH SHEAR STRESSES
D	FRONT PLATE	CHANGE BULKHEAD CONFIGURATION INCREASE PLATE THICKNESS TO 2.0 IN	HIGH BENDING STRESSES
E	SPAR PLATE	REMOVE AND REDUCE HOLE SIZES INCREASE PLATE THICKNESS TO 1.25 IN	HIGH PEAK STRESSES
F	BACK PLATE	CHANGE BULKHEAD CONFIGURATION INCREASE PLATE THICKNESS TO 2.0 IN	HIGH BENDING STRESSES
G	BULKHEAD PLATES (AROUND TUBE)	INCREASE PLATE THICKNESS TO 2.0 IN REDUCE HOLE SIZES	HIGH PEAK STRESSES

NOTES:

(1) See Figure 4-113 for letter identification.

Table 4-47 Preliminary Yoke Design Fatigue Case Margins of Safety

ID	Plate Thickness (in.)	Case	Alternating[1] Stress (psi)	Steady Stress (psi)	Allowable[2] Stress (PSI)	Margin of Safety
Front Plate In Corner	1	Y-Up	9,740	-10,071	5,000	-.487
Back Plate In Corner	1	Y-Up	3,847	2,846	5,000	.300
Center Spar Plate In Corner	1	Y-Up	6,884	-4,222	5,000	-.253
Top Plate In Corner	1	Y-Up	6,972	-5,568	5,000	-.280
Spar Plate In Corner At Holes	1	Y-Up	26,549	-12,241	8,000	-.699
Spar Plate Near Tube At Holes	1	X-Up	9,890	-2,308	8,000	-.191
Inside Plate at Teeter Bearing	1	X-Up	11,940	1,722	5,000	-.581
Outside Plate at Teeter Bearing	1	Y-Up	4,772	5,957	5,000	.048

(1) Half range alternating stress based on 99.99th percentile loads.
(2) AISC allowable stress.

Table 4-47 Preliminary Yoke Design Fatigue Case Margins of Safety
(Continued)

ID	Plate Thickness (in.)	Case	Alternating[1] Stress (psi)	Steady Stress (psi)	Allowable[2] Stress (PSI)	Margin of Safety
Bulkhead Plate Around Tube Near Holes	1	X-Up	10,500	-707	8,000	-.239
Bearing Tube at Forward Bearing	4	X-Up	4,952	5,446	5,000	.010

(1) Half range alternating stress based on 99.99th percentile loads.
(2) AISC allowable stress.

Table 4-48 Modified Yoke Design (4-Bay, Thickness Increases)

ID	Plate Thickness (in.)	Case	Alternating[1] Stress (psi)	Steady Stress (psi)	Allowable[2] Stress (PSI)	Margin of Safety
Front Plate In Corner	2	Y-Up	4,006	-4,142	5,000	.248
Back Plate In Corner	2	Y-Up	1,924	1,423	5,000	2.514
Center Spar Plate In Corner	1.25	Y-Up	5,507	-3,377	5,000	-.092[4]
Top Plate In Corner	1.5	Y-Up	4,524	-3,522	5,000	.105
Spar Plate In Corner	1.25	Y-Up	5,507	-3,377	5,000	-.092[4]
Spar Plate Near Tube At Holes	1.25	X-Up	7,904	-1,846	8,000	.012
Inside Plate At Teeter Bearing	2	X-Up	5,300	764	5,000	-.057[3]
Outside Plate At Teeter Bearing	2	Y-Up	2,386	2,979	5,000	1.096
Bulkhead Plate Around Tube Near Holes	2	X-Up	5,250	-353	8,000	.524
Bearing Tube At Forward Bearing	4	X-Up	4,952	5,446	5,000	.010

(1) Half range alternating stress based on 99.99th percentile loads.
(2) AISC allowable stress.
(3) Improved front plate skin effectiveness that will result in additional margin not included.
(4) Improved spar plate effectiveness that will result in additional margin not included.

Table 4-49 Simplified Yoke Design Fatigue Case Margins of Safety

ID	Plate Thickness (in.)	Case	Alternating[1] Stress (psi)	Allowable[2] Stress (psi)	Margin of Safety
Center Spar Plate in Corner	1.5	Y-Up	4,848	6,000	0.238
Spar Plate In Corner	1.5	Y-Up	4,893	6,000	0.226
Inside Plate At Teeter Bearing	3	X-Up	2,333	2,500	0.072
Front Plate In Corner	3	X-Up	5,400	6,000	0.111
Back Plate Near Bearing Tube	1.5	Y-Up	2,163	2,500	0.156
Top Plate In Corner	2	X-Up	5,400	6,000	0.111
Outside Plate At Teeter Bearing	1.5	Y-Up	1,186	2,500	1.108
Bulkhead Plate Shear Around Tube	2	X-Up	2,317	4,000	0.726
Bearing Tube at Forward Bearing	4	X-Up	4,089	8,000	0.956

(1) Half range alternating stress based on 99.99 percentile loads.
(2) AISC allowable stress.

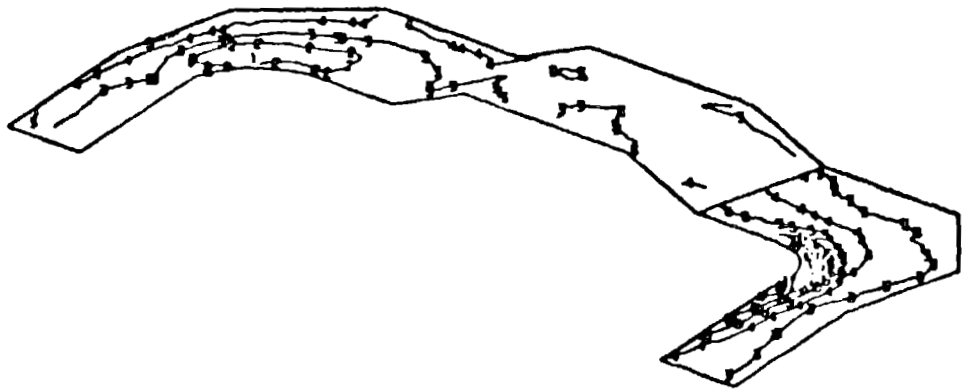

SYMBOL	VALUE
1	-1.155914E+03
2	-2.527607E+02
3	6.503923E+02
4	1.553545E+03
5	2.456698E+03
6	3.359852E+03
7	4.263004E+03
8	5.166156E+03
9	6.069309E+03
10	6.972469E+03

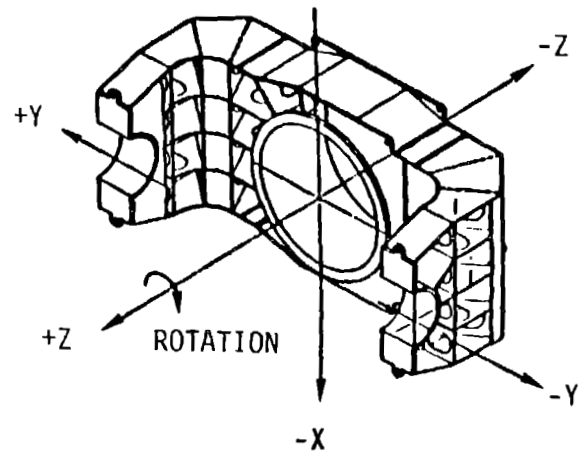

Figure 4-117. Top Plate Majprin Stress

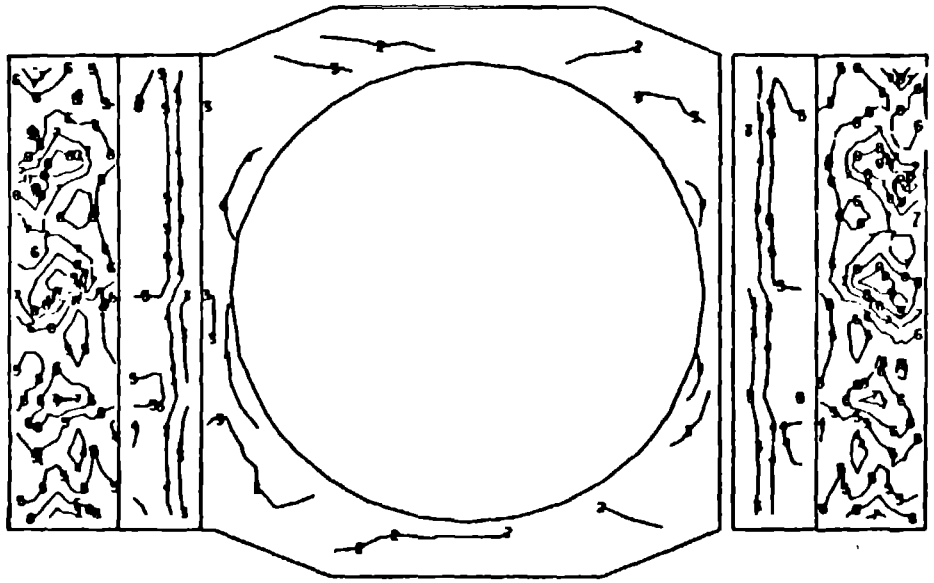

SYMBOL	VALUE
1	4.810447E+02
2	1.421082E+03
3	2.361118E+03
4	3.301155E+03
5	4.241191E+03
6	5.181227E+03
7	6.121262E+03
8	7.061297E+03
9	8.001332E+03
10	8.941379E+03

Figure 4-118. Front Plate Von Mises Stress

SYMBOL	VALUE
1	1.897026E+03
2	2.768448E+03
3	3.639871E+03
4	4.511293E+03
5	5.382715E+03
6	6.254137E+03
7	7.125559E+03
8	7.996980E+03
9	8.868402E+03
10	9.739832E+03

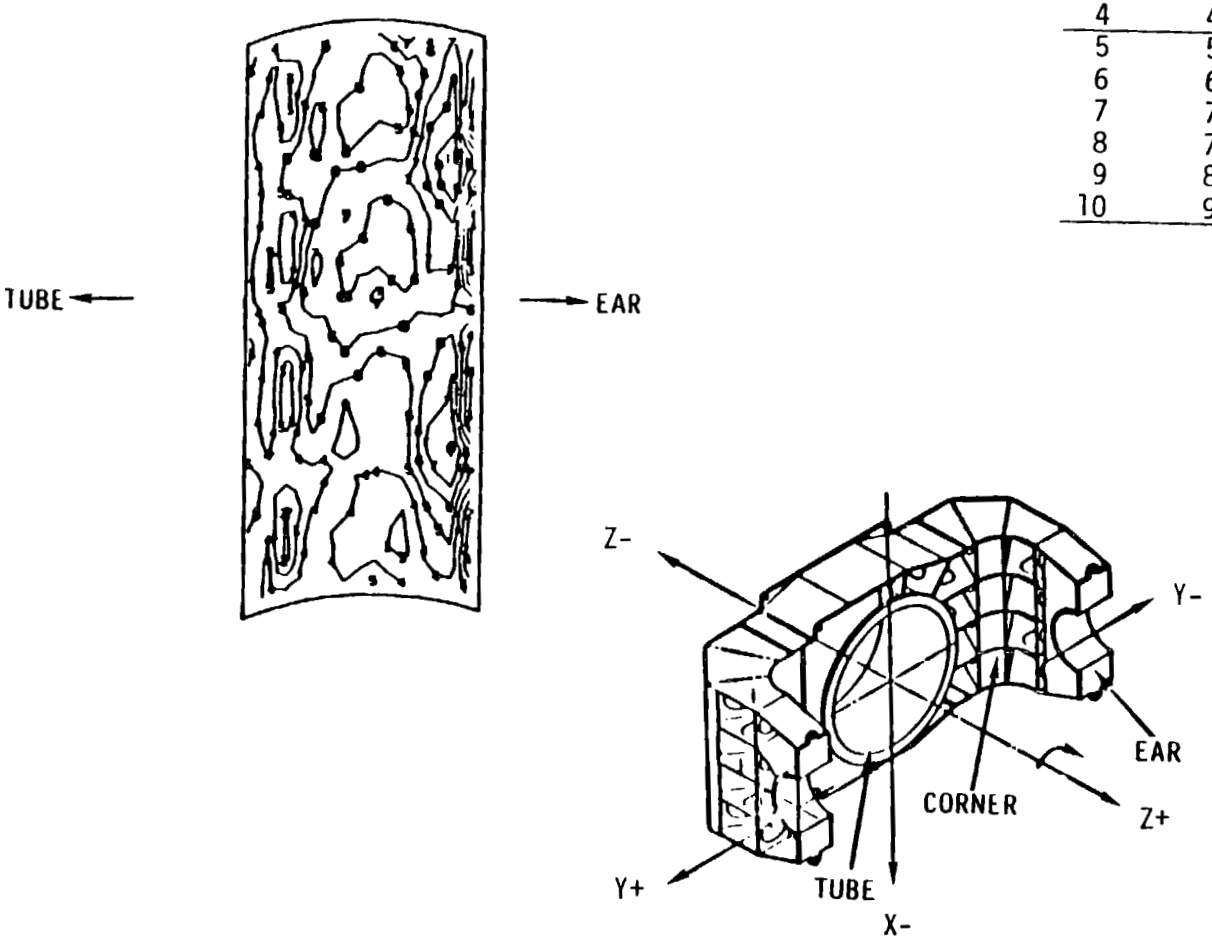

Figure 4-119. Majprin Stress Corner Inside Plate

70 in. from the load, has a higher reaction than the back plate, which is 120 in. from the load. The result is that the front plate has significantly higher stresses than the back plate, unless the plates are the same thickness.

Another effect occurs in the corner where the front plate is curved, with a 24 in. radius. The yoke tends to perform like a curved beam in this elbow. The stress distribution causes the surface with the smaller radius of curvature to encounter higher stress in bending than the surface with a larger radius of curvature. This effect also increases stresses in the front plate, and results in a non-linear elastic stress gradient across the spars.

A third effect was observed where the front plate deformed out-of-plane between the spar plates. Curved beams under in-plane moments stresses develop spar crushing or tearing forces perpendicular to the skin-flanges. Crushing occurs when the radius of curvature is reduced by applied loads. The skins in this structure are not fully effective. The NASTRAN results indicate stresses higher than can be found in curved beam calculations using the full cross-section of the yoke. The results also indicate noticeable, out-of-contour deformations.

The NASTRAN analysis shows that the stresses tend to concentrate in the corner of the elbow. These results are characterized typically in Figures 4-117, 4-118 and 4-119. The front, top, bottom and spar plates were shown to be deficient, as summarized in Table 4-47. Corrective measures were taken, to reduce stresses in the corner. The thickness of the front, back, top, bottom and spar plates were increased to 2.0, 2.0, 1.5, 1.5, and 1.25 in., respectively. The location of the access holes were changed from the spar plate in the corner to an area near the central bearing tube, which has lower calculated stresses. The effectiveness of these changes, which are summarized in Table 4-48, were calculated on a local basis.

Several studies determined whether the present 3-bulkhead design, with a 24-in. radius, should be changed. The studies showed that if the bend angle of the front face at each bulkhead was reduced, the stresses would decrease.

In addition, by adding straight sections, the stresses in the skins could be further reduced. Therefore, a 4-bulkhead configuration was developed, to replace the 3-bulkhead design and reduce the bend angle. However, a detailed finite element analysis of this configuration must be performed to determine its reliability. This analysis has not been performed.

The NASTRAN analysis identified other areas that required modifications. The inside and outside plates in the teeter bearing area of the ear were structurally deficient. The shear stresses were higher than expected because of socketing action of the teeter bearing capsule. The geometry is such that if the blade weight is P, stress equal to 1.36P acts on the inside plate and stress equal to .36P acts on the outside plate when the yoke is horizontal. This effect, and the presence of the spar plates around the teeter shell, tended to concentrate the stress at a few support points.

The width of the "ear", which is the distance between inside and outside plates, was increased to 42 in. instead of 28 in. The change resulted in a load distribution of 1.26P on the inside plate and .26P on the outside plate. The shear area of the plates was increased by extending the 2.0-in. thickness of the front and back plates into the teeter bearing area.

The bearing tube was acceptable according to the design criteria. However, the bulkhead plates which surround the tube were deficient. The thickness of these plates were increased to 2.0 in. and the sizes of the holes were reduced.

The roller bearing vendor recommended that the cylindrical roller bearing sets, 2 forward and 1 aft, which are located in the tube, be changed to one tapered set on each end. This recommendation was accepted. Accordingly, the tube details were modified. It is believed that these changes have not appreciably affected stresses in the tube.

However, the interaction between the tube and bulkhead plates is difficult to predict. Therefore, a finite element model is required to determine the

adequacy of this design. Table 4-48 summarizes the estimated fatigue margins for the preliminary yoke design with these modifications.

4.5.2.4 Preliminary Analysis Summary

A NASTRAN finite element structural analysis showed that several areas of the preliminary yoke design were deficient. Several changes to the structure, resulting in the four-bulkhead configuration, were implemented to bring the design into compliance. Another NASTRAN finite element analysis of similar complexity was required to verify the adequacy of the four-bulkhead design.

4.5.2.5 Simplified Yoke Design

A less complex yoke design was developed after the design of the four-bulkhead configuration was completed. The idea was to remove as many bulkhead plates as possible. This concept was based on reducing the complexity of the welding, inspection and assembly processes. These reductions in labor were expected to result in a lower cost and more reliable design.

4.5.2.6 Simplified Design Analysis

A linear elastic finite element model was developed using the MacNeal-Schwendler NASTRAN program, version 62A. The 794 grid, 1756 element model is shown in Figure 4-120. The left arm is a beam model for mass balance, loading and economy. The NASTRAN model was used to obtain estimates of the alternating half range stress for the same X-up and Y-up cases performed for the 4 bulkhead configuration. Consideration of the tapered roller bearings led to 120° of partial arc of contact boundary conditions inside the main tube.

The results of the analysis are shown in Table 4-49 and Figures 4-121, 4-122 and 4-123. The analysis showed that the highest stresses tend to concentrate

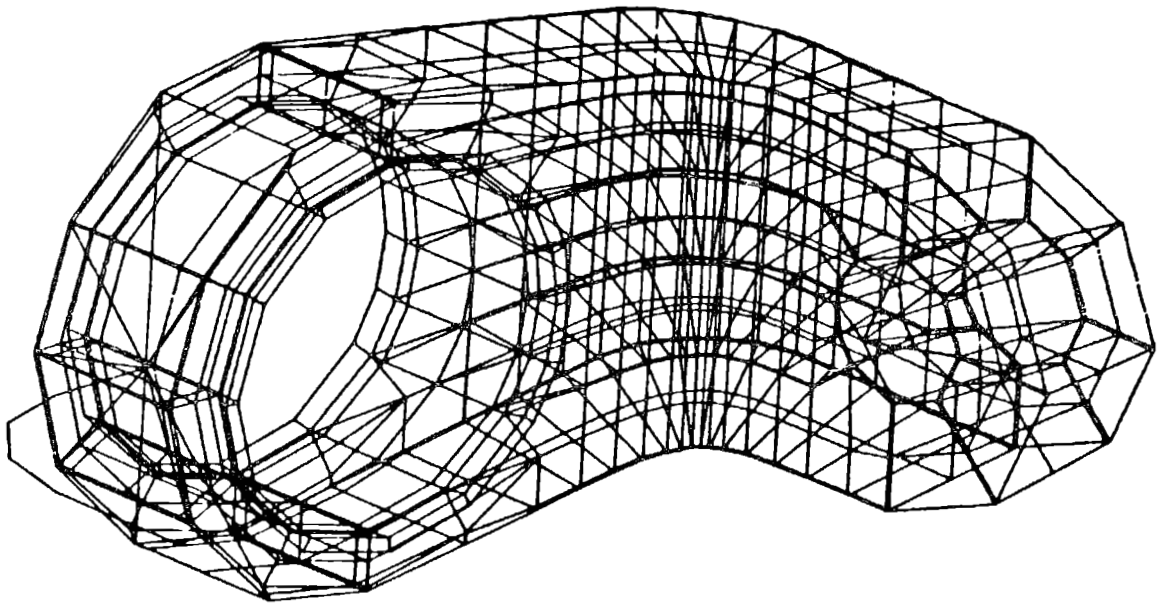

794 Grids
1756 Elements

Figure 4-120. Simplified Yoke Design, Preliminary NASTRAN Model

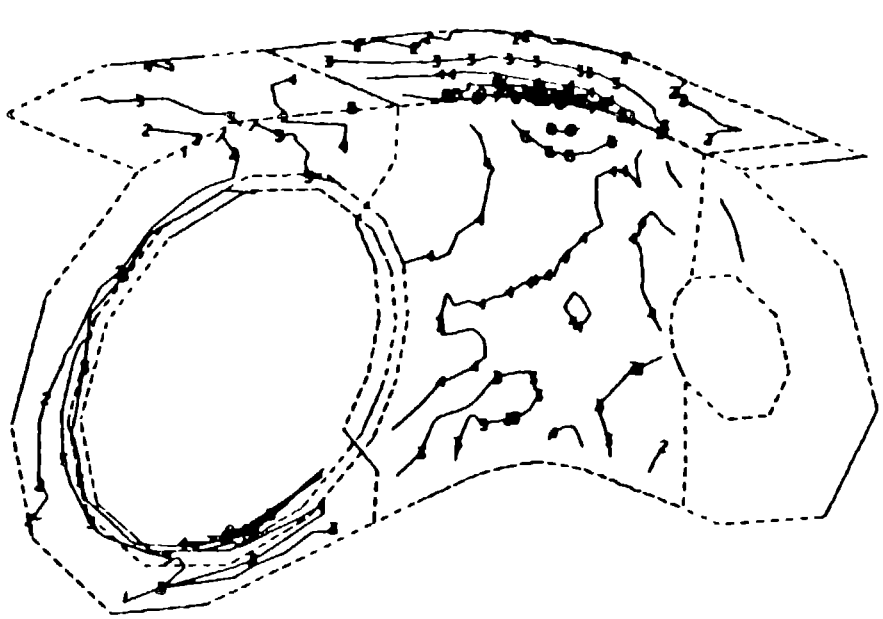

Figure 4-121 Front Skin and Spar 5, Major Principle Stress

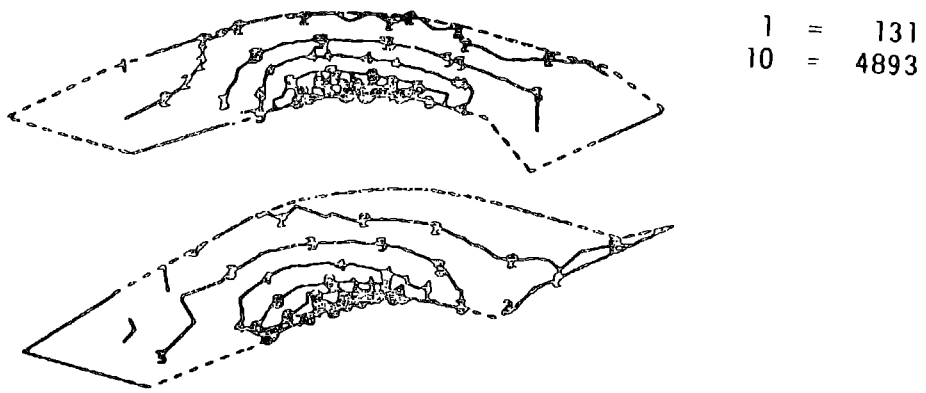

Figure 4-122 Spars 2 and 4, Major Principle Stress

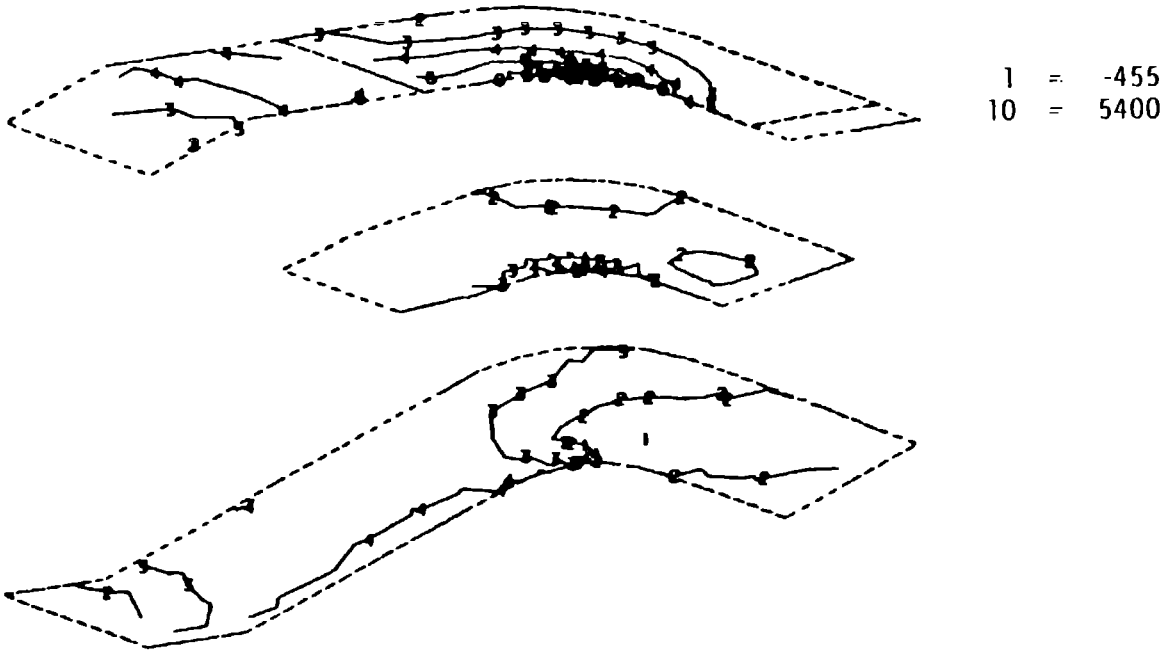

Figure 4-123. Spars 1, 3 and 5, Major Principle Stress

in the corner of the elbow. These results are characterized in Figures 4-121, 4-122 and 4-123.

The thickness of the front, back, top, bottom and spar plates was 3.0, 1.5, 2.0 and 1.5 in., respectively, in the simplified yoke design. The thickness of the front and spar plates had to be increased because of the absence of the bulkhead plates and the forward bias of the load path.

The bulknead plates provided support, which increased the effective width of the skins. The inefficiency caused by their absence contributes to the 50% increase in thickness of the front plate. However, the four-bulkhead design and the simplified yoke require the same amount of steel.

The analysis indicates that the simplified yoke design is acceptable. However, the mesh used in this finite element model may not be dense enough to verify the design. Another NASTRAN analysis, with a more refined mesh would verify the design.

4.5.2.7 Conclusions and Recommendations

The simplified design is the best of the two designs, because of the reduced complexity in the assembly, welding and inspection processes. A NASTRAN finite element structural analysis showed the simplified yoke design to be acceptable, as summarized in Table 4-49. A NASTRAN analysis, with a smaller mesh is required to verify the design.

4.5.3 TRADE-OFFS PERFORMED

The yoke design evolution involved trade-off analyses in rotor attachment methods, fabrication methods, structural design concepts, and materials. The evolution of the designs for the teeter bearing and teeter restrictors are described in sections 4.5.4 and 4.5.5. During the design of the wind turbine generator, several rotor support methods were considered. A yoke surrounding the entire blade was evaluated. An internal structure connected to the drivetrain through an opening in the blade skin was considered. Two teeter bearing assemblies attached to the blade by the bolsters and supported by the U-shaped yoke was finally chosen. Certain features of the yoke design were determined by this rotor support method. A central tube was required to interface with the main rotor bearings, and two cylindrical tubes were needed to house the teeter bearing assemblies. The yoke design involved connecting these assemblies to the central tube with a structure satisfying the design criteria. Four construction methods were considered in the design process: fabrication from rolled shapes, forging, casting, and welding. A built-up structure was eliminated because of the difficulty in obtaining the required torsional stiffness. Forgings, although they have excellent material quality and higher allowable stresses, were ruled out after consultations with various vendors. Forging an acceptable structural configuration would be prohibitively expensive. Casting the yoke structure was also considered. The ability to tailor wall thicknesses to reduce local stresses and the apparently lower cost were distinct advantages of casting. Discussions with two large casting vendors led to preliminary drawings of the concept. However, a castable steel with the required toughness at low temperatures was not identified when the project was terminated. This concept deserves further investigation should the project be resumed. Welding was the fabrication method chosen for the yoke. It afforded the optimum combination of versatility in material placement and producibility, using well-characterized materials and processes.

The yoke weldment design balanced structural design criteria, load paths, and producibility considerations. The enclosed box structure best satisfied these aims. The rectangular cross-section provided both bending and torsional stiffness with adequate internal reinforcement. Section 4.5.2 describes the

trade-off studies that evaluated the number and position of internal members and the shape of the "elbow" region of the yoke. Most attention was paid to limiting the location and number of welds in the low fatigue strength categories defined by the AISC. Different fabrication methods for the central tube were also considered. A ring forging was finally chosen as the fabrication method because the quality of the material was better. When the project was terminated, a tube rolled from plate and seam welded was being considered to reduce costs. This course should also be pursued if the program resumes.

The plate and forging steel used in the design were evaluated based on strength, notch toughness, formability, weldability, availability and cost. ASTM A633 Grade C and ASTM A508 Class 2 were chosen for the plate and forging materials, respectively. A633 Grade C is a normalized material. It was the preferred plate material for several reasons. Since the yoke is a weldment, A633 was chosen for its excellent weldability. The yoke design is also fatigue stress driven, so a high yield strength material is not required. The higher yield strength associated with quenched and tempered materials would have been diminished from the post weld heat treatment for stress relief. Finally, A633 Grade C, with the improved processing described in GE Specification 47A380062, exhibits the required notch toughness over the temperature range. A508 Class 2 was chosen for its weld compatibility with A633. It was not apparent that the required notch toughness value at low temperatures would be met at the center of the forging. Therefore, the present design restricts the operating temperature range of the yoke, subject to further review of actual material test data and further consideration of the consequences of a flaw or large crack involving the mid-thickness of the forging.

4.5.4 TEETER BEARINGS

The teeter bearings transmit rotor loads to the yoke, while allowing the blade to oscillate relative to the yoke. The main components of the load are the rotor thrust, weight and the torque that generates the wind turbine generator's power. The teeter motions are generally small during operation, usually less than $\pm 2°$. However, during startup and shutdown the angle could reach 7°.

Because of the small oscillating teeter motions, conventional rolling element bearings were eliminated in the early studies. Rolling element bearings could be used if the rollers were continually immersed in oil. But then the design would require a leak-proof oil seal, which would be subject to small oscillations, and must be easy to repair and replace. These requirements eliminated rolling element bearings.

Elastomeric and the teflon-fabric bearings remained under consideration. The teflon fabric bearing is a plain spherical bearing with teflon composite between the sliding surfaces. Recent advances in the technology of teflon material and the availability of standard large bearings with bores up to 75 in. made this style attractive. However, the reversal of loads in the teeter bearings, as the rotor goes through each cycle, caused complications. As teflon wears, the bearings allow more play. This wearing pattern necessitated a more complicated design. Preloaded bearings or a combination elastomeric thrust and teflon radial bearing were possibilities. Since the MOD-2 designs had used elastomeric bearings successfully, and no cost advantage could be shown for the teflon designs, an all elastomeric bearing was chosen in the final design phase.

The sizing of elastomeric bearings calls for specialized knowledge. Changes in the yoke and blade interfaces affected the design and packaging of the teeter bearings. A competitive procurement was used to select a vendor for the preliminary design and the winner was given a small design support contract.

A successful elastomeric teeter bearing design had the following requirements:

1. Replaceability: The design should allow the replacement of any component without removing the blade.
2. Inspectability: The exposed rubber surfaces should be easy to check visually for spalling or other signs of deterioration.
3. Protected Environment: The rubber surfaces should not be exposed to sunlight and air pollution.
4. Maintenance: Maintenance procedures should be minimal, for example, there should be no periodic lubrication requirement.
5. Assembly: The design should accommodate an easy rotor blade assembly.

The first requirement was the most important. Although the MOD-2 elastomeric bearings were tested and ran successfully for a short period, possible aging effects may not allow the entire 30-year life. Extensive testing would be much more expensive than replacement if the bearings could be replaced without removing the blade. Blade removal would require large cranes with long lead-time rentals and long shutdown times. If the blade could be temporarily supported by the yoke through a different load path while the bearing was replaced the process would be much quicker and cheaper.

Failures in elastomeric bearings on the MOD-5A would be caused by a slow deterioration of the surface. At the surfaces that experience the greatest stress, chunks would crack or spall, leaving telltale rubber grit. Cracks would propagate inward until separation was complete. Some periodic visual inspection (via borescope, if necessary) is the only inspection requirement. It is well known that elastomers exposed to sunlight, ozone and other air pollutants lose their properties. Usually the elastomer surfaces are coated and the surface area to volume ratio is small. However, environmental protection is prudent in view of the 30-year life requirement.

More teeter bearing requirements, for example, loads, teeter angles, are given in 47A380045 "Elastomeric Teeter Bearing Requirements Specification". The final design of the teeter bearing assembly is shown in figure 4-124 and 4-125.

Briefly, the assembly procedure takes the following steps:

1) The blade bolsters and the teeter pivot shaft are bonded to the blade in the field since the assembled blade is too big to ship. The bolster inserts are bonded with fixturing, so that the teeter axes are aligned and at the proper width.
2) The radial teeter bearing is assembled into the teeter hub and then mounted via the tapered shaft of the bolster insert to the blade. Temporary jack screws between the radial bearing inner race and the shelf of the hub allow a direct load path as the hydraulic tension pushes the assembly on the tapered V-shaft.
3) Measurements are checked so that the spacer ring can be ground to the right thickness. This allows the ears of the yoke to be preloaded via axial tension from the teeter pivot shaft, without shear strain on the radial bearing.
4) The yoke end caps are bolted to the hub with the split spacer ring in place.
5) The entire blade, teeter hub assembly and yoke caps are lifted to the hub height and mated to the yoke. The blade is secured by bolting the end caps to the yoke.
6) The thrust bearings are slipped over the teeter pivot shaft, followed by the Ringfeder^{TM} clamp. The hydraulic tensioners are preloaded the thrust bearing, the Ringfeder^{TM} clamp bolts are tightened, to secure the clamp, and the backup nut is installed.
7) The teeter motion limit width assembly is mounted and the protective cover bolted in place.

Studies of the bearing assembly showed that when the blade is vertical the weight, thrust and torque loads are transmitted through the radial bearing to the hub into the yoke. Both thrust bearings experience only the preload. When the blade is horizontal, only the thrust and torque loads are transmitted by the radial bearing. The lower thrust bearing experiences the axial preload plus half the blade weight. The upper bearing encounters the preload minus half the blade weight. With a preload greater than half the blade weight the

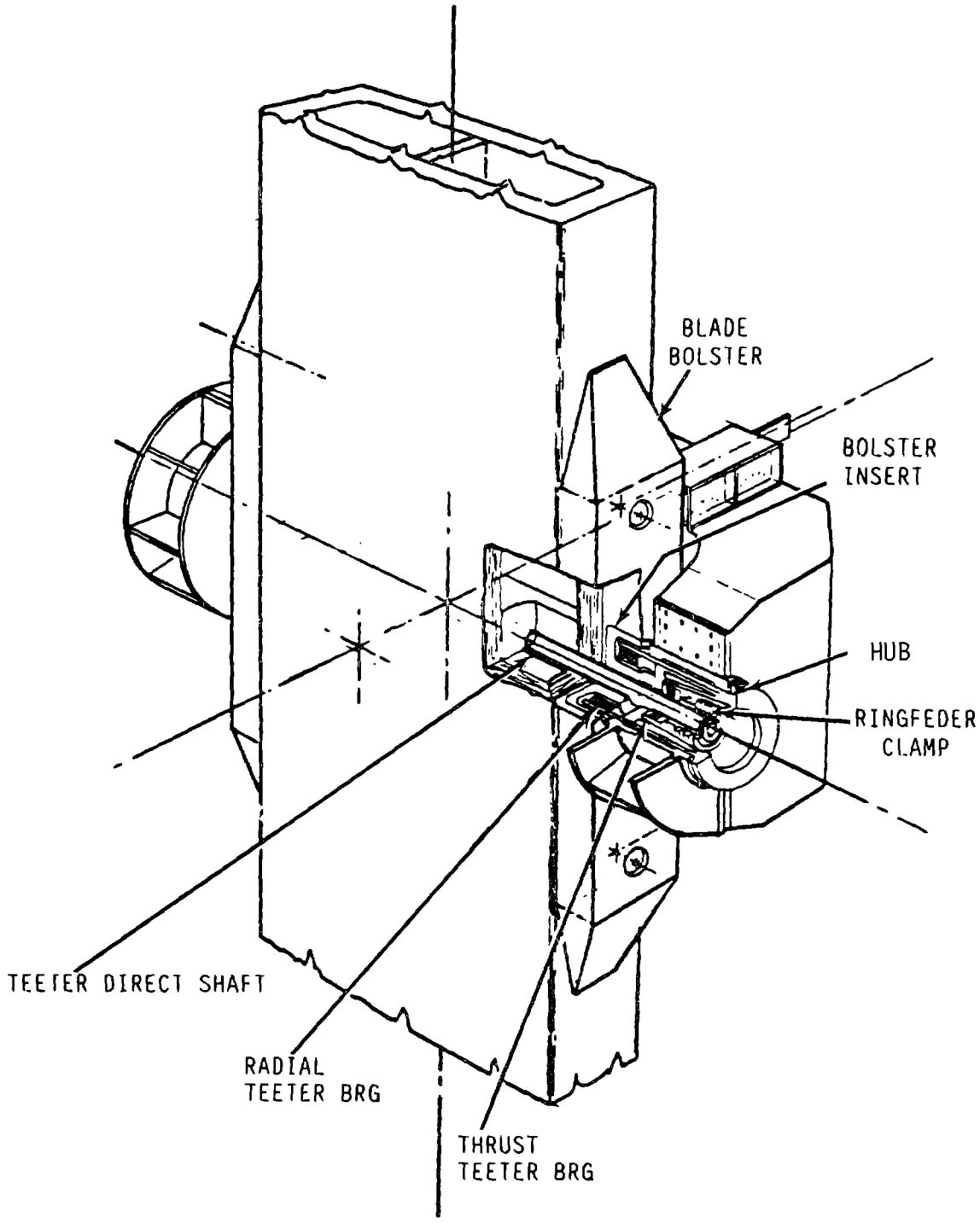

Figure 4-124. Teeter Bearing Arrangement

thrust bearings will always be in compression, which is necessary for long fatigue life.

Details of the elastomeric bearings are given in Figure 4-125a. The radial bearing is two concentric steel rings with rubber molding between the rings. Thin steel rings, called shims, are bonded in the rubber. The shims control the shape factor, which is the ratio of exposed surface area to volume. This ratio controls the bearing stiffness and strain properties. The thrust bearing is disk-shaped, with alternate layers of rubber and disk-shaped shims molded between the thick steel front and back rings. The back support disk is an integral part of the hub of the Ringfeder™ clamp. It has gussets to support the load properly.

4.5.4.1 Teeter Bearing Hub Structural Analysis

The elastomeric thrust bearing is subjected to a compression load of 270,000 lbs., by deflecting the bearing with a hydraulic jack and holding the preload with a plate and cylindrical structure, called the hub, as shown in Figure 4-125. The plate to which the bearing is molded is called the bearing load plate. It is reinforced with gussets. The bearing load plate is attached to the hub, which fits over the shaft, as shown in Figure 4-125b. The shaft is filled with a shrunk-in plug, to stiffen the shaft. The load on the bearing is maintained by securing the hub with a Ringfeder shrink ring and disc assembly, size 390-91.

The load is a steady 270,000 lbs., normal to the bearing load plate and an alternating 212,000 lbs., normal to the plate. The limit load is 482,000 lbs, the sum of the mean load and alternating load. The steady state load is induced by the elastomeric bearing preload and the alternating load is induced by the blade's weight during rotation.

The Ringfeder shrink ring and disc assembly provide pressure to the hub that attaches the load plate to the shafting. This pressure is a constant, radially inward force applied at the inner diameter of the shrink ring, as

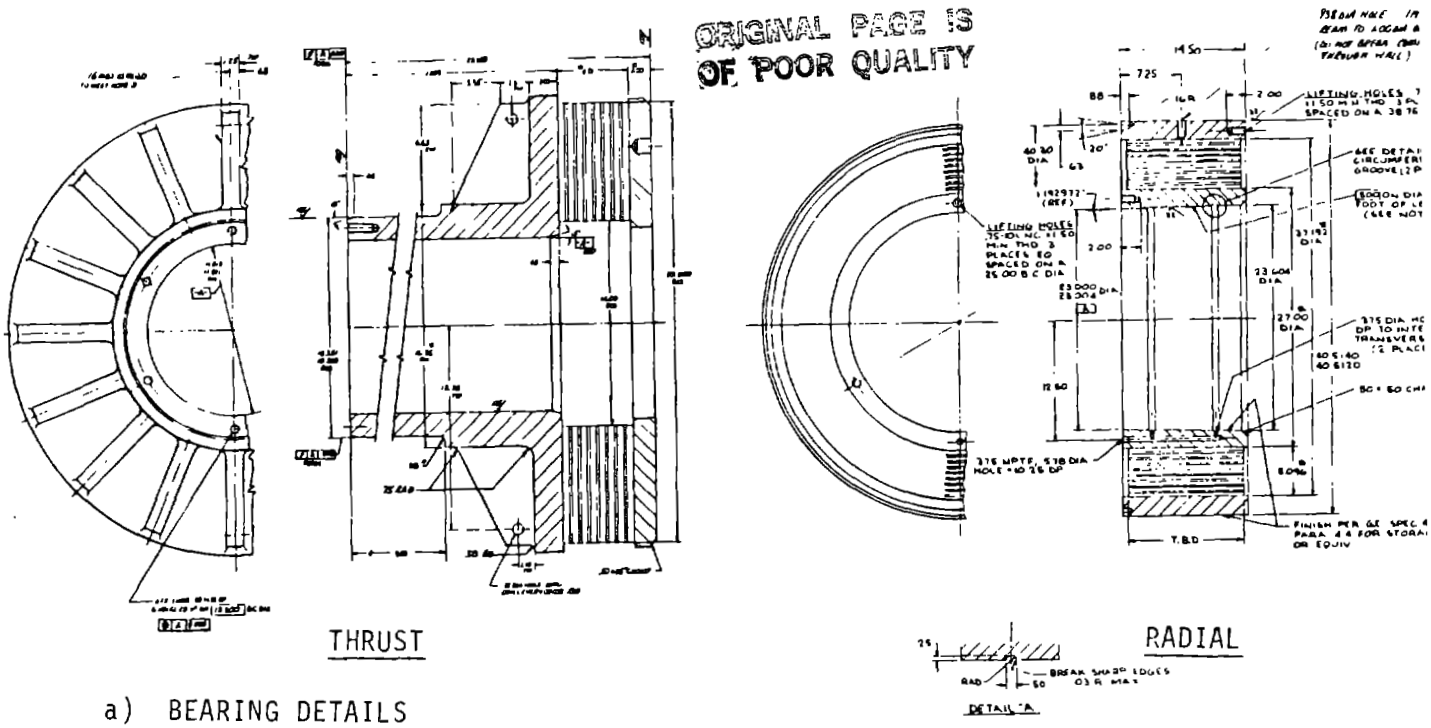

a) BEARING DETAILS

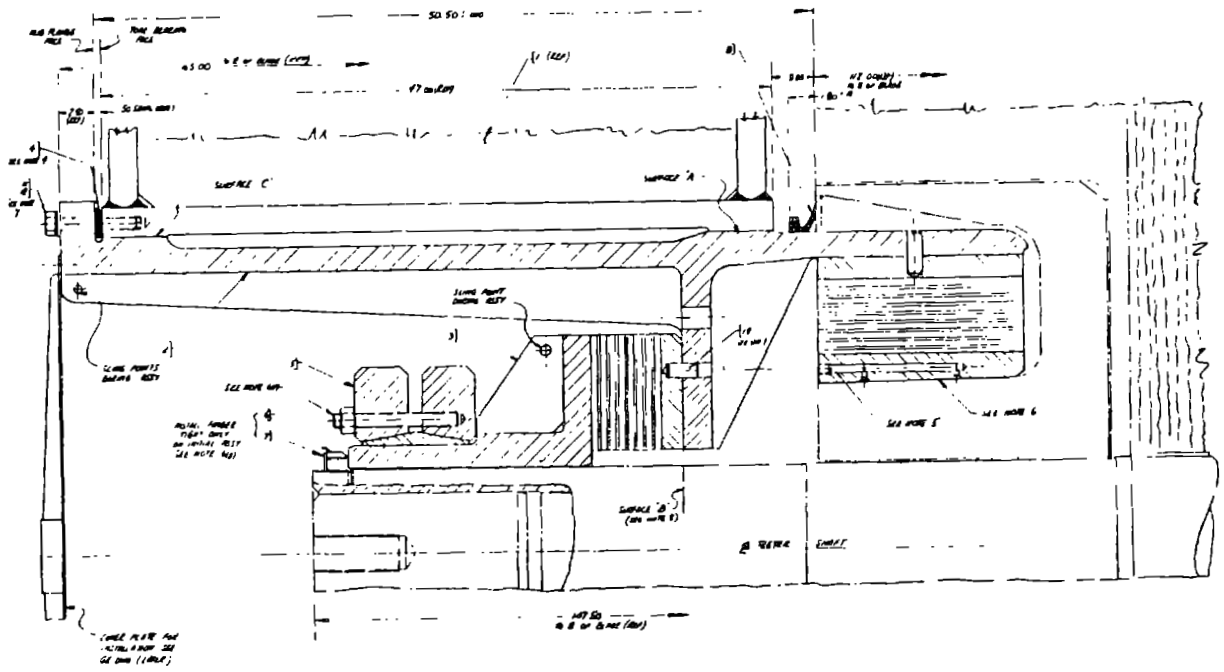

b) INSTALLATION

Figure 4-125 Teeter Bearing

shown in Figure 4-126. The pressure exerted by the shrink ring on the hub was calculated to be 28,902 psi.

A finite element model of the load bearing plate and hub was developed, using the "MACNEAL-SCHWENDLER" NASTRAN Program, Version 62A. The geometry and nomenclature are shown in Figures 4-127 and 4-128. The dimensions were varied until satisfactory stress levels were obtained.

The bearing load plate, the 16 gusset plates, and the hub were represented by CQUAD4 elastic plate elements. The stiffness of the shaft at the hub inner diameter, where the Ringfeder shrink ring contacts the hub outer diameter, was represented by a series of beam elements. The load in the X-direction was reacted at the end of the hub to simulate friction forces, as shown in Figure 4-126.

Three loading cases were considered: the limit load; the maximum alternating load; and the mean load.

The results of the finite element analysis are summarized in Tables 4-50 and 4-51 and Figures 4-129 through 4-133. The load on the bearing plate tends to develop membrane stresses on the gusset plates, as shown in Figure 4-133. The largest stresses result from the deflection pattern illustrated in Figure 4-130 and are approximately normal to the hub.

The gusset plate thickness was determined by the fatigue case loading. In a welded design, a principle stress range of 5,000 psi would be allowed at the capping interruption of the weld in the axial direction of the cylinder and in the radial direction of the flange.

Several vendors indicated that an integral design with no welding was feasible. Therefore, the gusset plates were designed to a maximum stress of 10,000 psi, 5,000 psi half range, and a minimum yield strength of 50,000 psi. A maximum semicircular flaw size of 0.05 in. was specified. This flaw size is compatible with the requirement that the yoke material must not exceed the crack growth threshold. A more complete discussion of design limits is given in Vol II, Section 9.0.

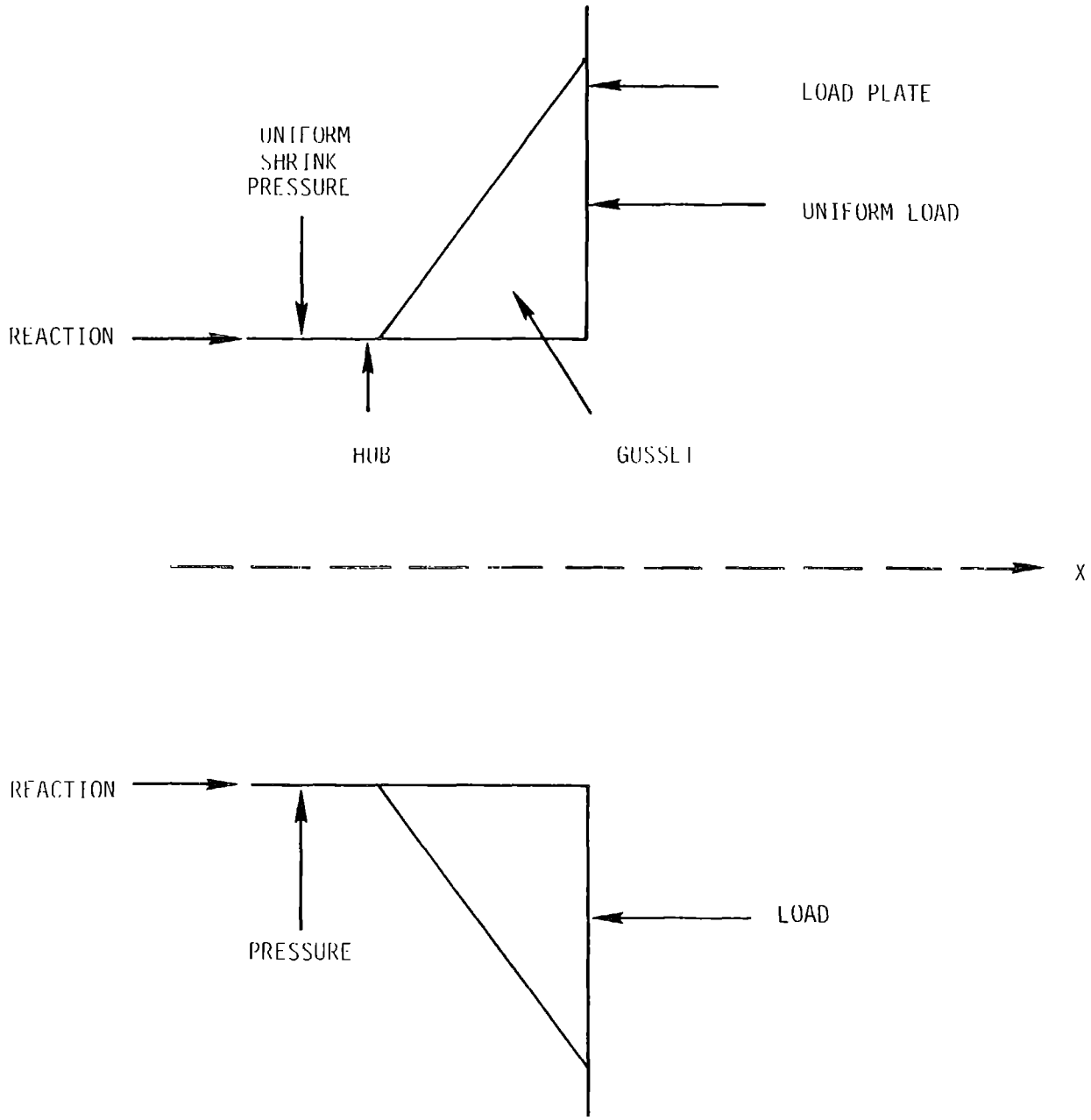

Figure 4-126. Load/Pressure Diagram

Figure 4-127. Hub, NASTRAN Linear Elastic Model
460 Elements - 324 Grids

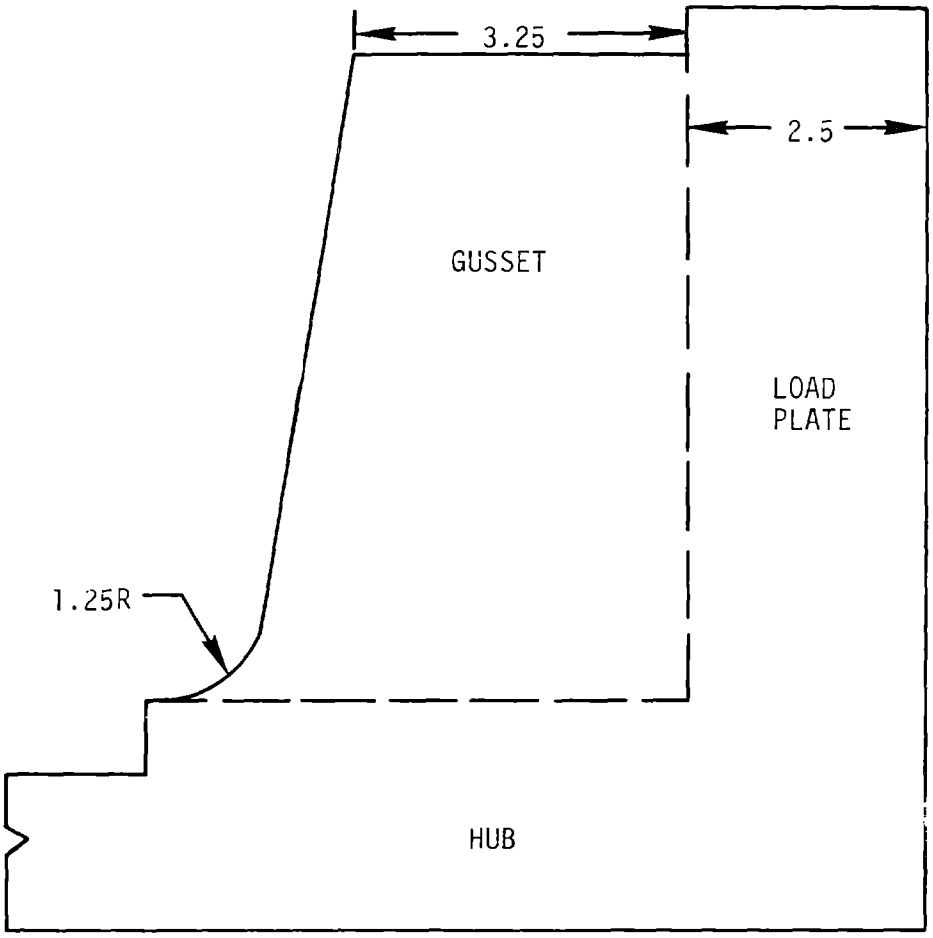

Figure 4-128. Hub Detail

Table 4-50 LIMIT LOAD CASE, MARGINS OF SAFETY

ID	MAXIMUM STRESS (PSI)	ALLOWABLE[1] STRESS (PSI)	MARGIN OF SAFETY
GUSSET PLATE	8,251	30,000	2.636
HUB RADIAL STRESS	-28,902	30,000	.038
HUB TANGENTIAL STRESS	-18,763	30,000	.599
LOAD BEARING PLATE	8,330	30,000	2.601

NOTES: (1) A MINIMUM YIELD STRENGTH OF 50,000 PSI IS REQUIRED.

Table 4-51 FATIGUE CASE, MARGINS OF SAFETY

ID	STEADY STRESS (PSI)	MAXIMUM[1] ALTERNATING STRESS (PSI)	ALLOWABLE[2] STRESS (PSI)	MARGIN OF SAFETY
LOAD BEARING PLATE	5,577	2,753	5,000	.816
HUB	1,295	3,016	5,000	.658
GUSSET PLATE	-3,374	4,947	5,000	.011

NOTES: (1) MAXIMUM ALTERNATING STRESS 99.99 PERCENTILE LOADS.
(2) ALLOWABLE STRESS BASED ON AISC DESIGN CRITERIA CATEGORY C.

11/29/83 MAX-DEF = 0.00030096
INCLINED VIEW FROM X AXIS ALL ELEMENTS AND SPIDERS

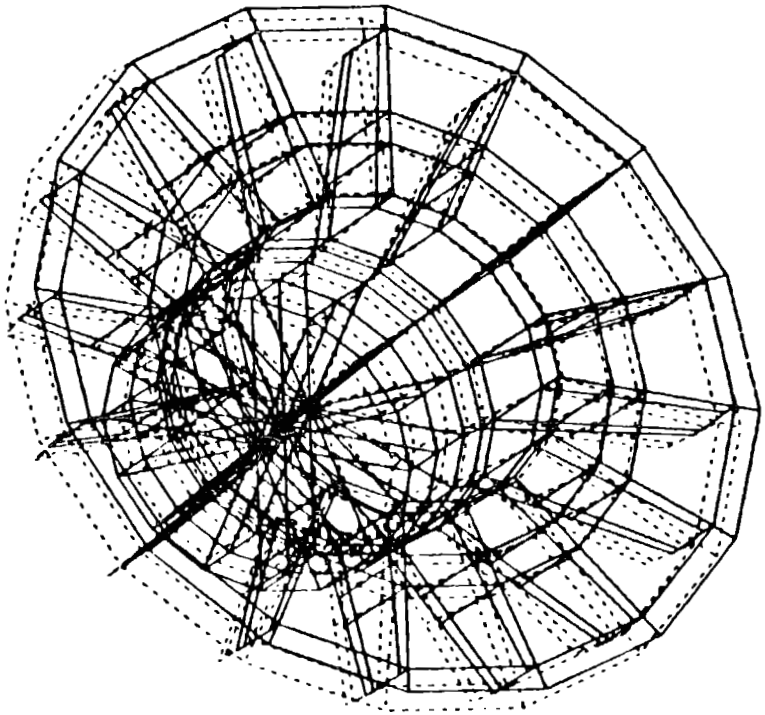

MEMBER RING4 TEETER BEARING LOAD RINGS
L SHAPED RING WITH GUSSET SUPPORTS
LIMIT LOAD CASE LOAD = 482000 LBS FIT PRESSURE = 28902 PSI
STATIC DEFOR. SUBCASE 1 LOAD 101

Figure 4-129. Hub Deflections

11/29/83 MAX-DEF = 0.00030096
VIEW FROM Z AXIS GUSSET 1 THETA = 0

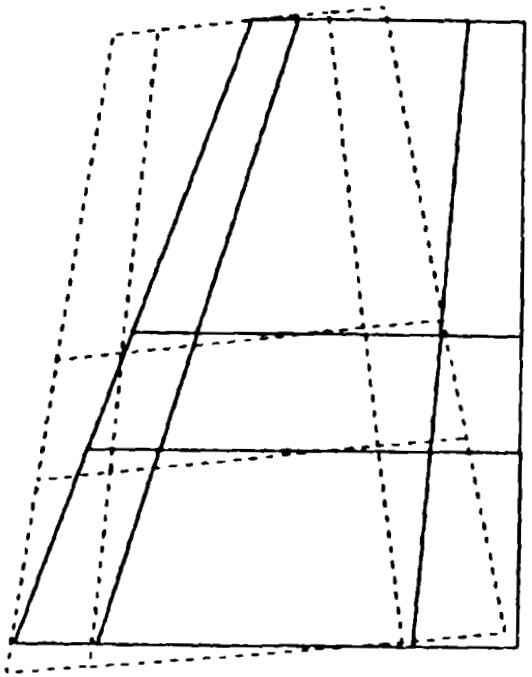

MEMBER RING4 TEETER BEARING LOAD RINGS
L SHAPED RING WITH GUSSET SUPPORTS
LIMIT LOAD CASE LOAD = 482000 LBS FIT PRESSURE = 28902 PSI
STATIC DEFOR STRESS SUBCASE 1 LOAD 101

Figure 4-130. Hub Deflection Detail

11/29/83
VIEW FROM X AXIS BEARING LOAD PLATE MAJPRIN STRESS

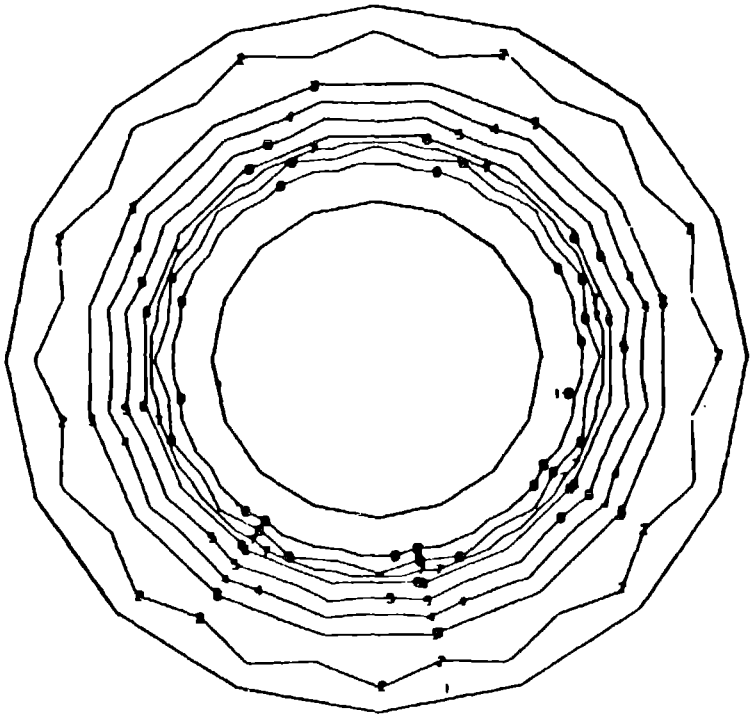

SYMBOL	VALUE
1	3.589684E+03
2	4.116398E+03
3	4.643113E+03
4	5.169828E+03
5	5.696543E+03
6	6.223258E+03
7	6.749973E+03
8	7.276687E+03
9	7.803402E+03
10	8.330133E+03

MEMBER RING4 TEETER BEARING LOAD RINGS
L SHAPED RING WITH GUSSET SUPPORTS
LIMIT LOAD CASE LOAD = 482000 LBS FIT PRESSURE = 28902 PSI
STATIC STRESS SUBCASE 1 LOAD 101

Figure 4-131. Hub Stress Contours

11/29/83
INCLINED VIEW FROM X AXIS HUB MINPRIN STRESS

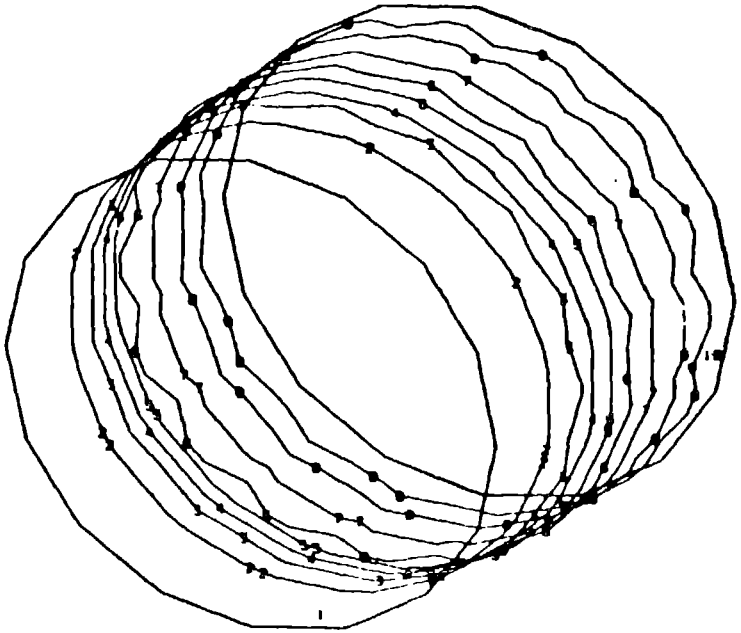

SYMBOL	VALUE
1	-1.876282E+04
2	-1.637641E+04
3	-1.399000E+04
4	-1.160359E+04
5	-9.217176E+03
6	-6.830766E+03
7	-4.444355E+03
8	-2.057946E+03
9	-3.284629E+03
10	-2.714867E+03

MEMBER RING4 TEETER BEARING LOAD RINGS
L SHAPED RING WITH GUSSET SUPPORTS
LIMIT LOAD CASE LOAD - 482000 LBS FIT PRESSURE = 28092 PSI
STATIC STRESS SUBCASE 1 LOAD 101

Figure 4-132. Hub Stress Contours

11/29/83
VIEW FROM Z AXIS GUSSET 1 THETA = 0 MINPRIN STRESS

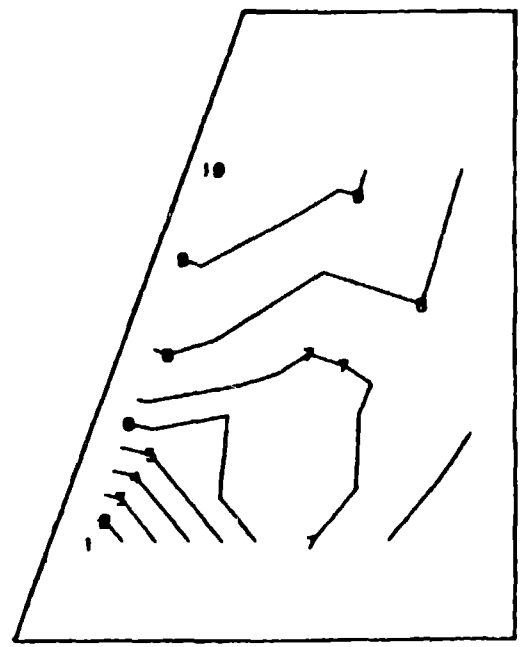

SYMBOL	VALUE
1	-4.946.379+03
2	-4.511762E+03
3	-4.077146E+03
4	-3.642530E+03
5	-3.207915E+03
6	-2.773299E+03
7	-2.338683E+03
8	-1.904067E+03
9	-1.469452E+03
10	-1.034837E+03

MEMBER RING4 TEETER BEARING LOAD RINGS
L SHAPED RING WITH GUSSET SUPPORTS
MAX ALT CASE LOAD = 212000 LBS FIT PRESSURE = 0 PSI
STATIC STRESS SUBCASE 2 LOAD 102

Figure 4-133. Hub Stress Contours, Detail

The design is shown in Figure 4-128. Margins of safety for the limit and fatigue load cases were calculated and are summarized in Tables 4-50 and 4-51.

Calculations determined the greatest stresses on each component for various cases. For the hub, the greatest stresses for the fatigue case are bending stresses parallel to the X axis, along the hub length. The greatest stresses for the limit load case are tangential stresses induced by the pressure of the shrink disc as characterized in Figure 4-132.

The greatest stresses in the bearing load plate were tangential stresses at the inner diameter, caused by the bending of the plate as characterized in Figure 4-131.

Radial and tangential stresses were calculated by thick-walled cylinder theory. This calculation was performed for the shaft when the Ringfeder shrink ring and disc were tightened and the plug was shrunk-fit. These stresses are summarized in Table 4-52.

The Ringfeder shrink ring and disc assembly provide pressure to the hub, which attaches the load plate to the shafting. This pressure is a constant radially inward force applied at the inner diameter of the shrink ring, as shown in Figure 4-126. A steady pressure of 28,902 psi was calculated to be the pressure exerted by the shrink ring on the hub.

The Ringfeder shrink disc, size 390-91, is supplied to the design by the Ringfeder corporation. The Ringfeder Corporation calculated that the disc's maximum torque capability was 561,125 ft-lbs and the maximum axial load capacity was 1,140,208 lbs.

The maximum torque load applied to the disc is 75,000 ft.-lbs., which is well below the design capability of 561,125 ft-lbs. The maximum load in the X direction, along the teeter shaft, as shown in Figure 4-126, is 482,000 lbs., which is also well below the design capability of 1,140,208 lbs. Therefore, the Ringfeder shrink disc, 390-91, is acceptable and well within design capability.

Table 4-52 SHRINK FIT STRESSES SHAFT AND PLUG STRESS SUMMARY

ID	DIAMETER	STRESS TYPE	STRESS (KSI)	MARGIN[1] OF SAFETY
SHAFT	OUTER	TANGENTIAL	-22.3	.345
SHAFT	INNER	TANGENTIAL	-20.6	.456
SHAFT	OUTER	RADIAL	-25.6	.172
SHAFT	INNER	RADIAL	-19.8	.515
PLUG	OUTER	TANGENTIAL	-19.8	.515
PLUG	OUTER	RADIAL	-19.8	.515

NOTES: (1) A MINIMUM YIELD STRENGTH OF 50,000 PSI WAS SPECIFIED.

4.5.4.2 Teeter Bearing Cylinder Analysis

The cylindrical shell which connects the yoke to the elastomeric radial teeter bearings was analyzed with a NASTRAN finite element model. As shown in Figure 4-134, symmetry was invoked with respect to the direction of the resultant radial force of the combined wind thrust and rotor torque loading. This resultant also included the appropriate weight according to the rotor orientation being analyzed. The compact length to diameter ratio, high radial shear loads and superposed loads along the cylinder axis but eccentric to the tube walls made the results of approximate beam calculations uncertain. The numerical model should accurately combine all effects.

The results of the numerical model are listed in Table 4-53 and the locations are indicated in Figure 4-134. This structure was designed to be cast, rather than welded, so Category C stress allowables were chosen. It can be seen that the maximum stress range is less than the 12 ksi allowable, except for the stress concentration at the web to cylinder, which is easy to correct by local geometry and thickness adjustments. The limit stress was compared to 60% of the tensile yield point of a typical casting alloy.

Table 4-53 Results of Numerical Model

	Limit		Fatigue	
Location	Stress (psi)	M.S.	Stress (psi)	M.S.
Flange	6,398	4.63	± 3,126	0.92
Cylinder Wall	14,940	1.41	± 5,152	0.16
Platform	5,158	5.98	± 2,318	1.61
Web Toe	24,430	0.47	± 11,260	-0.47
Web	9,872	2.65	± 5,165	0.16
Retaining Bolt	18,000	2.0	± 9,000	0.5

$$\text{M.S.} = \text{Margin of Safety} = \frac{\text{Allowable}}{\text{Actual}} - 1$$

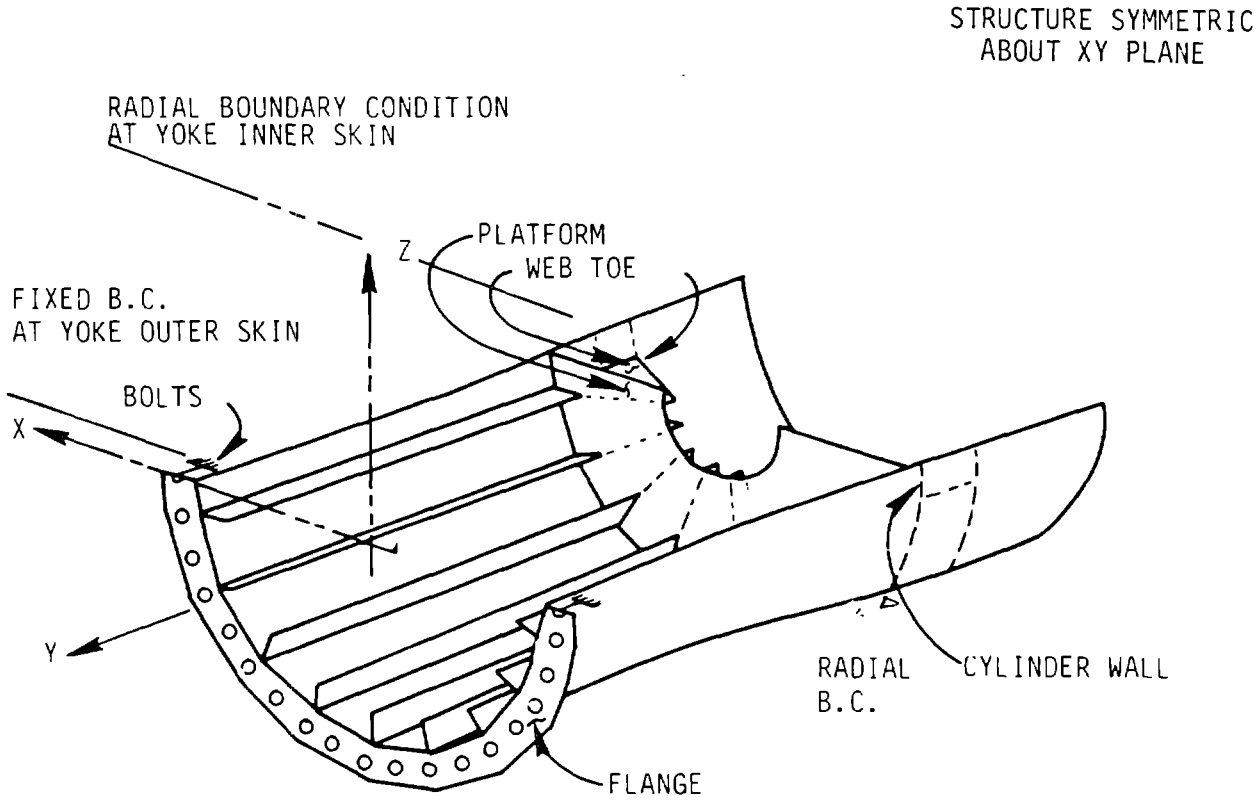

Figure 4-134. Finite Element Model of Teeter Bearing Cylinder and Location of Peak Stresses

The retaining bolt external stresses are compared to the allowables recommended by the AISC for high strength bolts with minimal prying action. These allowables require properly tightened bolts and depend on the continued existence of the friction capacity. The estimated friction capacity is 380 kips using a coefficient of 0.15 which should easily resist the limit load of 92 kips. However, if the joint loosens, bolt bending stress could reach 30 ksi. The design details and installation procedure must prevent bolt bending in order to assure good fatigue life.

4.5.5 TEETER RESTRICTOR ASSEMBLY

The teeter restrictor system dissipates teeter rotational energy, to limit the maximum teeter angle reached during operation. Any excessive unbalanced flapwise moments, which normally occur during startup or shutdown, are reacted by the force generated by the caliper brake assemblies on both sides of the teeter axis. The frictional force developed by the brakes is transmitted to the blade through a structural link connected to a pin retained by two structural rings bonded to the bolster, as shown in Figure 4-135. The brakes are applied in two stages, according to the magnitude of the teeter angle. The rubber bumper engages at a teeter angle of 7°, and makes solid contact with the yoke at the maximum angle of 9°.

Each of the two teeter restrictor assembly consists of two Goodyear SCL-38 brakes mounted in a tower structure, which is bolted to the yoke structure. The brakes are the same as those used in the yaw drive. The brakes grab the teeter links. One end of the link is mounted to the bolster support pin with spherical teflon fabric bearings. The other end is guided by cam rollers to maintain the proper orientation between the brake pads. The teeter links can be fixed to lock the blade in any position, by releasing hydraulic pressure in the brakes.

The primary trade-off study in the development of the teeter restrictor system concerned the active and passive designs. Two passive designs were considered. One design used a double-ended hydraulic actuator with the rod and head ends connected by a line containing a variable orifice. One end of the actuator rod was attached to the blade. Resistive force was provided by the pressure drop created by the fluid shuttling between the two cylinder ends as the rod was translated by the teeter motion of the blade. This damping system was not sufficient to prevent unacceptable teeter impact on the 9° hard stop at very low rotor speeds. Therefore, the second design added an elastic shock mount, which acted between 7° and 9°. This design prevented the 9° teeter stop impact, but produced higher teeter moment loads than the friction brake design for the worst case conditions. So the current friction brake design was adopted.

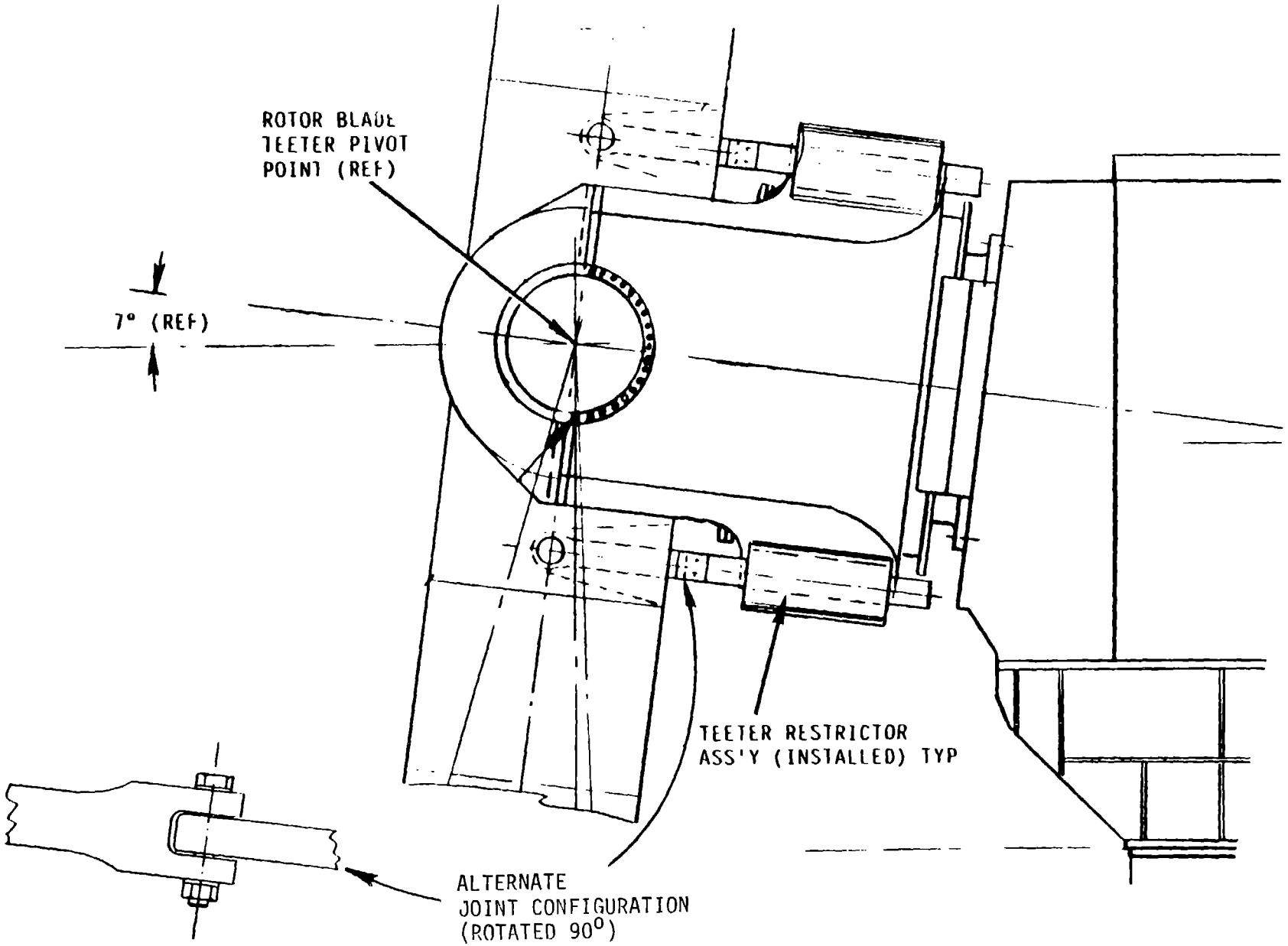

Figure 4-135. Teeter Restrictor Installation

Restrictor

The hydraulic schematic for the teeter restrictor system is shown in Figure 4-136. The rotor pump of the aileron system provides hydraulic power. The pump maintains pressure in two accumulators for the low and high brake stages. The low brake stage applies pressure to one brake, to exert a damping moment of 300,000 ft.-lb. This stage is applied by local control when the teeter angle exceeds ±2.5°. The high brake stage engages all eight brakes, to exert the maximum restraining moment of 2.4×10^6 ft.-lb. The high force brakes are applied by local control when the teeter angle exceeds ±5°. The interface between the control system and the teeter brake hydraulics is shown in Figure 4-137.

The different teeter brake modes are summarized as follows:

In state #1 no brakes are applied. This is the normal condition during blade rotation after an initial startup sequence. Both solenoid valves are continuously rated. They are electrically energized to remove hydraulic pressure from the brakes.

In state #2, the low force brakes are on. When teeter electrical control power is available, the low force teeter brakes are applied and released as a function of teeter angle (α_T), when $|\alpha_T|>2.5°$ or $|\alpha_T|<2.5°$. Local control at the yoke operates per switch SW1.

In state #3, the high force and low force brakes are on. When the system senses $|\alpha_T|>5°$, the local control switch (SW2), opens, removing power from the solenoid valve (V2), and applying the high force brakes. If these events occur during any automatic operating mode after the startup initialization sequence, the control system initiates a normal shutdown after it receives the high brakes on indication from the Sense A signal. Once they are applied, the high force brakes remain on by opening PS2, independently of subsequent teeter angle variations, as the shutdown progresses. As a backup, the control system monitors the analog signal and removes power, to apply the teeter brakes if the analog signal exceeds ±6.5°.

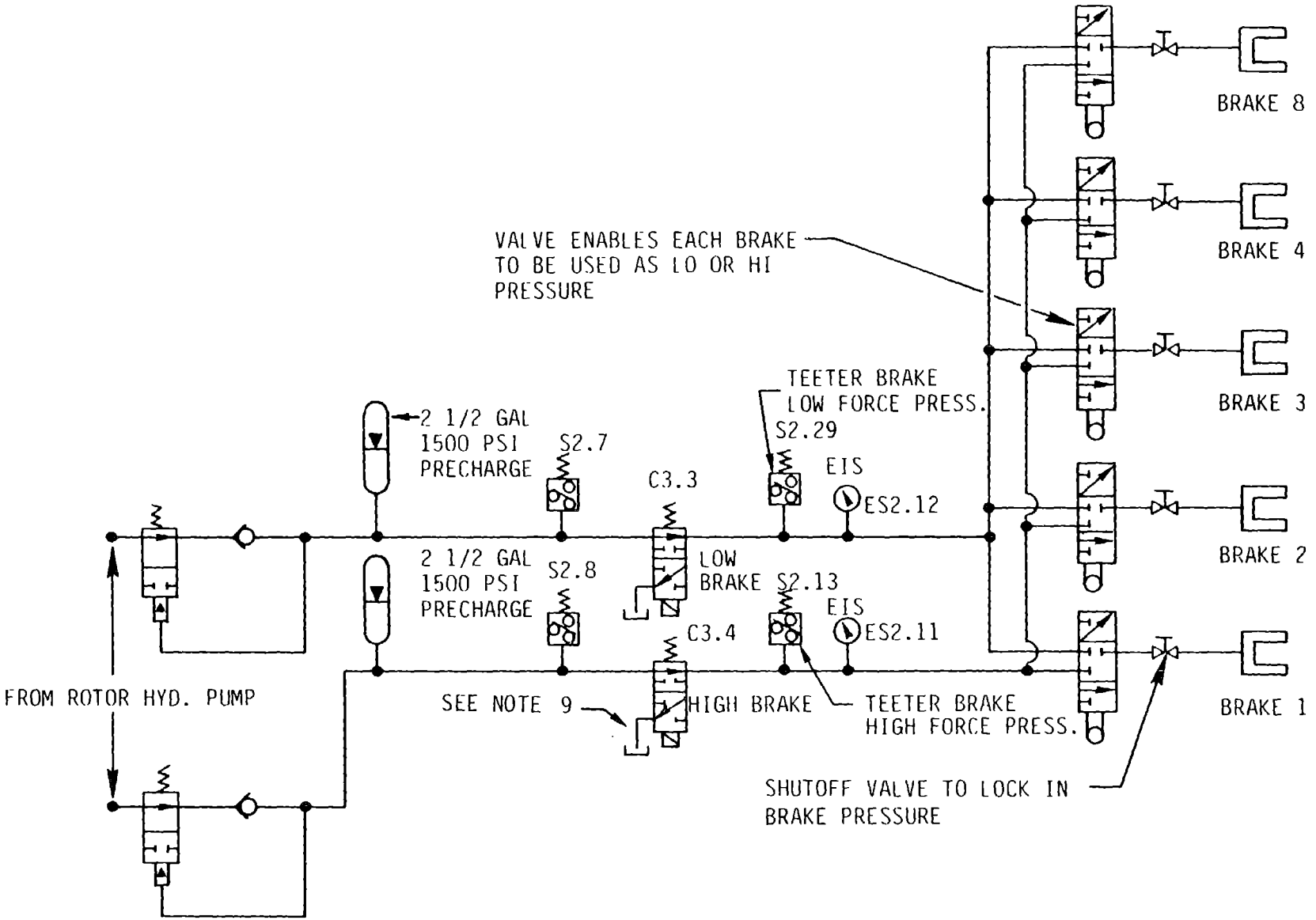

Figure 4-136. Teeter Restrictor Hydraulic Schematic

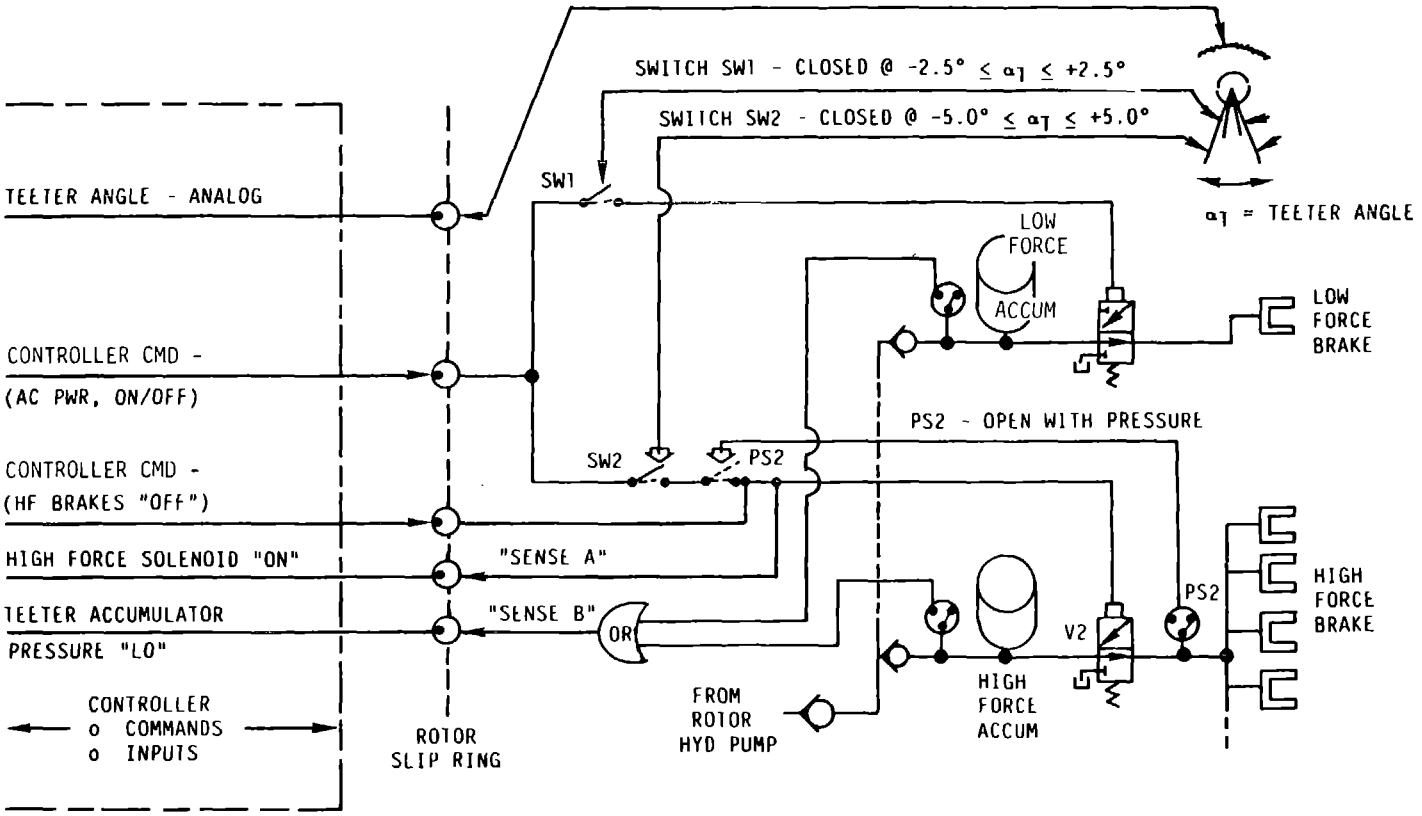

Figure 4-137. Teeter Brake Signal Interface

The portion of the teeter restrictor assembly that is mounted to the yoke is shown in Figure 4-138. The unit is formed by mounting two structural side plates to the pair of caliper brakes and bolting the entire assembly together with the two sets of brake assembly bolts. A top cover is added, and the assembly is attached to the yoke, with two bolts per corner. The roller assembly between the calipers guides the link and reacts the applied moment when only one brake is pressurized. The magnetic switch mounted in the rear of the assembly senses the teeter angle. The assembly is sealed from the environment by two flexible bellows attached to each end.

Bumper

According to the analysis of the dynamics of the wind turbine generator, the maximum teeter angle reached during operation, with the teeter restrictor systems functioning, is less then 6.5°. A bumper stop was incorporated in the yoke design to serve two functions: to provide a controlled impact point in the event of a teeter strike, and to serve as a "soft" stop to brace the rotor during maintenance. Figure 4-139(a) shows the bumper installed on the yoke. It is mounted using the two forward lifting holes on the yoke.

A detailed design of the bumper was not completed by the final report. The design spring rate is approximately 150,000 lb./ft. The bumper was expected to be of steel/elastomer construction, similar to the teeter bearing. Figure 4-139(b) shows a cross-section of the rotor pad bonded to the rotor. This pad engages the rubber at a 7° teeter angle and would completely compress the strip at 9°. A 2.4×10^6 ft.-lb. moment on the rotor would result from this enforced displacement.

Drag Link

The design for the drag link between the brakes and the bolster was reviewed, simplified and found to be satisfactory. A double lap shear bolted joint with preload could replace the machined clevis as shown in Figure 4-135. This

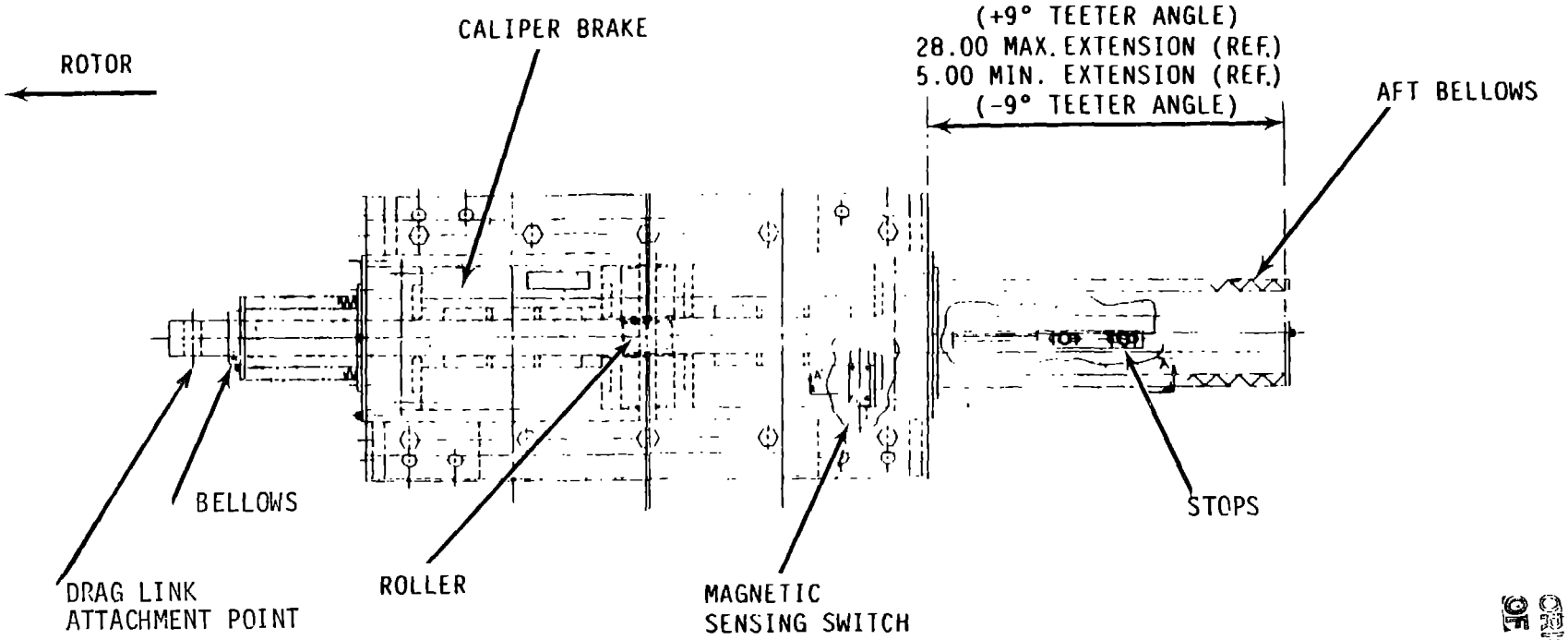

Figure 4-138. Teeter Restrictor System Assembly

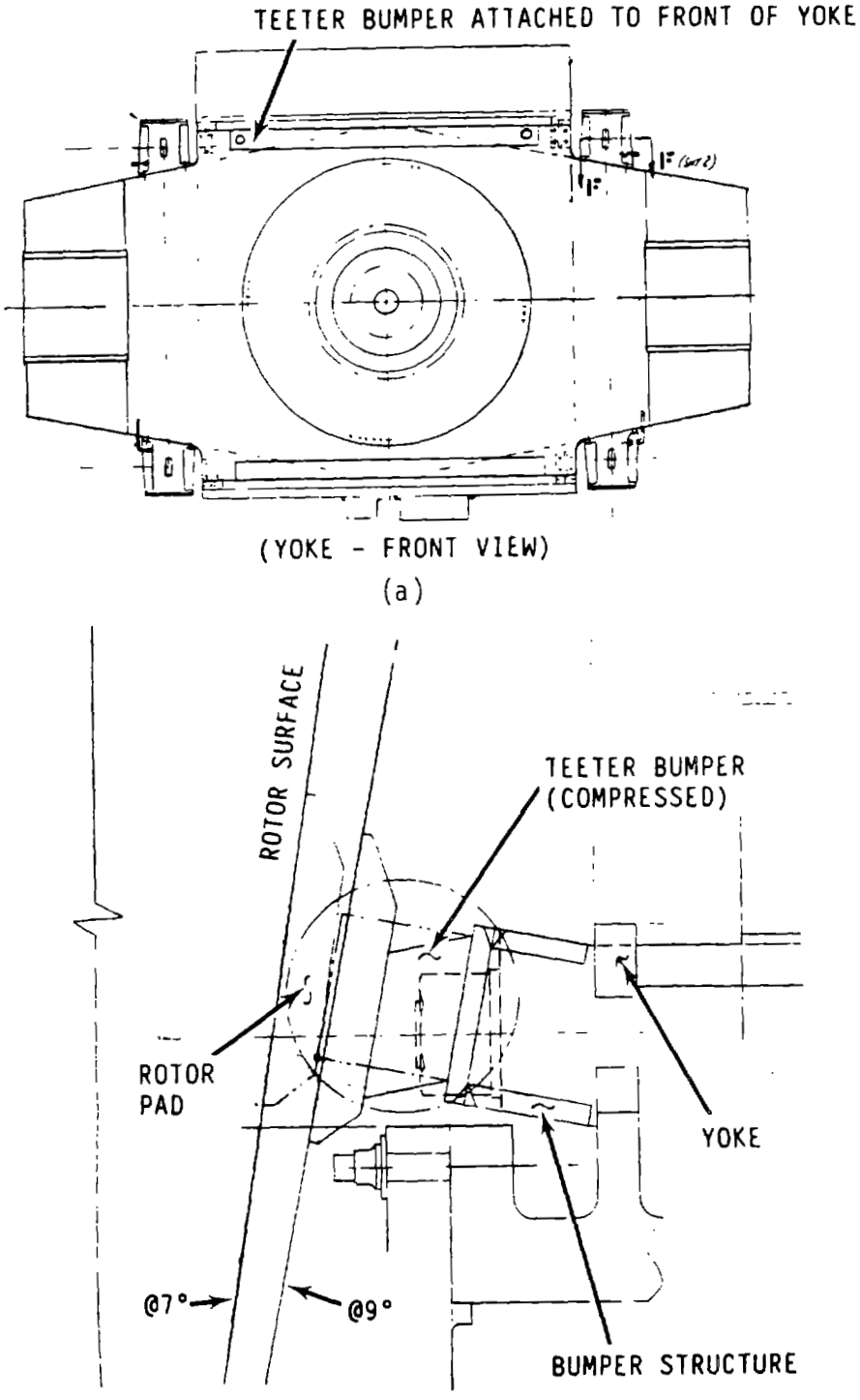

Figure 4-139. Teeter Bumper

assures clamping action which should have a friction capacity greater than the maximum brake load. The bolt could endure the brake load, even if the preload is lost, so the machined clevis with minimal clearances should also be satisfactory.

The maintenance free, self-aligning bearing was chosen because of wear considerations. It's maximum capacity is 1283 kip and its dynamic capacity is 653 kip, according to the catalogue. No stress analysis was conducted on this part. The brake calipers, their housing and its attachment to the yoke were also not analyzed.

The link alternately experiences tension and compression exerted by the caliper brakes. Relative deformations caused by the flapwise and chordwise bending of the blades impose bending stresses in two planes. The teeter motion also reorients the link while the brakes are clamping. This reorientation causes bending in the link, because the link motion includes a component transverse to the stroke as it slides through the calipers.

The fatigue loading from full-force teeter braking occurs less than 5×10^6 times in the expected 35,000 start-stop cycles. The maximum braking force occurs for a few cycles during inflow conditions at low rotor speed. In a tabular histogram in the teeter bearing specification (47A380045), the angle that triggers full-force braking is listed 110700 times in a spectrum of 1467300 cycles of teeter motion. Half-force brake action occurs in 1356600 cycles. No brake force is applied during normal operation at rated rotor speeds.

Pin -- The pin through the bearing can be hollow. Shear stress was the permanent design factor. The pin has an outer diameter of 6.3 in. and an inner diameter of 3.5 in. The pin can be designed to AISC Categories A for principle stress and F for shear stress. Figure 4-70 shows the lower 95% confidence bounds for stress vs. number of cycles (S-N) data described in references 4-5 and 4-7. The damage cycle ratio summation is given in Table 4-54.

Table 4-54 Damage Cycle Ratio Summation

APPLIED STRESS		MINIMUM LIFE		
BENDING	CYCLES	CYCLES	RATIO	SUMMATION
27014	110700	1300000	0.085	
13507	1356600	11000000	0.123	0.208
SHEAR				
11136	110700	714725	0.155	
5568	1356600	20188467	0.067	0.222

The pin is safe for the predicted duty. The load factor that will raise the shear damage ratio to 1.0 is calculated using the slope of the S-N curve.

$$F.S. = (0.222)^{-1/4.82} = 1.366$$

The pin's margin of safety is therefore 0.366.

Link -- The link was analyzed for stress and stability under simultaneous maximum brake drag, maximum relative deformations and maximum transverse drag from reorientation. The maximum combined stress is 11.9 ksi, near the brakes. Although column stability can be estimated to correspond to a critical stress of over 16 ksi, the AISC criteria for multiple loading may be more appropriate. The margin of safety for the AISC criteria is a positive 5% for a 2.75 by 8 in. section. The AISC criteria includes a factor of safety of at least 1.5 for the critical buckling stress level.

The link service splice is capable of carrying the load by friction alone or by bolt shear alone. Bolt shear and lap plate fatigue were calculated, assuming that the bolt lost the preload. The margin of safety in friction is +29%, in bolt shear is +18%, and in lap plate net section fatigue stress is zero for 2×10^6 cycles. When the net section fatigue was identified as the minimum margin, a more accurate estimate was made. The fatigue stress margin of safety for the expected two-force spectrum is 1.07 considering 110700 cycles at the 16 ksi stress range, 1356600 cycles at 8 ksi and category B data.

A category B weld could be used to attach the link to the bearing housing. The maximum stress range at this location will be about 12.0 ksi for an 8 by 2.75 in. section after bending stresses are considered. A "B" weld suggests a margin of safety of 1.22 for the two-force spectrum. This margin permits a welded design to be consistent as an alternative to the preliminary design, which is machined from one piece.

Bearing Housing at the Link End -- The bearing housing resembles a plate loaded in tension by a pin through a hole, as described in reference 4-8. The bearing's outer diameter of 9.055 in. is used as the diameter of the hole in the plate. A plate width of at least 13.175 in. is recommended. The plate thickness should be 3.14 in. The end distance should be at least 6.875 in.

In the housing, the teeter duty is expected to be 110700 cycles at 36 ksi and 1356600 cycles at 18 ksi. The damage ratio summation for category A is 0.47. A load factor of 1.25 would cause a damage ratio of 1.0. The stress margin of safety is 0.25.

STRESS MARGIN SUMMARY

Link Stability (Euler)	0.37+
Link Fatigue at B Weld	1.22
Link Splice Friction Capacity	0.29
Link Splice Bolt Capacity	1.38
Link Splice Bolt Fatigue (2×10^6 cyc at full force)	0.18
Link Splice Net Section Fatigue	1.07
Link End Bearing Housing Fatigue	0.25
Bearing Pin Fatigue	0.37

4.5.6 ROTOR HYDRAULIC SUBSYSTEM AND POWER CONNECTIONS

The rotor hydraulic subsystem provides hydraulic power to the aileron actuators and teeter restrictor brakes. The subsystem consists of a motor-pump set, several accumulators and associated control valving. The hydraulic subsystem is mounted on the yoke. Since the yoke rotates during the operation of the wind turbine generator, the hydraulic subsystem is subjected to centrifugal and alternating gravity loads. The design of the subsystem orientation and configuration takes this loading into account. The support structure was designed to survive the design life of the wind turbine generator, which is 4×10^8 cycles.

To power the ailerons, the subsystem pumps hydraulic fluid from the yoke-mounted reservoir into an accumulator. The fluid is then supplied through flexible hose running from the yoke to the blade, into tubing attached to the blade trailing edge. The hydraulic fluid supply at a pressure of 3000 psi flows through the tubing to the aileron accumulators and actuators, and finally returns to the reservoir during aileron motion.

To operate the teeter restrictor, the hydraulic subsystem maintains an accumulator pressure, which is applied to the caliper brakes by switch controlled valves when the teeter restrictor is required. The schematic describing the hydraulic subsystem is shown in Figure 4-140 (47E382440).

The pump and control valves of the rotor hydraulic system run on electrical power. Power is routed from the nacelle through the rotor slipring to wire conduits that run through the gearbox. The conduits continue through the core of the low speed shaft to the torque plate at the front of the yoke. The wires run through conduits from the torque plate to junction boxes mounted on the yoke, opposite the rotor hydraulic package. The pump motor receives power from one box. Also, control power is routed from the controls electronics cabinet in the nacelle, through the path described above, to another yoke junction box. This power operates the control valves and control functions associated with the aileron subsystem. The schematic describing this circuit for the ailerons is illustrated in Figure 4-141.

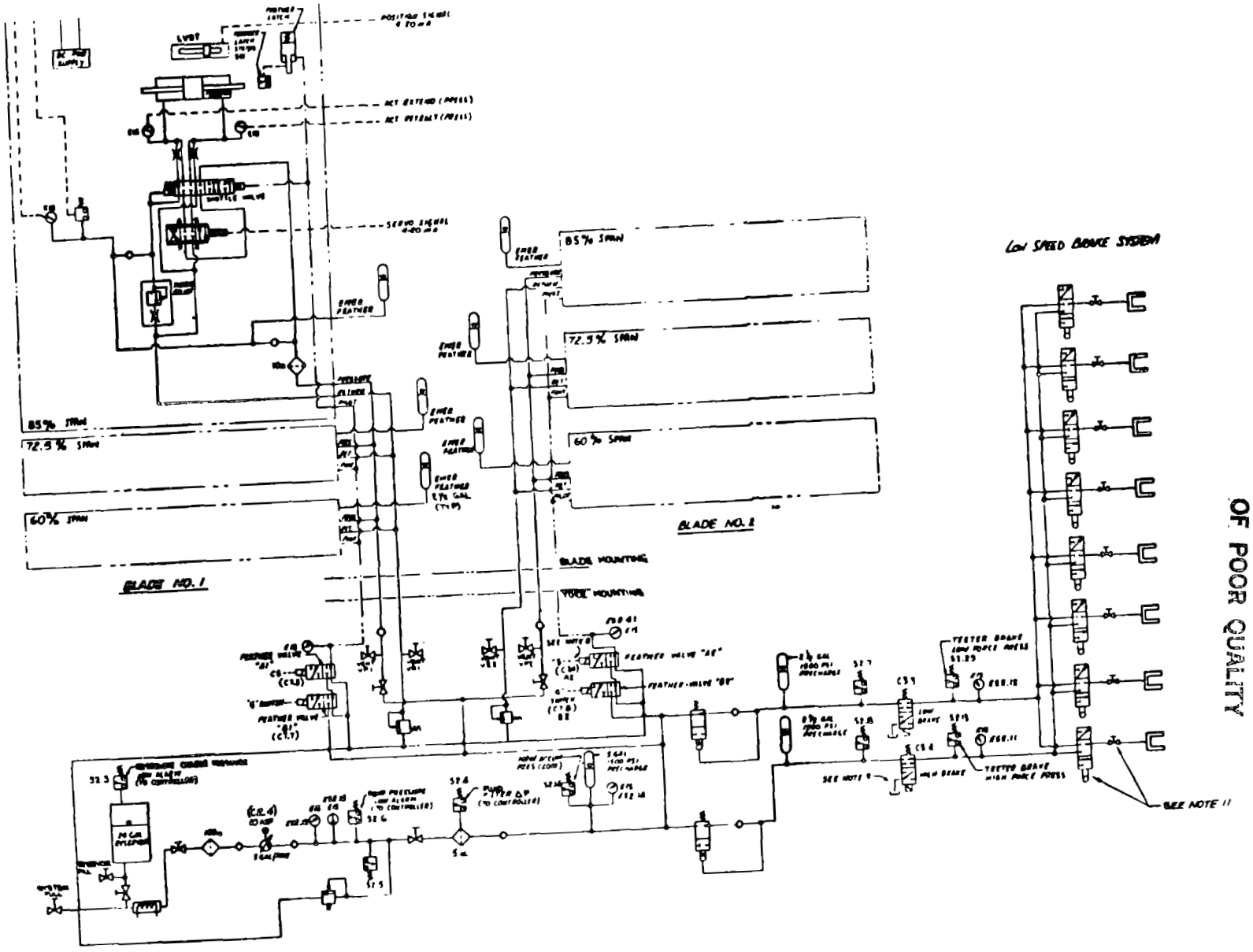

Figure 4-140. Rotor Hydraulic Schematic

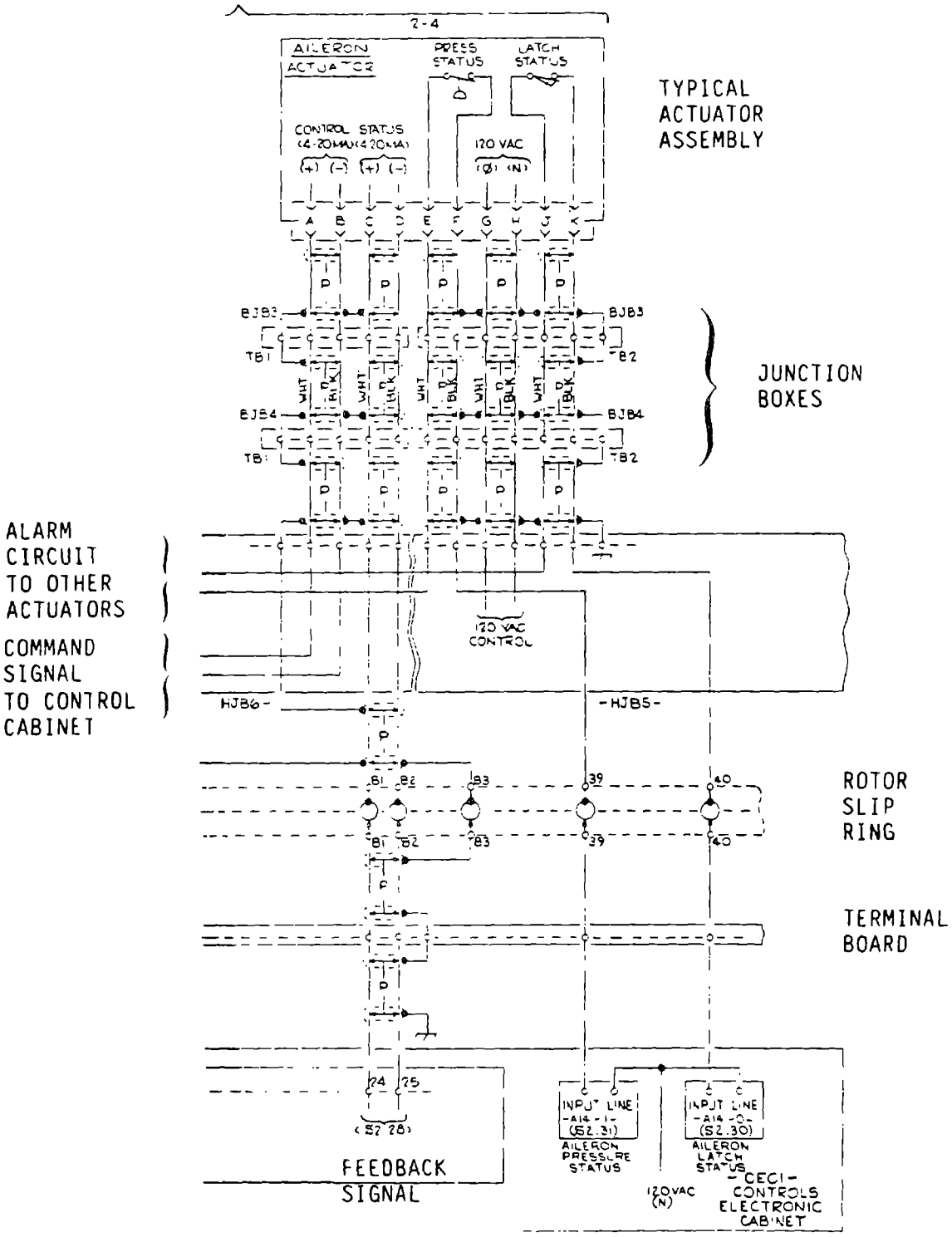

Figure 4-141. Rotor Control Schematic

4.5.7 LOW SPEED BRAKE

The aileron torque control reduces blade speed while the aileron is in the feathered position, but it cannot bring the rotor to a halt. A low speed shaft disc brake was incorporated into the design, for stopping the rotor. The brake can stop the rotor at speeds of 10 rpm and below. This brake also holds the rotor steady during maintenance and service of the rotor and drivetrain.

The brake assembly consists of a disc, mounted with slotted radial holes on the yoke, and a set of eight Goodyear SLC 19 calipers mounted on the rotor support adapter. The disc is made of ASTM A572 grade 50 steel plate, protected against corrosion on the active surface by a plasma sprayed coating of 442 stainless steel. The rest of the surface is painted with zinc-rich primer and corrosion protective paint.

When the brake is engaged it converts a considerable amount of energy from the rotating system to heat. To prevent thermal expansion, the disc is bolted to the yoke by means of slotted bolt holes that permit radial expansion without stress on the yoke. The expected temperature rise is 172°F when the brake absorbs all the kinetic energy of the rotor, which is turning at 10 rpm. The temperature rise is calculated as follows: for a rotor moment of inertia of 50×10^6 slug-ft^2 and a speed of 10 rpm, the kinetic energy of the rotor, KE, to be absorbed by the brake is:

$$KE = \frac{1}{2} (I) W^2$$

Where $I = 50 \times 10^6$ slug-ft^2

$$W = \frac{10 \text{ RPM} \times 2\pi \text{ rad/rev}}{60 \frac{\text{sec}}{\text{min}}}$$

$$W = \frac{1}{2} \times 50 \times 10^6 \times \left(\frac{10 \times 2\pi}{60}\right)^2$$

$$= 27{,}415{,}568 \text{ ft.-lb.} = 35{,}238.5 \text{ BTU}$$

For a disc weighing 2046 lbs., the average temperature increase will be:

$$\Delta T = \frac{Q}{C \times W} = \frac{35{,}238.5}{.1 \times 2046} = 172°F$$

In the MOD-5A service, the temperature gradient at the active surface will be below that experienced in the similar MOD-1 service. Since the low-speed brake on the MOD-1 performed acceptably, no further work was done in this area.

The holding and braking torque of the brake is a function of the area of the brake pistons, per caliper, the number of calipers, the action radius, the applied pressure and the coefficient of friction.

For double surface disc brakes, the braking torque, τ, can be expressed as;

$$\tau = 2 \mu APRN$$

where μ = friction coefficient, static = .4
dynamic = .3

A = Piston area/caliper, 32.5 $in.^2$

P = Hydraulic pressure, psi

R = Effective radius, 64 in.

N = Number of calipers, 8

At an applied hydraulic pressure of 3,000 psi, the MOD-5A low speed shaft brake has a holding torque of 39.94×10^6 in.-lb. and a braking torque of 29.95×10^6 in.-lb.

The resulting deceleration is obtained from the relationship $T = I\ddot{\theta}$

$$\ddot{\theta} = -\frac{T}{I} = \frac{-29.95 \times 10^6}{12 \times 50 \times 10^6} = -.04992 \text{ rad/sec}^2$$

Similarly, the time for the rotor to come to a complete stop from 10 rpm can be obtained from:

$$\dot{\theta} = \dot{\theta}_0 + \ddot{\theta}t$$

$$\dot{\theta}_0 = 10 \text{ rpm} = \frac{10 \times 2\pi}{60} \text{ rad/sec}$$

For $\dot{\theta} = 0$

$$\ddot{\theta} = -.04992 \text{ rad/sec}^2$$

$$t = \frac{10 \times 2\pi}{60 \times .04992} = 20.98 \text{ seconds}$$

After the brake is applied at 10 rpm, and assuming no additional energy was added to or taken out of the rotor by aerodynamic effects, the rotor will stop in about 21 seconds at a braking pressure of 3000 psi. The installation and design details of the brake are shown in Figure 4-142a.

4.5.7.1 Low Speed Holding Brake Stress Analysis

The layout of the low speed holding brake was analyzed using the NASTRAN finite element method. Stress outputs were used unchanged or were adjusted for notch factors, and compared to the applicable design criteria. The loading requirement was a holding capacity of 63 kips per brake and a stopping capacity of 44 kips per brake. As 35,000 start-stop cycles are expected, the design life of 500,000 cycles will include load cycles caused by turbulence when the rotor is parked.

The minimum margin in the analysis of the NASTRAN results is +0.04 in fatigue of the bolts for 500,000 cycles of loading from zero to 50 KIP at each of four brakes.

Figure 4-142b shows the model, and loading of the brake support. An 8 WF x 67 lb./ft. rolled steel beam was used, with a strip cut out of the web and groove welded back together, to reduce the height. The end ribs were 0.875 in. and the intermediate ribs were 0.5 in. A torque box was made by groove welding a 0.75 in. outer web to the edges of the flanges and ribs. Coping was used to avoid intersecting welds. Eight holes, 5 in. in diameter, allow access to the rotor for inspecting, cleaning, painting and tightening nuts. 1.25 in. bolts were used in the corners and the other 42 fasteners were 1.0 in. bolts. All bolts were SAE grade 5.

Flanges, webs and ribs were represented by the QUAD 4 element with membrane, bending and transverse shear properties defined. Beam elements represented the bolts. The bolt ends at the brake ring bottom flange had shear boundary conditions only. The ends 4 in. away, at the opposite face of the front

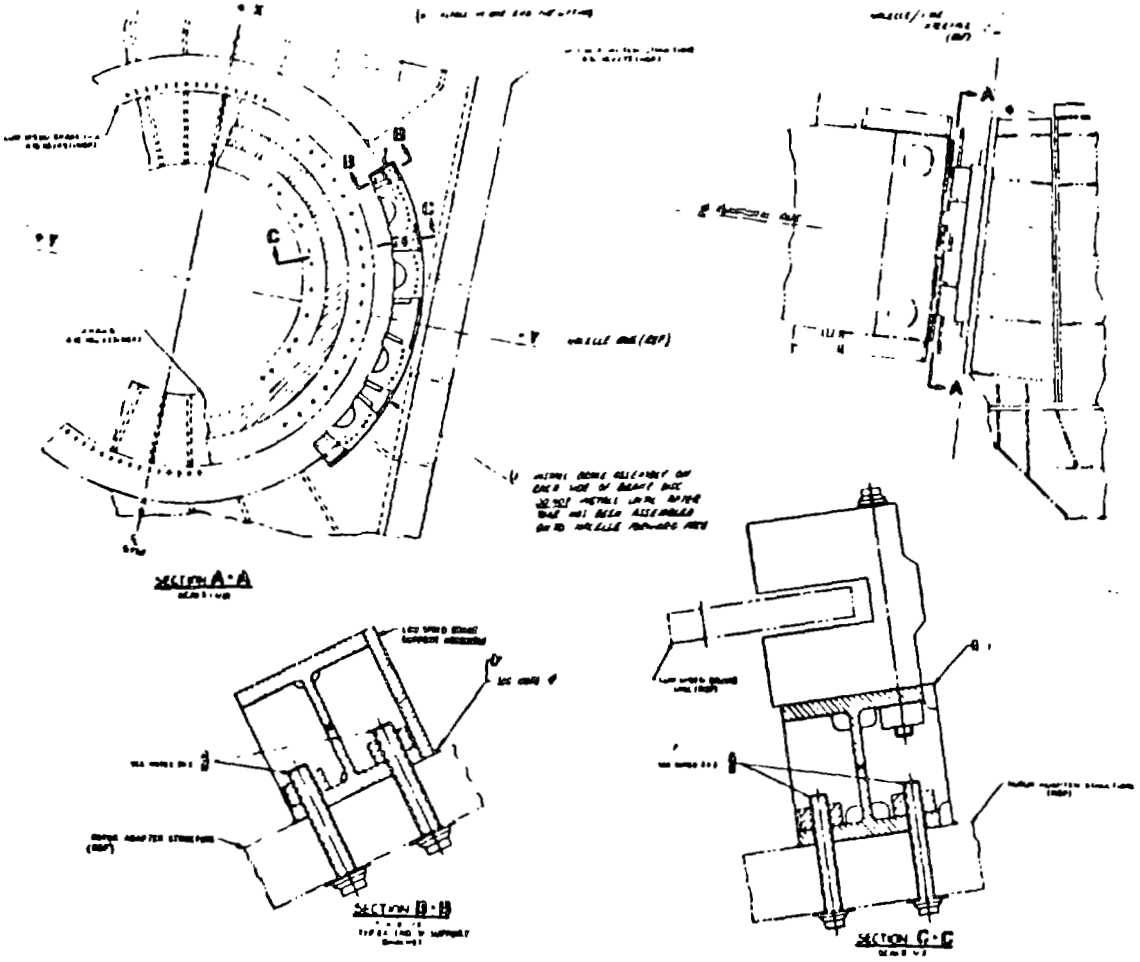

a) ARRANGEMENT & DESIGN

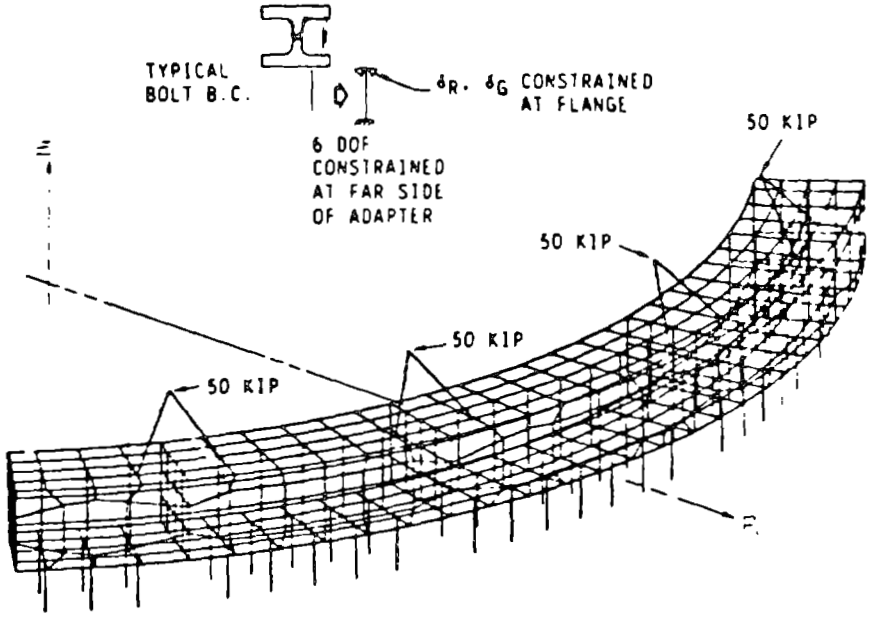

b) MODEL & LOADING

Figure 4-142 Rotor Brake Support

adapter plate, were constrained in all six directions. Thus, bolt stretching and bending were automatically calculated. Preload was not modeled.

Each brake was modelled as a rigid transfer spider. The mesh plot, Figure 4-142b, shows two members for each brake. Members to the compression side of the caliper attachment, which distribute the load to the eight grid joints adjacent to the left leg, were not plotted.

Toeing of the ring segment was supported by boundary conditions at the left edge and at the right inside corner. Other flange deflections that could bear on the adapter plate were less than 0.003 in., so they were not supported. Thus, the model is founded on the 46 bolts, as guided piers, and the toeing constraints. The model revealed an induced bending moment in the bolts, which led to a total stress 1.5 times the stress of direct tension in the corner bolts. Consideration of this stress, and shear in an interaction formula, led to a fatigue margin of safety of +0.04 for the 1.0 in. corner bolts. Consequently, the diameter of the corner bolts was changed to 1.25 in. to improve the margin of safety.

The load of 50 kips, which was 1.15 times the dynamic brake force, was chosen to be a load contingency factor.

The following allowables were used.

		BOLT SAE-5 92YP 120 UTS	BEAM & PLATE A572-G50 50YP 65 UTS
STATIC	TENSION	43.7 KSI	30 KSI
	SHEAR	13.7	17.4 KSI
FATIGUE	TENSION	21.85	13 KSI
($5x10^5$)	SHEAR	6.85	9 KSI

Table 4-55 Low Speed Brake Margin Summary

ITEM	STRESS-PSI	FATIGUE MS	STATIC MS
1.0 in. Bolts	20900	0.25	1.08
Top Flange Principle Stress	10379	0.25	2.89
Top Flange Shear	7688	0.17	1.25
Bottom Flange Principle Stress	9980	0.3	3.01
Bottom Flange Shear	2156	3.16	7.04
Web Principle Stress	9424	0.38	2.06
Outer Web Principle Stress	11894	0.09	1.52
Outer Web Shear	5667	0.58	2.06
Ribs Principle Stress	5687	1.28	4.27
Ribs Shear	2410	2.73	6.19
Friction Interface	252000 LB	-	0.98
Bolt Shear with Loss of Pl	31388 PSI	-	0.71

$$MS = \frac{ALLOWABLE}{PREDICTED} - 1$$

4.6 ROTOR SUPPORT BEARING SUBSYSTEM

The baseline rotor support system uses a stationary shaft, called the spindle, on which a pair of tapered roller bearings are mounted, separated by about 38 in. As shown in Figure 4-143, the bearings are arranged to react the moment and thrust loads that are generated by rotor weight, location and aerodynamic affects. The moment is resolved into radial and thrust loads at the forward and aft bearings. The forward bearing is closer to the center of gravity and experiences a downward radial load of about 1.1×10^6 lbs., while the aft bearing experiences an upward load of 6×10^5 lbs. and is the reaction point for the rated wind thrust load of about 230,000 lbs. The tapered roller bearings were chosen because they reduced the number of parts and simplified the installation.

The yoke rotates on the outer race, and the inner race is fixed on the spindle. The inner race is mounted with about .007 in. diametric clearance on the spindle and clamped in place. The outer race is press fit, with .005 -.010 in. interference into the yoke housing. The shoulders and clamping rings are designed to give the assembly about .020 in. axial clearance. This clearance provides the longest life expectancy under the required performance environment and a potential temperature differential of up to 40°F between the yoke and spindle.

4.6.1 NON-ROTATING SHAFT

The only function of the non-rotating shaft, called the spindle, is to support the rotor. Rotor torque is transmitted through the low speed shaft assembly. Consequently, the key rotor support element is not subjected to cyclical stress reversals, as a rotating support shaft would be. The support has, therefore, a good margin of safety under fatigue loads, and a larger margin under limit loads. The stress analysis of this part is discussed in Section 6.1, Volume III.

Basically, the spindle is a tube with a T-type flange bolted to the rotor support adapter. It contains flanges and shoulders for clamping and supporting the bearings. Because this unit is so important, it will be made from a one-piece forging of ASTM A508 Class 4B steel. Wall thicknesses minimize compliance of the bearing support to ensure long bearing life.

Corner relief at the shoulder minimizes any potential for fretting corrosion to start at that location. To further minimize the potential for fretting corrosion between the bearings and the spindle, the bearing seat will be plasma sprayed with a coating of copper-nickel-indium. This technique was developed and used successfully in large gas turbine bearings (Ref 4-10). The non-rotating shaft is shown in Figure 4-144, "Spindle Shaft, Rotor Support".

4.6.2 BEARINGS AND BEARING MOUNT

The objective of the design of the rotor bearing assembly was to develop a bearing configuration that could react the rotor loads using the fewest bearings. The rotor loads comprise rotor and blade weight, thrust, overturning moment and the dynamic loads induced by wind load and rotational effects. Several configurations were considered: 1) a pair of cylindrical roller bearings, separated by about 38 in., that would react the weight and overturning moment, and a crossed roller bearing that would react thrust, 2) a pair of cylindrical roller bearings and a conventional 2-row, cylindrical roller thrust bearing, 3) a cylindrical roller bearing at the forward position that would react one component of the moment load and a 2-row tapered roller bearing that would react the other moment load component and thrust, and 4) two cylindrical roller bearings arranged so that they react all loads. The latter configuration proved to be the least complex and most economical, so it was chosen for this application.

4.6.2.1 Bearing Design

Experience has shown that bearings should be as far apart as possible under moment loading conditions. The spacing placed the outboard faces of the bearings in a position shown in Figure 4-143. Tapered roller bearings were designed with a dynamic capacity so that the L-10 life* will reach 228×10^6 revolutions. This calculation was an integral part of the bearing life calculations provided by Torrington's GENROL computer program. Torrington Model G 3532A bearings were used in the forward location and G 3531A bearings were used in the aft location. These bearings, Figures 4-145A and 146, have a dynamic capacity of 6,013,000 lbs. and 4,092,000 lbs. respectively.

*(The L-10 life is the length of time after which 10% of the bearings will have failed, according to the manufacturer's definition of failure.)

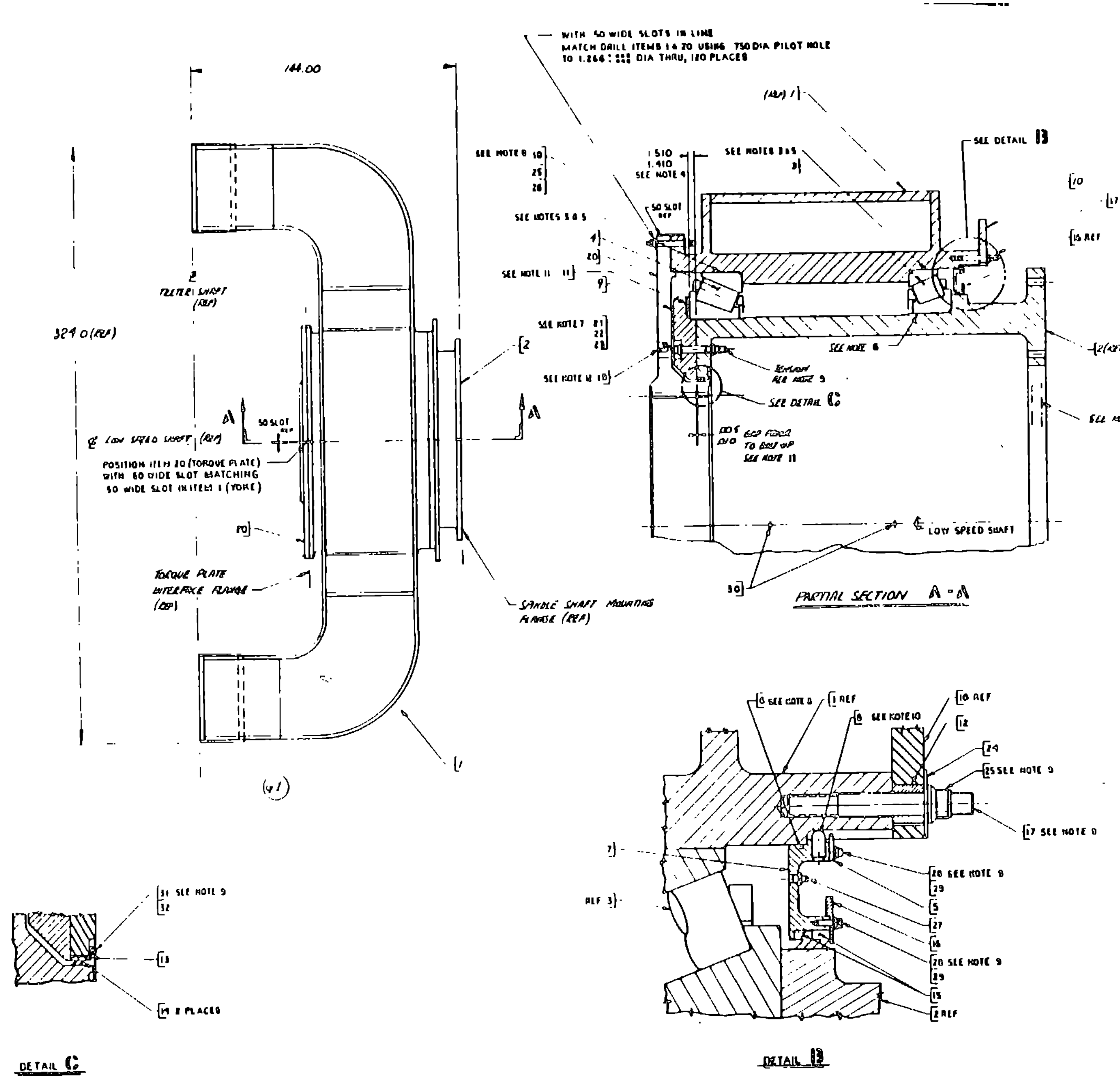

GENERAL NOTES

1. [illegible]
2. [illegible]
3. INSTALL BEARINGS AND SPINDLE SHAFT PER GE SPEC 47A305101.
4. [illegible]
5. [illegible]
6. [illegible]
7. [illegible]
8. INSTALL O'RINGS ITEM 6 INTO SEAL RETAINER ITEM 7 PRIOR TO INSTALLATION INTO YOKE BORE.
9. [illegible]
10. PRESS ANTI ROTATION PINS (ITEM 8) INTO ROTOR SEAL RETAINER, AFT (ITEM 7). PINS TO PROTRUDE FROM HOLE .375 MAX.
11. GRIND UNCHAMFERED FACE OF ROTOR BRG SHIM (ITEM 11) TO GIVE PRELOAD GAP OF .006 TO .010 INS MAX BETWEEN SPINDLE SHAFT (ITEM 2) AND ROTOR BRG RETAINER (ITEM 9).
12. PRESS FIT PLUG (ITEM 15) INTO TORQUE PLATE (ITEM 20) UNTIL FLUSH WITH OUTSIDE SURFACE.
13. ESTIMATED WEIGHT 120,000 LBS.

Figure 4-143 Yoke Spindle Assembly

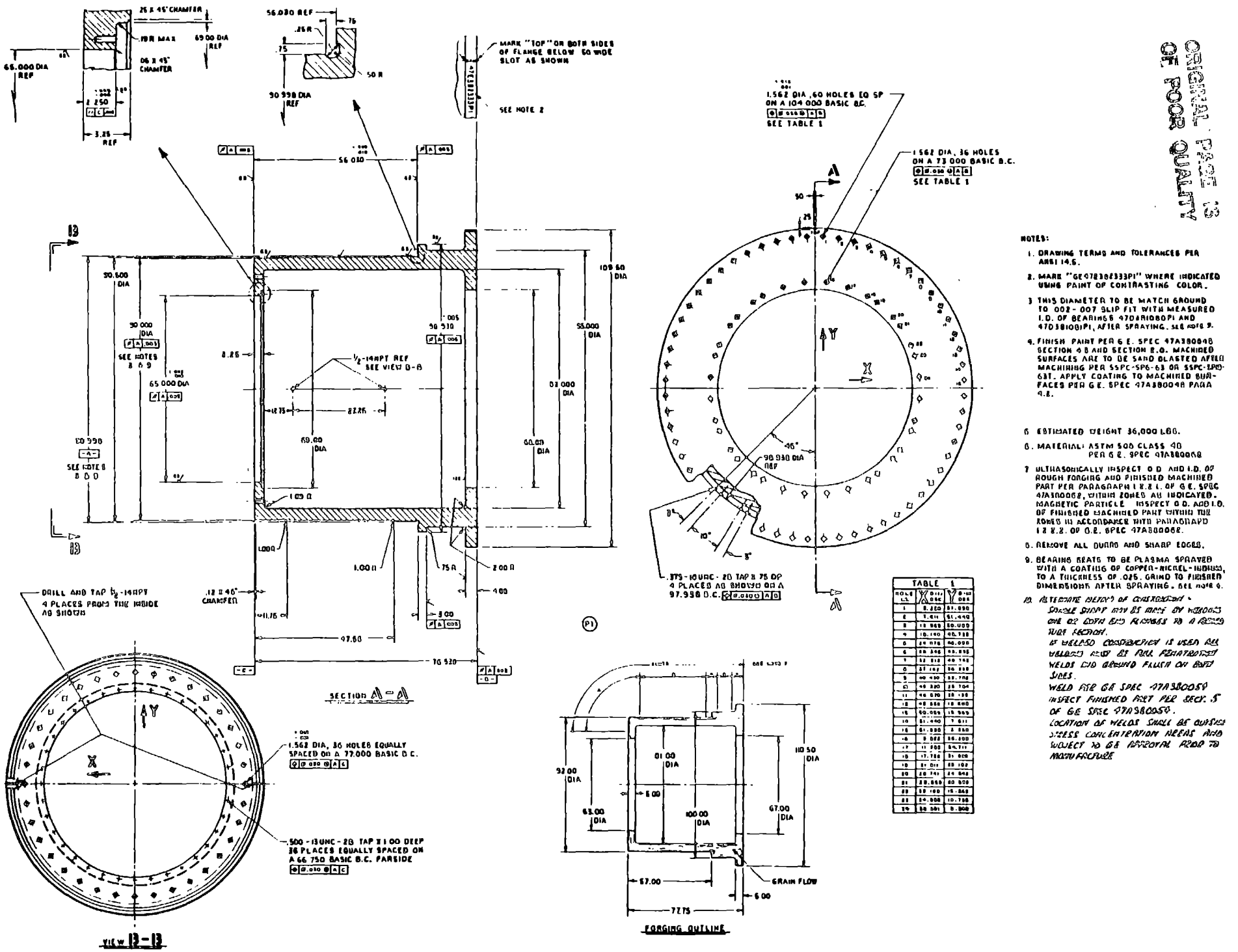

Figure 4-144 Spindle Shaft Rotor Support

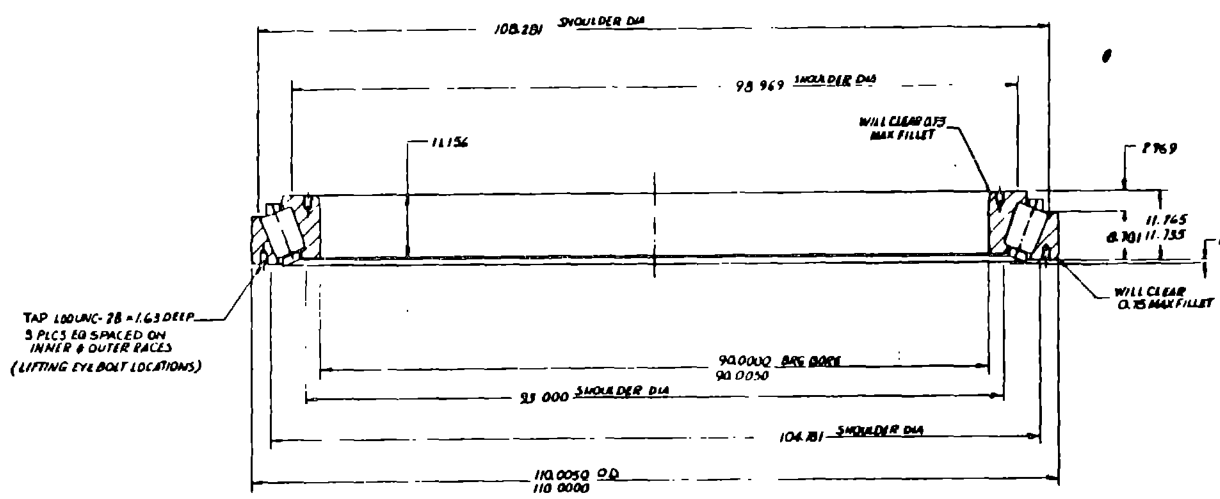

NOTES:

1- FOR DESIGN FABRICATION & INSPECTION REQMTS BEARING MUST CONFORM TO GE SPEC ... FOR INTERFACE & ASSY SEE DWG ...

2- MFG TOL (INCLUDING FLATNESS, CIRCULARITY, CONCENTRICITY, ETC) UNLESS OTHERWISE NOTED ON DWG OR SPEC TO BE PER MFR RECOMMENDED PRACTICES FOR LARGE TAPERED ROLLER BRGS.

3- PART TO BE MARKED WITH VENDOR'S IDENTIFICATION AND MARKED "0E47D361061P1" BY TAG.

4- EST BRG WT 8250 LBS.

5- DRAWING TERMS & TOLERANCES PER ANSI-Y14.5.

6- PERFORMANCE REQMT:

RACE ROTATION - ROTATING OUTER RACE, STATIONARY INNER RACE
RADIAL LOAD - 1,600,000 LBS WITH ... CYCLIC LOAD ...
THRUST LOAD - 388,000 LBS (INFREQUENT OCCURENCE)
RADIAL IMPACT - 3,000,000 MAX OF 2 SEC MAX DURATION OCCURRING 10,000 TIMES DURING LIFE OF BEARING (THIS IS DUE TO TEETER SNUBBER ACTION & IS NOT TO BE SUPERIMPOSED ON RADIAL LOAD)
ROTATION - 15.85 RPM, 25 RPM MAX
REVOLUTIONS - 228 x 10⁶
LIFE - 30 YEARS

Figure 4-145 Main Rotor Bearing - Forward

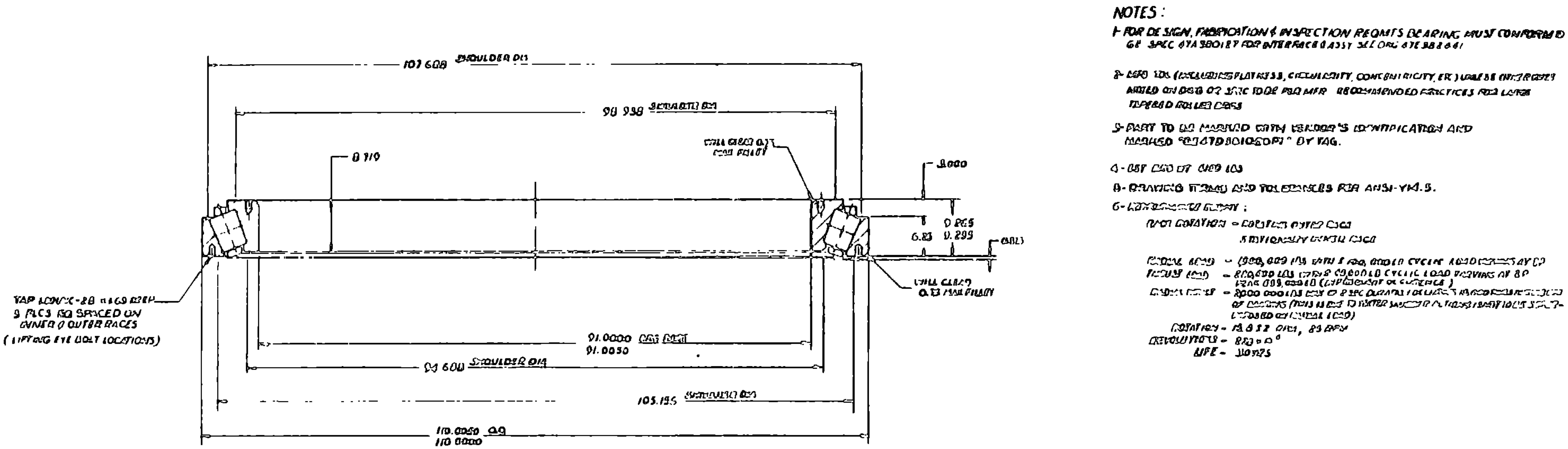

Figure 4-146 Main Rotor Bearing - Aft

Analyses conducted on the results of the GENROL program used specified loads and a speed of 15.35 rpm, the average operating speed. Note that these analyses were made either with the loads positioned as specified or with the loads shifted along the axis of rotation to the midpoint between the two bearings. For the shifted load, a moment load was added about the axis, perpendicular to both the loading axes.

The analyses confirmed that the same results are obtained with the specified load or the shifted load. The purpose of shifting the loads is to permit mechanical errors, such as out-of-roundness and torsional warp to be introduced into the bearing mounts. Three degrees of freedom were required for both loading conditions because of the limitations of the computer program. This prevented analyses of the effects of misalignment between the shaft and housing. However, this misalignment can be kept well under .0001 in., and is believed to be negligible.

It should be noted that the L-10 lives used from the GENROL calculations for all analyses were those made using an exponent of 3 in the load-life relationship. While an exponent of 4 may be used for a true line contact, the lower exponent is more conservative. The reliability calculations used the Weibull slope of 1.5 in all races.

To further enhance the bearing design, advanced technology was incorporated into the design of the contour of the roller crown. Torrington developed this technology to minimize the stress caused by contact between the roller and the raceway when the bearing is misaligned or skewed, and eliminate stress concentrations caused by loading rollers over the end of the roller. This roller profile was developed for both of the proposed bearings. This was based on the heaviest load computed by GENROL for zero internal radial clearance, and on a load equal to 20% of the dynamic capacity of the bearing. This value exceeds the bearing loads under specified operating conditions. Using these profiles, the contact stresses were calculated and plotted for the most heavily loaded inner race contact for a load of 20% of the dynamic capacity of the bearing and a bearing slope of .0005. These plots are shown in Figures 4-147 and 4-148.

STRESS (KPSI) VS. CONTACT AREA

JOB REF.: G-3531-A LOAD = BDC/5 BRG. SLOPE = .0005
RUN # : 5897
MAX PRES: 169903 PSI

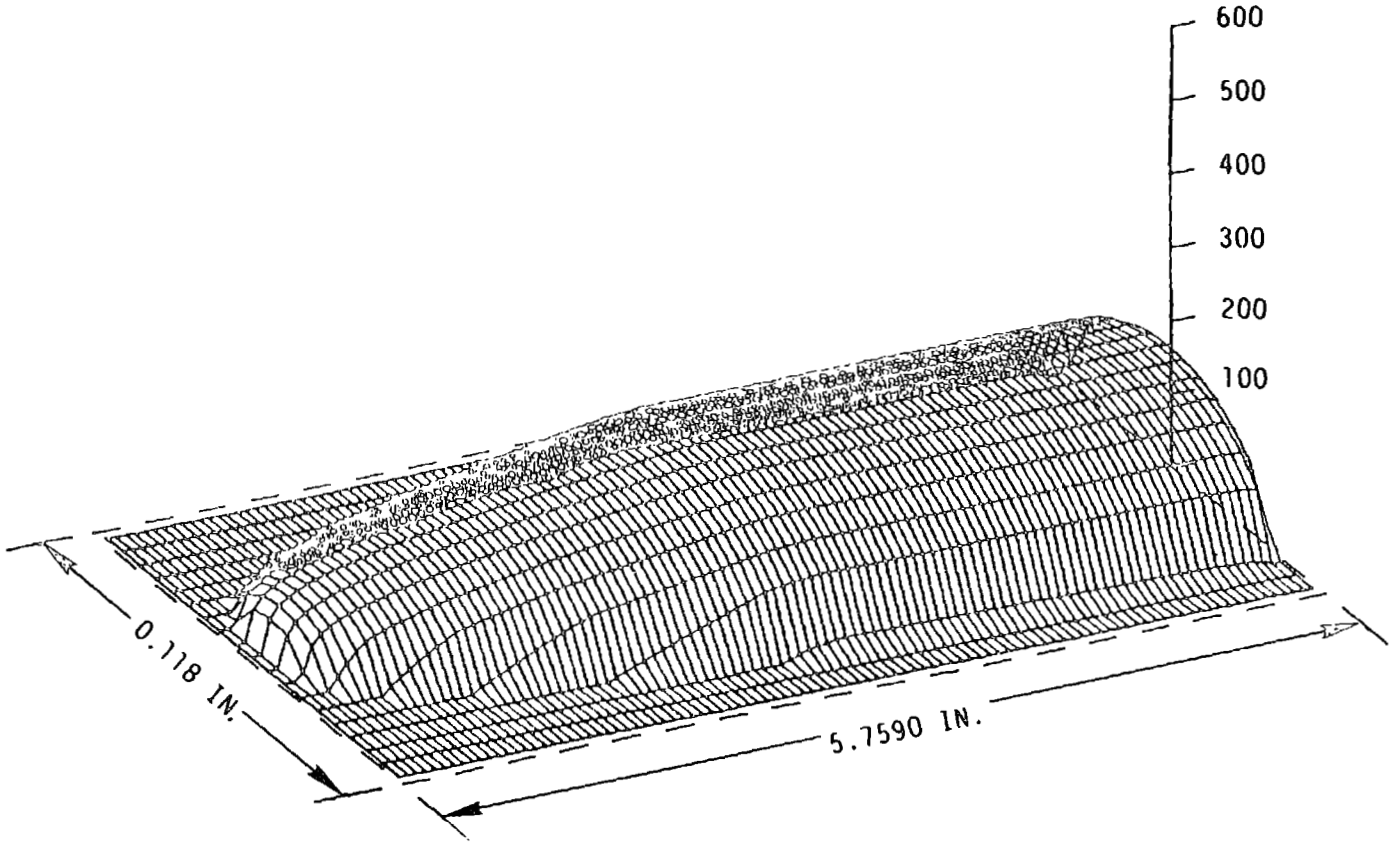

Figure 4-147 Contact Stresses

STRESS (KPSI) VS. CONTACT AREA

JOB REF.: G-3532-A LOAD C/P = 5 BRG. SLOPE = .0005 OPTROL
RUN # : 5896
MAX PRES: 174184 PSI

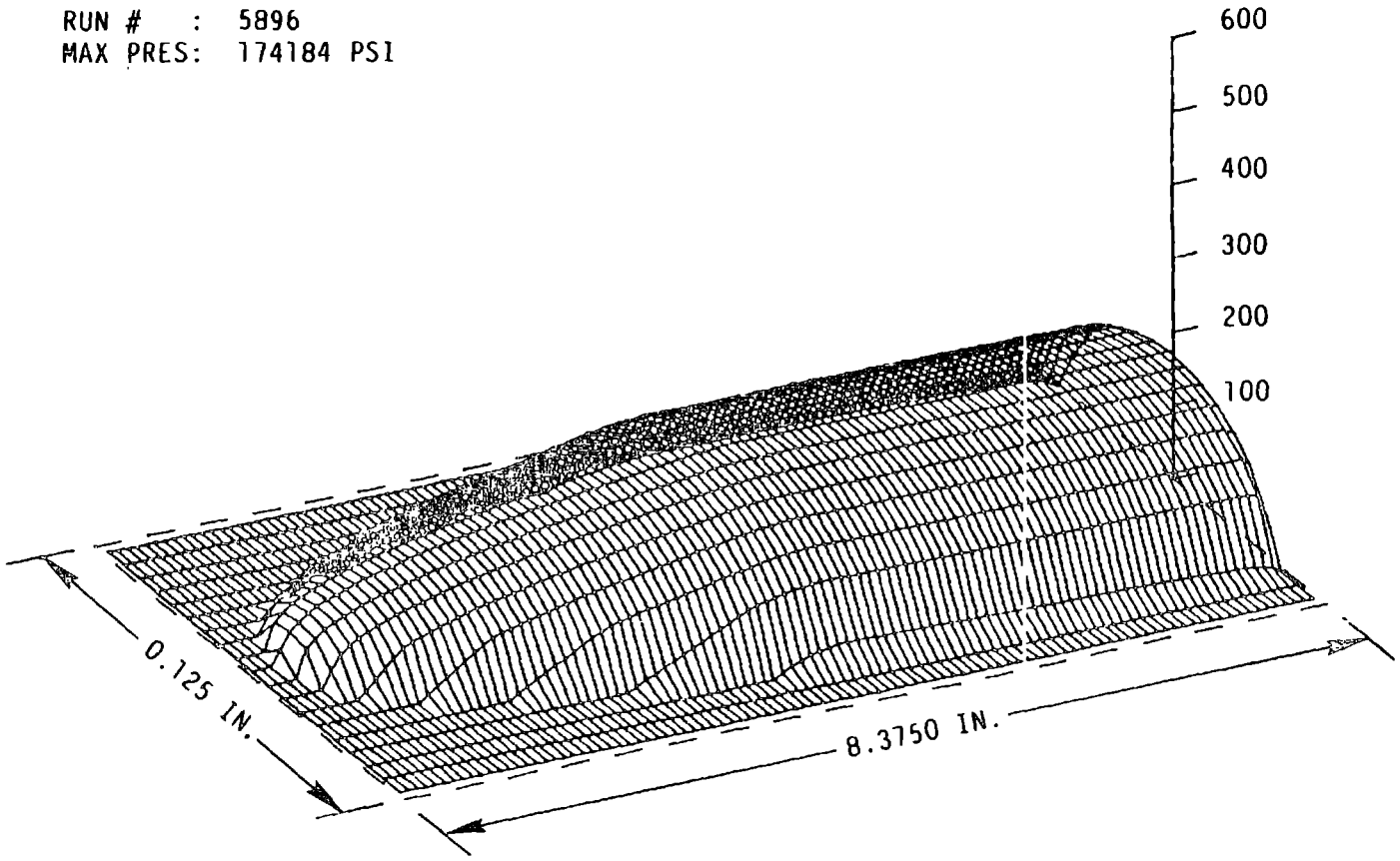

Figure 4-148 Contact Stresses

4.6.2.2 Flange Load

The roller contact surface of the inner race flange is part of a true sphere, ground to the radius calculated in the design of the bearing geometry. The end of the roller that contacts the flange is also part of a true sphere. The ratio of the radius of the roller end to the flange radius is known as the conformity. This ratio must be less than 1.0 for lubricant to provide a separating film. Contact stresses would be very high if the conformity were 1.0 or greater, particularly if mechanical errors, such as misalignment and skew affected the bearings. All bearing manufacturers consider conformity a proprietary value. Further analyses of the proposed bearing developed the maximum roller load against the flange and the contact pressure of the roller load, for loads of 20% of the bearing's dynamic capacity and a slope of .0005. Plots of the contact stresses are shown in Figures 4-149 and 4-150.

Similar bearings are used successfully in tunnel boring machines, where the loads are almost completely thrust and moment loads. Since the values for the flange load and pressure on the proposed bearings are within the range of values for tunnel boring units, the performance of the contacts between the bearing roller end and flange should be satisfactory.

4.6.2.3 Lateral Clearance

In order to determine the lateral clearance for this bearing system, the GENROL program used a series of varying lateral clearances, and maintained the specified axial and radial loads on the bearings along the inclined axes. The spacing between the bearings conformed to that shown in Figure 4-143. The L-10 life of the bearing system, computed in hours at 15.35 rpm, was converted to revolutions. The L-10 life equaled 228×10^6 revolutions over a range of lateral clearances, between approximately 0.013 in. preload and 0.028 in. endplay. A higher preload reduces the L-10 life rapidly, and greater endplay reduces the L-10 life less rapidly.

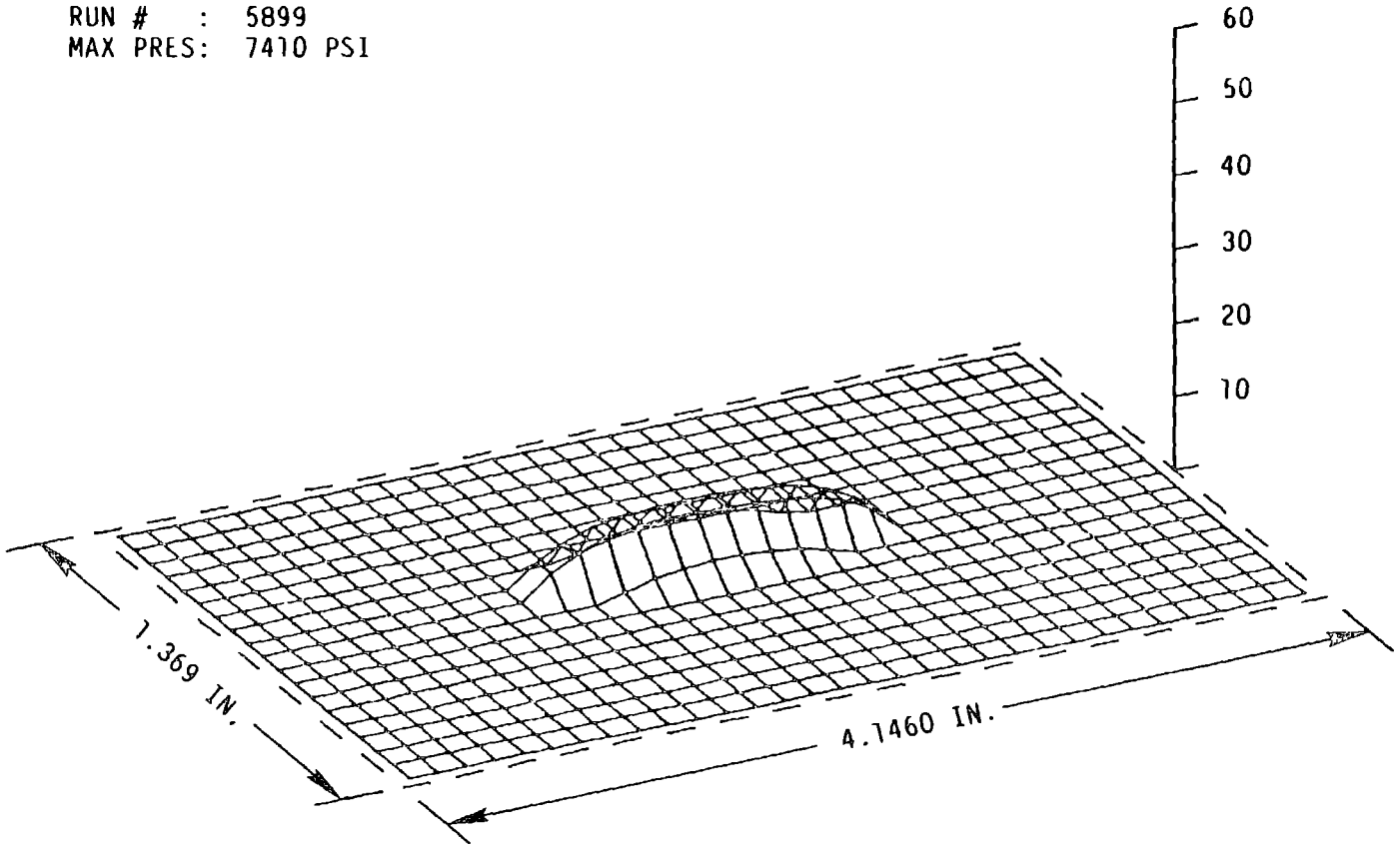

Figure 4-149 Contact Stresses - Flange

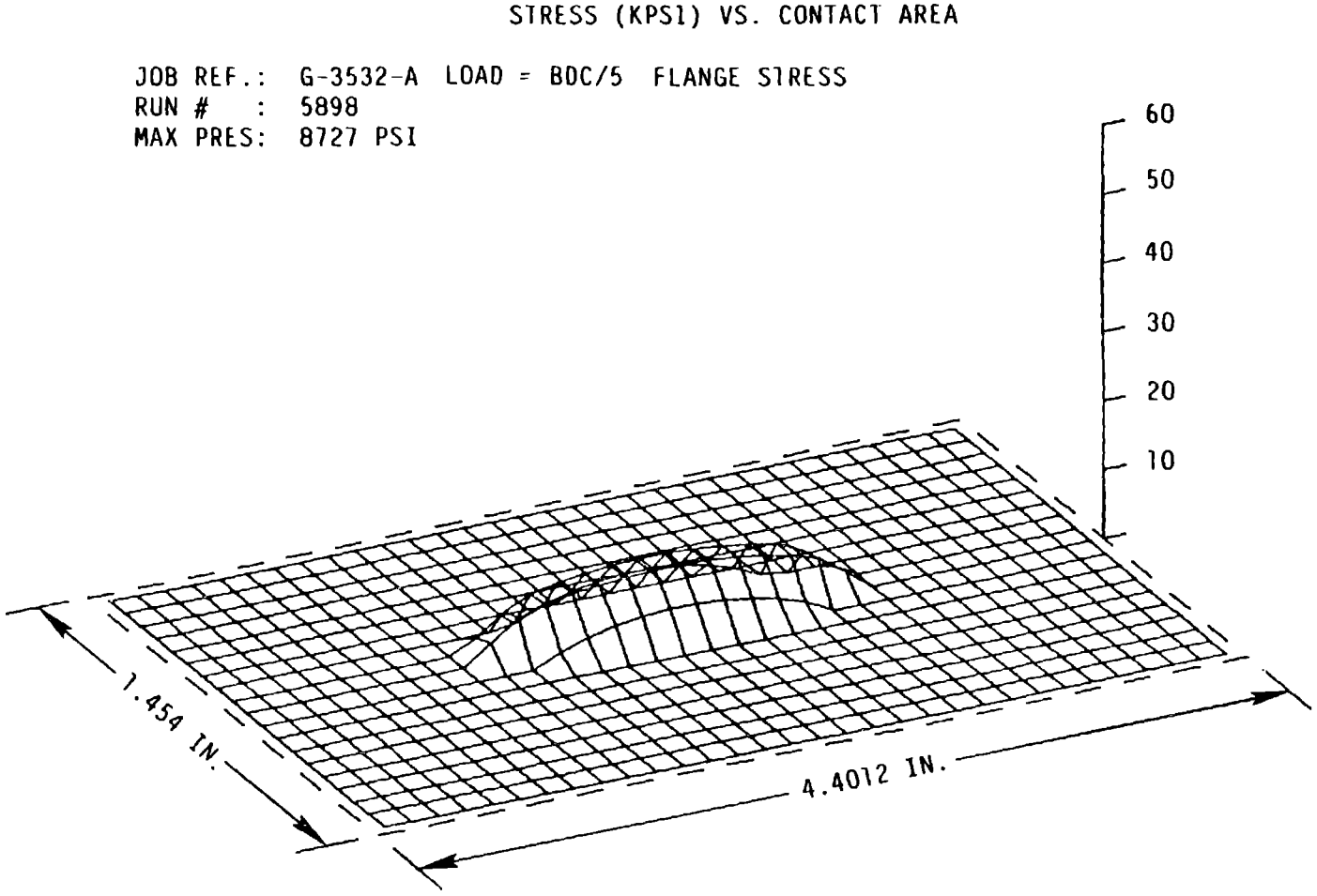

Figure 4-150 Contact Stresses - Flange

The temperatures of the bearing components affect the L-10 life of the bearing. A temperature gradient across the bearing section will cause the inner and outer races to expand, but at different rates. If the outer expands more than the inner, the internal radial clearance increases. The ratio of lateral clearance to radial clearance is 2.5 for the proposed bearings, so that the lateral clearance increases .0025 in for each .0010 in. increase in radial clearance. The differential expansion in internal radial clearance may be calculated as follows:

$R.C. = 6.5 \times 10^{6}$ P.D. x T.

R.C. = radial clearance
P.D. = pitch diameter = 100.7
T = the difference in temperature

The lateral clearance relation reduces to $L.C. = 1.636 \times 10^{-3}$ T. This relation is rigorous, assuming only that the temperature of each roller is halfway between that of the two races.

Bearing operation causes the bearing temperature to increase. The temperatures of two races increase at different rates; the inner race heats faster. At stabilized conditions the temperature of the inner race will be no more than 10°F above that of the outer race. This gradient will result in a maximum reduction of .016 in. in lateral clearance. Thus, a lateral clearance setting of 0.010 in. endplay, when the races are at equal temperatures would result in a lateral clearance of 0.006 in. preload when the inner race is hotter. This condition is nearly optimum.

Mechanical Errors

A preliminary analysis was made of the effect of torsional warp and out of roundness of the bearing races. Computer runs considered torsional warp of +0.0005 in./in. This analysis was made over a range of lateral clearances, and the results were compared with L-10 life data computed without torsional warp. This data is plotted in Figure 4-151. It shows very little reduction in the L-10 life at any value of lateral clearance. Torsional warp of up to .0005 in./in. can be considered negligible.

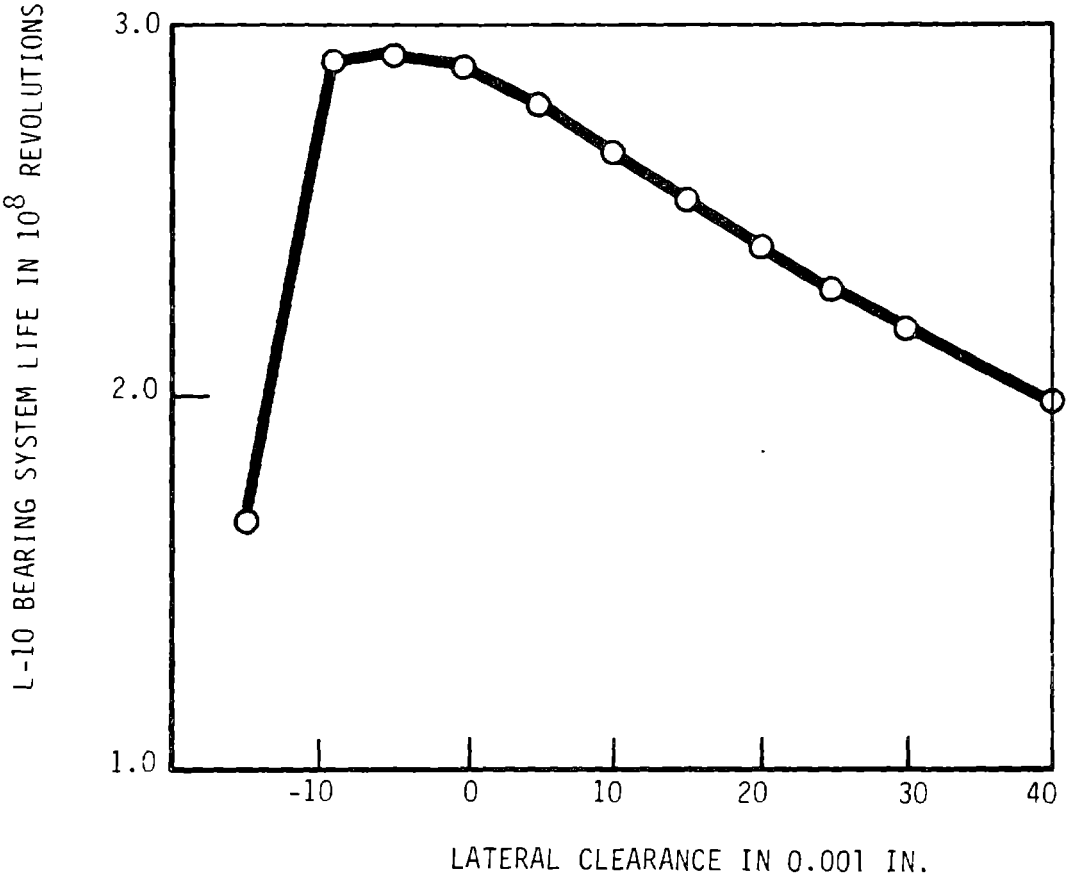

Figure 4-151 Bearing Life (L-10) vs Lateral Clearance

Bearing Mount

To assure a 30-year bearing life, under the load conditions created by the overhanging rotor mass, the bearing housing formed by the spindle and yoke was designed for maximum stiffness. For example, the total deflection of the spindle at the outboard bearing relative to the inboard bearing is only .00129 in. The resulting average bearing slope is only .0000282. Shoulders on the stationary spindle and rotating yoke clamp the bearing pair and locating centers. To install the yoke and spindle assembly, shrink fit the outer races into the yoke housing; seat them properly against the shoulders. Mount the inner race and roller and cage assembly of the inboard bearing on the spindle with .005 - .010 in. between the spindle and the inner race. With the rotating axis vertical, slip the yoke over the spindle, until the outer race of the aft bearing contacts the roller assembly. While Keeping the yoke concentric with the spindle, slip the inner race and roller and cage assembly of the outboard bearing on the spindle. Rotate the yoke, which sits on the spindle, two revolutions and tighten the preload snugly. With a jack, put a lateral load of 10,000 lbs. between the yoke and the spindle at the outboard end and measure the radial gap between the bearings over the circumference. Then put an equal load at the diametrically opposed location and measure the gap again. The gap should vary 10 $\pm$ 2 mils. Tighten the clamping bolts until that reading is obtained. Measure the gap between the spindle flange and the clamping ring.

Grind the measured amount off the bearing shoulder shim ring. Reinsert and tighten the bolt to the value indicated in Figure 4-143.

4.6.3 BEARING LUBRICATION SYSTEM

The baseline bearing lubrication system will be a centralized automatic grease lubrication system that will periodically inject grease into the bearing assembly at a rate that will consume about 55 gallons in one year. Although the injection pressure will be low, the lip seals will permit some grease to extrude. However, most of the grease will return to a collection container in the nacelle through a return line containing a check valve with a very weak spring-loaded check valve. The lubrication system is produced commercially by Lincoln St. Louis, Alemite and other vendors. The grease will have to meet certain oil viscosity requirements. To meet the life requirement, the grease

has to contain oil with a viscosity of 4600 SUS at 100°F and 220 SUS at 210°F. An example of a good grease is Mobilux EP111, manufactured by the Mobil Oil Co. It contains an oil soluble molybdenum additive that will not react with water to form corrosive compounds.

Oil lubricating systems were ruled out, because the seals do not provide a reliable barrier. Oil spills have occurred because of defective seals.

References

4-1 Manual of Steel Construction, 8th Ed., American Institute of Steel Construction ©1980

4-2 "Effect of Weldments on the Fatigue Strength of Steel Beams" J. W. Fisher, et. al., NCHRP Report #102, 1970, Transportation Research Board, Washington, DC

4-3 "Fatigue Strength of Steel Beams With Welded Stiffeners and Attachments", J. W. Fisher, et. al., NCHRP Report #147, 1974.

4-4 Fracture and Fatigue Control in Structures, L. T. Rolfe and J. M. Barsom, Prentice-Hall, Inc. ©1977.

4-5 Mechanics of Composite Materials, R. M. Jones, Scripta Book Company, ©1975

4-6 "Effect of Weldments on the Fatigue Strength of Steel Beams" J. W. Fisher, et. al., NCHRP Report #102, 1970, Transportation Research Board, Washington, DC

4-7 "Fatigue Strength of Steel Beams With Welded Stiffeners and Attachments", J. W. Fisher, et. al., NCHRP Report #147, 1974.

4-8 "Stress Concentration Factors Around a Central Circular Hole in a Plate Loaded Through a Pin in Hole", M. M. Frocht and H. N. Hill, J. Appl Mechanics, Vol. 7, No. 1, P. A-5, March, 1940.

4-9 "Probabilistic Design - Part I", E. Haugen and P. Wirsching. Machine Design, April 17, 1975.

5.0 DRIVE TRAIN SUBSYSTEM

5.0 DRIVETRAIN

The power generating torque is transmitted from the rotor to the generator by the drivetrain. The drivetrain consists of a low speed shaft and gear couplings, a speed-increasing gearbox and a high speed shaft with flexible couplings, as shown in Figure 5-1. The input speed varies between 13 and 17 rpm, with a maximum of 22 rpm. The input torque at the low speed shaft is 3.38×10^6 ft.-lb. The gearbox multiplies the speed by 82.14, so that the input to the generator varies between 1067 and 1396 rpm, with a maximum of 1800 rpm.

The rotor weight is supported by a separate yoke and spindle so that the drivetrain elements are not required to carry the rotor weight as a cantilever bending load. Thus, the low speed shaft transmits only torque from the rotor to the gearbox and stress reversals in the drivetrain are completely avoided during normal operation.

5.1 TORQUE PLATE

The torque plate connects the yoke to the low speed shaft. The plate is a large disc, with a splined inner diameter. The outer diameter of the disc is bolted to the yoke. The function of the torque plate is to transmit rotor torque from the yoke into the shaft. The torque plate and bolts were designed to resist the static loads exerted by the weight of the low speed shaft and couplings, and the dynamic torque loads exerted by the rotor.

A spline connection was selected to connect the low speed shaft to the torque plate and to the gearbox. The spline permits small angular motions of the connection without causing large bending stresses. A flanged gear coupling would provide the same relief, but with a more costly large flange. A solid bolted flange connection would produce unacceptable stress levels because of weight and alignment cyclic variations.

The emphasis of the design was on the splined coupling. A gear coupling with grease lubrication was chosen early in the design effort. Commercially available couplings were investigated, but the best cost and weight advantages were achieved by custom designing the splines using methods described in "When Splines Need Stress Control", by Darle W. Dudley (Product Engineering, 23

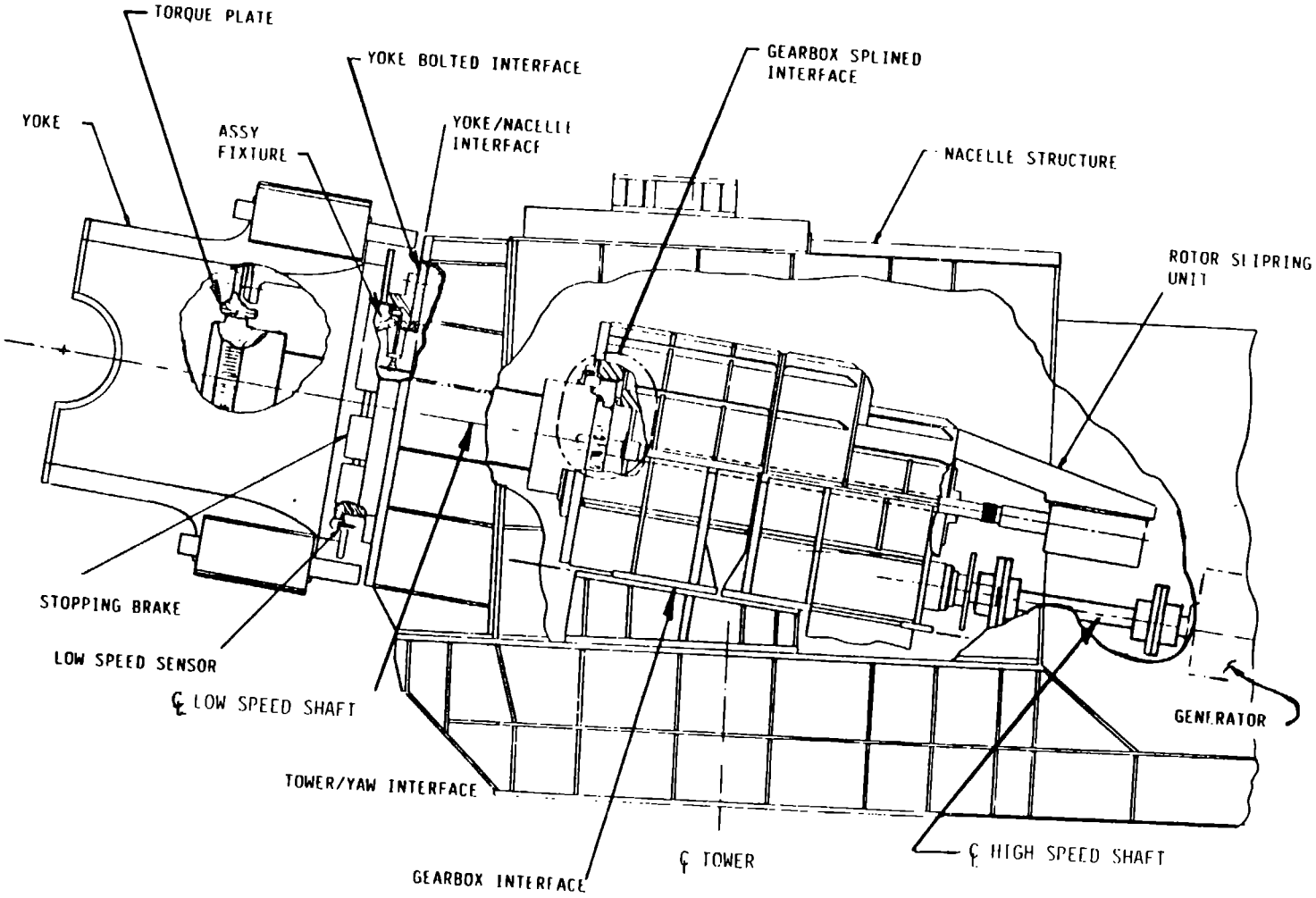

Figure 5-1 Drive Train Interfaces

Dec., 1957). Alternating and steady state stresses were considered in determining the size of the spline. The effective length of the spline is 7 in., at a pitch diameter of 57 in.. The base material is a hardenable steel with a minimum core hardness of 300 BHN, and is treated to a minimum surface hardness of R_C 46. The torque plate and the mating coupling hub are shown in Figure 5-2.

5.1.1 SUPPORTING STRESS ANALYSIS AND MARGINS OF SAFETY

First order calculations using design loads from a coupled dynamic analysis of the system predicted the stress in the torque plate. The friction capacity of the joint was 2.25 times the maximum torque (5.1×10^6 ft.-lb.), using a static coefficient of friction of 0.2. Close tolerance bolting controlled bolt bending if friction capacity is lost or overcome. 123 bolts, with a diameter of 1.25 in. were installed in holes 0.03 in. larger than the fastener's diameter. The bolts are 140 ksi UTS steel. The capacity of one third of the bolts under shear loads is 1.5 times the maximum torque.

The fatigue stress range at the fillet at the 70-in. diameter was 5075 psi. The fillets are sized for a static stress concentration of 2.2. The fatigue load range used was 4.36×10^6 ft.-lb. These were the largest shear fatigue stresses in the plate, which should easily tolerate a shear stress range of 12,000 psi. Therefore, the shear stress margin of safety was calculated to be 1.27. Calculations of the spline tooth bending stress range led to 15296 psi, which has a 0.6 margin of safety. The spline tooth shear stress range of 7291 psi has a 0.646 margin of safety.

5.2 LOW SPEED SHAFT AND COUPLINGS

The size of the low speed shaft was calculated for the transmission of 3.38×10^6 ft-lbs, with a ±20% alternating component at 2 per revolution for 1.74×10^8 revolutions. The shaft is hollow, with a 10-in. inner diameter, to permit electrical conduits to pass from the slipring on the generator end of the gearbox to the rotor mounted hydraulic power supply, control and instrumentation.

The shaft is a 180 in. long cylindrical forging, with a 32 in. outer diameter. It is made of forging grade material, ASTM A508 Class 4B. This

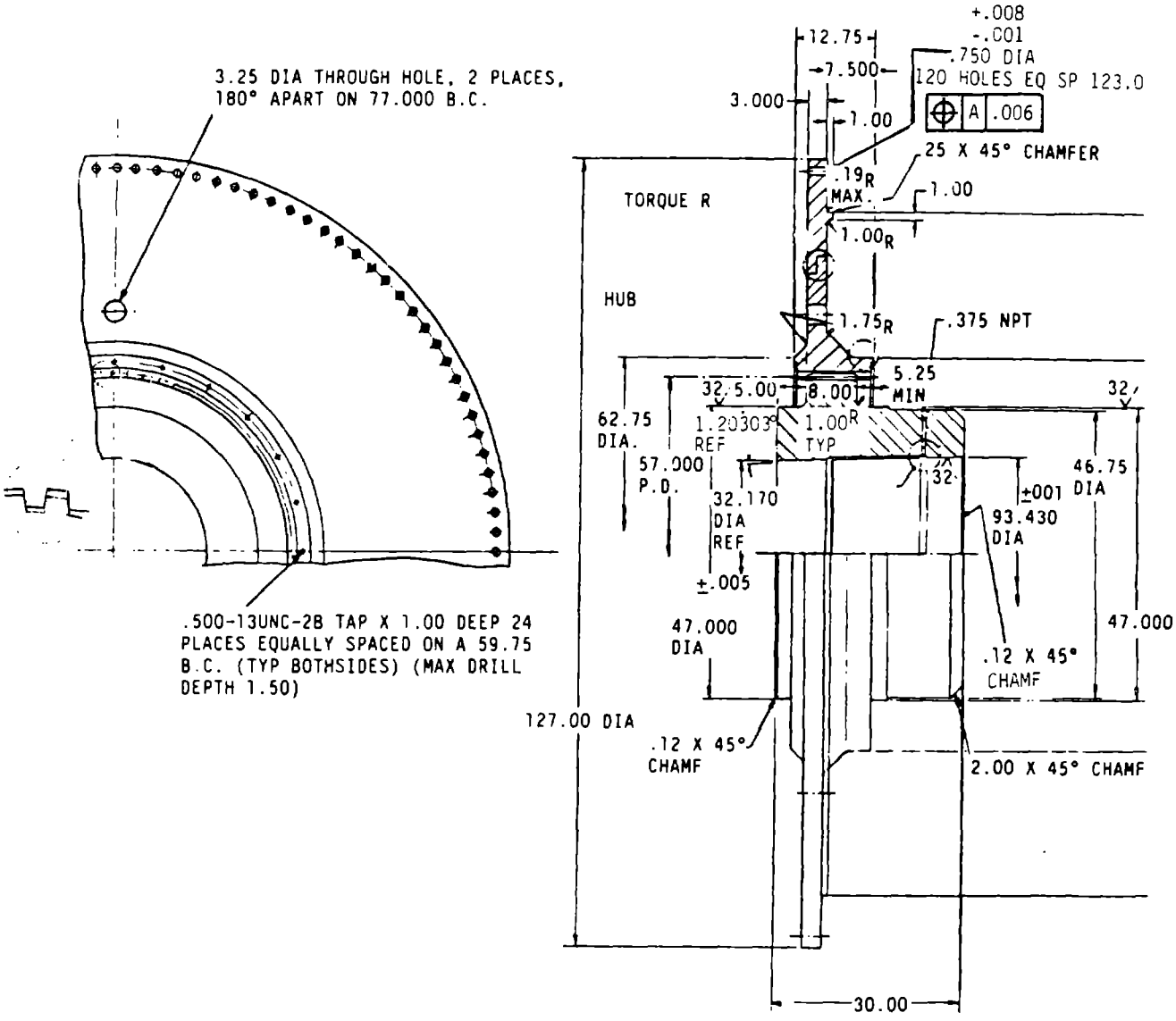

Figure 5-2 Torque Plate and Coupling

steel was the best combination of cost and strength for this application. A coupling hub is shrunk onto each end of the shaft. The shrink fit, with 0.07 in. radial interference, is designed to transmit twice the rated torque with a coefficient of friction of 0.15. To reduce stress raisers at the point where the hub terminates on the shaft body, the shaft and hub interface diameter was increased to 33.5 in. and a generous 0.75 in. radius was provided. The hub seat is tapered and the hubs are equipped with a hydraulic labyrinth to assist in disassembly. Pressure connections are provided on the outside of the hubs to pressurize the tapered annular region of the labyrinth shown in Figure 5-3. The pressure releases the shrink fit strain, lowers the friction coefficient, and produces an axial force caused by the taper. Hydraulic pressure above 13,000 psi applied to the hub will unseat the hub from the shaft.

Figure 5-3 shows the component and assembly design details. The hubs contain external splines designed to meet the requirements discussed in section 5.1.

5.2.1 HUB SHRINK FIT DESIGN

A hub that is shrunk onto a shaft will transmit torque across the interface through the large normal force produced at the interface, and the friction between the mating surfaces. The calculation of the torque begins with the classical equations:

$$F = fN \text{ and } T = FR \qquad [5\text{-}1]$$

where F is the friction force, f is the coefficient of friction, N is the normal force, T is the torque and R is the action radius. The coefficient of friction equals 0.15 for the interface of steel and steel.

In reference to Figure 5-4,

R_1 = inner radius of the shaft, 5.0 in

R_2 = outer radius of the shaft, also the inner radius of the hub, 16.75 in.

R_3 = outer radius of the hub, 23.5 in.

The normal force is the pressure at the interface radius, R_2, multiplied by the interface area, $2\pi R_2$ x hub length (L_H 30 in.).

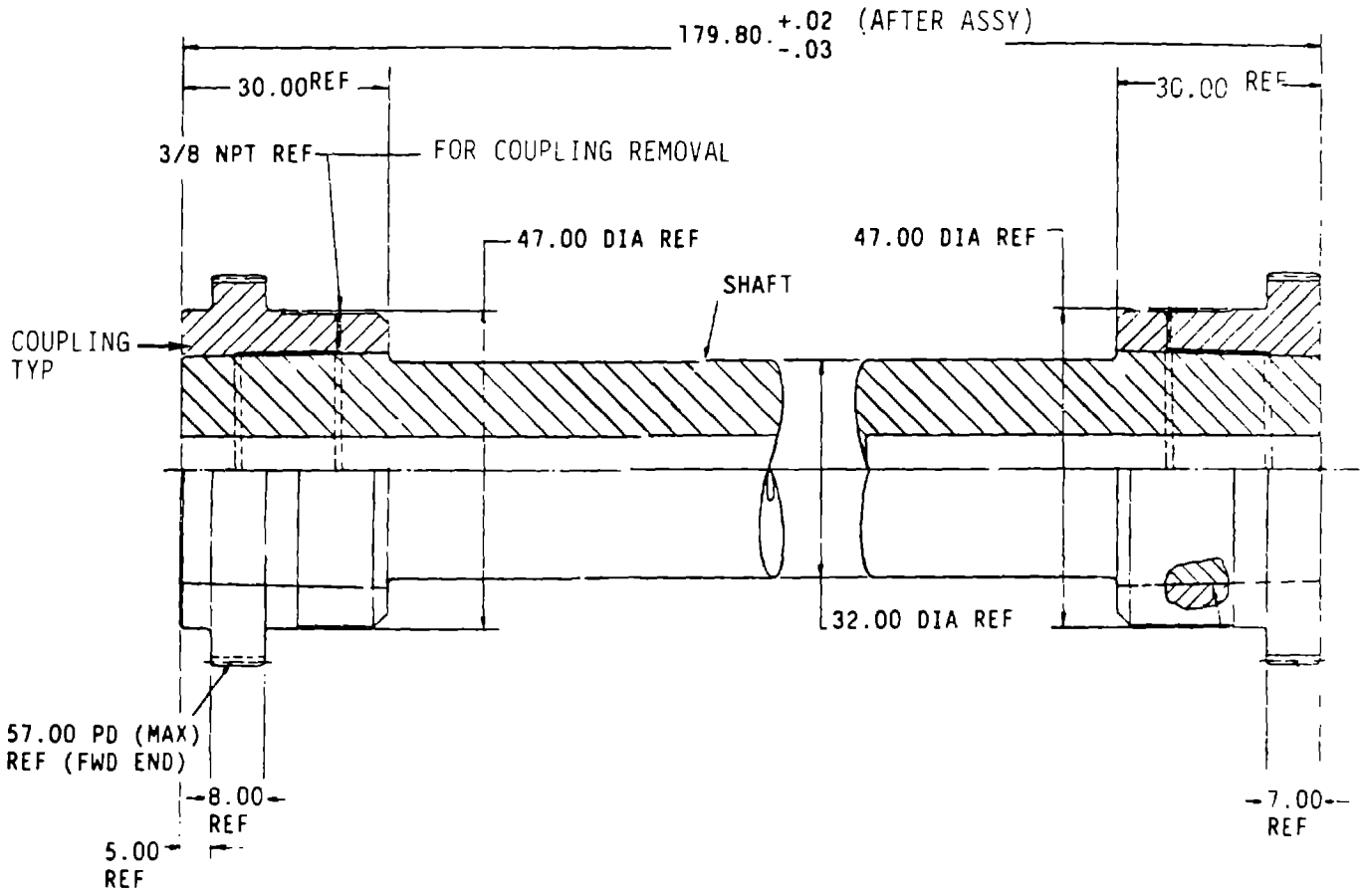

Figure 5-3 Low Speed Shaft

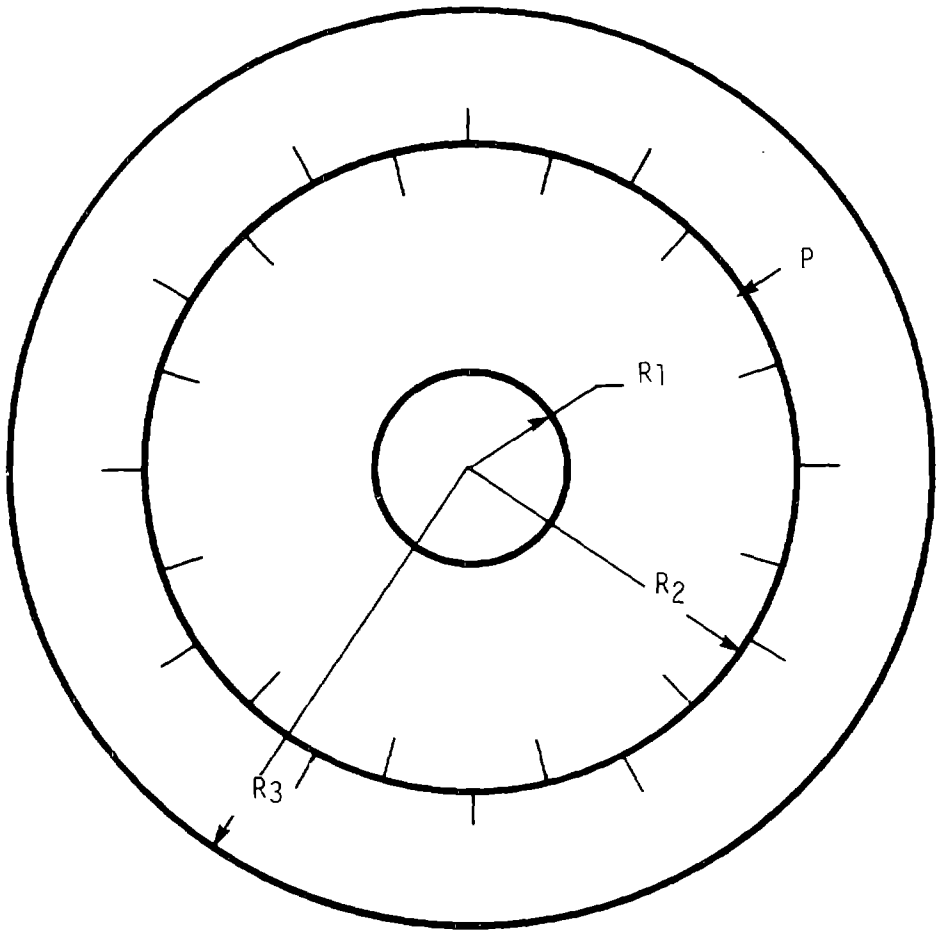

Figure 5-4 Relationship of the Hub Shrunk onto the Hollow Shaft

The rated torque is given as 3.38×10^6 ft.-lb., with a limit 10% above that. The Structural Design Criteria required the design of the friction fit to transmit a torque of 2.25 times the maximum, or 8.4×10^6 ft.-lb.

$$T = f \times 2\pi R_2 \times L_H \times P \times R_2 \qquad [5\text{-}2]$$

Solving for P yields [5-3]

$$P = \frac{T}{f \times 2\pi R_2^{\,2} \times L_H}$$

$$= \frac{8.4 \times 10^6 \times 12}{0.15 \times 2\pi \times 16.75^2 \times 30}$$

$$P = 12{,}710 \text{ psi}$$

Seely and Smith, on p. 34 of the 2nd edition of the "Advanced Mechanics of Materials" give an expression for the degree of interference necessary to produce this interface pressure.

$$S_1 = \frac{PR_2}{E}\left\{\left[\frac{R_3^{\,2} + R_2^{\,2}}{R_3^{\,2} - R_2^{\,2}}\right] + \mu\right\} \qquad [5\text{-}4]$$

where S_1 = increase in the internal radius of the hub to produce P
E = Young's Modulus, which equals 30×10^6 for steel
μ = Poisson's Ratio for steel, which equals 0.25

$$S_1 = \frac{12{,}710 \times 16.75}{30 \times 10^6} \; \frac{(23.75)^2 + (16.75)^2}{(23.75)^2 - (16.75)^2} + 0.25$$

$$S_1 = 0.023 \text{ in.}$$

Similarly $S_2 = \frac{PR_2}{E}\left\{\left[\frac{R_2^{\,2} + R_1^{\,2}}{R_2^2 - R_1^{\,2}}\right] - \mu\right\}$ [5-5]

where S_2 is the decrease of the outside radius of the shaft under an external pressure P.

Solving equation [5-5] yields a S_2 of 0.013 in.

The internal hub diameter of 33.430 in. and external shaft diameter of 33.500 in. reflect this condition within machining tolerances. The resultant tangential tensile stress in the hub is 38,900 psi, which compares favorably with the allowable of 45,000 psi for a steel with a core hardness of 320 BHN.

The assembly will be done at a hub temperature of 450°F above the temperature of the low speed shaft and setting the axial positions of the tapered fit based on precise measurements to obtain the desired interference.

5.2.2 SPLINE ANALYSIS

The design of the splines, which form the flexible part of the low speed shaft coupling, follows a method outlined in an article by Darle W. Dudley entitled "When Splines Need Stress Control", referenced in Section 5.1. The principal stresses are shear stresses in spline teeth, compressive stresses in spline teeth, and bursting stresses in the external spline hub. The article also discusses shear stresses in spline shafts. However, in this design the spline is cut into a hub that is shrunk onto a shaft, so the shaft stresses are discussed in section 5.2.1.

Dudley defined the allowable stresses, based on service conditions, surface finish and life expectancy. A spline design for which the calculated stresses do not exceed the allowables provides satisfactory service, if the splines receive proper lubrication and maintenance.

The following analysis is for the aft spline, at the interface of the shaft and gearbox. The aft spline contains 138 teeth on a 55.2-in. pitch diameter, and has a 7-in. face width. The forward spline, between the low speed shaft and torque plate, is slightly larger and has larger design margins. The external splines have a minimum crowning radius of 875 in.

Spline Teeth - shear

$$\text{shear stress, } S_s = \frac{4T\ k_m}{DN\ F_e\ t_c} \qquad [5\text{-}6]$$

T = equivalent torque, in.-lb = maximum torque $\times \sqrt[4]{\frac{\Sigma\ (\text{Load}^4 \times n)}{\Sigma n}}$
= 39.95×10^6 in.-lb.

k_m = load distribution factor, (max. load)/(average load) = 1.5

D = pitch diameter, 55.2 in.

n = number of cycles of a load level in the histogram

N = number of teeth

Load = torque in histogram normalized to maximum torque

F_e = effective facewidth, 6.65 in. (95% of actual)

t_c = chord thickness, .62 in.

$$S_s \quad \frac{4 \times 39.95 \times 10^6 \times 1.5}{55.2 \times 6.65 \times 0.62 \times 138} = 7632 \text{ psi}$$

The allowable shear stress, S_{sa}, is defined by Dudley as,

$$S_{sa} = S_s \frac{L_f}{K_a} \qquad [5\text{-}7]$$

Where S_s = maximum allowable shear stress for nitrided splines, 40,000 psi

L_f = life factor, .3 for unidirectional torque

K_a = application factor, 1.5 (intermittent shock)

$$S_{sa} = 40{,}000 \times \frac{.3}{1.5} = 8000 \text{ psi}$$

The calculated shear stress of 7632 psi compares favorably with the allowable of 8000 psi.

The spline compression stress for crowned splines is given as,

$$S_c = 2290 \sqrt{\frac{2T}{DNhr_2}} \qquad [5\text{-}8]$$

where h = tooth height, 0.4 in.
r_2 = crowning radius

The other variables, D, N, and T are the same as shown in equation [5-6].

The crowning radius, r_2, is calculated based on the angular misalignment and face width.

$$r_2 = \frac{F^2}{8A}, \text{ and} \qquad [5\text{-}9]$$

$$A = \frac{BF}{2}, \qquad [5\text{-}10]$$

where B = .002 in./in. maximum misalignment
F = 7 in. (actual face width)

Substituting $BF/_2$ for A in equation [5-9] yields the crowning radius,

$$r_2 = \frac{2F}{8B} = \frac{7}{4 \times .002} = 875 \text{ in.}$$

$$S_c = (2290) \sqrt{\frac{2 \times 39.95 \times 10^6}{55.2 \times 138 \times .4 \times 875}}$$

$$S_c = 12{,}536 \text{ psi}$$

The allowable spline compressive stress is defined as

$$S_{ca} = S_c \times \frac{Lw}{ka} \qquad [5\text{-}11]$$

where L_w, the life factor for wear is obtained from the equation

$$\text{Log}_{10}(L_w) = -.1507 \log_{10}(\text{number of revolutions}) + 1.2007 \qquad [5\text{-}12]$$

for 174×10^6 revolutions, $L_w = 1.298$
S_c = maximum compressive stress for nitrided splines, 16,000 psi
k_a = spline application factor, 1.5

The allowable spline compressive stress $S_{ca} = 16{,}000 \times \frac{1.298}{1.5} = 13{,}845$ psi

The calculated compressive stress is below the allowable stress for the service and life requirement.

The bursting stress of internal splines:

$$S_t = k_a k_m (S_1 + S_3) + S_2 \qquad [5\text{-}13]$$

$$\text{Radial force stress, } S_1 = \frac{T \tan \phi}{\pi D t_w F} \qquad [5\text{-}14]$$

where ϕ = pressure angle, 20°
t_w = wall thickness, 7 in.

$$S_1 = \frac{39{,}950{,}000 \times .36397}{\pi \times 55.2 \times 7 \times 7} = 1711$$

$$\text{Centrifugal force stress, } S_2 = .828 \times 10^{-6} (n^2) (2D_{ei}^2 + .424D_{ie})^2 \qquad [5\text{-}15]$$

Since the rotational speed in this application is very low, the centrifugal force stress, S_2 is virtually zero and can be ignored.

$$\text{Beam stress, } S_3 = \frac{4T}{D^2 F Y} \qquad [5\text{-}16]$$

where Y = form factor, 1.8 for internal teeth

$$S_3 = \frac{4 \times 39{,}950{,}000}{(55.2)^2 \times 7.0 \times 1.8} = 4162 \text{ psi}$$

$$S_T = 1.5 \times 1.5 (1711.2 + 4162.2) + 0$$
$$= 13{,}215 \text{ psi}$$

The allowable tensile stress is given by

$$S_{Ta} = S_T \times L_f \qquad [5\text{-}17]$$

where S_T = maximum allowable tensile stress for surface hardened (nitrided) steel, 45,000 psi

L_f = life factor, .3

S_{ta} = 45,000 x .3 = 13,500 psi

The calculated bending and tensile stresses do not exceed the allowables.

5.2.3 STRESS MARGINS OF SAFETY

The results of the stress analysis and margins of safety are shown in Table 5-1.

Table 5-1 Low Speed Shaft Stress Summary

ITEM	STRESS	MARGIN OF SAFETY
ROOT MEAN CUBED SHAFT FATIGUE PRINCIPLE STRESS IN FILLET	5649 $\pm$ 777 psi	0.94
CRACK GROWTH THRESHOLD STRESS RANGE IN SHAFT FILLET	14,405 psi	0.67
COUPLING FRICTION CAPACITY VERSUS TORQUE LIMIT WITH A COEFFICIENT OF FRICTION OF 0.2	11.2 x 10^6 ft-lb	1.20
HUB TANGENTIAL STRESS AT REMOVAL LABYRINTH VERSUS YIELD POINT	116,700 psi	0.16
SPLINE SHEAR	7,632 psi	0.04
COMPRESSION	12,536 psi	0.10
TENSION	13,215 psi	0.02

5.3 GEARBOX

The gearbox shown in Figure 5-5 and consists of three stages of speed increasers, with a speed increase ratio of 82.14. The first two stages are epicyclic, and the third stage is parallel shaft. This configuration was

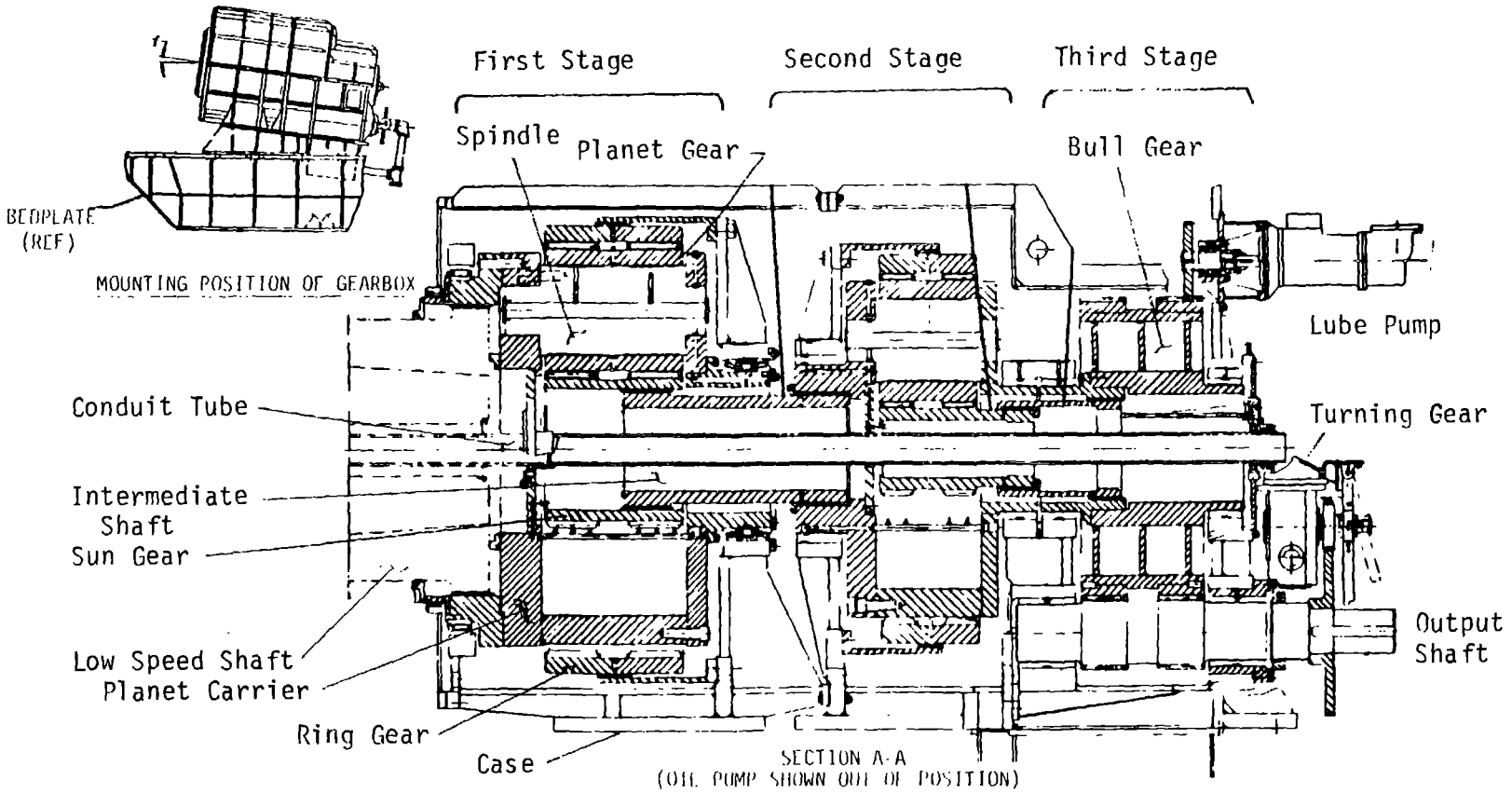

Figure 5-5 Gearbox Cross Section

chosen to provide the lowest gearing cost as described in Volume II, section 4. Epicyclic gears provide the lowest weight and cost per ft.-lb. of torque for the first and second stages. Parallel shaft gears provide the lowest cost for the third stage. The high-speed stage is a conventional parallel shaft design, consisting of a bull gear and pinion. The epicyclic stages evolved from the Stoechicht design, with an improved annulus ring support. In this design, the annulus rings are stationary, and are connected to the gearbox housing.

The input torque is applied to the planet carrier and the output is provided by the sun wheel. The low speed shaft, which provides the torque input, is connected to the planet carrier by a splined interface. The splined hub of the low speed shaft mates with an internal spline on the planet carrier. Between the first and second stages, the output shaft of the first stage sun gear drives the planet carrier of the second stage. The second stage sun drives the bull gear of the third stage. A conduit, which is concentric and rotates with the input shaft, passes through the entire gearbox and the bull gear shaft. All power, control and instrumentation wiring is routed from the nacelle to the rotor through this conduit and a slipring assembly mounted on the aft wall of the gearbox housing.

The gearbox housing is of welded steel plate with an integral oil reservoir below the third stage. The gearbox is foot-mounted on a pedestal that tilts the centerline of the unit 7° to the horizontal. Journal bearings are used wherever possible. Rolling element bearings are used only to react thrust.

5.3.1 PERFORMANCE REQUIREMENT

The gearbox was designed for strength and durability in accordance with AGMA Standard 411.02, "Design Procedure for Aircraft Engine and Power Take-off Helical Gears" and AGMA Information Sheet 217.01, "Gear Scoring Design Guide for Aerospace Spur and Helical Gear Parts". The life and duty cycle requirements defined in Tables 5-2 and 5-3 and Figure 5-6 were severe enough to warrant the requirements in the AGMA documents.

Table 5-2 Performance Requirements

Input Speed - Rated	16.8 rpm
Input Speed Range	13.70 rpm to 16.8 rpm
Speed Increaser Ratio	82.14
Rated Input Torque	3.38×10^6 ft-lb (10812 hp at 16.8 rpm) 1.49×10^6 ft-lb at 13.70 rpm
Service Factor	Consistent with 30-year life and duty cycle of Figure 5-6 and Table 5-3
Maximum Running Losses	3% at rated power (324 hp at 16.8 rpm)
Maximum Break-Away Torque	15,000 ft-lb (at low speed shaft)
Duty Cycle	See Table 5-3
Maximum No-Load Losses	1.5% of rating at rated input speed (162 hp at 16.8 rpm)
Direction of Rotation	Clockwise, looking at the low speed shaft

Table 5-3 Gearbox Torque Duty Cycle

TORQUE/RATED TORQUE	CUMULATIVE PROBABILITY	
	GEARS WITH RANDOM PHASING	GEARS WITH FIXED PHASING
.086	0.362×10^{-1}	0.659×10^{-2}
.173	0.129	0.461×10^{-1}
.259	0.248	0.158
.345	0.362	0.270
.388	0.415	0.326
.431	0.464	0.379
.475	0.509	0.428
.518	0.550	0.474
.561	0.587	0.517
.604	0.621	0.557
.647	0.653	0.593
.690	0.682	0.625
.734	0.709	0.655
.777	0.735	0.683
.820	0.761	0.710
.863	0.786	0.736
.906	0.811	0.762
.949	0.836	0.787
.992	0.861	0.812
1.036	0.884	0.838
1.079	0.905	0.863
1.122	0.924	0.887
1.165	0.940	0.909
1.208	0.952	0.928
1.251	0.963	0.943
1.295	0.971	0.955
1.338	0.978	0.965
1.381	0.984	0.973
1.424	0.988	0.980
1.467	0.992	0.985
1.51	0.994	0.989
1.553	0.996	0.993
1.640	0.998	0.997
1.726	0.999	0.999
1.812	0.100×10^{1}	0.999
1.899	0.100×10^{1}	0.100×10^{1}
1.985	0.100×10^{1}	0.100×10^{1}
ROOT MEAN FOURTH LOAD	.921 (WITH 30% MAX OVERLOAD)	.985 (WITH 30% MAX OVERLOAD)

RATED TORQUE = 3.38×10^{6}
TOTAL ROTOR CYCLES = 1.78×10^{8}
LOADS CONTAIN 1.15 CONTINGENCY FACTOR

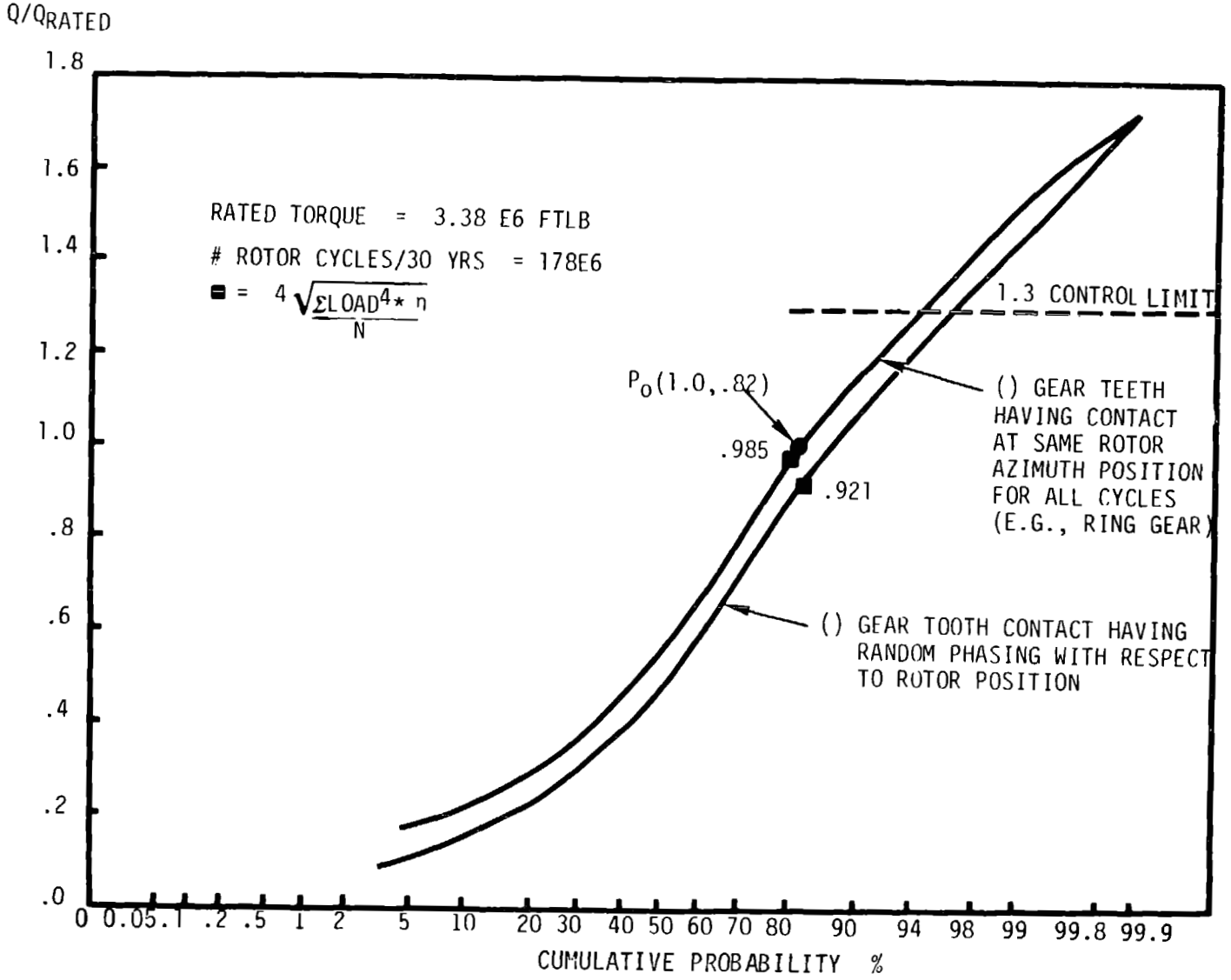

Figure 5-6 Total Drive Train Torque Level Probability Distribution

5.3.2 INTERFACES

5.3.2.1 Input

Torque is input to the first stage through a splined connection. The low speed shaft contains a splined hub that fits into a ring, with an internal spline, which is bolted to the first stage planet carrier. The rotation of the low speed shaft and planet carrier rotates the planetary gear. The splines are lubricated by the system that lubricates the gears and bearings in the gearbox with oil.

5.3.2.2 Output

The output shaft is integral with the third stage pinion. The third stage is a parallel shaft design, so that an electrical conduit can pass between the aft and forward ends of the gearbox. The shaft is supported by a pair of journal bearings straddling the pinion. A spur gear, 30 in. in diameter, is mounted on the shaft, outboard of the gearbox and interfaces with the rotor turning drive to position the rotor for maintenance. The output shaft interfaces with the high speed shaft and coupling assembly.

5.3.2.3 Mounting

The gearbox is mounted to the bedplate by a flanged connection. Reaction torque is transferred into bedplate through the flanged connection and the gearbox pedestal. The flange on the bedplate is included in the torque path from the annulus rings of the first and second stages.

5.3.2.4 Electrical Slipring Mount

A slipring transmits power, control and diagnostic instrumentation signals between the rotating, hub-mounted equipment and the stationary control boxes in the nacelle. The slipring is mounted on the aft end of the gearbox on a centerline concentric with the low speed shaft. The wires between the slipring and the low speed shaft are encased in a metal tube that rotates with the low speed shaft. To accommodate different rotational speeds of the tube and the second stage through which it passes, the tube is mounted on a bearing.

5.3.3 GEAR TOOTH STRESS AND LIFE ANALYSIS

The gears are rated per AGMA 420.04, Practice for Enclosed Speed Reducers or Increasers, at the rated input torque and speed. Since AGMA has established no procedures for calculating the J factor for internal gears, the J factor used for internal gear strength is that of a similar rack. This requirement is believed to be conservative.

The expected life of the gears was checked using the duty cycle shown in section 5.3.2, and the assumption that all loads in the duty cycle above 130% of normal should be applied at 130% because there is a torque limiting control in the system. A cumulative damage approach was used, using life factor curves calculated from AGMA 411.02 and extending these curves at the same slope beyond 10^{10} cycles.

Philadelphia Gear Company (PGC) routinely uses a program for studying the subsurface stress conditions of case-hardened gear teeth. A safety factor is calculated for the worst stress condition, compared to the design limits for a specified case depth, case hardness, and core hardness. To find the worst stress condition, the stress is calculated at incremental levels below the tooth surface and compared to material allowables. At varying levels below the surface, the material hardness varies, so calculated stresses and allowables also vary. This fact is taken into consideration in the program. The material allowables are derived from test coupons subjected to tensile stress, and converted to a unidirectional endurance limit and combined with a reliability factor and residual stress factor.

Tables 5-4 through 5-8 define all the pertinent gear parameters. These analyses were performed by GE and PGC, and confirmed by separate studies performed by Mr. Robert Errichello of Geartech, Inc., a consulting firm in Albany, California. Note that the gearing was evaluated for durability as well as strength. The large number of cycles during the design life required this wear-out evaluation.

Table 5-4 Gearing Specifications

Item	Low Speed Stage	Intermediate Stage	High Speed Stage
DPN	1.75	2.0	2.5
Face (in.)	22	13.5	18
Pressure Angle (deg.)	25	25	25
Center Distance (in.)	26.784	20.834	35.5
Ratio	3.767	4.966	4.393
Number of Planets	6	4	-
Helix Angle (deg.)	30	30	31.712
Overlap/Helix	3.06	2.15	7.53
PLV (ft./min.)	350.5	1118.4	4758.8

Table 5-5 Low Speed Stage

ITEM	Sun	Planet	Annulus
Teeth	43	37	119
Pitch Diameter (Ref) (in.)	28.373	24.414	78.52
Oversize (in.)	.401	.401	-.130
Material	4320 EFVD	4320 EFVD	4340 EFVD
Heat Treatment	Carburized	Carburized	Nitrided*
Hardness	58 R_C Case	58 R_C Case	49 R_C Case*
Compressive Stress (Actual) (psi)	114,555	114,555	72,100
Allowable Compressive (psi)	200,000	200,000	165,000
Bending Stress (Actual) (psi)	20,131	20,166	14,030
Allowable Bending (psi)	65,000	45,500	45,100
Safety Factor - Durability	3.048	3.048	5.237
Strength	3.229	2.256	3.214

*Nitriding of annulus gears to minimize potential for pitting from marginal lubrication. Gear rating based on thru-hardened 280 BHN min. core.

Table 5-6 Intermediate Stage

Item	Sun	Planet	Annulus
Teeth	29	42	115
Pitch Diameter (Ref) (in.)	16.743	24.249	66.394
Oversize (in.)	.347	.347	-.114
Material	4320 EFVD	4320 EFVD	4340 EFVD
Heat Treatment	Carburized	Carburized	Nitrided*
Hardness	58 R_C Case	58 R_C Case	49 R_C Case*
Compressive Stress (Actual) (psi)	129,277	129,277	68,144
Allowable Compressive (psi)	200,000	200,000	165,000
Bending Stress (Actual) (psi)	20,945	20,831	14,236
Allowable Bending (psi)	65,000	45,500	45,100
Safety Factor - Durability	2.393	2.393	5.868
Strength	3.103	2.184	3.168

Table 5-7 High Speed Stage

Item	Pinion	Gear
Teeth	28	123
Pitch Diameter (Ref.) (in.)	13.166	57.834
Oversize (in.)	.185	-.185
Material	4320 EFVD	4320 EFVD
Heat Treatment	Carburized	Carburized
Hardness	58 R_C Case	58 R_C Case
Compressive Stress (Actual) (psi)	133,742	133,742
Allowable Compressive (psi)	200,000	200,000
Bending Stress (Actual) (psi)	26,535	26,560
Allowable Bending (psi)	65,000	65,000
Safety Factor - Durability	2.236	2.236
Strength	2.450	2.447

Table 5-8 Life Study

SUMMARY FOR GEARING

Gear life checked by cumulative damage approach, using an extended life factor curve from AGMA 411.02
Goal: 176587. hr. (1.78×10^8 rotor cycles/30 years).

MEMBER	SAFETY FACTOR NEEDED TO REACH GOAL		ACTUAL SAFETY FACTOR		ACTUAL LIFE	
	Durability	Strength	Durability	Strength	Hours	Years
Low Speed Sun Pinion	1.839	1.408	3.048	3.229	5,656,140	960.9
Low Speed Planet	1.525	1.329	3.048	2.256	∞	∞
Low Speed Annulus	1.718	1.391	5.237	3.214	∞	∞
Intermediate Sun Pinion	2.146	1.485	2.393	3.103	459,638	78.1
Intermediate Planet	1.757	1.397	2.393	2.184	2,662,730	452.4
Intermediate Annulus	1.834	1.416	5.868	3.168	∞	∞
High Speed Gear	1.880	1.426	2.236	2.447	809,271	137.5
High Speed Pinion	2.226	1.502	2.236	2.450	184,225	31.3

5.3.4 SUBSURFACE STRESS ANALYSIS

Subsurface stress was analyzed to evaluate the stresses at various depths from tne surface of the flank of the tooth, to the center of the tooth at the pitch line.

Using PGC's "SSCON" Program, the contact stress, shear stress, principle stress, and the safety factor were calculated at various depths. The factor of safety at any point is equal to the allowable tensile stress, which was estimated by PGC, and divided by the principal tensile stress at that point. The allowable tensile stress at any given depth is a function of the hardness and residual stress, with a reliability factor of 1.78. The hardness and residual stress curves were established through typical material test data.

PGC's experience indicated that a minimum factor of safety should be 1.3 for continuous transmitted load conditions for good design. For intermittent peak load conditions, a minimum factor of safety of 1.0 may be satisfactory.

The gearing design is adequate, according to the subsurface stress criteria. The maximum stresses and the minimum safety factor are shown in Table 5-9.

Table 5-9 Subsurface Stress Analysis Summary

GEAR SET	MINIMUM SAFETY FACTOR				MAXIMUM TENSILE STRESS			
	Depth (in.)	Equivalent Tensile Stress (psi)	Combined Design Limit (psi)	Safety Factor	Depth (in.)	Equivalent Tensile Stress (psi)	Combined Design Limit (psi)	Safety Factor
High Speed Shaft								
Pinion	.145	41360	74348	1.8	.038	81018	149516	1.85
Gear	.144	41733	65011	1.56	.038	81013	149598	1.85
Intermediate Speed Shaft								
Sun	.034	77829	148420	1.91	.034	77829	148420	1.91
Planet	.034	77830	148420	1.91	.034	77830	148420	1.91
Low Speed Shaft								
Sun	.039	68830	148597	2.16	.039	68830	148597	2.16
Planet	.039	68830	148597	2.16	.039	68830	148597	2.16

5.3.5 GEAR MESH EHD FILM THICKNESS ANALYSIS

The elastohydrodynamic (EHD) film thickness of each gear mesh in the gearbox was analyzed. Based on the tooth geometry, tooth loading, and lubricant properties, this analysis determined the minimum oil film thickness between contacting gear teeth. Because lubricant properties change with temperature, the minimum film thickness was calculated within a range of $\pm 15°$ around the design temperature.

The film thickness is defined by the following equation:

$$x = \frac{h}{\sigma} \qquad [5\text{-}18]$$

Where,

x = film thickness

h = minimum EHD oil film

σ = composite surface roughness

Values of required x are plotted versus pitch line velocity in Figure 5-7.

The minimum acceptable film is based on composite tooth surface roughness modified with respect to pitch line velocity. As shown in Table 5-10, all meshes have an adequate oil film, even at temperatures above the design temperature.

References:

Akin, L.S. "EHD Lubricant Film Thickness Formulas for Power Transmission Gears". ASME Paper No. 73-LUB-21 Dawson and Higginson, Elastohydrodynamic Lubrication

Mobil Oil Corporation, Mobil EHL Guide Book, Third Edition - 1979 -1981.

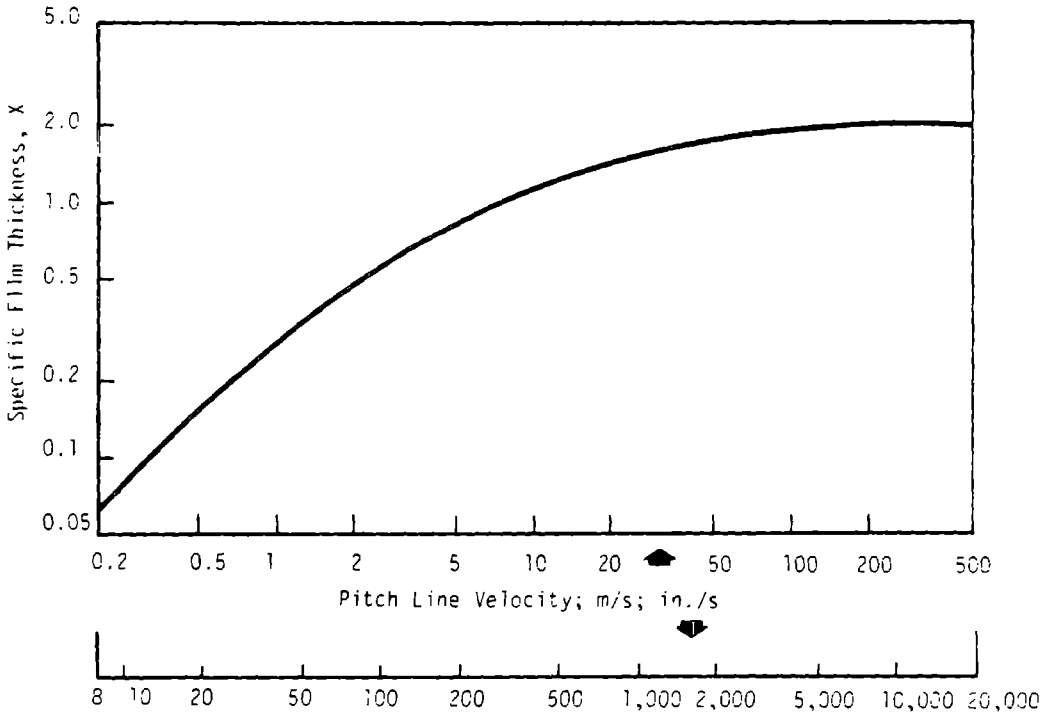

Figure 5-7 Film Thickness vs. Pitch Line Velocity

Table 5-10 EHD Oil Film Analysis

	EHD Film in.	Required Film in.	Safety Factor
High Speed Mesh	15.25×10^{-5}	4.3×10^{-5}	3.55
Intermediate Speed Sun-Planet Mesh	5.65×10^{-5}	2.7×10^{-5}	2.11
Intermediate Speed Planet-Annulus Mesh	9.36×10^{-5}	3.4×10^{-5}	2.75
Low Speed Sun-Planet Mesh	2.55×10^{-5}	1.27×10^{-5}	2.0
Low Speed Planet-Annulus Mesh	3.94×10^{-5}	1.7×10^{-5}	2.32

5.3.6 FLUID FILM BEARING ANALYSIS

Two complementary programs were used to determine the adequacy of the bearing and oil film. The first program, called INCOMP, was acquired from The Franklin Institute, Philadelphia, Pa. INCOMP provides a non-dimensional analysis that solves the Reynolds equation by a finite difference formulation over a grid network that represents the bearing area. For a given bearing geometry and film thickness distribution, sets of non-dimensional data are generated for various eccentricities and applied load angles. The non-dimensional data contains information on load capacity, power loss, side leakage, pad inlet flow, attitude angle and spring and damping coefficients.

The second program was developed by PGC, with guidance from The Franklin Institute. This program interpolates the raw, dimensionless data and performs a detailed heat balance analysis. The iterative process identified all final operating parameters of the actual bearing.

The operating parameters of all the fluid film bearings fall within generally accepted guidelines. See Figure 5-8 and Tables 5-11 and -12 for a summary of the results.

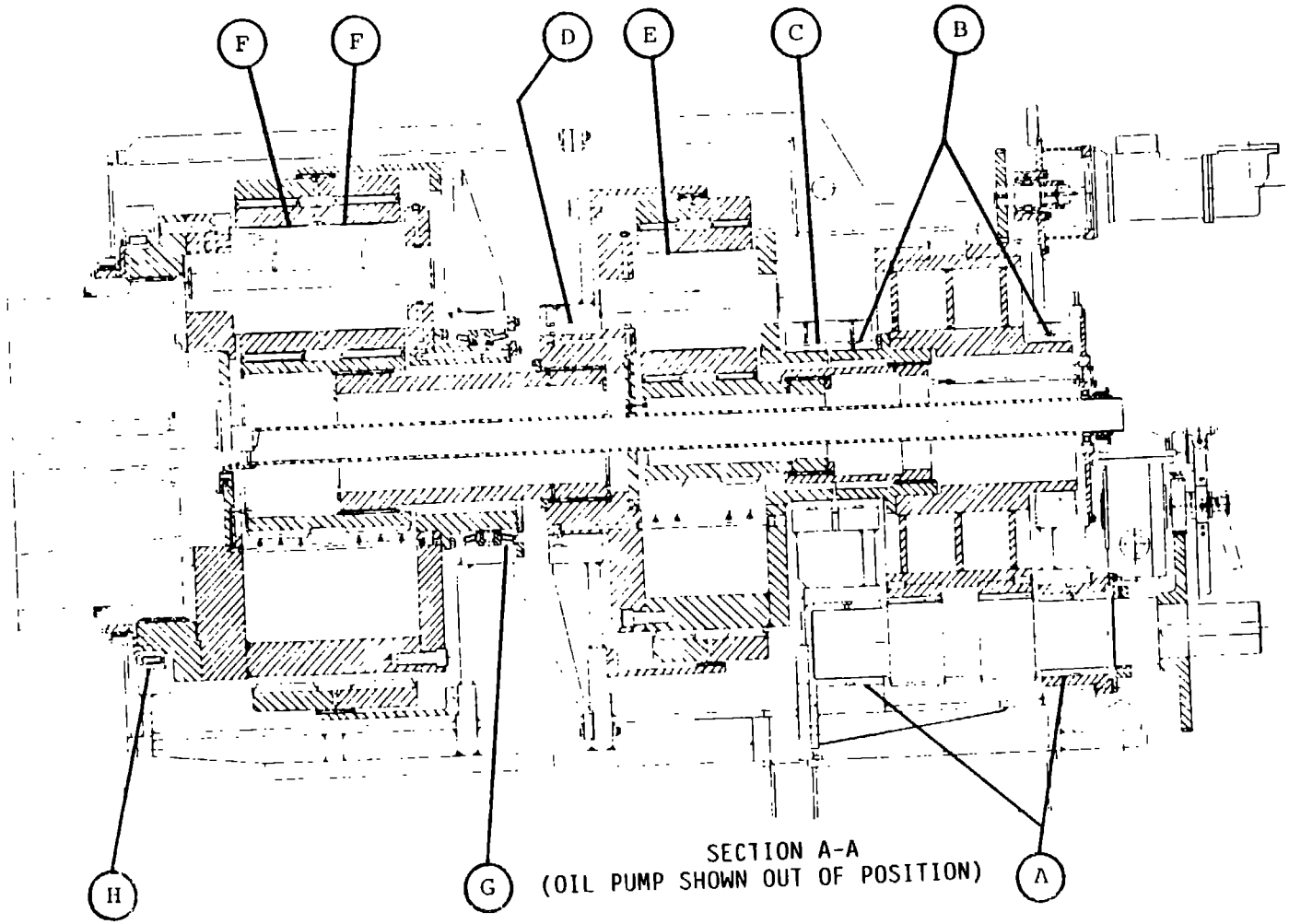

Figure 5-8 Bearing Identification Diagram

Table 5-11 Sleeve Bearing Performance

SUMMARY
(100% LOAD)

Ident. Letter	Bearing Location	Bearing Size Diameter X Length (in.) (in.)	Diameter Clear (in.)	Clear Diameter (in./in.)	Length Diameter (in./in.)	Speed (rpm)	Journal Velocity (ft./min.)	Load (lbs.)	Unit Load (psi)	Film Thickness (in.)	Temp Oil Out (F°)	Loss (hp)	Oil Required (gpm)	T (°F)
A	High Speed Pinion	11. x 10.5	.022	.002	.95	1381.	3977.	42750	370	.0037	152.7	27.3	10.4	37.7
B	High Speed Gear	24. x 6.	.020	.0008	.44	314	1973	48400	336	.0018	145.8	14.8	11.3	30.8
C	Intermediate Carrier	24. x 6.	.020	.0008	.25	64	402	15000	104	.0019	124.4	1.0	6.7	9.9
D	Intermediate Carrier	32. x 6.5	.018	.0006	.21	64	536	15000	72	.0024	129.6	2.0	5.6	14.6
E	Intermediate Speed Shaft Spindle	15.5 x 15	.012	.0008	.97	173	701	127352	548	.0015	152.3	3.7	1.3	37.0
F	Low Speed Shaft Spindle	17.25 x 12.25	.010	.0006	.71	54	244	124626	590	.0010	138.3	1.0	.7	23.3

OIL PROPERTIES
1165 SSU at 100°F, Inlet Temperature 115°F
131 SSU at 210°F

Supply Groove Pressure = 25 psi

Table 5-12 Sleeve Bearing Performance

SUMMARY
(130% LOAD)

Ident. Letter	Bearing Location	Bearing Size Diameter X Length (in.) (in.)	Diameter Clear (in.)	Clear Diameter (in./in.)	Length Diameter (in./in.)	Speed (rpm)	Journal Velocity (ft./min.)	Load (lbs.)	Unit Load (psi)	Film Thickness (in.)	Temp Oil Out (°F)	Loss (hp)	Oil Required (gpm)	T (°F)
A	High Speed Pinion	11. x 10.5	.022	.002	.95	1381.	3977.	55575	481	.0030	153.9	29.2	10.8	38.9
B	High Speed Gear	24. x 6.	.020	.0008	.44	314	1973	61500	427	.0016	147.4	15.6	11.3	32.4
C	Intermediate Carrier	24. x 6.	.020	.0008	.25	64	402	15000	104	.0019	124.4	1.0	6.7	9.9
D	Intermediate Carrier	32. x 6.5	.018	.0006	.21	64	536	15000	72	.0024	129.6	2.0	5.6	14.6
E	Low Speed Speed Shaft Spindle	15.5 x 15	.012	.0008	.97	173	702	165560	712	.0014	150.3	4.1	1.6	35.3
F	Low Speed Shaft Spindle	17.25 x 12.25	.010	.0006	.71	54	244	162000	767	.0008	140.0	1.0	.7	25.0

OIL PROPERTIES
1165 SSU at 100°F, Inlet Temperature 115°F
131 SSU at 210°F

Supply Groove Pressure = 25 psi

5.3.7 SPLINE STRESS ANALYSIS

All seven splines in the wind turbine gearbox -- the five case-hardened working splines and two through-hardened fixed splines -- were analyzed by the method presented by Darle Dudley in his paper, "When Splines Need Stress Control", publisned by Product Engineering, December 23, 1957. The fixed splines of the annuli coupling rings are designed in accord with Allen Gear design standards.

Each spline was analyzed for shaft shear stress, shear and compressive stresses in the spline tooth, and bursting stress of the internal splined hub.

The spline geometry and results of the stress calculations are shown in Tables 5-13, -14 and -15. Refer to Figure 5-9 for spline locations. Stresses were calculated both at rated loads and at 30% overload. The spline data was calculated using the methods discussed in section 5.2.

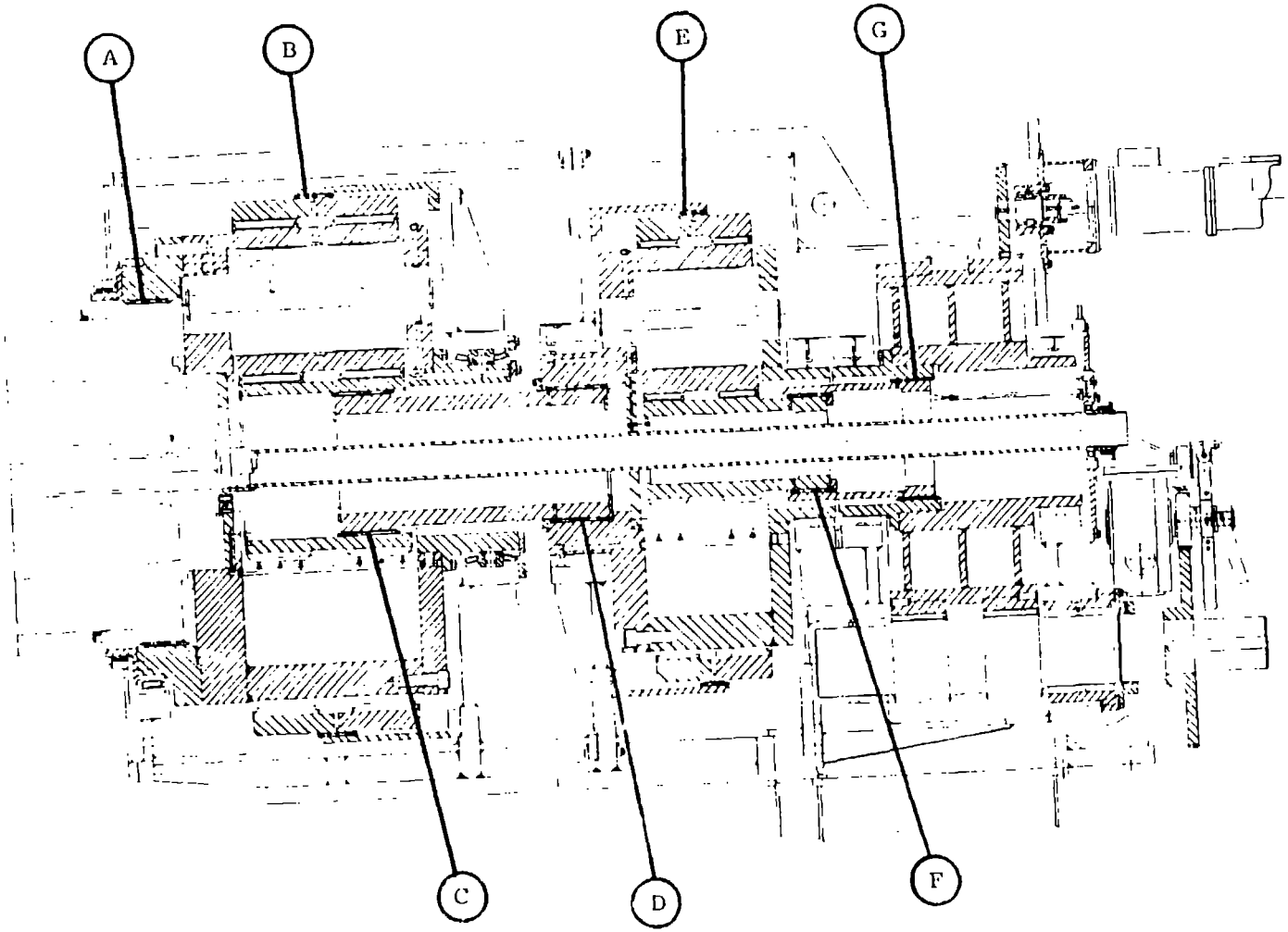

SECTION A-A
(OIL PUMP SHOWN OUT OF POSITION)

Figure 5-9 Spline Identification Diagram

Table 5-13 Spline Geometry

Ident. Letter	Location	Number of Teeth	Pitch (deg)	Pressure Angle (deg)	Pitch Diameter (in.)	Face (in.)	Crown Radius (in.)
A	Input Shaft	138	2.5/3.5	20	55.2	7.0	1880.
B	Low Speed Annulus Coupling	438	5/5	20	87.6	2.5 X 2	∞
C	Low Speed Sun Coupling	68	3/4	20	22.67	9.0	2025.
D	Intermediate Speed Input Shaft Coupling	64	3/4	20	21.33	9.0	2025.
E	Intermediate Speed Annulus Coupling	382	5/5	20	76.4	1.5 X 2	∞
F	Intermediate Speed Sun Shaft Coupling	62	4/5	20	15.5	7.0	1750.
G	High Speed Input Shaft Coupling	76	4/5	20	19.0	7.0	1139.

Table 5-14 Spline Stresses (psi)
At 100% Load

Ident. Letter	Location	SHEAR			COMPRESSIVE		BURSTING	
		Shaft	Spline	Allowable	Spline	Allowable	Spline	Allowable
A	Input Shaft	1396.	9998.	16667.	7632.	11600.	15901.	22500.
B	Low Speed Annulus Coupling	1101.	4451.	16667.	1812.	15000.	16959.	22500.
C	Low Speed Sun Coupling	7152.	12128.	20833.	9017.	11667.	20631.	27500.
D	Intermediate Speed Input Shaft Coupling	9615.	13669.	20833.	9529.	11667.	21039.	27500.
E	Intermediate Speed Annulus Coupling	357.	1708.	16667.	703.	15000.	5965.	22500
F	Intermediate Speed Sun Coupling	4605.	6601.	20833.	6217.	7467.	11970.	22500.
G	High Speed Input	4757.	4788.	16667.	6242.	7467.	7749.	22500.

Table 5-15 Spline Stresses (psi)
At 130% Load

Ident. Letter	Location	SHEAR			COMPRESSIVE		BURSTING	
		Shaft	Spline	Allowable	Spline	Allowable	Spline	Allowable
A	Input Shaft	1815.	12997.	16667.	8202.	11600.	20669.	22500.
B	Low Speed Annulus Coupling	1431.	5786.	16667.	2356.	15000.	22046.	22500.
C	Low Speed Sun Coupling	9297	15767.	20833.	10281.	11667.	26818.	27500.
D	Intermediate Speed Input Shaft Coupling	12500.	17770.	20833.	10865.	11667.	27350.	27500.
E	Intermediate Speed Annulus Coupling	464.	2220.	16667.	914.	15000.	7755.	22500
F	Intermediate Speed Sun Coupling	5987.	8581.	20833.	7089.	7467.	15541.	22500.
G	High Speed Input	6184.	6224.	16667.	7117.	7467.	10042.	22500.

5.3.8 SHAFT STRESS ANALYSIS

Shaft shear stresses were calculated for the rated load and for 30% overload. A summary of the results is given in Table 5-16. Refer to Figure 5-10 for the referenced shaft locations.

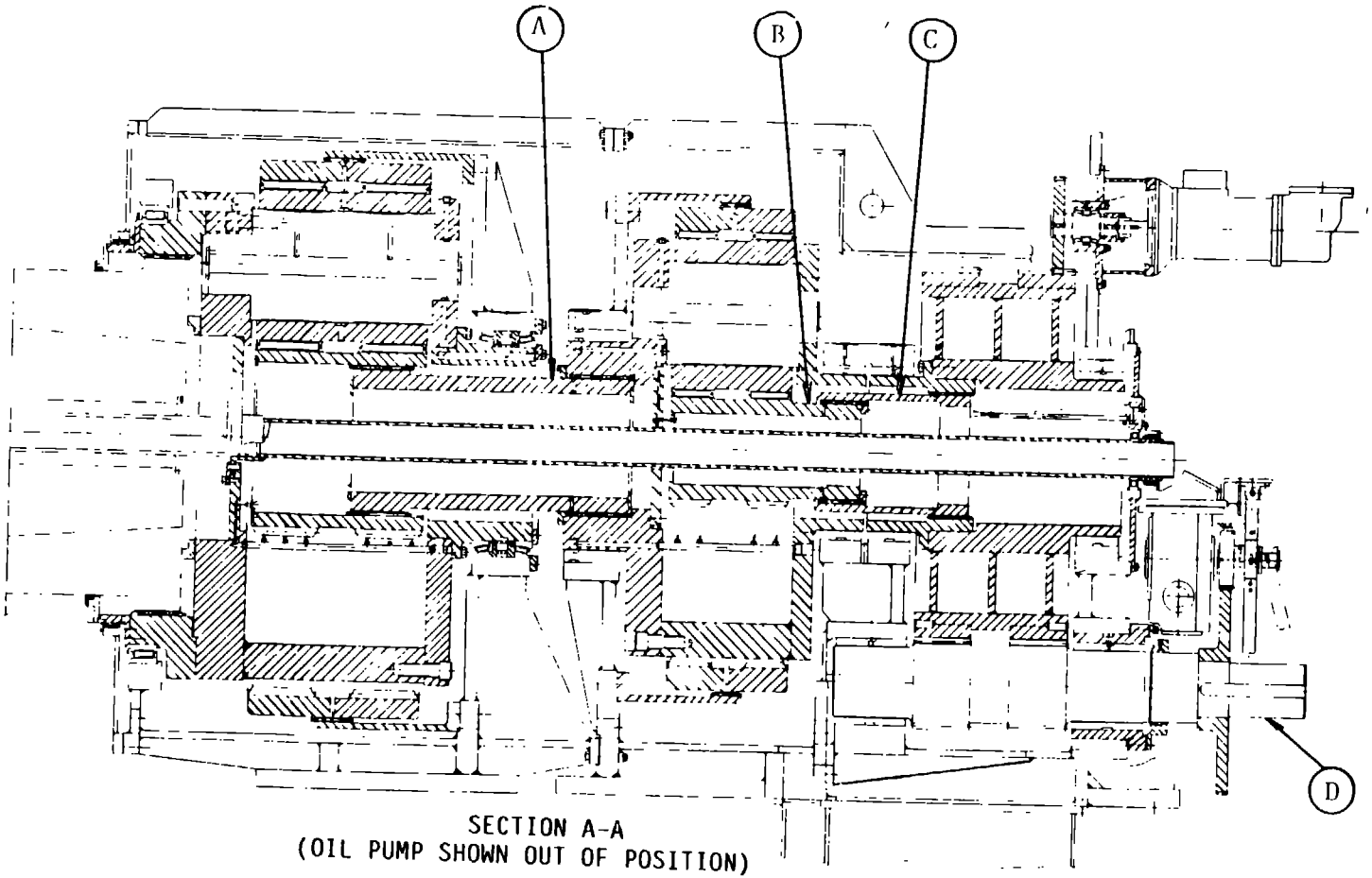

Figure 5-10 Shaft Identification Diagram

Table 5-16 Shaft Stresses (psi)

Ident. Letter	Location	At 100% Load		At 130% Load	
		Stress	Safety Factor	Stress	Safety Factor
A	Low Speed - Intermediate Speed Coupling Shaft	10119.	3.953	13154.	3.041
B	Intermediate Speed Sun Shaft	4982.	8.029	6476.	6.176
C	High Speed Coupling Shaft	5319.	7.520	6915.	5.784
D	Output Shaft	4278.	9.350	5561.	7.192

Service factors based on a shear yield stress of 40,000 psi.

5.4 GEARBOX LUBRICATION SUBSYSTEM

The gearbox lubrication subsystem, defined schematically in Figure 5-11, supplies filtered oil to the gearbox and aft low speed shaft spline at temperatures between 60°F and 115°F. This temperature range facilitates pumping the oil at the low temperature and maintains a minimum viscosity, consistent with requirements for journal bearing film thickness at the high temperature.

Two pumps are used. The electric motor-driven pump is used during start-up, until the wind turbine comes up to speed. Then the shaft-driven pump takes over. A pressure switch in the discharge line of the second pump determines when the first pump can be shut off. The motor-driven pump is also programmed to cut in if the shaft-driven pump fails. Loss of pressure in the discharge line of the shaft-driven pump determines its failure. Both pumps are Delaval IMO Type A3DH350. They can deliver 182 gpm against a 75 psi discharge pressure at a viscosity of 2000 ssu. Both pumps deliver the oil into a common line that contains a 40 micron Parker Rosean F3-400DC duplex filter, which is easy to maintain and service. The oil passes through a set of three Young Radiator Co. OCS-2000D-2P oil coolers, if the oil temperature exceeds 110°F. At temperatures below 110°F, the oil bypasses the coolers via the AMOT, thermostatically controlled, bypass valve. The oil flows into the manifold inside the gearbox, where it is distributed by a number of metering orifices into the bearing and gear meshes, and the splined shaft interface. The oil returns into the reservoir, which is mounted at the bottom of the gearbox. About 2 minutes of settling time is allowed for air bubbles to rise to the surface, before the oil resumes its travel through the subsystem.

5.4.1 INSTALLATION

The lubrication subsystem consists of the supply and conditioning module, mounted on a platform suspended below the bedplate, the distribution module inside the gearbox, the reservoir, which is integral with the gearbox, and the shaft-driven pump mounted on the gearbox.

The oil sump holds 360 gal. of oil. The sump is fitted with provisions for three sump heaters and associated thermostat ports, a suction strainer, low level switch and ports for two temperature transducers.

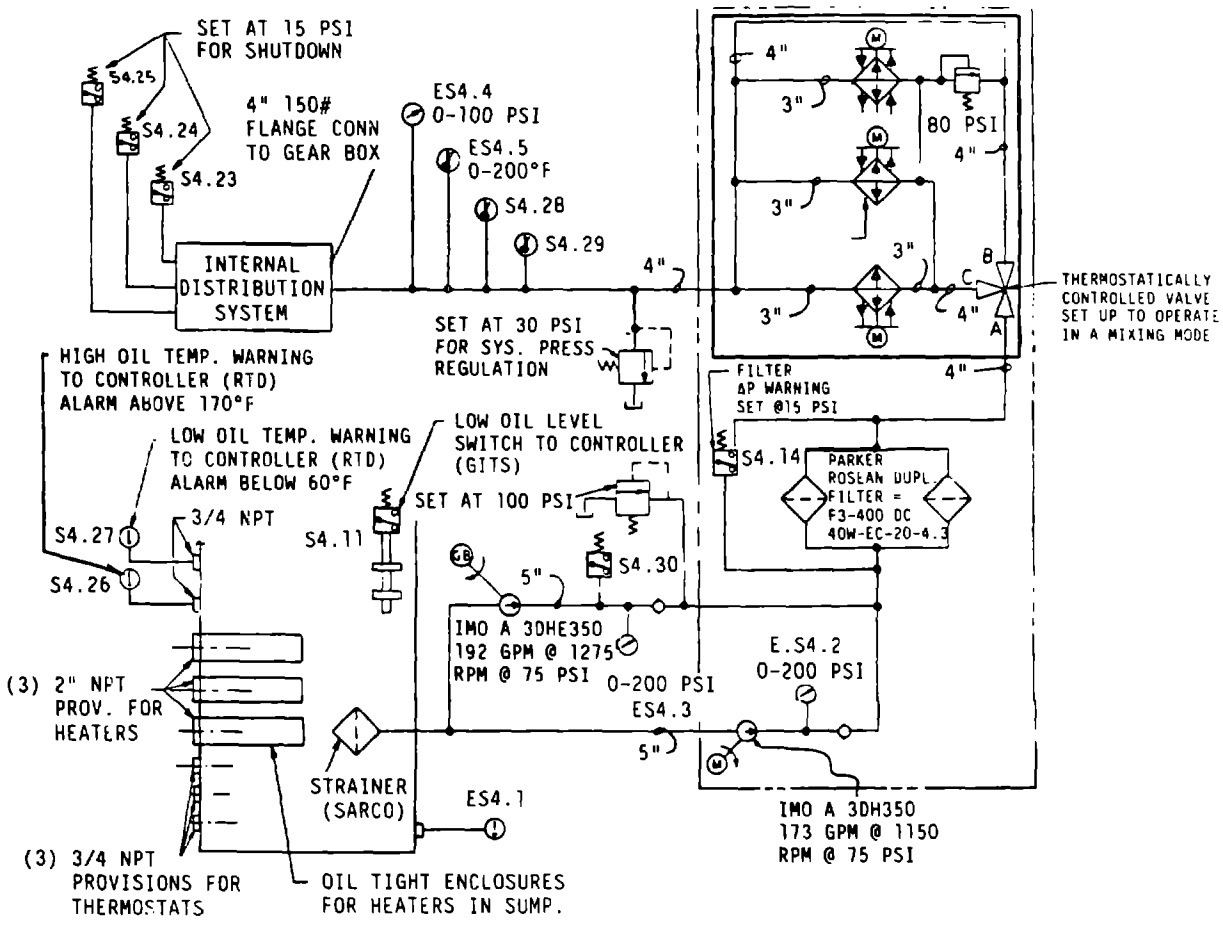

Figure 5-11 Gearbox Oil Lubrication Schematic

Oil is distributed to the gears, splines and bearings in the gearbox by a header 4 in. in diameter, running through the high speed section of the gearbox. The recommended lubricants are:

Mobil SHC 630
1165 SSU at 100°F
131 SSU at 210°F

All equipment on the lube platform is accessible by ladder from the nacelle for inspection and maintenance.

5.5 HIGH SPEED SHAFT AND COUPLING

The model 204 version of the high speed shaft design used splined gear couplings and a slip clutch to protect the drivetrain from torque overloads induced by wind gusts or a malfunctioning synchronous generator. When the generator was changed to a variable speed, wound rotor, induction generator, the need for a slip clutch was eliminated, because the generator became a torque limited component. Furthermore, experience indicated that in high speed applications, the gear-type couplings were prone to maintenance-related failures. Therefore, on the advice of consultants from the GE Medium Gas Turbine Department, the high speed shaft was redesigned with flexible disc couplings which are expected to be maintenance free and highly reliable.

The flexible disc couplings, unlike gear-type flexible joints, do not require lubrication or maintenance. The coupling selected for model 304.2 is produced by Zurn, Inc., Rexnord, and Dana Corp., and offers $\pm$.5° angular freedom and $\pm$3/8 in. axial play. This tolerance is very important, since the design needs to minimize thrust loading on the bearings of driving or driven members. The shaft is a hollow spool piece, which conserves weight. It is bolted to the couplings on either end by a flanged connection, so that removal is easy. Torque transmission between the driving and driven members and the respective couplings is by means of a square key. The couplings are installed with a slight interference fit.

The torque transmitted by the high speed shaft is about 39,750 ft-lb at 1,380 rpm. While the torque is limited by the variable speed generator to 10% above 39,750 ft-lb, the speed can go as high as 1,800 rpm during an overspeed condition with the generator unloaded. The flexible disc elements of the coupling were applied at a low than rated torque to assure a 30-year life (14 X 10^9 revolutions) in the expected duty cycle.

There was no detailed stress analysis support for the high speed shaft design because the loading was light in comparison with the catalogue ratings for the standard equipment selected. The equipment has a static torque capacity that is 4.5 times greater than the rated 40,000 ft-lbs. The expected root mean square alternating torque is only $\pm$ 3,400 ft-lb.

5.6 ROTOR SLIPRING ASSEMBLY

The rotor slipring assembly is required to transmit electrical power and control signal between the fixed nacelle and the rotating blades. Electrical power is required on the blades to drive the hydraulic pump that supplies hydraulic power to the aileron actuators. The control signals are similarly required to read and control aileron position and thereby control rotor speed.

The rotor slipring unit has quantities of rings as shown in Table 5-17.

Table 5-17 Rotor Slipring Assembly

Types of Rings	Rating	Number of Rings
Power Rings	80A, 600V	4
	25A, 600V	12
Control Rings	5A, 600V	39
Signal Rings	1A, 125V	45
Total Rings		100

Dimensions: 16 in. high, 54 in. long, 11 in. deep
Total Weight: 250 lb.

The slipring is bracket mounted on the back wall of the second stage of the gearbox. It is driven by a concentric conduit that penetrates the entire drivetrain, from the slipring to the rotor. A Flexonics bellows coupling connects the slipring rotor to the conduit. Additional definition of the rotor slipring assembly is in section 8.5.

5.7 ROTOR TURNING SUBSYSTEM

The gear increaser drive includes an externally mounted reduction gear for rotating the rotor at 1 rpm to assist maintenance and inspection. The "turning" reduction gear is a single helical worm gear drive enclosed in a welded steel housing. A small electric motor is integrally connected to the turning gear. It can rotate the entire geartrain and rotor in either direction.

The connection between the turning gear and main increaser is a spur gear wheel mounted on the high speed shaft extension of the increaser. A mating spur pinion is mounted on the low speed output shaft of the turning gear. The spur pinion has an integral collar that is linked to an engagement shifting yoke and lever.

This spur pinion can slide along its shaft, and can also lock into position to prevent disengagement while in operation. A protective Kirk interlock ensures secure operation and generates an electrical signal when opened. The electrical signal would be used in a permissive circuit to provide power to the motor, via the controller for operation of the turning subsystem.

To engage the turning gear, the rotor and shaft system must be stopped, the Kirk interlock opened, and the sliding pinion manually pushed to mesh with the spur gear wheel until it is locked into position. Then the electric motor can be either remotely activated through the controller or manually activated at the motor.

6.0 NACELLE SUBSYSTEM

6.0 NACELLE SUBSYSTEM

The nacelle subsystem is located between the rotor subsystem and the tower. The nacelle structurally supports all the elements of the rotor and drivetrain subsystems from the low speed shaft to the generator. It includes structural support elements and support equipment. An efficient structure was designed for the load path from the rotor support to the tower, capable of supporting the rotor weight and of reacting all mass unbalance and aerodynamic loads for 178 x 10^6 revolutions. The load path starts with the spindle, discussed in section 4.6.1, that holds the bearings that support the rotor and is bolted to the rotor support adapter. The adapter is mounted on the bedplate and is rigidly supported by the side and top structural plates. The speed increaser gearbox, the generator, the control equipment for rotor speed and power generation, and the power conditioning elements are mounted on the bedplate. A fairing over the bedplate protects the power equipment from the weather and is used to mount lightweight auxiliary equipment for ventilation and fire protection.

6.1 BEDPLATE

6.1.1 REQUIREMENTS

The bedplate provided a stiff foundation for all equipment mounted in the nacelle area. It must be particularly stiff in bending to avoid exceeding the limits of misalignment of the drivetrain and the flexible shaft couplings. Small deflections were confirmed by the analysis described in section 6.1.4.

6.1.2 DESIGN DEFINITION

The bedplate, including the rotor support structure, is shown in Figures 6-1 and 6-2. It consists of several major subassemblies: the base section, rotor adapter section, side and roof plate sections, and gearbox and generator pedestals. All rolled and plate stock of these components conform to ASTM 572 GR 50.

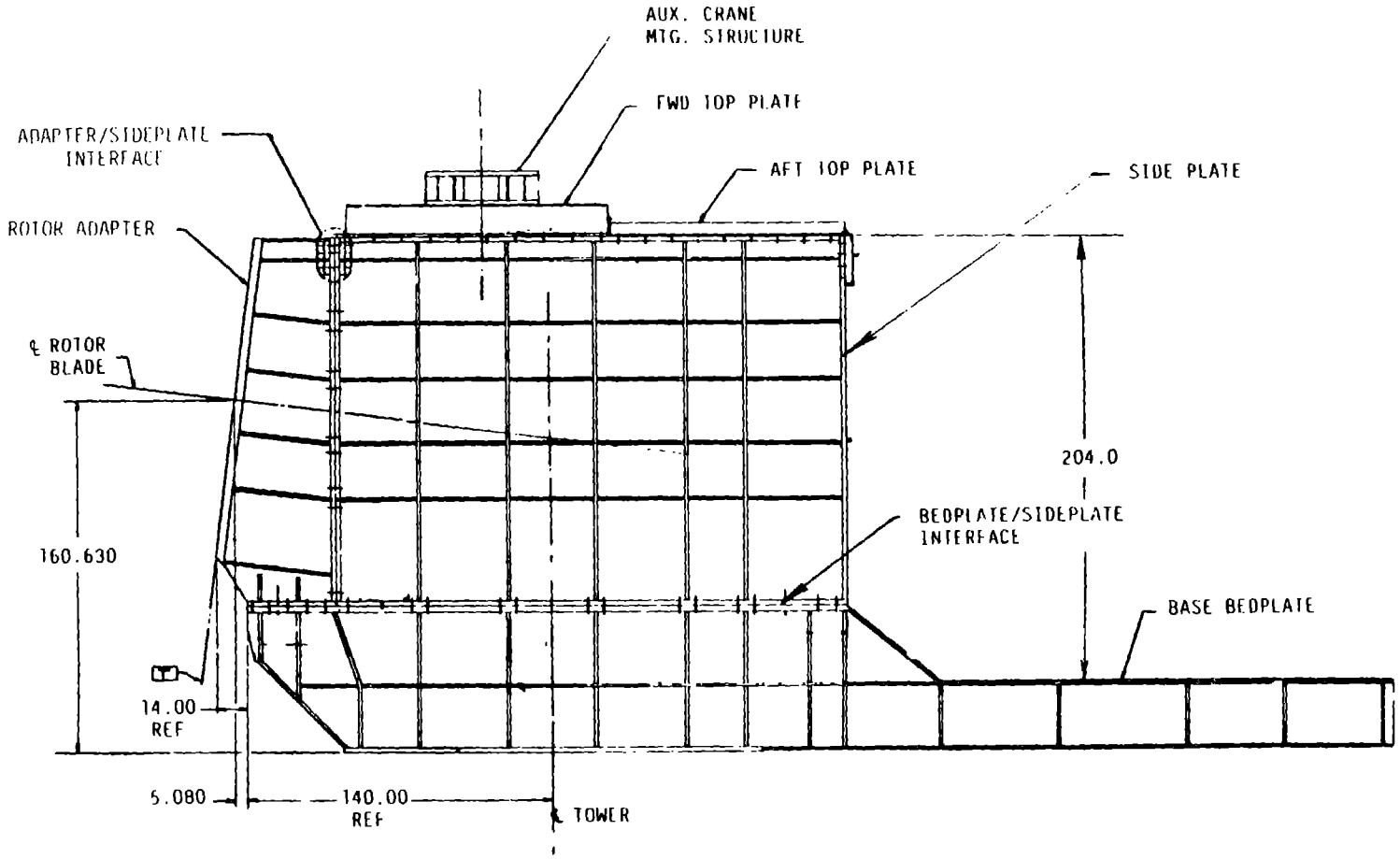

Figure 6-1 Bedplate and Rotor Support Structure

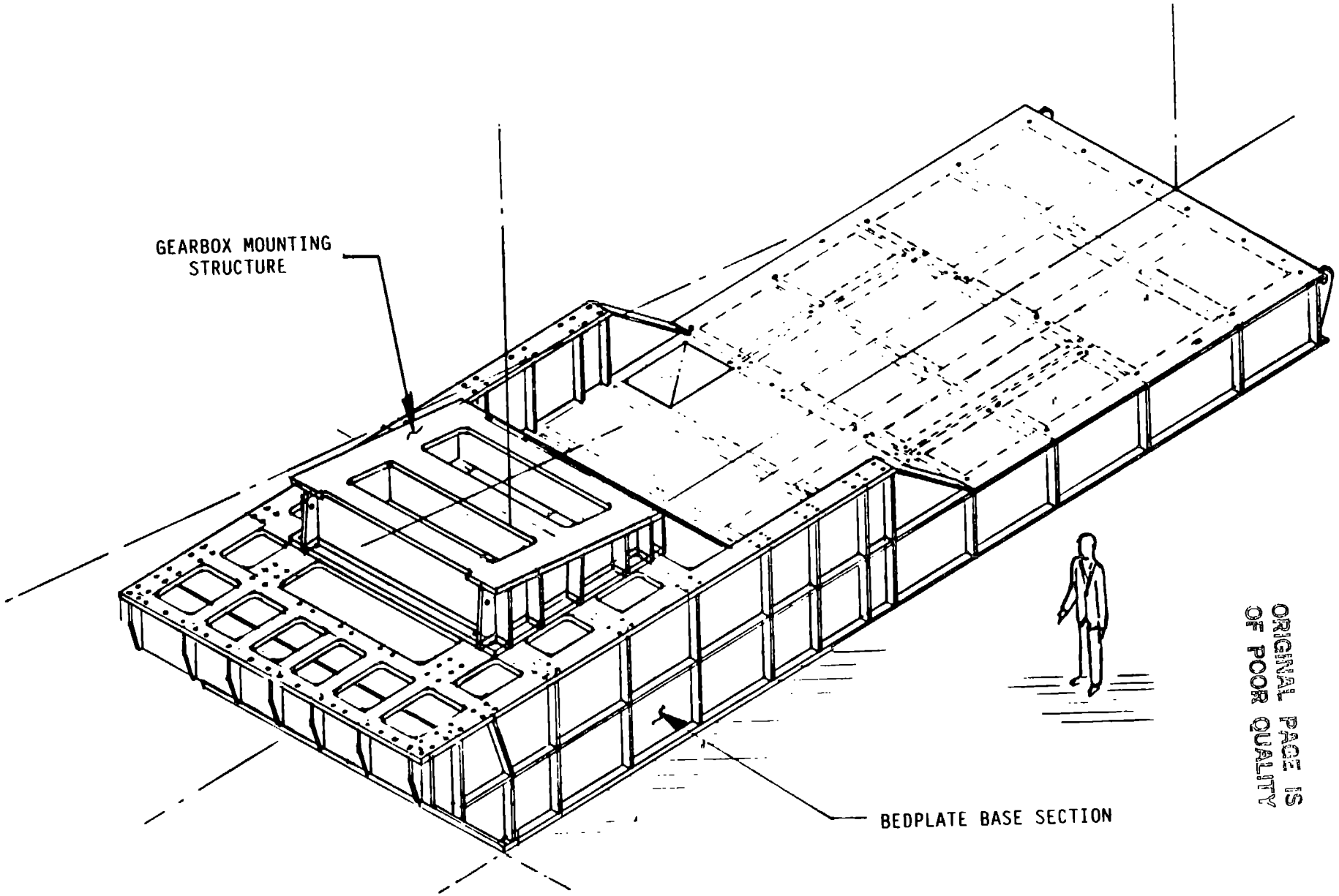

Figure 6-2 Bedplate and Rotor Support Structure, Base Section

6.1.2.1 Base Section

The base section, as shown in Figure 6-2, is built from welded plate and standard structural shapes, to form a rectangular, box-like structure. Transverse members distribute the principal loads to longitudinal beams and to the yaw structure interface. The longitudinal beams are cantilevered from the yaw interface to support the generator and electronic control equipment. Two hatches are incorporated in the base section, to provide access to the nacelle area from the upper level of the tower.

6.1.2.2 Rotor Adaptor Section

The rotor adaptor support section, shown in Figure 6-3, provides a transition from the circular rotor bearing spindle shaft to the square section of the upper bedplate structure. It is built from welded plate sections, with the fore and aft flat plate connected by a frustum section. Radial stiffening members connect the frustum section to the flat plate framing members. The rotor adaptor is bolted to the base section.

6.1.2.3 Side and Top Plates

Two rectangular side plates are bolted to the rotor adaptor and the bedplate base section. A two-piece roof plate is bolted across the side plates and rotor adaptor section. These members are constructed from welded plate sections, to form a multi-cruciform cross section.

The rotor adaptor is designed with enough stiffness so that it will not deform or because of the rotor weight if the roof sections are removed in order to remove the gearbox unit.

6.1.2.4 Mounting Structures

Two mounting pedestals are attached to the bedplate section for mounting the gearbox and generator. These pedestals were used to compensate for the 7° inclination of the rotor's rotational axis. The mounting structures are made from welded plate sections to form I-beam structures. The gearbox mounting structure is bolted to the bedplate section with bolts 2 in. in diameter and the generator mounting structure is bolted with bolts 1.25 in. in diameter.

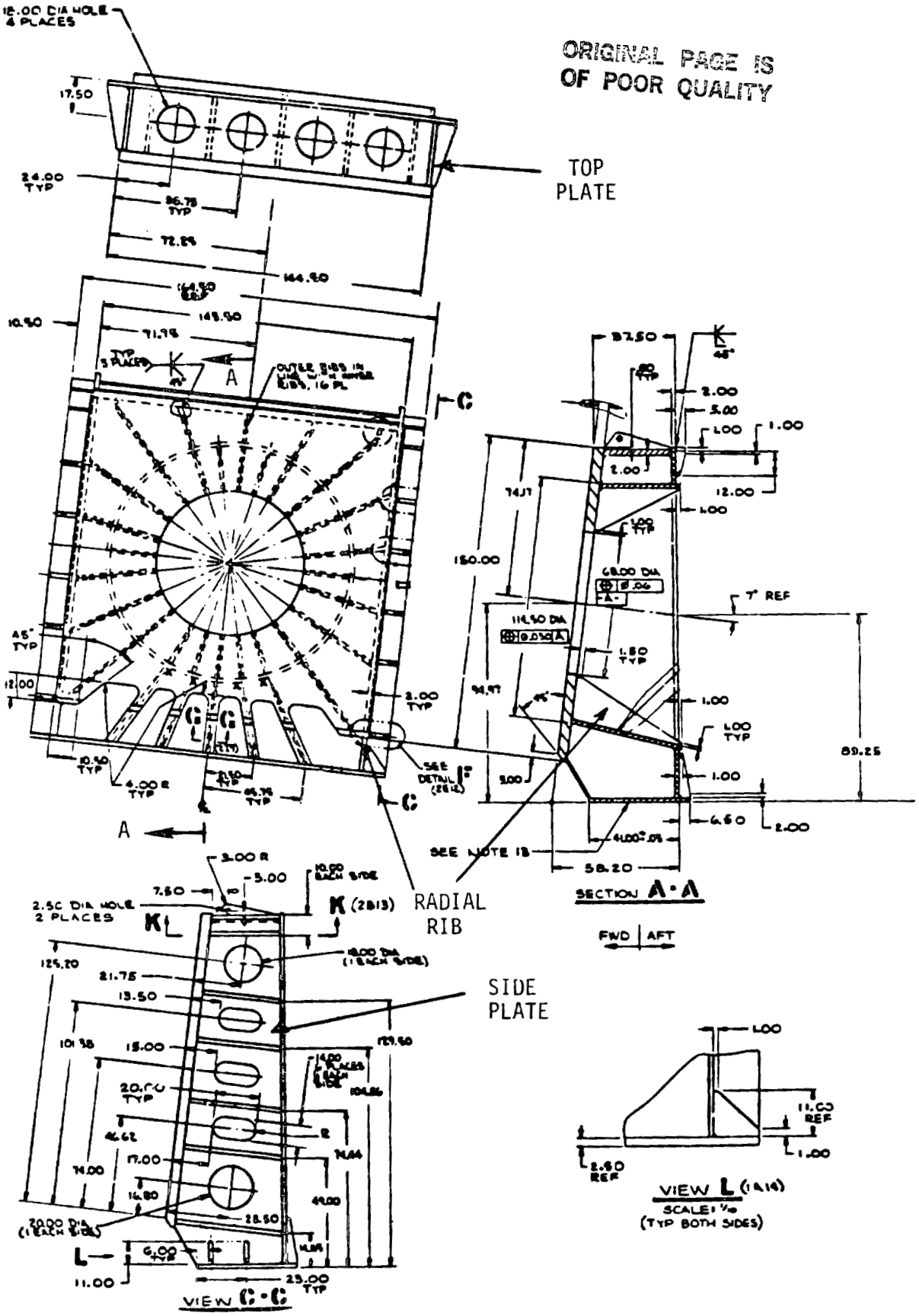

Figure 6-3 Rotor Support Adaptor Section

6.1.2.5 Assembly

The bedplate structure comprises four major subassemblies. Each steel weldment subassembly is designed in accordance with AISC requirements for fatigue-rated structures. The size of each assembly was determined for convenient shipping. All interfaces are bolted, so they can be assembled in the field. All interfaces were machined for good joint alignment.

The most important alignment in the bedplate assembly maintains the mounting face of the rotor adapter structure perpendicular to the mounting pads of the gearbox. This alignment makes sure that the rotor assembly, located by the rotor spindle hub forward face, is perpendicular to the low speed shaft of the gearbox. Alignment is obtained by making a final machine cut of the rotor adapter structure after it is installed to the bedplate. Tolerances on this alignment will result in a change in slope of the drive shaft between the rotor and the gearbox and are accommodated by the flexible gear coupling halves on the drive shaft. The drive shaft couplings also permit some lateral misalignment between the two mounting surfaces.

Misalignments between the gearbox mounting feet and the low speed stub shaft can be corrected, by machining the bedplate mounting surfaces. However, the horizontal mounting pads also allow shimming to reduce this misalignment. Precise grinding is not required; a tolerance of 0.10 in. over the 100 in. diameter of the rotor adapter structure results in a slope error of 1 in 1,000. This error is well within the capability of the shaft coupling, which can tolerate 0.5° per engagement, to accommodate dynamic deformation of the bedplate.

Since the drive shaft couplings also accept some longitudinal misalignment, tolerances that locate the gearbox with respect to the rotor adapter structure in the longitudinal direction are not as important. There is no final machining of the bedplate assembly.

6.1.3 ROTOR SUPPORT STRUCTURE STRESS ANALYSIS

6.1.3.1 Loads

The loads were determined by the analysis discussed in sections 7.0 through 7.5 in Volume II. Loads simulating various operating conditions were taken at the interface between the nacelle and low speed shaft. Fatigue and limit loads were considered in this analysis. These loads are summarized in Tables 6-1 and 6-2 and Figure 6-4.

6.1.3.1.1 Analysis

The analysis of the rotor support structure combined the spindle, adapter, and gearbox enclosure in one finite element model, shown in Figure 6-5. The spindle structure consists of a cylinder and flanges, shown in Figure 6-6. The adapter structure, shown in Figure 6-7, consists of a top plate, bottom plate, side plates, back plate, front plate, cylinder, and radial reinforcing ribs. The gearbox enclosure consists of reinforced sidewall plates, which are called the right and left support, and a removable cover. A side sectional view of these three substructures is shown in Figure 6-8. The relation of the rotor support structure to the yoke and bedplate is shown in Figure 6-9.

The rotor support structure transmits all loads, except drivetrain torque, from the yoke to the bedplate. The central yoke tube exerts reactions on the spindle cylinder through the tapered roller bearings. These reactions are transferred to the enclosure and the adapter through bolted connections. The enclosure is attached to the bedplate with bolted connections.

A linear elastic finite element model was developed using the "MacNeal-Schwendler" NASTRAN Program, Version 62A. The model and nomenclature, with 1855 grid points, and 3726 elements, described in Figure 6-5, represented the structure of the spindle, adapter, and enclosure, which function together to transfer loads to the bedplate.

The loads were applied to the model at the reaction points of the forward and aft tapered roller bearing sets. The rigid elements distribute forces and moments from the system's dynamic loading centroid at the nacelle and low speed shaft interface, which has five degrees of freedom, to these reaction points.

Table 6-1

Limit Loads Applied at the Nacelle
and Low Speed Shaft Interface

	Vx (lbs.)	Vy (lbs.)	Vz (lbs.)	Mx (in-lb)	My (in-lb)
Extreme Wind, 130 mph	$-.6417 \times 10^6$	0	$.385 \times 10^6$	0	-51.12×10^6
Normal Shutdown, 60 mph	$-.6659 \times 10^6$	$.0569 \times 10^6$	$-.1024 \times 10^6$	-3.312×10^6	-105.02×10^6
Normal Shutdown, 60 mph Modified	$-.6659 \times 10^6$	$.0569 \times 10^6$	$-.1024 \times 10^6$	-62.65×10^6	-45.68×10^6
Control Malfunction, 60 mph	$-.6682 \times 10^6$	$.0087 \times 10^6$	$-.524 \times 10^6$	2.774×10^6	-68.03×10^6

Table 6-2

Limit Loads Applied at the Nacelle
and Low Speed Shaft Interface

	Vx (lbs.)	Vy (lbs.)	Vz (lbs.)	Mx (in-lb)	My (in-lb)
99.99th percentile Type 1 and 2					
Mean	$-.641 \times 10^6$	$.627 \times 10^3$	$-.227 \times 10^6$	$.1033 \times 10^6$	-66.48×10^6
Alternating	$.0228 \times 10^6$	$.489 \times 10^4$	$.0902 \times 10^6$	2.028×10^6	1.464×10^6
50.0th percentile Type 1 and 2					
Mean	$-.641 \times 10^6$	$.627 \times 10^3$	$-.227 \times 10^6$	$.1033 \times 10^6$	-66.48×10^6
Alternating	$.0108 \times 10^5$	$.319 \times 10^4$	$.008 \times 10^6$	1.056×10^6	$.5688 \times 10^6$
RMC Type 1 and 2					
Mean	$-.641 \times 10^6$	$.627 \times 10^3$	$-.227 \times 10^6$	$.1033 \times 10^6$	-66.48×10^6
Alternating	$.0131 \times 10^6$	$.326 \times 10^4$	$.0122 \times 10^6$	1.147×10^6	$.6084 \times 10^6$
Type 3					
Mean	$-.638 \times 10^6$	$-.0102 \times 10^6$	$-.165 \times 10^6$	-1.608×10^6	-66.84×10^6
Alternating	$.0190 \times 10^5$	$.0184 \times 10^6$	$.150 \times 10^6$	2.964×10^6	1.908×10^6

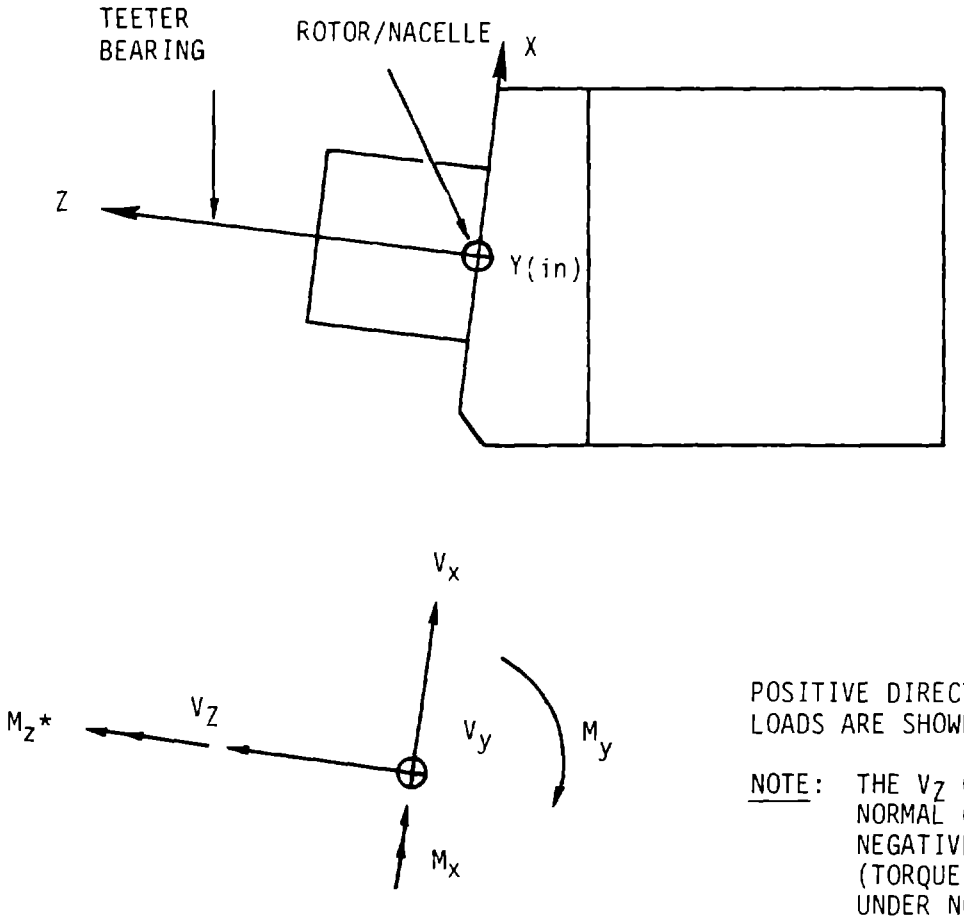

POSITIVE DIRECTIONS OF APPLIED LOADS ARE SHOWN.

NOTE: THE V_Z OR THRUST LOAD UNDER NORMAL OPERATION HAS A NEGATIVE SIGN. ALSO THE M_Z (TORQUE) AND THE V_x LOADS UNDER NORMAL OPERATION HAVE NEGATIVE SIGNS.

Figure 6-4 Coordinate System for Applied Loads

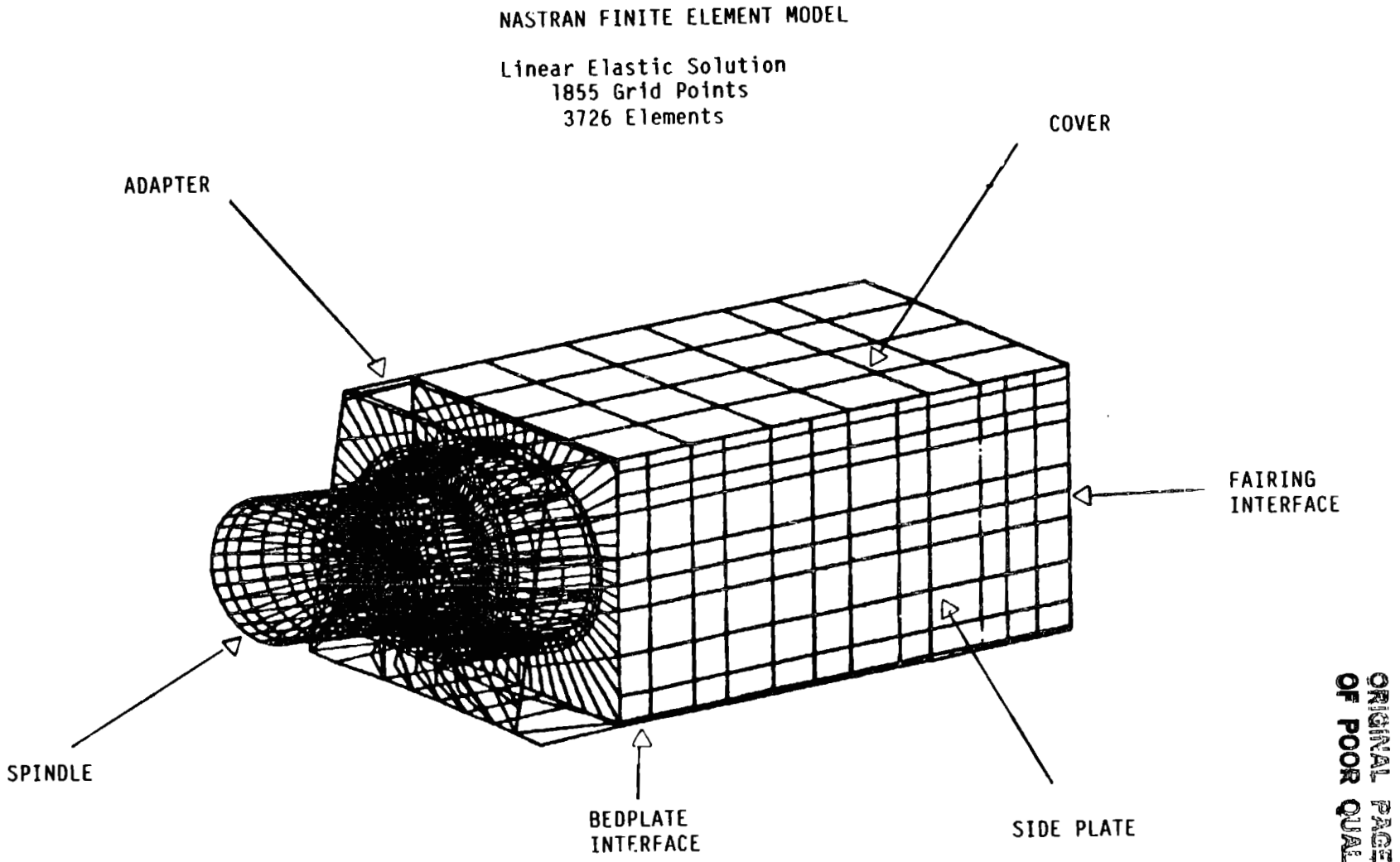

Figure 6-5 Rotor Support Finite Element

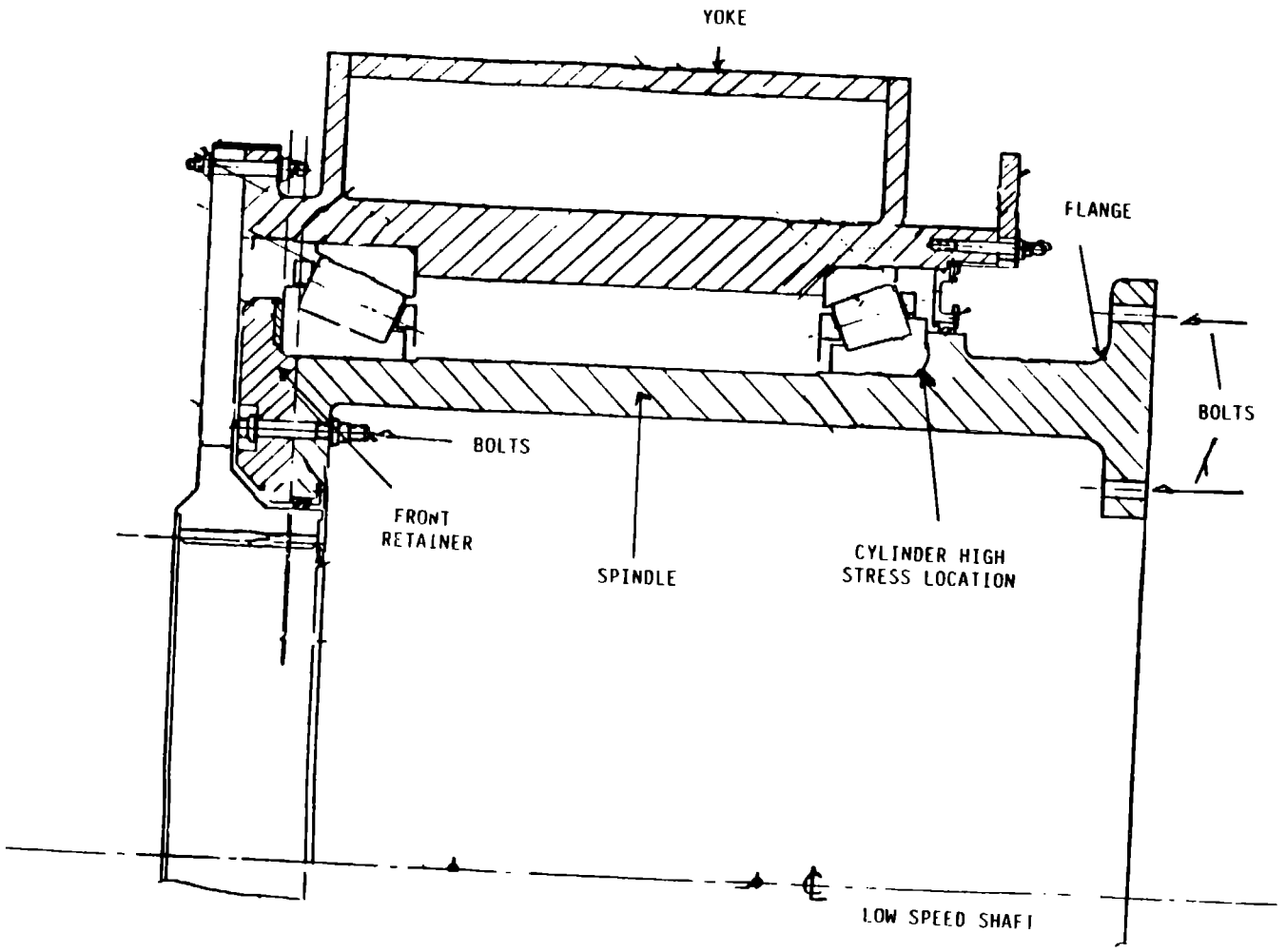

Figure 6-6 Relationship of Spindle and Yoke via Tapered Roller Bearing Set

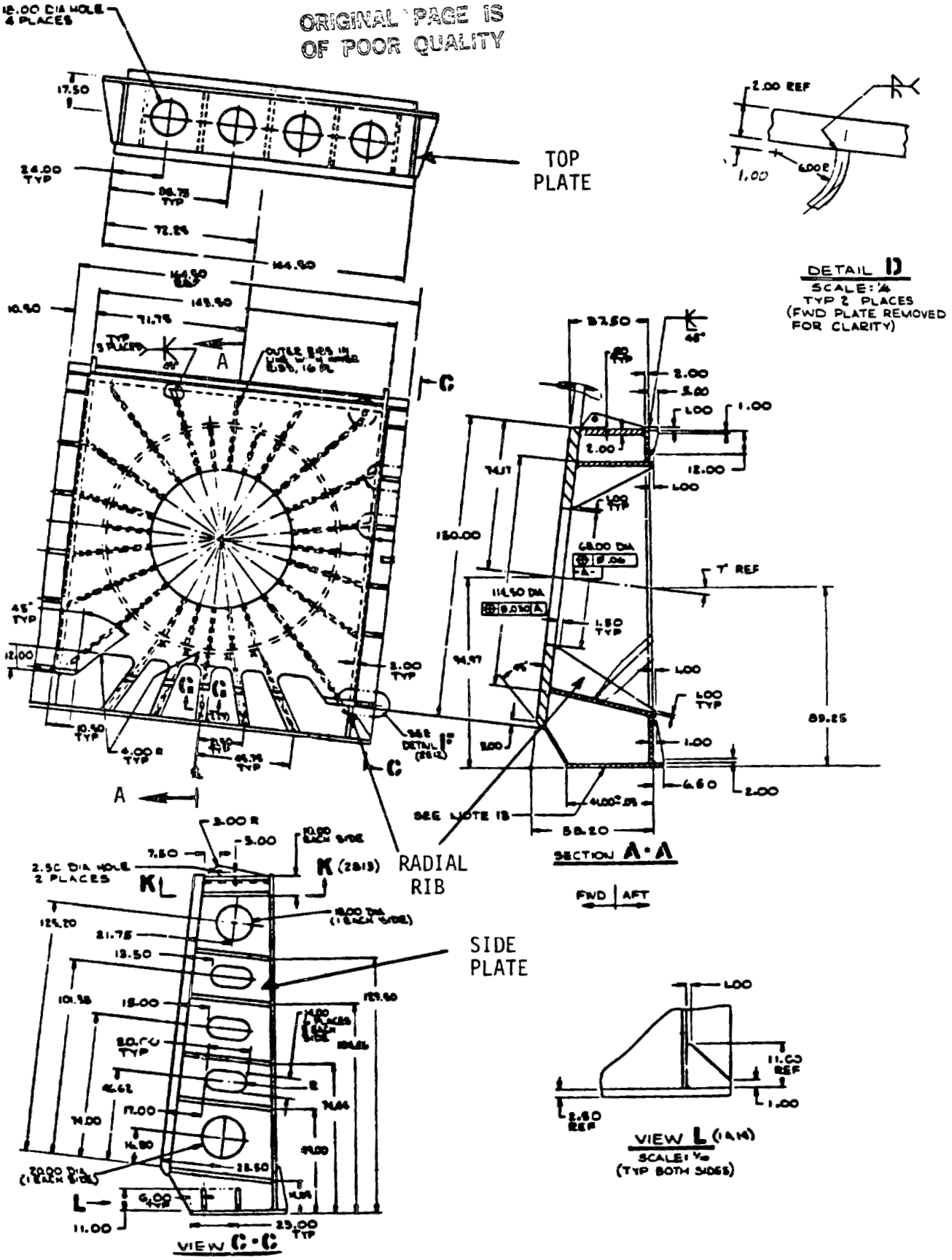

Figure 6-7 Adapter Weldment

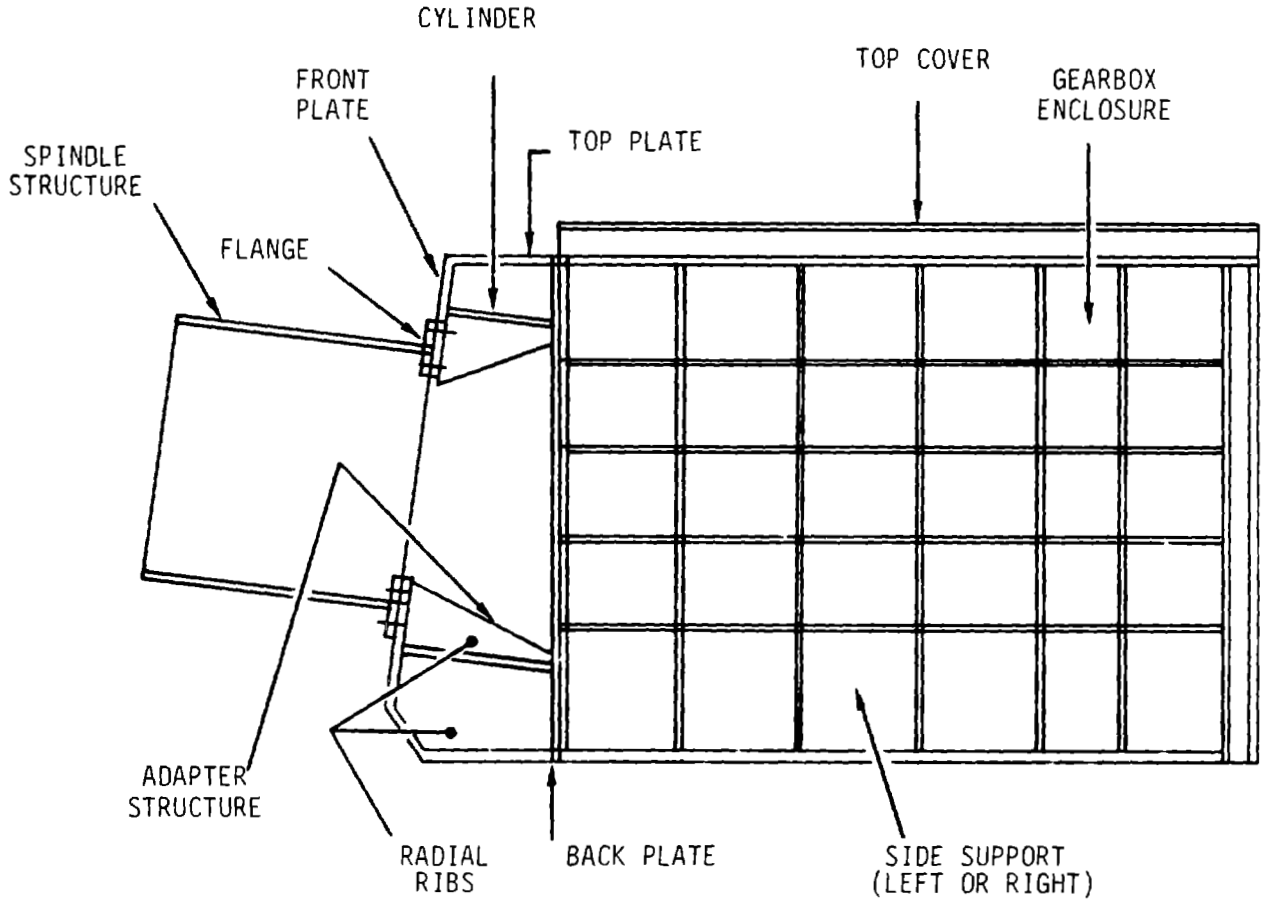

Figure 6-8 Cross-Sectional View Through Central Vertical Plane

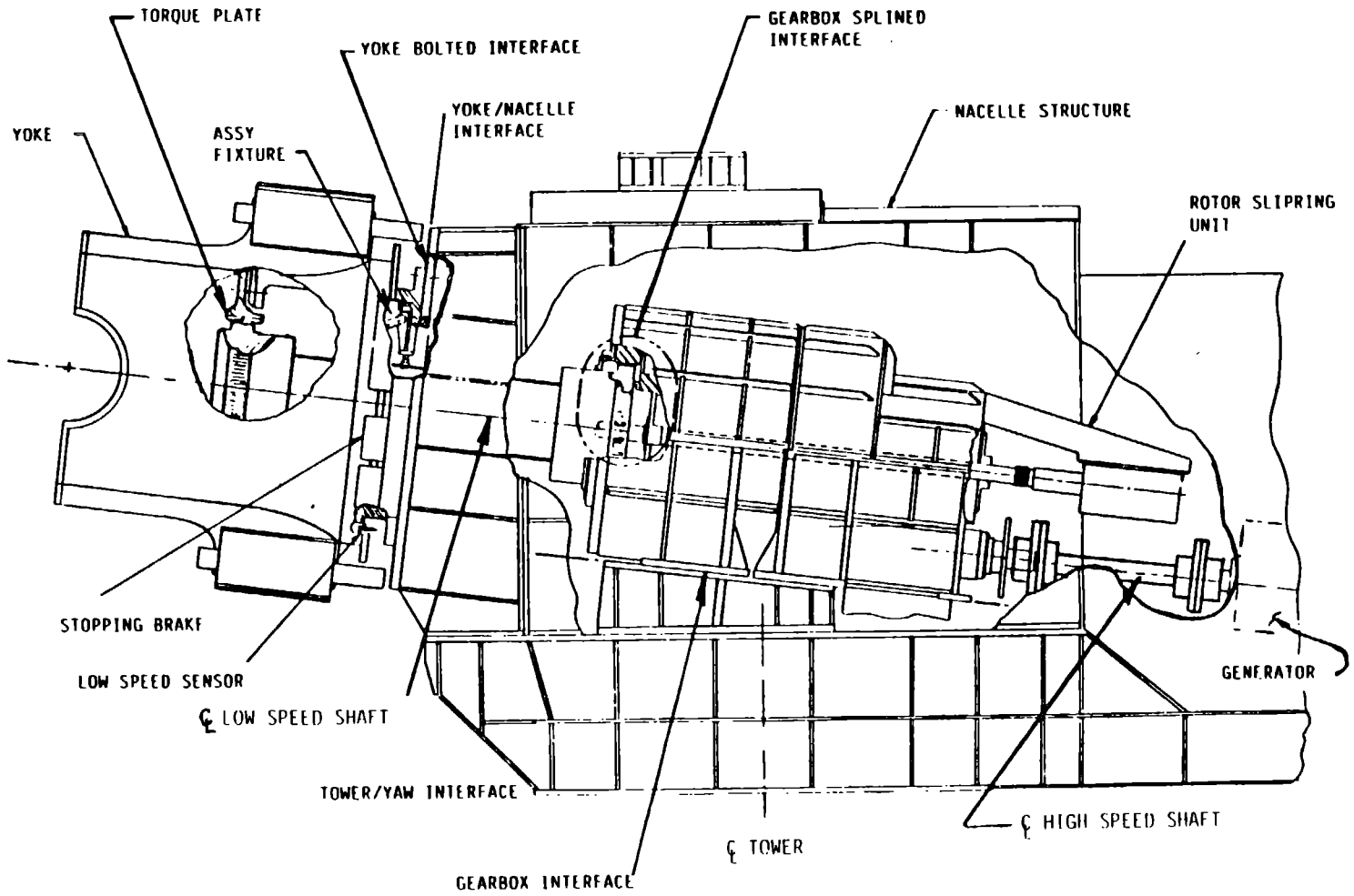

Figure 6-9 Structural Relationship

These rigid elements simulated the loading directions, the pressure distribution, and the geometry of the tapered roller bearings using a special coordinate system and point load transfer oriented to simulate the roller contact angles.

Steady, alternating, and limit load stresses for the fatigue cases and limit load cases were obtained from the NASTRAN results. The minimum fatigue and limit load margins of safety were determined from the loading conditions shown in Tables 6-1 and 6-2. However, the model did not show peak stresses in several areas where local stress concentrations were important. These regions were evaluated by local analyses, starting with the loads and stresses obtained from the NASTRAN analysis.

The structural margins of safety were calculated to the limit load and root mean cubed (RMC) fatigue criteria, as discussed in section 9 of Volume II. Minimum margins of safety were calculated to be 0.0 and .07 for the limit load and RMC fatigue cases, respectively.

The NASTRAN results were scanned to find the peak stresses for the limit load and RMC fatigue load cases. They are summarized in Tables 6-3 and 6-4. The minimum margin of safety was calculated to be 1.0 and .37 for the radial ribs in the adapter structure, for the limit and RMC fatigue cases, respectively.

The minimum margin of safety was calculated to be .04 for the doubler plates, shown in Figures 6-10 and 6-11, and .07 for the front bearing retainer, shown in Figure 6-8, from the local analyses for the limit and RMC fatigue cases, respectively. The results of these calculations are summarized in Tables 6-5 through 6-7.

The bolting was analyzed in accordance with the guidelines of the Structural Design Criteria, included in section 9 of Volume II. Bolting was specified to be 140 ksi UTS, fatigue-rated, alloy steel bolts. The bolting satisfied the guidelines of the Structural Design Criteria guidelines for prying action, preload, bolt strength, thread design, and other considerations. The minimum

Table 6-3

NASTRAN Analysis for the Limit Load Case
Margin of Safety

	Calculated Stress (psi)	Allowable Stress (psi)	Margin of Safety
SPINDLE STRUCTURE			
SPINDLE	7,239	30,000	3.14
FLANGE	12,577	30,000	1.38
ADAPTER STRUCTURE			
FRONT PLATE	7,991	30,000	2.75
CYLINDER	6,893	30,000	3.35
TOP PLATE	8,283	30,000	2.62
RADIAL RIB	14,944	30,000	1.01
BACK PLATE	7,787	30,000	2.85
GEARBOX ENCLOSURE			
TOP COVER	2,675	30,000	10.21
RIGHT SIDE SUPPORT	6,353	30,000	3.72
LEFT SIDE SUPPORT	6,194	30,000	3.84

Table 6-4

NASTRAN Analysis for the RMC Fatigue Load Case
Margin of Safety

	Steady[1] Stress (psi)	Alternating Stress (psi)	Allowable Stress (psi)	Margin of Safety
SPINDLE STRUCTURE				
SPINDLE	4,455	89	182	1.05
FLANGE	8,550	158	251	.59
ADAPTER STRUCTURE				
FRONT PLATE	5,386	110	212	.93
CYLINDER	3,984	67	143	1.13
TOP PLATE	4,955	33	66	.99
RADIAL RIB	10,140	223	306	.37
BACK PLATE	4,435	156	303	.94
GEARBOX ENCLOSURE				
TOP COVER	1,615	14	36	1.57
RIGHT SIDE SUPPORT	3,778	52	114	1.20
LEFT SIDE SUPPORT	3,758	73	158	1.16

NOTES: 1. Steady stresses increased by 10,000 psi to compensate for potential residual stresses when calculating allowable stresses in welds.

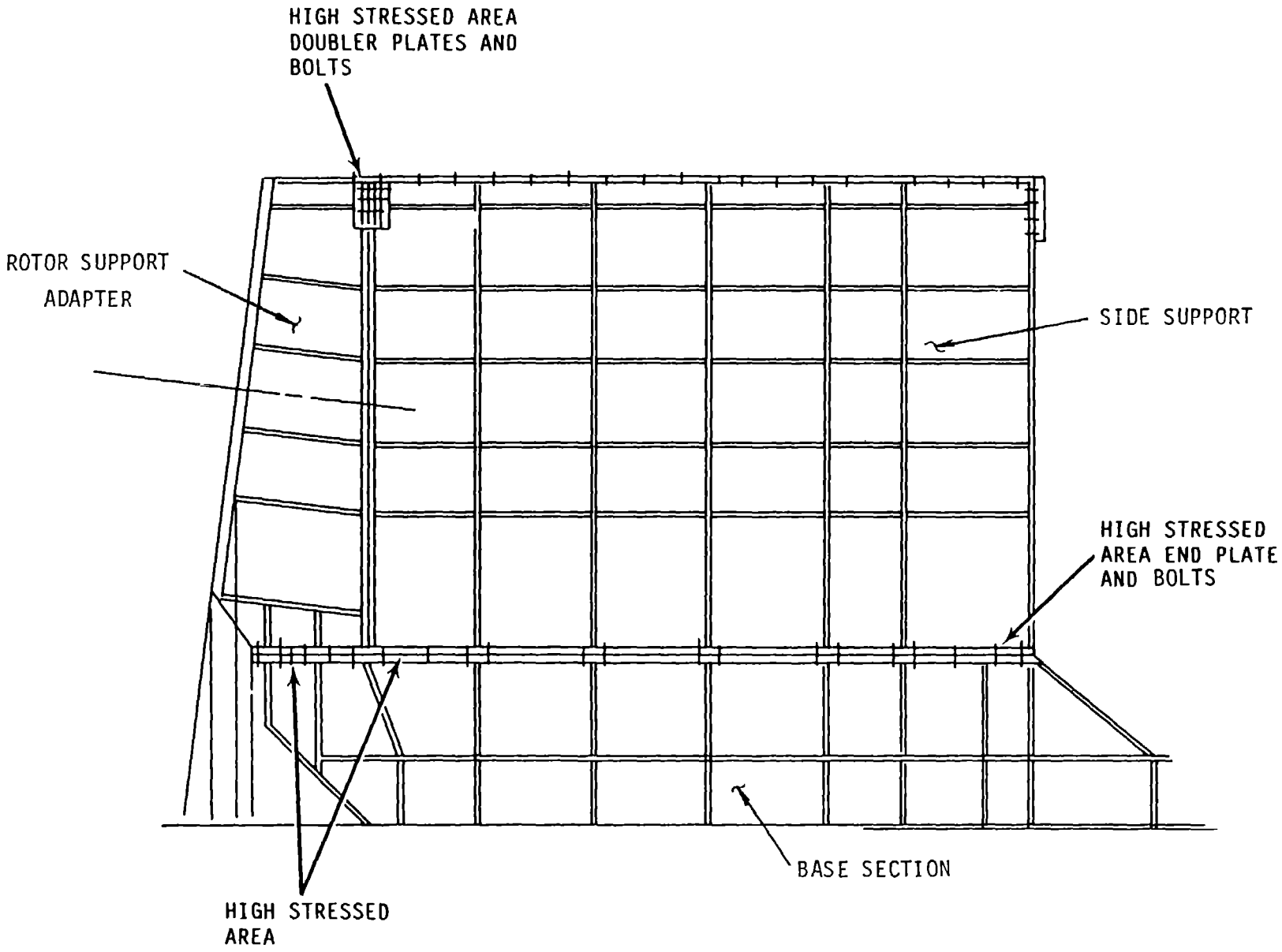

Figure 6-10 Important Bolt Locations

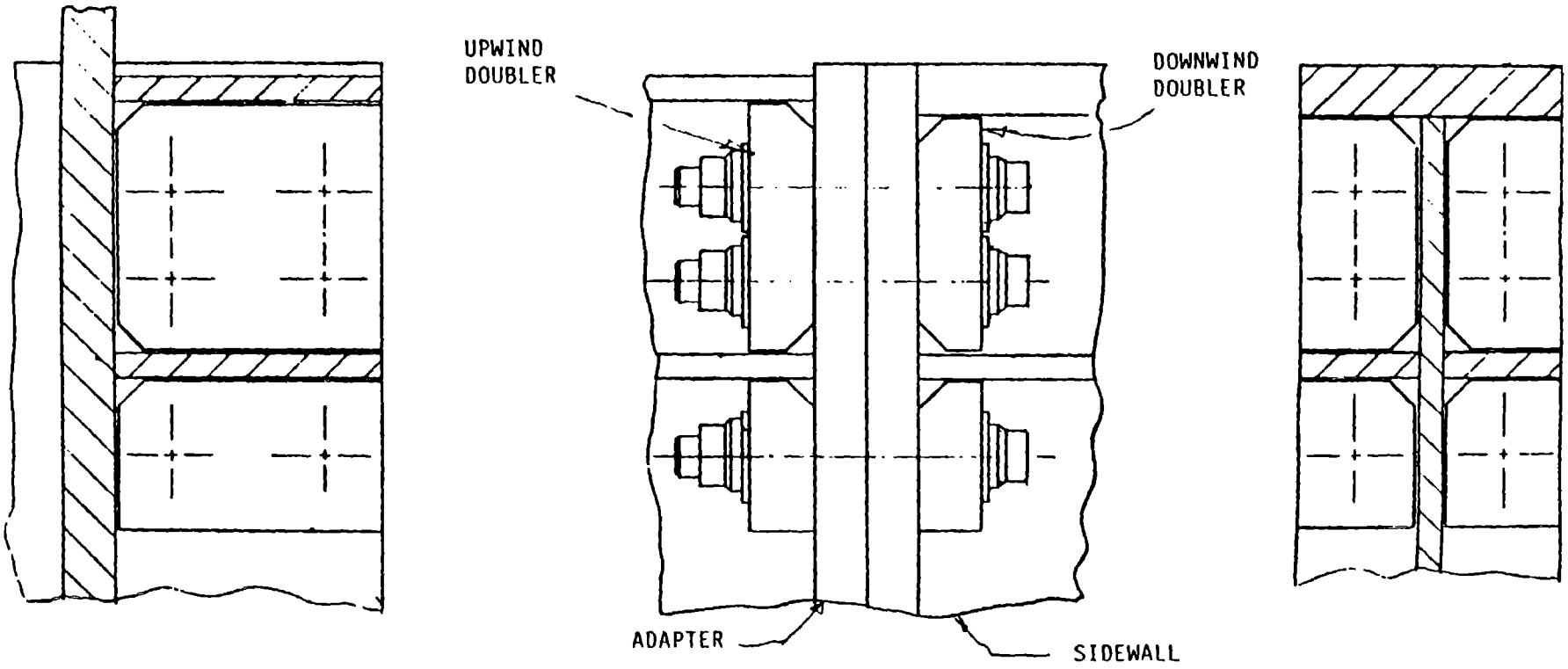

Figure 6-11 Doubler Plates and Bolts

Table 6-5

Spindle Structure
Margin of Safety for the Limit Load Case

	Calculated Stress (psi)	Allowable Stress (psi)	Margin of Safety
Front Bearing Retainer	20,905	30,000	.43
Front Bearing Retainer 1.5 in. diameter bolts(1)	89,385	95,400	.06
Adapter to Spindle 1.5 in. diameter bolts(1)	65,821	95,400	.44

Margin of Safety
RMC Fatigue Load Case

	Steady Stress (psi)	Alternating Stress (psi)	Allowable Stress (psi)	Margin of Safety
Cylinder	19,494	391	1,080	.48
Flange	24,237	419	840	1.00
Front Bearing Retainer	26,887	542	580	.07
Front Bearing Retainer 1.5 in. diameter bolts(1) 18.10		47,222	89	1,700
Adapter to Spindle 1.5 in. diameter bolts(1) 24.97		35,323	77	2,000

NOTES: 1. Alloy Steel Bolt 140 UTS.

Table 6-6

Adapter Structure
Margin of Safety for the Limit Load Case

	Calculated Stress (psi)	Allowable Stress (psi)	Margin of Safety
Adapter to Bedplate			
Bolt Diameter: 1.5 in.	38,719	38,090[1]	0.0
Top Plate with Cutouts[2]	4,732	20,000	3.22
Side Plate with Cutouts[2]	8,054	30,000	2.72

NOTES: (1) Based on shear bolt allowable.
(2) Cutouts shown in Figure 6.
(3) Alloy Steel Bolt 140 UTS.

Table 6-7

Gearbox Enclosure
Margin of Safety for the Limit Load Case

	Calculated Stress (psi)	Allowable Stress (psi)	Margin of Safety
Adapter to Side Support 1.25 in. diameter bolts(1)	49,026	53,473	.09
Adapter to Side Support Upper Corners with Doubler Plates 1.25 in. diameter bolts(1)	49,028	59,370	.21
Adapter Back Plate Upwind Doubler Plate	31,342	33,000	.04
Sidewall Flange to Adapter Downwind Doubler Plate	23,002	33,000	.43
Side Support to Bedplate 1.5 in. diameter bolts(1)	59,721	28,084	1.12
Side Support to Bedplate End Plate	21,153	33,000	.56

NOTES: (1) Alloy steel bolt 140 UTS.

margin of safety was calculated to be 0.0 for the limit load case in shear for the bolting that secures the adapter to the bedplate at the center of the bottom of the back plate.

The loads in the spindle attempt to separate the flange from the adapter structure. The stresses tend to peak near the flange end of the spindle, where the cantilevered structure is fixed by the bolts. A local NASTRAN analysis confirmed that there is minimal prying action in this joint. The largest stresses occurred in the fillet geometries of the flange and aft bearing. These stresses are summarized in Table 6-5 for the limit load and RMC fatigue load cases.

The forward bearing is secured with a retainer structure, which is bolted to the spindle as shown in Figure 6-6. The stresses in the retainer and bolting were calculated in a local analysis and are summarized in Table 6-5.

The adapter structure is loaded by the reactions of the bolts connected to the spindle. The loads induce bending, membrane, and shear stresses to the various members, depending on their orientation. The loads are transferred from the adapter to the enclosure and bedplate structures through bolted connections.

The bolting between the bedplate and adapter has a margin of safety of 0.0 for the limit load in shear. This margin of safety is the result of the distortion of the adapter caused by the overhung rotor dynamic moment. The stresses and margins of safety in the cutouts of the top plate and side plates were calculated for the limit loads. They are summarized in Table 6-6. Fatigue stresses at the cutouts result in large margins of safety. The other members of the adapter were analyzed satisfactorily using the NASTRAN results. They are summarized in Tables 6-3 and 6-4.

The gearbox enclosure reacts the loads from the adapter and transfers them to the bedplate. The large overturning moment resulting from the rotor's dynamic weight tends to load the upper corners closest to the adapter and the lower corners closest to the fairing, as shown in Figure 6-7.

The most important stresses in these regions were caused by the limit loads. The RMC fatigue stresses were small. The flanges in the upper corners were reinforced with doubler plates, as shown in Figures 6-10 and 6-11. The calculations, which are summarized in Table 6-7, show a minimum margin of safety of 0.04 for the doubler plates. Margins of safety for the other sections of enclosure structure were analyzed satisfactorily from the NASTRAN results. They are summarized in Tables 6-3 and 6-4.

C-6

6.1.4 BEDPLATE AND GEARBOX MOUNTING PEDESTAL STRESS ANALYSIS

The gearbox mounting and bedplate structures were evaluated using a finite element model of the design. Two finite element models of the final design were created and analyzed using the MacNeal-Schwendler MSGMESH pre-processor to generate the models, and the NASTRAN solution format to generate linear static solutions. One model represented the gearbox mounting structure and the central region of the bedplate model shown in Figure 6-12. This model was used to determine the approximate load paths to the interface between the bedplate and yaw, to determine the sizes of the members that support the gearbox and to determine the approximate distribution of bolt loads at the yaw interface. Another model represented the bedplate, shown in Figure 6-13. This model was used to determine stresses at the weld locations and to predict bolt loads at each of the important interfaces.

Loading was applied according to the results of the rotor mount analysis, which predicted the distribution of forces at each bolt in the interface between the yaw and the bedplate. The distribution of gearbox footing forces was estimated by the Philadelphia Gear Corporation (PGC).

The entire bedplate structure was divided into 32 sub-structural regions. Using this method, locations of maximum stress could be identified conveniently. A separate elemental plot set was created in the finite element model, to correspond with each of the regions. For the fatigue analysis, contour plots of maximum Hencky-von Mises stresses were generated for the average mean and the root-mean-cubed (RMC) loading conditions. For each region, the maximum absolute values of mean and alternating stresses were located. An additional mean stress of 10 ksi was used, to account for a maximum potential residual tensile stress of .20 Fy that may be present, although the specified post weld heat treatment process is supposed to relieve it.

Curves were plotted for the various AWS/AISC weld categories shown in Figure 6-14. This data was based on the allowable alternating-cycle intercept stress (CIS) values listed in Table 9-2 of Volume II. The alternating stress and mean stress coordinate was plotted on the graph and compared with the

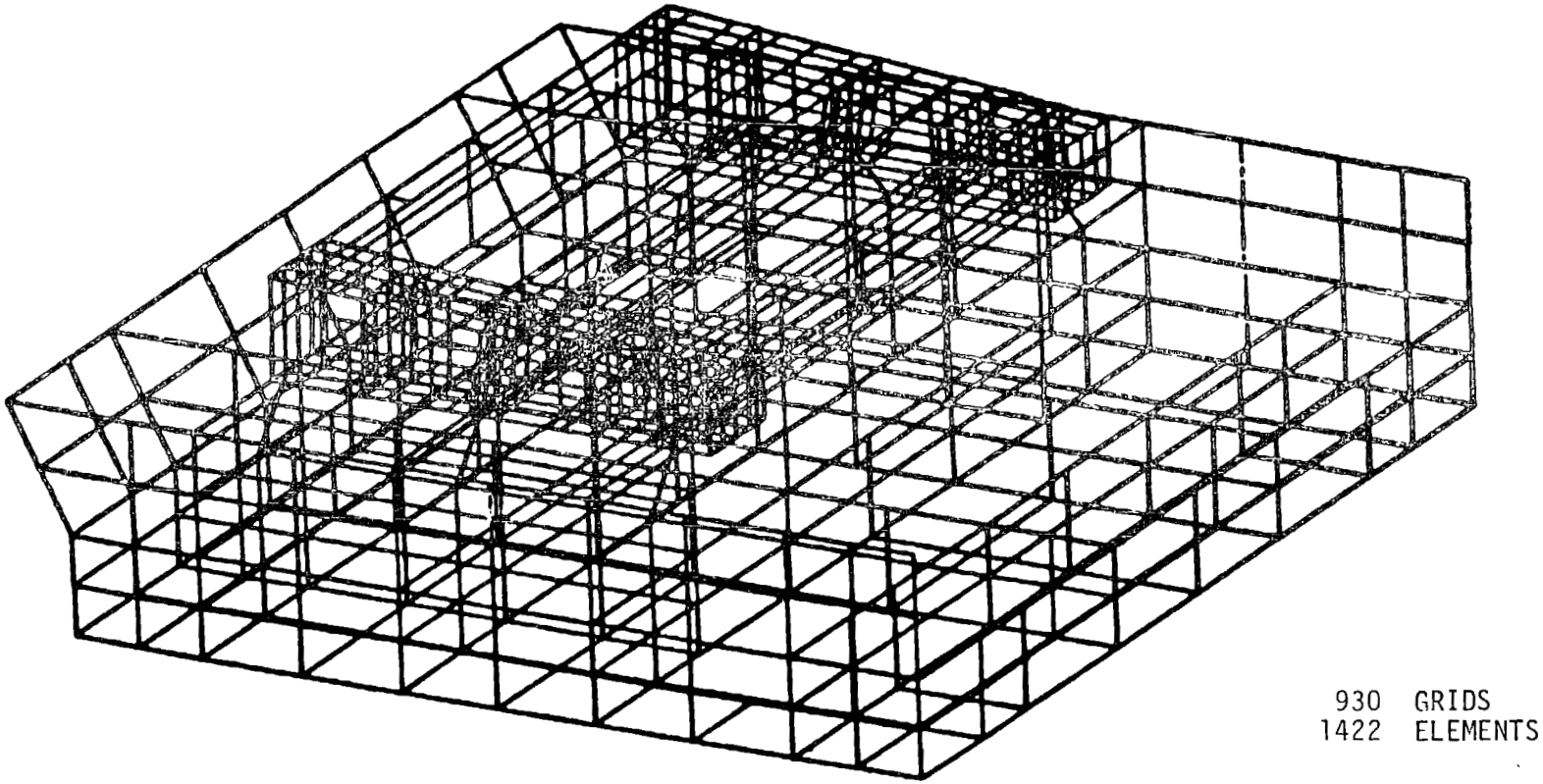

Figure 6-12 Design Development of the Finite Element Model for the Gearbox Mounting Structure and Central Bedplate Region

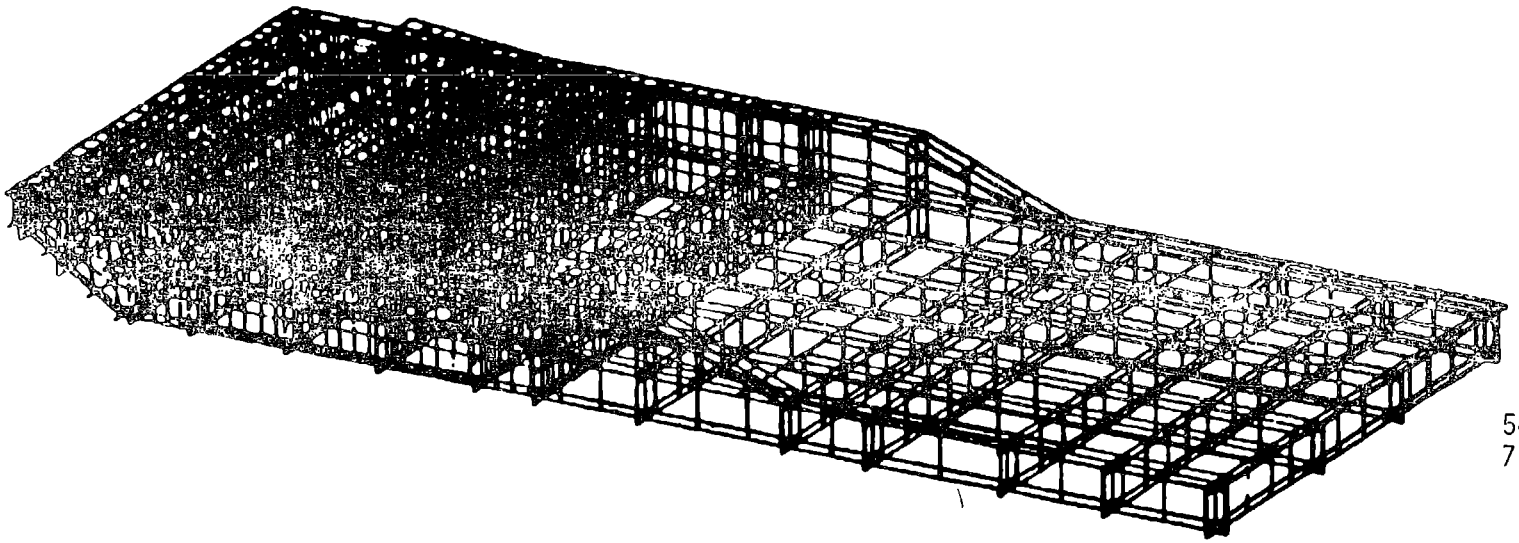

Figure 6-13 Detailed Finite Element Model of the Bedplate

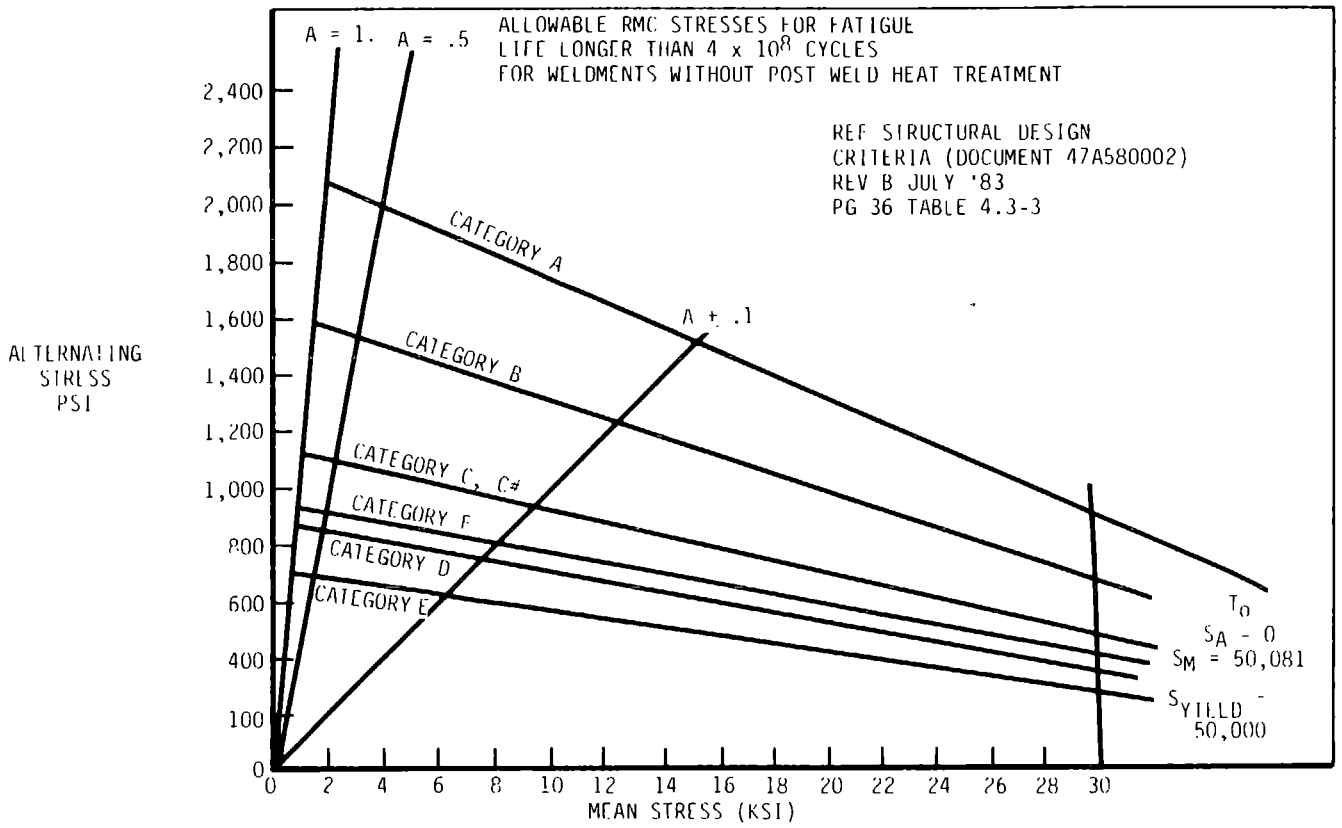

Figure 6-14 Allowable RMC Stresses for Fatigue Life Longer than 4 x 10^8 Cycles for Weldments Without Post-Weld Heat Treatment

allowable stress for the weakest welded fabrication detail in the region. In most cases, this coordinate fell in Category E, and provided a substantial margin of safety for the design fatigue life of 4×10^8 cycles.

When this method did not yield a positive margin of safety for a region, each element in that region was examined individually. The mean tensile stress was checked against the corresponding elemental RMC alternating stress. Margins of safety were determined in accordance with the applicable AWS/AISC weld category stress allowables in Table 9-2 of Volume II, and are listed in Table 6-8 for the structural regions.

The allowable maximum working stress was established, by the AISC and the Design Criteria, as .60 Fy for flexure and .40 Fy for shear. The stresses obtained from the critical limit load case were used for checking purposes. The positive margins of safety for the most highly stressed regions are listed in Table 6-9. Since the critical case used for the stress check is based on a combination of loads that occurs rarely, arising from a normal shutdown from 60 mph and a maximum drivetrain torque of 5.10×10^6 ft-lb. caused by a cycloconverter mishap, the margins may be higher than those listed.

An additional stress check determined whether the following criteria were met:

1. $(\sigma_{mean} + \sigma_{alternating} + \sigma_{residual}) \leq Fy$
2. $(\sigma_{limit} + \sigma_{residual}) \leq Fy$

The formulae are satisfied; so no cycles, not even infrequent ones, will cause the stress level to exceed the elastic limit. Thus, the introduction of any permanent set into the structural elements is unlikely.

AISC's basic provisions to prevent plate buckling, in sections 1.9, 2.7 and Appendix C of ref. 2, were reviewed. Width-to-thickness ratios for stiffened and unstiffened plates were checked and found to satisfy stability criteria for the expected maximum stress levels. The AISC allowables were based on the elastic buckling expression for plates in compression, similar to the Euler equation for columns, and were derived as $F_{cr} = k \dfrac{\pi^2 E}{12 (1-\mu^2)(b/t)^2}$.

Table 6-8. RMC Fatigue Stress Summary for Important Structural Regions

STRUCTURAL REGION	CRITICAL DETAIL	ELEMENT	APPLICABLE WELD CATEGORY	RMC ALTERNATING STRESS,(PSI)	MEAN TENSILE STRESS,(PSI)	ALLOWABLE CIS ALTERNATING STRESS,(PSI)	MARGIN OF SAFETY
FLOOR, +Y CENTER SECTION	TERMINATION OF WELD AT VERTICAL WEB-TO-FLOOR CONNECTIONS	230238	E	431	16,200	480	0.11
LONGITUDINAL WEBS,-Y FORWARD SECTION (CANTILEVER)	ROLLED BEAM CUT-OUTS GROOVE WELD AT BLENDED PARTS, 6 in. > R $\geq$ 2 in.	20059	D	667	10,200	700	0.05
GEARBOX SUPPORT STRUCTURE	WEB-TO-FLANGE WELD TERMINATIONS	762389	E	521	12,900	521	0.0
	STIFFENER-TO-WEB WELDED CONNECTIONS	772376	C	831	13,900	831	0.0
HIGH FLANGES, FORWARD SECTION (CANTILEVER)	GROOVE WELD AT BLENDED PARTS, 24 in. > R $\geq$ 6 in.	22476	C	506	23,500	602	0.19

Table 6-9. Limit Stress Summary for Important Structural Regions

STRUCTURAL REGION	CRITICAL DETAIL	MAX. LIMIT STRESS (PSI)	ALLOWABLE LIMIT STRESS (PSI)	MARGIN OF SAFETY
GEARBOX SUPPORT STRUCTURE	TOP FLANGE PARENT MATERIAL AT CENTRAL GEARBOX CONNECTION	15,990	30,000	.88
LONGITUDINAL WEBS, -Y FORWARD SECTION (CANTILEVER)	PARENT MATERIAL ADJACENT TO WELD AT FLOOR	26,210	30,000	.14
LATERAL WEBS FORWARD SECTION (CANTILEVER)	PARENT MATERIAL ADJACENT TO WELD AT FLOOR	21,590	30,000	.39

The relative stockiness of the plates and the strategic placement of stiffeners provided positive margins of safety against buckling throughout the structure.

Bolted connections were checked for critical limit and fatigue loads and required preloads were determined. They are listed in Table 6-10. The axial and shear loads were obtained from the NASTRAN finite element model. Forces of single point constraint, for example, the reaction points, provided the bolt loads at the yaw interface. The grid point force balance output at the gearbox and gearbox mounting structure interfaces defined the resultant bolt loads at these locations. The bolts were designed and analyzed using VDI 2230 (ref. 3 and 4) to estimate joint compliance and the fraction of load fluctuation in the pretensioned bolt. The AISC code (ref. 2 and 5) and recent fatigue data that accounts for the effects of bolt diameter and thread forming (ref. 6) were also used.

The bolt pattern at the yaw interface is illustrated in Figure 6-15. The important bolt locations are also noted on the figure.

The computed values of maximum deflections were within the tolerances needed to avoid distortions. The stiffness requirements listed in section 4.2.2 of the Design Criteria (ref. 1) were satisfied. The maximum deflection under the critical limit load subcase was 0.146 in. In normal operation, the largest absolute deflection caused by a combination of mean and maximum alternating loads was 0.087 in. In both the mean and limit instances, the maximum displacement occurred at the front lip. Under the maximum alternating loads the displacement occurred at the top flange of the gearbox mounting structure, which is where the largest portion of the torque load is transmitted by the gearbox.

Great care was taken to incorporate details that are not sensitive to the cyclical loading of the wind turbine generator. During the investigation, the design was modified to improve the margins of safety. The generous radii for cut-outs, large, smooth coping at beam intersections, and gradual transitions between plates of different thickness, enhance the fatigue resistance of the structure. Tables 6-8 and 6-9 indicate the calculated margins of safety

Table 6-10. Bedplate Bolt Summary

INTERFACE	BOLT DIAMETER	CRITICAL BOLT LOADS (lbs. x 10^3)			MARGINS OF SAFETY		REQUIRED PRELOAD (lbs. x 10^3)
		LIMIT	MEAN	ALT.	LIMIT	FATIGUE	
GEARBOX/ MOUNT STRUCTURE	2.25	T = 134.8 V = 31.5	T = 46.8 V = 11.7	T = 94.8 V = 20.8	.04	.02	225
MOUNT STRUCTURE/ BEDPLATE	2	T = 70.4 V = 42.9	T = 23.2 V = 38.4	T = 47.6 V = 16.1	.53	.75	120
BEDPLATE/ YAW	1.75	T = 62.0 V = 26.7	T = 23.1 V = 13.6	T = 19.8 V = 3.0	.24	2.2	112

BOLTS ARE: HIGH STRENGTH (UTS = 140 KSI) WITH THREADS ROLLED AFTER HEAT TREATMENT.
LIMIT MARGINS OF SAFETY BASED ON AISC CRITERIA.
FATIGUE MARGINS OF SAFETY BASED ON VDI 2230 CRITERIA (REF. 3).
PRELOAD REQUIREMENTS BASED ON VDI 2230 CRITERIA (REF. 3).
CRITICAL BOLT LOADS DERIVED FROM NASTRAN ANALYSES.
T = TENSILE LOAD, V = SHEAR LOAD

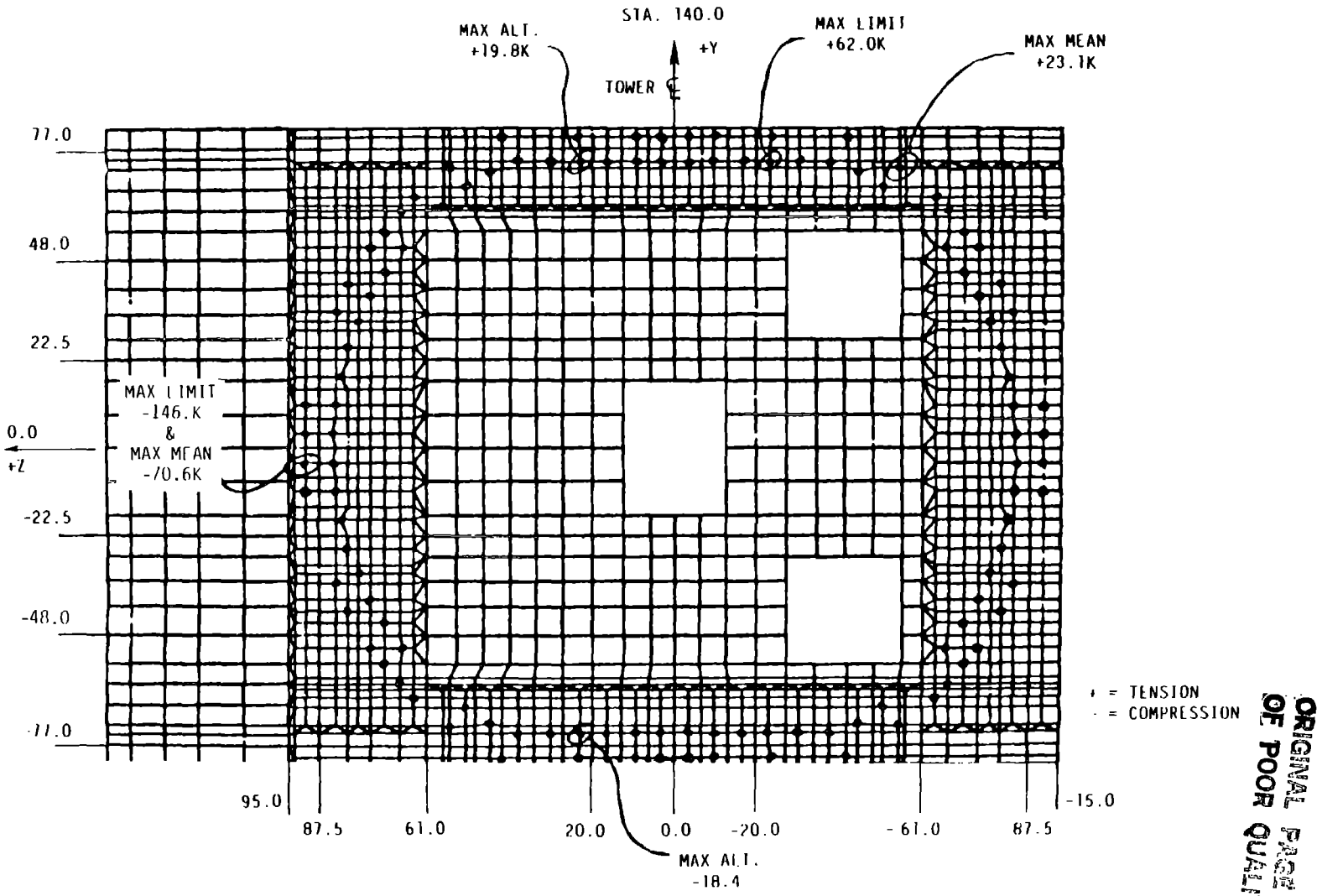

Figure 6-15 Yaw Interface Bolt Pattern and Maximum Loads

resulting from the recommended structural modifications. The tables also summarize the important design factors by loading type. In general, however, the structural members that are in the direct load path of the torque transmitted through the gearbox are critical for both limit and fatigue cases. The additional recommendations, illustrated in Figure 6-16, are primarily detailed fabrication drawing revisions that will bring the locations shown into compliance with the Design Criteria, and will greatly improve the structural reliability. The following recommendations pertain to other construction and maintenance features:

- Preload high-strength bolts, in accordance with the schedule in Table 6-10, for each of the major interfaces. Bolts should never be tensioned beyond 75% of their yield strength.

- Bolts must be installed with a precision tensioner and rechecked for the specified preload after 24 hours. After 100 hours of operation, the bolts must be checked again. Bolts should be checked at regular intervals thereafter. The schedule is to be determined for the Operation and Maintenance Specification.

- The top cut-out plate in the gearbox region should be one piece, to avoid longitudinal welds along the main sidewall flanges (Figure 6-16).

- Longitudinal beams (Y = $\pm$ 48.0) should be continuous between stations 160.0 and 524.0, to improve the support for the cantilevered portion of the structure (Figure 6-16), which supports the generator and other equipment.

- All attachments that are to be used for lifting and erection should be made with high-strength bolted connections, rather than welds.

- The material should be ASTM 572 GR 50 or ASTM A633 GR C steel. Since the sulfur content is required to be less than .020% and Al-Si deoxidation practice is specified, tearing in the sheet is almost impossible.

- All bolts must be high strength material (UTS=140 ksi) with threads rolled after heat treatment. For corrosion protection, the bolts must be coated with a ceramic-filled, baked-on PTFE fluorocarbon resin similar to STAND-COTE.

- The flux-cored arc welding process is preferred, for the following reasons:

    1) Best arc stability
    2) Fewer defects caused by lack of fusion
    3) Less potential of porosity
    4) Smoother weld bead with better wash on fillets

- Replace 45° chamfer with quarter circles in corners of internal stiffeners, as shown in the detail of Figure 6-16.

- Use E7018 electrodes (iron-powder, low hydrogen)

- Smoothness of flame-cut edges should be less than 1000 in. RMS in accordance with ASA B46.1-1962 surface texture nomenclature.

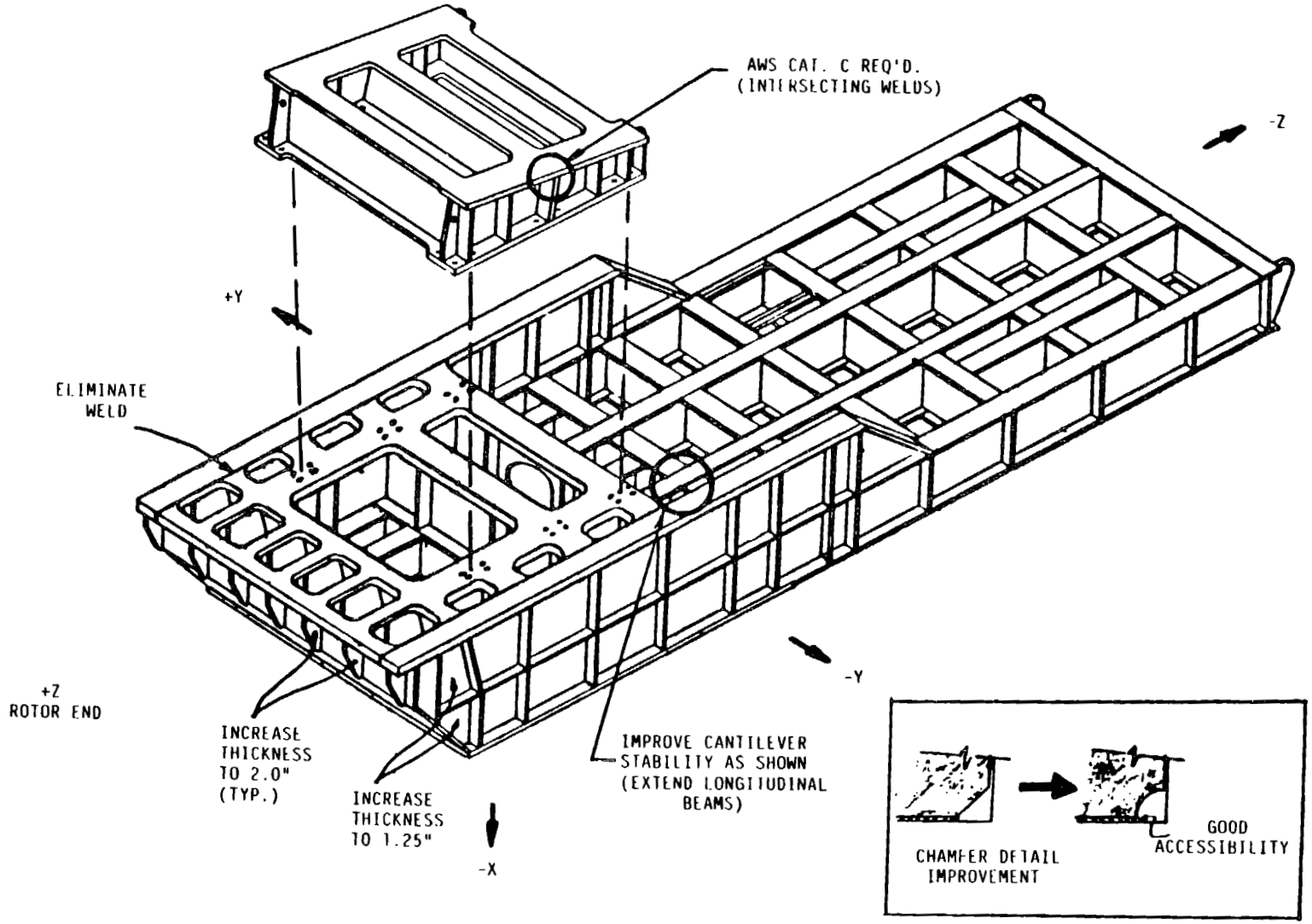

Figure 6-16 Recommended Modifications for Bedplate and Gearbox Support Structure

6.2 CRANE

6.2.1 GENERAL LIGHT MAINTENANCE AND INSPECTION

General, scheduled and periodic maintenance is designed to be carried out without a large external crane system. Replacement lube oil and fresh bearing grease can be brought aboard by external winching from the lube platform or via the elevator. Bolts, welds and wear can be inspected from the platforms, described in section 6.4, or the yaw platform or the nacelle area. The design provides access to all rotating bearing seals, splined couplings and electronic gear.

6.2.2 REPAIR AND MAINTENANCE

Although the wind turbine is designed for a 30-year life, some parts will need to be replaced before the end of the 30 years. In the first machines, the probability of replacement may be high, because of the uncertainties of the design. A crane with a capacity of 10,000 lb. was designed into the system.

6.2.2.1 The Crane

A rigid boom, turret-mounted crane can be installed on top of the forward rigid roof section of the nacelle rotor torque box section as a customer option.

Made by the Devault Company, the crane has a 30-ft. fixed boom, and a 5-ton capacity with the boom horizontal, boom elevation motion from 0° to 80° and 360° traversal capability. This crane is used for the basic installation, as shown in Figure 6-17. Other cranes made by various manufacturers, could be installed at the discretion of the customer, subject to the limitations of the nacelle support structure.

The rated speed of the crane winch is 120 ft/min. A single ball hook and 17-strand cable with a .75 in. diameter are used. The drum capacity is sufficient to reach the ground from the top of the nacelle, approximately 300 ft. of cable. All power drives are electro-hydraulic drive systems, controlled from one station, and are located on the side of the crane pedestal. All drive systems are self-contained in the crane envelope. Electrical power is supplied to the crane from the nacelle. The crane boom is "stayed" to the nacelle roof when not in use, as shown in Figure 6-17. The estimated weight of the crane subsystem is 10,000 lbs, and the shipping modules are 245 cu. ft.

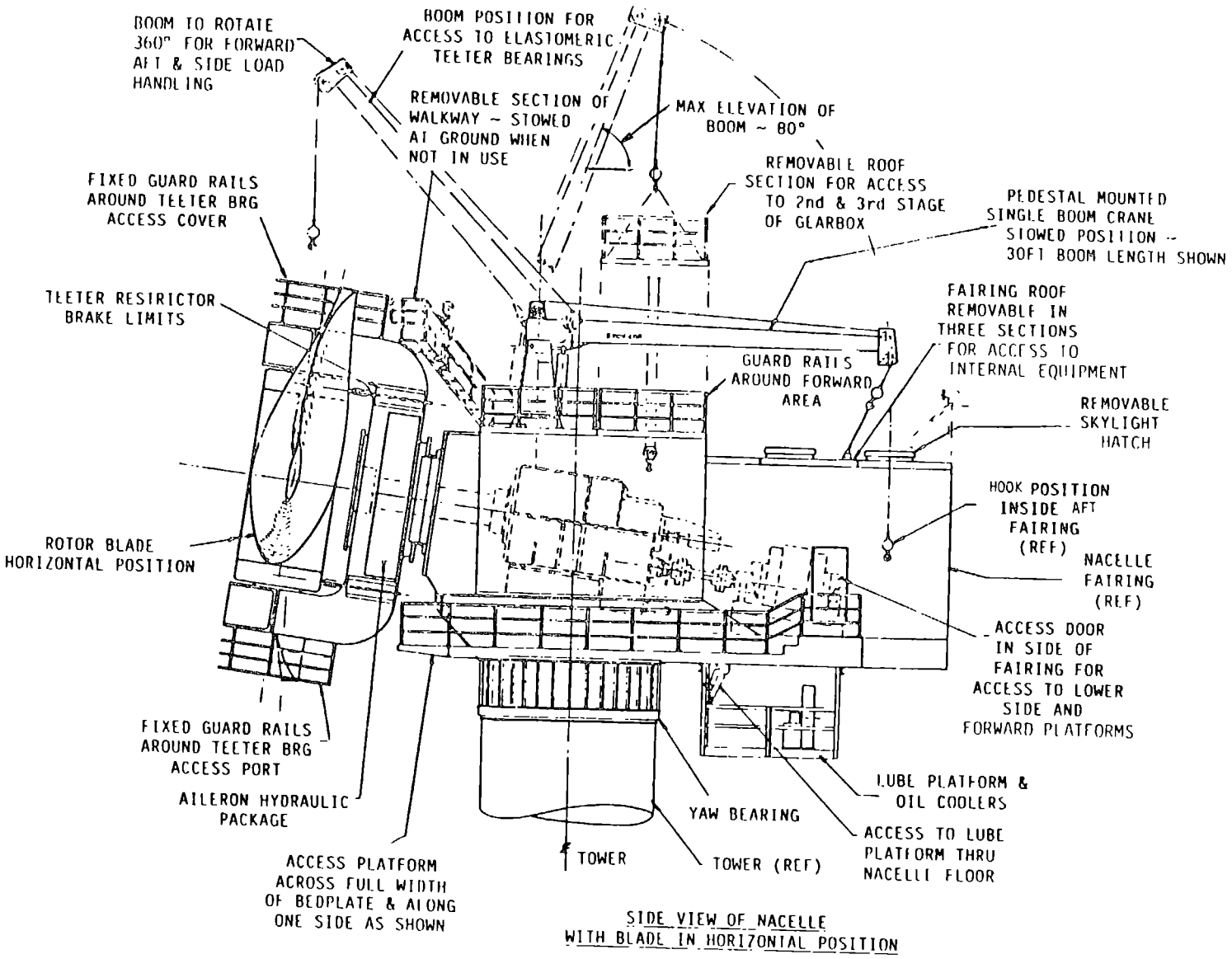

Figure 6-17 Crane and Walkway Installation

6.2.2.2 Crane Use

The externally mounted crane is primarily intended for changing the elastomeric teeter bearings. The teeter subsystem was designed so that the radial and thrust bearings could be removed without removing the rotor.

The crane may be used to:

(1) Remove the aft gearbox cover for access to the 2nd stage planetary system and to the 3rd stage parallel drive system. The cover is estimated to weigh 5,000 lbs. Access to the 1st stage planetary system requires that the gearbox be removed.

(2) Remove the high speed drive shaft assembly. Its estimated weight is 3,000 lbs.

(3) Remove the rotor slipring system. Its estimated weight, including the bracket mount, is 1,000 lbs.

(4) Remove the high voltage cabinet or the control electronics cabinet. They are estimated to weigh 3,000 lbs. and 2,500 lbs. respectively.

(5) Lift miscellaneous tools, equipment, and pumps that are too large and cumbersome to be transported in the elevator.

6.2.2.3 Crane Mounting

The crane is mounted on the forward roof section of the nacelle torque box. This roof section is designed to support the crane system and to react a maximum lift of 10,000 lbs at a 30 ft. boom radius.

The crane mounting is a simple flange connection containing 36 bolts of 7/8 in. diameter. The roof section is reinforced, to transmit the support and reaction loads to the side walls of the rotor torque box.

Safety railings are installed around the periphery of the roof area enclosing the crane location.

6.3 FAIRING

6.3.1 GENERAL DESCRIPTION

The nacelle fairing is a secondary structure that protects nacelle-mounted equipment from weather, supports the externally-mounted wind sensors and aircraft hazard lights and provides filtered air to the inside of nacelle. It does not carry any rotor support loads.

6.3.2 STRUCTURE

The fairing structure is designed to be shipped in modules, and to be easily assembled. It is a three-sided, box-like structure, with a roof section. It attaches to the aft face of the nacelle torque box and the bedplate. All joints are sealed and weatherproofed. The roof and wall sections are in three pieces, with skylights in the two aft roof sections. Exhaust air from the generator is vented through one side wall and fresh air is drawn in through the bedplate bottom. Air is filtered to remove airborne particulates and salt.

The fairing is standard commercial construction for lightweight mobile buildings. A sandwich construction consists of standard steel channel sections that are covered with galvanized steel sheets, inside and out. All joints are bolted with standard steel nuts, bolts and washers, and sealed with commercial caulking througnout the jointed area. All fairing sections contain individual lifting lugs for assembly and handling.

Electrical conduits are installed through the walls for wall outlets and lighting. Brackets are permitted on the inside of walls, to store nacelle equipment.

6.3.3 FAIRING DESIGN CRITERIA

Tne fairing is designed using commercial design practices. The loads were based on a maximum horizontal wind pressure of 68 lbs. per sq. ft., 50 lbs. per sq. ft. of ice or snow on the roof and a wind uplift loading of 51 lbs. per sq. ft. No permanent deformation is permitted at the design load and no failures are allowed at 1.5 times the design load.

6.3.4 FINISH

Logos will be determined by the customer. The interior is primed and painted white.

6.4 WORK PLATFORMS

6.4.1 GENERAL DESCRIPTION

For entry to, and exit from, the nacelle, platforms, ladders and walkways provide safe and reliable passage for workers. Platforms at various staging areas in the yaw and nacelle area, ladders linking these platforms, and walkways past equipment are also provided. All platforms, ladders and

walkways are clearly marked and are designed according to the standards of the Occupational Safety & Health Acts, and the American National Standards for Fixed Ladders, ANSI A14.3.

6.4.2 YAW AREA

There are three tower and yaw platforms located near the top of the tower. The lowest of the three is the staging platform for the elevator. The middle platform is for access to and maintenance of the elevator drive. The upper platform is for access to and maintenance of the yaw drive system.

The upper yaw platform is attached to the lower yaw structure. The lower two tower platforms float, hung by steel cables from the inboard stiffeners of the lower yaw, to eliminate penetration and attachment to the upper tower shell sections. The platform base frames are welded and bolted steel channel sections covered by standard 9-in. or 12-in. wide commercial steel decking. Cut-outs were added to the decking for workers to pass through, for access to the elevator, electrical wire ways and the installation of the yaw slipring.

The upper and middle platforms are connected by a standard fixed ladder, at only one location. For access between the upper yaw platform and the nacelle unit, two ladder sections are provided. These two ladders are suspended from the bedplate so they rotate during yaw maneuvers. All platform surfaces are coated with non-skid coating. These platforms are illustrated in section 7.3 of this volume.

6.4.3 NACELLE AREA

A removable floor grating is fitted throughout the generator area of the bedplate. All electrical wireways are routed beneath this floor. The grating is supported by local brackets in the bedplate structure.

A hatch is provided in the floor for access to the lube oil platform, which is hung from beneath the bedplate structure.

A fixed ladder is attached to the inside of the rotor side plate, forward of the gearbox, for access to the roof area. Removable floor grating is installed along the gearbox, for access to the low speed shaft area. The removable floor gratings also provide access to the yaw and bedplate interface bolts.

6.4.4 ROOF AREA

A natch is provided in the forward left corner of the forward roof section. Guard railings are provided around the entire periphery of the roof, and non-skid coating marks walk ways around the auxiliary crane area. A forward, overhung deck is installed for access to the yoke-mounted equipment.

6.5 AUXILIARY SUBSYSTEM

6.5.1 GENERATOR COOLING AIR FILTRATION

Adequate cooling for the variable speed generator, based on vendor practice, requires about 100 cfm of air across the generator for each kW of loss. The losses, which are converted to heat, amount to about 3% of the generated power. At a rating of 7,500 kW, 225 kW must be carried away by cooling air. At 100 cfm/kW, the total flow is 22,500 cfm. The generator has built-in fans to move 22,500 cfm against 12 in. water gauge pressure, while it is operating. An auxiliary fan with a rating of 10,000 cfm provides cooling air to the generator during low speed motoring. This auxiliary fan is a Buffalo Forge S, model #29A9, which runs at 1,750 rpm.

In a sea coast environment like Hawaii's, the air must be filtered to reduce tne salt concentration. Tests conducted by General Public Utilities defined tne salt concentration at about .25 miles inland from ocean surf. The maximum concentration is about 0.2 ppm for a wind speed of 40 mph blowing on shore. GE's Gas Turbine Division found similar data. The mean crystal size was 10 microns, and 95% of the crystals are larger than 2 microns, in a 15 mph wind. This data was used to design filters.

Several filters were required to deliver air with a maximum salt content of .005 ppm in this environment. RIGA-FLOW by Farr Company of Los Angeles, and the high efficiency Acropac Air Filter by Cambridge Filter Corporation of Syracuse meet these requirements. These filters will block 99.7% of the 2-micron particles. For larger particles, the efficiency is higher. Air flows into these filters at 500 fpm, which requires a total projected flow area of 45 square ft. The filter elements are approximately 12 in. deep. A mechanical separator ahead of the bank of filters separates any salt-bearing moisture droplets from the incoming air. The device generally consists of vertically oriented hooked vanes, mounted parallel to the air stream. The vanes force the air to change direction several times as it flows through the

array. Any droplets in the air stream will attach to the vanes, unable to follow the undulations of the air stream because of the water. The water migrates to a hook-like trough on the vane, and flows down along the hook to a catch trough below the separator. The filters and separators are located underneath the bedplate, just below the generator and above the lube oil platform. The filters will be serviced from the lube platform.

6.5.2 FAIRING VENTILATION

Air enters the nacelle through openings in the forward side walls and exits through a Buffalo Forge Type "S" 29A9, or equivalent, exhaust fan in the aft bulkhead of the fairing. Air filters and water separators, are installed at inside walls of the inlet vents. Motorized louvers at the inlet vents and exhaust port create an air-tight seal, which meets the requirements of a Halon fire protection system.

6.5.3 NACELLE FIRE PROTECTION SYSTEM

In the event of a fire within the confine of the nacelle, a total flooding Halon 1301 (bromotrifluoromethane) fire extinguishing system will be used to quell the flames. Although most of the material in the nacelle is not combustible, the use of petroleum-based hydraulic and lubrication oils, and electrical equipment insulation, made a fire suppression system necessary. Since the system is based on Halon, which is denser than air, the entire nacelle was designed to allow a charge of Halon in a 5% uniform concentration to be maintained in the nacelle for 10 minutes. The system was designed to meet requirements of the Factory Mutual Approval Guide. One hundred ninety (190) pounds of Halon 1301 is stored in a cylindrical steel container suspended from the ceiling of the fairing. The self-contained unit has a fill valve, pressure gauge, discharge valve, initiator, safety cap and the necessary cabling and interconnects to the smoke detector, fire alarm and motorized louvers. A horn is used to sound the pre-discharge and discharge warnings to personnel. The motorized louvers are closed on discharge to maintain the concentration.

REFERENCES

1 Sweet, V. T.; "Structural Design Criteria For Mod-5A Wind Turbine Generator, Rev. B": Document #47A380002, Rev. B, July 1983.

2 "Specification for the Design Fabrication and Erection of Structural Steel for Buildings"; American Institute of Steel Construction, Eight Edition, November, 1978.

3 Aaronson, S. F.; "Analyzing Critical Joints", Machine Design; January 21, 1982.

4 "Systematic Calculations of High-Duty Bolted Joints"; VDI-Verlag GmbH; Standard VDI 2230; West Germany; October, 1977.

5 "Specification for Structural Joints Using ASTM A325 or A490 Bolts"; Research Council on Structural Connections; April, 1978.

6 Crispell, C.; "New Data on Fastener Fatigue", Machine Design; April 22, 1982.

7.0 TOWER AND FOUNDATION SUBSYSTEM

7.0 TOWER AND FOUNDATION SUBSYSTEMS

7.1 OVERALL DESIGN DESCRIPTION

The tower and foundation subsystem is a simple, clean design, shown in Figure 7-1. The tower is a welded steel plate cylindrical shell with a conical base. The cone tapers from a base diameter of 22.5 ft. to a diameter of 14.5 ft. at the 50-ft. elevation point. At this point, there is a formed piece, called the knuckle section, making a transition between the cone and the cylinder. The tower is 224.73 ft. high at the yaw bearing interface. The 6-ft. section of the tower below the yaw bearing is called the lower yaw adapter; the section above the yaw bearing is called the upper yaw adapter. Both are prefabricated. The basic tower is made of sections, and most of the sections are slightly less than 10 ft. high. The sections are factory rolled, shipped to the site, welded into can sections about 30 ft. long, and lifted onto the tower for a circumferential weld.

The tower is bolted to a reinforced concrete spread foundation. The foundation size depends on the soil properties of the site. The foundation is designed for a generic site with minimum allowable soil bearing pressure of 4,000 psi, no drainage problems, and a minimum effective modulus of elasticity of 5,000 psi. These properties were specified in the statement of work and are representative of many possible sites. A circumferential base plate, ring and anchor bolt chairs form a transition between the base and the foundation.

An elevator mounted inside the tower provides access to the nacelle. A ground level access door, internal platforms, emergency ladder and cableway/wire conduit are contained in the tower. These items and the yaw drive subsystem are mounted inside the tower to protect them from weather. The elevator structure is used to support the wiring. Stress concentration in the main tower shell were avoided by designing the elevator structure to be supported only at the yaw platform and base.

The tower design had to meet safe stress levels, and had to give the system the proper dynamic frequencies. It is a "soft" tower design, in that the first system bending frequency is about 0.34 Hz. This frequency is between the one and two per revolution forcing frequencies of the blade. This frequency, as shown by the dynamic analysis, lowers the system fatigue loads,

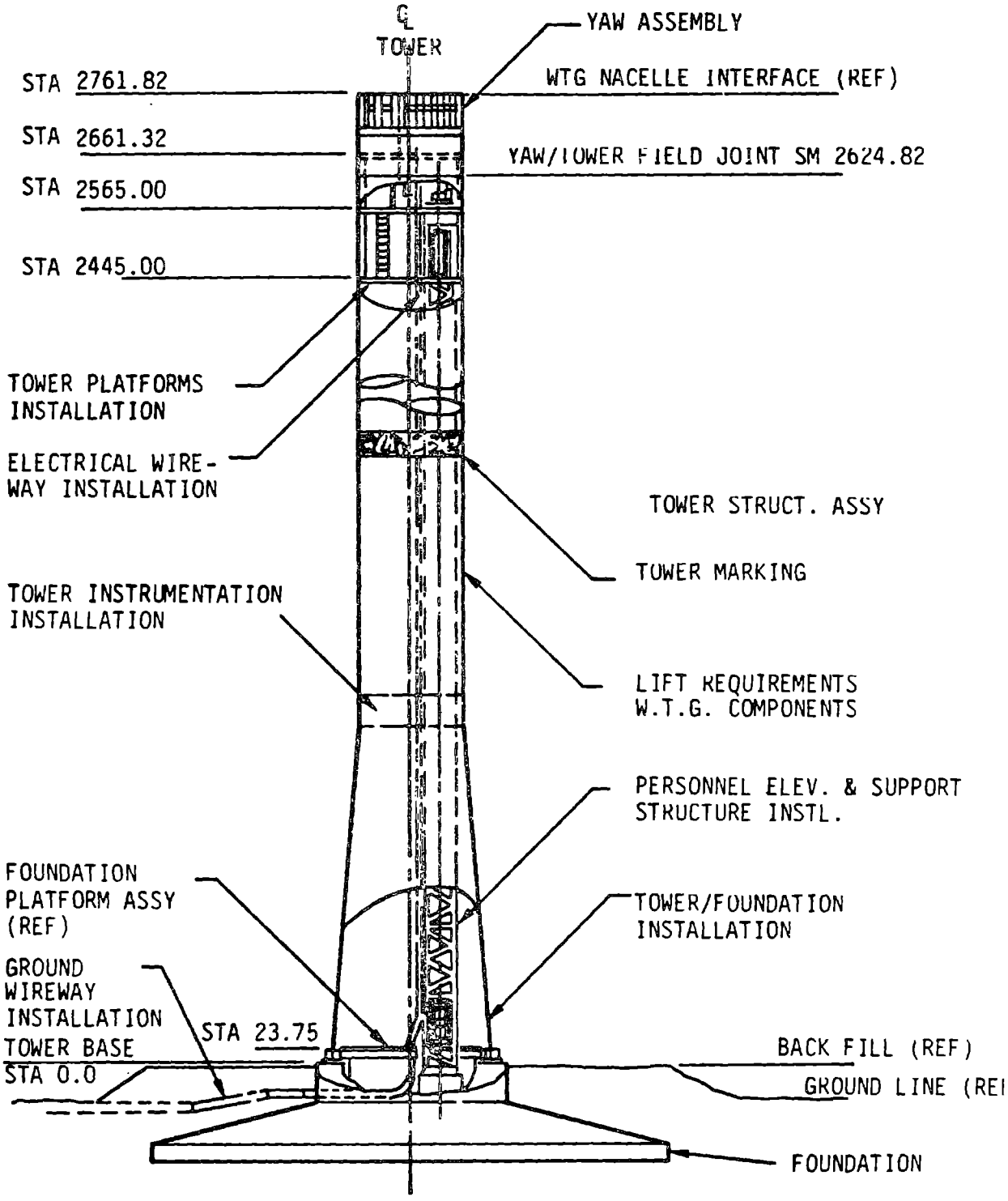

Figure 7-1 Tower and Foundation

not only for the tower, but for the whole system. Several parameters can tune the system: 1) the base diameter and height of the conical base, 2) the basic cylinder diameter, 3) the tower height, 4) individual section thicknesses and 5) the tower material. In the conceptual and preliminary design phases, the basic geometry was determined by trade-off studies. The tower diameter was set at 14.5 ft. for acceptable limit load stress in the transition knuckle between the cylindrical and conical sections with maximum material thickness. Design of the yaw bearing and yaw drive subsystem proceeded after the diameter was set. Frequency tuning of the tower bending mode was mainly done by adjusting tower height, one of the most sensitive parameters.

Several tower trade-off studies were made during the conceptual design. These studies covered such topics as tower height, door design, foundation types, field versus factory fabrication, paint systems, attachment of platforms, rock anchors, erection schemes, and basic materials. Manufacturing trade-off studies are discussed furtner in section 10.

In the early design phases, the material trade-off study selected A572-GR50, a 50 ksi yield steel. Later, a 60 ksi yield steel was chosen to allow thinner sections, which were needed for final tuning the tower bending mode to a lower frequency. Because of the low design temperature of -40°F and the 60 ksi yield, a quenched and tempered steel, A678 GR B was chosen. The material was selected on the basis of price, weldability, formability, toughness, and surface preparation. This material is the plate specification equivalent to A537, Class 2, a nuclear code steel. There was good fabrication experience with this steel.

The tower and foundation are designed to meet hurricane limit load and operating cyclic load conditions. The design driver for the tower and foundation is the hurricane limit load condition. In this case, the blade is assumed to be downwind of the tower and broadside to the wind, so that the large shear and overturning moment are added to the nacelle dead weight moment and tower drag forces. The critical failure mode was found to be local inelastic buckling of the wall sections. In addition, there are several welds near the knuckle section that have nearly zero margins in fatigue, requiring

the use of high quality AISC category "B" welds. Several other limit load situations such as overspeeds and unusual shutdowns were analyzed and did not have a significant impact on the tower design.

Seismic loads for Zone 3 were added to the normal operating loads per the Uniform Building Code (UBC). Using the UBC procedures, which distribute additional lateral loads, the seismic margins were shown to be higher than the hurricane margins. Ice and snow loads also were found to be of little consequence.

The design was checked for vibration of the tower induced by the wind. It is well established that a tall, smooth cylinder can, in certain, steady wind conditions, develop a swaying motion with a large amplitude. At the critical wind speed the vortices that shed from the cylinder alternate at a frequency in phase with the first bending natural tower frequency, inducing a positive feedback. The vortices induce a lift force perpendicular to the wind direction, which reverses as the vortices shed from opposite sides of the cylinder. Thus, the swaying motion builds up perpendicular to the wind direction. The first case to be checked was the fully assembled wind turbine generator. For this case, the natural frequency is 0.34 Hz and the critical wind speed is 15.3 mph. At this low wind speed lift forces are small and tower motions are negligible. The isolated tower, which must be protected during assembly, was the second case. This case can be more troublesome, according to calculations and field experience with the MOD-2. The natural frequency of an isolated MOD-5A tower is about 1.0 Hz and the critical wind speed is 46 mph, which can result in significant lift forces and tower motions. Although the MOD-5A tower should not have amplitudes of motion as large as those of the MOD-2 according to comparative calculations, the temporary strake arrangement used on the MOD-2 was also used on the MOD-5A. This strake arrangement consists of suspended boat bumpers on the outer surface of the tower in a spiral fashion. The strakes break up the vortex pattern, to prevent vibratory build-up. They are easy to remove once the wind turbine generator is fully assembled.

7.2 TOWER STRUCTURE DETAILS

7.2.1 TOWER BASE

The tower is bolted to the foundation by 96 2.5-in. anchor bolts embedded in

the foundation. The stresses in the tower immediately above the base are distributed shell stresses. These stresses must become concentrated at the point loads applied by the bolts. A method similar to the method used in large flanged pipe connections makes this transition. As shown in Figure 7-2, vertical gussets on each side of the bolt end in a continuous back-up ring. The gussets and ring design are called the anchor bolt chair. Since the tower is large compared to a flanged pipe, the anchor chairs are also used on the inside. This distributes the loads with comparatively little shell or base plate bending, consequently the thickness of these components was reduced. Less material in the basic shell compensates, to some extent, for the additional internal anchor chair material and welding.

The size of the anchor chairs and base plate was determined by Chicago Bridge and Iron (CBI), using a standard design procedure. However, as reported in section 7.4.5, a finite element model analysis of the anchor bolt system was made. The purpose of the analysis was to determine bolt loads and stresses in the chairs.

The door is near the base. The reduction of basic shell material must be compensated for by reinforcing the door opening in the base. The door opening design was done by CBI, using a beam section method. A thicker plate was also specified for the cone segment containing the door to reduce the basic shell stress and minimize the potential for reinforcement weld stress concentrations exceeding allowables. A finite element analysis of the door opening was not done for the first unit. Figure 7-3 shows the details of the fabricated angle sections that act as side posts and form a lintel above the door. The angles are made from the basic tower material, rather than hot rolled angles or beams of a different material. This design avoids the possible problems of welding two different steels.

There is a large radius where the top of the side posts contact the tower shell. The large radius reduces the stress concentration to an American Institute of Steel Concentration (AISC) "C" weld category (ref. 7-9) with a margin of safety for fatigue of 0.06. This margin is based on the assumption that the door sees all the highest fatigue tower stresses, which is the worst case. Actually, the door is located at 90^{o} from the prevailing wind direction, so that it will most frequently be on, or near, the neutral axis.

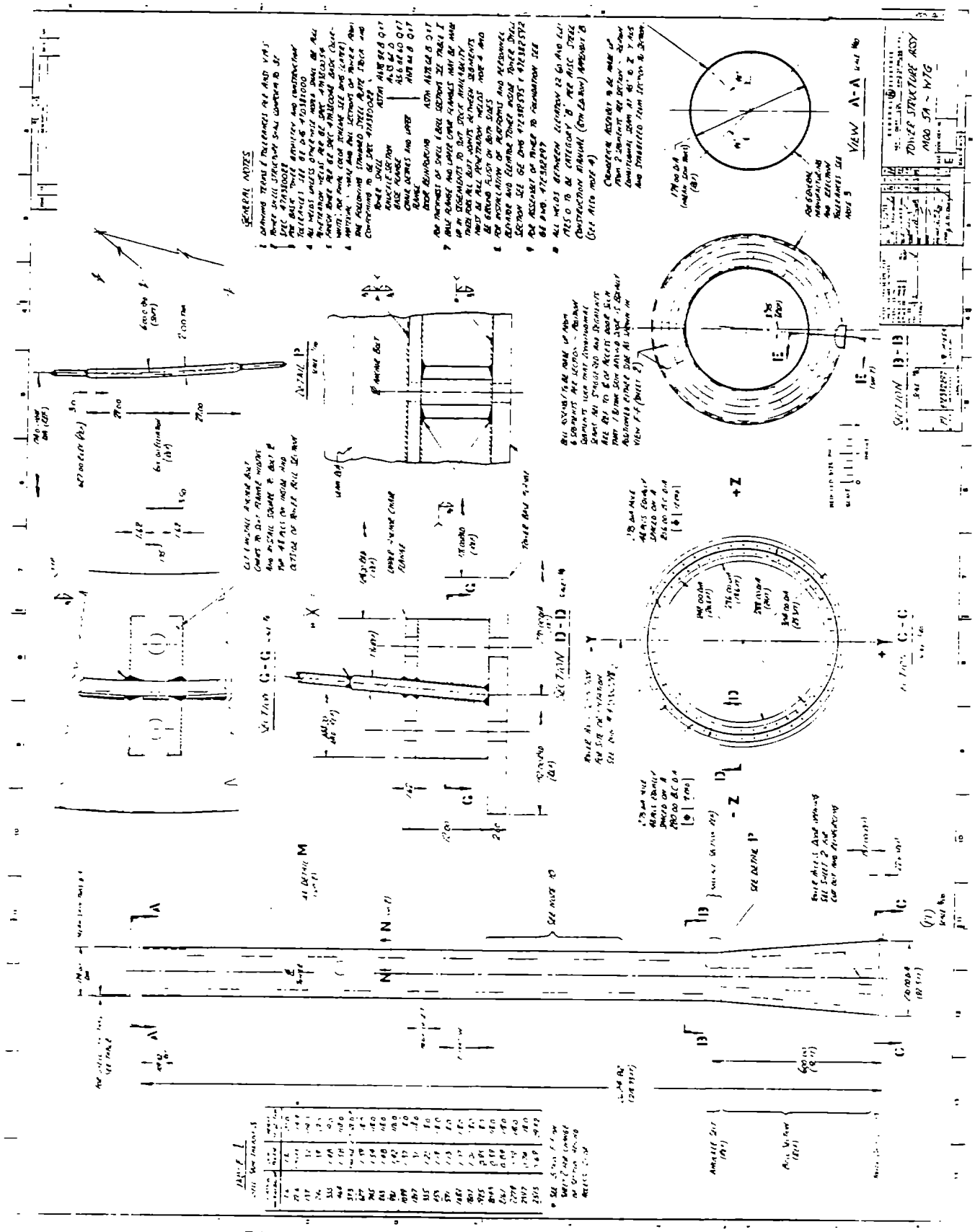

Figure 7-2. Tower Base - Chair Details

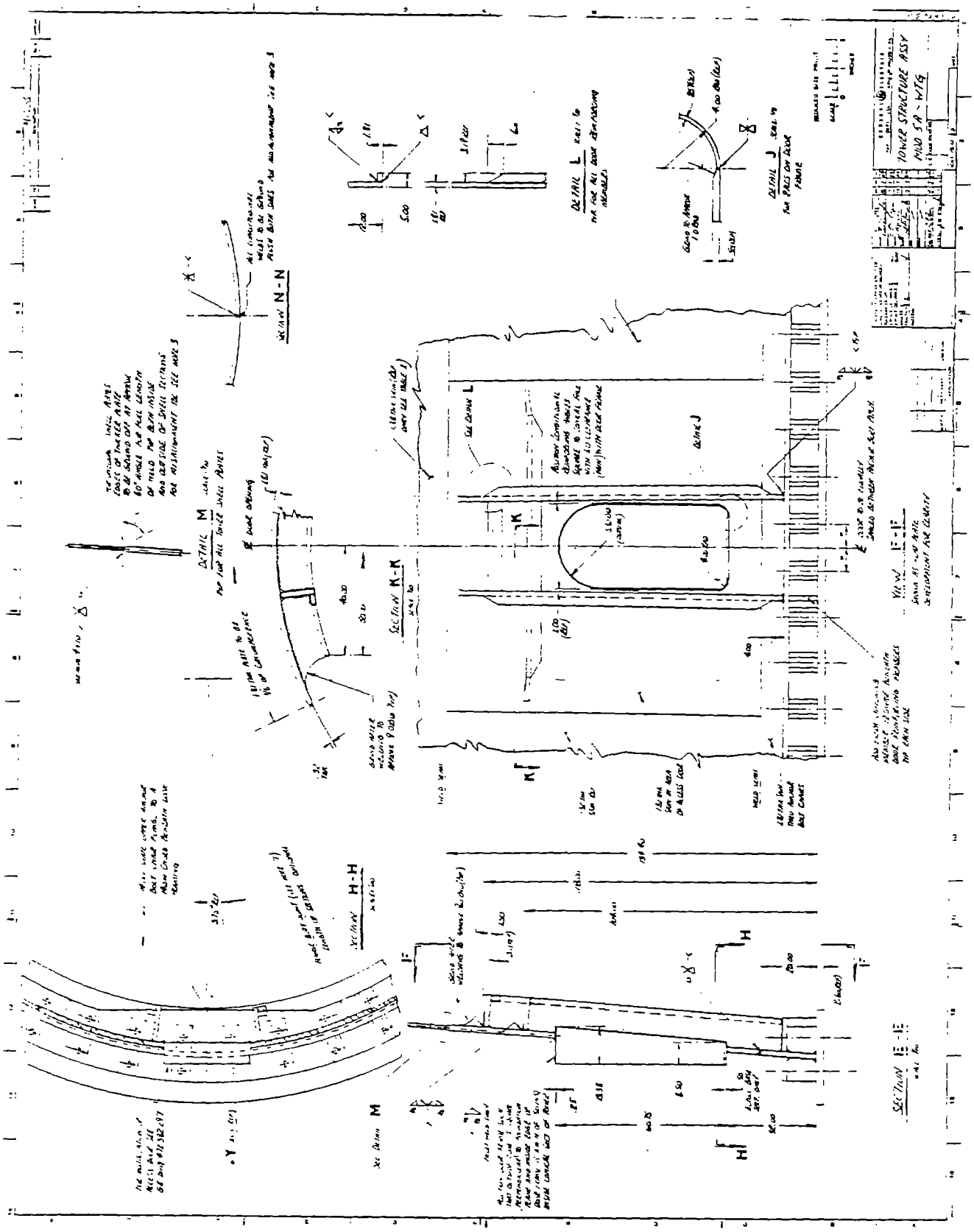

Figure 7-3. Tower Access Door Details

Thus, the actual margin can be considerably higher than the calculated margin, depending on the local site wind direction characteristics.

7.2.2 TOWER SHELL ALLOWABLE STRESSES

The tower shell was designed to both avoid inelastic local buckling from hurricane limit loads and avoid stressing welds to fatigue allowables during operation. Fatigue design criteria are described in section 9, Vol. II, Design Criteria. Local buckling criteria were determined by CBI and GE, using chimney liner design procedures (ref. 7-1) as a guide, since the tower is a thin wall cyclinder with radius-to-wall thickness ratios similar to liners. The allowable stress is based on a 1.25 safety factor.

Local buckling design, which predominates for the MOD-5A geometry, is different from Euler buckling of long cyclinders. Removal of the so-called Euler critical load allows long columns to snap back, whereas local buckling in the inelastic region is irreversible. The design also takes into account the effect of the tower weight on critical buckling, by modifying the Euler constant, as suggested by Timeshenko and Gere (ref. 7-2, pg. 100).

The ration of the radius to the wall thickness ($t/_R$) of the MOD-5A tower design ranges from about 50 to 150. According to Timeshenko and Gere (ref. 7-2, pg. 458), the theoretical buckling stress for thin elastic cylinders in compression is:

$$\sigma_{cr} = .606\ Et/_R \text{ (psi) where } t = \text{thickness of the wall} \qquad [7.1]$$

R = radius

E = tangent modulus of elasticity

This theoretical stress is for a cylinder with no initial imperfections, no residual stresses, and for idealized loading conditions. This theoretical stress is reduced by a capacity reduction factor to account for realistic conditions. The factor for a large ration of radius to wall thickness equals .206 in the CBI design procedure, so that $\sigma_{cr} = 0.125\ Et/_R$. For small values of $t/_R$, σ_{cr} will exceed the proportional limit of steel, and a plasticity reduction factor is used. Finally, for very small ratios the shell will not buckle; instead, it will yield in straight compression.

The ASCE/CBI design method accounts for these factors as shown in Figure 7-4, where the factor Y is the Euler reduction and the factor X accounts for the three regions of radius to wall thickness ratios, with the capacity and plasticity factors built into the three formulas for X. For the baseline material the allowable stresses for 1.0 and 1.25 factors of safety are shown in Figure 7-5, as a function of the radius to wall thickness ratio using the ASCE/CBI method.

During the design, CBI and consultants from Lehigh University brought to light more recent data than that on which the ASCE method was based, and newer design curves. A paper by C. D. Miller (ref. 7-3) summarizes the test data on fabricated or welded cylinders with the appropriate radius to wall thickness ratios. All the pertinent data from ref. 7-3 are plotted in Figure 7-5. In the figure, the data points are normalized by plotting the ratio of test stress to the theoretical stress, with Euler buckling accounted for. The data are mostly for mild steels, 30 to 50 ksi, with one point at 100 ksi. The ASCE/CBI method used here is restricted to 60 ksi yield or stronger steels. The more recent data points were taken at the University of Alberta (ref. 7-4). The figure shows that the current design curves are conservative, since all the data falls above the ASCE curve, except at a radius to wall thickness ratio of 0.25, which is not in the range of the MOD-5A tower's $t/_R$. The structural design criteria permits use of a 1.25 factor of safety with the supporting test data noted above.

There are other design procedures that have allowable curves nearer the data, such as the 1.0 factor of safety. These procedures include an ASME method (ref. 7-5), the API method (ref. 7-6) and the DNV method (ref. 7-7). These methods are slightly less conservative than the ASCE method, but their use would provide little benefit, since fatigue, rather than buckling stresses would become the design driver in many sections of the tower.

APPENDIX A

CRITICAL STRESS FOR AXIAL COMPRESSION*

$$\sigma_{cr} = XY$$

$$X = \frac{1}{8} E \frac{t}{R} \qquad 0 \leq \frac{t}{R} \leq 8 \frac{F_p}{E}$$

$$X = [F_y - K_s(F_y - F_p)] \qquad \frac{8F_p}{E} < \frac{t}{R} < \frac{20F_y}{E}$$

$$X = F_y \qquad \frac{t}{R} < \frac{20F_y}{E}$$

$$Y = \frac{493{,}200}{F_y \left(960 + \left(\frac{K_1}{.5R}\right)^2\right)} \qquad y \leq 1.0$$

E = Modulus of Elasticity

F_y = Yield Stress (ksi)

F_p = Proportional Limit

t = Thickness

R = Shell Radius

1 = Distance from top to point being considered.

K = 2.0

r = Radius of Gyration

$$K_s = \frac{\frac{20F_y}{E} - \frac{t}{R}}{\frac{20F_y}{E} - \frac{8F_p}{E}}$$

* THESE FORMULAS HAVE BEEN TAKEN FROM THE DESIGN AND CONSTRUCTION OF STEEL CHIMNEY LINERS, PUBLISHED BY THE AMERICAN SOCIETY OF CIVIL ENGINEERS WITH THE EXCEPTION THAT THE EQUATION FOR Y AND THE LIMITS OF $\frac{K_1}{r}$ HAVE BEEN MODIFIED.

NOTE: THESE FORMULAS ARE BASED ON 60 KSI YIELD MATERIAL MAXIMUM.

Figure 7-4 Critical Stress for Axial Compression

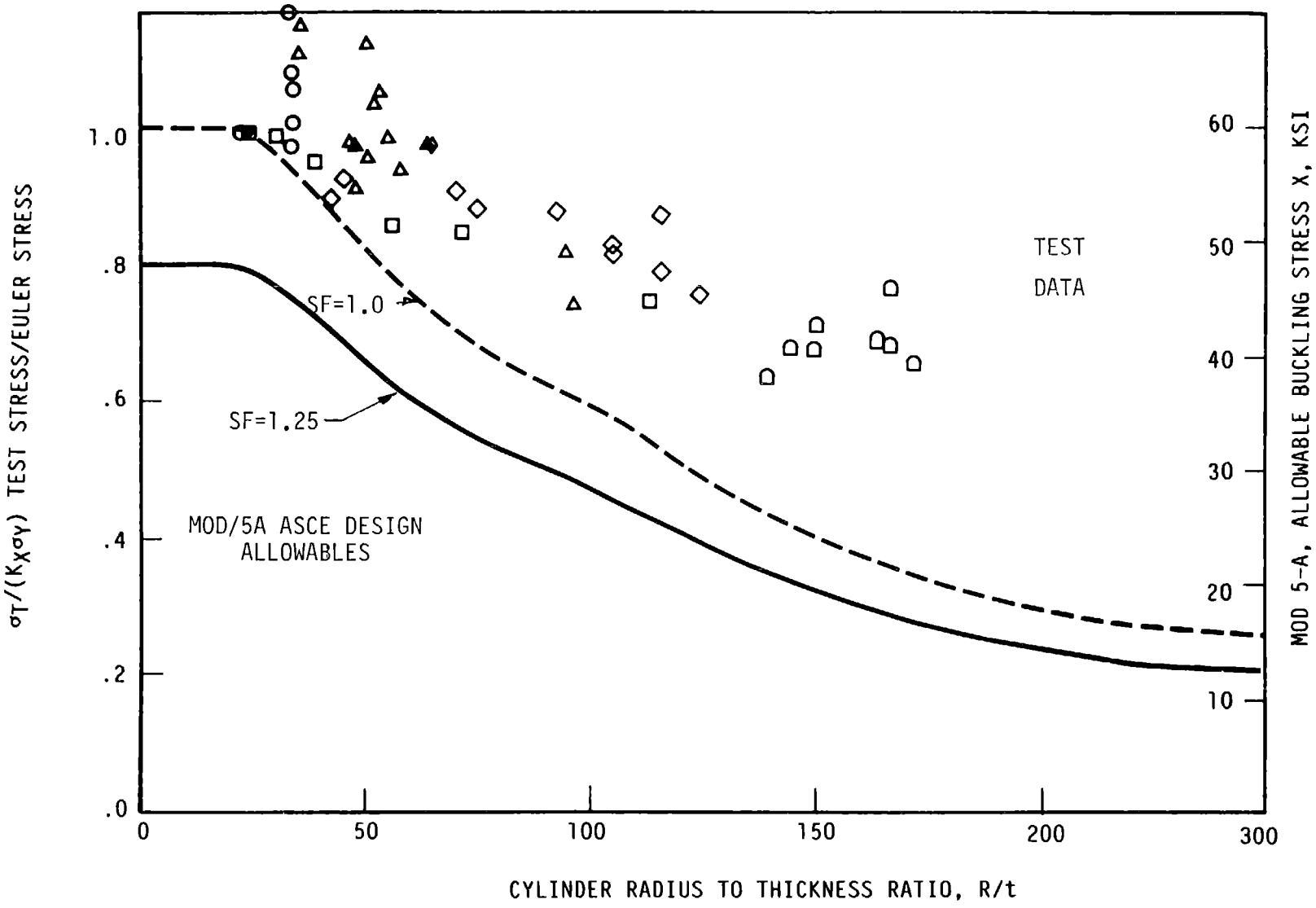

Figure 7-5 Allowable Buckling Stress

All the test data cited is for simple compression. The MOD-5A tower experiences mostly bending compression. Timeshenko (ref. 7-7) points out that computing the exact bending solution of critical buckling is complicated. But he concludes that a conservative result is obtained, assuming that the tower buckles when the sum of the bending and uniform compressive stress equals that of the critical uniform compressive stress. He cites one theoretical example for which the exact calculation was done for a radius to wall thickness ratio of 228. In this example the pure bending was 30% stronger. He also cites experimental data, from 1934 aircraft tubular configurations, in which the critical stress in bending is about 1.4 times the axial-compressive data.

Therefore, considering the tower as a beam column, the maximum combined compressive stress is not directly compared to the critical local buckling stress. The bending and axial compressive stresses were combined by the interaction formula to determine allowable stress.

$$\frac{f_a}{F_a} + \frac{f_b}{F_b} \leq 1.0 \qquad [7.2]$$

Where f_a and f_b are the computed axial and bending stresses, F_b is the allowable stress per the ASCE method and F_a is the same stress, but lowered by a slenderness reduction factor. The latter accounts for overall column buckling and its value is given by the AISC method in Figure 7-4. The effect of the slender column reduction is small, since f_a is small compared to f_b.

Finally, the applicability of the data depends on the quality of the construction. The allowable imperfections for the MOD-5A fabrication are slightly larger than allowed by the ASME method (per Code Specification Subsection NE-4220), but are compatible with the test specimens and the other design standards. Also, the effect of imperfections appears to be less significant in the inelastic zone according to recent test data. To quote Professor Ostapenko (ref. 7-8), "Thus, one may conclude that geometric imperfections do not reduce the local buckling stress in this range as significantly as is generally believed". The study of test data has shown a general trend toward more scatter at higher radius-to-wall thickness ratios. The increased scatter is assumed to be due to the stronger influence of imperfections at higher ratios. Also, aircraft design procedures call for higher factors of safety with larger radius-to-wall thickness ratios, presumably for the same reason.

7.2.3 CYLINDER AND CONE SECTIONS

Each section of the tower has a slightly different thickness. In this type of steel construction different thicknesses minimize the material costs, but on the MOD-5A different thicknesses are also used for the purpose of frequency placement. It might be supposed that ordering plate to a few standard thicknesses would reduce costs, but this is not so. The steel mill sells steel by weight, and will roll steel to any thickness. However, plate widths must be standard, so the height of each section was set at slightly less than 10 ft. A standard width is 10 ft., but some allowance is needed for edge preparation and development of the projected cone segments.

The thicknesses of the tower sections were determined by the hurricane load and each girth weld was checked for fatigue. The final results of the thickness design procedure are given in Tables 7-1 and 7-2. Paragraph 7.2.2 justified the use of a buckling design factor of 1.25. The procedure used a factor of 1.375 because fatigue margins near the knuckle were negative. The third column is the thickness of the tower between the height in column 1 to the next lower height, for example, from a height of 2696.82 in. to a height of 2624.82 in., the shell thickness is 0.750 in. This section weight is 8,410 lbs. The total tower shell weight, including the 34 in.-wide base plate, is 560,730 lbs. The weight of the anchor chairs and door reinforcement should be added to this weight, for a total weight of 579,000 lbs., exclusive of the upper yaw housing, elevator, elevator structure, cableways and platforms.

The fatigue check of each circumferential seam weld is given in Table 7-2. Each seam is checked by the crack growth threshold method. The results appear in column 2 and 3. Column 2 contains the maximum alternating stress for the start-stop cyclic load. The allowable stress for an AISC Category "B" weld is 8,000 psi, which is exceeded in four girth welds. Consequently, the structural design criteria requires that those four seams be checked by the crack initiation stress (CIS) method. These results are shown in columns 5, 6 and 7. Column 4 shows the smallest plate thicknesses at each seam. In the cone this is the lower section of the abutting sections; in the cylinder it is the higher section, except in the case of the highest seam where the lower yaw section is thicker.

Table 7-1

Tower Thickness Schedule for Limit Load (Buckling Design

INPUT E, YIELD STRENGTH, PROP. LIMIT STRENGTH, & F.S (psi)
29000, 60, 36, 1.375
INPUT SHEAR, VERTICAL FORCE AND MOMENT AT TOWER TOP (lb., ft.lb.)
436.2, 1060, 204640

H (IN.)	DIA. (IN.)	T (IN.)	TOT. WT. (KIPS)
2696.82	174.00	0.750	8.41
2624.82	174.00	0.690	20.33
2514.00	174.00	0.740	33.81
2397.00	174.00	0.790	48.34
2279.00	174.00	0.840	63.78
2161.00	174.00	0.890	80.14
2043.00	174.00	0.950	97.60
1925.00	174.00	1.010	116.17
1807.00	174.00	1.070	135.84
1689.00	174.00	1.130	156.62
1571.00	174.00	1.190	178.49
1453.00	174.00	1.250	201.47
1335.00	174.00	1.310	225.55
1217.00	174.00	1.370	250.74
1099.00	174.00	1.420	276.84
981.00	174.00	1.480	304.05
863.00	174.00	1.540	332.36
745.00	174.00	1.590	361.59
627.00	174.00	2.000	378.42
573.00	178.32	1.580	407.26
464.00	195.76	1.480	436.79
355.00	213.20	1.390	466.90
246.00	230.64	1.320	497.74
137.00	248.28	1.250	530.69
22.60	266.38	1.810	539.38
2.60	269.58	34.000	560.73
0.00	270.00	0.000	560.73

BASE MOMENT = 127150.224524 KIP-FT

Table 7-2

Check of Tower Weld Seams for Fatigue

FATIGUE CHECK FOR TOWER: FINAL DESIGN TOWER MARCH, 1984

	My (TYP III)	Mz (TYP III)	My (RMC)	Mz (RMC)
TOP	2420000 ft.lb.	2650000	329000	347000
BASE	31000000 Typ.	10100000	4560000	3220000

SEAM HEIGHT (in.)	STRESS TY III (psi)	B WELD M.S.	ACTUAL THKNSS (in.)	STRESS RMC (psi)	B WELD M.S.	THKNSS REQ'D (in.)
0.0	295	26.13	34.00	50	30.69	1.073
2.6	3861	1.07	1.81	661	1.42	0.748
22.6	5653	0.42	1.25	968	0.65	0.756
137.0	6262	0.28	1.25	1071	0.49	0.837
246.0	6622	0.21	1.32	1132	0.41	0.934
355.0	7084	0.13	1.39	1211	0.32	1.052
464.0	7588	0.05	1.48	1296	0.23	1.199
573.0	8227	-0.03	1.58	1404	0.14	1.387
627.0	8401	-0.05	1.59	1433	0.12	1.424
745.0	8233	-0.03	1.54	1403	0.14	1.351
863.0	8107	-0.01	1.48	1380	0.16	1.277
1099.0	7771	0.03	1.37	1320	0.21	1.130
1217.0	7612	0.05	1.31	1291	0.24	1.057
1335.0	7439	0.08	1.25	1259	0.27	0.983
1453.0	7250	0.10	1.19	1224	0.31	0.910
1571.0	7043	0.14	1.13	1186	0.35	0.838
1689.0	6814	0.17	1.07	1144	0.40	0.765
1807.0	6562	0.22	1.01	1097	0.46	0.692
1925.0	6280	0.27	0.95	1044	0.53	0.620
2043.0	5964	0.34	0.89	985	0.62	0.548
2161.0	5542	0.44	0.84	906	0.77	0.476
2279.0	5074	0.58	0.79	818	0.95	0.404
2397.0	4553	0.76	0.74	719	1.23	0.333
2514.0	3983	1.01	0.69	607	1.63	0.262
2624.8	3163	1.53	0.69	453	2.53	0.196

The root mean cubed (RMC) stress at each seam is obtained by the worst case moment combination. M_Y and M_Z are assumed to peak at the same time and at the same axis at top and bottom, so that the vector sum is the actual peak tower moment. These assumptions are conservative, but for partial span control blades the actual combination of M_Y and M_Z was only slightly larger than the maximum individual moment component. It is assumed that the same combination would be approximately true for the final tower with aileron controlled blades. Hence, instead of the computed minimum margin in fatigue at location 627 of 0.12 the effective margin may be much greater.

Positive margins were needed because the margins shown in Table 7-2 do not include any seam mismatch stress concentration effects. The category B weld, per AISC standards, is for a butt weld ground flush but with no discontinuities, or a slope no greater than 2.5 to 1. (Ref. 7-9, Figure B1, No. 10, 12, 13).

Welds in large structures can pucker or bend in or out and this condition must be controlled. The construction methods and allowable tolerances, therefore, affect the actual stress field at the girth welds. To control this, the Tower Specification requires that "Seam mismatch in girth welds shall not exceed the smaller of one-tenth the minimum plate thickness or 1/10 in." CBI did not complete a finite element model study of the seam mismatch problem, but felt that the results they obtained confirmed the formula found by Gurney (ref. 7-10) as shown in Figure 7-6. To minimize the discontinuity, the basic tower design was changed from a constant outer diameter to a constant mean diameter. From the formula and tolerances, at the lowest margin fatigue section, in the worst case e = 0.10 in., t = 1.59 in., and, therefore, K_t = 1.19. After reviewing all the factors, it was concluded that the margin in fatigue would be positive. Strain gage data would be taken at the knuckle seam of the first tower to confirm that the actual loads (strains) corresponded to the predicted loads (strains).

7.2.4 KNUCKLE SECTION

At a height of 50 ft. there is a transition between the conical base and the cylindrical tower sections. The change in shell shape causes a stress concentration at a place where the fatigue margin is the lowest. Often such an intersection is reinforced by rolled structural ring shapes. Such a welded reinforcement would be, at best, a AISC "C" category, but the tower design is based on a "B" category with higher allowable stress. A wall thickness increase was not acceptable. The solution was to use a formed knuckle section for a smooth transition between the cone and the cylinder. Chicago Bridge and Iron (CBI) used this design in water tower designs. They have a standard procedure for determining the size of such a knuckle section. The applied loads produce stresses in the longitudinal direction. The shape change also causes circumferential stresses which are proportional to the longitudinal stress times the ratio of the developed radii, as shown in Figure 7-7.

These components of stress are checked in an intersection formula per CBI's procedure. In the final design, the required thickness was 2 in. for the 50 ksi yield material. A633 Gr C steel was selected for the knuckle since the section would be built of hot formed segments. These segments would be welded together and heat treated as a welded assembly. If the basic tower material A678 Gr B was used, with 60 ksi yield, the entire assembly would require a quench and temper after the hot forming. This could have led to unacceptable distortion. A knuckle section of A633 steel would be normalized, thus avoiding quenching distortion.

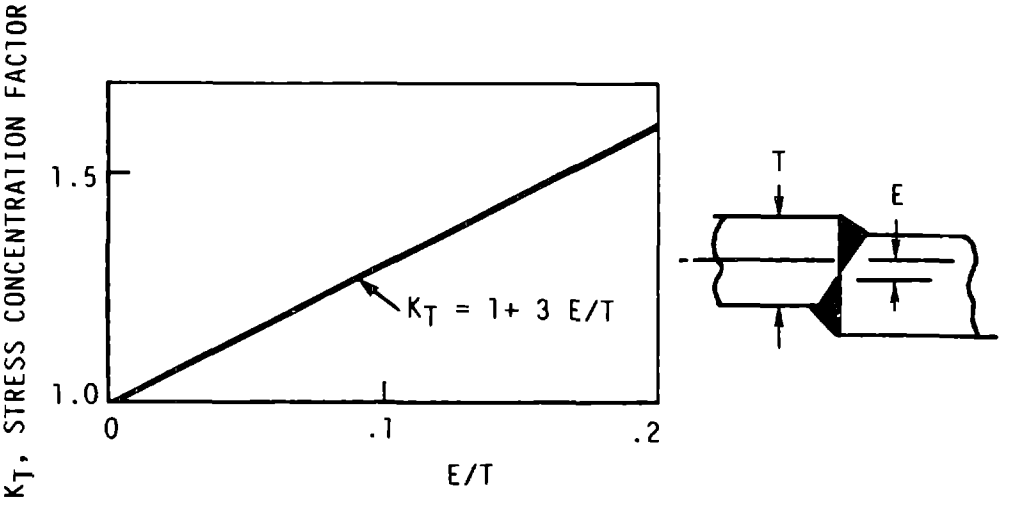

Figure 7-6 Seam Mismatch Stress Concentration Factor

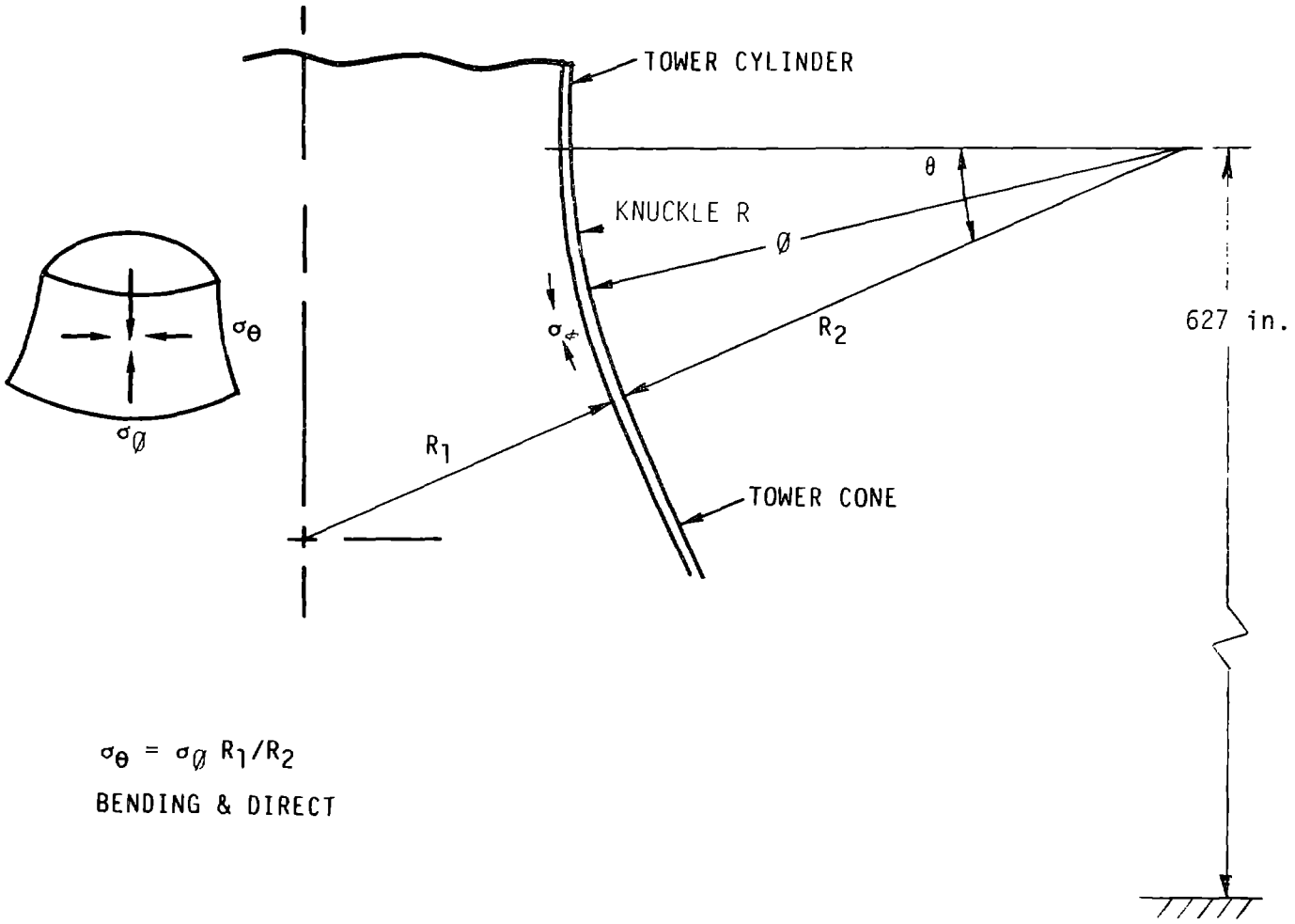

Figure 7-7 Knuckle Section Stress

7.3 ELEVATOR AND PLATFORMS

During the final design, the state OSHA's of California and Hawaii were contacted for elevator approval, since the first MOD-5A's would probably be installed in these states. They declared the low cost cable climbing elevator used on MOD-0A, MOD-1 and MOD-2 would not be acceptable for permanent use on a production wind turbine generator. They suggested elevators that met the requirements of Part XV of ANSI/ASME A17.7-1982. Part XV, entitled "Special Purpose Personnel Elevators", applies to elevators permanently installed to provide vertical transportation only to authorized personnel and their tools and equipment. Because of its limited use on the MOD-5A, many of the more restrictive provisions of A17.1 would not apply. The California OSHA supplied a list of elevator manufacturers, who were requested to provide the MOD-5A elevator design.

The provisions of Part XV require a maximum floorspace of 9 ft^2, maximum speed of 100 ft./min., and maximum capacity of 650 lbs. This was acceptable for the MOD-5A, as all heavy components in the nacelle would be handled by the nacelle crane. The components in the yaw area, except for the slipring, could be transported in the elevator. There were four types of elevators allowed, but the rack-and-pinion and traction types seemed economical and well suited for this application.

The traction elevator has been used for a long time in grain elevator towers. It consists of a large sheave with a 180^{o} cable loop at the top of the tower. One side of the cable supports the elevator cab and the other side supports a counter-weight. The sheave is driven by a motor via a 60:1 gear box and is held with a failsafe brake.

The rack-and-pinion elevator uses a motor driven pinion mounted on the cab roof that pulls the cab up and down the long rack. The latter elevator is becoming more popular, because it is more reliable and easier to maintain. Usually these elevators are used in exposed, high use applications, such as large, chimmney-mounted devices.

After the bids were reviewed, a traction elevator was selected. The MOD-5A application is totally enclosed and the elevator would not be used enough

for lower maintenance costs to balance the higher initial cost of the rack-and-pinion elevator. The choice was affected by the means of support of the two types. The traction elevator requires guide rails for the cab and counter-weight. These must be supported at least every 10 ft. An enclosed elevator support structure meets this requirement, and the structure also serves as support for the emergency ladder, power and signal conduits and internal lighting fixtures. This frees the main tower from welded or bolted bracketry that would create stress concentrations and possibly initiate fatigue cracks. The rack-and-pinion elevator requires a mast that needs lateral support and by itself is not large enough for mounting of all the conduits and a ladder.

The key elements of the elevator are shown in Figure 7-8. The elevator car is totally enclosed. The top of the car has an escape hatch. The car contains the controls and an interior light. The governor attachments are shown on the right side of the car. If the three .5-in. wire rope support cables break, the governor senses a falling speed greater than 175 fpm, and applies the safety brakes. The safety brakes are "dog" brakes, which clamp to the guide rails and safely stop the falling car.

The installation details of the elevator support structure are shown in Figure 7-9. Although a full scale layout shows an apparently very slender column, local buckling influenced the design of the structure more than overall buckling. The structure was designed per AISC sections 1.6.1, "Combined Axial Compression and Bending", Sec. 1.8, "Stability and Slenderness Ratios" and Sec. 1.1.8 "Built-up Compression Members". A dynamic analysis of the elevator support structure should be made before installation.

The elevator structure would be welded in the factory in 39-ft. segments, shipped to the site, and assembled as the tower is erected. The structure is elastically mounted to the foundation on rubber pads, as shown in Figure 7-9, because of the deflection at the top of the tower. In a hurricane, the deflection at the yaw bearing is about 30.5 in., but under normal operating conditions the deflection should be less than $\pm$ 5.5 in.

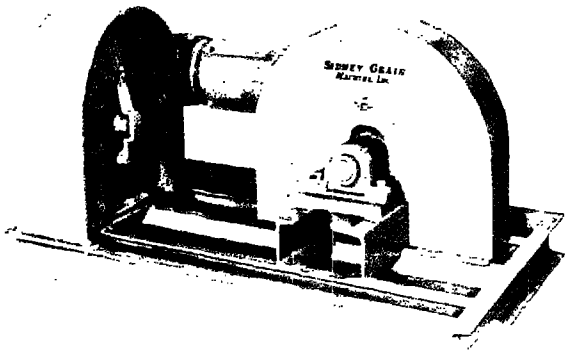

DRIVE ASSEMBLY

A TWO H P MOTOR WITH A MAGNETIC BRAKE PROVIDES THE HOISTING WORKS FOR THE SIDNEY LINE" ELEVATORS. THIS DRIVE ALONG WITH THE HOISTING CABLES SHEAVE. OUTBOARD BEARING AND DOWN SPEED GOVERNOR ARE MOUNTED ON A HEAVY DUTY CHANNEL IRON FRAMEWORK THE MOTOR IS AVAILABLE IN TOTALLY ENCLOSED, NON-VENTILATED OR EXPLOSION PROOF ALL MOVING PARTS OF THE DRIVE ARE PROTECTED BY ENCLOSED GUARDS

CAR

SHOWN IS THE 300 LB CAPACITY ONE MAN ONLY CAR ALSO AVAILABLE ARE 500 LB CAPACITY TWO MAN CARS ALL UNITS ARE DESIGNED AND MANUFACTURED TO CONFORM WITH THE CODE REQUIREMENTS OF THE STATE IN WHICH THEY ARE TO BE INSTALLED ALL MODELS ARE EQUIPPED WITH A BROKEN AND/OR SLACK CABLE SAFETY SYSTEM AS WELL AS A DOWN SPEED GOVERNOR SAFETY SYSTEM THESE SYSTEMS AUTOMATICALLY APPLY THE CAR SAFETIES, LOCKING THE CAR TO ITS GUIDE RAILS IN THE EVENT OF CABLE FAILURE OR OVERSPEED THE CAR IS COMPLETELY ENCLOSED ON THREE SIDES WITH A BI FOLD DOOR IN FRONT CARS ARE AVAILABLE WITH DOORS IN FRONT AND BACK. POLYETHYLENE CAR GUIDES ARE PROVIDED FOR SMOOTH QUIET OPERATION AND ELIMINATE ANY POSSIBILITY OF SPARKING IN HAZARDOUS ATMOSPHERES CARS ARE SHIPPED WITH ALL CONTROLS MOUNTED AND PRE-WIRED TO A TERMINAL BOX UNDER THE PLATFORM

CALL US FOR THE CODE REQUIREMENTS IN YOUR AREA.

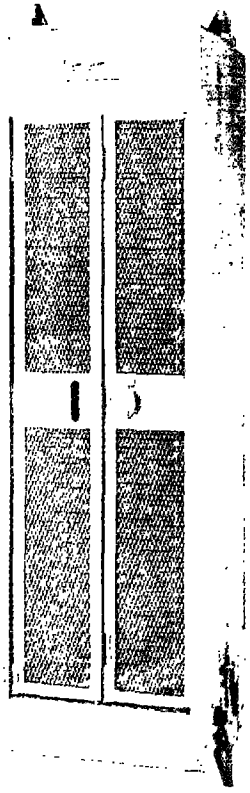

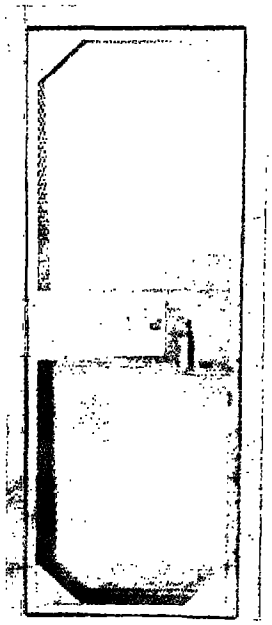

LANDING DOOR

LANDING DOORS ARE FURNISHED AS STANDARD EQUIPMENT FOR ALL LANDINGS THESE DOORS CONSIST OF FORMED CHANNEL FRAMES WITH ALL STEEL EXPANDED METAL SWING DOORS AVAILABLE IN LEFT OR RIGHT HAND SWING HORIZONTAL OR VERTICAL SLIDING DOORS ARE ALSO AVAILABLE INCLUDED WITH ALL LANDING DOORS S AN ELECTRO-MECHANICAL LOCKING DEVICE WHICH LOCKS THE DOOR WHEN THE CAR LEAVES THE LANDING AND UNLOCKS IT WHEN THE CAR ENTERS THE LANDING AN ELECTRIC CONTACT SWITCH WILL NOT ALLOW THE CAB TO MOVE IN EITHER DIRECTION UNLESS THE LANDING DOOR IS CLOSED AND LATCHED

CONTROLLER

THE ELECTRICAL BRAINS OF THE SPECIAL PURPOSE PERSONNEL ELEVATOR IS HOUSED IN THIS NEMA 12 FUSED DISCONNECT PANEL THE CONTROLLER WILL ACCEPT 240 OR 480 VOLTS AND IS EQUIPPED WITH ALL THE LATEST ELECTRICAL SAFETY DEVICES REQUIRED ON ELEVATORS THE PANEL IS COMPLETE WITH A TRANSFORMER WHICH REDUCES THE CONTROL CIRCUIT VOLTAGE TO 120 VOLTS A PHASE REVERSE RELAY, ANTI WELDING RELAY, REVERSING STARTER WITH OVERLOAD PROTECTION AND CONTROL CIRCUIT RELAYS ALL COMPONENTS ARE PRE-WIRED TO A NUMBERED TERMINAL STRIP ALL OTHER ELECTRICAL CONTROLS, SUCH AS THE TERMINAL AND FINAL LIMIT SWITCHES AND UP/DOWN BUTTONS FOR EACH LANDING, ARE PART OF THE PACKAGE

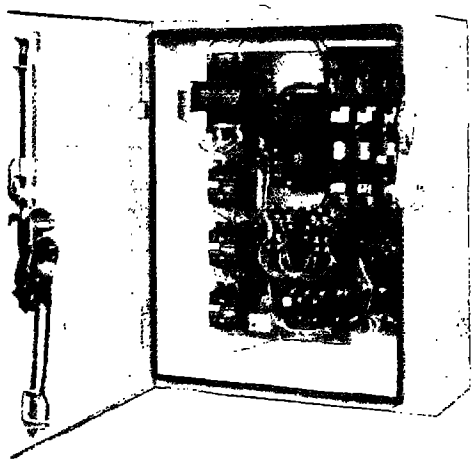

Figure 7-8 Elevator Components

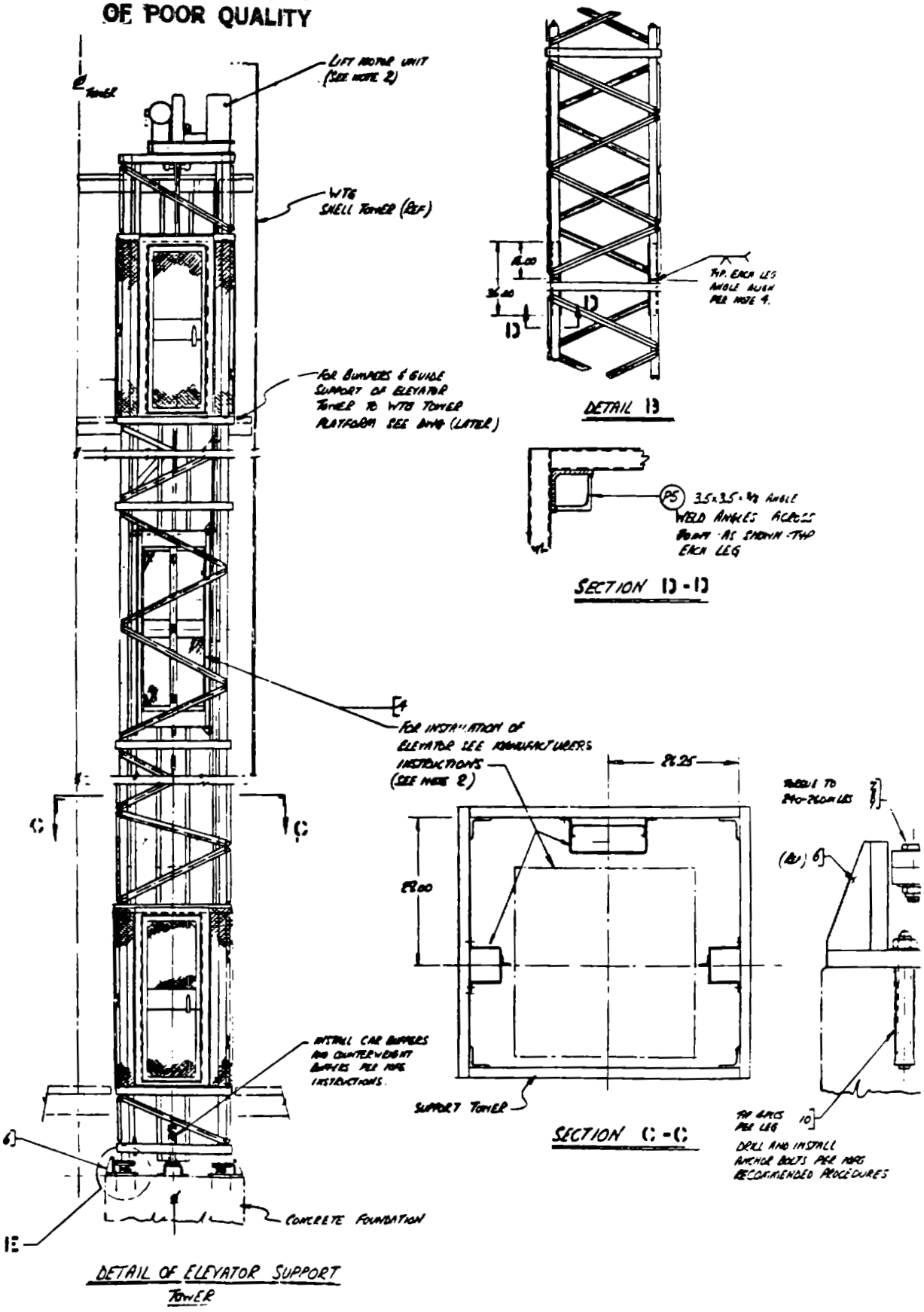

Figure 7-9 Elevator Installation

If the base of the structure was rigidly tied to the foundation, stresses in the structure near the base would exceed weld allowables. The rotational spring constant of the elastomeric pads was calculated to be about 120 x 10^6 in. lb./rad. This limits the shear force at the top landing to an acceptable 345 lb. for the hurricane deflection.

Platforms are needed at the bottom and top elevator landings. The lower platform covers the foundation's circular pit within the ring wall. This pit provides the necessary space for the power cabling in the foundation, and doubles as the elevator inspection pit. All the platforms use interlocking steel floor decking and the individual decking strips are bolted to the H-beam framework for easy removal.

Near the top of the tower are three platforms, which are shown in Figures 7-10 and 7-11. Workers leave the elevator at the level of the elevator top platform. A set of stairs provides access to the elevator inspection platform. Both platforms can be used for storage, but the main use of the higher platform is for inspecting, lubricating, and maintaining the elevator's drive assembly. From the inspection platform, either of two ladders provides access to the yaw area. There are two openings in the yaw platform, since one opening, in certain nacelle orientations, could be blocked by the yaw hydraulics package. Both the elevator landing and inspection platforms are hung from the lower yaw structure using wire rope cables with clevis end fittings. This design avoids any welding or bolting to the tower to support platform loads. Rubber pads are fitted between the tower and the platforms for stability and to prevent any impact.

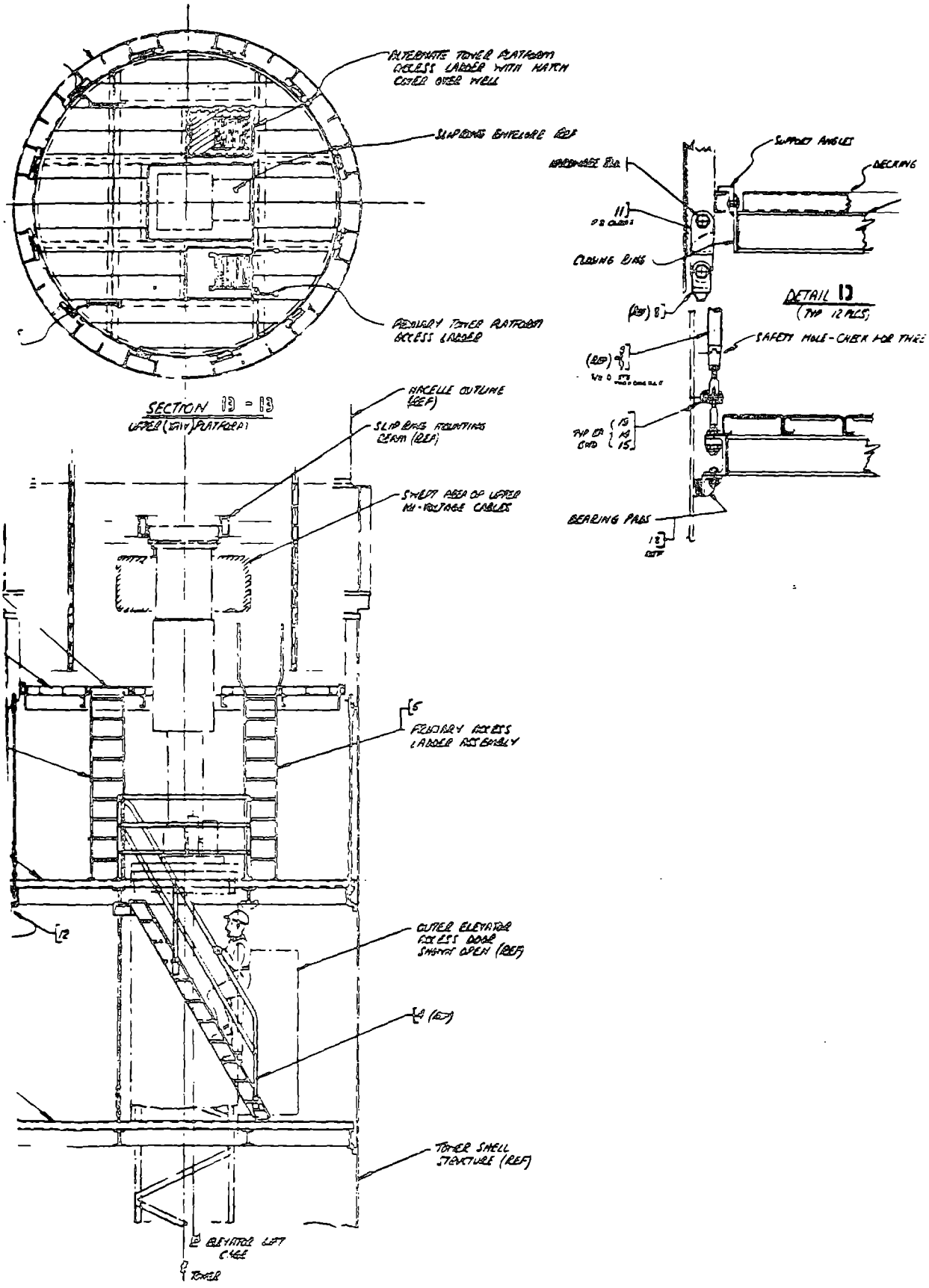

Figure 7-10 Upper Platform by Slipring

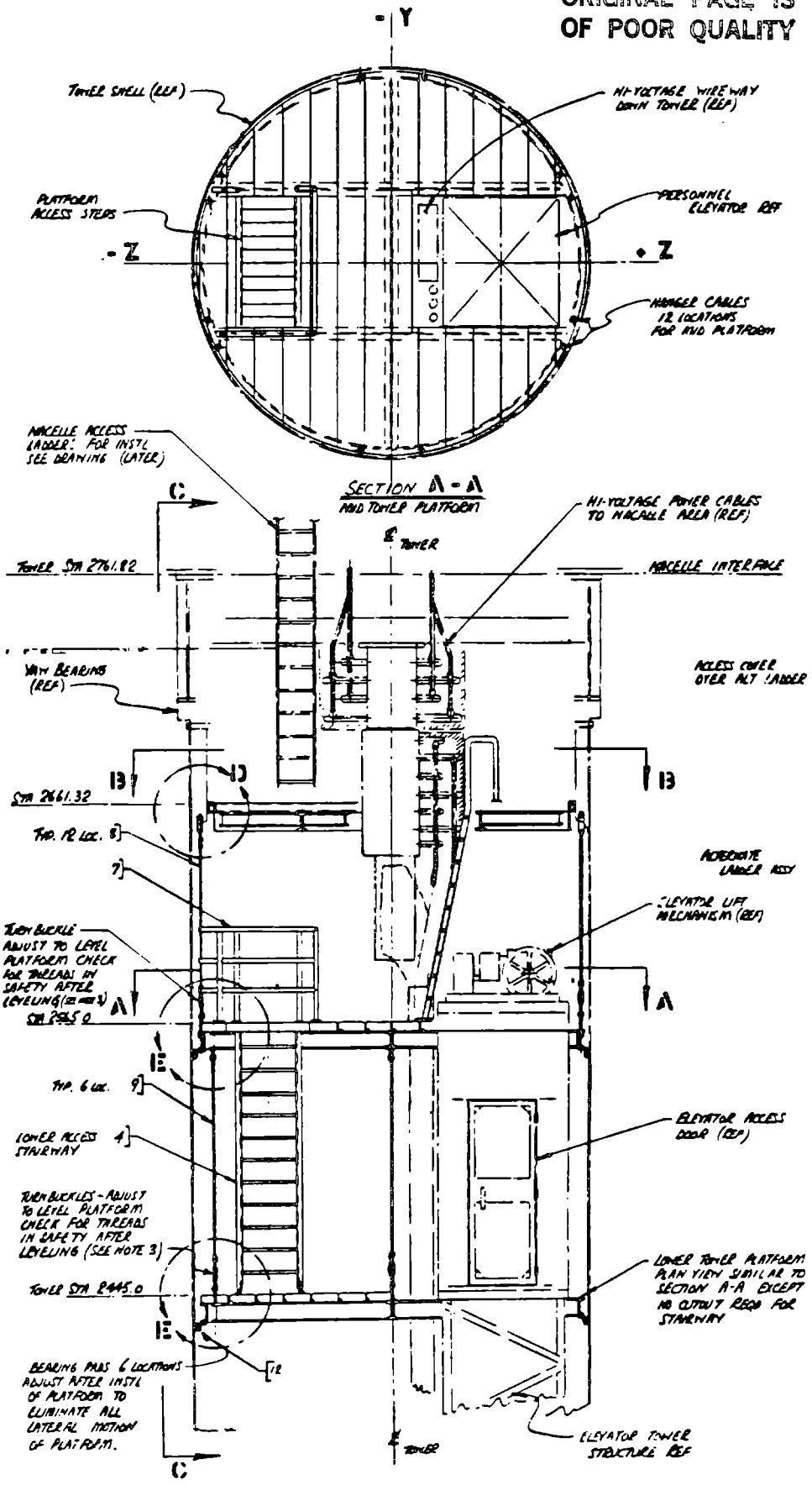

Figure 7-11 Upper Platform by Elevator

7.4 FOUNDATION

7.4.1 REQUIREMENTS

The function of the foundation is to transmit the loads from the tower into the soil. Soil can have a wide range of characteristics, so a generic foundation design for all sites is impractical. However, some soil properties were assumed for the foundation trade-off studies.

The site was assumed to be near Cleveland, OH during the preliminary design. The generic site had a generally flat terrain and the substrate had no unusual or unsuitable features. To a depth of 15 ft. the soil consisted of very stiff to hard brown, sandy, silty clay with gravel and shale fragments. Split spoon penetrations of 20 to 60 blows per ft. were assumed, increasing with depth. A minimum allowable bearing pressure of 4,000 psi, no drainage problems, and a minimum effective modulus of elasticity of 5,000 psi were also assumed.

The conceptual trade-off studies and the spread foundation design were developed by CBI simultaneously with the tower design. The final design of the foundation was done by C. F. Braun of Alhambra, CA. The scope of the work included:

1.) establishing generic foundation design criteria for the MOD-5A
2.) a conceptual design for the selected prototype site
3.) reviewing the final CBI foundation design

Only the first task was completed by C.F. Braun, because the project did not enter the fabrication phase. The report of this work is in Appendix A. The first section deals with geotechnical requirements for a soils investigation, and describes the site exploration, soil boring, lab tests and reporting requirements for the soils engineer. The second section lists the criteria for the foundation design. Most of the criteria are included in the Tower and Foundation Specification and are discussed further in this section.

The foundation meets the applicable industry standards, noted in refs. 7-11 through 7-16. The scope of each standard is defined by its title. The American Concrete Institute (ACI) and Portland Cement Association (PCA) are the sources for concrete and rebar standards.

The standards do not cover all the requirements for wind turbine generators. For example, fatigue data on the anchor bolts, concrete and rebar usually end at about 10^7 cycles. The MOD-5A would run for 40 x 10^7 cycles. There was no consideration as to how much of the fluctuating applied load is actually applied to the anchor bolts. Both CBI and C. F. Braun indicated that ACI 215R and PCA RD059D1D are the only relevant standards, and that for the stress ranges predicted these standards should be acceptable. To determine load sharing by the bolts, a finite element model analysis was conducted. The results of this study are reported in section 7.4.5.

The foundation design criteria requires total settlement of less than 1.0 in. and differential settlement with a slope of less than 1:250, during the 30-year life of the wind turbine generator. C. F. Braun suggested that the peak rocking motion be limited to 10^{-4} radians. However, a value for peak rocking motion was not selected because in effect, limiting the rocking motion limits the rigid body spring constant and limits the decrease in the system rocking frequency. A decrease in the rocking frequency is desirable, since the tower frequency, as shown in Section 7.2, is slightly higher than the optimum.

Results from early parameter studies on the effect of the foundation diameter and soil properties are shown in Figure 7-12. In the range of expected soil moduli for good sites, E >15,000, different foundation radii will have a small, but beneficial effect. Only near the minimum acceptable soil modulus, given in the Statement of Work, would the frequency drop excessively. For the baseline foundation, with a radius equal to 36 ft., the drop is acceptable. But if the rocking motion is limited to 10^{-4} radians as C. F. Braun recommended, the foundation would have to be much larger. The rotational spring constant for a circular spread foundation (ref. 7) is given by:

$$K_\Theta = \frac{ED^3}{6(1-\nu^2)} \quad \text{where } E = \text{Soil Modulus}, \ \nu = \text{Soil Poisson's ratio}, \ D = \text{Foundation Diameter} \qquad [7.3]$$

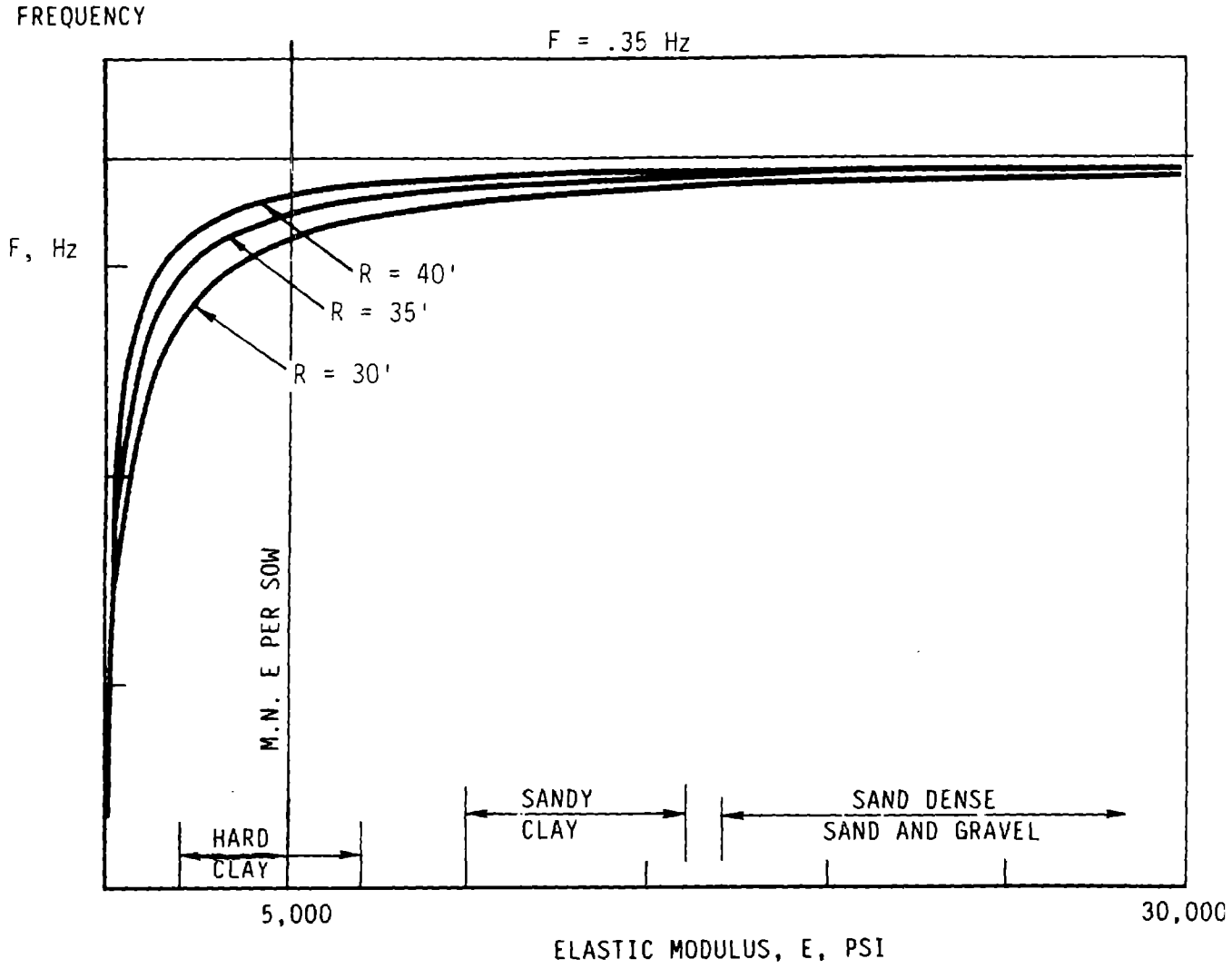

Figure 7-12 Effect of Size and Modulus on System Frequency

For the peak rocking moment of 24 x 10^6 ft-lb, $K_\theta \geq 24 \times 10^{10}$ ft-lb per radian. Solving for D with E = 5,000 psi and ν = .4 yields:

$$D \geq \left[\frac{6(1-.4^2) \times 24 \times 10^{10}}{5{,}000 \times 144}\right]^{1/3} = 118.9 \text{ ft.} \qquad [7.4]$$

This is 65% larger than the 72 ft. baseline diameter. While a larger foundation is necessary for soil with a low modulus, a very large diameter can be avoided if the rocking angle is not specified. An evaluation of the acceptable rocking angle will be required for each site. The evaluation will include rocking frequency and other soils engineering.

7.4.2 TRADE-OFF STUDIES

During the conceptual design, CBI's studies indicated that the circular spread foundation was the most cost effective type of foundation. Piles and deep piers were applicable only in certain locations. C. F. Braun also studied the foundation designs, and reached the same conclusions. Their rationale is summarized in Section 6 of the Foundation Design Criteria, found in Appendix A. Other studies by CBI dealt with using mass production techniques to lower the foundation cost. However, they concluded that unless many wind turbine generators are to be erected on the same site, the foundation design or manufacturing techniques could not lower the installed cost.

7.4.3 BASELINE FOUNDATION DESCRIPTION

The baseline circular spread foundation is shown in Figure 7-13. Its outer diameter is 72 ft., 8 in., with a ring wall outer diameter of 26 ft. 4 in. The tower anchor bolts are embedded in the 4 ft.-thick ring wall. The ring wall and elevator support block are poured after the basic foundation, but both are tied to the base by rebar.

The rebar in the mat portion of the foundation weighs about 126,000 lbs. The overall density is 140 lbs./cubic yard, about average for this type of foundation. The density in the ring wall is significantly higher, because of the greater rebar content.

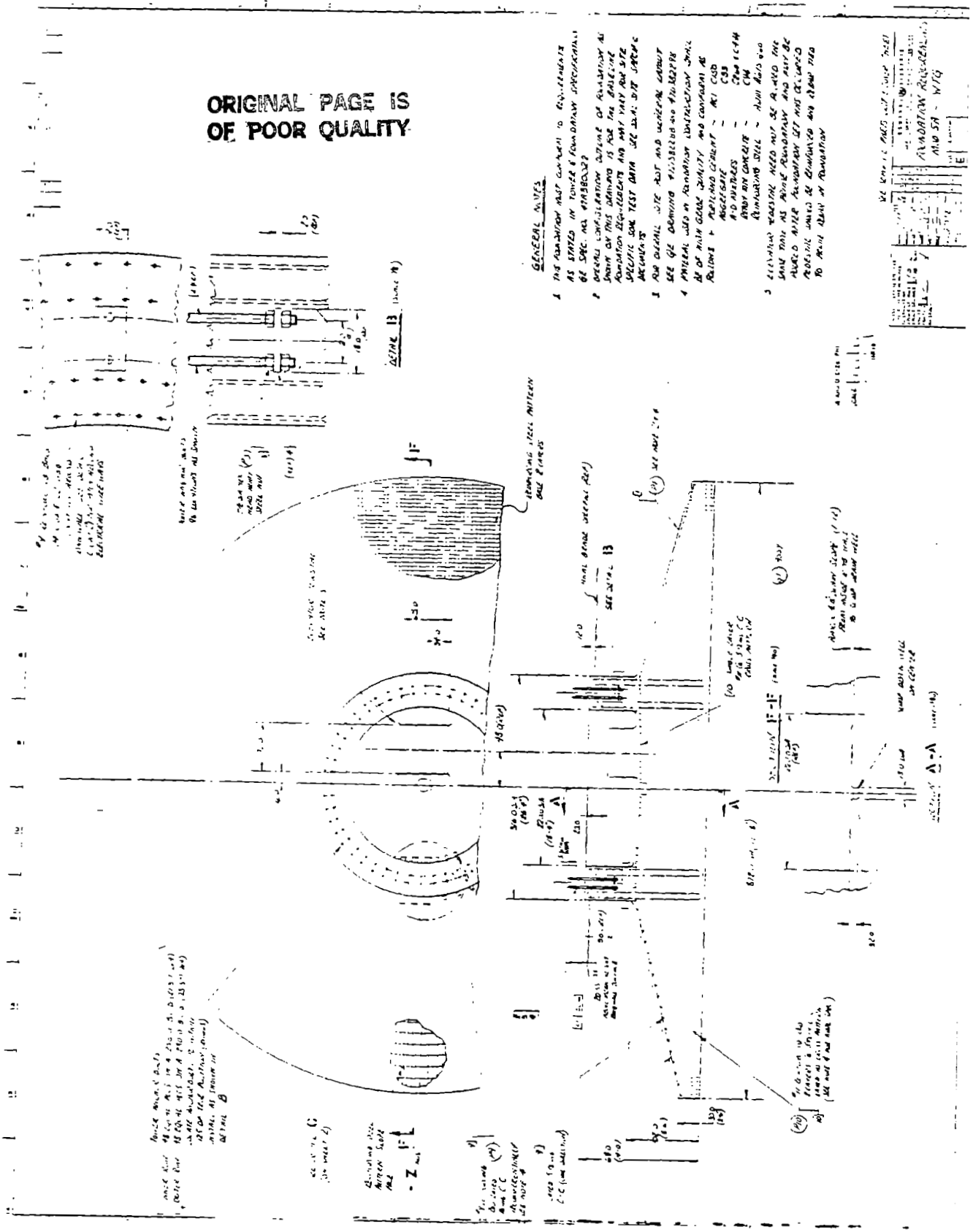

Figure 7-13. Foundation

The ring wall is penetrated by three rectangular wire way conduits and three conduits as shown in Figure 7-14. Those pipes and conduits pass power and control signals from the elevator support structure to the trench way on the outside, which leads to the control enclosure. The pit enclosed by the ring wall is sloped toward the center, where a small sump pit is placed. Provision is made for a portable sump pump to dispose of inner tower condensation runoff, if necessary.

There are 96 2.5 in. anchor bolts embedded in the ring wall. These are high strength, fatigue resistant bolts, which meet the ASTM A193 B7 requirements. The threads are rolled after heat treatment, to provide good fatigue life.

7.4.4 FOUNDATION STRESSES

Stresses were checked against allowables at the nine locations shown in Figure 7-15. The loads imposed by the tower are also shown. In certain cases, the dead weight loads of the foundation and soil overburden must be added to the tower loads. CBI used proprietary computer codes to make size estimates, and extensive hand calculations to check for fatigue. The diameter was driven by the requirement to keep the maximum soil bearing pressure within allowables. The soil bearing was checked for two conditions: maximum operating load, and maximum hurricane or any other limit load that would occur only once or twice in the lifetime. For the operating loads, the foundation may not allowed uplift, as shown by the pressure distribution in Figure 7-15. The integrated pressure for the distribution shown over the area must be equal to the sum of the tower load (V) and the dead weight of the foundation and soil overburden. Also, the net upward force of the soil acting through the centroid must balance the moment caused by the tower (M) and shear force (H) times the height. Therefore, only one unique pressure distribution is possible.

Using the pressure distributions, the thickness dimensions of the mat were found by iteration until concrete shear, rebar flexural tension, and centerline stresses were within allowables. Formulas and design curves from ACI 318-77 Ultimate Strength Method and concrete design textbooks (ref. 7-18) were used. CBI used formulas and design curves from standard design procedures. The ring wall rebar and dimensions were similarly sized.

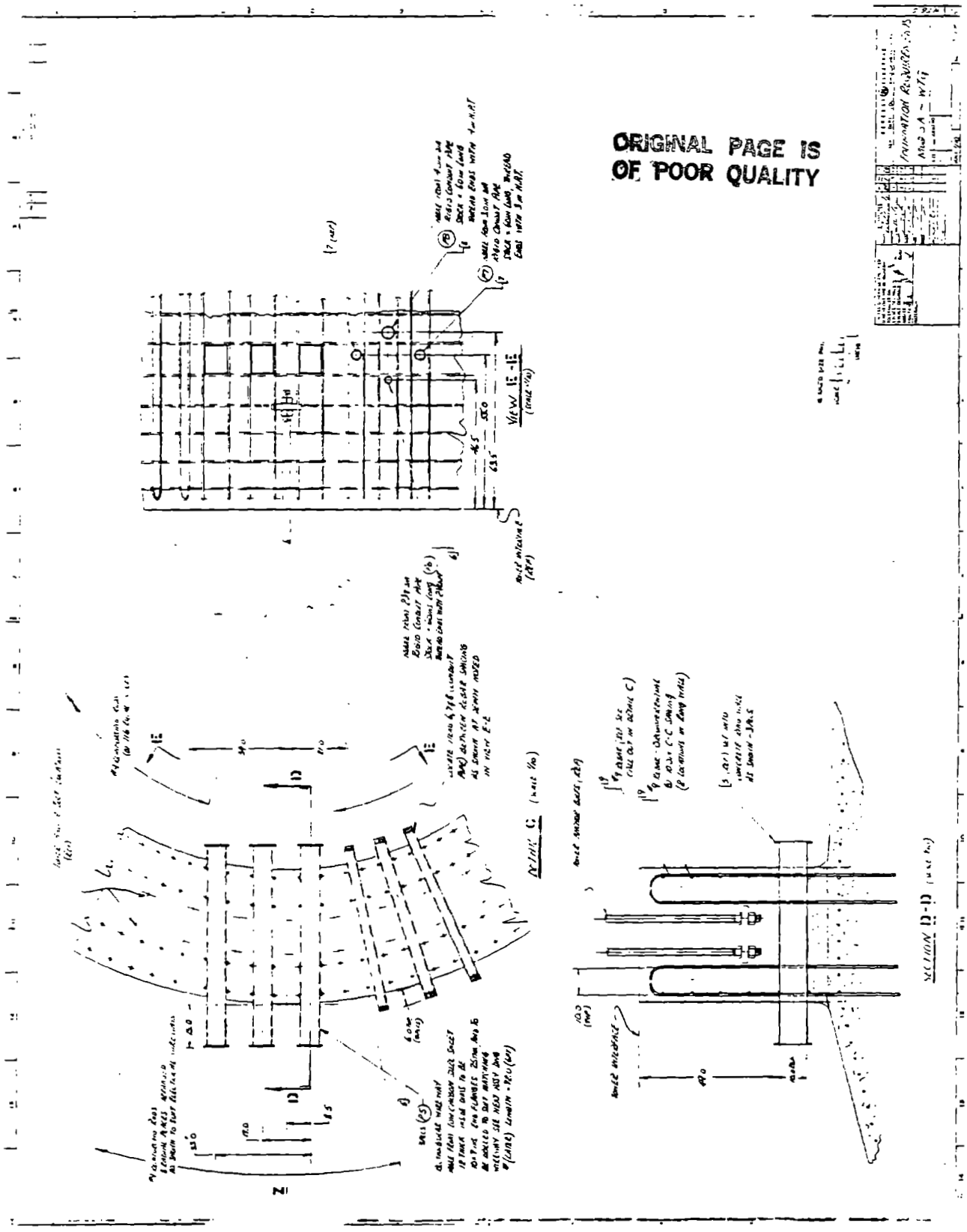

Figure 7-14. Conduit Through Foundation

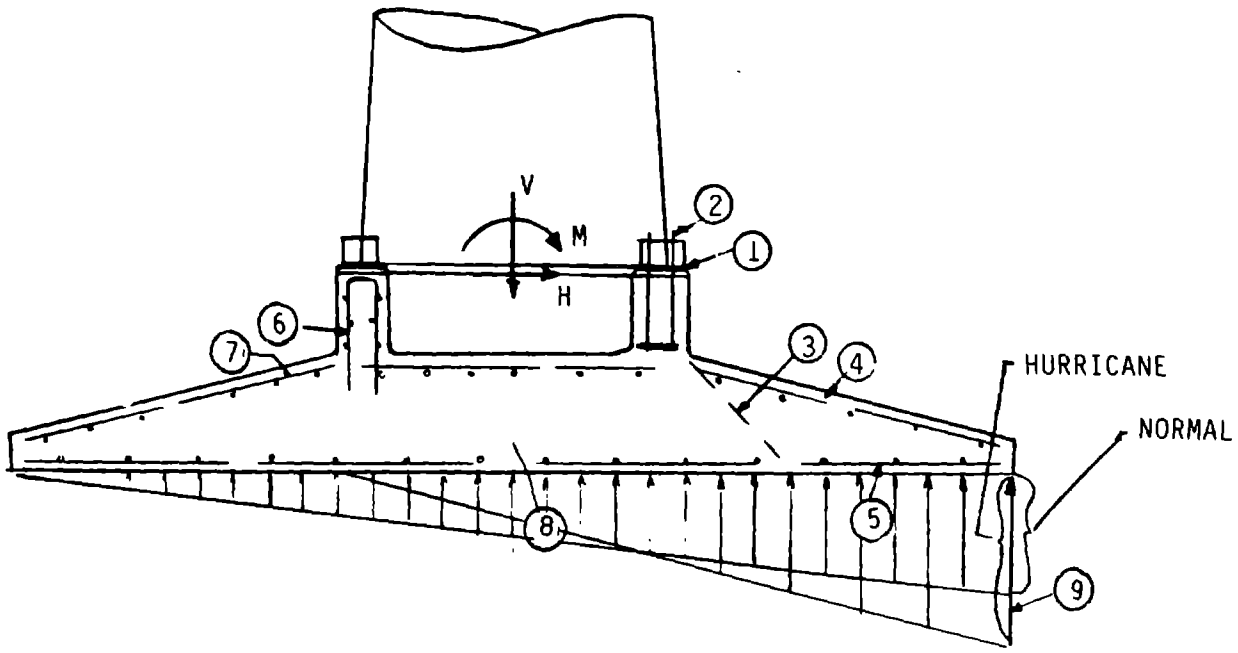

Figure 7-15 Foundation Stress Analysis

Because of the high cycle fatigue nature of wind turbine generators, the methods of checking the design for fatigue are of special interest. The allowable range stresses for the various foundation components were computed as follows:

1. Steel Reinforcement:

   From the PCA Bulletins RD 059.01J and RD 045.01E the following is recommended:

   $$f_r = 21 - .33 f_{min} + 8 (r/h) \qquad [7.5]$$

   Where f_r = maximum stress range allowable in ksi
   f_{min} = minimum stress in ksi (tensile positive sign compression negative sign)
   r/h = ratio of base radius to height of rolled deformation (use .3 when unknown)

   The various manufacturers of rebar have different deformation characteristics that produce minor changes in fatigue strength.

2. Concrete Shear:

   From ACI 71-10, Section 3.1.1

   $$V_r = (1 - V_{min}/V_c) * V_c/2 \qquad [7.6]$$

   Where V_r = allowable shear stress range
   V_{min} = minimum shear stress
   V_c = shear stress capacity of concrete

3. Concrete Compression:

   Again from ACI 71-10, Section 3.1.1

   $$f_r = (1 - f_{min}/.75 f'_c) + .4 f'_c \qquad [7.7]$$

   Where f_r = allowable stress range
   f_{min} = minimum stress
   f'_c = concrete compressive strength

4. Bond Stresses:

   From ACI SP-41, if the maximum bond stress due to cyclic loadings is less than 40% of the static bond stress, unlimited fatigue cycles are assumed.

5. Soil Bearing:

   The allowable pressure range will be determined by the laboratory tests recommended by the geotechnical engineer. These tests will vary for each site.

In several of these formulas, the minimum stress is used and normally operates to increase the allowable if it is compressive. For conservatism, since the wind turbine generator could yaw 180° from any rest or operating position, the minimum stress used was the largest tensile stress at the pertinent part of the foundation. If all the pertinent areas are in compression the minimum value would be set to zero.

The same formulas that were used to check the static stresses were used for the stress range, by substituting the load range for the applied load. The load range was the largest of either the Type I and II combination or the Type III range loads. Both values were determined by the dynamic analysis of the wind turbine generator, reported in Volume II, Sections 6 and 7.

7.4.5 ANCHOR BOLT STRESSES

Great care was taken in the design of the anchor bolts since they will be embedded into the ring wall and would be very difficult to replace. State of the art bolted joint analysis indicated that proper design and preload greatly reduces the risk of fatigue failure. As explained by references 7-19 and 7-20, the relative stiffness of the bolts and clamped parts affects how much of an applied load that a preloaded bolt will see.

Technical literature explains how to estimate the relative stiffness of the bolt and the clamped joint for standard bolted joints, such as pipe flanges or automotive connecting rods. However, the literature does not cover systems like the foundation anchor bolt system, which clamps through 4 ft. of reinforced concrete and a steel anchor chair. A finite element model was constructed and analyzed for this part of the foundation and tower. The results of the analysis estimated the load sharing capabilities of the joint.

A 3.75° segment of the ring wall and anchor chairs was modeled as shown in Figure 7-16. The anchor bolt elements were lowered in temperature to simulate the preload force that would normally be applied. A uniform load was applied to the top elements of the tower shell. Because concrete cracks under low tension, concrete elements under tension greater than 100 psi were sequentially released. The final run indicated the applied load distribution between the bolt load and the grip load.

The finite element model was also used to quantify the assumed concrete stiffness, by changing the elastic properties of the unreinforced concrete and reinforced concrete elements. The results of the study are summarized in Table 7-3.

Table 7-3

FEM Anchor Bolt Load Summary

Case	Anchor Bolt	Preload F_v	Applied Load F_{ax}	Total Load F_s	Working Load $F_{sa} = F_s - F_v$
H	Inner Bolt	244.6	100	249.4	4.8
	Outer Bolt	245.4	100	250.0	4.6
L	Inner Bolt	237.5	100	243.5	6.0
	Outer Bolt	238.4	100	244.2	5.8

Load in kips Case H is for concrete with $E = 3.50 \times 10^6$ psi. Case L uses $E = 2.625 \times 10^6$ psi.

A contingency factor of 25% is assumed in the following bolt fatigue life analysis because up to a 15% uncertainty exists in assumptions made in the finite element model analysis.

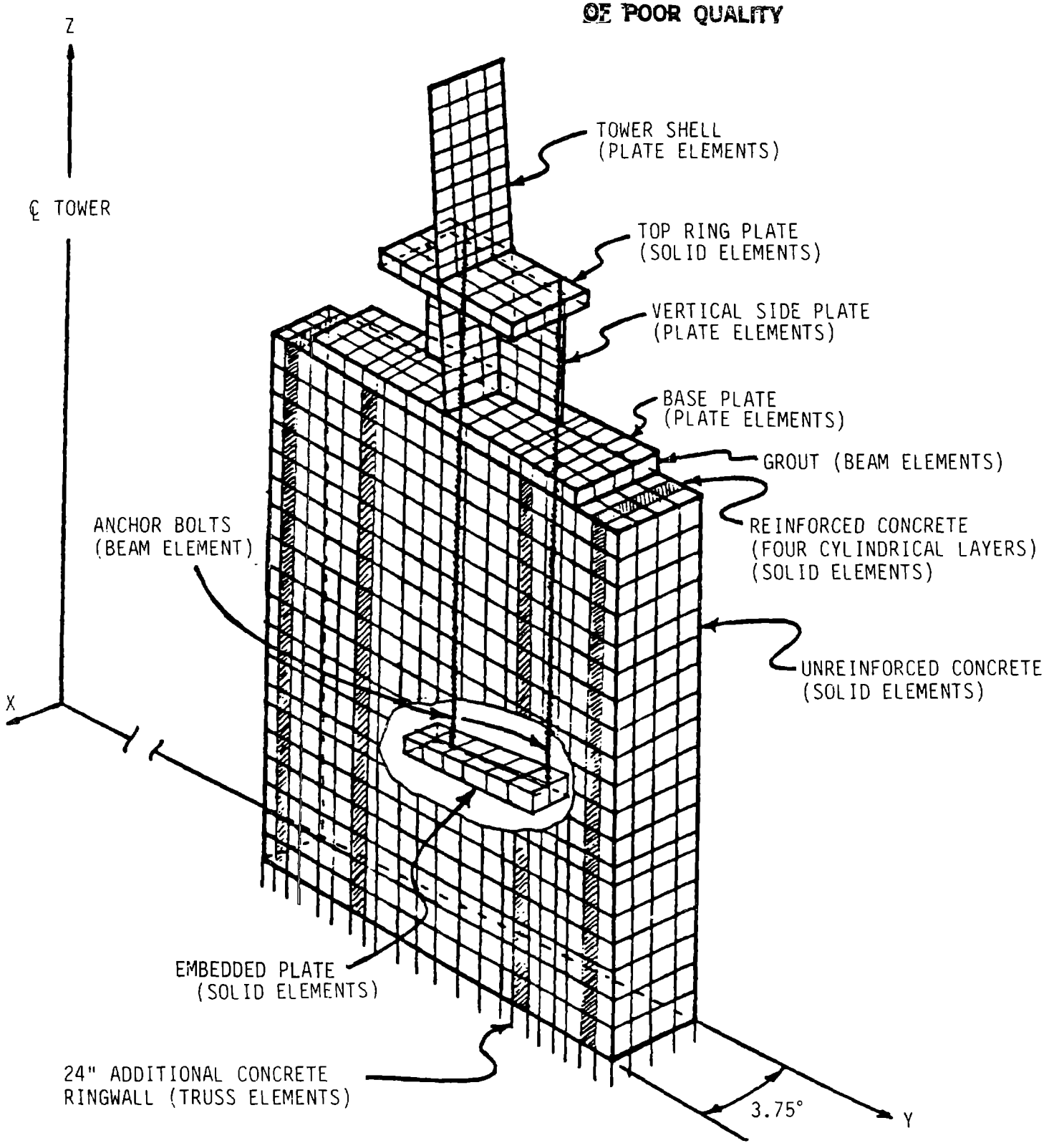

Figure 7-16 Finite Element Model of Anchorage System

The fatigue life of the bolts was checked by the CIS method according to the Structural Design Criteria (Section 9, Volume II). The root mean cubed vector sum of the M_y and M_z half range moment at the base is 5.58×10^6 ft-lb. Using the standard design formula:

$$F_{ax} = \frac{4M}{NC} - \frac{W}{N} \qquad [7.8]$$

Where F_{ax} = applied load per bolt
M = overturning moment
N = number of equally spaced bolts
C = average diameter of bolt circles
W = axial or dead weight force

$$F_{ax} = \frac{4 \times (\pm\ 5.58 \times 10^6)}{96 \times 22.5} - \frac{(\pm\ 13{,}000)}{96}$$

F_{ax} = 10,469 lb. (worst case combination)

Using a resiliency ratio (r), which is defined as the working load divided by the applied load, of 0.075 and a bolt prying factor (p) of 1.25, the thread stress for the 2.5-in. bolt is:

$$S = F_{ax}\, rp/A \qquad [7.9]$$

$$S = \frac{10{,}469 \times .075 \times 1.25}{4.44} = 221 \text{ psi}$$

The allowable RMC stress is 600 psi, following the recommendation of ref 7-21, based on the testing of large anchor bolts under various conditions. C. F. Braun suggested using category "D". This suggestion is supported by the extrapolation of other fatigue data for smaller standard bolts. In either case, the anchor bolt fatigue margin is quite large.

The bolts are designed for the hurricane limit load condition. This load is slightly more than the preload on the most heavily loaded bolt, as indicated by CBI's finite element model analysis. By the design formula:

$$F_{ax} = \frac{4 \times 121 \times 10^6}{96 \times 22.5} - \frac{1.56 \times 10^6}{96} = 207{,}824 \text{ lb.}$$

The bolt stress with a 1.25 prying factor is 58,500 psi, an acceptable 83.5% of the proof load.

7.5 AUXILIARY SYSTEMS AND SUBSYSTEMS

There are several platforms at the the top of the elevator. The platforms provide access to the yaw drive system, which keeps the rotor and nacelle pointed into the wind. The large yaw bearing enables the nacelle to rotate with minimal friction. To allow the yaw drive to be assembled and checked in the factory, the upper and lower yaw structures, immediately above and below the yaw bearing, are assembled in the factory, rather than in the field with the rest of the tower.

The yaw slipring is also mounted in this area. The slipring transmits power and control signals between the rotating nacelle and the fixed tower. The slipring is described in more detail in Section 8.5.

The drive components had to be protected, as far as possible, from the outside. The yaw bearing, slipring, yaw hydraulics, elevator, etc. are located inside the yaw section to protect them from weather and to provide access for maintenance as shown in Figure 7-17.

7.5.1 YAW STRUCTURES

The yaw structure and yaw bearing are assembled together as shown in Figure 7-18. The lower yaw structure is a relatively simple weldment. The material is A678 Gr B steel, which is compatible with the material of the main tower, to which it is welded. The cylindrical shell supports the brake disk of the yaw drive system, which supports the yaw bearing. Internal stiffeners, placed every 10 degrees, transfer the loads from the disk to the cylindrical structure. Holes near the bottom of the stiffeners allow the structure to be tied to the factory floor, and are used to hang the elevator platforms. The stiffeners have a bottom radius of 6 in. to reduce weld stress concentration. The weld between the stiffener and the shell must be ground, so that the weld will fit in the AISC "C" category.

Although the stress analysis for the tower indicates that "C" category welds

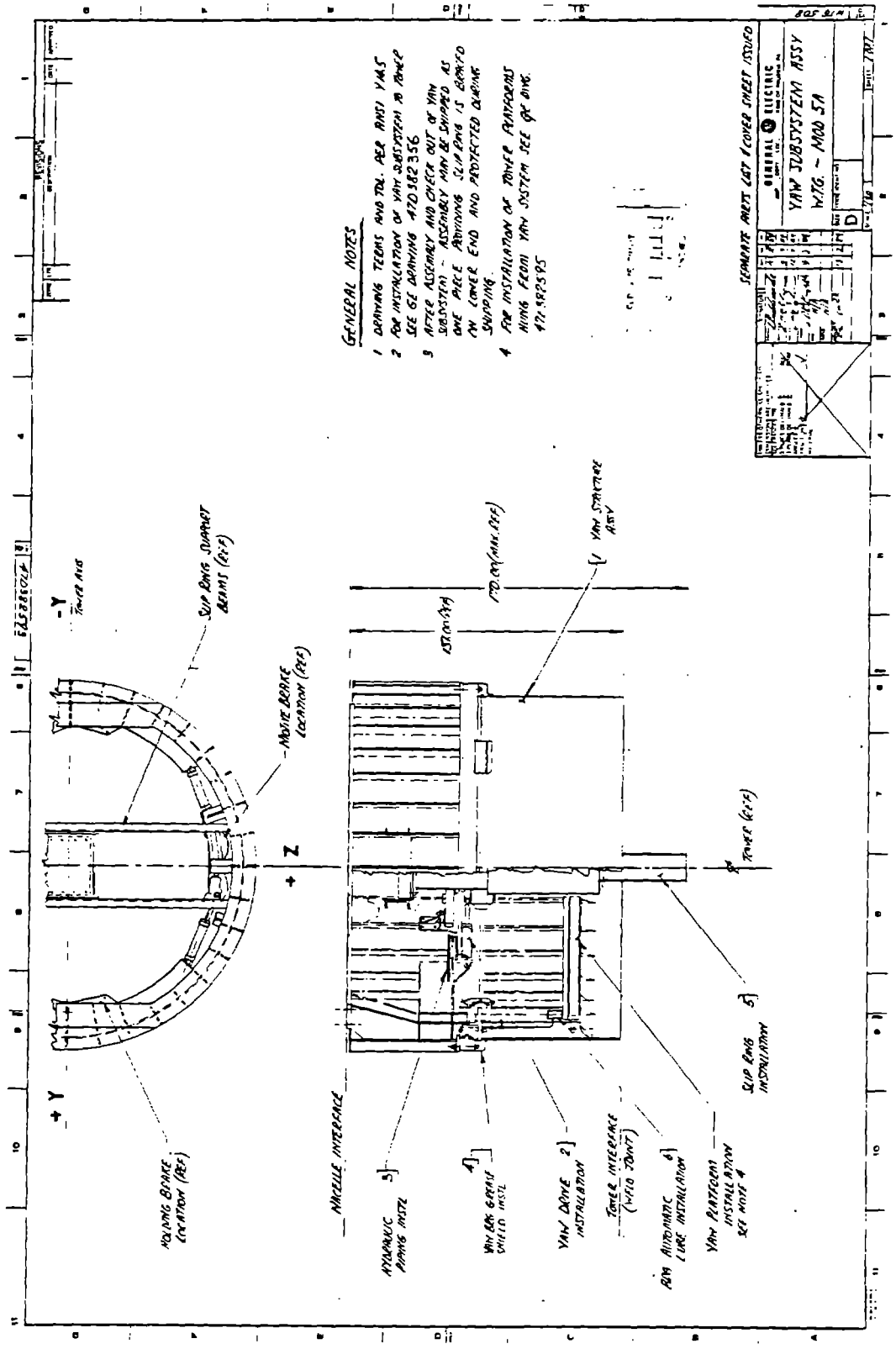

Figure 7-17. Yaw Subsystem Assembly

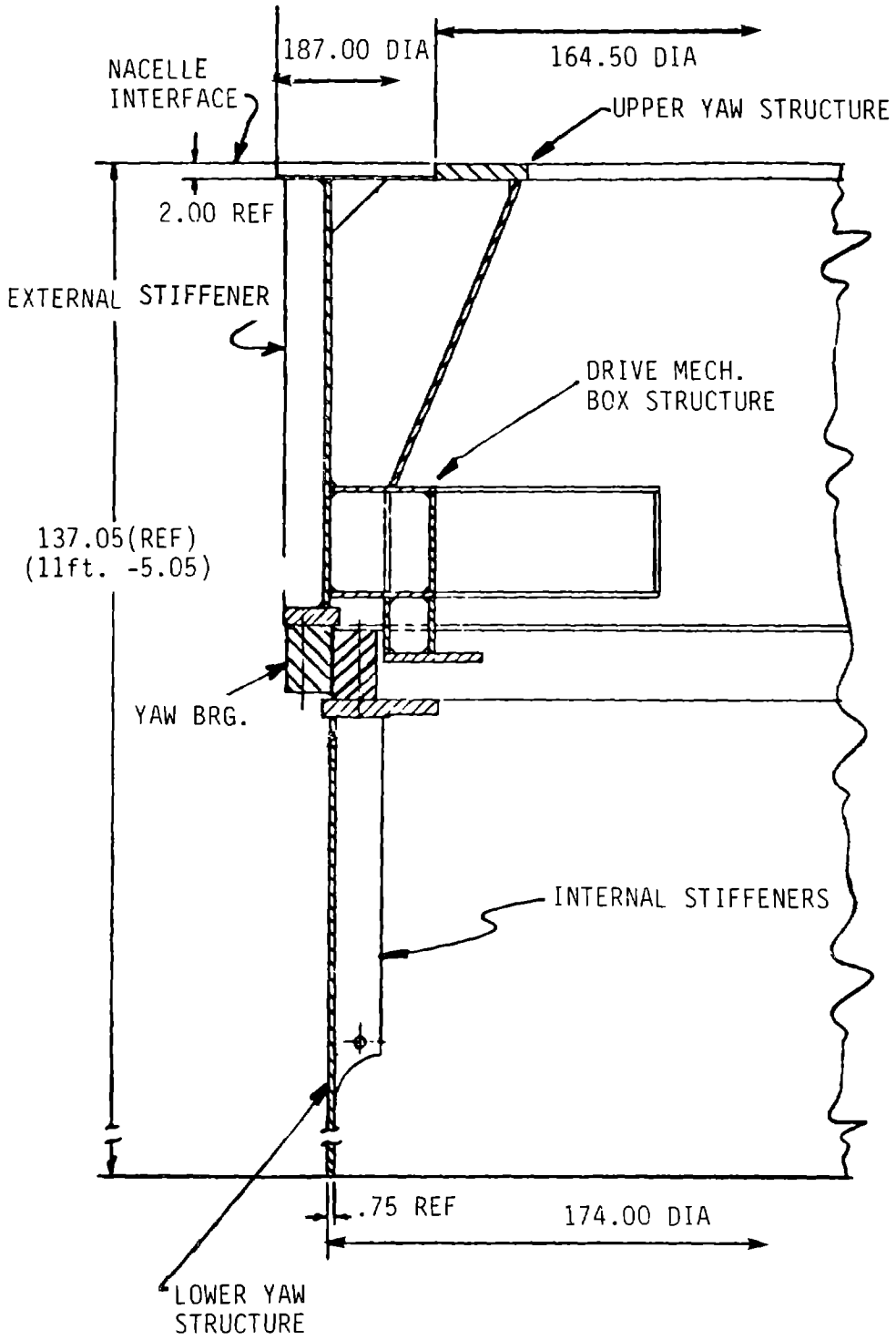

Figure 7-18 Yaw Structure Assembly

are not required at the top of the tower, the more stringent weld category was chosen because of the uncertainty in the load predictions and in the finite element model analysis of local stress concentrations in the yaw structures. The stress analysis quantified stress ranges at weld details, including load peaking through the yaw bearing. The wall thickness was increased from .625 in. to .75 in. Analysis showed that the thickness of 0.75 in. was adequate, based on the CIS fatigue criteria.

Because the upper yaw structure is so complex, it was designed as a weldment. The upper yaw must transfer loads from the rectangular bedplate to the circular yaw bearing. The yaw drive forces and dead weight loads must also be accommodated. The bedplate is not uniformly stiff, like the tower. The effect is noted in the plots of yaw bearing bolt loads, shown in Figure 7-21. More severe load peaking occurs at the top of the structure. To compensate for the load peaking, the yaw structure was strengthened, above the size that a hand analysis using theoretical load distributions would stipulate.

On the Y axis, shown in Figure 7-18, supporting structures for the yaw stationary brakes are required. A box structure that follows the contour of the cylinder for approximately $\pm$ 50^{o} is used. At each end of the box, structure that holds the ends of the yaw drive cylinders is added. In this segment, there are internal gussets that vary in shape between the rectangular nacelle bolting surface and the circular yaw bearing mounting ring. On the Z-axis the gussets are uniform in shape. Three gussets on each side are used to mount the yaw drive's moving brake track. The hydraulic power supply for the yaw drive is mounted in two packages and attached to the internal gussets near the Y axis.

The design of the upper yaw structure was driven by fatigue, so 60 ksi yield material was not required. A572 Gr 50 steel is specified, with good weldability, tougnness, a fine grain, and a restricted vanadium content.

7.5.2 YAW BEARING

A bearing allows the nacelle to rotate relative to the tower, to keep the rotor pointed into the wind. The bearing supports the weight of the nacelle, and can withstand a large overturning moment. Once the bearing is installed, it will be difficult to repair or replace. For these reasons, and because of its high cost, the bearing is a key component.

The bearing is located about 56 in. below the bedplate, between the upper and lower yaw structures, as shown in Figure 7-18. The location of the yaw bearing is a compromise between the packaging and loading constraints. If the bearing was located just below the nacelle, the loads caused by some limit load overturning moments would be smaller. However, the uneven distribution of loads, caused by the non-uniform stiffness of the bedplate, would be worse. The packaging of the yaw drive and slipring would also be adversely affected by the change in bearing location.

The yaw bearing is a three-row, rolling element bearing, commonly called a slewing ring bearing. This type of bearing is often used in large cranes, antennas, excavators and other machinery, in which low rotational speeds are required. There are several other types of rolling element bearings: the single-row four-point-contact ball bearing, and the crossed roller bearing. The three-row bearing can withstand the largest overturning moment for a given bearing diameter. The bearing diameter was determined by the tower diameter, since any structural transitions would add to the bearing's cost. The three-row bearing transmits the loads with the least distorting force. The ball and crossed roller type bearings induce side forces proportional to the axial loads, which distort the yaw structures. The three-row bearing also has the lowest frictional torque, although this was not an important consideration.

Other types of bearings were considered during the conceptual design. A simple journal bearing with Teflon pads created too much friction, and because the large overturning moment causes the direction of the load to reverse around the circumference, the bearing design became complicated. The reversing load also complicates the design of an air film bearing, and the large loss of gas would require a very large compressor and storage system.

A kingpost bearing design, using two separated bearings with smaller diameters, available from catalogs, would unacceptably cramp the area needed for the slipring and yaw drive.

Potential slewing ring bearing vendors were questioned about the possibility of integrating the bearing into the yaw structures. The conclusion was that the design was feasible, but the design and development costs would be high. Any changes in the design would be expensive. Consequently, the standard slewing ring bearing was chosen. There were at least four potential vendors, so that cost would be competitive.

The integrated design requirements for the bearing are specified in a document written with the aid of the Franklin Research Center (FRC), in Philadelphia, Pa. FRC has engineering expertise in large bearings, and first worked with GE during the selection of the MOD-1 bearings. FRC also aided in the bearing selection during the MOD-5A program.

The design of slewing ring bearings is different from the design of standard rolling element bearings, in that speeds are very slow, load paths differ, and structural deformations are important. The outer race of the three-row bearing has a nose ring that is subject to bending stress. A crack through this part could lead to a catastrophic failure of the bearing, and if the bearing failed, the nacelle would fall off the tower.

The load and stress considerations are shown in Figure 7-19. The two main load components, the overturning moment and the axial force, are shown. A radial or shear force, caused by rotor thrust, also occurs when the wind turbine is operating. This component is relatively small and is absorbed by the radial row of rollers.

On the left side of the bearing, as shown in Figure 7-19, the moment and axial components combine. The load path runs through the nose ring of the outer race, and the bottom, or support, row of rollers, and into the lower yaw structure. In the figure, the critically stressed points are labelled a and b. At a, the bending tensile stresses of the nose ring are magnified by the

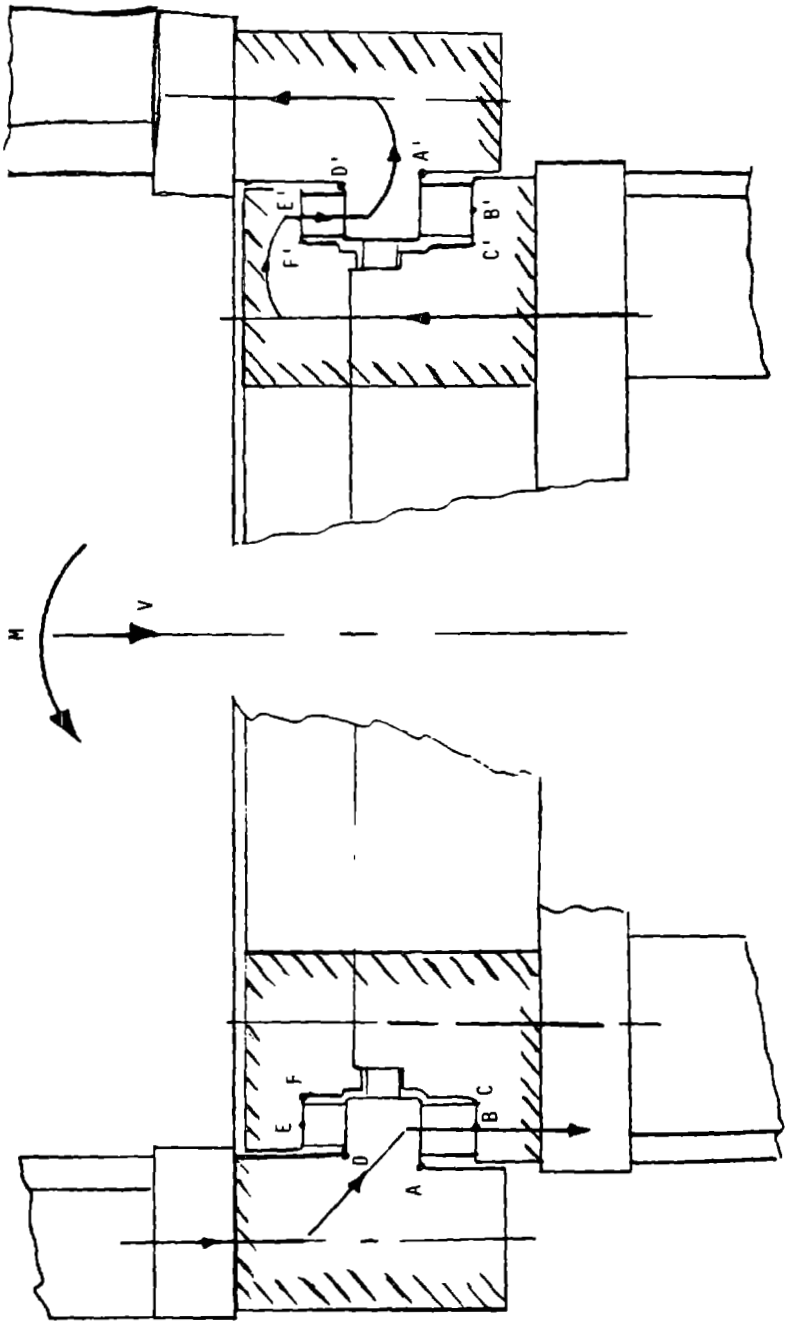

Figure 7-19 Bearing Load Paths

stress concentration of the corner. At c, the stress is considerably less because the load bends the bottom ring less, since it is backed up by the lower yaw flange. At b, large contact stresses occur in both the roller and inner race. The roller is made of a high quality material, which can be hardened all the way through, so contact stress is not a problem. All the bearing races are made from ring forgings of a 4340 type material, which has through hardness properties of about $38R_C$. The raceway surface is induction hardened to $58\text{-}60R_C$. Because the hardening extends only about 0.190 in., contact stresses, including shear stresses, are checked well into the core against allowable compressive and shear stresses.

The moment component is usually larger than the axial component. Consequently, the load path, as shown on the right side in Figure 7-19, is different from the left side and goes through the upper, or retaining, row. The critical points are d', e' and f'. However, the load is less than the load on the left side, since the axial and moment components subtract, rather than add. At e' stresses are not a problem, and d' will be at a lower stress than a, since the load is lower and the geometry similar. At f', however, there is no backup support like that at c on the left side.

The preceding analysis is straightforward for limit loads, because stresses are directly compared to allowables. For fatigue considerations, there are three sources of cyclic loads. The variations of the moment and vertical load components, which occur during wind turbine operation, are one source. These loads are analyzed like the limit loads, using cyclic loads and fatigue allowables for the high cycle fatigue. The second and third sources come from nacelle rotation, which is assumed to be less than 30,000 cycles. The rotation is the second source of fatigue; point c becomes c' after a 180^o rotation, and the load changes appropriately. Note that points b, c, e and f go from different maximum tensile values to nearly zero stress. Points a and d on the nose ring go through stress reversal, but the tensile stress at a is greater than the compressive stress at a' because the load is smaller on the right. The final source of fatigue loads comes from the variation in raceway loading since the rollers are not continuous. In the figure the stress at a is maximized when the line of roller contact is in the same plane. As the roller moves, the stress decays until a is midway between two rollers, then it

builds again for the next roller. For every complete nacelle rotation the number of cycles is N/2, where N is the number of rollers. The range of this stress is small compared to the other load cycles and can be ignored if the crack growth threshold fatigue approach is used. However, since the stresses at a, d and f exceed the 24 ksi required by the AISC category A, the CIS approach was used to check fatigue. For the worst case assumption, the fatigue histogram has 359 x 10^6 cycles defined by the operating loads, 30,000 load cycles from rotation and 30,000*N roller load cycles.

The effect of the non-uniform structural support for the bearing must be considered. The yaw structures were analyzed by the finite element method, with a simple representation of the bearing. The mesh at the bearing is shown in Figure 7-20. The mesh at the bearing rollers, elements 401 to 220, transmits loads in all directions, whereas the actual bearing can only transmit radial loads in compression. The radial distortion calculation was, therefore, smaller than it actually is, but this should have only a small effect in the axial direction.

The axial force transmitted at various positions around the bearings circumference is plotted in Figure 7-21, for both the finite element model and the theoretical model. The loading is for the hurricane limit loads, defined as of January 1983. The distortions from the theoretical model occur because of hard point intersections of the bedplate's side beams and the upper yaw housing. On the rotor side of the nacelle, where the dead weight nacelle moment and blade drag moment add to the dead weight force, the peak load per inch is magnified by a factor of 1.52. On the other side there is a magnification factor of 1.68. For the rest of the analysis, all theoretical loads are assumed to actually produce peak loads 1.75 times larger.

NODE	R	Z
20101	81.87	70.0
11001	87.0	70.8
40101	87.0	74.25
110001	87.5	78.5
120101	92.5	78.5

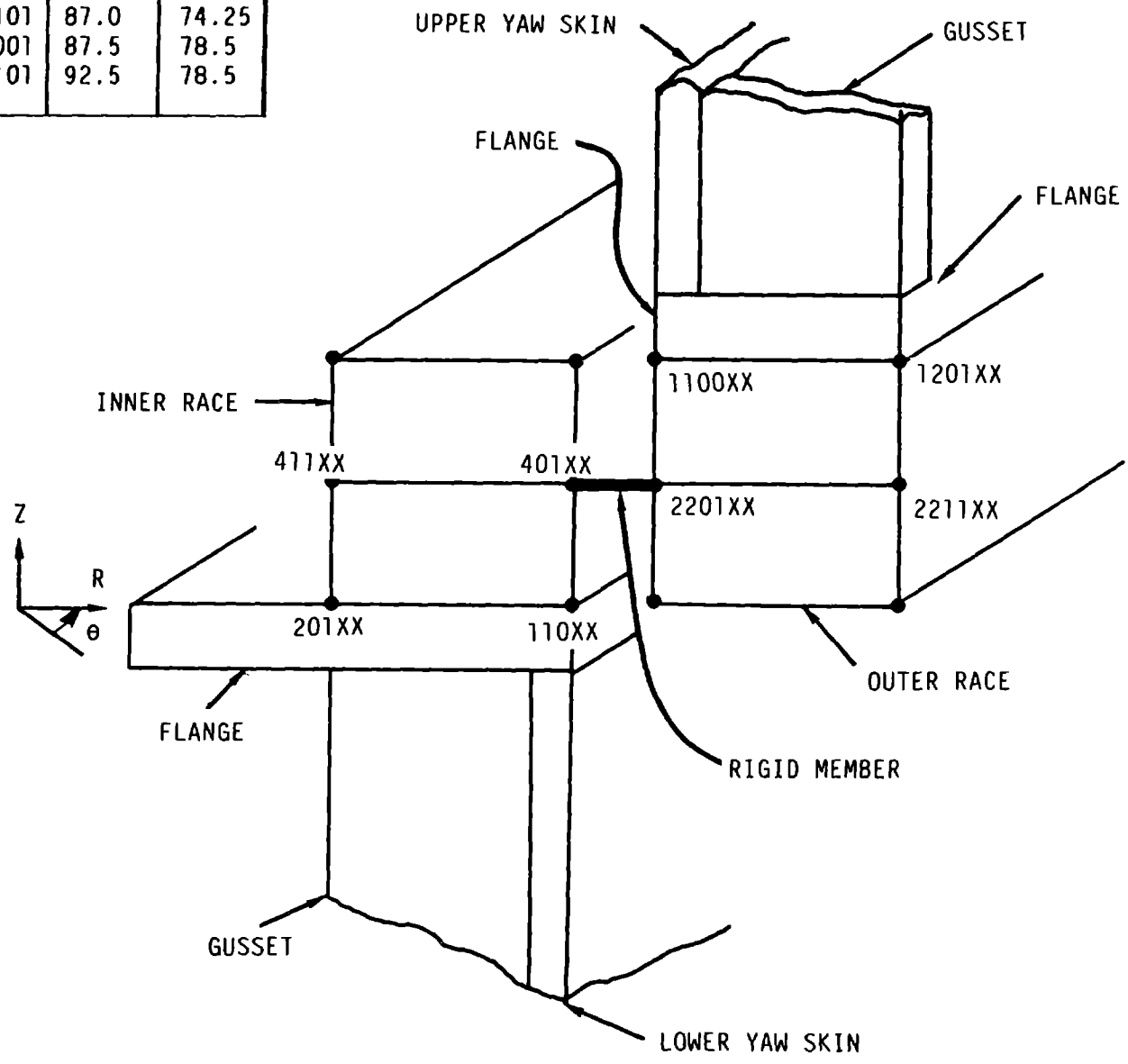

SECTION A-A

Figure 7-20 Bearing Stress Model

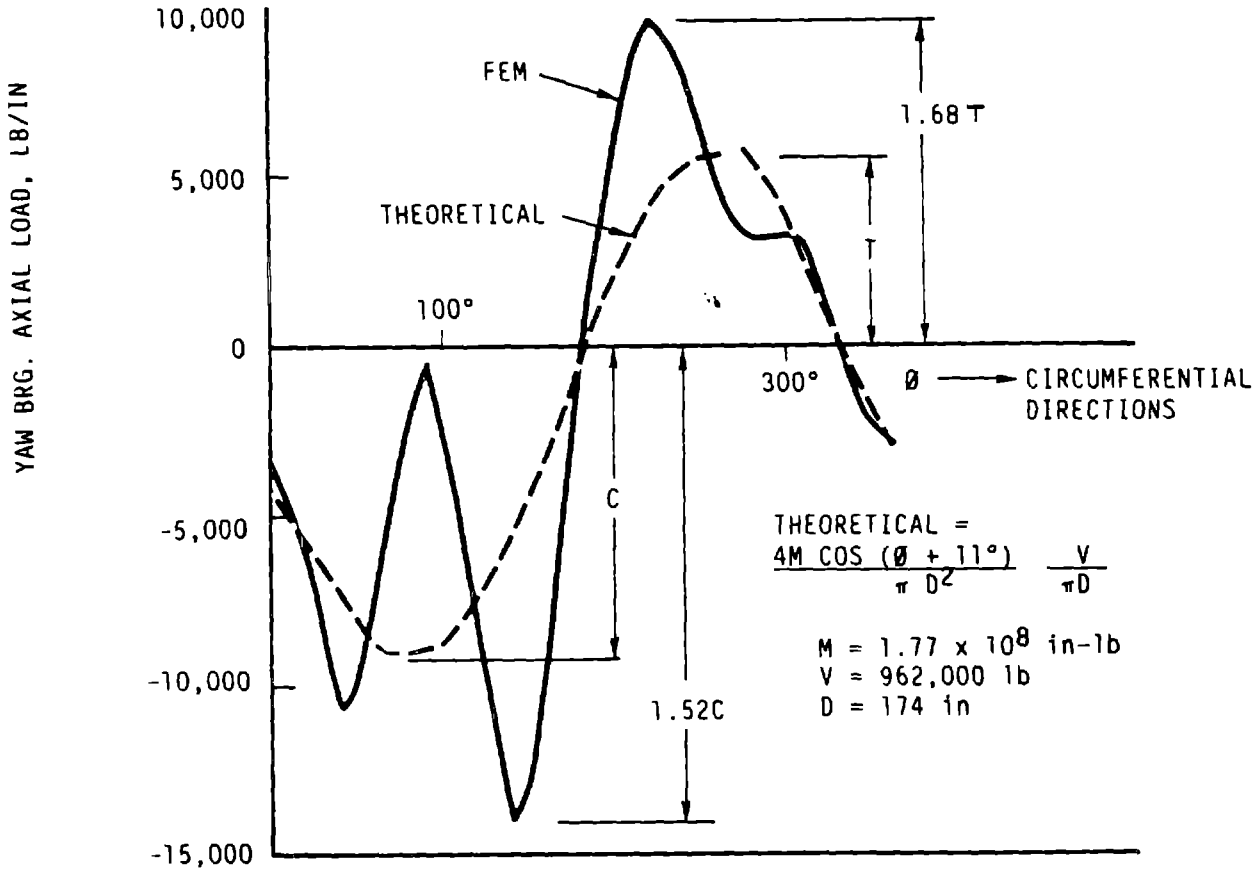

Figure 7-21 Bearing Loads

The bearing stresses under the latest hurricane loads are summarized in Table 7-4. An analysis should plot subsurface shear versus depth. This plot would ensure that allowables are not exceeded at any depth. Previous load analyses have done this and the margins shown in the table are adequate.

The nose ring and retaining ring stresses, at points a and f' of Figure 7-19, are shown in Table 7-5. The bending stress is usually computed by bearing manufacturers, assuming that the roller load is uniformly distributed along the direction of the circumference. In this table, however, stress was computed at the root of the ring cantilever with roller line loads spaced as shown in Figure 7-22. This analysis increases the stress peak by about 50%, and shows the stress halfway between the rollers at about half the peak. This stress gives the one per roller cyclic stress during nacelle rotation.

As shown in both tables, good margins of safety exist for all conditions.

Table 7-4

Yaw Bearing Stresses Under Hurricane Load Conditions

	SUPPORT ROW	RETAINER ROW	RADIAL ROW
Race diameter, d_m, in.	174.01	173.62	171.06
Roller diameter, D, in.	1.575	1.26	.984
Roller length, l, in.	1.575	1.26	.985
No. of Rollers, N	297	362	447
Roller load/in, p, lb/in	24,497	15,526	3,502
Hertz Stress, σ_c, ksi (Note 1,3)	398	354.2	296.5
Hertz M.S.	.45	.63	.96
Contact Width, b, in.	.039	.028	.018
Case Depth, h, in.	.197	.197	.100
Max. Subsurface, Shear, τ_{yz}, ksi	120	106.3	89
Shear M.S. (Note 2)	.59	.79	1.13
Core Interface, Shear, τ_{yz}, ksi	38.3	24.8	26.0
Core M.S. (Note 2)	.57	1.42	1.30

NOTES:
1) The Hertz stress allowable is 580 ksi per AFMBA
2) The shear stress allowable is 190 ksi in case, and 60 ksi in core
3) Assumes 58 - 60 RC case
4) The formulas for stress are found in Roark or Sealy and Smith

Table 7-5

Yaw Bearing Bending Stresses, Limit Load and Fatigue

	NOSE RING pt. a	RETAINING RING pt. f'
Depth, t, in.	2.216	1.728
Width, l, in.	1.839	1.504
Limit Load per in.	17,815	6,305
Bending Stress, σ_b, ksi	26.69	12.70
σ_bx K_t (= 2.0), ksi	53.37	25.40
M.S. (2)	1.25	3.72

Cycles	Fatigue Load, $\sigma_b x k_t$		
359 x 10^6	RMC (range), psi	1,615	1,708
30,000	1 per rev, psi (Note 1)	0	13,544
30,000 * N/2	1 per roller, psi	10,839	6,772
RMC (Total), psi (Note 3)		2,711	2,135
M.S.		.75	1.22

(1) The nose ring does not unload as nacelle rotates

(2) Core properties of σ_y = 120 ksi were used

(3) Range stress for AISC "A" category is 4,740 psi

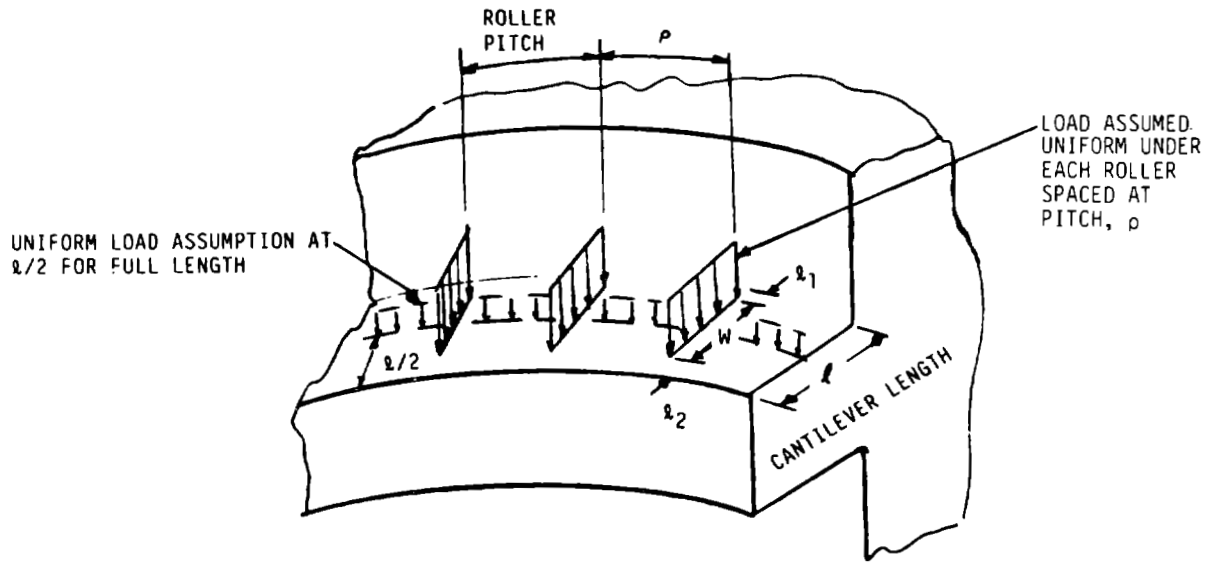

Figure 7-22 Comparison of Nose Ring Load Assumptions

7.5.3 YAW DRIVE AND HYDRAULIC SUBSYSTEM

The yaw drive provides the motive power to rotate the nacelle and the clamping force to hold the nacelle in alignment with the wind. The drive can operate in the standby enable, startup, or run modes of the control system. In the first two modes, the rotor does not turn. The requirements of the system are to:

1. provide the required operating and stationary torques,
2. meet the dynamics requirements of the system, by having proper stiffness,
3. limit the rotational speed, to avoid gyroscopic effects.

The requirements stipulated a low-cost, reliable system that could tolerate misalignments caused by structural deflections and manufacturing tolerances.

The traditional yaw drive solution is a geared motor driving a large gear, usually cut right into a race of the yaw bearing. This solution has a reasonable cost, and the drive operates smoothly. Still, misalignment problems can occur. For the MOD-5A a simpler, push-pull drive was chosen. A variation of the push-pull drive was used in one MOD-0A machine. The MOD-0A system's dynamics were the reason for using this type of drive. The drive had better stiffness characteristics than the geared drive used on other MOD-0A machines. NASA indicated the MOD-0A drive worked well, and that corrosion was the biggest concern. The yaw drive is entirely enclosed on the MOD-5A, so this concern was eliminated.

The operation of the push-pull yaw drive is shown in Figure 7-23. The top of the lower yaw housing is a large disk. The lower part of the yaw bearing is mounted on the outside of the disk. The inside of the disk acts as a horizontal brake disk. Two sets of hydraulic caliper brakes grab this disk. Two groups of two brakes, separated by 180°, are called the holding brake set. They are mounted directly on the upper yaw housing. They inhibit yaw motion when energized. The other two groups of two brakes, separated by 180°, are called the motive brake set. They are located 90° from the holding brakes, and are mounted on segments of circular track bolted to the upper yaw housing. They are called the motive brakes because they move the nacelle. Two hydraulic cylinders on each end of each motive brake group move the brakes freely along the track when the brakes are not energized.

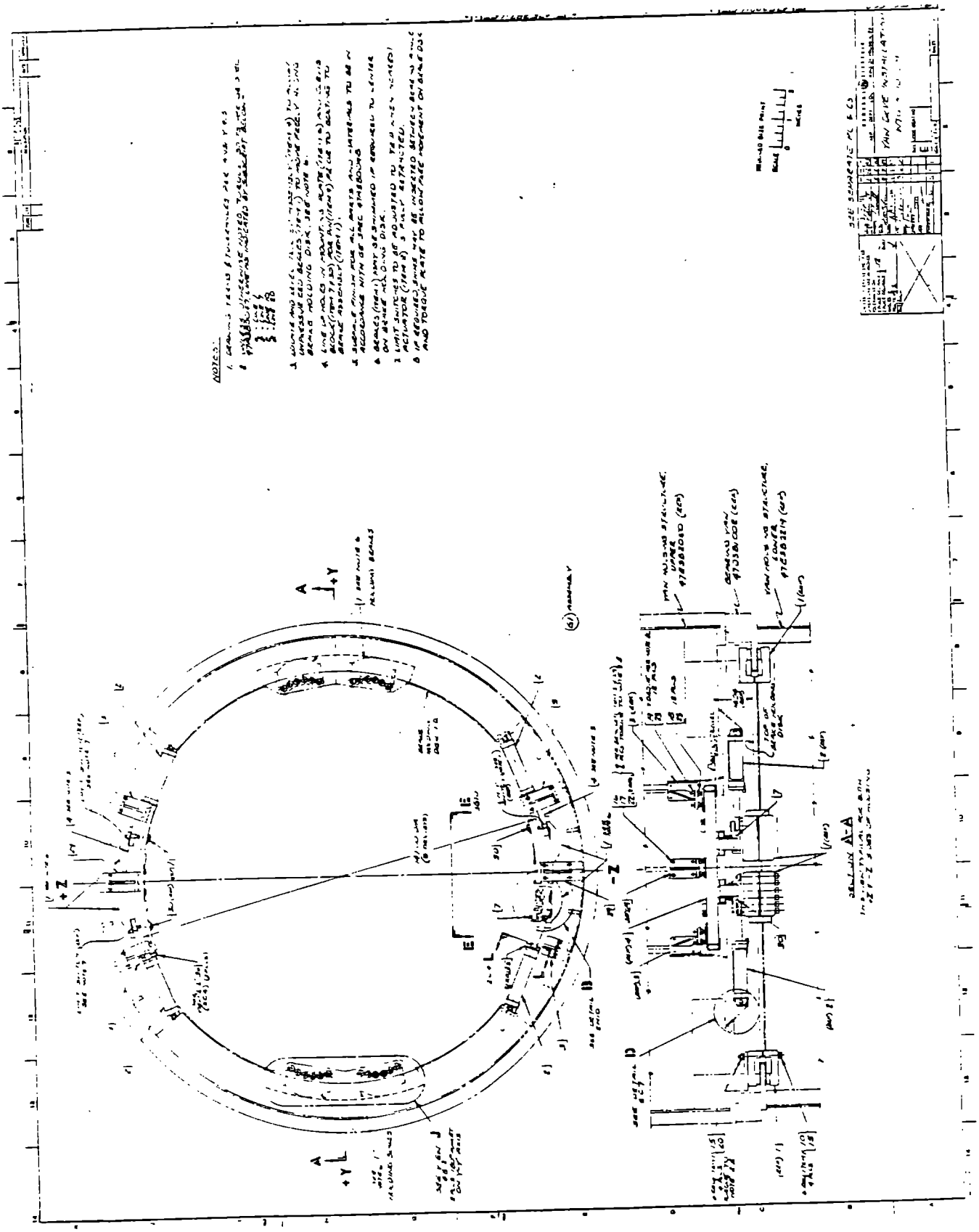

Figure 7-23. Yaw Drive Subsystem

The controller operates the yaw drive by energizing and de-energizing hydraulic valves. When the holding brakes are de-energized, the motive brakes are energized and the cylinders are pressurized, and the cylinders pull and push the nacelle relative to the tower. At the end of the cylinder's stroke a limit switch signal tells the controller to 1) energize the holding brake, 2) de-energize the motive brake and 3) reverse the flow into the cylinders. The nacelle is held while the motive brakes travel to the other end of the circular track. When the brakes reach the end of the track, another limit switch reverses these steps, and the nacelle moves again. Each of the four cylinders has a 4 in. bore, a 2 in. rod, and a 15 in. stroke. As 1 in. on each end is for limit switch overtravel, 13 in. of the stroke is active. Each inch of cylinder stroke provides .77° of nacelle rotation. The nacelle rotates approximately 10° in either direction, then stops while all four cylinders retract before the next cycle. Each end of the cylinders is cushioned to reduce stop loads. The cylinder that retracts most quickly waits for the other set's limit switch to close. That is, when the cylinders are retracting the controller responds only when both limit switches close. However, on the drive stroke, the controller responds when either closes, since power must be removed once either set reaches the end of its stroke.

In section A-A of Figure 7-23, note that the cylinders do not attach at the center of the brake's plane of action. The cylinders rotate the brakes relative to the track and to the brake disk. To limit the rotation, the outer brake pad retainers were replaced with a heavier piece that has minimal clearance relative to the disc. With the end plates separated by 38 in., the rotation is limited to less than 0.03° and only small forces are generated, to avoid damage to the disk.

The hydraulic flow to the cylinder is controlled by a piping restriction and the drive normally rotates the nacelle at .40°/sec., for an average speed of .20°/sec. This speed can be held for the first 6 minutes (~72°) of motion; then it reduces to .30°/sec., for an average of .15°/sec.

A 14-gallon accumulator enables the system to operate at the initial high speed. After six minutes of continuous operation, the accumulator is depleted

and the speed is limited by the rate of flow of the pump. Note that system pressure will drop to the accumulator charge pressure of 1300 psi after the six minutes of continuous motion. This pressure should be high enough, since tne wind turbine would not be rotating during a large yaw manuever. When the wind turbine is rotating and delivering power, the yaw drive torque must overcome a torque proportional to the drivetrain torque because of the seven degree tilt of the rotor.

Hydraulic power for the yaw drive is supplied by a power supply module consisting of a 4.5 gpm, 3000 psi rotary piston pump and a 10 hp, 1800 rpm, 480 V, 3Ø 60 Hz electric motor assembly, a 30-gallon reservoir, suction and discharge filters and an immersion heater. This assembly is mounted on a structural subplate providing the necessary rigidity for transportation and handling. An oil level switch in the reservoir warns against loss of fluid. A pressure switch, at the discharge point of the pump, indicates that the pump is delivering fluid. A relief valve in the pump's discharge line protects the system against excess pressure.

A separate control package contains the switching valves, diagnostic and warning sensors and back-up accumulators necessary to convert the control signals into force and motion by the brakes and actuators. Additional valves in the control package provide control for the low speed shaft brakes. The schematic diagram detailing the function and operation of the yaw drive hydraulics is shown in Figure 7-24.

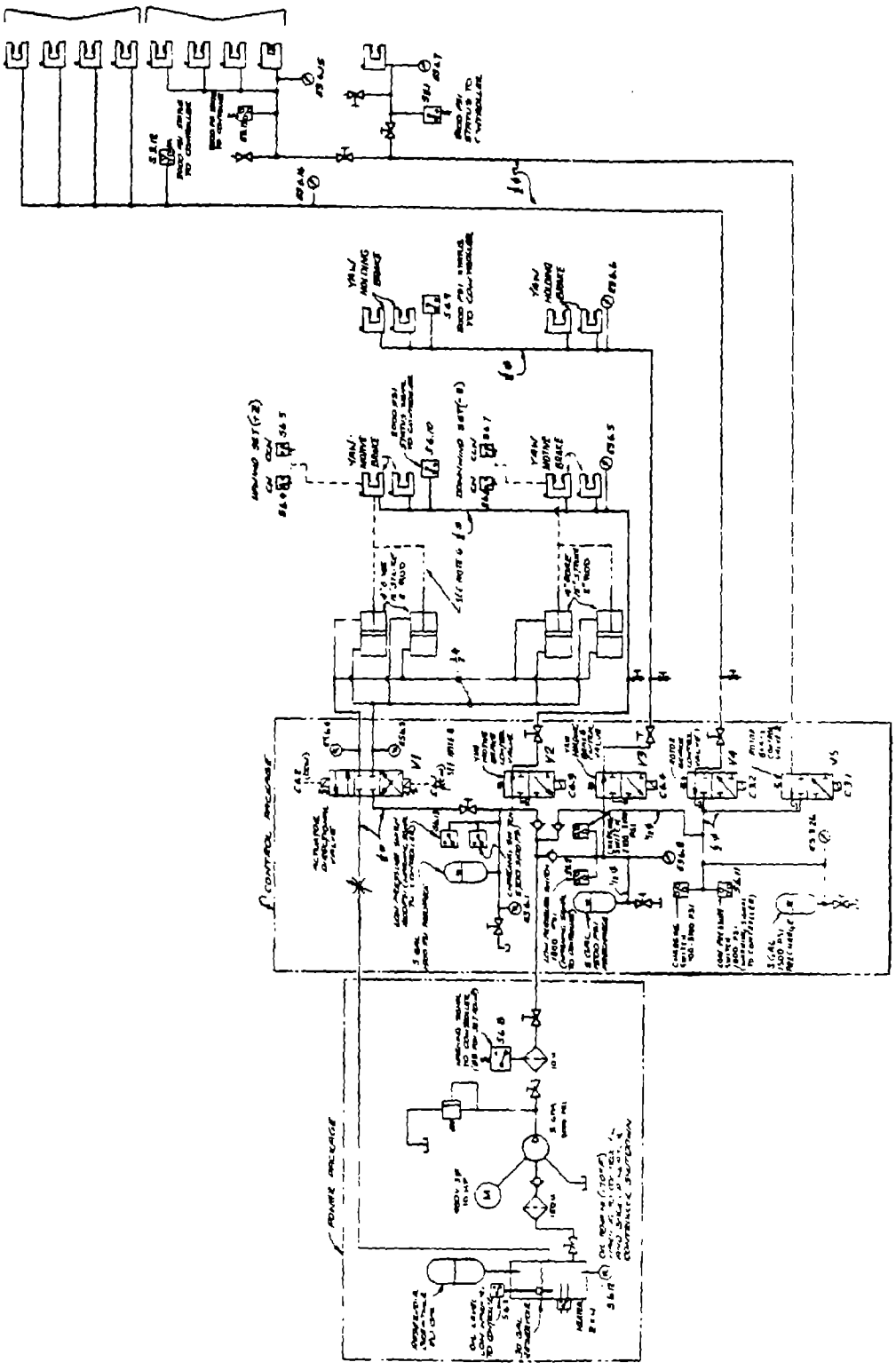

Figure 7-24 Yaw Hydraulic Subsystem

REFERENCES:

7-1 Design and Construction of Steel Chimney Liners, Am. Soc. of Civil Engineers, 1975, pg. 70-71.

7-2 Timeshenko, S. D. and Gere, J. M., Theory of Elasaic Stability, 2nd Ed., McGraw Hill, 1961.

7-3 "Summary of Buckling Tests on Fabricated Steel Cylindrical Shells in USA" Miller, C. D., Offshore Structure Engineering, Vol. III, Edited by Harding et al, Gulf Publishing Co., 1982.

7-4 "Local Buckling of Thin-Wall Tubular Steel Members", Stephens, M. J., et al CE Report 103, University of Alberta, Edmonton, Alberta Feb. 1982.

7-5 American Society of Mechanical Engineers, Boiler and Pressure Vessel Code Case N-284, "Metal Containment Shell Buckling Design Methods," Supplement #2 to Nuclear Code Case Book, 1980.

7-6 American Petroleum Institute, "Recommended Practice for Planning, Designing, and Constructing Fixed Offshore Platforms," API RP 2A, Eleventh Edition, Jan. 1980.

7-7 Det Norske Veritas, Rules for the Design Construction and Inspection of Offshore Structures, Appendix C, 1977.

7-8 Ostapenko, A. "Local Buckling of Welded Tabular Columns", Stability of Structures Under Static and Dynamic Loads Colloquim, May, 1977. Published by ASCE.

7-9 "Manual of Steel Construction", American Institute of Steel Construction, 8th Edition, 1980.

7-10 Gurney, T. R. "Fatigue of Welded Structures", Cambridge U. Press, pg. 93.

REFERENCES: (CONT.)

7-11 ACI 215 R-74 "Considerations for Design of Concrete Structures Subjected to Fatigue Loading

7-12 ACI SP-41 "Fatigue of Concrete"

7-13 PCA Bulletin RD 059.01E "Design of Reinforced Concrete for Fatigue"

7-14 PCA Bulletin RD 045.01E "Fatigue Strength of High-Yield Reinforcing Bars"

7-15 ACI 318-77 "Building Code Requirements for Reinforced Concrete"

7-16 AISC Specification for Design, Fabrication and Erection of Structural Steel for Buildings, & AISC Code of Standard Practice, 1980

7-17 Richert, F.E. Jr et al "Vibrations of Soils and Foundations", Prentice Hall

7-18 Winter, Geo. and Nilson, A.H. "Design of Concrete Structures" 9th Ed., McGraw-Hill, 1979

7-19 Aaronson, S.F. "Analyzing Critical Joints", pg. 95, Machine Design, Jan. 21, 1983

7-20 VDI 2230 Standard, "Systemative Calculation of High-Duty Bolted Joints", October 1977

7-21 Frank, K.H. "Fatigue Strength of Anchor Bolts", ASCE Journal of the Structural Division,June 1980

ABBREVIATIONS

A	Amperes
AAO	average annual outage time
AASHTO	American Association of State Highway and Transportation Officials
ac	alternating current
ACI	American Concrete Institute
A/C	aircraft
AGMA	American Gear Manufacturers Association
AILSTAB	Aileron Stability Analysis
AISC	American Institute of Steel Construction
ASCE	American Society of Civil Engineers
ASCII	American Standard for Computer Information Interchange
ASTER	a computer program
ASTM	American Society for Testing Materials
AWG	American Wire Gauge
AWS	American Welding Society
baud	the rate of transmission of data from one part of computer to another
BESD	backup emergency shutdown
CBI	Chicago Bridge and Iron
CD	coefficient of drag
CDS	controls data system
CEC	control electronics cabinet
ccw	counterclockwise
cfm	cubic feet per minute
CGT	crack growth threshold
CI	cut-in
CIS	cycle intercept stress
CMD	command
COE	cost of energy
COV	coefficient of variation
CPU	central processing unit
CRT	cathode ray tube
CVN	Charpy V-notch test
dc	direct current
DOE	Department of Energy

ECL	Eptak control language
EHD	elastohydrodynamic
EMC	equivalent moisture content
ES	engineering instrumentation system
EPTAK	trade name for controller from Eagle Signal Division of Gulf and Western Industries
EMI	electromagnetic interference
ESD	emergency shutdown
FMEA	failure modes effects analysis
fpm	feet per minute
fpy	failures per year
FRP	glass fiber-reinforced plastic
ft.	feet
g	a unit of acceleration, equal to 32 ft/sec or 9.8 m/sec
G	giga, a prefix meaning one billion
gal.	gallons
GBI	Gougeon Brothers Incorporatedde
GETSS	GE Turbine System Analysis
GETSTAB	a computer program
gpm	gallons per minute
Hz.	Hertz
IITRI	Illinois Institute of Technology, Research Institute
I/O	input/output
in.	inch
ISM	input signal manager
k	kilo, a prefix meaning 1000
kips	a unit of force or weight, kilopounds, or 1000 pounds
ksi	a unit of stress, kips per square inch, or 1000 psi
kV	kiloVolts, or 1000 Volts
kW	kiloWatt or 1000 Watts
kWh	kiloWatt-hours, or 1000 Watt-hours
lbs.	pounds
lb/MDGL	pounds per 1000 square feet of double glue line
LEFM	linear elastic fracture mechanics
LMC	laminae moisture content
LVDT	linear variable differential transformer

m	milli, a prefix meaning .001
M	mega, a prefix meaning 1,000,000
mA	milliAmperes, or .001 of an Ampere
MC	moisture content
ml	milliliter
mpn	miles per hour
mps	meters per second
MTBF	mean time between failures
MTTR	mean time to repair
MS	structural margin of safety
m/sec	meters per second
mps	meters per second
MUX	multiplexer
MW	megaWatt, or one million Watts
MWA	megaWatt-Amperes, or a million Watt-Amperes
N	Newton, the unit of force in the metric system
NASA	National Aeronautics and Space Administration
NASTRAN	a computer program
NDT	Nil-ductility transition
NEMA	National Electrical Manufacturers Association
N-m	Newton-meter, the unit of moment in the metric system
NSD	normal shutdown
O&M	operating and maintenance
OIS	operational information system
OSM	output signal manager
P	per revolution
PCS	pitch change system
PGC	Philadelphia Gear Corporation
PSC	partial span control
PIR	progarm information report
PLV	pitch line velocity
ppm	parts per million
PROM	programmable read only memory
psf	pounds per square feet
psi	pounds per square inch
PWHT	post-weld heat treatment
QAERO	a computer program

R	ratio of actual stress to allowable stress, or minimum fatigue stress cycle to maximum fatigue stress cycle
rad/sec	radians per second
RAM	random access memory
RAM	reliability, availability, and maintainability
RFP	request for proposal
RMC	root mean cubed
ROM	read only memory
rpm	revolutions per minute
RT	room temperature
SCAMP	Stiffness Coupling Approach Modal-Synthesis Program
SCI	Structural Composites, Incorporated
SIM-5A	a computer code for control system analysis
S_{min}	minimum stress
S_{max}	maximum stress
S-N	stress vs. number of cycles
SOW	Statement of Work
STRAP	Static Row Analysis Program
ssu	Saybolt univeral seconds
TBD	to be determined
TBR	to be resolved
TFT	transverse filament tape
TRAC	Transient Rotor Analysis Code
tty	teletype
TVI	television interference
UBC	Uniform Building Code
UPS	uninterruptible power supply
UDRI	University of Dayton Research Institute
V	Volts
Vac	alternating voltage
Vdc	constant voltage
W	Watts
WEPO	Wind Energy Project Office
WTG	wind turbine generator
WT	weight
WINDLD	a computer program
WINDOPT	a computer program

1. Report No.	2. Government Accession No.	3. Recipient's Catalog No.
NASA CR-174736		

4. Title and Subtitle	5. Report Date
MOD-5A Wind Turbine Generator Program Design Report Volume III - Final Design and System Description Book 1	August, 1984
	6. Performing Organization Code
7. Author(s)	8. Performing Organization Report No.
	10. Work Unit No.
9. Performing Organization Name and Address General Electric Company Advanced Energy Programs Department P.O. Box 527 King of Prussia, PA 19406	11. Contract or Grant No. DEN 3-153
	13. Type of Report and Period Covered Contractor Report
12. Sponsoring Agency Name and Address U.S. Department of Energy Conservation and Renewable Energy Division of Wind Energy Technology Washington, D.C. 20545	14. Sponsoring Agency Code DOE/NASA/0153-3

15. Supplementary Notes

Final report. Prepared under Interagency Agreement DE-AI01-79ET20305. Project Manager, T.P. Cahill, Wind Energy Project Office, NASA Lewis Research Center, Cleveland, Ohio 44135

16. Abstract

This report documents the design, development and analysis of the 7.3MW MOD-5A wind turbine generator covering work performed between July 1980 and June 1984. The report is divided into four volumes: Volume I summarizes the entire MOD-5A program, Volume II discusses the conceptual and preliminary design phases, Volume III describes the final design of the MOD-5A, and Volume IV contains the drawings and specifications developed for the final design.

Volume III, Final Design and System Description, describes the performance and characteristics of the MOD-5A wind turbine generator in its final configuration. Each subsystem - the rotor, drivetrain, nacelle, tower and foundation, power generation, and control and instrumentation subsystems - is described in detail. The manufacturing and construction plans, and the preparation of a potential site on Oahu, Hawaii, are documented. The quality assurance and safety plan, and analyses of failure modes and effects, and reliability, availability and maintainability are presented.

17. Key Words (Suggested by Author(s))	18. Distribution Statement
Renewable energy; Wind energy Wind power; Variable speed generator Wind turbine design; Wind turbine system; Wood rotor blades; Large scale wind turbine	Unclassified - unlimited STAR Category - 44 DOE Category - UC-60

19. Security Classif. (of this report)	20. Security Classif. (of this page)	21. No. of pages	22. Price*
Unclassified	Unclassified		

*For sale by the National Technical Information Service, Springfield, Virginia 22161